DISSERTATION

THE DEVELOPMENT OF NEW SYNTHETIC METHODS AND TECHNIQUES USING STRONG BRØNSTED BASES

Submitted by

Garrett A. Hoteling

Department of Chemistry

In partial fulfillment of the requirements

For the Degree of Doctor of Philosophy

Colorado State University

Fort Collins, Colorado

Summer 2024

Doctoral Committee:

Advisor: Jeffrey Bandar

Garret Miyake
Carmen Menoni
Christie Peebles

ABSTRACT

THE DEVELOPMENT OF NEW SYNTHETIC METHODS AND TECHNIQUES USING STRONG BRØNSTED BASES

Brønsted bases are indispensable tools in synthetic chemistry and, as such, deprotonation serves as a ubiquitous mode of molecular activation. By pushing the boundaries of what is possible within the acid-base reaction paradigm, unique synthetic methods and techniques can be developed. The work described in this thesis focuses on gaining a fundamental understanding of strong-base chemistry in efforts towards the development of new base-promoted synthetic methods. Herein, Brønsted bases have been investigated in two ways; 1) the design and application of benchtop-stable precatalyst salts for valuable organic superbases; and 2) the implementation of base-promoted halogen-transfer to develop benzylic oxidative coupling reactions with alkyl (hetero)arenes.

This dissertation consists of five chapters. Chapters One and Three provide background and motivation for the work disclosed in this dissertation. Chapters Two, Four and Five represent project areas I have developed with Chapter Two adapted from published work and Chapters Four and Five as drafts of unpublished work. Below is a list of the chapters including a summary of the content for each.

Chapter One describes the importance of organic superbases and their relevance to the synthetic community and the Bandar Group as a whole. Presnted here will be the various classes of superbases and their unique properties that dinstinguish them from other classes of bases. Additionally, applications and known limitations to use of these bases will be discussed here.

Chapter Two describes work along with Dr. Stephen J. Sujansky on the development of benchtop-stable organic superbase salts and the method for their facile *in situ* activation. Here, air-sensitive organic superbases form salts when mixed with carboxylic acids that are indefinitely stable on the benchtop. When combined with an epoxide additive, the carboxylate will react to open the epoxide and generate an alkoxide that can neutralize the superbase conjugate acid. This strategy is effective at promoting catalytic Michael-type additions and polymerizations as well as stoichiometric substitution and Pd-catalyzed cross-coupling reactions. This strain-release mechanism not only provides an accessible precatalyst for air-sensitive superbases but provides a new opportunity for controlling base concentration *in situ*.

Chapter Two describes the development of the Bandar Group's base-promoted halogen transfer research program. The history and importance of this mechanistic platform will be discussed as well as previous reports in the area by our group. In this chapter, the mechanism of base-promoted halogen-transfer is described, which enables the exchange of weakly acidic C–H bonds for C–X bonds that can be subsequently substituted with a pronucleophile *in situ*. This section will also provide the necessary background and motivation for Chapters Four and Five.

Chapter Four describes the development of a new method for the synthesis of benzylic amines from alkyl (hetero)arenes. The development, optimization, and scope investigation of this reaction are described herein. The results of this work represent the first general approach for benzylic C–H amination, functioning on a broad scope of alkyl (hetero)arenes and amine coupling partners.

Chapter Five describes the use of base-promoted halogen-transfer to enable alkyl (hetero)arene desaturation. With ethyl- and longer alkyl-substituted arenes, after benzylic halogenation, elimination takes place in the presence of excess base, a process that is competitive

with the substitution protocol described in Chapter Two. Here, this reactivity has been exploited to develop a general desaturation technique for alkyl (hetero)arenes. Under desaturation conditions, an amine pronucleophile can be added, at which point β-addition followed by subsequent desaturation affords the β-aryl enamine, which is a diversifiable functional handle. This chapter describes the development of desaturation, cascade enamine formation, and the modification of enamine products.

ACKNOWLEDGEMENTS

There are many people I would like to thank for helping and providing support for me during my journey in graduate school. I would like to begin with the Bandar Group, as I have worked closely with you all each and every day since I got here. I could not have asked for a better group of chemists to have worked with over the years, thank you for always being there to help me out. Whether it was talking through ideas in the office, helping me work through presentations, and especially the brewery trips and the overly competitive nature of our group outings, I would not trade a single day of it. I would like to specifically thank Kendelyn and Leidy, we joined this group together and have gone through and grown so much, thank you for being incredible colleagues and friends. For those who were here before I joined the group, Tom, Shawn, and Tyler who, even though you were not my direct mentors, you were incredibly supportive and influential on me. I learned so much from you and would not be where I am today without your guidance. Steve, I do not know even where to start, I owe so much of my progress and development to you. You have been an amazing mentor and friend who made this process so much easier, especially when we were stuck on the night shift during the pandemic. Thank you for grinding out the superbase precatalyst project, it was truly an honor to develop that project with you from the ground up, and see it finally come to fruition all these years later.

To all those who have come and gone since joining the lab, I want to thank you as well. First, I would like to thank Faith for being honestly the most positive person I have ever met. Your constant support has gotten me through a lot of tough days, so thank you. Mike, thank you for everything you taught me while you were here, I am still practicing a lot of the techniques to this day. Cristian, you have been an amazing friend and desk neighbour, thanks for always being down

to talk movies and food, it always made the days easier to get through. As for the younger students, Alex, Nick, Vivian, Kayla, and Viet, you have taught me a lot as well, especially what it takes to be an effective mentor, keep pushing I am excited to see what is in store for you all.

The next person I would like to thank is my advisor, Jeff Bandar. Thank you so much for giving me the chance to do research in your lab, I truly could not have asked for a better advisor and mentor. Thank you for your tireless effort and support, going through presentations, reports, and papers with me to make them the best they could be. You have been and always will be a great mentor and I am so excited to see what you and the group can accomplish moving forward.

I would next like to thank my amazing friends, Luke, Fran, Alex, Dakota, and Brennan, for their love and support during this whole process. Luke and Fran, thank you for the last three years of living together, I could not have asked for better roommates, it has been a real pleasure. Luke and Alex, thank you for helping me find my love for cooking, for going in three ways on a ssmoker to live out our dream of making brisket, and for always giving me something to look forward to doing. Dakota, thank you for being the best concert buddy anyone could ever ask for, I will always cherish our memories of going to as many shows together as we could, even driving five hours out to Aspen in the middle of February. Brennan, you are truly an amazing friend and thank you so much for getting us all into playing D&D, it really brought us all closer together. You are all more than just friends, we have truly been a family here in Colorado and you have helped me learn and grow so much as a person.

Outside of CSU, thank you Mom and Dad, you are amazing parents and have taught me how to be both a good person and a hard worker. I would not be where I am today if it were not for you both. Thank you to Grammy and Grampy for always being there providing unconditional

support. Thank you to Abbey and Colin, and my niece and nephew Lyla and Jesse, I am truly honored to have you as family and thank you for all you have done to support me through this.

Finally, the last person I would like to thank is my amazing girlfriend, Macayla. Thank you for taking this chance with me five years ago to pack up our lives and move across the country to Colorado. You have been here for me every step of the way and I cannot thank you enough for all you have done for me. We have grown so much together since moving here and I have cherished every moment of it. Thank you also for committing with me to getting our dog, Edison. He has been such an amazing part of our lives, and I am so happy we made the decision to get him four years ago, he is the best dog in the world. I am so excited to see what we have in store for us next, and I could not be happier to do it together.

TABLE OF CONTENTS

CHAPTER ONE

ORGANIC SUPERBASES AND THEIR UTILITY IN SYNTHETIC METHODOLOGY

1.1 Chapter Overview

Deprotonation is one of the most fundamental ways one can activate a molecule, thus making Brønsted bases indispensable tools in synthetic chemistry. For a given application, the exact choice of base can be of critical importance as its properties often dictate reaction outcomes.[1] The Bandar Group focuses on utilizing strong Brønsted bases in order for activation of weakly-acidic substrates in order to discover new and innovative synthetic methods. One such class of strong Brønsted bases is organic superbases, which are at the cutting-edge of modern synthetic chemistry due to a number of unique properties.[2,3] This chapter focuses on establishing the relevance and importance of organic superbases to provide motivation for Chapter Two, the development of shelf-stable precatalysts of organic superbases which, once added to solution, spontaneously generate the freebase for use in reaction applications. I worked in tandem on this project with Dr. Steve Sujansky who effectively laid the necessary groundwork for this method.

1.2 Background for Organic Superbases

Organic superbases are defined as neutral organic compounds possessing a pK_a, value greater than that of the Proton Sponge® (18.6, referenced in MeCN solvent).[2-5] The high basicity of organic superbases is derived from their ability to delocalize the positive charge upon protonation throughout the entire molecule.[4-7] The strength of the base is, in turn, determined by what degree this positive charge can be distributed. Many organic compounds can be classified as organic superbases and some common subsets of these structures include amidines, guanidines,

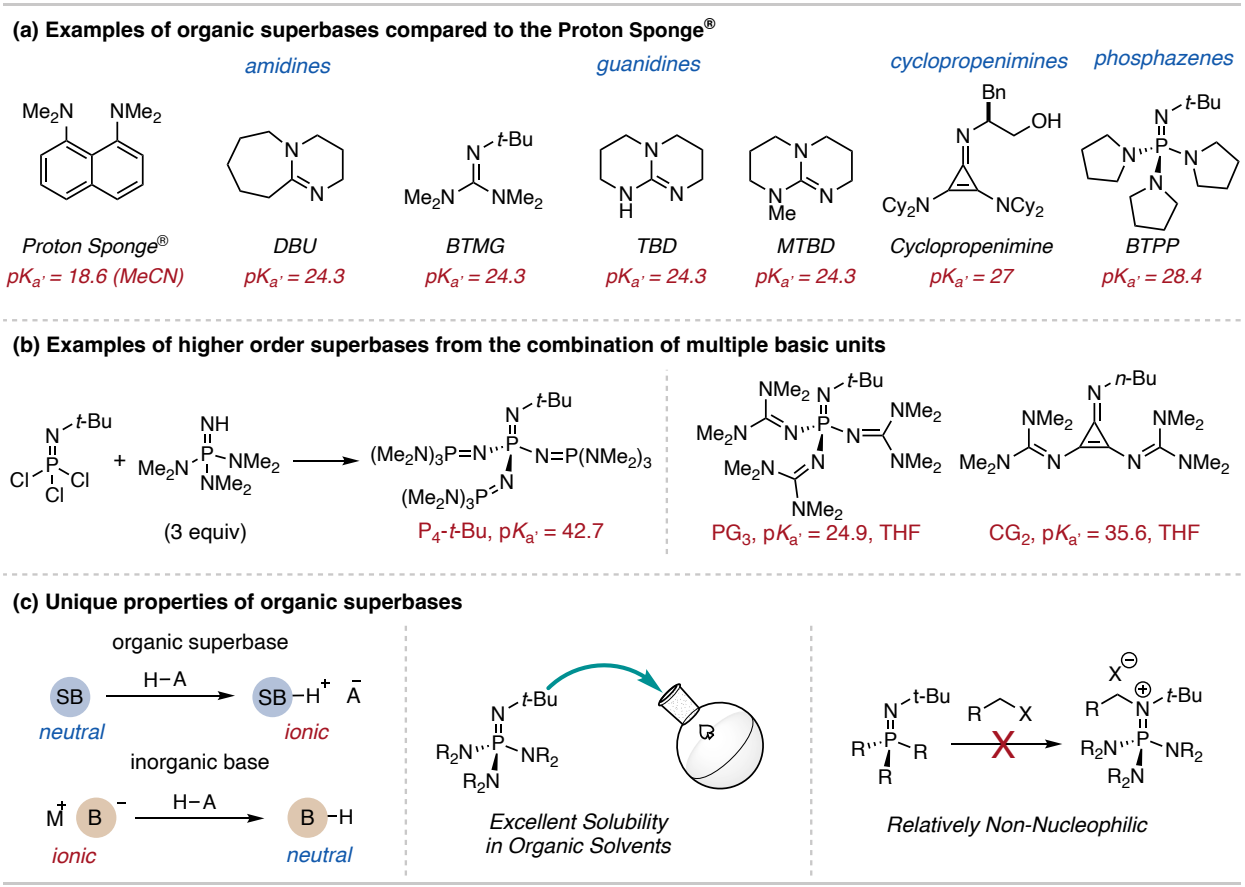

Figure 1.1: Examples of organic superbases and their unique properties

cyclopropenimines, and phosphazenes, with examples shown in Figure 1.1a.[2,5,6,8] Higher-order superbases can be synthesized by combining multiple superbasic units together to access a more basic compound. An example of this is with P_4-*t*-Bu, which features three P_1 phosphazene units appended to an iminophosphorane core structure, leading to a large increase in basicity ($pK_{a'}$ for P_1-*t*-Bu = 27 *vs* $pK_{a'}$ for P_4-*t*-Bu = 42.7, measured in MeCN).[6,9] This modularity has also been exploited in the synthesis of PG_3, where three guanidine unites are linked to an iminophosphorane core and higher order cyclopropenimine superbases where two guanidine subunits are combined with a cyclopropenimine core (Figure 1.1b).[10,11]

Organic superbases form stable conjugate acid ion pairs when combined with a strong acid, a fundamental contrast to commonly used anionic bases that form neutral conjugate acids (Figure

1.2a). This fundamental difference leads to a number of unique and desirable properties associated with organic superbases.[3] Due to their neutral structure, organic superbases are highly soluble in organic media, especially nonpolar solvent systems. Additionally, these bases are relatively non-nucleophilic, generally only acting as a Brønsted base in reaction applications. Finally, upon protonation superbases form large conjugate acid cations leading to a loose ion pair and a more "naked" and nucleophilic counteranion (Figure 1.1c). It is because of these properties that organic superbases have been engaged in a number of cutting-edge reaction applications such as reaction discovery, metal-catalyzed cross-coupling reactions, and high-throughput experimentation.[3] Section 1.4 of this chapter will highlight some examples of reactions that utilize organic superbases.

1.3 Relevance and Background of Phosphazene Superbases

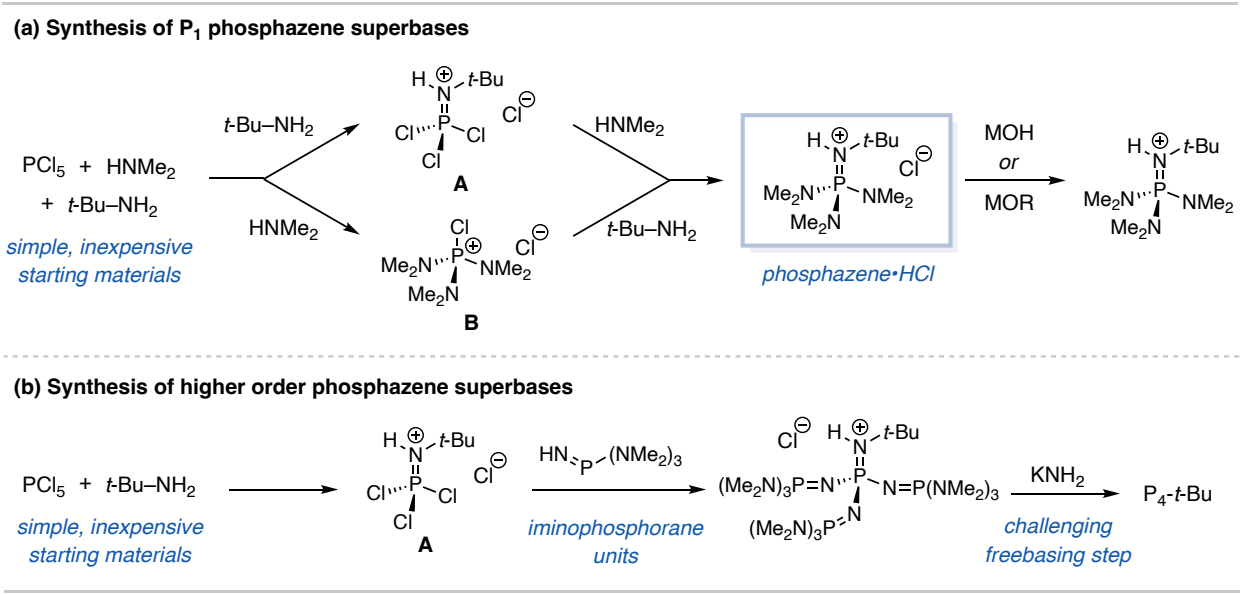

Figure 1.2: Synthesis of phosphazene superbases

The phosphazene class of superbases represent the strongest of the commercially available superbases spanning a broad range of basicity (pKa' = 27 – 43 in MeCN).[4] Phosphazenes were first discovered by Schwesinger in the late 1980s, however their use was limited in synthetic

applications.[12,13] The R-groups on the head imino nitrogen as well as the flanking amino nitrogens has led to derivatives of phosphazenes, including chiral variants to promote asymmetric transformations.[5,6,14] The synthesis of these bases is relatively straightforward, common starting materials like phosphorus pentachloride and alkyl amines can be employed. In the case of P_1 superbases, the primary amine (i.e., *tert*-butylamine) that represents the head nitrogen of the iminophosphorane is reacted with PCl_5 to generate intermediate **A**, which is subsequently reacted with excess of a secondary amine (i.e., dimethylamine), furnishing the phosphazene•HCl salt (Figure 1.2a). Alternatively, the reaction of the secondary amine with PCl_5 can be performed first (intermediate **B**), followed by reaction with the secondary amine to access the phosphazene•HCl salt. The freebase can then be generated by simply treating the phosphazene•HCl salt with hydroxide or alkoxide followed by distillation for purification. Moving from P_1 to P_2 and P_4 superbases, the synthesis to the phosphazene•HCl salt remains largely the same, replacing secondary amines with N–H iminophosphorane units (Figure 1.2b). However, with these higher order superbases, the neutralization and purification steps become more challenging. With P_4-*t*-Bu, the final neutralization step requires the use of hazardous potassium amide (KNH_2), with further discussion on this challenge in Section 1.5.[6]

Phosphazene superbases are very important to the Bandar Group as we have developed numerous methods utilizing P_4-*t*-Bu in the context of catalytic styrene functionalization reactions as the group's first developed area of research. In 2018, the group reported the use of catalytic P_4-*t*-Bu for the first general approach to the anti-Markovnikov addition of alcohols to styrene derivatives (Figure 1.3, left).[15] The hypothesis for this work was that use of P_4-*t*-Bu should be uniquely enabling for this reaction as its high basicity ($pK_{a'}$ = 30.2 in DMSO) and large size should lead to full deprotonation of an alcohol pronucleophile ($pK_{a'}$ = 28-32 in DMSO). The loose

coordinating nature of the P$_4$-*t*-Bu conjugate acid leads to a highly reactive alkoxide nucleophile that adds into the styrene derivative. It was found that this reaction is general to a wide scope of alcohols and styrene derivatives. In 2022, our group in a computational collaboration with the Paton Group at Colorado State University, reported a deep mechanistic investigation into this transformation.[16] Insights from these studies provided improved reaction conditions and expanded the substrate scope of compatible coupling partners.

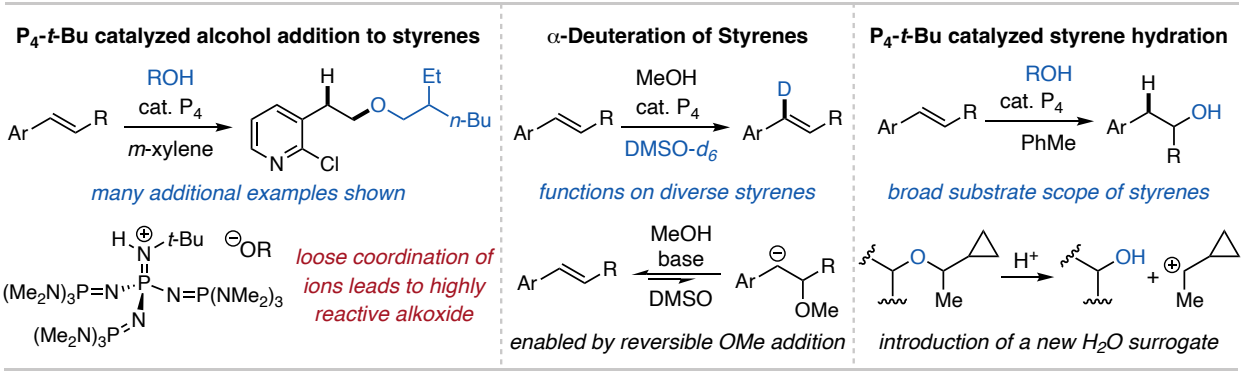

Figure 1.3: Synthetic methods employing catalytic P$_4$-*t*-Bu developed by the Bandar Group

This reactivity was further exploited for a styrene hydration protocol using a novel water surrogate that can be deprotected upon acidic workup of the reaction (Figure 1.3, middle).[17] In the initial report, it was observed that use of DMSO as a solvent caused the reaction to be highly reversible. A former member of the Bandar Group, Dr. Tom Puleo, discovered that this phenomenon could be exploited, which led to the development of the first method for α-selective deuteration of styrene derivatives in which methanol adds to the styrene, followed by deuteration and subsequent elimination of the alcohol (Figure 1.3, right).[18] The development of these methods highlights the importance of phosphazene superbases not only for the Bandar Group, but more broadly for synthetic methods development by exploiting their unique reactivity.

Beyond the use of P$_4$-*t*-Bu for these styrene functionalization reactions, this base has inspired two other research areas within our group. The first is a reductive coupling strategy for

the defluorofunctionalization of trifluoromethylarenes. The initial discovery in this field was made by a former member of the Bandar Group, Dr. Chaosheng Luo when he was attempting to deprotonate and functionalize difluoromethylarenes with allylsilane electrophiles (Figure 1.4, left). It was discovered that P$_4$-*t*-Bu was acting as a Lewis base to activate the allyl silane, which eventually led to the use of common fluoride salts to activate allyl silanes for defluorallylation of trifluoromethylarenes.[19] Since this seminal report, this defluorofunctionalization strategy has been expanded by Dr. Shawn Wright, another former member of the Bandar Group, through the use of formamides to trap the reactive intermediates to create a difluorobenzylic hemiaminal, a highly diversifiable functional handle.[20]

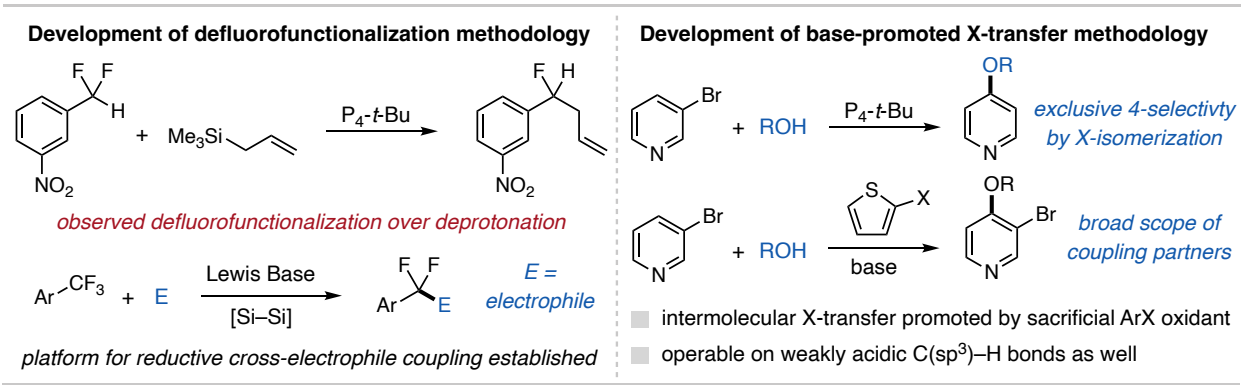

Figure 1.4: Other research areas in the Bandar Group inspired by initial findings with P$_4$-*t*-Bu

In addition to this reductive coupling platform, P$_4$-*t*-Bu has also been used to establish a third research area in our group, base-promoted halogen-transfer for oxidative coupling reactions. Here, Dr. Tom Puleo observed exclusive 4-position selectivity when attempting to promote S$_N$Ar reactivity on 3-bromopyridine, which was found to be due to intramolecular halogen transfer (Figure 1.4, right). Tom ultimately found that use of KO-t-Bu as a base can promote this halogen isomerization when coupled with a subsequent substitution reaction on a wide variety heteroarene substrates.[21] Since this seminal report, the group has expanded this reactivity using intermolecular halogen transfer to functionalize weakly acidic C–H bonds such as heteroarenes and electron-

deficient C(sp^3)–H bonds, and more recently, C(sp^3)–H bonds featured in benzylic and alpha carbonyl positions of molecules.[22-24] Chapter Three will describe in more detail the development of this field and Chapters Four and Five will describe my contributions to establishing new methodology with this mechanistic platform.

1.4 Example Reactions that Utilize Organic Superbases

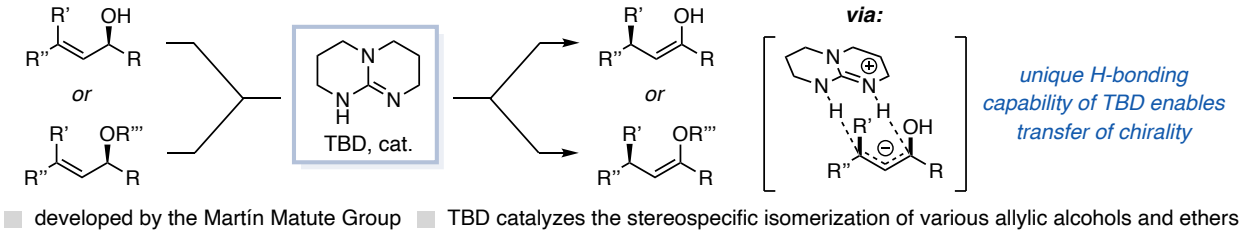

Figure 1.5: Use of TBD superbase for allylic alcohol isomerization

As mentioned, organic superbases have been engaged in a variety of useful reactions, and of the many examples five are highlighted here in this section. I have selected these five examples to cover the spectrum basicity of organic superbases, with most attention focused on phosphazene superbases due to their synthetic utility and interest to the Bandar Group. The first of these examples is the base-catalyzed stereospecific isomerization of allylic alcohols developed by the Martín-Matute Group in 2016 (Figure 1.5).[25] They found that use of the guanidine base TBD is important to the success of this reaction; when compared to other common bases of similar strengths TBD gave consistently higher yields and stereocontrol. The reason for the enhanced reactivity using TBD was attributed to an intimate ion pair formed between the allylic anion and conjugate acid of the base, which efficiently transfers the stereochemical information. The ability for the protonated TBD to act as both a H-bond donor and acceptor makes it uniquely well-suited to enable this reaction.

The next example for the use of organic superbases is the seminal report on cyclopropenimine bases by Bandar and Lambert in 2012.[8] In this report, asymmetric Michael

additions using glycine imine and acrylate Michael acceptors is disclosed. Key to the success of this reaction is the chiral alcohol appended to the head imino nitrogen of the base which, through H-bonding interactions, brings together the coupling partners in a specific orientation, resulting in selectivity for one enantiomer of the product (Figure 1.6). This reaction was shown to be operable on a variety of Michael acceptors with high yield and *ee*. The high basicity and mode of enantiocontrol featured here have enabled subsequent asymmetric transformations reported by the Lambert Group.[11,26-28]

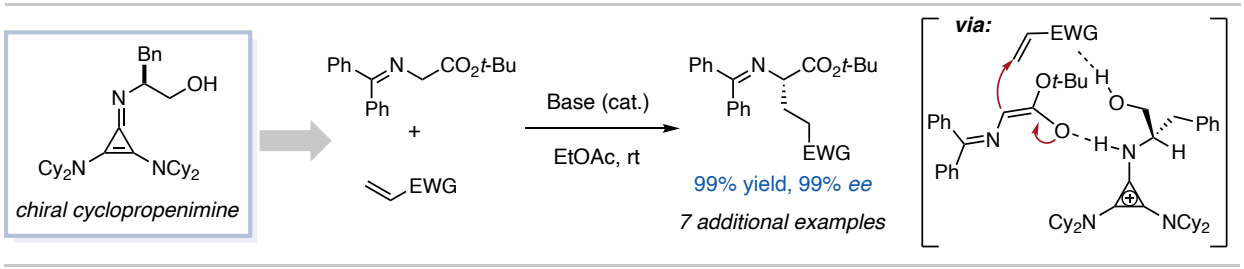

Figure 1.6: Use of cyclopropenimines for asymettric Michael additions by the Lambert Group

Moving into the phosphazene class of superbases, the next example is the use of BTPP for alcohol deoxyfluorination utilizing sulfonyl fluorides developed by the Doyle Group (Figure 1.7).[29-31] This reaction is very prone to side reactions, with alcohol elimination and base sulfonylation being the most predominant ones. In their seminal report, the authors found that use of amidine and guanidine superbases help to minimize these side pathways and promote effective deoxyfluorination. However, the ideal base, sulfonyl fluoride, and reaction conditions were found to be highly substrate dependent. In order to rapidly screen reaction conditions, the Doyle Group exploited the homogeneous reaction conditions enabled by organic superbases to implement machine learning-assisted high-throughput experimentation (HTE). Through this investigation, they found BTPP is very well suited at promoting these reactions for a broad scope of aliphatic alcohols. The large *t*-Bu group on the iminophosphorane nitrogen makes BTPP non-nulceophilic while still maintaining high basicity to promote this reaction while avoiding the unproductive side

reactions. This application showcases how the unique features of organic superbases are strategically utilized to enable useful transformations.

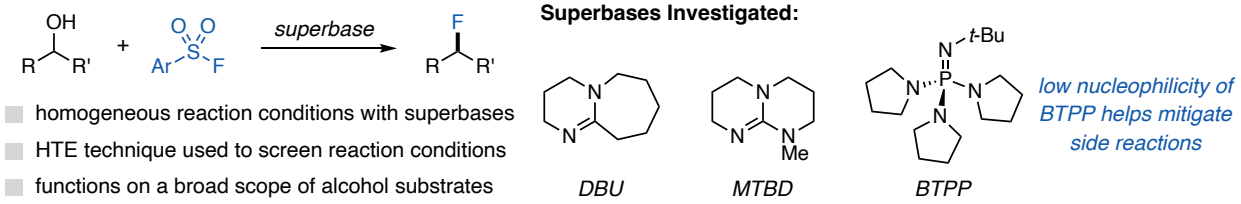

Figure 1.7: Use of organic superbases for alcohol deoxyfluorination by the Doyle Group

Higher order phosphazene superbase possess higher basicity and therefore can be used for a wider range of useful reaction applications. One such application is the use of P_2-Et in Pd-catalyzed cross-coupling reactions developed by scientists at Merck in 2015. The two main reasons why P_2-Et was employed in this reaction were (1) it is a relatively non-nucleophilic base that is unlikely to competitively bind to the Pd catalyst and inhibit the reaction and (2) the high solubility of the base enables homogeneous room temperature reaction conditions required for the implementation of HTE. Through this rapid condition screening, the authors found that P_2-Et is compatible with a series of Pd catalysts and ligands to promote a wide variety of C–C, C–O, and C–N coupling reactions. This protocol was utilized for the synthesis of a complex and base-sensitive pharmaceutical target, highlighting the importance of utilizing phosphazenes for cutting-edge reaction applications (Figure 1.8).

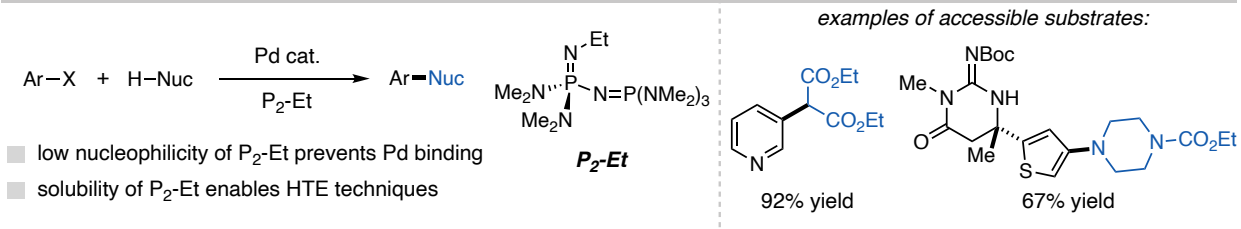

Figure 1.8: Use of P_2-Et for Pd-catalyzed cross coupling reactions by Dreher and coworkers

A fifth example of the utility of organic superbase is in the use of catalytic P_4-*t*-Bu to enable the amination of methoxy(hetero)arenes developed by the Kondo Group in 2019 (Figure 1.9).[33]

Similar to work developed by our group for hydroetherification of styrene derivatives, the utilization of P_4-*t*-Bu here can fully deprotonate a variety of amine pronucleophiles, leading to a loosely coordinated and thus highly reactive nucleophile that can undergo the desired S_NAr reaction. This reaction takes advantage of methoxyarenes, which are prevalent and abundant functional groups that are typically not considered to be reactive functional groups in this manner. A wide variety of amines and electron-deficient methoxyarenes are compatible with this transformation, providing a complementary approach to other methods for aromatic C–N bond formation.[34-37] Additionally, in prior work to this report the Kondo group disclosed similar reactivity for the aromatic methoxy-alkoxy exchange reaction.[38] This example highlights the power of using high order organic superbases to enable unique and useful reactions.

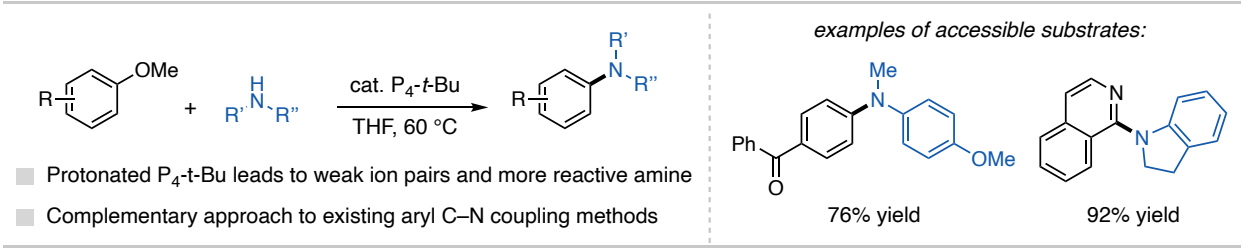

Figure 1.9: Use of P_4-*t*-Bu for the amination of methoxyarenes by the Kondo Group

1.5 Limitations of Organic Superbases

Discussed up to this point has been the synthetic utility and advantages of using organic superbases in place of more commonly employed inorganic base counterparts. Despite the precedent and potential of these bases, they possess significant limitations and drawbacks that stifle their translation from small-scale discovery settings to more widespread adoption by the chemistry community. These limitations include challenging preparation and handling, air and moisture sensitivity, and high cost. These challenges will be discussed in this section within the context of the different classes of organic superbases.

Beginning with the amidine and guanidine class of superbases, their lower basicity leads to relatively facile synthesis and general commercial availability. Figure 1.10a shows this in the context of the synthesis of DBU, which can be purchased relatively cheap ($0.42/g, $65/mol, from Millipore Sigma).[39] Other bases in this class, like BTMG and TBD for example, are similarly easy to synthesize and are cheap.[40] Despite this, these bases are prone to hydrolysis under aqueous conditions, which leads to a loss in basicity and a propensity to engage in side reactions when employed in reaction applications (Figure 1.10b).

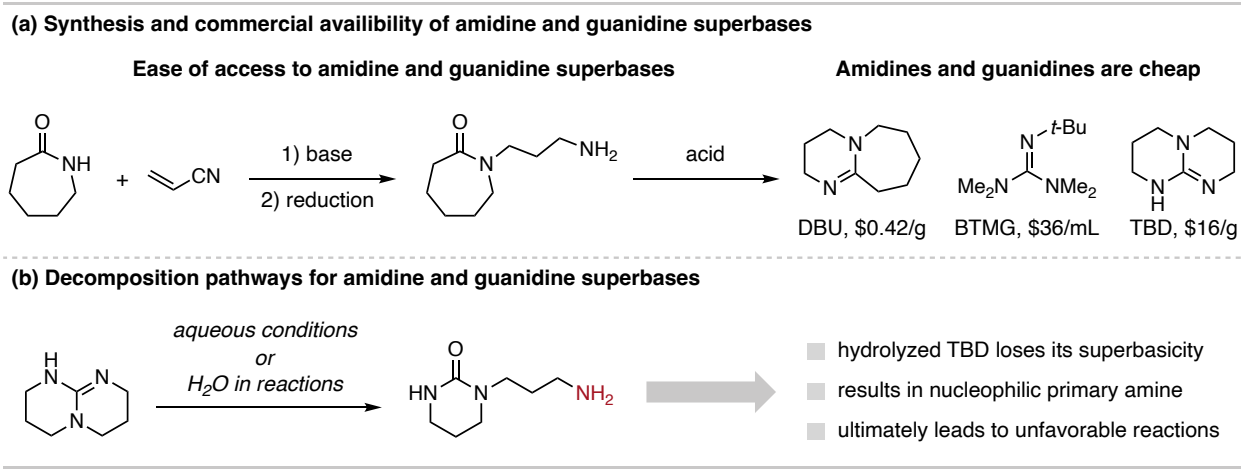

Figure 1.10: Limitations associated with amidine and guanidine superbases

Moving up in basicity to the cyclopropenimine class of organic superbases, they are relatively easy to synthesize from readily available starting materials and are commercially available, most often sold as the protonated HCl salt (Figure 1.11).[8,11] In practice, these bases can be challenging to use because they must be activated prior to use and in their freebase form, they are prone to decomposition over time. This ultimately leads to very limited application of these bases compared to other classes of organic superbases.

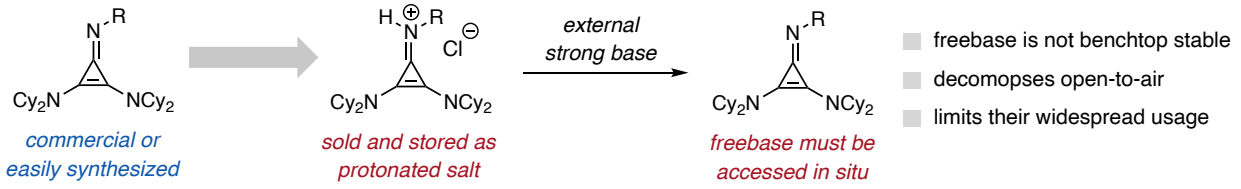

Figure 1.11: Limitations associated with cyclopropenimine superbases

Phosphazenes, the most basic and commonly employed class of organic superbase, accordingly have rather significant limitations for their use. The final freebasing step in the synthesis of higher order superbases the is often challenging and potentially hazardous, as described in Section 1.3. With P_4-*t*-Bu for example, access to the freebase requires the use of potassium amide in liquid ammonia, which is pyrophoric when exposed to air making this a dangerous reaction to perform.[9] Lower order phosphazenes like P_1 and P_2 variants do not require the use of such hazardous bases for their neutralization, however isolation and handling of the intermediates and products must be fully conducted air-free, which adds challenges and considerations to preparation.[5,6] An alternative approach to the generation of the P_4-*t*-Bu freebase was reported by Hoge in 2019 where its hydrate salt can be neutralized under repeated subjection reduced pressure and high heat. This method is ultimately unideal as the preparation of HP_4-*t*-Bu•OH is nontrivial.[42] For the synthesis of P_1-*t*-Bu, upon generation of the freebase the product must be isolated *via* distillation high temperature and low pressure, harsh conditions that can lead to superbase decomposition if not monitored carefully (Figure 1.12a). With P_2-*t*-Bu, a similar procedure is utilized to isolate the pure superbase, however it is even more challenging as P_2 bases are less volatile than P_1 bases, leading to even harsher distillation conditions.

In addition to the challenging synthesis of phosphazenes, they are known to be rather air and moisture sensitive (Figure 1.12b). Phosphazenes are known to undergo an irreversible decomposition pathway with carbon dioxide in the atmosphere to generate a phosphoramide, a

process that P_1 superbases are especially prone to with this process taking place over the course of a week when exposed to ambient conditions.[43] Though higher order superbases like P_2 and P_4 variants are known to undergo this decomposition pathway as well, with their higher basicity they are more prone to react with moisture in the air to form highly stable hydrate salts that are challenging to recover.[42] This ultimately leads to phosphazenes being limited in commercial availability and very expensive (BTPP: \$29/mL, \$8780/mol; P_2-*t*-Bu solution: \$73/mL, \$15,954/mol; P_4-*t*-Bu solution: \$58/mL, \$36,400/mol, from Millipore Sigma), limiting the accessibility of this class of superbases.

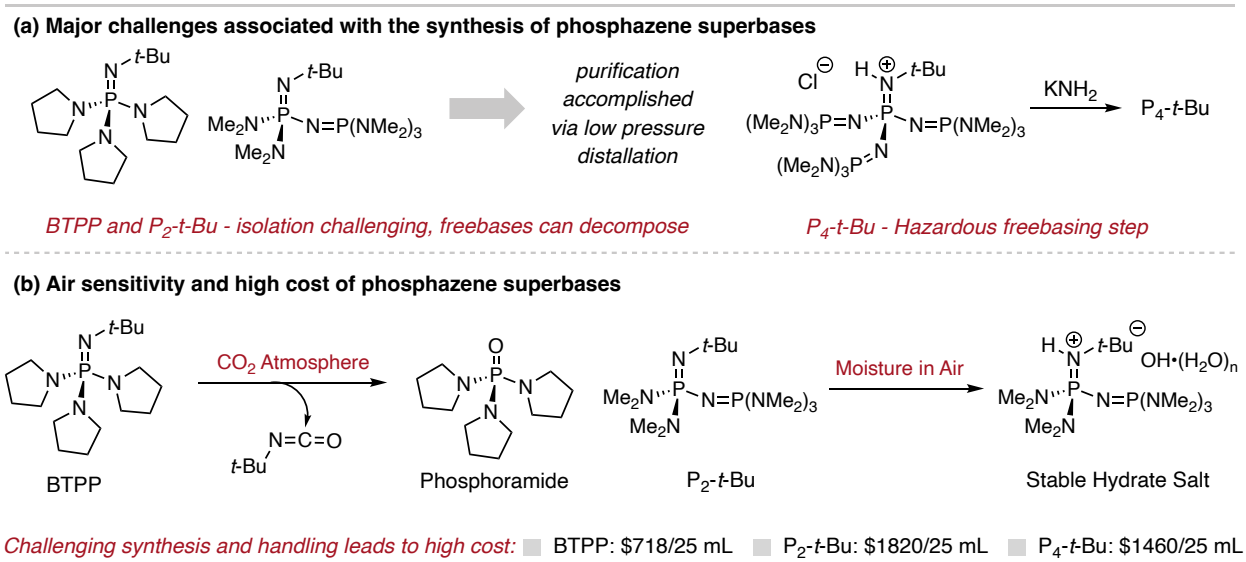

Figure 1.12: Challenges in the synthesis and handling of phosphazene superbases

1.6 Conclusion

This chapter provides background on the utility and importance of organic superbases in synthetic methodology. These bases are used in diverse applications where their unique properties are exploited to enable reactions that would not be possible with alternative strong Brønsted bases. Despite this utility, organic superbases have a series of limitations that prevent more widespread utilization, a challenge that I sought to address when I joined the Bandar Lab. Chapter Two describes my efforts in developing shelf-stable organic superbase precatalysts that spontaneously

generate the freebase when added to solution. The development of these precatalysts ultimately led to new and unique opportunities for base-promoted methodology that are not possible with the current way strong-base chemistry is conducted. Alternative superbase structures have been studied, however they are outside the scope of this dissertation and the main focus will be on phosphazene superbases.

REFERENCES

[1] For selected reviews on the utility of strong bases and their structural effects on reactivity, see: (a) Henderson, R. K.; Hill, A. P.; Redman, A. M.; Sneddon, H.F. Development of GSK's Acid and Base Selection Guides. *Green Chem.* **2015**, *17*, 945-949. (b) Haag, B.; Morison, M.; Ila, H.; Malakhov, V.; Knochel, P. Regio- and Chemoselective Metalation of Arenes and Heteroarenes Using Hindered Metal Amide Bases. *Angew. Chem. Int. Ed*. **2011**, *50*, 9794-9824. (c) Mulvey, R. E.; Mongin, F.; Uchiyama, M.; Kondo, Y. Deprotonative Metalation Using Ate Compounds: Synergy, Synthesis, and Structure Building. *Angew. Chem. Int. Ed.* **2007**, *46*, 3802–3824. (d) Collum, D. B.; McNeil, A. J.; Ramirez, A. Lithium Diisopropylamide: Solution Kinetics and Implications for Organic Synthesis. *Angew. Chem. Int. Ed.* **2007**, *46*, 3002-3017. (e) Patel, C. K.; Banerjee, S.; Kant, K.; Sengupta, R.; Aljaar, N.; Malakar, C. C. Roles of Alkali Metals tert-Butoxide as Catalysts and Activators in Organic Transformations. *Asian J. Org. Chem.* **2023**, *12*, e2023003. (f) Rathman, T. L.; Bailey, W. F. Optimization of Organolithium Reactions. *Org. Process Res. Dev*. **2009**, *13*, 144–151.

[2] Superbases for Organic Synthesis: Guanidines, Amidines, Phosphazenes and Related Organocatalysts; Ishikawa, T., Ed.; Wiley, Chichester, UK, 2009.

[3] Puleo, T. R.; Sujansky, S. J.; Wright, S. E.; Bandar, J. Organic Superbases in Recent Synthetic Methodology Research. *Chem. Eur. J*. **2020**, *27,* 4216 – 4229.

[4] Kaljurand, I.; Saame, J.; Rodima, T.; Koppel, I.; Koppel, I. A.; Kögel, J. F.; Sundermeyer, J.; Köhn, U.; Coles, M. P.; Leito, I. Experimental Basicities of Phosphazene, Guanidinophosphazene, and Proton Sponge Superbases in the Gas Phase and Solution. *J. Phys. Chem. A* **2016**, *120*, 2591−2604.

[5] Vazdar, K.; Margetić, D.; Kovačević, B.; Sundermeyer, J.; Leito, I.; Jahn, U. Design of Novel Uncharged Organic Superbases: Merging Basicity and Functionality. *Acc. Chem. Res.* **2021**, *54*, 3108−3123.

[6] Schwesinger, R.; Schlemper, H.; Hasenfratz, C.; Willaredt, J.; Dambacher, T.; Breuer, T.; Ottaway, C.; Fletschinger, M.; Boele, J.; Fritz, H.; Putzas, D.; Rotter, H. W.; Bordwell, F. G.; Satish, A. V.; Ji, G.-Z.; Peters, E.-M.; Peters, K.; von Schnering, H. G.; Walz, L. Extremely Strong, Uncharged Auxiliary Bases; Monomeric and Polymer-Supported Polyaminophosphazenes (P2- P5). *Liebigs Ann*. **1996**, 1055 – 1081.

[7] Leito, I.; Koppel, I. A.; Koppel, I.; Kaupmees, K.; Tshepelevitsh, S.; Saame J. Basicity Limits of Neutral Organic Superbases. *Angew. Chem. Int. Ed*. **2015**, *127*, 9394 –9397.

[8] Bandar, J. S.; Lambert, T. H. Enantioselective Brønsted Base Catalysis with Chiral Cyclopropenimines. *J. Am. Chem. Soc*. **2012**, *134*, 5552−5555.

[9] Schwesinger, R.; Kondo, Y. Phosphazene Base P_4-*t*-Bu. Encyclopedia of Reagents for Organic Synthesis. 2010. DOI: 10.1002/047084289X.rp150.pub2.

[10] Kolomeitsev, A. A.; Koppel, I. A.; Rodima, T.; Barten, J.; Lork, E.; Röschenthaler, G.-V.; Kaljurand, I.; Agnes Kütt, A.; Koppel, I.; Mäemets, V.; Leito, I. Guanidinophosphazenes: Design, Synthesis, and Basicity in THF and in the Gas Phase. *J. Am. Chem. Soc*. **2005**, *127*, 17656-17666.

[11] Nacsa, E. D.; Lambert, T. H. Higher-Order Cyclopropenimine Superbases: Direct Neutral Brønsted Base Catalyzed Michael Reactions with α-Aryl Esters. *J. Am. Chem. Soc*. **2015**, *137*, 10246−10253.

[12] Schwesinger, R. Chimia **1985**, *39*, 269 – 272.

[13] Schwesinger, R.; Schlemper, H. Peralkylated Polyaminophosphazenes- Extremely Strong, Neutral Nitrogen Bases. *Angew. Chem. Int. Ed. Engl*. **1987**, *26*, 1167 – 1169.

[14] Krawczyk, H.; Dzięgielewski, M.; Deredas, D.; Albrecht, A.; Albrecht, Ł. Chiral Iminophosphoranes – An Emerging Class of Superbase Organocatalysts. *Chem. Eur. J.* **2015**, *21*, 10268-10277.

[15] Luo, C.; Bandar, J. S. Superbase-Catalyzed anti-Markovnikov Alcohol Addition Reactions to Aryl Alkenes. *J. Am. Chem. Soc*. **2018**, *140*, 3547−3550.
[16] Luo, C.; Alegre-Requena, J. V.; Sujansky, S. J.; Pajk, S. P.; Gallegos, L. C.; Paton, R. S.; Bandar, J. S. Mechanistic Studies Yield Improved Protocols for Base-Catalyzed Anti-Markovnikov Alcohol Addition Reactions. *J. Am. Chem. Soc.* **2022**, *144*, 9586–9596.
[17] Pajk, S. P.; Qi, Z.; Sujanksy, S. J.; Bandar, J. S. A base-catalyzed approach for the anti-Markovnikov hydration of styrene derivatives. *Chem*. *Sci*., **2022**, *13*, 11427-11432.
[18] Puleo, T. R.; Strong, A. J.; Bandar, J. S. Catalytic α-Selective Deuteration of Styrene Derivatives. *J. Am*. *Chem*. *Soc*. **2019**, *141*, 1467–1472.
[19] Luo, C.; Bandar, J. S. Selective Defluoroallylation of Trifluoromethylarenes. *J. Am. Chem. Soc.* **2019**, *141*, 14120–14125.
[20] Wright, S. E.; Bandar, J. S. A Base-Promoted Reductive Coupling Platform for the Divergent Defluorofunctionalization of Trifluoromethylarenes. *J. Am. Chem. Soc.* **2022**, *144*, 29, 13032–13038.
[21] Puleo, T. R.; Bandar, J. S. Base-catalyzed aryl halide isomerization enables the 4-selective substitution of 3-bromopyridines. *Chem. Sci.* **2020**, *11*, 10517-10522.
[22] Puleo, T. R.; Klaus, D. R.; Bandar, J. S. Nucleophilic C–H Etherification of Heteroarenes Enabled by Base-Catalyzed Halogen Transfer. *J. Am. Chem. Soc.* **2021**, *143*, 12480–12486.
[23] Bone, K. I.; Puleo, T. R.; Bandar, J. S. Direct C–H Hydroxylation of N-Heteroarenes and Benzenes via Base-Catalyzed Halogen Transfer. *J. Am. Chem. Soc.* **2024**, *146*, 9755–9767.
[24] Bone, K. I.; Puleo, T. R.; Delost, M. D.; Shimizu, Y.; Bandar, J. S. Direct Benzylic C–H Etherification Enabled by Base-Promoted Halogen Transfer. *ChemRxiv preprint, DOI: 10.26434/chemrxiv-2024-fvrc1.*
[25] Martinez-Erro. S.; Sanz-Marco, A.; Gómez, A.; Vázquez-Romero, A.; Ahlquist, M. A. G.; Martín-Matute, B. Base-Catalyzed Stereospecific Isomerization of Electron-Deficient Allylic Alcohols and Ethers through Ion-Pairing. *J. Am. Chem. Soc*. **2016**, *138,* 13408−13414.
[26] Bandar, J. S.; Lambert, T. H. Cyclopropenimine-Catalyzed Enantioselective Mannich Reactions of t-Butyl Glycinates with N-Boc-Imines. *J. Am. Chem. Soc.* **2013**, *135*, 11799-11802.
[27] Bandar, J. S.; Sauer, G. S.; Wulff, W. D.; Lambert, T. H.; Vetticatt, M. J. Transition State Analysis of Enantioselective Brønsted Base Catalysis by Chiral Cyclopropenimines. *J. Am. Chem. Soc.* **2014**, *136*, 10700-10707.
[28] Seibel, Z. M.; Bandar, J. S.; Lambert, T. H. Enantioenriched α-Substituted Glutamates / Pyroglutamates via Enantioselective Cyclopropenimine-Catalyzed Michael Addition of Amino Ester Imines. *Beilstein J. Org. Chem.* **2021**, *17*, 2077-2084.
[29] Nielsen, M. K.; Ugaz, C. R.; Li, W.; Doyle, A. G. PyFluor: A Low-Cost, Stable, and Selective Deoxyfluorination Reagent. *J. Am. Chem. Soc*. **2015**, *137*, 9571−9574.
[30] Nielsen, M. K.; Ahneman, D. T.; Riera, O.; Doyle, A. G. Deoxyfluorination with Sulfonyl Fluorides: Navigating Reaction Space with Machine Learning. *J. Am. Chem. Soc*. **2018**, *140*, 5004−5008.
[31] Żurański, A. M.; Gandhi, S. S.; Doyle, A. G. A Machine Learning Approach to Model Interaction Effects: Development and Application to Alcohol Deoxyfluorination. *J. Am. Chem. Soc.* **2023**, *145*, 7898–7909.
[32] Santanilla, A. B.; Christensen, M.; Campeau, L.-C.; Davies, I. W.; Dreher, S. D. P_2Et Phosphazene: A Mild, Functional Group Tolerant Base for Soluble, Room Temperature Pd-Catalyzed C–N, C–O, and C– C Cross-Coupling Reactions. *Org. Lett.* **2015**, *17*, 3370-3373.

[33] Shigeno, M.; Hayashi, K.; Nozawa-Kumada, K.; Kondo, Y. Organic Superbase t-Bu-P4 Catalyzes Amination of Methoxy(hetero)arenes. *Org. Lett.* **2019**, *21*, 5505–5508.
[34] Ruiz-Castillo, P.; Bucwhald, S. L. pplications of Palladium-Catalyzed C−N Cross-Coupling Reactions. *Chem. Rev.* **2016**, *116*, 12564−12649.
[35] Forero-Cortés, P. A.; Haydl, A. M. The 25th Anniversary of the Buchwald−Hartwig Amination: Development, Applications, and Outlook. *Org. Process Res. Dev*. **2019**, *23*, 1478−1483.
[36] Monnier, F.; Taillefer, M. Catalytic C–C, C–N, and C–O Ullmann-Type Coupling Reactions. *Angew. Chem. Int. Ed.* **2009**, *48*, 6954 – 6971.
[37] Terrier, F. *Modern Nucleophilic Aromatic Substitution*; John Wiley & Sons, Inc.: Weinheim, Germany, 2013.
[38] Shigeno, M.; Hayashi, K.; Nozawa-Kumada, K.; Kondo, Y. Phosphazene Base tBu-P4 Catalyzed Methoxy–Alkoxy Exchange Reaction on (Hetero)Arenes. *Chem. Eur. J*. **2019**, *25*, 6077-6081.
[39] Oediger, H.; Möller, F.; 1,5-Diazabicyclo[5.4.0]undec-5-ene, a New Hydrogen Halide Acceptor. *Angew. Chem. Int. Ed. Engl*. **1967**, *6*, 76.
[40] Boyd, D. W.; Eswarakrishnan, V.; Hickenboth, C. R.; Karabin, R. F.; McCollum, G. J.; Minch, B. A.; Moriarity, T. C.; Zawacky, S. R. Method for producing bicyclic guanidines by use of a cyclic urea. Patent Number US20090281314 date **2009**-11-12.
[41] Hyde, A. M.; Calabria, R.; Arvary, R.; Wang, X.; Klapars, A. Investigating the Underappreciated Hydrolytic Instability of 1,8-Diazabicyclo[5.4.0]undec-7-ene and Related Unsaturated Nitrogenous Bases. *Org. Process Res. Dev*. **2019**, *23*, 1860−1871.
[42] Weitkamp, R. F.; Neumann, B.; Stammler, H. G.; Hoge, B Generation and Applications of the Hydroxide Trihydrate Anion, [OH(OH2)3]-, Stabilized by a Weakly Coordinating Cation. *Angew. Chem. Int. Ed*. **2019**, *58*, 14633 –14638.
[43] Courtemanche, M.-A.; Légaré, M.-A.; Rochette, É.; Fontaine, F.-G. Phosphazenes: efficient organocatalysts for the catalytic hydrosilylation of carbon dioxide. *Chem. Commun.*, **2015**, *51*, 6858–6861.

CHAPTER TWO

A STRATEGY FOR THE CONTROLLABLE GENERATION OF ORGANIC SUPERBASES FROM BENCHTOP-STABLE SALTS

2.1 Chapter Overview

This chapter discusses my efforts in the development of shelf-stable superbase precatalysts. This project is motivated by the fact that despite the utility of organic superbases, there are significant practical imitations to their use such as difficult preparation and air and moisture sensitivity, which is discussed in detail in Chapter One. The development of an effective precatalyst for these bases not only makes them easier to use but introduces new reactivity with a novel precatalyst activation strategy. I worked very closely with Steve on this project and when I joined the Bandar Group in 2019, he was laying the groundwork for our initial system.

Our initial precatalyst system involved the development of superbase carboxylate salts that would undergo decarboxylation to generate CO_2 and the active superbase. Though this initial method ultimately was met with little success, we found that the use of epoxide-strain release can help drive superbase neutralization. For this project, we focused on BTPP and P_2-*t*-Bu superbases as they are commercially available and commonly used for reaction discovery and methods development. The eventual goal of this project is to develop an effective precatalyst system for P_4-*t*-Bu, the strongest commercially available superbase, and to investigate the development of new superbases. This chapter will discuss our development of this epoxide-opening activation mechanism and its utilization in a number of reaction applications. Steve mainly focused on the development of the BTPP precatalyst system and I mainly focused on the development of the P_2-

t-Bu precatalyst system. The principles discussed in this chapter can translate to the development of more compatible precatalyst systems operable on stronger organic superbases in ongoing work being conducted in the Bandar Group.

2.2 Motivation for the Development of Organic Superbase Precatalysts

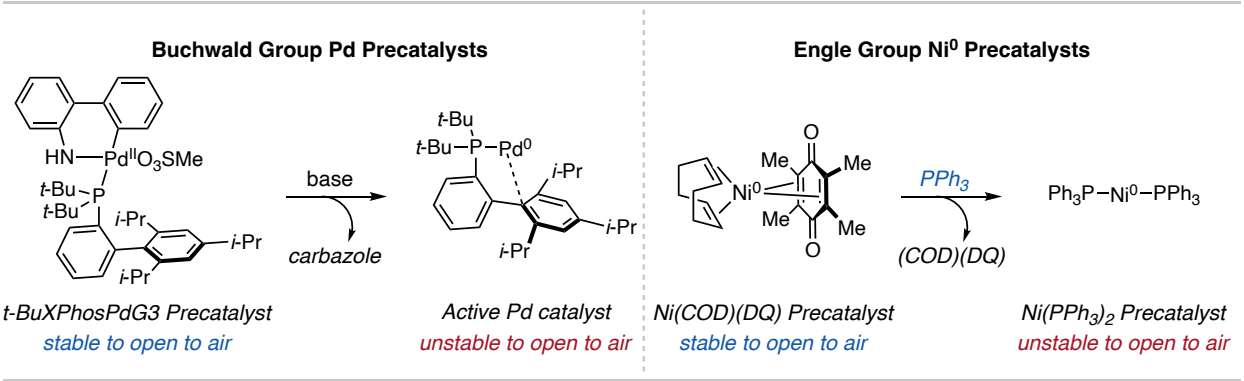

Figure 2.1: Examples of precatalysts for transition metal catalysts

As previously mentioned in Chapter 1, organic superbases are highly reactive compounds that suffer from air instability.[1,2] It is known that other highly reactive compounds in synthetic methodology also suffer from general air instability leading to hazardous working conditions with reagents like organolithium bases or decomposition in the case of transition metal catalysts.[3-5] A strategy for overcoming this challenge is through the development of a precatalyst, which is a stable form of the active catalyst that is activated upon addition to a reaction solution. This effectively makes conducting reactions with air-sensitive compounds more practical and facile. The most prevalent class of reagents precatalysts have been designed for are transition metal catalysts, due to the prevalence and impact of their use in cross-coupling reactions.[6] Two examples of precatalysts developed for transition metals include the Buchwald Pd precatalysts and the series of Ni precatalysts developed by the Engle Group (Figure 2.1).[5,7,8] In the case of the Buchwald precatalyst, the active catalyst is the Pd^0 species, however this form is highly air and moisture sensitive. The precatalyst exists as a Pd^{II} oxidative-addition complex that once put into solution

with a base, undergoes reductive elimination to form the active Pd^0 catalyst. In contrast, Engle and coworkers developed stable Ni^0 precatalysts through the implementation of stabilizing ligands that once put into solution, undergo ligand exchange to generate the active catalyst.

Given the air and moisture instability of organic superbases, we reasoned that this precatalyst concept could be applied to create practical, benchtop-stable versions of these bases. In order to develop effective precatalyst strategy for organic superbases, the mechanism for activation must take place spontaneously in solution (Figure 2.2). A unique feature of organic superbases is that they form stable salts upon protonation, which is a key distinction from commonly used inorganic bases that become neutral upon protonation. This is exemplified by the tetrafluoroborate salt of P_4-*t*-Bu (HP_4-*t*-Bu•BF_4), which we have stored open-to-air on our benchtop, and it has remained unchanged and stable for five years (Figure 2.2).

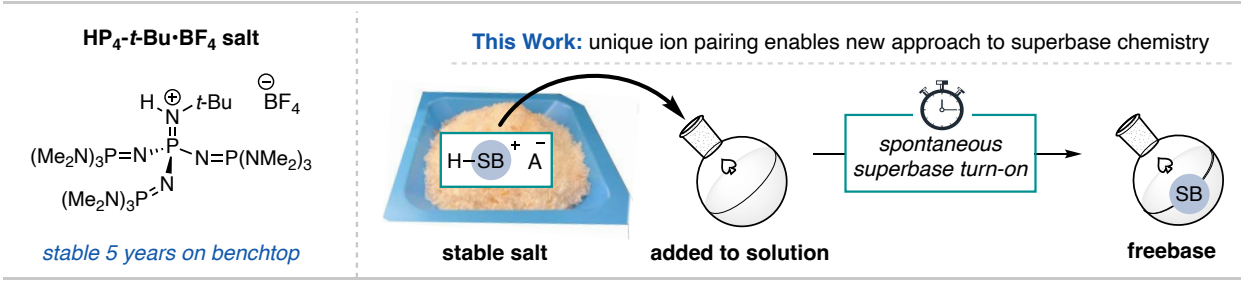

Figure 2.2: Stability of protonated superbases and the exploitation of this for a benchtop-stable precatalyst

In order to effectively utilize this distinct feature of organic superbases, deprotonation of the conjugate acid must be facilitated *in situ*. Overall, for an effective precatalyst, we wanted to avoid use of a separate, stronger base to solution. In our group's report on base-catalyzed anti-Markovnikov hydroetherification of styrene derivatives, the authors disclosed the use of KO-*t*-Bu to deprotonate HP_4-*t*-Bu•BF_4 and utilize the freebase on the benchtop (Figure 2.3, left).[9] Although this presented an immediate solution to *in situ* facilitation of conjugate acid deprotonation, for our precatalyst strategy we wanted to avoid the use of a separate, stronger base to generate the freebase. This would ultimately shift the burden onto this additional base for an ultimately ineffective

precatalyst. To address this, we hypothesized that the counteranion of the protonated superbase salt could be used as a functional handle to facilitate the necessary deprotonation.

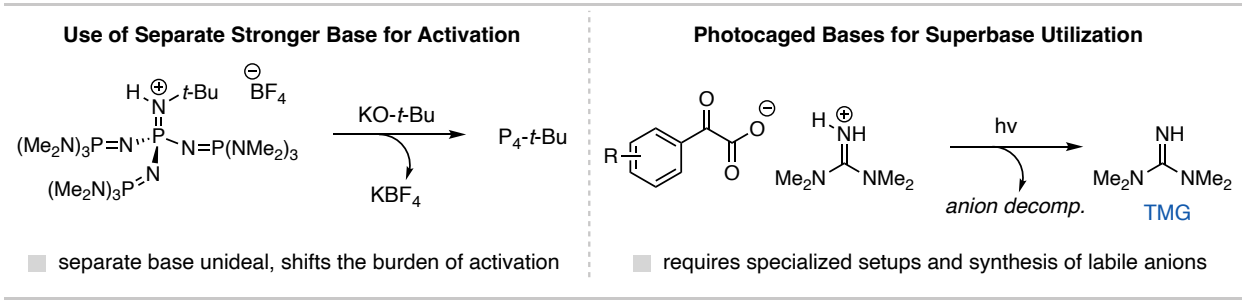

Figure 2.3: Current approaches to activate shelf-stable superbase salts *in situ*

For this strategy to work, the deprotonation reaction must be coupled with a driving force as the reaction is going from a low-energy protonated base to a high-energy freebase, a thermodynamically challenging transformation. In this context, the counteranion could be engaged in an exergonic reaction that facilitates deprotonation and the formation of an inert byproduct. The exploitation of the superbase conjugate acid salt counteranion has been reported previously in the context of photocaged bases.[10,11] Here, photoinduced counteranion decomposition leads to base decomposition, however, this approach has thus far only been used for photocuring applications and has yet to be applied towards synthetic methods (Figure 2.3, right). Additionally, utilization of a photochemical deprotonation mechanism would be unideal to the requirement of specialized reaction setups for success. Therefore, we sought to accomplish this using an alternate, thermal approach to facilitate deprotonation. Section 2.3 discusses our first generation precatalyst where we utilized a decarboxylation approach to generate the freebase from benchtop-stable carboxylate salts.

2.3 Decarboxylation Strategy for Organic Superbase Precatalysts

Our first approach to developing an effective superbase precatalyst and activation strategy was to utilize carboxylate salts that, once added to solution, would decarboxylate to generate CO_2

and a carbanion, which would deprotonate the superbase conjugate acid. Here, the release of CO_2 gas would serve as the driving force necessary for the activation strategy. In 2001, Schroeder and coworkers disclosed the decarboxylation of polyfluorobenzoic acids using organic superbases (Figure 2.4).[12] The combination of these reagents resulted in the formation of CO_2, polyfluorobenzene, and the unprotonated superbase. This reaction proceeds through superbase deprotonation of the carboxylic acid, followed by decarboxylation and proton transfer from the protonated superbase to the aryl carbanion. In this report, the authors investigated the rates of decarboxylation using various organic superbases such as the Proton Sponge® ($pK_{a'}$ = 18.6, MeCN), TMG ($pK_{a'}$ = 23.3, MeCN), MTBD ($pK_{a'}$ = 24.3, MeCN), and P_2-Et ($pK_{a'}$ = 32.9, MeCN). This precedent shows the potential of utilizing a decarboxylation strategy for activation of a superbase precatalyst salt. For the development of this project, we targeted BTPP and P_2-*t*-Bu phosphazene superbases as they are commercially available and are among the most commonly used superbases for reaction discovery and methods development. Steve did the initial work with this decarboxylation study before I joined the Bandar Group in 2019.

When developing these precatalyst salts, we wanted to make sure we generated a free-flowing, crystalline powder as this is the most practical form of a precatalyst to use. Here, we investigated a series of carboxylate structures in order to find ones that formed crystalline solids with BTPP and P_2-*t*-Bu. We began this investigation with perfluorobenzoic acids; however, these did not form solid salts with the bases (salts **1** and **2**) and were not further studied. Steve found that triphenylacetic acid, which would result in the triphenylmethyl carbanion upon decarboxylation, form stable salts with BTPP and P_2-*t*-Bu (Figure 2.4b, salts **3** and **4**). With stable salts in hand, the next step was to subject them to reaction conditions and track their ability to activate and generate the freebase. Using BTPP salt **3** to first investigate this, the salt was dissolved in DMSO-d_6 and

reaction progress was tracked by ^{1}H and ^{31}P NMR spectroscopy. Under these conditions, Steve found that although rapid and efficient decarboxylation takes place, only phosphoramide and no freebase was observed by ^{31}P NMR spectroscopy (Figure 2.4c). As described in Chapter One, phosphazene bases are prone to decomposition in the presence of CO_2, the byproduct of this reaction, and will form this phosphoramide. When I joined Steve on this project, we were investigating ways to sequester this CO_2 from the reaction as it is formed, in order to make a decarboxylation method viable.

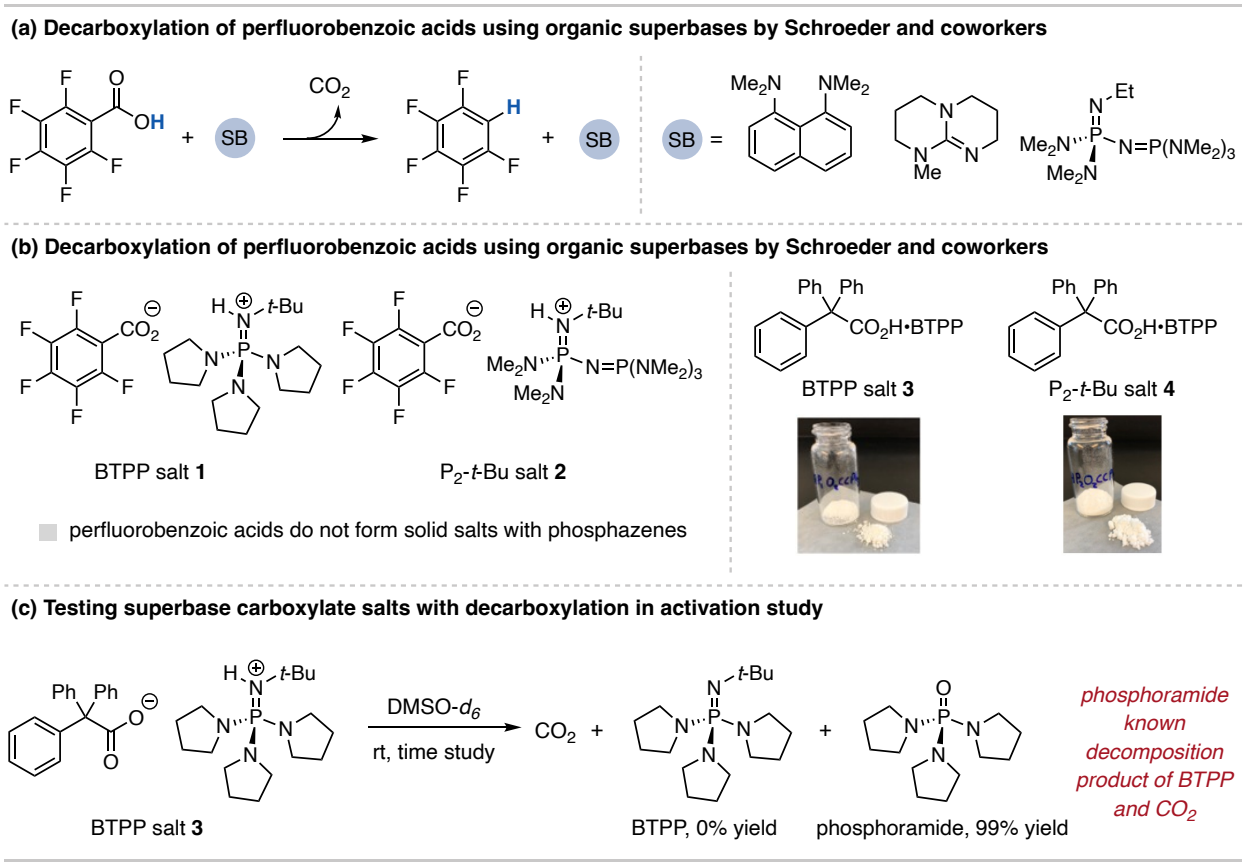

Figure 2.4: Inspiration and application of a decarboxylation strategy for superbase prectatalysts

The solution we found for this challenge was inspired by work reported by Kleij and coworkers in 2019 for the synthesis of 5-membered cyclic carbonates by the reaction of CO_2 and epoxy alcohols using DBU or TBD as a basic catalyst (Figure 2.5a).[13] Based on this reactivity, we reasoned that an epoxy alcohol additive could be introduced to the superbase carboxylate salt

precatalyst activation reaction to sequester the CO_2 before it can react unfavorably with the phosphazene. Steve initially tested this with glycidol **5** added to solution with BTPP salt **3** and found efficient formation of BTPP freebase by ^{31}P NMR and one equivalent of the cyclic carbonate **6** by ^{1}H NMR spectroscopy (Figure 2.5b). When I joined the lab, I began investigating the structure of this epoxy alcohol and the effects on the efficiency of CO_2 capture. We found that derivatives of phenyl glycidol were well suited for rapid reaction with CO_2, with **7** being best for this due to the electron-deficient aryl ring.

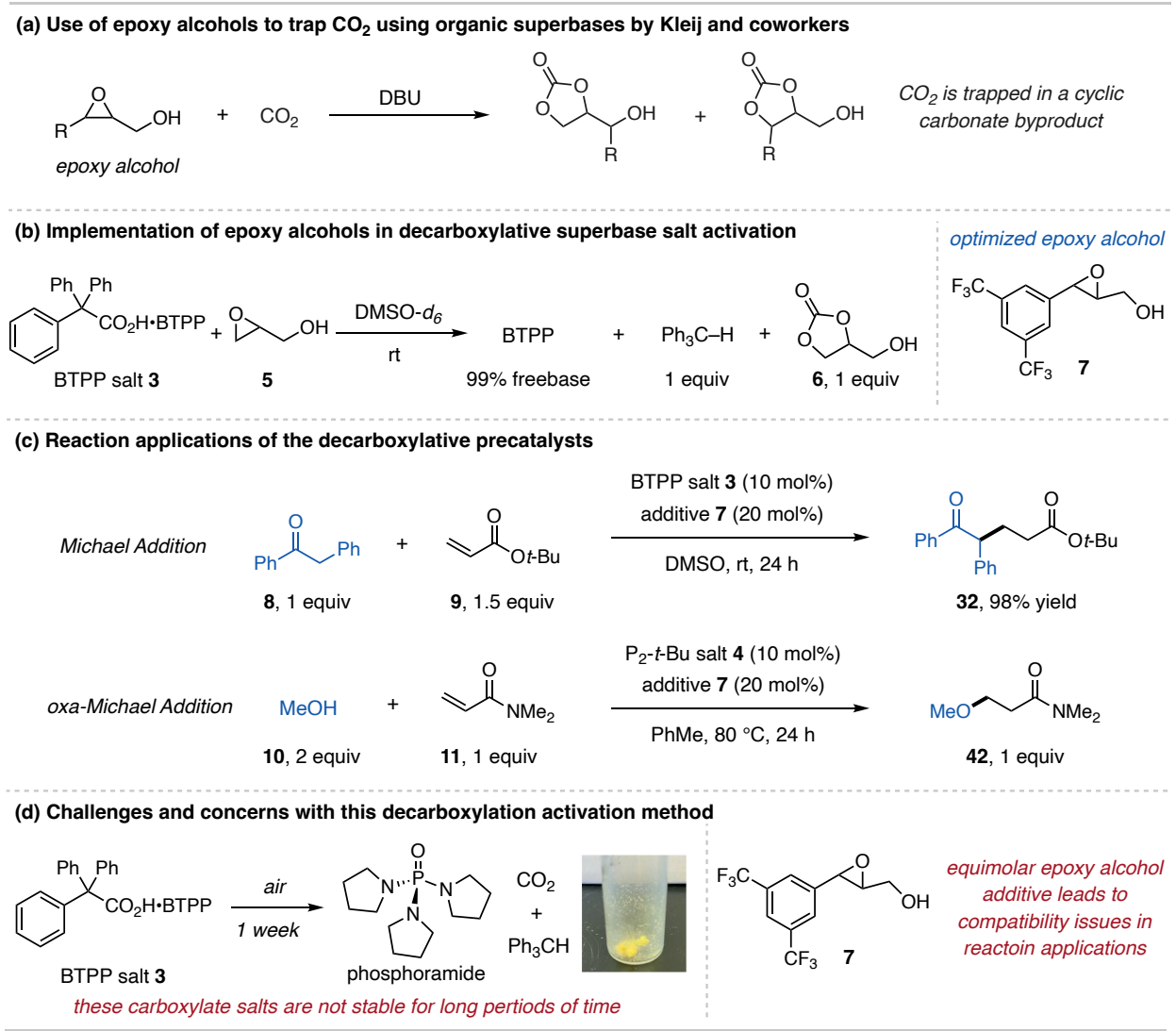

Figure 2.5: Development and eventual challenges with epoxy alcohol CO_2 trap for decarboxylation activation method

With efficient CO_2 capture enabling this decarboxylation strategy, we next tested the ability of this system to act as a precatalyst in reaction applications (Figure 2.5c). This was tested with the Michael addition between deoxybenzoin (**8**) and tert-butyl acrylate (**9**) for BTPP and the oxa-Michael addition between methanol (**10**) and *N,N*-dimethylacrylamide (**11**) for P_2-*t*-Bu. Good yields for both of these test reactions were obtained, indicating the high potential for this precatalyst and activation method for organic superbases.

Considering the overall feasibility of this system, we next investigated the overall stability of the carboxylate salts over time. We found that when exposed to ambient conditions (room temperature and exposed to air), salts **3** and **4** were stable for one week before actively decarboxylating and becoming sticky yellow masses (Figure 2.4d). Additionally, with the necessity of equimolar amounts of the epoxy alcohol additives, applications beyond these test reactions proved to be challenging. Overall, these concerns led us to moving on from this decarboxylation method to a new activation method using stable carboxylate salts, which will be discussed in Section 2.4.

2.4 Development of Epoxide-Opening Method for Precatalyst Activation

2.4.1 Concept of Using Epoxide Ring-Strain Release for Precatalyst Activation

Despite the concerns and ultimate incompatibility of this decarboxylation, we were able to draw inspiration from it for our next generation precatalyst activation method. The driving force for precatalyst activation was the decarboxylation of the counteranion, however, for the rapid and efficient trapping of the resultant CO_2 with an epoxy alcohol, a separate driving force is at play. In this mechanism, once the alcohol reacts with the CO_2, the subsequent carboxylate opens the epoxide ring, releasing the ring strain energy (~27 kcal/mol)[14] which provides the driving force

for the cyclization reaction (Figure 2.6a). With this, we reasoned that the release of epoxide strain energy could be utilized independently from decarboxylation as an activation method.

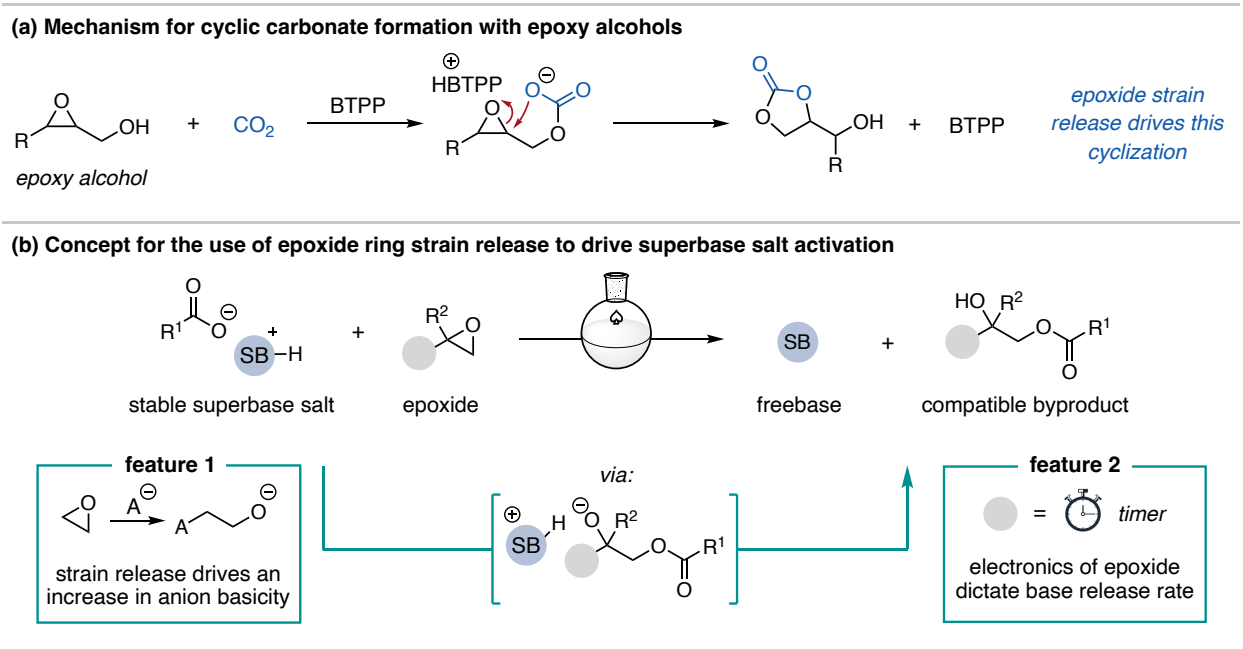

Figure 2.6: Use of epoxide ring strain release to drive superbase salt activation

With decarboxylation no longer a necessary component of activation, we no longer needed to target counteranions that were prone to decarboxylation. With the burden of activation shifted to the epoxide, we were able to just focus on the benchtop stability of the superbase conjugate acid salt, which opened up many more possibilities for structural investigation. This system is effective because, by definition, the counteranion of any stable salt is incapable of directly neutralizing the conjugate acid.[15] Therefore, activation will only take place once the epoxide additive is added to solution, followed by ring opening by the carboxylate anion that releases the strain energy to generate an alkoxide in solution (Figure 2.6b). This generated alkoxide is sufficiently basic enough ($pK_{a'}$ = 28 – 32, DMSO) to deprotonate the neutralize the superbase for use in reaction applications.[16] In principle, the epoxide can be stored independently for easy variation, premixed with the salt for convenience or incorporated into the salt structure itself, so long as activation takes place only in solution. Additionally, the epoxide structure and electronics can be varied in

order to gain influence over the rate of the activation reaction, a concept discussed later in this Section. We first investigated this system for BTPP and after gaining preliminary results, Steve focused on further developing the BTPP precatalyst system and I focused on developing an effective system for the more basic P_2-*t*-Bu phosphazene base.

2.4.2 Initial Results and Development of the BTPP Precatalyst System

As stated, with this system more stable phosphazene carboxylate salts can be investigated as the counteranion no longer needs to be prone to decarboxylation. As such, drawing inspiration from the crystallinity of phenylacetic acid salts, Steve tested a series of phenylacetic acid derivatives and found that blocking the alpha-position of the carboxylic acid with a fused cyclopropane ring led to a crystalline solid, BTPP salt **16** (Figure 2.7a). Importantly, when stirred at elevated temperatures for a prolonged period of time this salt does not decarboxylate and remains stable, indicating that it should be compatible with this activation method.

We next used this salt in a series of activation studies with various epoxide additives by stirring them together in DMSO-d_6, followed by NMR spectroscopic analysis. Here, we look at the percentage of freebase formation by ^{31}P NMR spectroscopy, where we can observe both the protonated and freebase for BTPP, and byproduct formation by ^{1}H NMR spectroscopy using an internal standard to quantify. Initially, we investigated aryl-substituted epoxides synthesized from styrene derivatives, with an example using phenyl oxirane **17** in Figure 2.7b. Here, we observe 50% conversion to BTPP freebase as well as formation of two isomers of the byproduct (**A** and **B**) that total 61% yield. Importantly, in these studies we observe byproduct within 5-10% of freebase formation, indicating byproduct formation is an effect of precatalyst activation, while also giving us multiple reliable ways to analyze freebase formation.

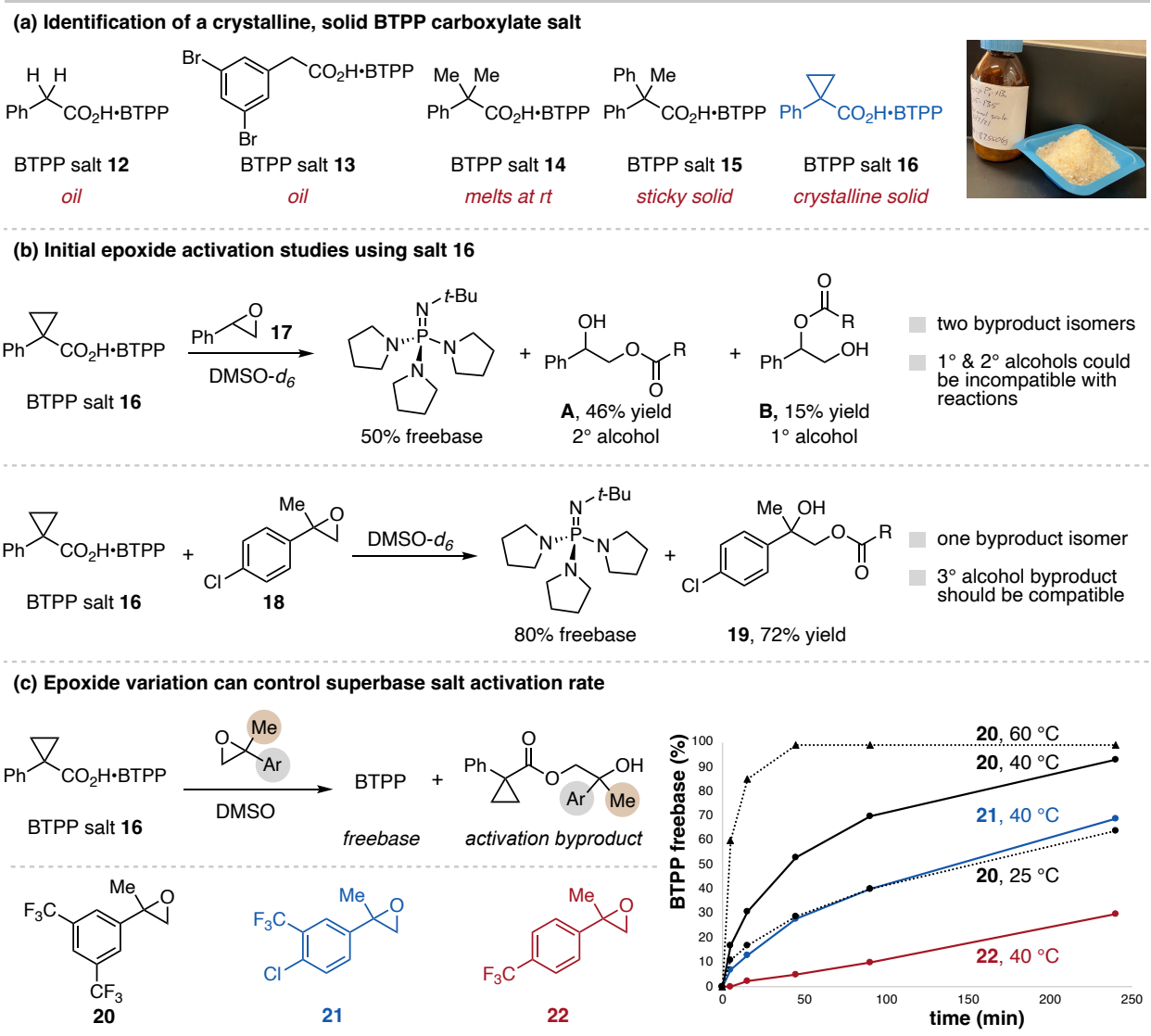

Figure 2.7: Identification of a stable BTPP precatalyst salt and the development of epoxide-opening activation

With this result, we drew two major conclusions. The first is that phenyl oxirane **17** was likely not electrophilic enough to be an effective additive, and that if we wanted to achieve quantitative freebase formation, we would need to investigate more electrophilic epoxides. The second conclusion was that under the reaction conditions, two isomers of the byproduct were forming, leading to secondary and primary alcohols. Steve and I realized that these byproduct isomers may not be inert as desired and led us to developing epoxide **18**, which features a methyl group in the alpha position and a chlorine withdrawing group on the aryl ring. When we reacted

this epoxide with BTPP salt **16**, we observed 80% freebase generation as well as 73% formation of byproduct **19**, which was subsequently isolated and confirmed to be the tertiary alcohol isomer, which should be inert and more compatible than the secondary or primary alcohol byproducts.

At this point, Steve continued developing this system for BTPP and I moved on to working with P_2-*t*-Bu. In this further investigation, Steve continued to vary the electronics of the aryl ring and found epoxide structures that lead to quantitative freebase formation (**20**-**22**). It was found that by changing the electronics of the aryl ring, the rate at which BTPP salt **16** activation takes place is influenced, and that the rate can be slowed down by using less electrophilic epoxides (Figure 2.7c). Additionally, condition variation like choice of solvent and reaction temperature can also influence the rate of precatalyst activation, providing many options for control over this method. This presents an opportunity to effectively control the rate of strong base addition to a reaction solution by simply varying the epoxide additive or conditions. This contrasts the current method for achieving this which is through manual slow addition or by use of a syringe pump, where this epoxide-opening activation method provides a more practical alternative.

2.4.3 Development of the P_2-t-Bu Precatalyst System

With initial groundwork for the BTPP precatalyst system laid, it was important to develop an effective system for stronger superbases, like P_2-*t*-Bu. Stronger phosphazenes find use in more frequent and diverse reaction applications such as Pd-catalyzed cross couplings, polymerization reactions, and HTE techniques.[17] As such, a benchtop-stable precatalyst for stronger superbases could make these applications easier as well as streamline research of new base-promoted transformations. To begin, a slight variation of the carboxylate structure led to P_2-*t*-Bu salt **23** as a crystalline, free-flowing powder. To assess how much freebase and byproduct were formed in activation studies using salt **23**, NMR spectroscopic analysis was again utilized. However, unlike

with BTPP, with P_2-*t*-Bu the protonated and freebase are not observable at the same time *via* ^{31}P NMR spectroscopy and as such I had to develop a method for estimating the amount of freebase formed in an activation study. I accomplished this by preparing standards of known ratios of protonated to free P_2-*t*-Bu and analyzing them by ^{31}P NMR spectroscopy. Each activation study was assessed against these standards to estimate the range of freebase formation, with more details in Appendix A. Additionally, ^{1}H NMR spectroscopy was used to quantify the amount of byproduct formed after activation, which was consistent with the amount of freebase estimated with the described technique.

In order to activate salt **23**, I began with using α-methylated, aryl-substituted epoxide additives since these epoxide structures were shown to be effective for BTPP precatalyst salt activation. Figure 2.8a shows an example activation study using epoxide **18** where only 50% generation of P_2-*t*-Bu and 50% yield of byproduct **24** were observed. To try and improve this activation, I tested several other epoxide structures (examples in Figure 2.8a) as well as increased temperature, concentration, reaction time, and changes in solvent choice. In all cases, the activation did not exceed 50% conversion to the freebase. It became clear that this was a systematic challenge with aryl-substituted epoxides and that I needed to figure out the cause of it.

To elucidate the cause of this problem, I considered the differences between P_2-*t*-Bu and BTPP and their activation. As a stronger base, P_2-*t*-Bu is higher in energy than BTPP and, as such, it is a higher energy base. Because of this, the driving force provided by the opening of aryl-substituted epoxides may not be sufficient to drive complete activation of the P_2-*t*-Bu precatalyst. To further investigate this, I set up time studies for the forward activation reaction as well as the reverse activation reaction, where commercial P_2-*t*-Bu was reacted with an equivalent of byproduct **24** and epoxide **18**, where the formation or consumption of **24** was tracked by ^{1}H NMR

spectroscopy. The results of this experiment show that the forward and reverse reactions converge over time at 50% of byproduct **24**, which indicates that this activation reaction has established equilibrium and that with aryl-substituted epoxides we would never be able to achieve greater than 50% activation (Figure 2.8b).

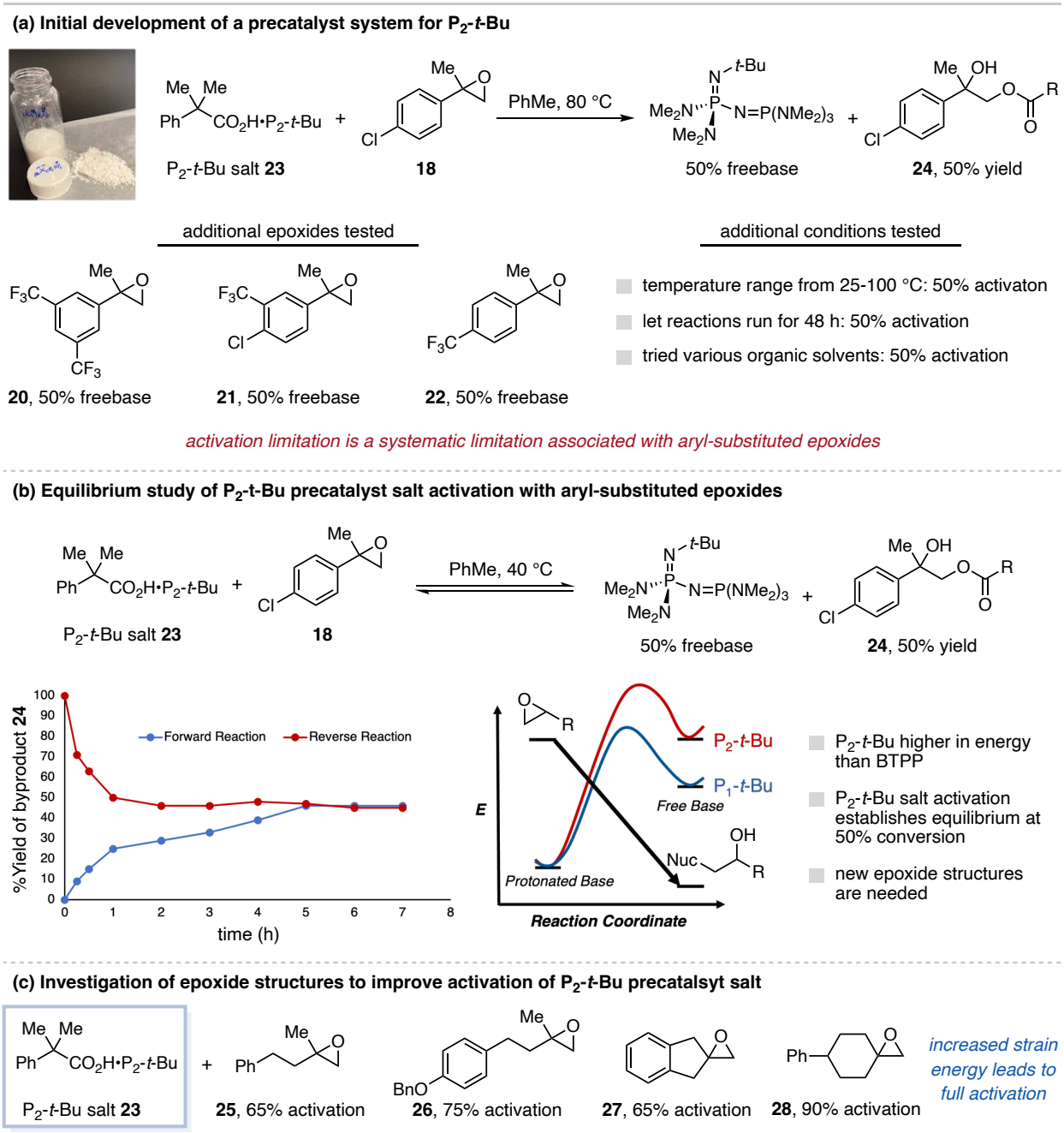

Figure 2.8: Development of an epoxide-opening activation for P_2-*t*-Bu precatlyst salts

In order to overcome this thermodynamic limitation, I considered epoxide structures that would be higher in energy and provide a greater driving force. I found that use of aliphatic epoxides instead of aryl-substituted epoxides led to an increase in freebase formation (Figure 2.8c, **25** and **26**). Use of spirocyclic aliphatic epoxides also lead to an increase in freebase formation, and use of epoxide **28** lead to 90% conversion to P_2-*t*-Bu and byproduct from salt **23**. I reasoned that the improvements using epoxide **28** were due to an increase in strain energy with the fused cyclohexane ring that would provide a greater driving force to overcome the larger energy gap difference between P_2-*t*-Bu and its conjugate acid.[18-20]

2.4.4 Improvements Made to the Practicality of this Precatalyst System

After developing effective precatalyst systems for both BTPP and P_2-*t*-Bu, we identified two areas where the practicality of the system required improvement. For the first area, up until this point, the phosphazene salt and epoxide have been stored separately and mixed in solution. Although this approach is well suited for controlling precatalyst activation with varying epoxide structures, an ideal way to utilize this system would be to store the precatalyst and salt in one vial. This would provide the maximum "ease-of-use" as the superbase precatalyst can be utilized in a single-addition protocol to achieve spontaneous activation. In order for this to work, both the precatalyst salt and epoxide must be crystalline solids, to avoid premature reaction before added to solution. I began by investigating this for the P_2-*t*-Bu, as the epoxide **28** is a solid, providing a good place to start. For this investigation, P_2-*t*-Bu salt **23** was manually mixed with an epoxide additive in a sealed glass vial using a metal spatula and stored in a benchtop desiccator open to air. Over the course of the storage time, the vial was opened periodically and mixed with a metal spatula to mimic more frequent use (Figure 2.9, left). The mixture was then assessed for longevity by physical inspection as well as ^{1}H and ^{31}P NMR spectroscopy for decomposition or activation.

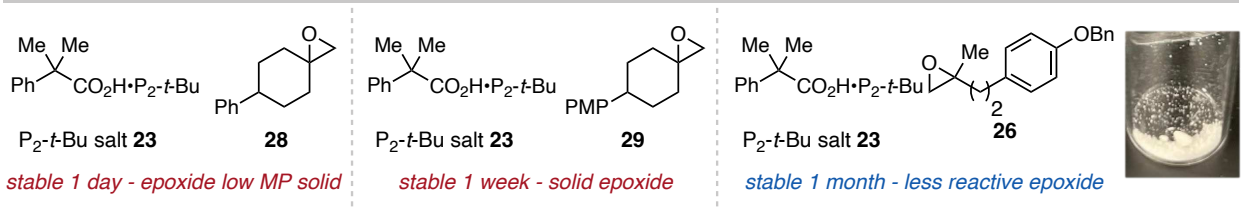

Figure 2.9: Development of an all-in-one precatalyst for P_2-*t*-Bu salt 23

When salt **23** and epoxide **28** are combined together, the mixture only lasts for one day before turning they reacted together and formed an oil. The short lifetime of this mixture is likely due to epoxide **28** being a low-melting point solid that does not form a stable mixture. I synthesized an analogue of epoxide **28** with a *p*-methoxyphenyl group in place of the phenyl group (**29**), which provided a crystalline solid epoxide. When I combined salt **23** with epoxide **29**, the mixture had a longer lifetime of one week, however, after that it turned into an oil and showed precatalyst activation (Figure 2.9, middle). This indicated that this core epoxide structure was likely too reactive and so I moved towards aliphatic epoxides which are presumably less reactive as a less conversion to freebase is observed when they are utilized in activation studies. With this, I found that epoxide **26** forms a solid mixture with salt **23** that is stable for up to 1 month on the benchtop, and indefinitely in the freezer (Figure 2.9, right). In activation studies, this all-in-one precatalyst provides the same amount of freebase as the separately stored salt and epoxide. Additionally, the all-in-one precatalyst was utilized in reaction applications, discussed in Section 2.6, where it performed just as well as the use of separately stored salt **23** and epoxide **28**. We investigated an all-in-one precatalyst for the BTPP system, but we could not find a solid aryl-substituted epoxide that was compatible to make this mixture.

The second area we identified for improvement comes with the overall stability of the superbase salts. With BTPP salt **16** and P_2-*t*-Bu salt **23,** we tested their stability by storing them in sealed glass vials on the benchtop, in a desiccator, and in a freezer over the course of six months.

While stored, 3 times per week the vials containing the salts were opened and the salts were mixed around using a metal spatula to mimic heavy usage. We found that these salts were stable over time and had no change in physical or spectral features and performed just as well in reaction applications, described in Sections 2.5 and 2.6.

For the vast majority of the year, Fort Collins has a very dry climate, so much so that a hygrometer in our lab does not register above the detection limit for most of the year. However, on days when the humidity was high (50-60%), we noticed the salts would clump together and stick to the spatula when weighing them out. We reasoned this was due to the salts being hygroscopic, a problem that would be exacerbated in labs in less dry climates where the relative humidity can much higher (80-90%). In order to test the effects of this, we stored salts **16** and **23** in glass chambers with controlled humidity of 84% to see how quickly they would absorb water. We observed formation of oil hydrates in each case after 24 hours being stored uncapped at 84% humidity. This process occurs much more rapidly on weigh paper, within an hour the salts have completely formed hydrates. In order to resolve this challenge, we investigated two solutions; 1) a salt restoration procedure and 2) developing new salts for BTPP and P_2-*t*-Bu that are less hygroscopic.

The first solution that we found to address this limitation was the use of an azeotrope to remove the water from the salts *in vacuo*. This restoration procedure exploits the fact that the hygroscopic nature of the carboxylate salts differs from freebase decomposition, as neutral phosphazenes react with CO_2 or absorb water and are impossible or challenging to restore, respectively. Figure 2.10a shows the recovery of salts **16** and **23** by dissolving the hydrates in PhMe followed by concentration *in vacuo* repeated three times. For each, the recovered mass matches the starting mass of the salts, and the water is absent on a ^{1}H NMR spectrum. This

recovery strategy serves as a quick solution to water absorption by the salt, however, in order to truly improve the system alternate superbase salts needed to be found that were less hygroscopic.

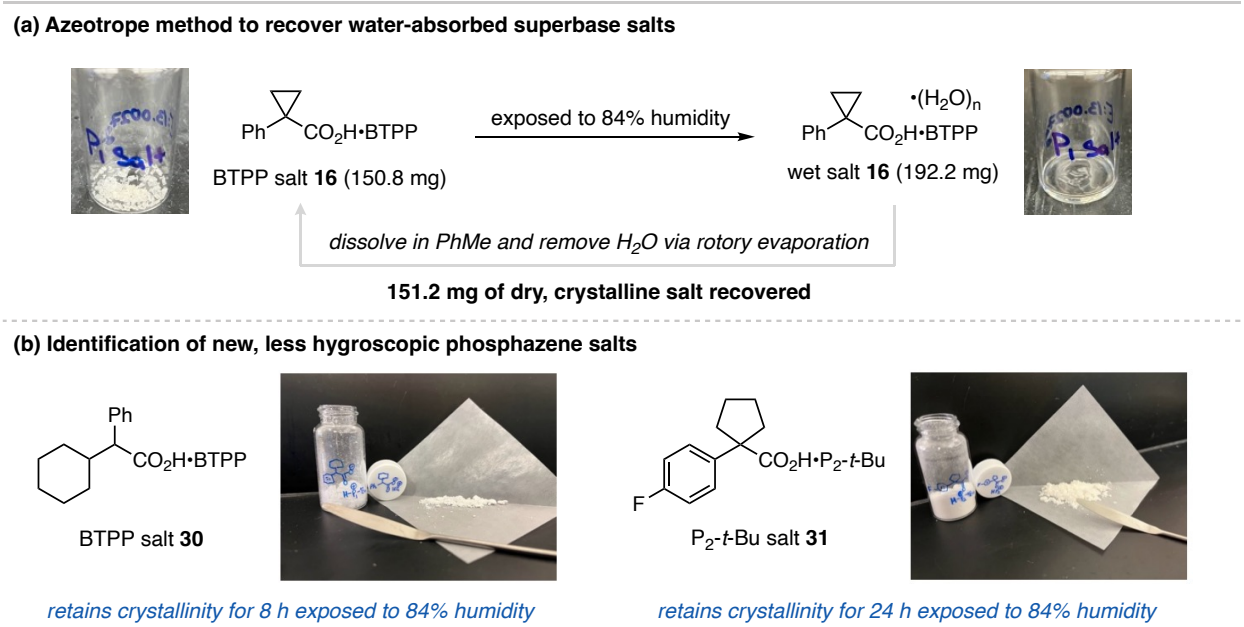

Figure 2.10: Strategies for overcoming hygroscopicity of phosphazene precatalyst salts

In this regard, I investigated a vast range of carboxylate anions that form less hygroscopic salts with BTPP and P_2-*t*-Bu. Each time I found a combination that resulted in a crystalline solid salt, I would store it in a glass vial and on weigh paper inside the 84% humidity chamber to see how long it would remain solid before becoming an oily hydrate. I found that BTPP salt **30** and P_2-*t*-Bu salt **31** are much more stable, lasting 8 and 24 hours on weigh paper in the 84% humidity chamber, respectively (Figure 2.10b). These salts were used in reaction applications compared to BTPP salt **16** and P_2-*t*-Bu salt **23** and were found to function exactly the same. Sections 2.5 and 2.6 will discuss the application of the BTPP and P_2-*t*-Bu precatalyst systems., We utilized BTPP salt **16** and P_2-*t*-Bu salt **23** for these applications, however, based on results comparing these salts to **30** and **31**, we believe there should be no loss of reactivity utilizing the less hygroscopic salts.

2.5 Applications of the BTPP Precatalyst System

2.5.1 Catalytic Application of the BTPP Precatalyst System in Michael-Type Reactions

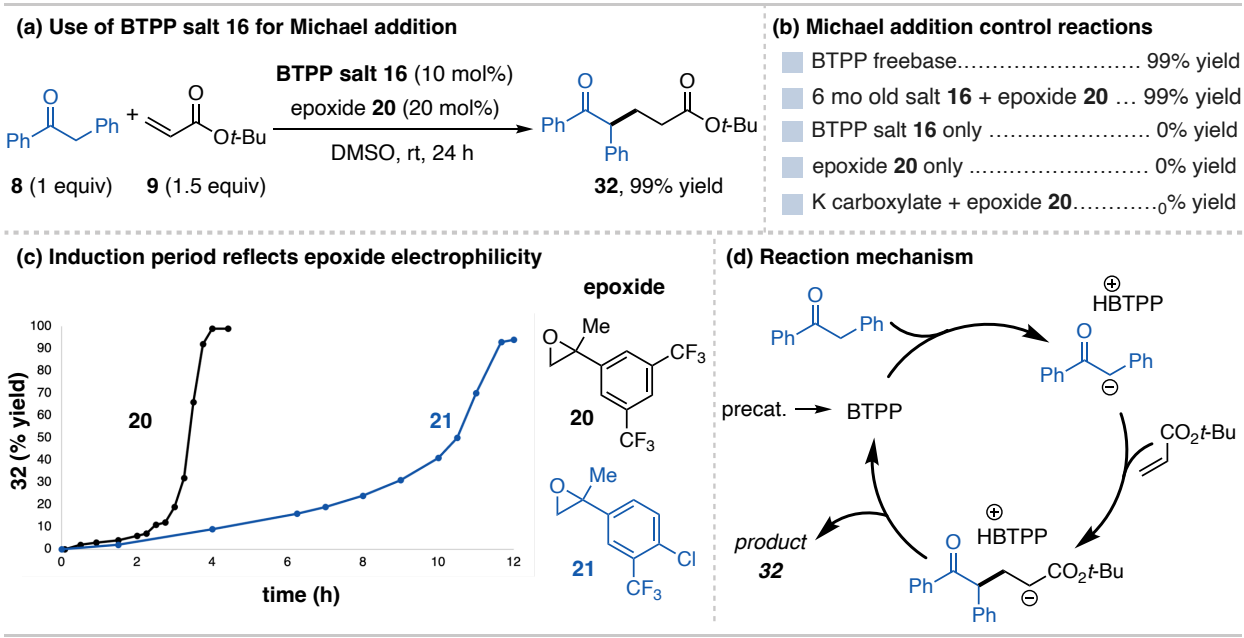

Figure 2.11: Use of BTPP salt 16 in the Michael addition reaction

After developing precatalyst systems for BTPP and P_2-*t*-Bu, we next wanted to assess their efficacy and compatibility as surrogates for these bases in reaction applications. We first showcased this in catalytic applications of the BTPP precatalyst system. The first reaction we targeted was the Michael addition, utilizing the same model reaction between deoxybenzoin (**8**) and tert-butyl acrylate (**9**) as in Section 2.3. For this model reaction, simple addition of BTPP salt **16** and epoxide **20** to solution with the substrates at room temperature leads to 99% yield of the addition product (**32**), matching the use of commercial BTPP (Figure 2.11). This provides a more practical alternative to utilizing commercial BTPP, where the reaction must be setup in a N_2-filled glovebox where BTPP must be stored. Control experiments show that neither BTPP salt **16** nor epoxides on their own promote this reaction (Figure 2.11a). The fact that the combination of potassium carboxylate of BTPP salt **16** with epoxide **20** also does not promote this reaction indicates BTPP is a necessary component of the precatalyst system. Furthermore, use of six-month-old BTPP salt **16** still provides high yield of **32**. Consistent with a precatalyst activation process, time profiles for this reaction show induction periods of different lengths, depending on

the electrophilicity of the epoxide (Figure 2.11a). Also shown in Figure 2.11a is the proposed catalytic cycle for this reaction where the precatalyst activates to generate BTPP, followed by deprotonation of **8** and facilitation of conjugate addition to **9**. Finally, proton transfer regenerates the active freebase as well as the product **32**.

Figure 2.12 shows a representative scope of products accessible using this method. Steve investigated the Michael addition products including the use of acrylates and acrylamides, the use of glycine-derived Schiff base (**33**), boronic ester containing nucleophiles (**34**), and ketones with a β-substituted acrylate (**35**). Beyond the Michael addition, I found a series of other enolate-addition reactions are possible with the use of BTPP salt **16** and epoxide **20**. These include an aldol and Mannich addition as well as a Mannich addition-elimination reaction (**36-39**). Overall, this demonstrates the generality and versatility of the BTPP precatalyst system.

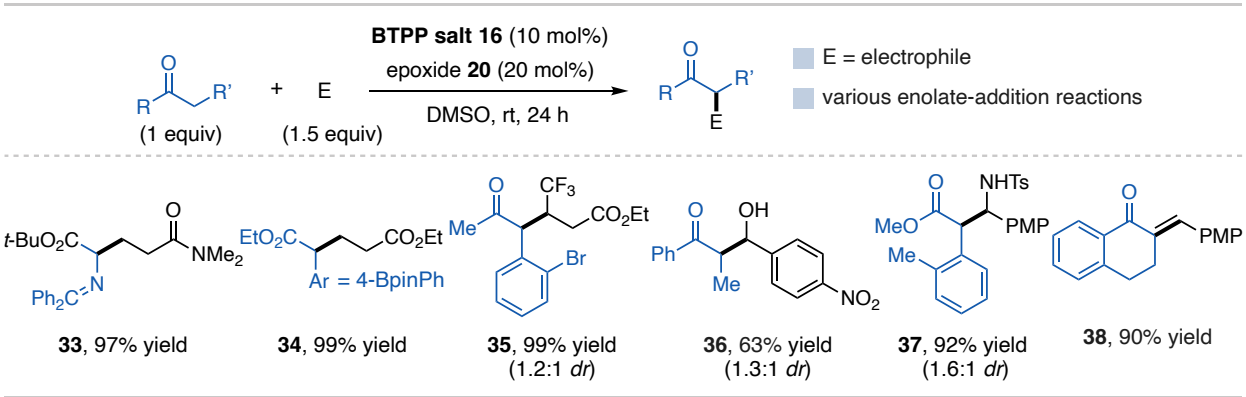

Figure 2.12: Scope of the Michael addition reaction

2.5.2 Catalytic Application of the BTPP Precatalyst System in Ester Amidation Reactions

The next application we targeted was the amidation of esters using amino alcohols, which represent prevalent reactions and functional groups in the development of pharmaceutical compounds.[21] In 2013, the Jamieson Group reported the amidation of esters using P_1 superbases where the use of organic superbases led to improved yields over commonly used inorganic bases.[22,23] When Steve set up this reaction with ester **39** and aminoalcohol **40** utilizing BTPP salt

16 and epoxide **20**, he observed no product formation (Figure 2.13). After further investigation, he found that the precatalyst activation process was being inhibited by the aminoalcohol and to address this, developed a simple preactivation protocol where BTPP salt 16 and epoxide **20** are stirred together in DMSO at 80 °C for five minutes. This effectively makes a solution of the BTPP freebase, which can be transferred to a solution of starting materials to catalyze the reaction. When Steve employed this procedure, he observed 94% yield of **41**, effectively solving the limitation with this reaction. Similar control reactions as described in Section 2.5.1 were run for this reaction and provide support for the BTPP generated from the precatalyst being the active catalyst. Figure 2.13b shows a scope of additional amidated products in excellent yields.

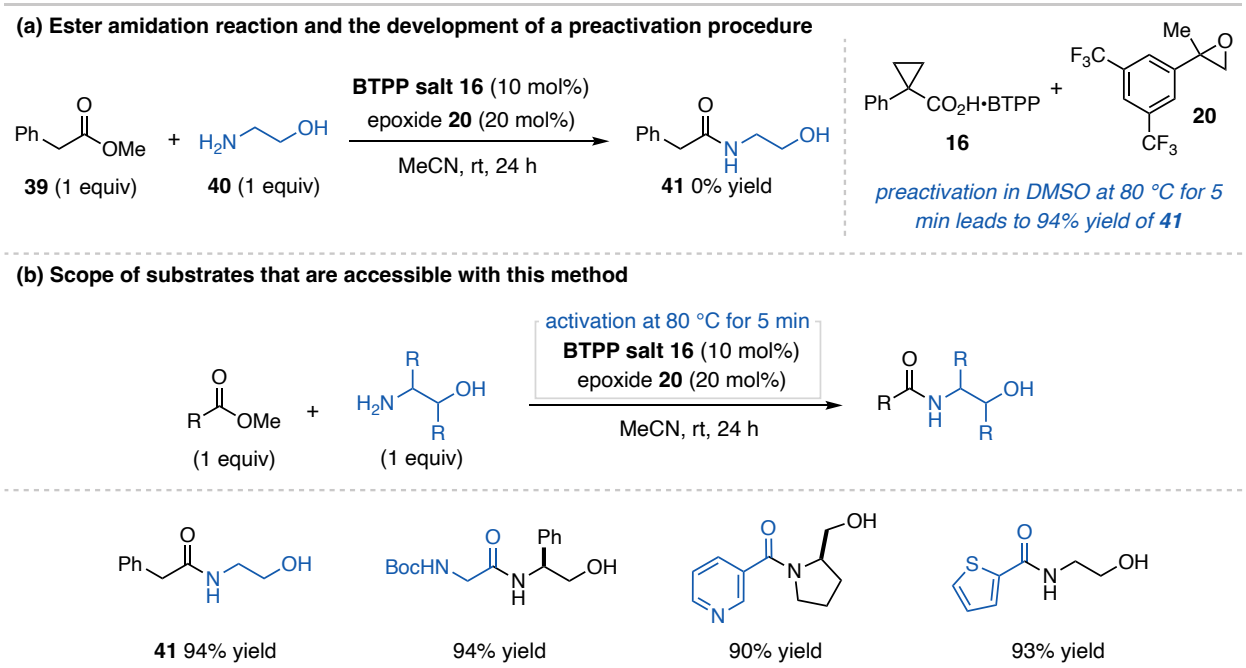

Figure 2.13: Application of BTPP precatalyst system in ester amidation with aminoalcohols

2.5.3 Stoichiometric Application of the BTPP Prereagent System in Alcohol Deoxyfluorination

Beyond catalytic applications of this system, it is important to show the efficacy of BTPP salt **16** and epoxide **20** can be an effective surrogate for commercial BTPP in a stoichiometric context. This provides a good test for this system as this application would require full generation

of the freebase. For this, we targeted the alcohol deoxyfluorination reaction developed by the Doyle group using BTPP.[24] This application was targeted not only to utilize the prereagent system stoichiometrically, but to test the compatibility of the system with a highly electrophilic sulfonyl fluoride and the 3° alcohol byproduct with fluorinating conditions. When Steve initially tried this reaction adding BTPP salt **16** and epoxide **20** to solution with the alcohol substrate and sulfonyl fluoride, he observed no product. When he employed a similar preactivation protocol, switching out DMSO with THF for the solvent, he observed good yields of fluorinated products and no deoxyfluorination of the 3° alcohol byproduct, showing its compatibility. Figure 2.14 shows a representative scope of deoxyfluorinated products, demonstrating the generality of this approach to access alkyl fluorides from readily available starting materials. Additionally, control reactions were run that strongly support that BTPP is the active catalyst in these reactions.

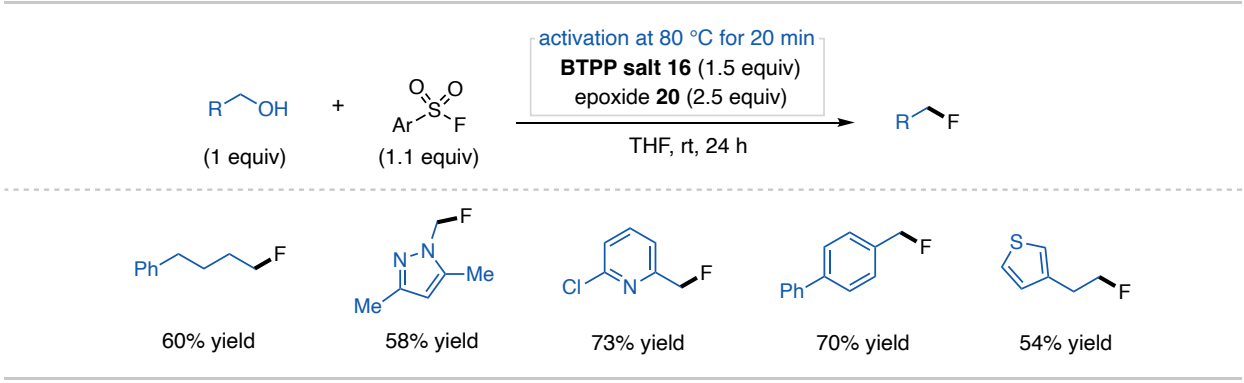

Figure 2.14: Application of BTPP precatalyst system in alcohol deoxyfluorination reactions

2.6 Applications of the P_2-*t*-Bu Precatalyst System

2.6.1 Catalytic Application of the P_2-t-Bu Precatalyst System in oxa/aza-Michael Additions

While Steve developed reaction applications for the BTPP precatalyst system, I focused on investigating applications of the P_2-*t*-Bu precatalyst system. The first reaction I targeted was the oxa/aza-Michael addition, which is known to be a challenging but highly useful reaction.[25-27] The major challenge with this reaction is its reversibility, requiring the use of strong non-coordinating

bases that can operate in nonpolar media, which makes organic superbases ideal catalysts. The simple addition of P_2-*t*-Bu salt **23** and epoxide **28** to a solution of methanol (**10**) and *N,N*-dimethylacrylamide (**11**) leads to a high yield of product **42**, similar to the use of commercial P_2-t-Bu in a glovebox (Figure 2.15a). Notably, use of the all-in-one precatalyst (P_2-*t*-Bu salt **23** and epoxide **26** stored together) or six-month-old P_2-*t*-Bu salt **23** also provide high yield of **42**. Control experiments show that neither P_2-*t*-Bu salt **23** nor epoxides on their own promote this reaction (Figure 2.15a). Importantly, use of the potassium carboxylate of salt **23** with epoxide **28** does not promote this reaction on their own, indicating the *in situ* generated 3° alkoxide is not capable of promoting this reaction and P_2-*t*-Bu is necessary. Figure 2.15b shows a scope of additional substrates obtained with this method, including additional oxa-Michael additions using an alkynol (**43**) and adamantane methanol (**44**) with various acrylamides and aza-Michael additions using *N*-heterocycles with β-substituted acrylates and styrene derivatives (**45** and **46**).

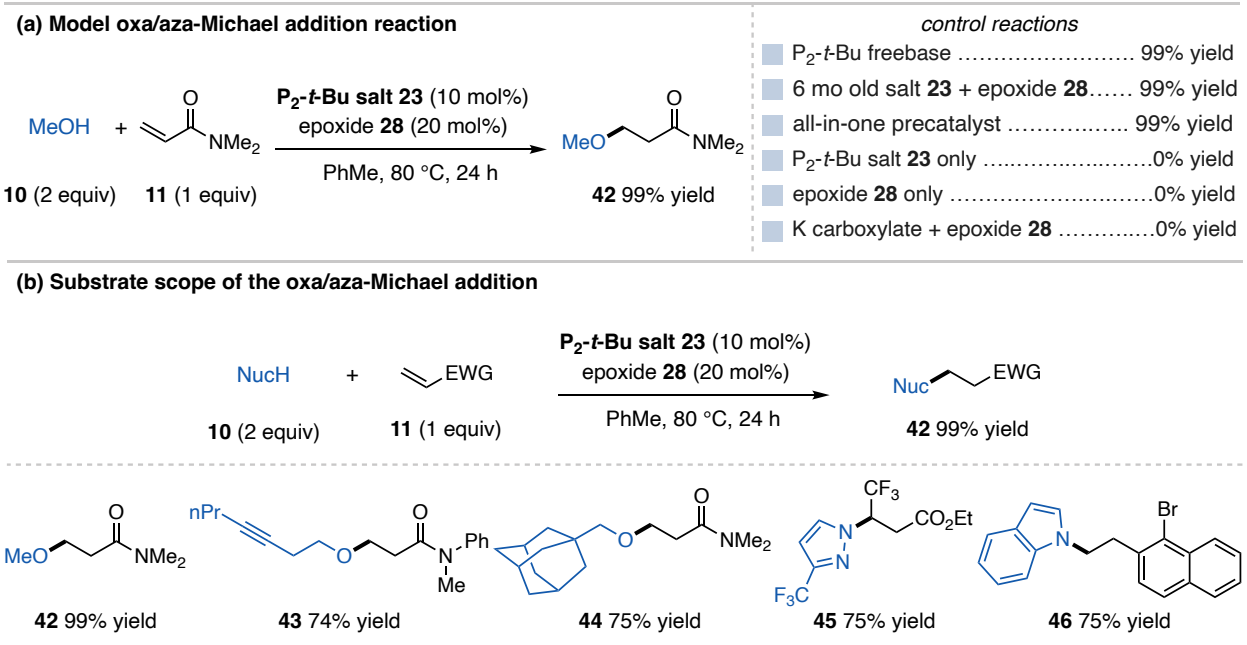

Figure 2.15: Use of P_2-*t*-Bu preactalsyt system in the oxa/aza-Michael addition

2.6.2 Catalytic Application of the P_2-t-Bu Precatalyst System in Polymerizations

An important application of phosphazene superbases is their use as organocatalysts for anionic polymerization reactions.[28,29] Phosphazenes are highly desirable in this context due to their high basicity and low nucleophilicity. In this regard, phosphazenes can easily convert protic compounds (i.e., alcohols, thiols, and amides) into nucleophilic initiators. The loose coordination of ion pairs with phosphazene bases can also be advantageous over other cations like lithium, as it leads to a more active anionic chain end for the polymerization process. Because of the importance of phosphazenes in polymerization reactions, I sought to utilize the phosphazene precatalysts with the epoxide activation method to promote polymerization reactions.

The reaction I targeted was the polymerization of ε-caprolactone (**47**), which has been shown with P_2-*t*-Bu as an organocatalyst by the Hadjichristidis Group in 2014.[30] In addition to literature precedent, polycaprolactone is well known to be a biodegradable and biocompatible material that is being investigated as an alternative to commonly utilized plastics. This has implications biomedical implants as well as drug-delivery technology, making the synthesis of this material incredibly important.[31-33] I ran the polymerization of ε-caprolactone (**47**) in PhMe using P_2-*t*-Bu salt **23** and epoxide **28** with benzyl alcohol (BnOH, **48**) as the initiator at room temperature (rt) and observed no formation of the polymer product. In comparison, the use of commercial P_2-*t*-Bu results in 97% conversion to polycaprolactone (**49**). I reasoned that this was due to the fact that the activation of P_2-*t*-Bu salt **23** with epoxide **28** is very inefficient at rt, thus prohibiting polymerization. To overcome this, I implemented a preactivation protocol where the salt **23** with epoxide **28** were premixed in PhMe at 100 °C for thirty minutes prior to addition to a solution of monomer and initiator. Under these conditions, I observed 92% conversion to polycaprolactone, which shows this precatalyst method can be effectively used for polymerization reactions (Figure 2.16a).

Despite the success of utilizing a preactivation method, I still desired to accomplish this reaction with a one-pot procedure. The solution to this challenge came from considering initial activation studies using aryl-substituted epoxides. Even though they only lead to at most 50% activation of P_2-*t*-Bu salt **23**, this process can easily take place at rt, which is the required temperature for polymerization. In a catalytic application, complete activation of the precatalyst is not required so long as there is sufficient formation of P_2-*t*-Bu for the reaction to take place. So, when P_2-*t*-Bu salt **23** and epoxide **20** are added to solution with monomer and initiator, 90% conversion to polycaprolactone **49** is observed (Figure 2.16b). This reaction is set up using a Schlenk manifold line without the need to further purify starting materials before reaction. Additionally, this material was precipitated and isolated for characterization to confirm its identity by ^{1}H NMR spectroscopy and evaluate molecular weight, with Mn = 14.9 kDa, Đ = 1.07.

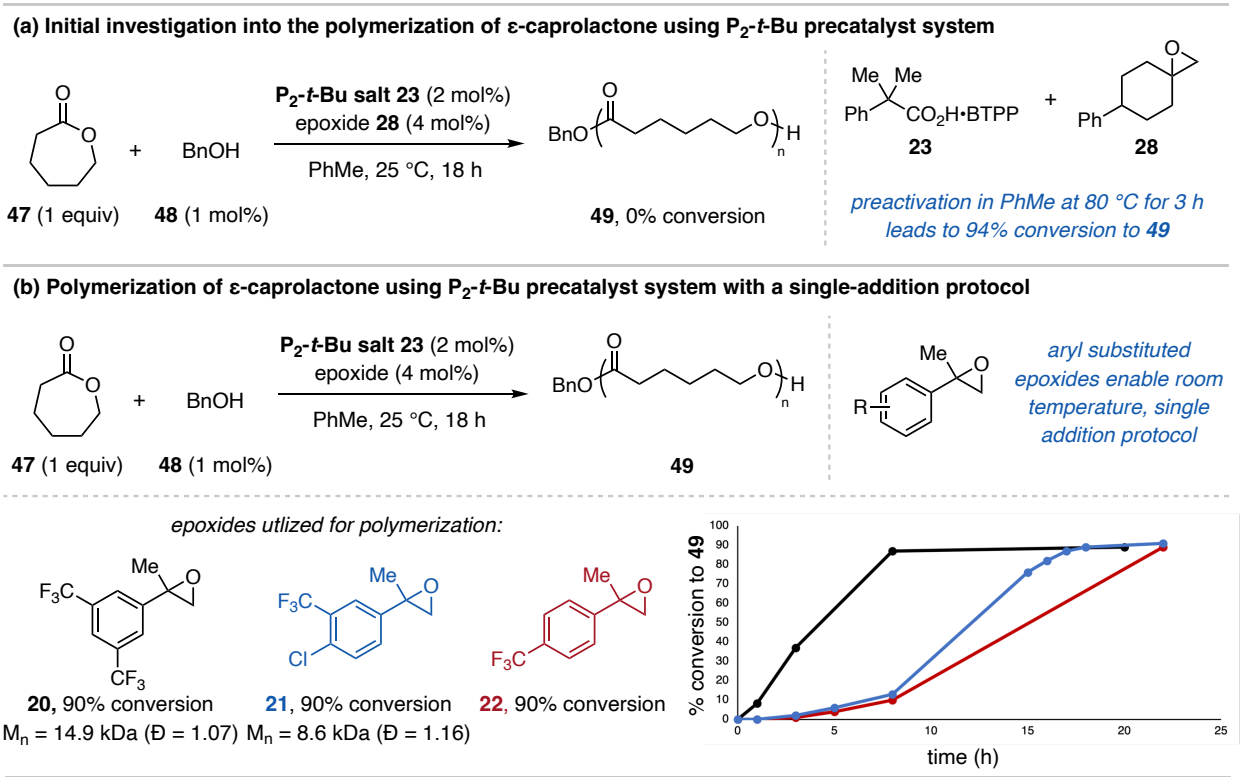

Figure 2.16: Application of P_2-t-Bu precatalyst system in the polymerization of ε-caprolactone

With the ability to utilize the aryl-substituted epoxides, variation of the electronics of the aryl ring should influence the rate of the polymerization reaction, as seen for variable induction periods for the Michael addition in Section 2.5. The Fors Group has shown that by controlling the rate of initiator addition to a polymerization reaction, they could control the physical properties of the resulting material.[34] I reasoned that by varying the identity of the epoxide additive, a similar phenomenon could occur where epoxide electrophilicity can dictate initiation rate and thus material properties. Figure 2.16c shows time profiles for the use of three different epoxide structures where a clear difference in rate is observed along with differences in the physical properties of the material. This method has the potential to gain controllable access to an important polymeric material with a general and simple protocol. This work has been established for disclosure within this organic superbase project and could lead to a number of useful methods for polymerization reactions.

2.6.3 Stoichiometric Application of the P_2-t-Bu Prereagent System in S_NAr Reactions

As with the BTPP precatalyst system, it is important to show that the P_2-*t*-Bu precatalyst system can act as a prereagent for stoichiometric applications. For this application, I targeted the nucleophilic aromatic substitution (S_NAr) reaction, which represents a versatile way to substitute aryl C–X bonds with diverse pronucleophiles. This represents an emerging application of P_2-superbases as they have been shown through HTE techniques to act as mild bases to uniquely enable challenging S_NAr reactions.[35] I performed a series of detailed control studies to probe the active basic promotor for this reaction, with more information in Appendix A, which provide support for P_2-*t*-Bu being the active base. The prereagent system promotes SNAr for a broad range of *O*-, *N*-, and *C*-based pronucleophiles with various aryl-halide coupling partners, shown in Figure

2.17 (**51**-**56**). Substrate **53** shows an example for the regioselective synthesis of a complex substrate that is enabled by the use of P_2-*t*-Bu.

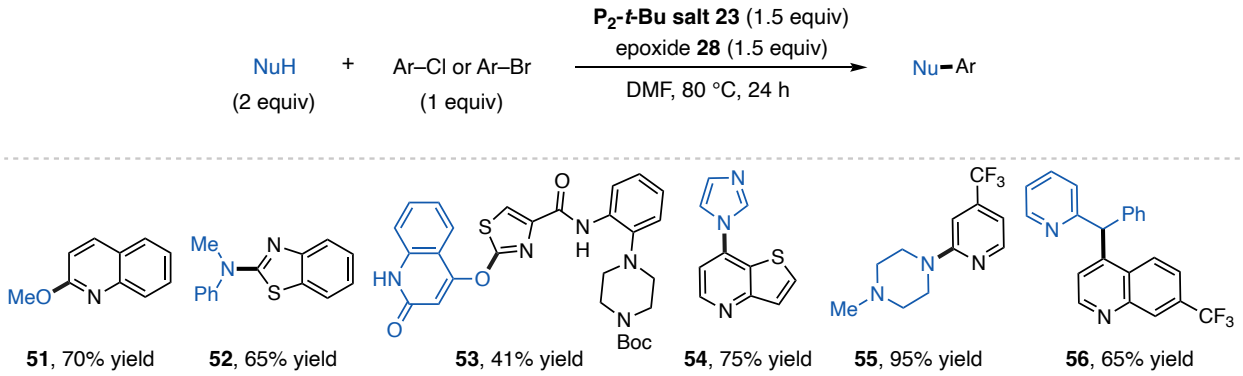

Figure 2.17: Use of the P_2-*t*-Bu prereagent system in the S_NAr reaction

2.6.5 Stoichiometric Application of P_2-t-Bu Prereagent System in an Enolate-Type Alkylation Reaction

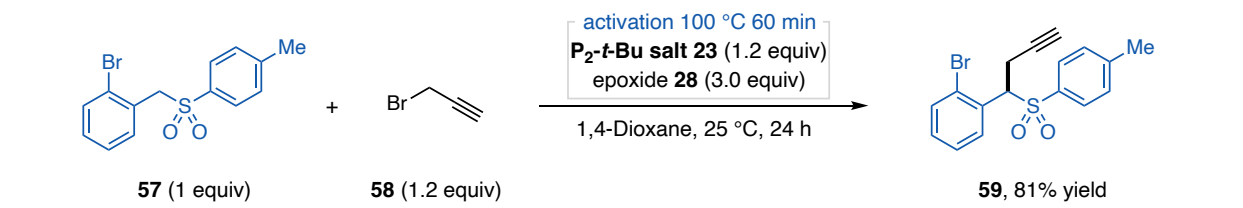

Figure 2.18: Use of the P_2-*t*-Bu prereagent system in benzyl sulfone enolate-type alkylation

For an additional example for the use of the P_2-*t*-Bu prereagent system in a stoichiometric context is in an enolate-type alkylation reaction with a 2-bromobenzyl sulfone (Figure 2.18). This reaction was reported for use of P_2-Et to promote a number of alkylation reactions using **57**, and I reasoned that the P_2-*t*-Bu prereagent could be used as an alternative base-promoter.[36] I targeted the reaction of **57** with propargyl bormide (**58**) to furnish alkylated product **59**. Due to this reaction taking place at room temperature, I developed an effective preactivation strategy where P_2-*t*-Bu salt **23** and epoxide **28** were stirred together in 1,4-dioxane prior to transfer to the reaction solution.

This was successful in giving 81% yield of **59**, demonstrating further efficacy of this system in stoichiometric applications.

2.6.5 Stoichiometric Application of Phosphazene Prereagent Systems in Pd-Catalyzed Cross-Coupling Reactions

Pd-catalyzed cross-coupling reactions represent one of the most utilized classes of reactions in the pharmaceutical industry.[1] A very useful and widely employed subclass of these reactions include Pd-catalyzed aryl aminations to furnish a wide variety of C–N coupled products. These reactions require basic conditions to proceed, either with strong metal alkoxides or silylamides at rt or metal carbonates at elevated temperatures.[37] The drawback here is that the use of inorganic bases provides to heterogeneous reaction conditions that could lead to challenges in reproducibility, especially when scaling the reaction. Organic superbases present an ideal alternative to these inorganic bases as they possess similarly high basicity but are highly soluble in organic media. In 2015, scientists at Merck reported the use of P_2-Et to enable homogeneous reaction conditions HTE to investigate a wide variety of Pd-catalyzed cross-coupling reactions. this represented the first general method to employ organic superbases for this type of application.[38] Since this report, Merck scientists have further explored P_2-Et for complex coupling reactions using HTE techniques (Figure 2.18a).[35] In 2018, the Buchwald group used DBU and novel AlPhosPd catalyst to enable coupling of aryl halides and triflates to various amine pronucleophiles. In this report, the authors found through mechanistic studies that slow addition of the DBU base was beneficial for a number of substrates, due to the Pd being more electropositive due to the bulky AlPhos ligand donating less electron density.[39] This beneficial effect from slow addition of base will be discussed further in Section 2.7.

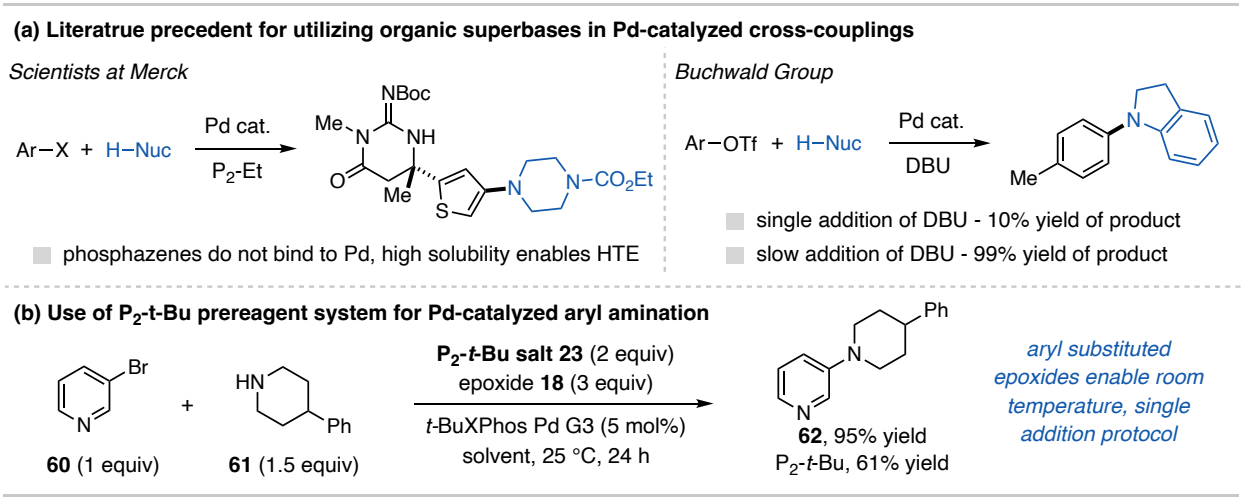

Figure 2.19: Precedent for use of phosphazenes in Pd-catalysis and implementation of P_2-*t*-Bu prereagent system

These reports inspired us to investigate the use of organic superbase prereagents to promote Pd-catalyzed cross coupling reactions. This reaction application was studied by Steve, and I came in to help after he had investigated much of the scope. To begin, Steve selected the model reaction disclosed by Merck scientists, the coupling of 3-bromopyridine (**60**) and 4-phenylpiperidine (**61**) to synthesize **61**. Using the *t*-BuXPhos Pd G3 precatalyst and commercial P_2-*t*-Bu in THF at rt, he obtained a 61% yield of **61**. Use of P_2-*t*-Bu salt **23** with epoxide **28** resulted in 0% yield of 59, which is not surprising since epoxide **28** will not efficiently activate salt **23** at rt. Use of a preactivation method with salt **23** and epoxide **28** led to 85% yield of **61**, demonstrating the prereagent system is compatible with this reaction. Ideally, however, this reaction could be done at rt with a single-addition protocol using aryl-substituted epoxides that are known to activate salt **23** at rt. We hypothesized that in a stoichiometric application, since the base is irreversibly consumed as it is generated, the equilibrium of the activation process will be shifted as the base is removed, thus achieving full activation. This was indeed the case and with a single-addition protocol using P_2-*t*-Bu salt **23** with epoxide **20**, we observed 95% yield of **23**, with a full equivalent of the activation byproduct observed by ^{1}H NMR spectroscopy (Figure 2.18b). We note that the yield of this reaction using the prereagent system is higher than use of commercial P_2-*t*-Bu, a result

that is fully addressed in Section 2.7. A full set of control reactions were run, detailed in Appendix A, which provide support that the active basic promoter for these reactions is P_2-*t*-Bu generated from the prereagent system.

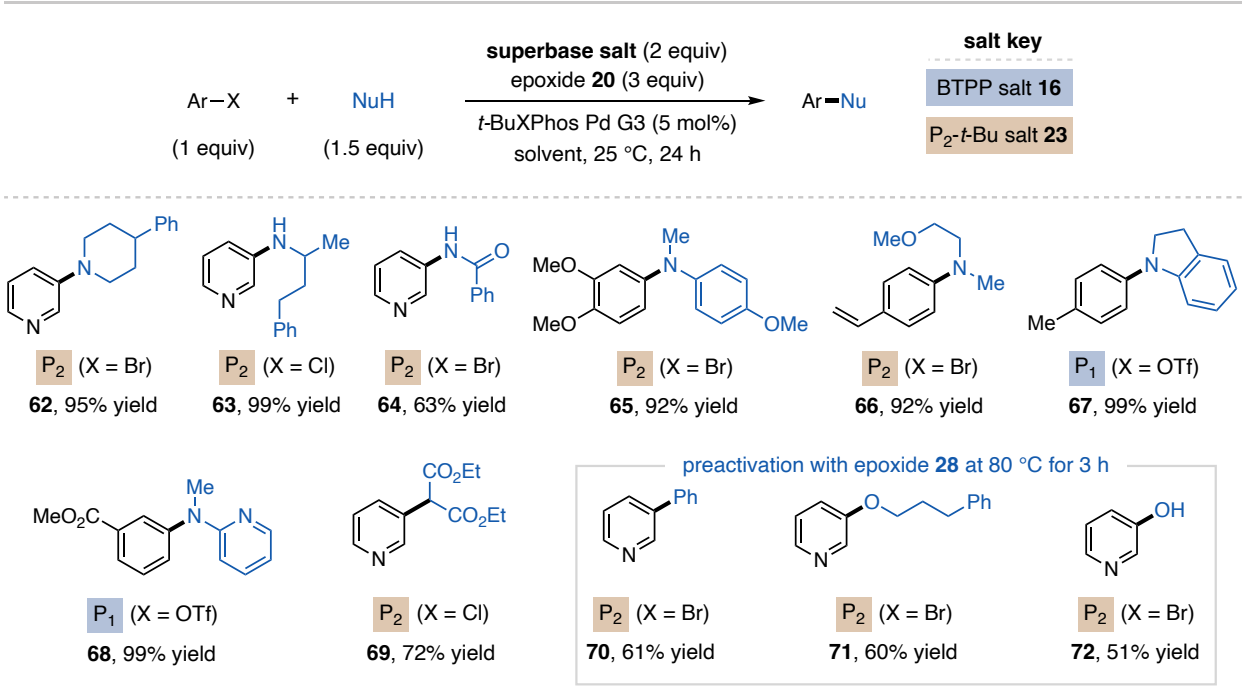

Figure 2.20: Precedent for use of phosphazenes in Pd-catalysis and implementation of P_2-*t*-Bu prereagent system

We next moved on to investigate a substrate scope for this reaction (Figure 2.19). This strategy is effective at coupling aliphatic amines with aryl bromides and chlorides (**62**, **63**). Benzamide can be used as a pronucleophile (**64**), and electron rich anilines and aryl halides are tolerated (**65**). 4-bromostyrene can be used as an effective coupling partner (**66**), a substrate that could potentially undergo competitive base-promoted hydroamination. Steve also found that BTPP salt **16** can be used to promote coupling reactions between anilines and aryl triflates (**67**, **68**). P_1 superbases are underexplored in the literature for cross-coupling reactions and this could provide access to a general application of these bases in this context. Merck scientists also showed examples of C–C and C–O coupling under these conditions, so we explored substrates to showcase this as well. Substrate **69** shows the use of diethylmalonate as a compatible pronucleophile. In

reactions that involve alcohols or water, the pronucleophile interferes with the prereagent activation procedure and as such a preactivation protocol must be employed where P_2-*t*-Bu salt **23** and epoxide **28** are stirred together in PhMe for 1 h at 80 °C, after which this solution is transferred to a vial containing the starting materials. With this procedure, C–C coupling *via* PhBPin (**70**, H_2O as an additive) in a Suzuki reaction is possible as well as C–O coupling with an alcohol (**71**) and water (**72**) as the pronucleophile. Added benefits associated with the application of organic superbases in Pd-catalysis will be discussed in Secion 2.7.

2.7 Unique Opportunities Enabled by Superbase Precatalysts

2.7.1 Improved Synthesis and Recovery of Organic Superbases as Carboxylate Salts

Throughout the development of these phosphazene superbase precatalysts, we have noticed a number of added benefits unique to this method that were not possible with commercial superbases. The first of these benefits is in the synthesis and recovery of air-sensitive superbases as carboxylate salts. For the salts synthesized in this report, they were made by stirring the commercial superbase with a carboxylic acid to form the ion pair. However, with this method the superbase salt can be synthesized directly, without ever needing to access the reactive freebase and thus never having to keep the system air-free. This was demonstrated by Steve with the synthesis of BTPP salt **16** on a 75 mmol scale beginning from phosphorus pentachloride (Figure 2.20a). Here, PCl_5 is reacted with *t*-$BuNH_2$, followed by reaction with pyrrolidine to access the BTPP•HCl salt without needing to isolate the intermediate. The BTPP•HCl salt is then subjected to anion metathesis with carboxylate **73,** where the chloride is exchanged for the carboxylate anion and through recrystallization, pure BTPP salt 16 was obtained in 61% overall yield (>20 g). This procedure provides streamlined and efficient access to phosphazene superbases and has the potential to enable rapid study of new phosphazene bases, especially chiral variants.

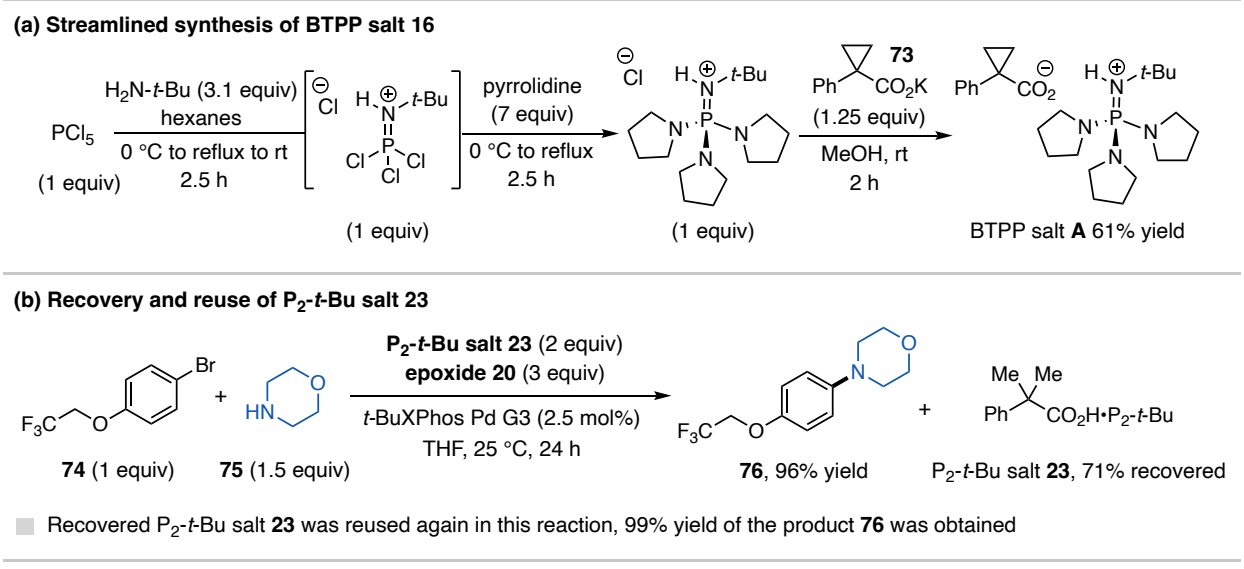

Figure 2.21: New synthetic capabilities enabled by superbase precatalysts

In addition to streamlined synthesis of phosphazenes, this procedure also enables the recovery of these air-sensitive bases upon completion of a reaction. This is especially important given the high cost of these bases (discussed in Chapter 1, Section 1.5), as their recovery as of now has not been investigated or reported. With this protocol, after a reaction is complete, the mixture can be washed with aqueous HCl to generate the phosphazene•HCl salt that will go into the aqueous layer. The HCl salt can be then obtained concentrated or simply extracted with a mixture of isopropanol and chloroform. This HCl salt can then undergo anion metathesis with the potassium carboxylate salt to regenerate the phosphazene precatalyst salt. This process is especially important in stoichiometric applications where multiple equivalents of the base are used at once. Recovery of P_2-*t*-Bu salt **23** was demonstrated in the Pd-catalyzed coupling of **74** and **75** to furnish **76**. After reaction, the previously described recovery procedure was used and 71% recovery of P_2-*t*-Bu salt **23** was obtained (Figure 2.20b). This salt was subsequently reused in the same reaction, benchmarked against freshly synthesized salt **23**, and in each case 99% yield of **76** was observed, indicating no loss in reactivity for this recovered salt. Overall, this protocol provides

streamlined access to and recoverability of unstable phosphazene superbases, something that was not possible before the development of this method.

2.7.2 Opportunity for Reaction Rate Control of Pd-Catalyzed Cross-Coupling Using the Prereagent Method

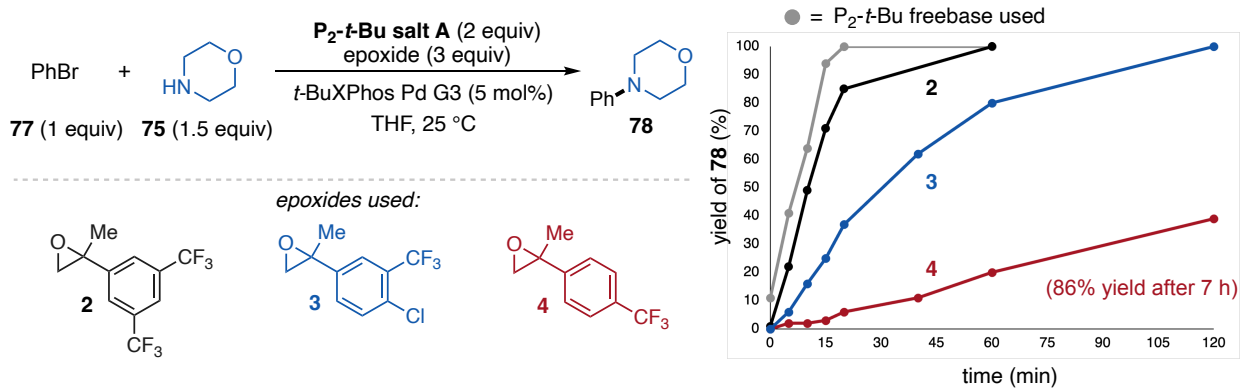

Figure 2.22: Reaction rate control by choice of epoxide structure

As mentioned in previous sections, the electrophilicity of the epoxide used for precatalyst activation can influence the rate at which this takes place and ultimately the rate of a potential reaction application. We have observed this in the context of the Michael addition, where the length of the induction period is controlled by the choice of epoxide, and in the polymerization of ε-caprolactone (**49**) where the reaction rate was controlled by the choice of epoxide, leading to varied material properties. In the context of Pd-catalyzed cross couplings, two main benefits can be considered for this application. The first is that with an *in situ* "slow addition" of base, a potential exotherm, which is known for Pd-catalyzed reactions, could be mitigated, ultimately making this method a safer alternative to traditional single-addition protocols.[40] The second is that for reactions where the presence of strong base is necessary but also potentially problematic, as in the case of base-sensitive substrates, this technique could enable challenging coupling reactions. This concept is further discussed below in Section 2.7.3.

This concept was tested using the coupling of bromobenzene (**77**) and morpholine (**7**), where time profiles tracking the formation of **78** by ^{1}H NMR spectroscopy (Figure 2.21). Here, we compared the use of commercial P_2-*t*-Bu to the use of P_2-*t*-Bu salt **23** with epoxides **20**, **21**, and **22**. We found that P_2-*t*-Bu and salt **23** with epoxide **20** have similarly rapid reaction rates. As the electrophilicity of the epoxide decreases going from **20** to **22**, the rate of the reaction also decreases, and we start to observe an induction period indicative of slower prereagent activation. In Section 2.7.3 below, we exploit this protocol to enable coupling reactions with base-sensitive systems.

2.7.2 Use of in situ Slow Base Release to Enable Challenging Coupling Reactions of Base Sensitive Substrates

In our substrate investigation for the Pd-catalyzed cross coupling reaction, we noticed several cases where the use of the prereagent lead to higher yields than use of commercial P_2-*t*-Bu. Figure 2.22a shows some examples of this (**62**, **66**, **79**-**82**) with varying differences between the yields obtained using the freebase and prereagent system. We reasoned that this yield improvement could be due to two major factors. The first is that the P2-t-Bu is competitively binding to the Pd catalyst, and that with the prereagent method, the slow-release of base is beneficial to stifling this competitive binding. This phenomenon was investigated by Buchwald and coworkers in 2019 report where they found benefits to slow addition of the DBU base, which helped to mitigate the competitive binding of the base to the catalyst.[41] A second possibility is that the substrates are base sensitive, and that base-mediated decomposition leads to loss in reactivity or species that can favorably bind with the Pd catalyst. This was investigated in the context of five-membered ring heterocycles by Buchwald and coworkers in 2019 where they found a more mild NaOTMS base lowered substrate decomposition and use of the specialized GPhos ligand resisted catalyst

deactivation by competitive binding.[42] In this case, slow addition of base from the prereagent activation method could help mitigate decomposition and competitive binding pathways as well.

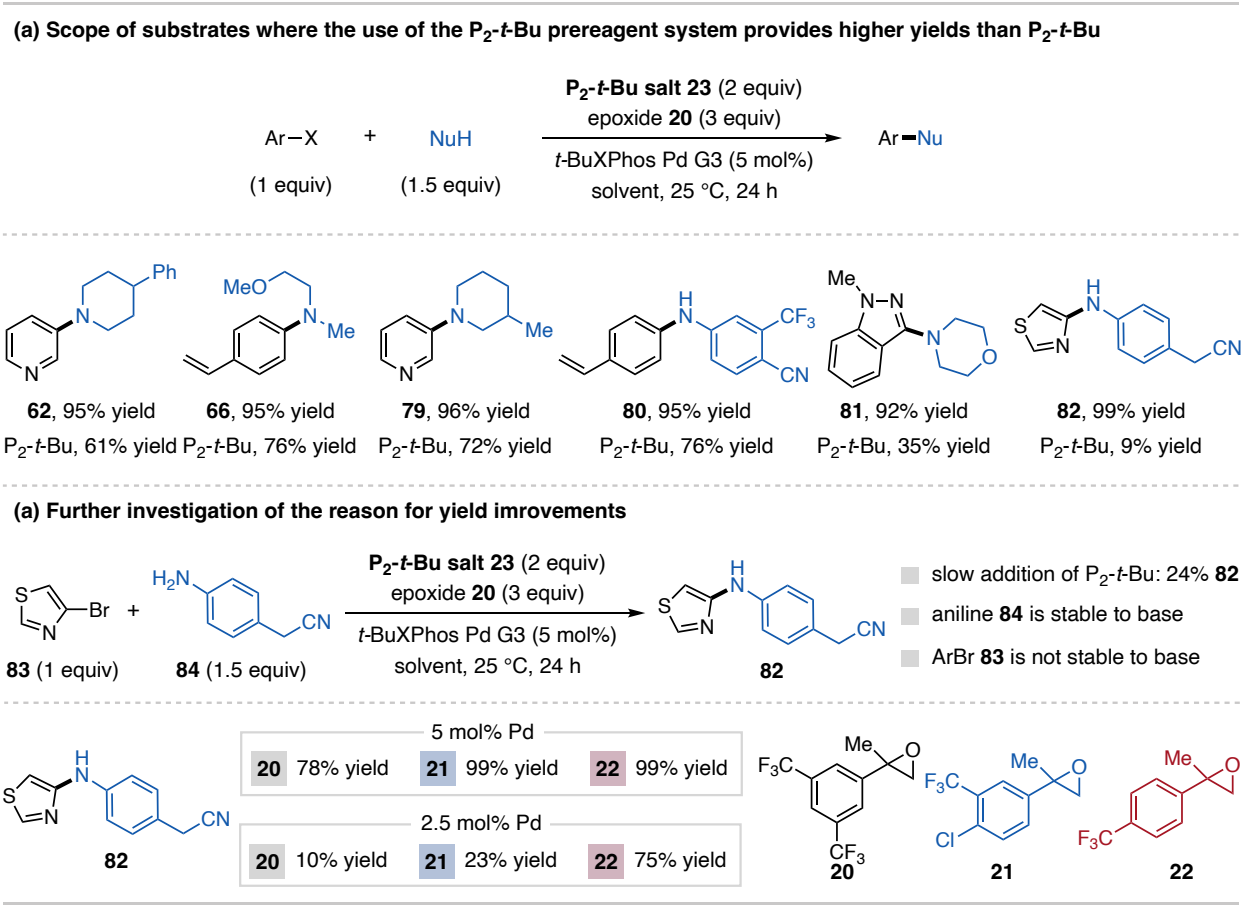

Figure 2.23: Improvements to Pd-catalyzed cross-coupling yields with epoxide-controlled slow base release

Substrate **82** shows the most drastic difference in yield between the prereagent system and commercial P$_2$-*t*-Bu, so we studied this substrate further to elucidate the reason behind this. We investigated the stability of aryl bromide **83** and aniline **84** in the presenece of P$_2$-*t*-Bu, independent of the Pd catalyst. We found that **83** undergoes decomposition and **84** remains untouched (further details in Appendix A), which could be an explanation for the low yield using P$_2$-*t*-Bu. In a separate control reaction, I conducted the reaction **83** and **84** with manual slow addition of P$_2$-*t*-Bu over the course of fifteen minutes, where I observed an increase in yield from 9% to 24% of **82**. This indicates that this reaction is very sensitive to the initial concentration of base in solution. I next

investigated the effects of epoxide structure on the results of this reaction when the P_2-*t*-Bu prereagent is utilized. Utilizing the fastest activating epoxide, **20**, leads to 78% yield of **82** whereas slower activating epoxides **21** and **22** lead to 99% yield of the product. I next lowered the catalyst loading of Pd from 5 mol% to 2.5 mol%, as a lower loading of Pd should be more sensitive to the concentration of base. Here, I noticed a much more pronounced trend, with epoxide **20** only giving 10% yield of product and **21** only giving 23% yield, indicating these epoxides activate too rapidly. However, use of epoxide **22** lead to 75% yield of **82**, providing support that the slow addition of P_2-*t*-Bu enabled by the prereagent system is critical for obtaining high yields for these substrates. Overall, this epoxide-opening activation method provides unprecedented reactivity through an *in situ* slow addition technique controlled by epoxide electrophilicity.

2.8 Conclusion

In summary, the strategy presented here provides access to organic superbases from benchtop-stable carboxylate salts. Drawing inspiration from an initial decarboxylation method, we developed an epoxide-opening method to activate these salts. These salts, with epoxide additives, are effective precatalysts and prereagents for BTPP and P_2-*t*-Bu using standard Schlenk manifold protocols. The salts are easy to prepare, recyclable and can be regularly handled open to air. We described several scenarios where a preactivation procedure is required to illustrate potential challenges that may be encountered and how they can be addressed when using these salts. Improved activation systems are currently under development, including for the stronger P_4-*t*-Bu superbase. The precatalyst systems have the potential to accelerate the discovery of new superbases, superbase-promoted applications and their use by a wider community. More broadly, the mechanistic ability to regulate superbase introduction to solutions presents a myriad of possibilities for improving or manipulating base-promoted reactivity, a prospect that we are

currently pursuing in numerous contexts. This project area has been brought to completion and has been published in *Chemical Science* in 2024 (Sujansky, S. J.; Hoteling, G. A.; Bandar, J. S. *Chem. Sci.* **2024**, Advance Article, highlighted as Pick of the Week).

REFERENCES

[1] Weitkamp, R. F.; Neumann, B.; Stammler, H. G.; Hoge, B Generation and Applications of the Hydroxide Trihydrate Anion, [OH(OH2)3]-, Stabilized by a Weakly Coordinating Cation. *Angew. Chem. Int. Ed*. **2019**, *58*, 14633 –14638.

[2] Courtemanche, M.-A.; Légaré, M.-A.; Rochette, É.; Fontaine, F.-G. Phosphazenes: efficient organocatalysts for the catalytic hydrosilylation of carbon dioxide. *Chem. Commun.*, **2015**, *51*, 6858–6861.

[3] Rathman, T. L.; Schwindeman, J. A. Preparation, Properties, and Safe Handling of Commercial Organolithiums: Alkyllithiums, Lithium sec-Organoamides, and Lithium Alkoxides. *Org. Process Res. Dev*. **2014**, *18*, 1192–1210.

[4] Collum, D. B.; McNeil, A. J.; Ramirez, A. Lithium Diisopropylamide: Solution Kinetics and Implications for Organic Synthesis. *Angew. Chem. Int. Ed*. **2007**, *46*, 3002 – 3017.

[5] Biscoe, M. R., Fors, B. P.; Buchwald, S. L. A New Class of Easily Activated Palladium Precatalysts for Facile C-N Cross-Coupling Reactions and the Low Temperature Oxidative Addition of Aryl Chlorides. *J. Am. Chem. Soc.* **2008**, *130*, 6686-6687.

[6] Campeau, L.-C.; Hazari, N. Cross-Coupling and Related Reactions: Connecting Past Success to the Development of New Reactions for the Future. *Organometallics* **2019**, *38*, 3−35.

[7] Surry, D.S.; Buchwald, S. L. Dialkylbiaryl phosphines in Pd-catalyzed amination: a user's guide. *Chem. Sci.* **2011**, *2*, 27-50.

[8] Tran, V. T.; Li, Z. Q.; Apolinar, O.; Derosa, J.; Joannou, M. V.; Wisniewski, S. R.; Eastgate, M. D.; Engle, K. M. Ni(COD)(DQ): An Air-Stable 18-Electron Nickel(0)–Olefin Precatalyst. *Angew. Chem. Int. Ed.* **2020**, *59*, 7409 –7413.

[9] Luo, C.; Bandar, J. S. Superbase-Catalyzed anti-Markovnikov Alcohol Addition Reactions to Aryl Alkenes. *J. Am. Chem. Soc*. **2018**, *140*, 3547−3550.

[10] Suyama, K.; Masamitsu, S. Photobase Generators: Recent Progress and Application Trend in Polymer Systems. *Prog. Polym. Sci.* **2009**, *34*, 194-209.

[11] Zivic, N.; Kuroishi, P. K.; Dumur, F.; Gigmes, D.; Dove, A. P.; Sardon, H. Recent Advances and Challenges in the Design of Organic Photoacid and Photobase Generators for Polymerizations. *Angew. Chem. Int. Ed.* **2019**, *58*, 10410–10422.

[12] Gierczyk, B.; Wojciechowski, G.; Brzezinski, B.; Grech, E.; Schroeder, G. Study of the decarboxylation mechanism of fluorobenzoic acids by strong N-bases. *J. Phys. Org. Chem*. **2001**, *14*, 691–696.

[13] Sopeña, S.; Cozzolino, M.; Maquilón, C.; Escudero-Adun, E. C.; Belmonte, M. M.; Kleij, A. W. Organocatalyzed Domino [3+2] Cycloaddition/Payne-Type Rearrangement using Carbon Dioxide and Epoxy Alcohols. *Angew. Chem. Int. Ed*. **2018**, *57*, 11203 –11207.

[14] Morgan, K. M.; Ellis, J. A.; Lee, J.; Fulton, A.; Wilson, S. L.; Dupart, P. S.; Dastoori, R. Thermochemical Studies of Epoxides and Related Compounds *J. Org. Chem*. **2013**, *78*, 4303−4311.

[15] Bordwell, F. G. Equilibrium acidities in dimethyl sulfoxide solution. *Acc. Chem. Res.* **1988**, *21*, 456–463.

[16] Olmstead, W. N.; Margolin, Z.; Bordwell, F. G. Acidities of water and simple alcohols in dimethyl sulfoxide solution. *J. Org. Chem*. **1980**, *45*, 3295–3299.
[17] Puleo, T. R.; Sujansky, S. J.; Wright, S. E.; Bandar, J. Organic Superbases in Recent Synthetic Methodology Research. *Chem. Eur. J*. **2020**, *27,* 4216 – 4229.
[18] Carlson, R. G.; Behn, N. S. Conformational Preference of the Oxiran Group in Cyclohexanespiro-oxiran. *Chem. Commun.* **1968**, 339-340.
[19] Hrenar, T.; Primožič, I.; Fijan, D.; Majerić Elenkov, M. Conformational Analysis of Spiro-Epoxides by Principal Compnent Analysis of Molecular Dynamics Trajectories. *Phys. Chem. Chem. Phys.* **2017**, *19*, 31706-31713.
[20] Alabugin, I. V.; Kuhn, L.; Krivoshchapov, N. V.; Mehaffy, P.; Medvedev, M. G. Anomeric effect, hyperconjugation and electrostatics: lessons from complexity in a classic stereoelectronic phenomenon. *Chem. Soc. Rev.* **2021**, *50*, 10212–10252.
[21] Brown, D. G.; Boström, J. Analysis of Past and Present Synthetic Methodologies on Medicinal Chemistry: Where Have All the New Reactions Gone? *J. Med. Chem*. **2016**, *59*, 4443−4458.
[22] Caldwell, N.; Jamieson, C.; Simpson, I.; Tuttle, T. Organobase-Catalyzed Amidation of Esters with Amino Alcohols. *Org. Lett.* **2013**, *15*, 2506- 2509.
[23] Caldwell, N.; Campbell, P. S.; Jamieson, C.; Potjewyd, F.; Simpson, I.; Watson, A. J. B. Amidation of Esters with Amino Alcohols Using Organobase Catalysis. *J. Org. Chem.* **2014**, *79*, 9347-9354.
[24] Nielsen, M. K.; Ugaz, C. R.; Li, W.; Doyle, A. G. PyFluor: A Low-Cost, Stable, and Selective Deoxyfluorination Reagent. *J. Am. Chem. Soc*. **2015**, *137*, 9571−9574.
[25] Nising, C. F.; Bräse, S. Recent Developments in the Field of oxa-Michael Reactions. *Chem. Soc. Rev.* **2012**, *41*, 988-999.
[26] Kennemur, J. L.; Maji, R.; Scharf, M. J.; List, B. Catalytic Asymmetric Hydroalkoxylation of C−C Multiple Bonds. *Chem. Rev.* **2021**, *121*, 14649–14681.
[27] Müller, T. E.; Hultzsch, K. C.; Yus, M.; Foubelo, F.; Tada, M. Hydroamination: Direct Addition of Amines to Alkenes and Alkynes. *Chem. Rev.* **2008**, *108*, 3795–3892.
[28] Boileau, S.; Illy, N. Activation in Anionic Polymerization: Why Phosphazene Bases are Very Exciting Promoters. *Prog. Polym. Sci*. **2011**, *36*, 1132-1151.
[29] Liu, S.; Ren, C.; Zhao, N.; Shen, Y.; Li, Z. Phosphazene Bases as Organocatalysts for Ring-Opening Polymerization of Cyclic Esters. *Macromol. Rapid Commun*. **2018**, *39*, 1800485.
[30] Alamri, H.; Zhao, J.; Pahovnik, D.; Hadjichristidis, N. Phosphazene-Catalyzed RingOpening Polymerization of ε-caprolactone: Influence of Solvents and Initiators. *Polym. Chem*. **2014**, *5*, 5471-5478.
[31] Ikada, Y.; Tsuji, H. Biodegradable polyesters for medical and ecological applications. *Macromol. Rapid Commun.* **2000**, *21*, 117-132.
[32] Nair, L. S.; Laurencin, C. T. Biodegradable polymers as biomaterials. *Prog. Polym. Sci.* **2007**, *32*, 762–798.

[33] Woodruff, M. A.; Hutmacher, D. W. The return of a forgotten polymer—Polycaprolactone in the 21st century. *Prog. Polym. Sci.* **2010**, *35*, 1217–1256.

[34] Gentekos, D. T.; Dupuis, L. N.; Fors, B. P. Beyond Dispersity: Deterministic Control of Polymer Molecular Weight Distribution. *J. Am. Chem. Soc*. **2016**, *138*, 1848−1851.

[35] Gesmundo, N. J.; Sauvagnat, B.; Curran, P. J.; Richards, M. P.; Andrews, C. L.; Dandliker, P. J.; Cernak, T. Nanoscale Synthesis and Affinity Ranking. *Nature* **2018**, *557*, 228-232.

[36] Costa, A.; Nájera C.; Sansano, J. M. P2-Et-Mediated Deprotonation of ortho-Halobenzyl Sulfones: Synthetic Applications of Zwitterionic Synthons. *Synlett* **2001**, *12*, 1881-1884

[37] Meyers, C.; Maes, B. U. W.; Loones, K. T. J.; Bal, G.; Lemierè , G. L. F.; Dommisse, R. A. Study of a New Rate Increasing "Base Effect" in the Palladium-Catalyzed Amination of Aryl Iodides. *J. Org. Chem*. **2004**, *69*, 6010−6017.

[38] Shigeno, M.; Hayashi, K.; Nozawa-Kumada, K.; Kondo, Y. Phosphazene Base tBu-P4 Catalyzed Methoxy–Alkoxy Exchange Reaction on (Hetero)Arenes. *Chem. Eur. J*. **2019**, *25*, 6077-6081.

[39] Dennis, J. M.; White, N. A.; Liu, R. Y.; Buchwald, S. L. Breaking the Base Barrier: An Electron-Deficient Palladium Catalyst Enables the Use of a Common Soluble Base in C−N Coupling. *J. Am. Chem. Soc*. **2018**, *140*, 4721–4725.

[40] Yiang, Q.; Babij, N. R.; Good, S. Potential Safety Hazards Associated with Pd-Catalyzed Cross-Coupling Reactions. *Org. Process Res. Dev.* **2019**, *23*, 2608-2626.

[41] Dennis, J. M.; White, N. A.; Liu, R. Y.; Buchwald, S. L. Pd-Catalyzed C–N Coupling Reactions Facilitated by Organic Bases: Mechanistic Investigation Leads to Enhanced Reactivity in the Arylation of Weakly Binding Amines. *ACS. Catal*. **2019**, *9*, 3822-3830.

[42] Reichert, E. C.; Feng, K.; Sather, A. C.; Buchwald, S. L. Pd-Catalyzed Amination of Base-Sensitive Five-Membered Heteroaryl Halides with Aliphatic Amines. *J. Am. Chem. Soc*. **2023**, *145*, 3323-3329

CHAPTER THREE

BACKGROUND AND MOTIVATION FOR BENZYLIC C–H FUNCTIONALIZATION *VIA* BASE-PROMOTED HALOGEN TRANSFER

3.1 Chapter Overview

Deprotonation serves as one of the most ubiquitous strategies for molecular activation in synthetic organic chemistry. In the Bandar Group, we focus on gaining a fundamental understanding of the acid-base reaction paradigm in order to drive the development of new base-promoted methods. Our goal is to push the boundaries of traditional base-promoted chemistry and discover new capabilities of strong bases for new reactivity. This is an important goal as new and simplified routes to forge important chemical bonds are highly desirable for the continued development of bioactive pharmaceuticals and agrochemicals. In Chapter Two, I discussed the development of organic superbase precatalyst salts, which provided me and the group with a deeper understanding of base-promoted reactivity. In this Chapter, I will discuss the development and research within another project area in our group devoted to the development of new C–H functionalization reactions through base-promoted halogen transfer.

Within this area of research, I have established two new reaction platforms, the benzylic amination of alkyl (hetero)arenes and the desaturation of alkyl (hetero)arenes that can be coupled with cascade functionalization reactions. This Chapter will discuss the background and relevance for these transformations, including the importance of the products and current state-of-the-art methods to achieve similar transformations. In addition to this, I will discuss the history and

development of base-promoted halogen transfer by our group and the current state of this area within our group.

3.2 Importance and Significance of Benzyl Amines

Amines are very important functional groups in synthetic and medicinal chemistry, both in building blocks and complex bioactive molecules.[1-3] Amines are sought after due to beneficial properties such as the ability to act as both H-bond donors and acceptors, which is useful for binding abilities of bioactive compounds. Benzylic amines represent an interesting class of amines that are prevalent in pharmaceutical compounds such as filgotinib for rheumatoid arthritis treatment, duvelisib for leukemia treatment, and evocalcet for hyperparathyroidism (Figure 3.1). The introduction of amines and other heteroatoms to drug molecules *via* late-stage functionalization has been well studied in order to investigate the potential benefits of additional heteroatoms.[4,5]

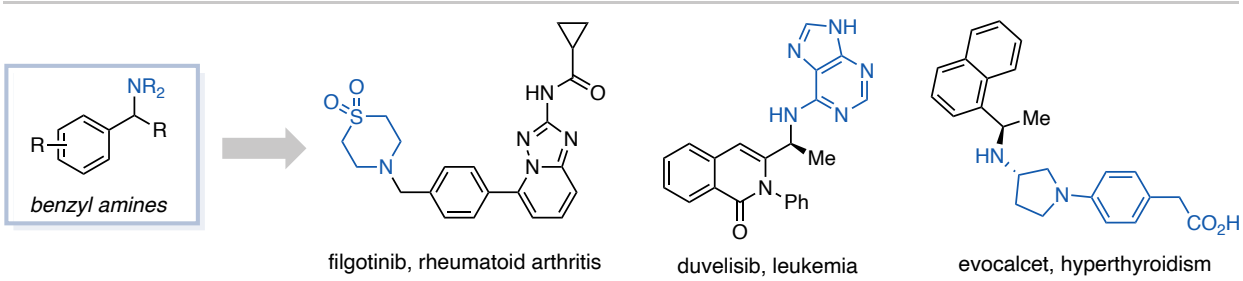

Figure 3.1: Prevalence of benzyl amines in pharmaceutical compounds

Figure 3.2a shows an example of benefits imparted by the introduction of a benzylic amine to penicillin G to make ampicillin.[6,7] Penicillin G is highly effective against gram-positive bacteria, however, it is ineffective against gram-negative bacteria due to low membrane permeability. It was found that by introducing the amine to the benzylic position, membrane absorption of the drug was significantly enhanced, allowing ampicillin to be effective at fighting both gram-positive and -negative bacteria, leading to a more generally useful drug. In a similar vein, the White Group in

2018 reported a Mn-catalyzed benzylic C–H amination protocol that functions on a wide variety of alkyl arenes.[8] In this report, they showcased the introduction of benzyl amines to a number of pharmaceutical compounds, with examples shown in Figure 3.2b.

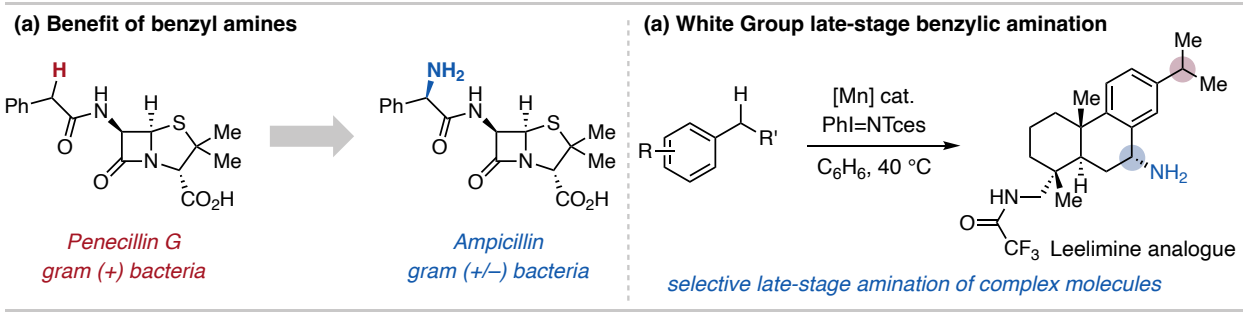

Figure 3.2: Beneficial effects for the installation of benzyl amines in pharmaceutical compounds

The benefits of benzylic amines in pharmaceutical compounds warrants further investigation in the development of new compounds. As such, a facile and broad method for their synthesis is highly desirable. Chapter Four will discuss my efforts in developing the first general method for coupling any amine with a benzylic C–H bond. The next Section of this Chapter will discuss current methods for benzylic C–H amination to provide context for the method I have developed.

3.3 Methods to Achieve Benzylic C–H Amination of Alkyl (Hetero)Arenes

3.3.1 Benzylic C–H Amination Utilizing Protected Ammonia Surrogates

There are two main approaches for achieving direct benzylic C–H amination, the first being the use of a protected ammonia surrogate as coupling partners towards the synthesis of primary amines which, after deprotection, could be further functionalized to other amine products. The other approach is more direct, coupling any amine partner to an alkyl (hetero)arene and accessing these diverse amine products in one step, as opposed to multiple (Figure 3.3). The first of these two methods, the use of a protected ammonia surrogate, has been more thoroughly developed. A major drawback with this approach is the use of ammonia surrogates like azides or tosyl groups,

which can be hazardous to work with or difficult to remove after reaction, respectively. [9-14] Additionally, these methods can only access primary amines, necessitating additional synthetic steps and purifications to access a diverse scope of products. Despite this, methods that utilize this approach are still very useful and of the many published works in this area, I will highlight five here to provide an overview of this area.[15-17]

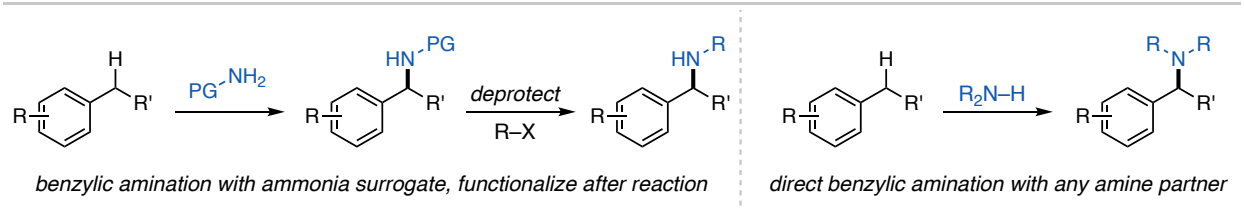

Figure 3.3: Two approaches to benzylic C–H amination

The first method was reported by the Dauban Group in 2006 for diastereoselective intermolecular C–H amination of alkyl arenes (Figure 3.4).[18] Here, they utilize a rhodium catalyst to facilitate amination from a chiral sulfonamide nitrene precursor. From previously reported work, the group found that the combination of sulfonamides and hypervalent iodine compounds results in iminoiodanes, which serve as nitrene donors for the Rh catalyst to facilitate C–H aziridination with various vinyl arenes.[19] In this report, the authors utilized this approach to aminate alkyl arenes of with various electronics and functional groups. A notable limitation of this transformation is that heteroaryl alkenes aside from 2-ethylthiophene are not included in the scope.

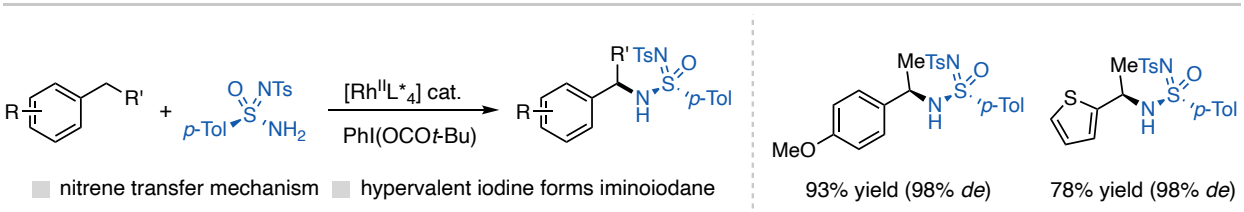

Figure 3.4: Rh catalyzed nitrene transfer developed by the Dauban Group

Another method for achieving benzylic C–H amination using an ammonia surrogate was reprted in 2017 by the Arnold Group (Figure 3.5).[20] In this report, the authors engineered an

enzymatic Fe catalyst based on cytochrome P450 monooxygenase, which is an enzyme that plays a key role in the metabolism of xenobiotics such as drug compounds.[21] Using this Fe catalyst with tosyl azide (TsN_3) as a nitrene source, nitrene transfer for benzylic C–H amination is achieved. This method functions on a scope of alkylbenzene derivatives with variation of the arene electronics and alkyl chain composition. However, a notable restriction of this method is a lack of diverse methylarenes and no incorporation of *N*-heteroarene substrates.

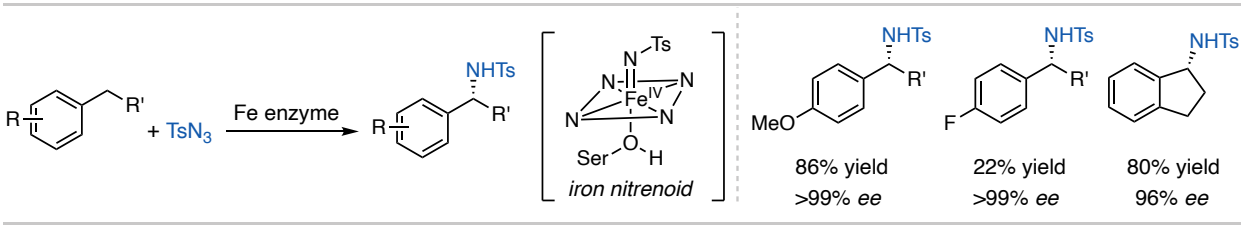

Figure 3.5: Engineered cytochrome P450 enzyme catalyzed benzyl amination developed by the Arnold Group

The next method of note is the Mn-catalyzed benzylic amination for late-stage functionalization developed by White and coworkers in 2018 (Figure 3.2b).[8] This reaction proceeds *via* a nitrene-transfer mechanism using an iminoiodane nitrene precursor, similar to the processes described above. The power of this method lies in its ability to functionalize complex drug molecues, demonstrating high functional group tolerance and site selectivity with multiple compounds featuring multiple benzylic C–H bonds. Although pyridines are featured in the substrate scope of this protocol, it must be protected by the addition of a Lewis acid to avoid unfavorable reactivity with the catalyst.

The next featured method was developed by the Lambert Group in 2021 for the electrophotocatalytic Ritter-type amination of alkyl arenes (Figure 3.6).[22] Cyclopropenium ions, pioneered by the Lambert Group, are photoexcited leading to oxidation of the alkyl arene followed by deprotonation and a second oxidation to get to the benzyl cation, which is trapped with acetonitrile. This product is then hydrolyzed to obtain the N-acyl benzylamine, which are easily

deprotected to the primary amine. This protocol is tolerant of a variety of functionalities including *N*-heterocycles, with examples of site selectivity when multiple benzylic sites are available.

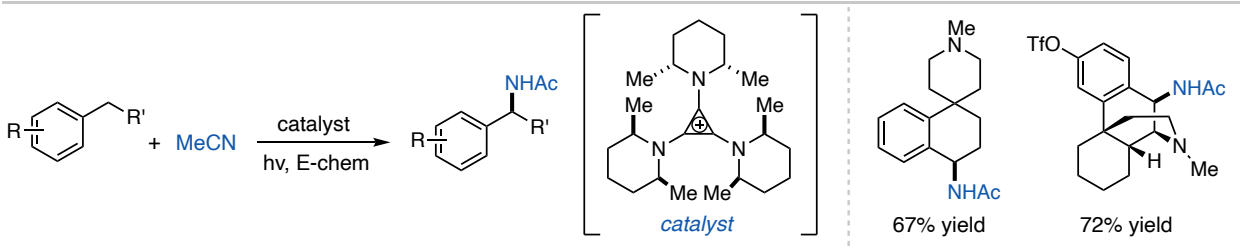

Figure 3.6: Electrophotocatalytic Ritter-type reaction using cyclopropenium ion catalyst by the Lambert Group

The final example to be discussed here was reported by the Zhaou Group for cationic Cu-catalyzed enantioselective benzylic C–H amination.[23] In this method, *t*-Bu peroxide is used to oxidize the alkyl arene. The resultant benzyl radical can coordinate to the Cu catalyst, where benzamide is already bound. Through reductive elimination, the C–N coupled product is obtained. This reaction is made enantioselective by use of a chiral bisoxazoline (BOX) ligand. A variety of alkyl arenes and benzamide coupling partners were showcased, however, alkyl heteroarenes are absent in this protocol.

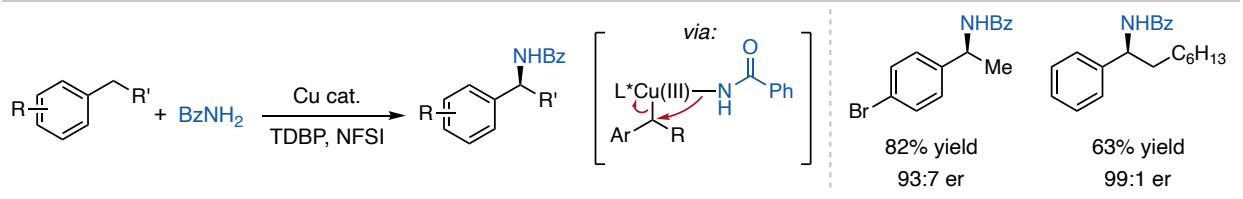

Figure 3.7: Cu-catalyzed enantioselective benzylic amination developed by the Zhao Group

Overall, these five methods give an overview of current approaches to benzylic C–H amination using ammonia surrogates. Though useful methods, a general method that does not rely on transition metals, nitrene chemistry, or complicated reaction setups is highly desirable. Currently, our group is developing a method for direct C–H amination to access primary benzylamines that addresses substrate scope limitations using our base-promoted halogen transfer methodology, described in Section 3.7.

3.3.2 Benzylic C–H Amination Utilizing Diverse Amine Coupling Partners

In the previous section, I described a range of methods for achieving benzylic amination using ammonia surrogates, resulting in primary benzylamines. A more appealing approach to this transformation is the direct coupling of any amine to a benzylic C–H bond. Compared to the previous approach, there are far fewer methods reported for engaging primary and secondary amines and anilines in this process. There have been methods that report some examples benzylic C–H amination, but this section will focus on methods that are devoted entirely to this transformation.[24-26]

One of the most utilized benzylic C–H amination reactions is the Hoffmann−Löfler−Freitag reaction, which was first developed by Hoffmann in 1879 and expanded upon by Löfler and Freitag in 1909 (Figure 3.8).[27,28] This reaction utilizes N-halo aliphatic amines that undergo homolytic cleavage to form the N-centered radical, followed by a 1,5-hydride shift with the alkyl chain. This is followed by C–X bond formation and cyclization to form the pyrrolidine. This has been a heavily used reaction and since its development, chemists have pushed the boundaries of compatible substrates.[29-31] For this reaction, benzylic positions are typically engaged due to the stabilization of the carbon-centered radical formed in the mechanism. Although this is a well-utilized reaction, the process is restricted to cyclization reactions and the availability of the alkyl *N*-halo amine precursor.

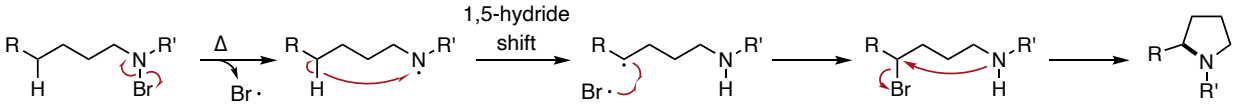

Figure 3.8: Mechanism of the Hofmann-Löffle-Freytag reation

The Stahl group has disclosed multiple benzylic C–H oxidation strategies, two of which, published in 2023, will be discussed here for benzylic amination. The first approach is through

heterobenzylic C–H chlorination followed by amine substitution of this product.[32] Here, upon activation of the *N*-heterocycle with a Lewis acid, benzylic deprotonation takes place followed by trapping of this intermediate with an electrophilic halogen source. The halogenated product can then be coupled with a series of amines and azoles for benzylic amination(Figure 3.9a). This protocol successfully engages *N*-heterocycles in a benzylic amination protocol, a substrate class that is not compatible with alternate routes described previously. Some drawbacks to this method include restriction to N-heterocycles by nature of the mechanism and the fact that this is a two-step protocol where the amine is added to the reaction after the halogenated intermediate is formed.

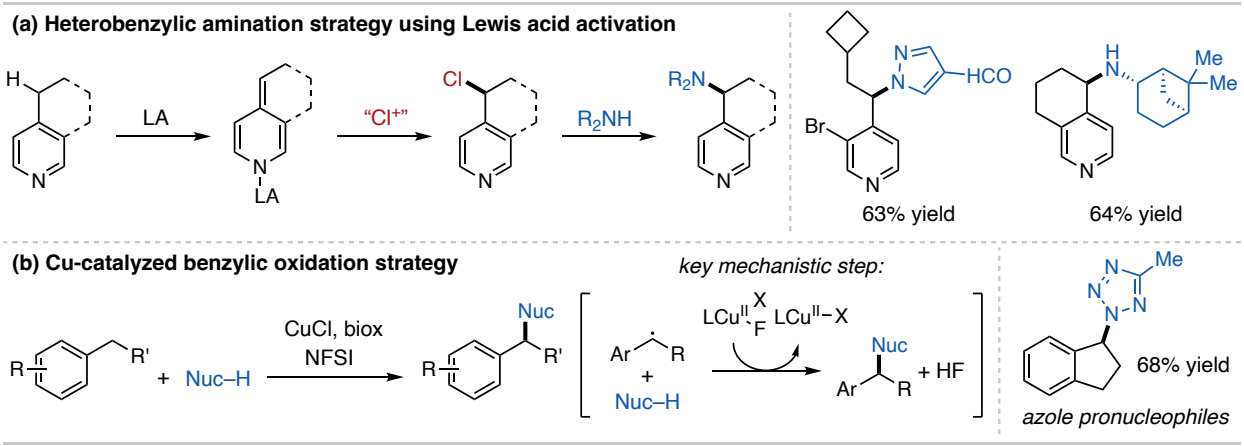

Figure 3.9: Stahl Group approaches to benzylic C–H amination

The second approach by the Stahl group involves Cu catalyzed benzylic oxidation using NFSI, followed by C–N bond formation (Figure 3.9b).[33] The key to this reaction is the use of redox buffers to convert the off-cycle stable Cu–NSI complex back to the active Cu catalytic species to enable productive reactivity. This protocol is used to furnish new C–O, C–S, and C–N bonds in the benzylic position. The majority of *N*-pronucleophiles utilized for this reaction include azole heterocycles and amides, with select examples of amines presented. This method is general to a variety of alkyl(hetero)arene substrates, but the limitation to mostly azole or amide pronucleophiles ultimately restricts this method.

The next method for benzylic C–H amination was developed by the Musacchio and coworkers in 2023.[34] In this report, photocatalytic homolysis of *N*-alkyl pyridinium salts leads to HAT of a benzylic C–H bond followed by oxidation of this benzylic radical by the photocatalyst. This generated benzylic carbocation is then trapped with an azole pronucleophile (Figure 3.10). This method is limited to alkyl arene substrates that can stabilize a benzylic carbocation, so electron-deficient arenes and heteroarenes are not tolerated. Additionally, azoles are the only demonstrated pronucleophile for this transformation, where use of multiple amine types would be ideal.

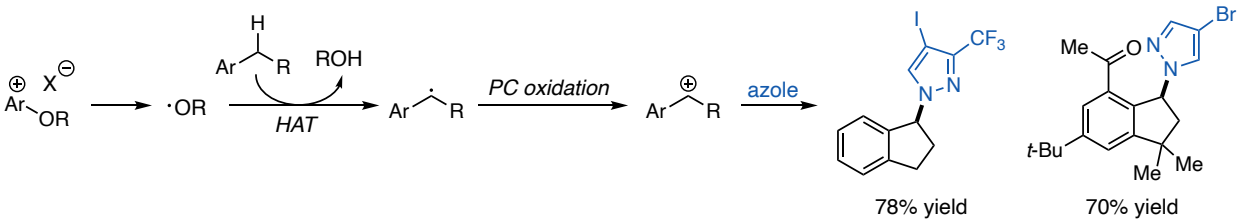

Figure 3.10: Photoredox-catalyzed benzylic C–H azolation developed by the Musacchio Group

Another method for benzylic C–H amination was developed by the Powers Group in 2022 using their developed *N*-aminopyridinium salt chemistry.[35] This method was first developed for the aziridination of vinyl arenes, but Powers and coworkers found that with alkyl arenes, these reagents could be leveraged for amination.[36] In this method, benzylic C–H oxidation is achieved followed by amination with *N*-aminopyridinium salts. Following isolation, the aminated products are engaged in Ni-catalyzed cross-coupling with arylboronic acids to access a variety of benzylic aniline products (Figure 3.11). Although this provides access to a wide variety of products, the method is unappealing due to the need for two separate protocols with long reaction times and sometimes impractical conditions.

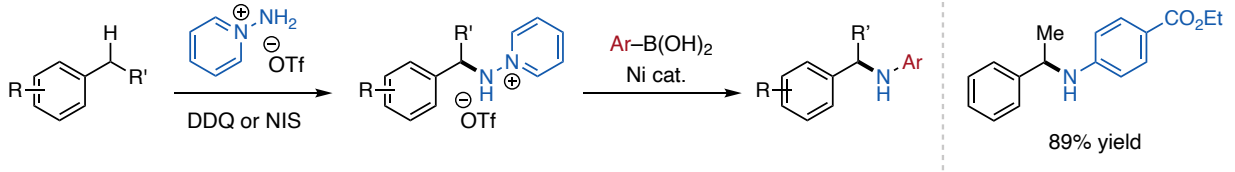

Figure 3.11: Powers Group approach to benzylic amination with *N*-aminopyridinium salt coupling

The next method was developed by the Kumar Group in 2015 for intramolecular cyclization to synthesize *N*-aryl-isoindolinones (Figure 3.12).[37] This method follows a similar mechanism to the Hoffmann−Löfler−Freitag reaction, where the amide is halogenated followed by homolysis and a 1,5-hydride shift. Benzylic C–X bond formation takes place, and the reaction is finished with an S_N2 cyclization. This reaction shows broad functional group tolerance on the amide nitrogen portion, but rather restricted on the arene portion. Additionally, the starting materials must be presynthesized, which leads to a less general protocol.

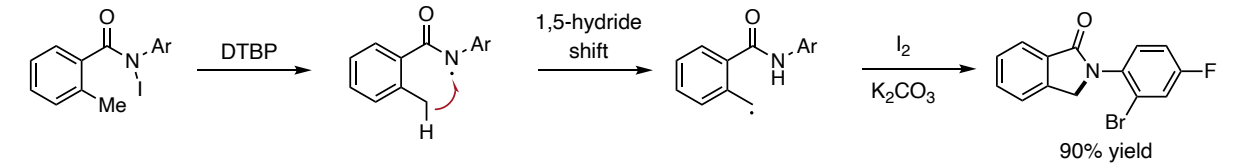

Figure 3.12: Kumar Group intramolecular benzylic C–H amination

While methods do exist for direct benzylic C–H amination, there are clear limitations to each approach. In Chapter Four of this dissertation, I describe my development of a direct and general benzylic C–H amination protocol using base-promoted halogen transfer. This protocol is guided by C–H acidity whereas established methods typically rely on C–H bond strengths, which provides access to a broad substrate scope and interesting site selectivity.

3.4 Importance and Significance of Vinyl (Hetero)Arenes

While investigating the benzylic amination protocol I developed, described in Chapter Four, I discovered that when alkyl (hetero)arenes are utilized, desaturation from elimination of the benzyl halide is a competitive side pathway. This leads to highly valuable vinyl (hetero)arenes and

the discussion of the preliminary work I have established in this area is in Chapter Five. This Section is intended to provide background on this functional group and its importance in synthetic and medicinal chemistry.

Alkenes are ubiquitous functional groups in organic chemistry that have been well studied as building blocks for the synthesis of more complex molecules.[38] Vinyl arenes represent one class of alkenes that are engaged in a number of useful transformations (Figure 3.13a).[39] There have been many methods developed for the synthesis of these substrates, with the Wittig reaction being the most common, accessing the vinyl arene from a benzaldehyde.[40] Section 3.5 will cover current routes for accessing vinyl arenes through alkyl arene desaturation.

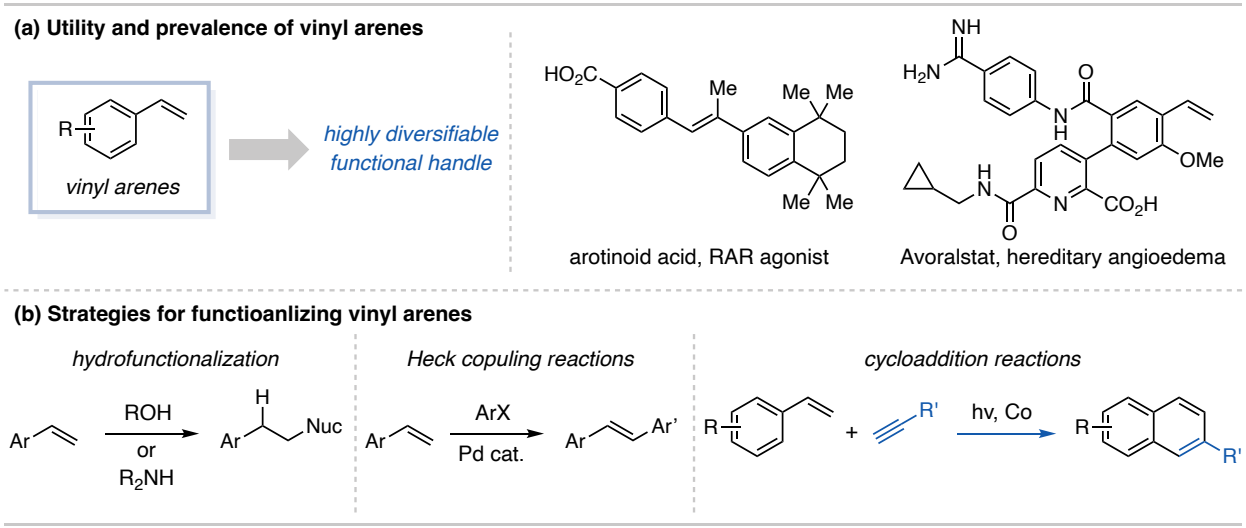

Figure 3.13: Prevalence of vinyl arenes and selected strategies for their functionalization

Besides serving as building blocks towards the synthesis of complex molecules, vinyl (hetero)arenes are also appear in these compounds, with example pharmaceutical compounds such as arotinoid acid as a RAR agonist and Avoralstat for treatment of hereditary angioedema (Figure 3.13a). The utility of vinyl arenes most often comes in their use in functionalization reactions. Some examples of common alkene functionalization reactions include hydroetherification[41]

(example developed by the Bandar Group in 2018) and hydroamination[42], transition metal cross-coupling[43], and cycloaddition[44] reactions (Figure 3.13b).

3.5 Methods to Achieve Desaturation of Alkyl (Hetero)Arenes

Direct desaturation of alkyl (hetero)arenes presents an ideal route to access vinyl (hetero)arenes due to their prevalence in both simple and complex molecules (Figure 3.14). This section aims to provide background for the current landscape of methods to achieve this transformation, as well as discuss related transformations that exploit desaturation of carbonyl compounds. Historically, this approach is taken in the synthesis of styrene for polymerization through the dehydrogenation of ethylbenzene in the vapor-phase with an iron oxide catalyst.[45] This process is overall impractical and is not suited for other alkyl arenes.

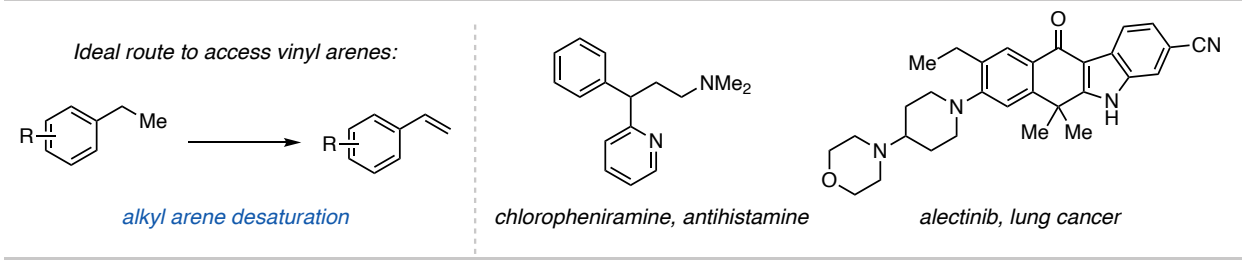

Figure 3.14: Alkyl arenes as an ideal precursor to vinyl arenes through direct desaturation

The current state-of-the-art approach for achieving alkyl arene desaturation is in the Ni-catalyzed method developed by the Newhouse Group in 2020.[46] In this reaction, the Ni catalyst undergoes oxidative addition with a sacrificial 2-bromothiophene oxidant, after which transmetalation occurs from the Zn-activated alkyl arene. β-Hydride elimination affords the product, and the catalyst reductively eliminates the thiophene, followed by reactivation with another equivalent of the oxidant. This protocol operates on a wide variety of alkyl heteroarenes, with examples shown in Figure 3.15. Less active alkyl arenes are unfortunately not tolerated under these reaction conditions. In 2021, Newhouse and coworkers followed up on this report and exploited the desaturation reactivity for further functionalization of the products using similar

activated alkanes, showing the further utility of this method. This concept of exploiting the alkene product as a diversifiable functional handle will be further discussed in Chapter Five.

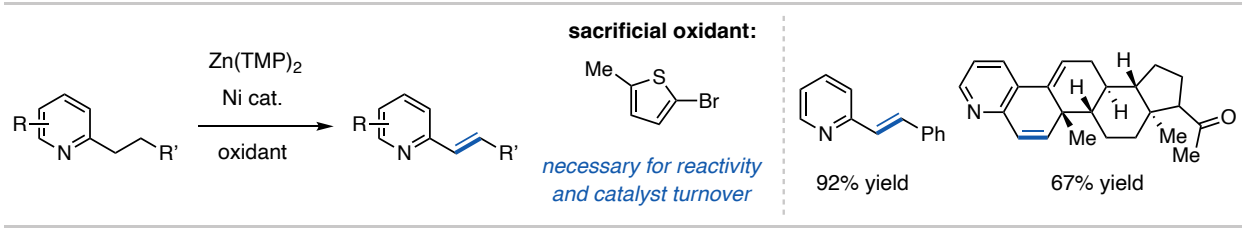

Figure 3.15: Newhouse Group Ni-catalyzed alkyl arene desaturation

Another useful method for direct alkyl arene desaturation was developed by the Jin and Nozaki Groups in 2022 (Figure 3.16).[48] Here, TEMPO is used as a catalyst to generate the benzylic radical *via* hydrogen atom transfer (HAT), followed by C–O bond formation and subsequent elimination to furnish the vinyl arene product. The TEMPO catalyst is then regenerated by reaction with oxygen under ambient conditions. This reaction is demonstrated on a series of ethylbenzene and -pyridine substrates. The drawback with this transformation is the presence of an acetophenone byproduct that forms as a result of the benzyl radical reacting with oxygen, an unavoidable side reaction.

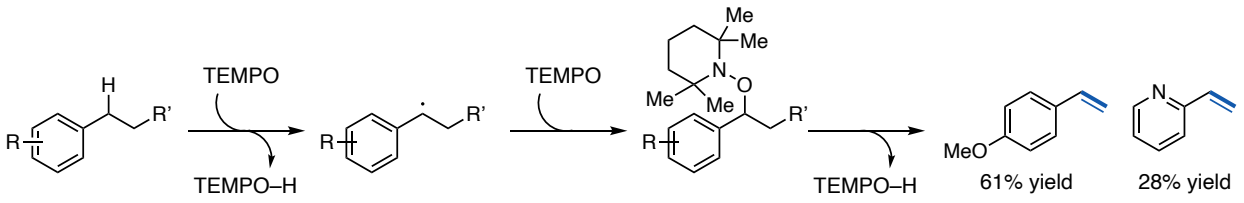

Figure 3.16: TEMPO catalyzed alkyl arene desaturation by Jin and Nozaki

The next method for this transformation was developed by the Xu and Huang Groups in 2021 (Figure 3.17).[49] In this method, the authors exploit dual photoredox and cobalt catalysis where the photocatalyst oxidizes the benzylic position of the alkyl arene followed by binding of the resultant radical to the cobalt center. β-Hydride elimination affords the desaturated product, and the cobalt catalyst is then reduced by the photocatalyst, regenerating the active catalysts for

each half of the cycle. The authors show a broad substrate scope of alkyl (hetero)arenes as well as related activated alkanes such as alkyl ethers, amides, and carbonyl compounds. The major drawback to this method is the requirement of both transition metal and photoredox catalysts.

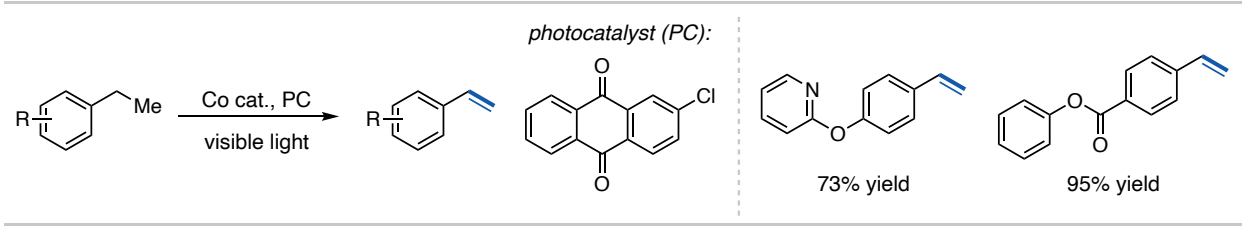

Figure 3.17: Xu and Huang Co-photocatalytic approach to alkyl arene desaturation

Related to the alkyl arenes, there has also been work reported in the desaturation of other activated alkyl systems, examples of which have been highlighted in this section in discussed methods. In this regard, the Stahl and Leonori Groups have pioneered the oxidation of cyclohexanone derivatives for the synthesis of phenols (Figure 3.18).[50,51] In each case, the authors report iterative desaturation processes that lead to the synthesis of phenols, a process that is exploited differently in each case. The Stahl group utilizes this method to synthesize unconventional phenols such as those with *meta* functionality, which would be challenging to access with typical *o/p* directing capability of phenols. The Leonori Group includes the addition of a secondary amine, which initially reacts with the cyclohexanone to form an enamine, that undergoes the iterative desaturation process, resulting in anilines. Recently, the Leonori group published a separate protocol utilizing the same desaturation method to synthesize heteroaryl amines from cyclohexanone derivatives.[52] This new report greatly expands the scope and utility of this methodology. Chapter Five briefly discusses my investigation of this iterative desaturation protocol for aromatic heterocycle synthesis using our halogen transfer approach.

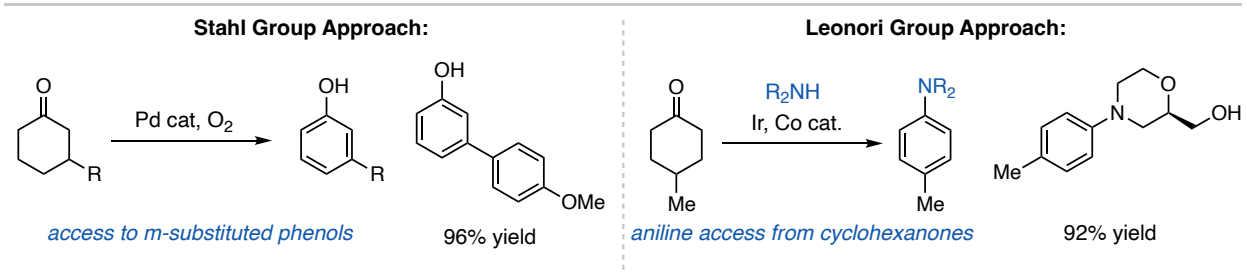

Figure 3.18: Stahl and Leonori cyclohexanone desaturation strategies

3.6 Development of the Base-Promoted Halogen Transfer Research Program

This section describes the development of the base-promoted halogen transfer research program within our group. This research area was established by Tom in our group and, as discussed in Chapter One, this area was really started with initial findings with organic superbases. Tom was attempting to enable challenging S_NAr reactions with 3-bromopyridine using P_4-*t*-Bu, but instead of obtaining the 3-substituted product, he observed the 4-substituted product (Figure 3.19a). The results of this reaction indicate that the halogen is isomerizing on the molecule under basic conditions. This behavior has been seen before, first reported by Nord and coworkers in 1951 and 1953 where they observed 2-bromo- and 2-iodothiophene disproportionate into the corresponding tetrahalothiophene under basic conditions (Figure 3.19b).[53,54] Since this initial finding, other groups have reported similar observations with haloarenes, prompting Bunnett and coworkers in the 1970s to investigate the mechanism of this phenomenon.[55] In these studies, they proposed two potential mechanisms by which this isomerization could take place, through an aryne intermediate or through intermolecular halogen transfer. These studies eventually led to the determination that intermolecular halogen transfer, termed "halogen dance" by Bunnett, as the likey and now accepted mechanism for this process (Figure 3.19c).

With this in mind, Tom next tested other aryl halides under basic conditions with P_4-*t*-Bu and observed disproportionation to a mixture of isomers with an example using 2-bromobenzotrifluoride shown in Figure 3.19d. Tom next reasoned that this typically uncontrollable

process could be leveraged for a selective substitution reaction as the different isomers of haloarenes possess different S_NAr reactivities. In this regard, the first method disclosed by our group in this area was developed, the 4-selective etherification of 3-bromopyridines enabled by base-catalyzed halogen isomerization (Figure 3.19d).[56]

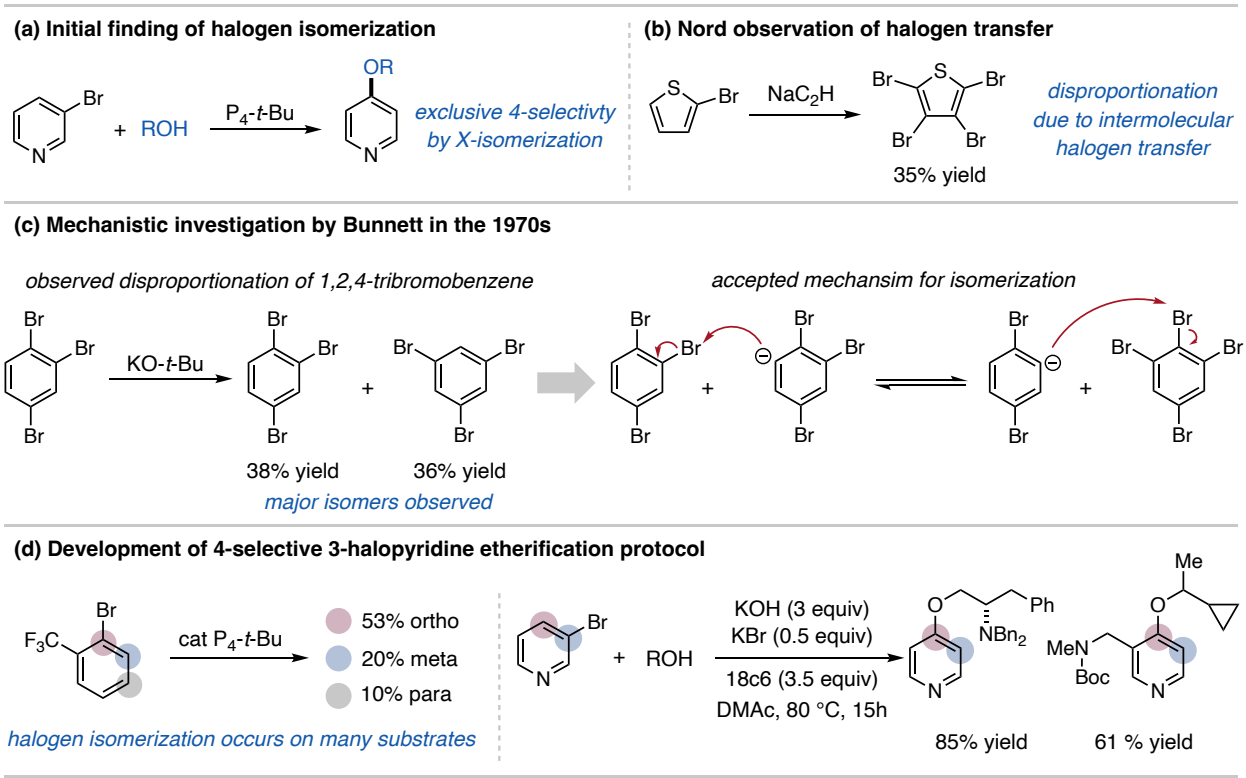

Figure 3.19: Development of the halogen-transfer reasearch program and initial work

After this initial report and based on the accepted mechanism of the "halogen dance", Tom reasoned that and intermolecular process could be effective. Here, base can be used to deprotonate a weakly acidic aryl C(sp^2)–H bond followed by halogen transfer from a sacrificial halogen oxidant to furnish a new aryl C–X bond that can be coupled with an S_NAr reaction *in situ*. Using 2-halothiophenes as sacrificial oxidants and alcohols for etherification, Tom found that this mechanism can be exploited for net aromatic C–H etherification (mechanism in Figure 3.20).[57] This method is general for a variety of alcohols and heteroarene coupling partners. Under the same mechanism, Tom and another member of the Bandar Group, Kendelyn Bone, found that by use of

2-phenyl ethanol, after etherification a base promoted elimination takes place to give the hydroxylated heteroarene. Additionally, Kendelyn found that this reactivity extends to electron-deficient benzenes to expand the scope of this protocol (Figure 3.20).[58]

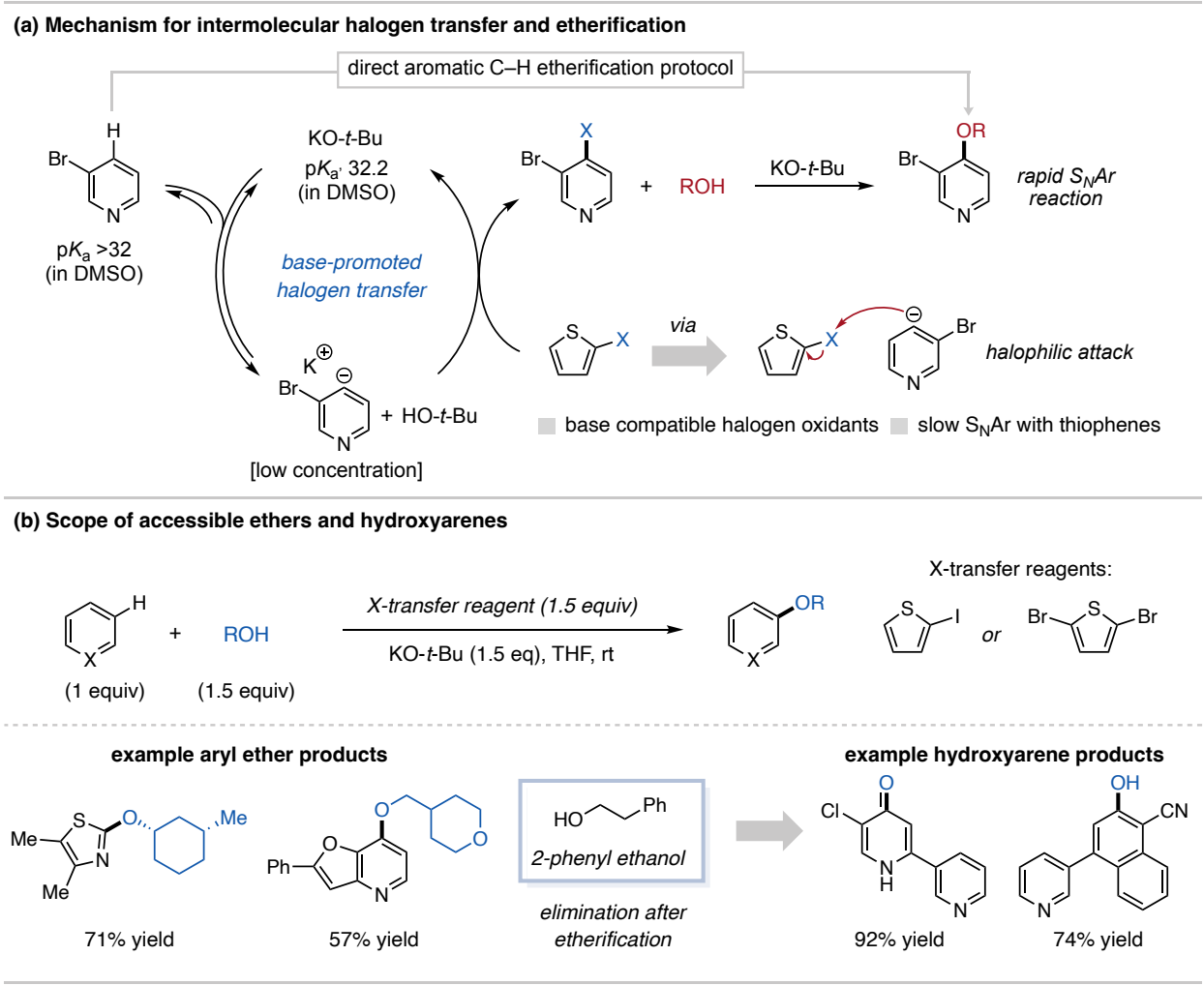

Figure 3.20: Development of intermolecular aromatic C–H functionaliztion *via* bas-promoted halogen transfer

With this process, we can effectively treat C–X bonds like C–H bonds and, under basic conditions, can maneuver them between molecules. Based on this, our group considered if other weakly acidic C–H bonds could be engaged in this transformation, like C(sp^3)–H systems. We recently disclosed the use of base-promoted halogen transfer to enable benzylic C(sp^3)–H etherification, a process that is notoriously challenging using traditional metalation/halogenation approaches due to unavoidable dimerization that occurs (Figure 3.21).[59,60] The key to success using

the halogen transfer approach is the synergistic relationship between the deprotonation, halogenation, and substitution step. In this mechanism, the benzyl anion is formed in transient amounts and is immediately trapped by the halogen oxidant, followed by substitution, obviating the buildup of benzyl halide and anion necessary for dimerization.

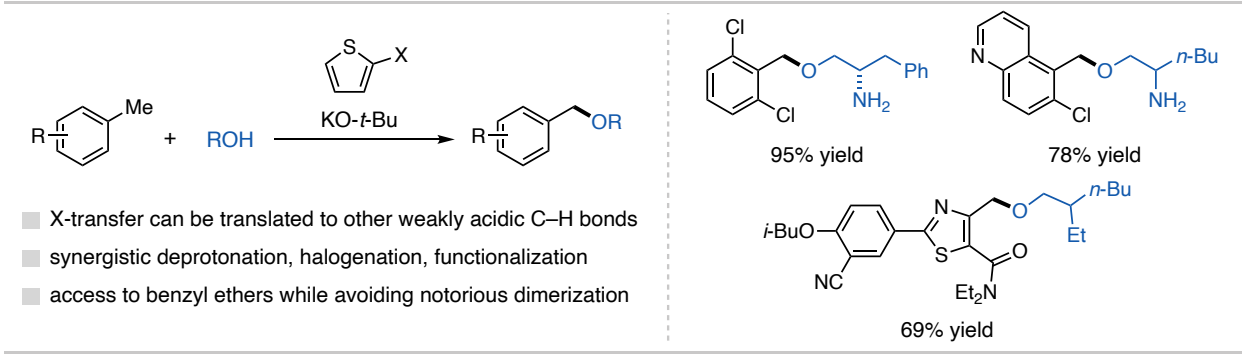

Figure 3.21: Base-promoted X-transfer enabled benzylic C–H etherification

3.7 Current State of Base-Promoted Halogen Transfer Methodology

The application of base-promoted halogen transfer is an ongoing area of research within our group. This section will give a brief overview of ongoing projects in this area (Figure 3.22), while Chapters Four and Five discuss my work in this field. For benzylic functionalization, I have developed a method for the coupling of alkyl (hetero)arenes with a variety of amine pronucleophiles. In a similar method, a graduate student in our group, Vivian Nguyen, has developed the ability to utilize silylamides as both the base and nucleophile to afford benzyl silylamine products. Through simple workup procedures, this method provides facile access to a variety of benzylic primary amines. With these benzylic functionalization protocols, we have observed many cases of site selectivity when multiple benzylic positions are available in one molecule. Two graduate students, Kayla Constantini and Alex Curtis, are working on understanding the origins of this selectivity and the potential for switchability through the collaboration of experimental and computational work.

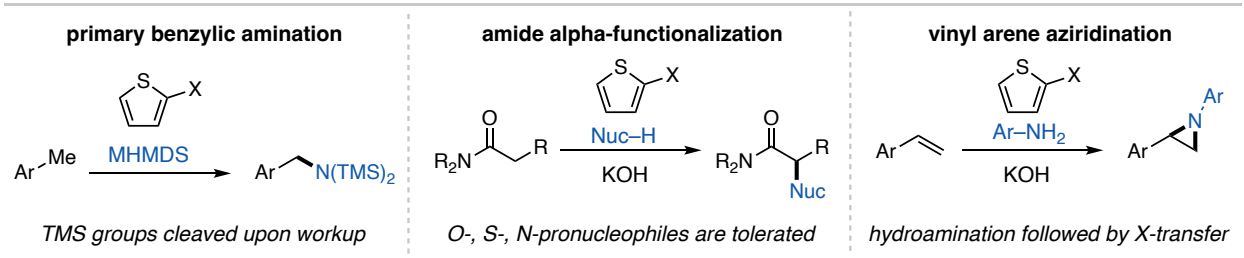

Figure 3.22: Current state of the halogen transfer research area in the Bandar Group

Branching away from aromatic compounds, another graduate student in the Bandar Group, Faith Kidd, is investigating the α-heteroatom functionalization of amides. In this protocol, halogen transfer takes place after enolate formation, followed by substitution with a variety of alcohol, thiol, and amine pronucleophiles. Cristian Vásquez Tapia Vera, a graduate student in our group, has been investigating alternate mechanisms for anion formation that could react under halogen transfer conditions. He found that primary anilines will undergo hydroamination with styrene derivatives, followed by base-promoted halogen transfer to the benzylic position, where an intramolecular cyclization reaction can occur for aziridine synthesis. This represents the current ongoing work in this area of research within our group.

3.8 Conclusion

This chapter provides background for the importance of benzylic C–H functionalization, specifically in the context of amination and desaturation protocols. These are two well-studied areas of research with current limitations that I am working to address using our group's base-promoted halogen transfer reaction platform. The development of this research area is described, showing the utility of halogen transfer, which has led to many ongoing projects within the group and continues to push the boundaries of possible C–H functionalization reactions.

REFERENCES

[1] Vine, L. E.; Schomaker, J. M. Amination, Back to Basics. *Nature Chem.* **2022**, *14*, 1093-1094.

[2] Amines: Synthesis, Properties, and Applications; Lawrence, S. A., Ed.; Cambridge University Press, Cambridge, U.K., 2004.

[3] Afanasyev, O. I.; Kuchuk, E.; Usanov, D. L.; Chusov, D. Reductive Amination in the Synthesis of Pharmaceuticals. *Chem. Rev.* **2019**, *119*, 11857−11911.

[4] Cernak, T.; Dykstra, K. D.; Tyagarajan, S.; Vachal, P.; Krska, S. W. The medicinal chemist's toolbox for late stage functionalization of drug-like molecules. *Chem. Soc. Rev.* **2016**, *45*, 546-576.

[5] Stepan, A. F.; Mascitti, V.; Beaumont, K.; Kalgutkar, A. S. Metabolism-guided drug design. *Med. Chem. Commun*. **2013**, *4*, 631-652.

[6] Acred, P.; Brown, D. M.; Turner, D. H.; Wilson, M. J. Pharmacology and Chemotherapy of Ampicillin – a New Broad-Spectrum Penicillin. *Brit.J.Pharmacol.* **1962**, *18*, 356-369.

[7] Richter, M. F.; Drown, B. S.; Riley, A. P.; Garcia, A.; Shirai, T.; Svec, R. L.; Hergenrother, P. J. Predictive compound accumulation rules yield a broad-spectrum antibiotic. *Nature* **2017**, *545*, 299-304.

[8] Clark, J. R.; Feng, K.; Sookezian, A.; White, M. C. Manganese-catalysed benzylic C(sp^3)–H amination for late-stage functionalization. *Nature Chem.* **2018**, *10*, 583-591.

[9] Treitler, D. S.; Leung, S. How Dangerous Is Too Dangerous? A Perspective on Azide Chemistry. *J. Org. Chem*. **2022**, *87*, 11293−11295.

[10] *Sodium Azide, ReagentPlus®, ≥99.5%*; CAS RN: 26628-22-8; S2002, Millipore Sigma: Miamisburg, OH: March 02, 2024. https://www.sigmaaldrich.com/US/en/sds/sial/s2002?userType=undefined (accessed 2024-05-22).

[11] Azides and Nitrenes: Reactivity and Utility; Scriven E. F., Ed.; Academic Press, Cambridge, MA, 2012.

[12] Tat, J.; Heskett, K.; Satomi, S.; Pilz, R. B.; Golomb, B. A.; Boss, G. R. Sodium azide poisoning: a narrative review. *Clin. Toxicol.* **2021**, *59*, 683-697.

[13] Javorskis, T.; Orentas, E. Chemoselective Deprotection of Sulfonamides Under Acidic Conditions: Scope, Sulfonyl Group Migration, and Synthetic Applications. *J. Org. Chem.* **2017**, *82*, 13423−13439.

[14] Sun, P.; Weinreb, S. M. *tert*-Butylsulfonyl (Bus), a New Protecting Group for Amines. *J. Org. Chem*. **1997**, *62*, 8604-8608.

[15] Collet, F.; Dodd, R. H.; Dauban, P. Catalytic C–H amination: recent progress and future directions. *Chem. Commun.* **2009**, 5061-5074.

[16] Ramirez, T. A.; Zhao, B. Shi, Y. Recent advances in transition metal-catalyzed sp^3 C–H amination adjacent to double bonds and carbonyl groups. *Chem. Soc. Rev.* **2012**, *41*, 931-942.

[17] Cho, S. H.; Kim, J. Y.; Kwak, J.; Chang, S. Recent advances in the transition metal-catalyzed twofold oxidative C–H bond activation strategy for C–C and C–N bond formation. *Chem. Soc. Rev.* **2011**, *40*, 5068-5083.

[18] Liang, C.; Robert-Peillard, F.; Fruit, C.; Müller, P.; Dodd, R. H.; Dauban, P. Efficient Diastereoselective Intermolecular Rhodium-Catalyzed C–H Amination. *Angew. Chem. Int. Ed*. **2006**, *45*, 4641–4644.

[19] Fruit, C.; Robert-Peillard, F.; Bernardinelli, G.; Müller, P.; Dodd, R. H.; Dauban P. Diastereoselective rhodium-catalyzed nitrene transfer starting from chiral sulfonimidamide-derived iminoiodanes. *Tetrahedron-Assymetr.* **2005**, *16*, 3484-3487.

[20] Prier, C. K.; Zhang, R. K.; Buller, A. R.; Brinkmann-Chen, S.; Arnold, F. H. Enantioselective, intermolecular benzylic C–H amination catalysed by an engineered iron-haem enzyme. *Nature Chem.* **2017**, *9*, 629-634.

[21] Urlacher, V. B.; Eiben, S. Cytochrome P450 monooxygenases: perspectives for synthetic application. *TRENDS Biotechnol.* **2006**, *24*, 324-330.

[22] Shen, T.; Lambert, T. H.; C−H Amination via Electrophotocatalytic Ritter-type Reaction. *J. Am. Chem. Soc*. **2021**, *143*, 8597-8602.

[23] Dai, L.; Chen, Y.-Y.; Xiao, L.-J.; Zhou, Q.-L. Intermolecular Enantioselective Benzylic C(sp^3)–H Amination by Cationic Copper Catalysis. *Angew. Chem. Int. Ed*. **2023**, *62*, e202304427.

[24] Morofuji, T.; Shimizu, A.; Yoshida, J.-i. Direct C–N Coupling of Imidazoles with Aromatic and Benzylic Compounds via Electrooxidative C–H Functionalization. *J. Am. Chem. Soc*. **2014**, *136*, 4496–4499.

[25] Hasyeoui, M.; Chapple, P. M.; Lassagne, F.; Roisnel, T.; Cordier, M.; Samarat, A.; Sarazin, Y.; Mongin, F. Lateral Deprotometallation-Trapping Reactions on Methylated Pyridines, Quinolines and Quinoxalines Using Lithium Diethylamide. *Eur. J. Org. Chem.* **2023**, *26*, e202300555.

[26] Shimojo, H.; Moriyama, K.; Togo, H. A One-Pot, Transition-Metal-Free Procedure for C–O, C–S, and C–N Bond Formation at the Benzylic Position of Methylarenes. *Synthesis*, **2015**, *47*, 1280-1290.

[27] Hofmann, A. W. Piperidine and pyridine. *Ber. Dtsch. Chem. Ges*. **1879**, *12*, 984−990.

[28] Löffler, K.; Freytag, C. New method for the formation of N-alkylated pyrrolidines. *Ber. Dtsch. Chem. Ges.* **1909**, *42*, 3427−3431.

[29] Wappes, E. A.; Fosu, S. C.; Chopko, T. C.; Nagib, D. A. Triiodide-Mediated δ-Amination of Secondary C–H Bonds. *Angew. Chem. Int. Ed*. **2016**, *55*, 9974 –9978.

[30] Martínez, C.; Muñiz, K. An Iodine-Catalyzed Hofmann–Löffler Reaction. *Angew. Chem. Int. Ed*. **2015**, *54*, 8287 –8291.

[31] Becker, P.; Duhamel, T.; Stein, C. J.; Reiher, M.; Muñiz, Cooperative Light-Activated Iodine and Photoredox Catalysis for the Amination of Csp^3–H Bonds. *Angew. Chem. Int. Ed*. **2017**, *56*, 8004 –8008.

[32] Maity, S.; Lopez, M. A.; Bates, D. M.; Lin, S.; Krska, S. W., Stahl, S. S. Polar Heterobenzylic C(sp^3)–H Chlorination Pathway Enabling Efficient Diversification of Aromatic Nitrogen Heterocycles. *J. Am. Chem. Soc*. **2023**, *145*, 19832–19839.

[33] Chen, S.-J.; Krska, S. W.; Stahl, S. S. Copper-Catalyzed Benzylic C–H Cross-Coupling Enabled by Redox Buffers: Expanding Synthetic Access to Three-Dimensional Chemical Space. *Acc. Chem. Res*. **2023**, *56*, 3604–3615.

[34] Das, M.; Zamani, L.; Bratcher, C.; Musacchio, P. Z. Azolation of Benzylic C–H Bonds via Photoredox-Catalyzed Carbocation Generation. *J. Am. Chem. Soc*. **2023**, *145*, 3861–3868.

[35] Roychowdhury, P.; Herrera, R. G.; Tan, H.; Powers, D. C. Traceless Benzylic C−H Amination via Bifunctional N-Aminopyridinium Intermediates. *Angew. Chem. Int. Ed.* **2022**, *61*, e202200665.

[36] Tan, H.; Samanta, S.; Maity, A.; Roychowdhury, P.; Powers, D. C. *N*-Aminopyridinium reagents as traceless activating groups in the synthesis of *N*-Aryl aziridines. *Nature Commun.* **2022**, *13*, 3341.

[37] Verma, A.; Patel, S.; Meenakshi, Kumar, A.; Yadav, A.; Kumar, S.; Jana, S.; Sharma, S.; Prasad, C. D.; Kumar, S. Transition metal free intramolecular selective oxidative C(sp^3)–N coupling: synthesis of *N*-aryl-isoindolinones from 2-alkylbenzamides. *Chem. Commun.* **2015**, *51*, 1371-1374.

[38] Beller, M.; Seayad, J.; Tillack, A.; Jiao, H. Catalytic Markovnikov and anti-Markovnikov Functionalization of Alkenes and Alkynes: Recent Developments and Trends. *Angew. Chem. Int. Ed.* **2004**, *43*, 3368-3398.

[39] (a) Yin, X.; Li, S.; Guo, K.; Wang, X. Palladium-Catalyzed Enantioselective Hydrofunctionalization of Alkenes: Recent Advances. *Eur. J. Org. Chem.* **2023**, *26*, e202300783. (b) Zhu, Y.; Liao, Y.; Jin, S.; Ding, L.; Zhong, G.; Zhang, J. Functionality-Directed Regio- and Enantio-Selective Olefinic C–H Functionalization of Aryl Alkenes. *Chem. Rec.* **2023**, *23*, e202300012.

[40] Wittig, G.; Schookopf, U. Triphenylphosphinemethylene as an olefin-forming reagent. *Chem. Ber.* **1954**, *97*, 1318-1330.

[41] Luo, C.; Bandar, J. S. Superbase-Catalyzed anti-Markovnikov Alcohol Addition Reactions to Aryl Alkenes. *J. Am. Chem. Soc*. **2018**, *140*, 3547−3550.

[42] Müller, T. E.; Hultzsch, K. C; Yus, M.; Foubelo, F.; Tada, M. Hydroamination: Direct Addition of Amines to Alkenes and Alkynes. *Chem. Rev.* **2008**, *108*, 3795–3892.

[43] Heck, R. F.; The Mechanism of Arylation and Carbomethoxylation of Olefins with Organopalladium Compounds. *J. Am. Chem. Soc.* **1969**, *91*, 6707-6714.

[44] Zhang, G.; Lin, Y.; Luo, X.; Hu, X.; Chen, C.; Lei, A.; Oxidative [4+2] annulation of styrenes with alkynes under external-oxidant-free conditions. *Nature Commun.* **2018**, *9*, 1225.

[45] Lee, E. H. Iron Oxide Catalysts for Dehydrogenation of Ethylbenzene in the Presence of Steam. *Catal. Rev.: Sci. Eng*. **1974**, *8*, 285−305.

[46] Zhang, P.; Huang, D.; Newhouse, T. R. Aryl-Nickel-Catalyzed Benzylic Dehydrogenation of Electron-Deficient Heteroarenes. *J. Am. Chem. Soc*. **2020**, *142*, 1757−1762.

[47] Huang, D.; Newhouse, T. R. Dehydrogenative Pd and Ni Catalysis for Total Synthesis. *Acc. Chem. Res*. **2021**, *54*, 1118−1130.

[48] Ito, T.; Seidel, F. W.; Jin, X.; Nozaki, K. TEMPO as a Hydrogen Atom Transfer Catalyst for Aerobic Dehydrogenation of Activated Alkanes to Alkenes. *J. Org. Chem*. **2022**, *87*, 12733−12740.

[49] Zhou, M.-J.; Zhang, L.; Liu, G.; Xu, C.; Huang, Z. Site-Selective Acceptorless Dehydrogenation of Aliphatics Enabled by Organophotoredox/Cobalt Dual Catalysis. *J. Am. Chem. Soc.* **2021**, *143*, 16470−16485.

[50] Iosub, A. V.; Stahl, S. S. Palladium-Catalyzed Aerobic Dehydrogenation of Cyclic Hydrocarbons for the Synthesis of Substituted Aromatics and Other Unsaturated Products. *ACS Catal.* **2016**, *6*, 8201−8213.

[51] Dighe, S. U.; Julia, F.; Luridiana, A.; Douglas, J. J.; Leonori, D. A photochemical dehydrogenative strategy for aniline synthesis. *Nature* **2020**, *584*, 75-81.

[52] Corpas, J.; Caldora, H. P.; Di Tommaso, E. M.; Hernandez-Perez, A. C.; Turner, O.; Azofra, L. M.; Ruffoni, A.; Leonori, D. A general strategy for the amination of electron-rich and electron-poor heteroaromatics by desaturative catalysis. *Nat. Catal.* **2024**, *24*.

[53] Vaitiekunas, A.; Nord, F. F. Tetrabromothiophene from 2-Bromothiophene by means of Sodium Acetylide in Liquid Ammonia. *Nature*, **1951**, *168*, 875–876.

[54] Vaitiekunas, A.; Nord, F. F. Studies on the Chemistry of Heterocyclics. XXII. Investigations on the Mechanism of Reactions of 2-Thienyl Halides with Sodium Amide and Sodium Acetylide in Liquid Ammonia. *J. Am. Chem. Soc.*, **1953**, *75*, 1764–1768.

[55] Bunnett, J. F. Base-catalyzed halogen dance, and other reactions of aryl halides. *Acc. Chem. Res.* **1972**, *5*, 139–147.

[56] Puleo, T. R.; Bandar, J. S. Base-catalyzed aryl halide isomerization enables the 4-selective substitution of 3-bromopyridines. *Chem. Sci.* **2020**, *11*, 10517-10522.

[57] Puleo, T. R.; Klaus, D. R.; Bandar, J. S. Nucleophilic C–H Etherification of Heteroarenes Enabled by Base-Catalyzed Halogen Transfer. *J. Am. Chem. Soc.* **2021**, *143*, 12480–12486.

[58] Bone, K. I.; Puleo, T. R.; Bandar, J. S. Direct C–H Hydroxylation of N-Heteroarenes and Benzenes via Base-Catalyzed Halogen Transfer. *J. Am. Chem. Soc.* **2024**, *146*, 9755–9767.

[59] Bone, K. I.; Puleo, T. R.; Delost, M. D.; Shimizu, Y.; Bandar, J. S. Direct Benzylic C–H Etherification Enabled by Base-Promoted Halogen Transfer. *ChemRxiv preprint, DOI: 10.26434/chemrxiv-2024-fvrc1.*

[60] Blangetti, M.; Fleming, P.; O'Shea, D. F. Homo- and Hetero-oxidative Coupling of Benzyl Anions. *J. Org. Chem*. **2012**, *77*, 2870–2877.

CHAPTER FOUR

DIRECT BENZYLIC C–H AMINATION OF ALKYL ARENES ENABLED BY BASE-PROMOTED HALOGEN TRANSFER

4.1 Chapter Overview

A major research area in the Bandar Group involves exploiting base-promoted halogen transfer (X-transfer) in order to activate weakly-acidic C–H bonds. Chapter Three details our group's development of this area as well as the transformations we have published, and ongoing projects. I began working in this research area in 2023 and at this time the group had published two methods for aromatic functionalization, with a third in development published in 2024.[1-3] Also at this time, group members were developing benzylic C–H etherification methodology to expand reactivity from C(sp^2)–H bonds to C(sp^3)–H bonds.[4] This chapter discusses my efforts to expand the scope and capabilities of benzylic C–H functionalization through the development of a benzylic C–H amination protocol that functions on a broad range of alkyl arene and amine coupling partners.

4.2 Reaction Discovery and Optimization

4.2.1 Motivation and General Overview

I began working in the area of X-transfer in our group on benzylic functionalization and I identified two major limitations that needed to be addressed. The first of these limitations was that amines were not compatible pronucleophiles under established X-transfer conditions whereas alcohols and thiols are well tolerated (Figure 4.1a). As stated in Chapter Three, benzylic amines are highly valuable substructures, but currently there is no general way to access them with a

simple protocol. I believed that a base-promoted approach using X-transfer could be the ideal solution to finding a general benzylic amination approach and, as such, I was motivated to investigate why amines were limited to overcome this challenge.

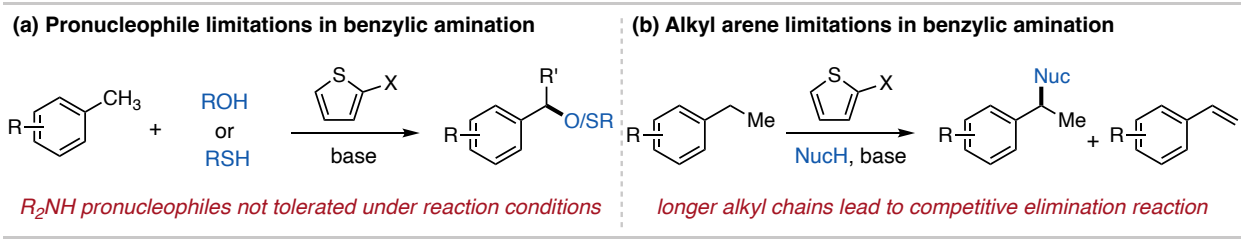

Figure 4.1: Current limitations with benzylic C–H functionalization methodology

The second limitation I identified was that our current benzylic functionalization methodology was limited to methylarenes with no examples of longer-chain alkyl arenes (Figure 4.1b). The main reason behind this limitation is competitive elimination upon benzylic halogenation under strong basic conditions.[5-7] Additionally, there is an added steric factor and decreased acidity at the benzylic position with these reagents which could make them more challenging to access. It would greatly improve the utility of our group's benzylic C–H functionalization methodology to be able to incorporate longer-chain alkyl arenes by expanding the scope of accessible substrates. This would also improve the applicability of this method towards late-stage modification of pharmaceutical compounds as more benzylic positions on molecules would be available. Due to the potential power of utilizing any alkyl arene substrate, I was motivated to overcome this limitation to expand the scope of benzylic C–H functionalization *via* X-transfer.

Figure 4.2 shows the proposed mechanism for the benzylic amination of alkyl arenes by base-promoted halogen transfer, based off of the accepted mechanism proposed by our group for etherification reactions.[3,4] Here, the benzylic position of the alkyl arene is deprotonated by either an alkoxide or silylamide base followed by X-transfer with a sacrificial halogen oxidant. The

resultant benzyl halide is substituted by an amine *in situ* for net C–H amination. Key to this reaction is the synergistic relationship between the deprotonation, halogenation, and substitution steps. In this regard, I found that the compatibility of the substrate, base, and X-transfer reagent is critical, and that careful selection of each component and their combination leads to the overall success of this transformation. Although I investigated benzylic C–H amination of methyl and alkyl arenes concurrently and insights from each helped the development of the other, they will be discussed separately in this Section.

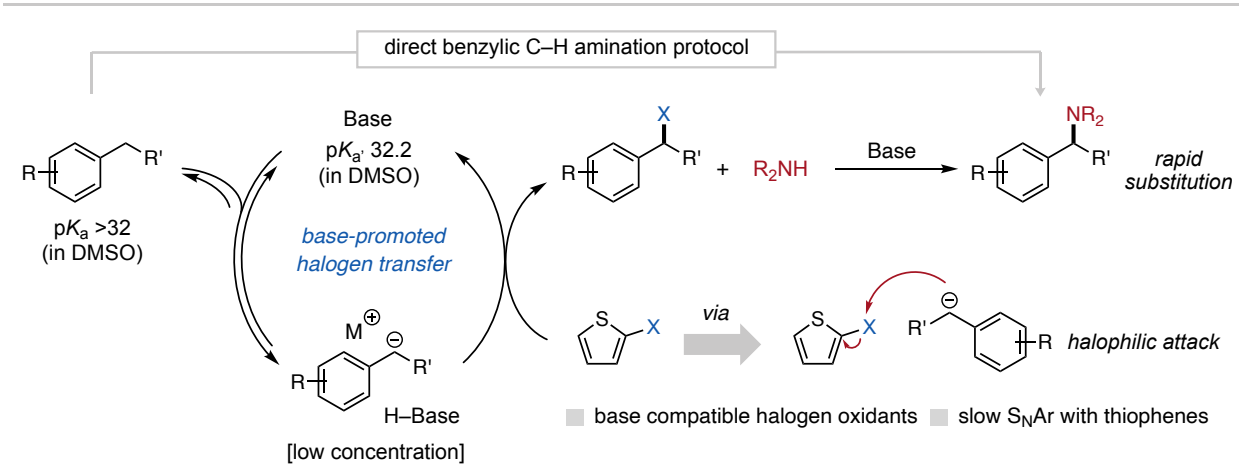

Figure 4.2: Proposed mechanism for benzylic C–H amination *via* base-promoted X-transfer

4.2.2 Development of Benzylic C–H Amination with Alkyl Arenes

I am beginning the discussion of reaction development with longer-chain alkyl arenes as much of the key insights and advances were made while investigating these substrates. I began this investigation using 2-ethylpyridine (**1**) as a model alkyl arene and *N*-methylaniline (**2**) as a model amine (Figure 4.3a). I began this investigation with aniline pronucleophiles as they have similar acidity to alcohols (pK_a = 27 – 33, measured in DMSO), which have been shown to be effective pronucleophiles for our reported etherification reactions.[8,9] For the X-transfer reagent, I began with 2-bromothiophene (**3**) as it is commercially available and has been shown to be effective as an oxidant in previous reports.[2-4] Thus, the first iteration of this reaction run using the

mentioned reagents in THF as a solvent at 60 °C for 18 h. Using 1 equivalent of **3** and 1.5 equivalents of KO-*t*-Bu as the base, I observed 7% of benzyl amine **4** along with a variety of additional products, including 2% of vinyl arene **5**, 21% homobenzylic amine **6**, and 21% enamine **7**, with 49% leftover **1** to account for all of the mass balance.

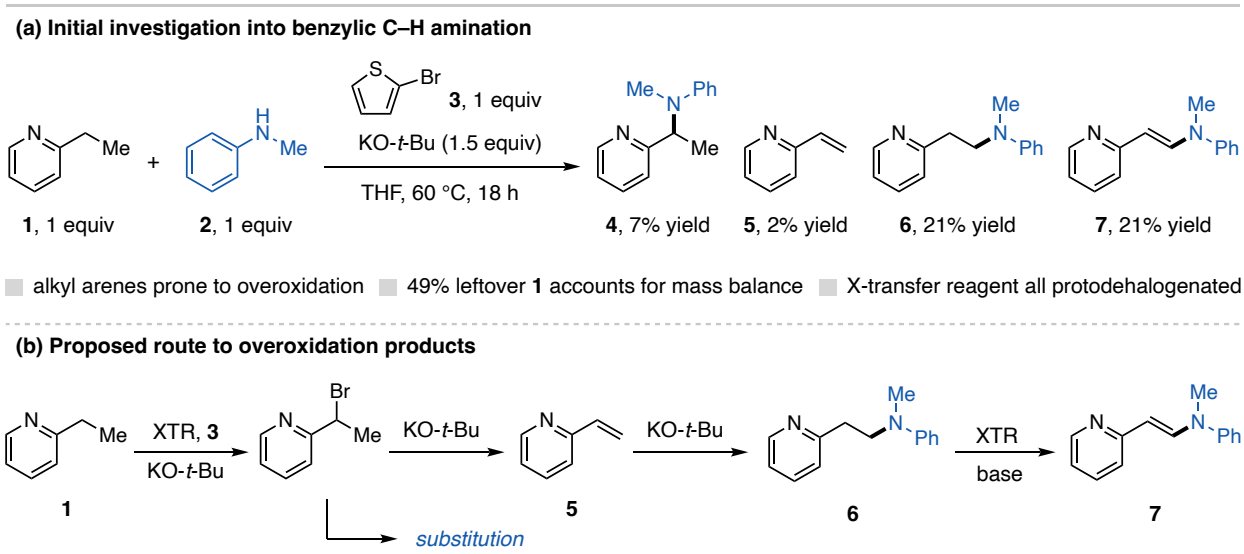

Figure 4.3: Initial investigation into benzylic amination and observation of overoxidation

Side products **5**-**7** form *via* the competitive elimination pathway from the benzylic halide intermediate. Figure 4.3b shows the proposed mechanism for the formation of each of these side products. Upon deprotonation and halogenation of the benzylic position of **1**, base-promoted elimination can occur, leading to the formation observation of vinyl arene **5**, albeit in very low yield. Vinyl arenes are often engaged in the synthesis of more complex molecules, and as such they are reactive species under our reaction conditions.[10-12] A common approach to functionalizing alkenes is through hydroamination with an amine pronucleophile, and with **2** present in solution base-promoted hydroamination of **5** leads to the formation of homobenzylic amine **6**. Finally, **6** can undergo subsequent benzylic halogenation, followed by base-promoted elimination to form enamine **7**. The formation of these side products provides insight into the challenge of engaging longer-chain alkyl arenes in benzylic C–H functionalization protocols, however, I viewed this not

as a limitation but as an opportunity. I reasoned that by intentionally targeting the elimination process that this reaction could be exploited for the desaturation of alkyl arenes. Chapter Five will discuss my efforts in establishing the area of desaturation coupled and cascade alkene functionalization within the Bandar Group.

I took two key insights from this first experiment, the fact that about 49% of **1** remains after the completion of the reaction and that all of X-transfer reagent **3** has been converted to the dehalogenated thiophene. This product is the result of productive X-transfer, however, it can also form *via* protodehalogenation under reaction conditions, resulting in complete consumption of the X-transfer reagent before **1** is fully reacted.[13,14] Additionally, in previous reports we have observed the disproportionation of thiophene X-transfer reagents *via* the halogen dance mechanism described in Chapter Three. This led us to investigate more base-stable X-transfer reagents that will last longer under reaction conditions so that productive reactivity can occur.

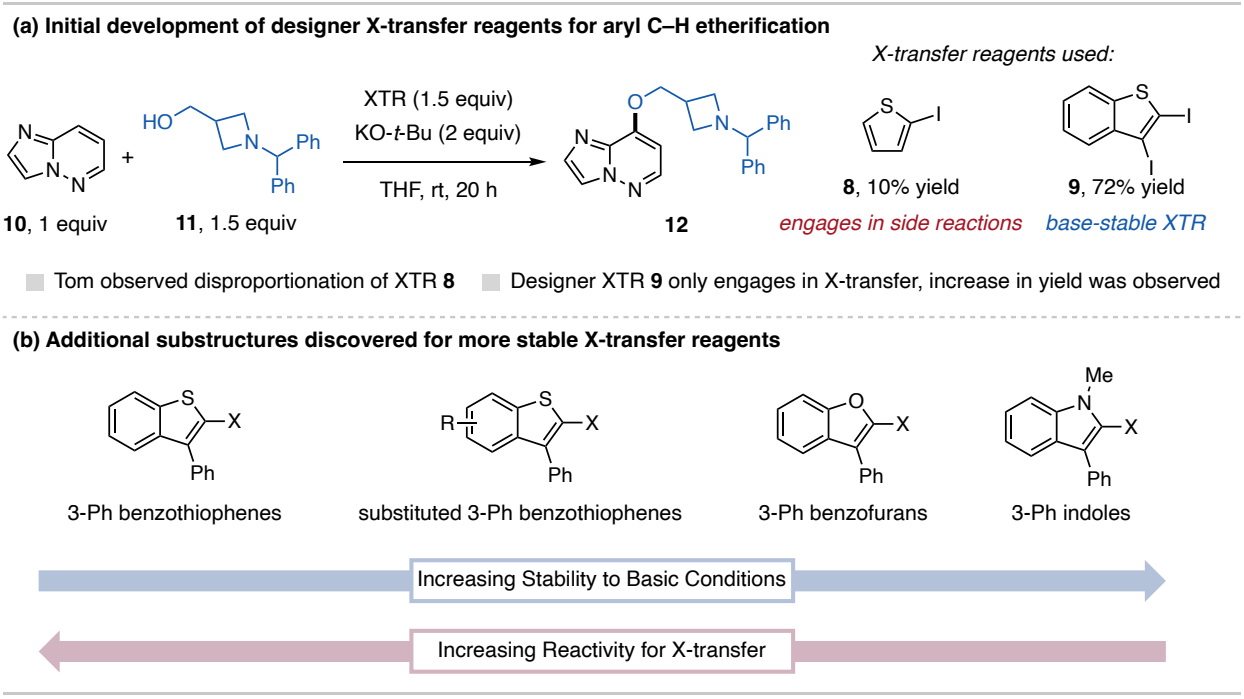

Figure 4.4: Development of designer X-transfer reagents with increased base stability

This area in our group was stated by Tom, who investigated 3-substituted benzothiophene **9** where all acidic C–H bonds have been blocked by substituents, thus preventing unproductive side pathways with the X-transfer reagents.[2] He showcased the improvements associated with this new X-transfer reagent in the reaction between **10** and **11**, comparing the efficacy of **9** and commercial 2-iodothiophene (**8**). Here, Tom found an increase in yield from 10% to 72% of **12** when 8 is used as the X-transfer reagent over **9** (Figure 4.4a). Beyond the use of **8**, our group has developed many other designer X-transfer reagents that provide additional base and reagent compatibility to enable our ongoing research in this area. Figure 4.4b highlights the four main structural scaffolds for our designer X-transfer reagents, including 3-phenylbenzothiophenes, functionalized 3-phenylbenzothiophenes, 3-phenylbenzofurans, and 1-methyl-3-indoles primarily engineered by a former postdoc in our lab, Dr. Mike Delost. These designer X-transfer reagents play a key role in the development of the alkyl arene C–H amination.

Based off of the insights gained from the initial investigation into the synthesis of **4**, I next utilized more base-stable benzothiophene X-transfer reagent **13**. I utilized 2 equivalents of **13** here to ensure enough was present for productive reaction of the starting materials. Unfortunately, the results of this reaction showed 0% yield of **4**, with increased 48% yield of vinyl arene **5**, 5% of **6**, and 10% of **7**, with 33% leftover **1** (Figure 4.5a). Although the X-transfer reagent was indeed more stable with 0.6 equivalents left after the reaction, it is more suited for desaturation pathways over substitution.

I next moved back to utilizing 2-bromothiophene (**3**) as the X-transfer reagent as it promotes less desaturation and investigated a more nucleophilic aniline (**14**) in order to more favor substitution over elimination. I increased to 2.5 equivalents of both the X-transfer reagent and base to hopefully provide enough excess to fully convert the starting material (**1**). Under otherwise

unchanged reaction conditions, I observed 4% of the benzyl amine product **15**, 3% elimination (**5**), 12% homobenzylic amine **16**, and 43% enamine **17**, with 33% unreacted **1** (Figure 4.5b). Unfortunately, hydroamination and enamine formation are also positively correlated with an increase in nucleophilicity of the aniline, so simply changing the identity of the aniline would not lead to high yield of the benzyl amine. Additional empirical optimization such as temperature, solvent choice, and reaction stoichiometry variation was performed which did not improve the yield of amine **17**.

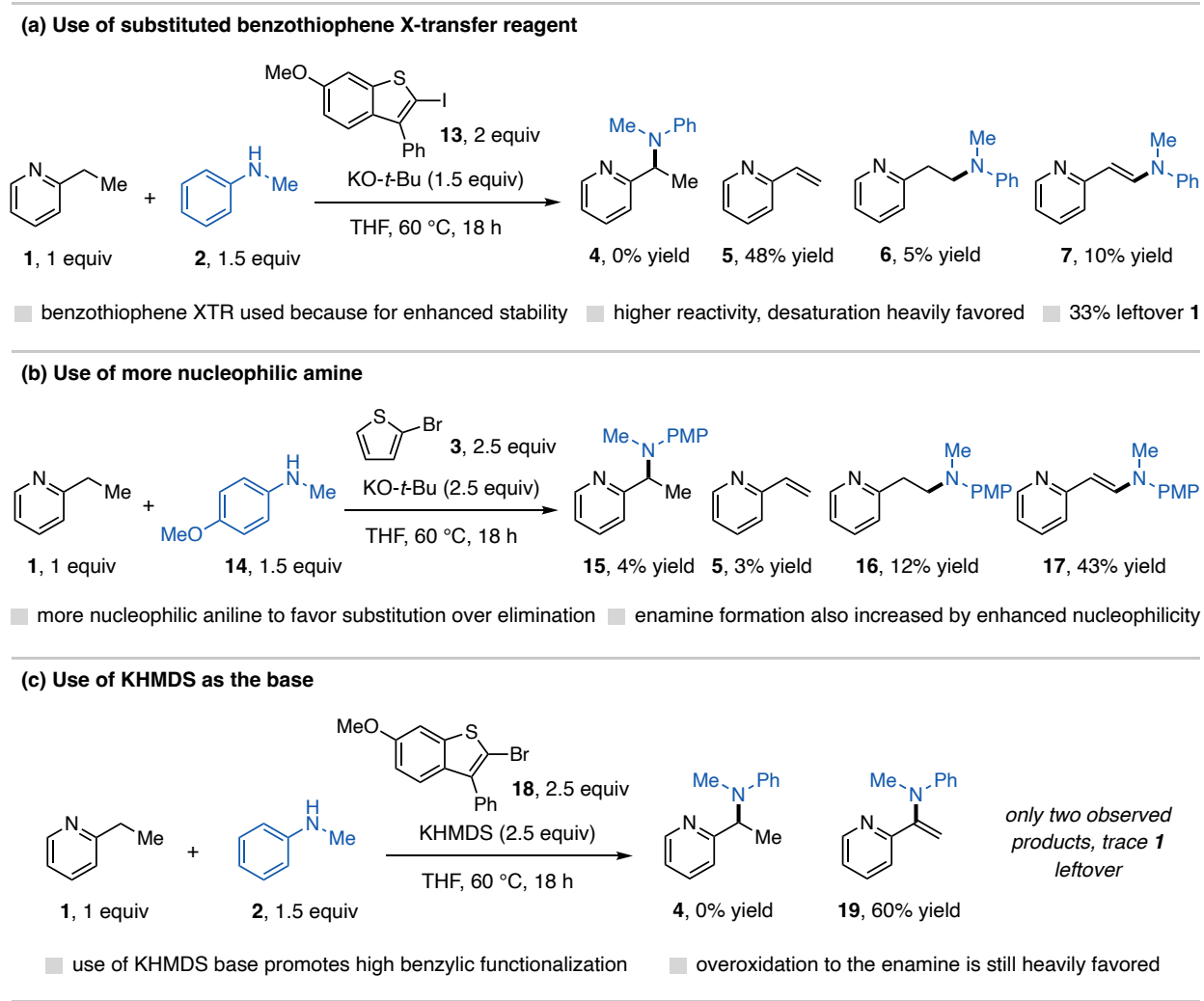

Figure 4.5: Reaction Optimization for exclusive α-functionalization

It became clear that these reaction conditions were heavily favoring desaturation products and that more significant changes would need to be made to promote benzylic amination. Chapter Five discusses further development of these conditions with the goal of high yielding desaturation and enamine formation. Up until this point, the base used in the reaction has been held constant using KO-*t*-Bu. I considered alternate bases to use in this reaction and decided on KHMDS. Although KHMDS is less basic than KO-*t*-Bu, there are many beneficial features that enhance its reactivity and utility.[15,16] The steric bulk of the KHMDS makes it relatively non-nucleophilic and the silyl groups aid in its solubility in more nonpolar media where the base primarily exists as a relatively reactive dimer.[17-20] Overall, this makes KHMDS an interesting and effective alternative to other strong metal-coordinated bases. Again using 2-ethylpyridine (**1**) and *N*-methylaniline (**2**) as model substrates, I employed 2.5 equivalents of X-transfer reagent **18** and KHMDS in THF at 60 °C for 18 h (Figure 4.5c). Here, I observed exclusive formation of α-enamine **19** in 60% yield with no other products and trace amount of leftover **1**. Product **19** is likely the result of benzylic amination followed by subsequent X-transfer and elimination. This was a key result in that even though the use of KHMDS did not result in the formation of benzylamine **4**, the observation of **19** shows that substitution is favored over elimination after the initial X-transfer, and that overoxidation likely results from too active of reaction conditions. From here, my goal was to optimize this reaction to stop after formation of benzylamine **4** and in Chapter Five I discuss the optimization of this reaction for α-enamine **19** formation.

The first approach I took to optimizing this reaction with KHMDS as the base was to target the X-transfer reagent to try and mitigate overoxidation. When Mike was investigating alternate X-transfer reagent structures, he found that more base-stable reagents were inherently less reactive towards transferring their halogen. One such example is X-transfer reagent **20**, which Mike found

remains unaffected when stirred with base in ethereal solvents. With its stability, **20** can be used at higher temperatures and as such the amination of 2-ethylpyridine (**1**) with 4-methoxy-N-methylaniline (**14**) was run at 85 °C using DME as a solvent. With 2.5 equivalents of the X-transfer reagent and KHMDS base, I observed 34% yield of benzylamine **15** and 31% of enamine **21** as the only products (Figure 4.6a). Under the same reaction conditions, three additional substrates were investigated including 2-propylpyridine (**22**) to investigate longer alkyl chains, 1-ethylnaphthalene (**23**) to investigate less activated arenes, and ethylbenzene (**24**) to investigate completely unactivated systems. These substrates resulted in 56%, 41%, and 5% yields, respectively, with no formation of desaturated products (Figure 4.6a).

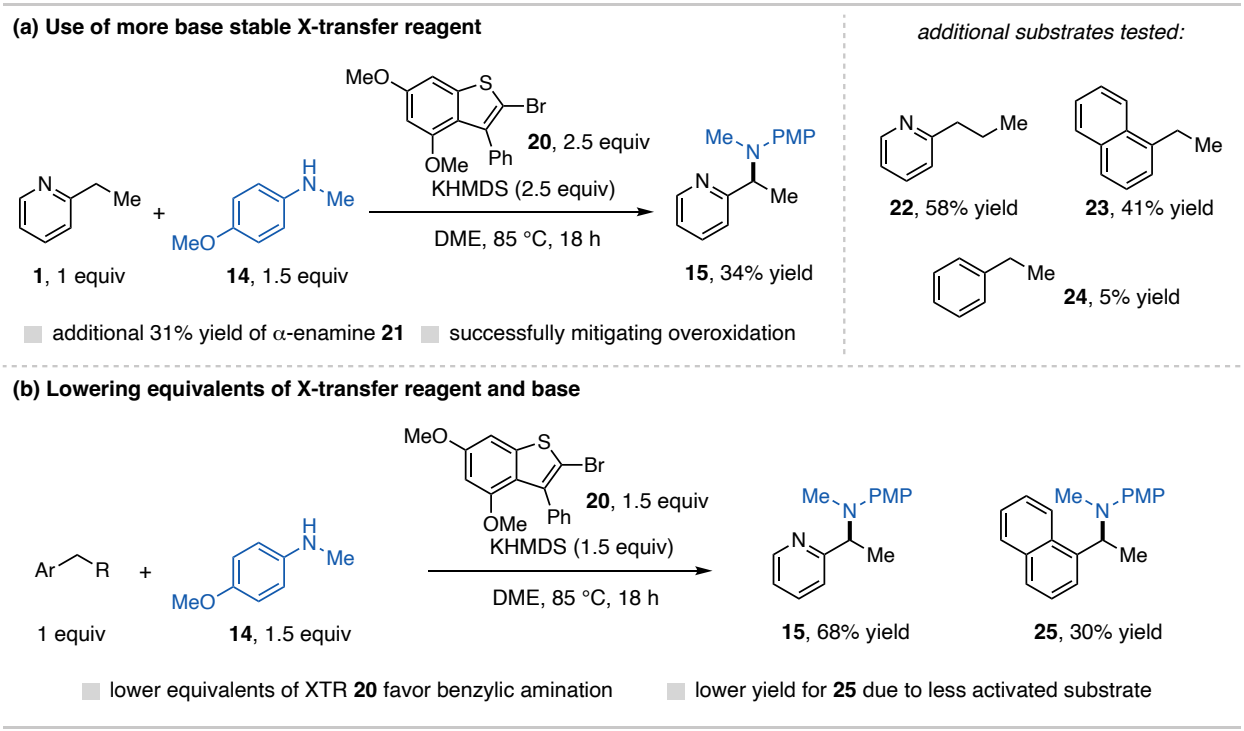

Figure 4.6: Further optimization and initial scope investigation for benzylic amination

These results were encouraging as this was the first time I had observed significant formation of the benzylic aminated product. With 2-ethylpyridine (**1**) still prone to overoxidation under these conditions, my next attempt at reaction optimization was to decrease the equivalents of X-transfer reagent and base used in order to suppress the second X-transfer process that takes

place for enamine formation. I lowered the amount of X-transfer reagent and base from 2.5 to 1.5 equivalents and investigated the effect of this on both 2-ethylpyridine (**1**) and 2-ethylnaphthalene (**23**). For the reaction with 2-ethylpyridine (**1**), I observed 68% yield of **15** with 6% α-enamine **19**, indicating effective suppression of overoxidation with lower loading of X-transfer reagent **20**. For the reaction with and 1-ethylnaphthalene (**23**), I observed 30% yield of **25**. This slight decrease in yield is likely due to 1-ethylnaphthalene (**23**) being a less activated and therefore less reactive substrate than 2-ethylpyridine (**1**) that benefits from more forcing conditions.

My next goal was to further optimize these two reactions separately as it became clear that activated substrates like alkyl heteroarenes and unactivated substrates like ethylbenzene derivatives would require separate conditions for high yield. Beginning with alkyl heteroarenes, I found that the reaction could be run at 40 °C, which also helps suppress the formation of desaturation side products. Figure 4.7 shows a small scope of products accessible using this method with incorporation of extended alkyl chains (**26**), fused cyclic systems (**27** and **28**), and alternate heterocycles (**29** and **30**) to show the initial generality of this protocol.

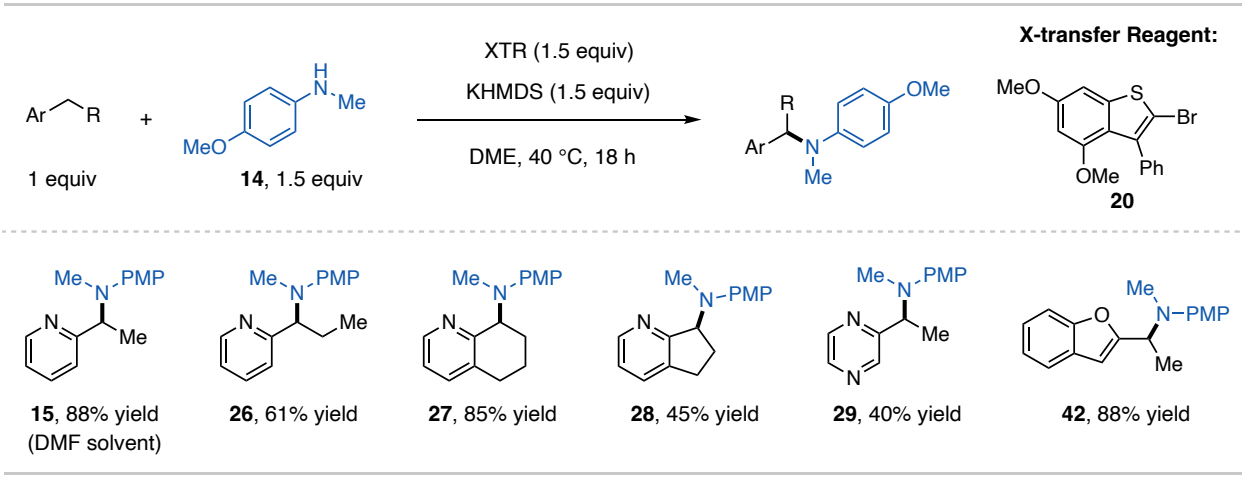

Figure 4.7: Initial substrate scope of activated alkyl arenes. Yields determined by ^{1}H NMR spectroscopy.

I next moved on to the optimization of less activated alkylbenzene derivatives. Here I used 1-ethylnaphthalene (**23**) as a model substrate with 2-methoxy-N-methylaniline (**31**), which

provided more consistent results. With the ability to apply stronger conditions to these substrates, I investigated the use of more polar solvents and 18-crown-6 ether additives to generate a more active base in solution. Use of DMF as the solvent with 18-crown-6, this reaction can be run at room temperature, which improves the practicality of this reaction. Using X-transfer reagent **20**, I observed 68% yield of benzylamine **32** (Figure 4.8a). Attempts to improve the yield of this reaction using empirical optimization of reaction conditions was unsuccessful, prompting me to investigate what was limiting the yield.

When I was isolating **25** by preparatory thin-layer chromatography (prep TLC) to confirm the identity of the product by ^{1}H NMR spectroscopy, I also independently isolated an amine side product from the reaction. This amine side product featured all of the amine peaks by ^{1}H NMR, only shifted downfield and is present in the crude ^{1}H NMR spectrum. With no other peaks present, the identity of this product is likely either the *N*-halo amine or the amine dimer, which results from the amine reacting with the *N*-halo amine. It is known that *N*-methylanilines can undergo dimerization with an electrophilic halogen source, making this a plausible pathway under base-promoted X-transfer conditions.[21] This pathway is problematic as it unproductively consumes both the amine and X-transfer reagent, thus hindering productive amination (Figure 4.8b).

Considering how to overcome this limitation, I reasoned that X-transfer reagent **20** is too active, leading to reaction between it and aniline **31**. This required me to identify less reactive X-transfer reagents to stifle unproductive side reactions. When Mike was synthesizing new structures for X-transfer reagents, he found that alternate heteroatoms led to more stable and less reactive reagents, like benzofurans and indoles. Figure 4.8c shows the conditions for this reaction, which was run at 40 °C due to account for the lower reactivity of X-transfer reagents **32** and **34**. Both X-transfer reagents were successful in suppressing side reactivity with aniline **31**, however, the **34**

led to significantly higher yield. With this side pathway successfully avoided, I could now optimize this reaction using X-transfer reagent **34** to obtain a higher yield of **32**. Figure 4.8d shows the results of this optimization where this reaction can be run at room temperature with DME as the solvent, resulting in 90% yield of benzylamine **32**.

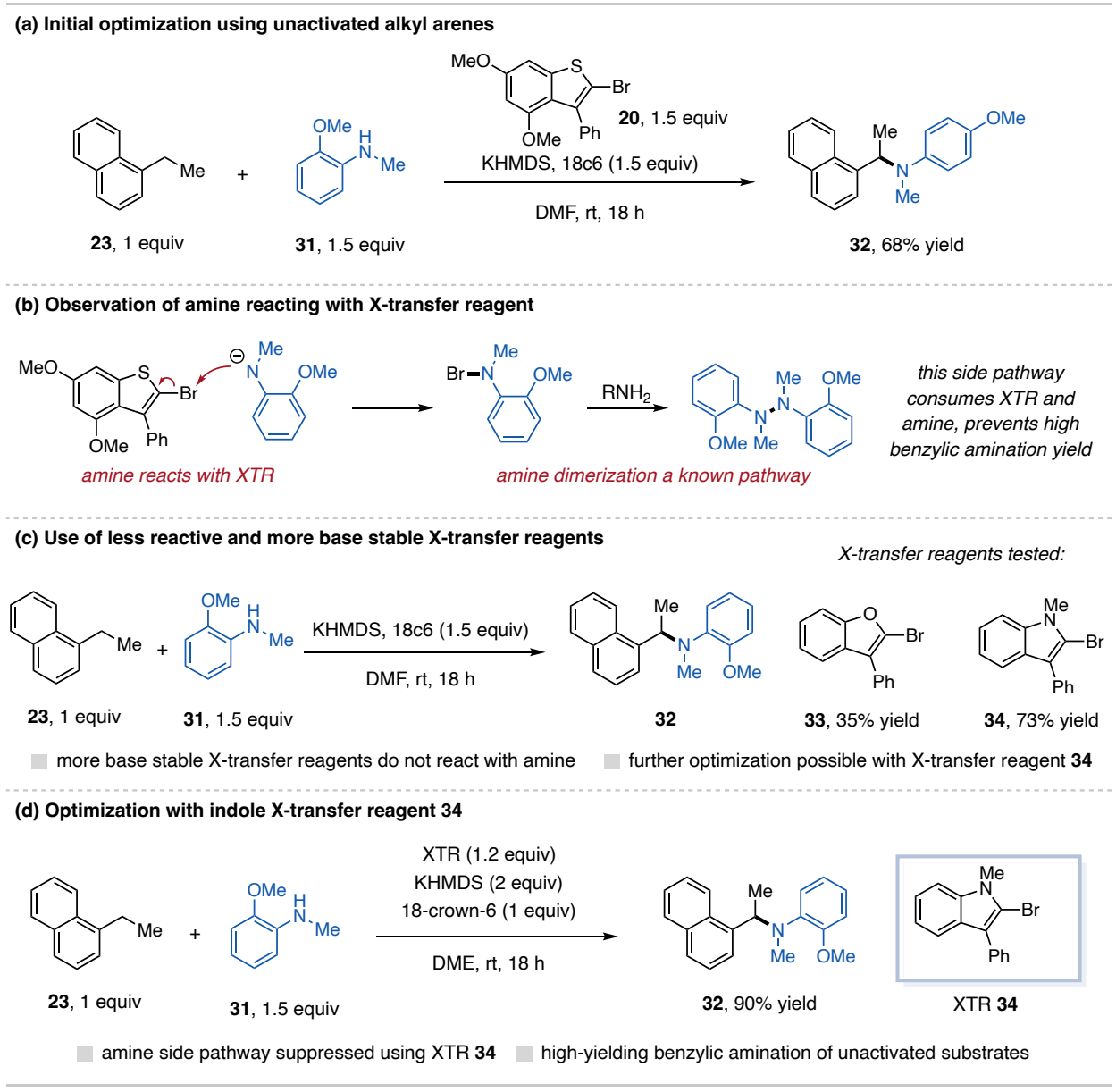

Figure 4.8: Optimization of benzylic C–H amination conditions for unactivated alkyl arenes

With the success of utilizing X-transfer reagent **34** for unactivated alkyl arenes, I next wanted to investigate its efficacy using more activated alkyl heteroarenes. Using conditions from

Figure 4.8d, I tested three substrates (**35-37**) and found that use of **34** led to decreased yields using *N*-heterocyclic substrates (Figure 4.9a). I did not observe the formation of any amine side products, indicating this decrease in yield was not due to this unproductive pathway. Instead, the yield decreases were likely due to substrate instability over time under basic reaction conditions, as very low mass balance was observed in each case. In order to overcome this, I reasoned that for more activated substrates, use of a more reactive X-transfer reagent would increase the rate of the amination, leading to product formation before decomposition. This was indeed the case and when I utilized X-transfer reagent **38** I observed 90% yield of **36** and 85% yield of **37** (Figure 4.9b). With ethyl substituted heteroarenes such as **1**, overoxidation becomes competitive again with a more active X-transfer reagent (65% yield of **35** and 21% enamine). This challenge, however, can be mitigated by use of less active thiophene X-transfer reagents like **20**, as shown previously.

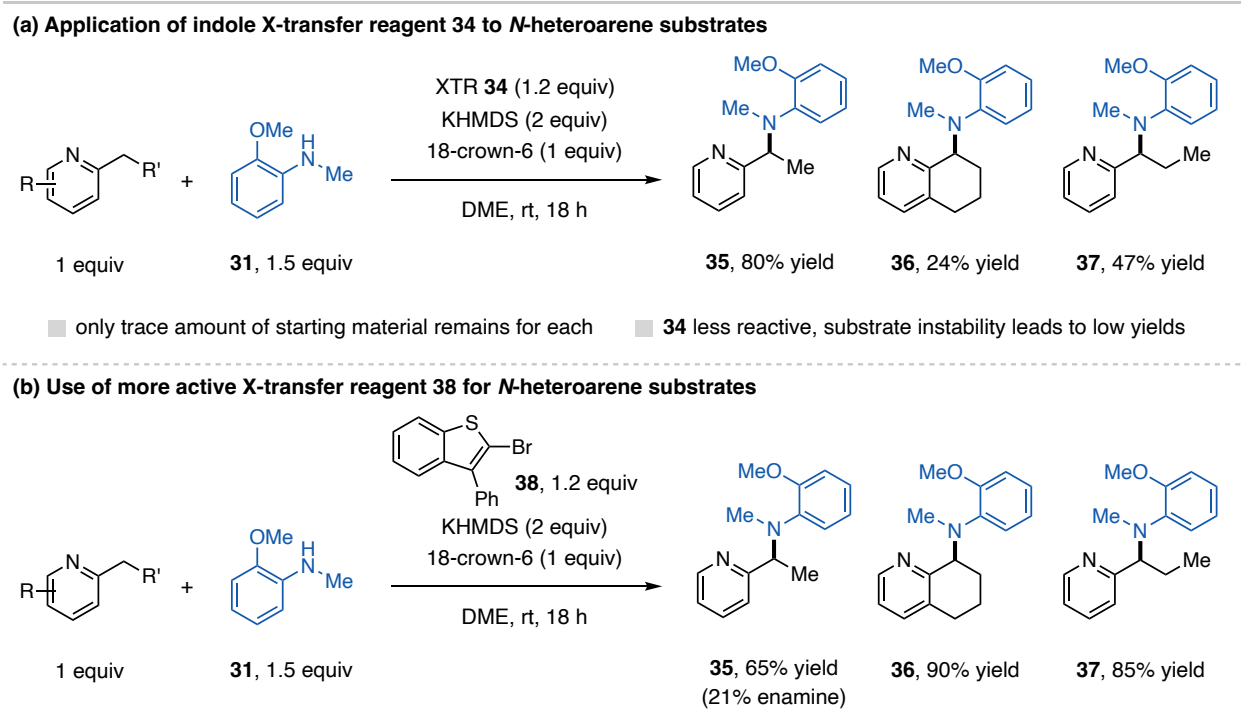

Figure 4.9: Improved reaction conditions for *N*-heteroarene substrates

4.2.3 Development of Benzylic C–H Amination with Methyl Arenes

As previously mentioned, the optimization of methyl arenes and longer-chain alkyl arenes took place concurrently. In this Section, I will discuss the optimization of reaction conditions to incorporate methyl arenes in this reaction with much of the focus on two substrates. However, I found that in general, slight variations to the reaction conditions are necessary to obtain good yields for different substrates, making it difficult to obtain a general set of conditions for multiple substrates. Despite this, I was able to find a variety methyl arene substrates for benzylic amination, most of which will be discussed in Section 4.3.

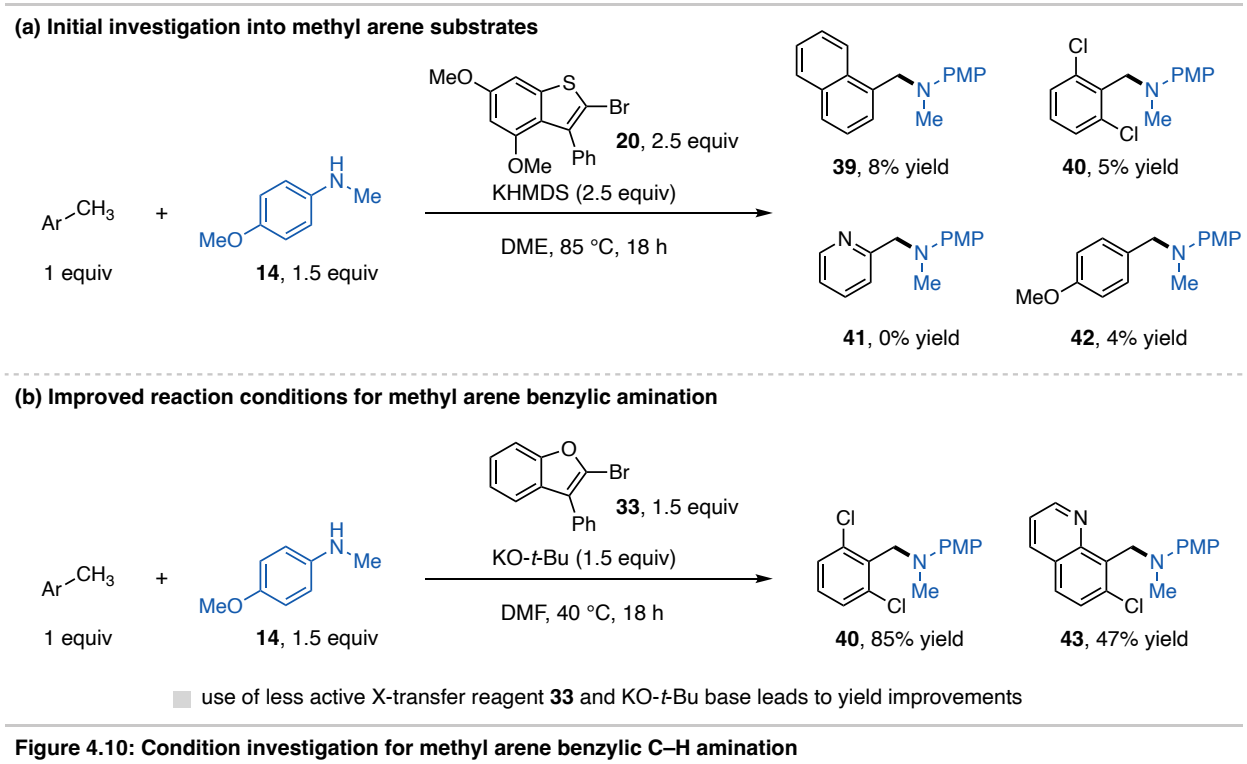

Figure 4.10: Condition investigation for methyl arene benzylic C–H amination

I first screened methyl arenes for benzylic amination when I discovered conditions that led to high yields using longer-chain alkyl arenes (Figure 4.6). Under these conditions I screened four methylarene substrates with a range of electronic properties to see what substrates would be operable. Unfortunately, under these conditions I only observed trace amounts of the benzyl amine products (**39**-**42**, Figure 4.10a). With no need to consider any over oxidation products with methyl

arenes, less care needed to be taken with reaction conditions to prevent it. Therefore, I next revisited KO-*t*-Bu as a base in polar DMF as the solvent with substrates **40** and **43**. Here, I observed 85% yield of **40** and 47% of **43**, providing the first observation of efficient amination of methyl arenes (Figure 4.10b).

Based off of these initial results, I further investigated each of these alkyl arenes using aniline **31**, as this aniline proved to be more consistent and will be utilized in scope investigation in Section 4.3. Drawing inspiration from the optimized conditions, I found that use of 1 equivalent of 18-crown-6 and 1.5 equivalents of X-transfer reagent **33** with DME as the solvent leads to 90% yield of **44**, however only 45% yield of **45** (Figure 4.11a). I next investigated condition optimization to increase the yield of **45**. Here, I found that use of NaHMDS as the base at room temperature in DME leads to 88% yield of **45**, showcasing the necessity of slightly varied reaction conditions for different substrates (Figure 4.11b).

There is one more substrate I would like to highlight in this Section, substrate **46**. This substrate is relatively unactivated as compared to **44** and **45** which allowed me to investigate a potentially more challenging reaction. Using conditions that provided high yield for **45**, I observed 0% yield of 47 with 98% of the methyl arene starting material leftover, indicating this substrate is not reactive under these conditions. However, when I switched to using X-transfer reagent 35 and KO-t-Bu as the base, I observed 50% yield of **46**. In the cases of these three substrates (**44**-**46**), it became clear that for methyl arenes it is very important to consider the compatibility of the substrate, X-transfer reagent, and base in order to optimize the compatibility of the deprotonation halogenation and substitution steps of this transformation. Methyl arenes are also seemingly more sensitive to this than longer-chain alkyl arenes, leading to individual substrate optimization for methyl arenes whereas alkyl arenes benefit from general conditions. After establishing reaction

optimization, the scope of this reaction was investigated for both alkyl arenes and amine coupling partners, discussed in Section 4.3.

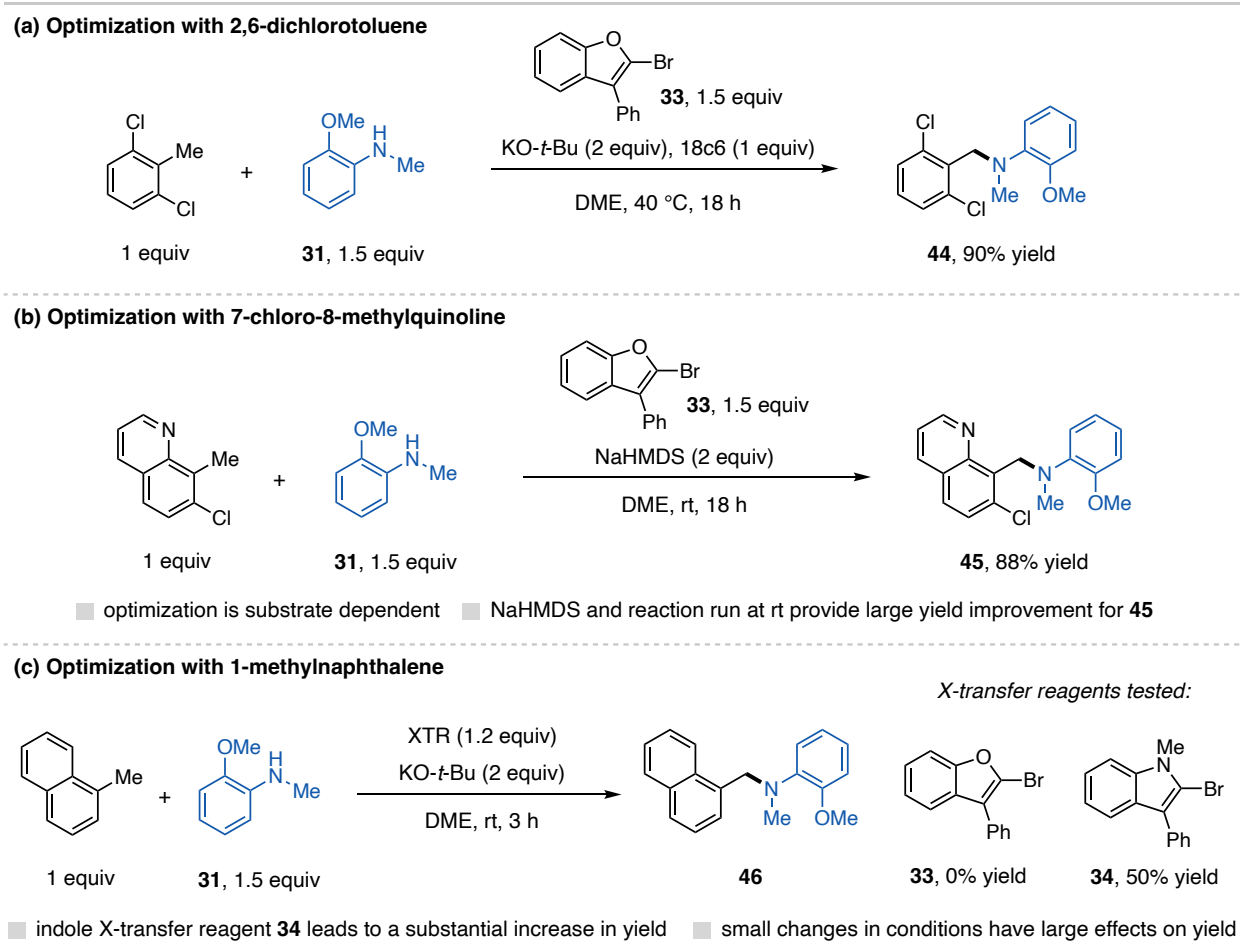

Figure 4.11: Substrate-dependent optimization of methyl arene substrates

4.3 Substrate Scope

After optimizing conditions for selected substrates as described in Section 4.2, I next moved on to investigate a scope of substrates that can be obtained with this reaction. Figure 4.12 shows the compilation of this scope, split into two parts to highlight investigation of alkyl arene substrates and investigation of compatible amines. In general, a variety of alkyl arenes and amines are shown in this scope to demonstrate functional group tolerance and interesting selectivity.

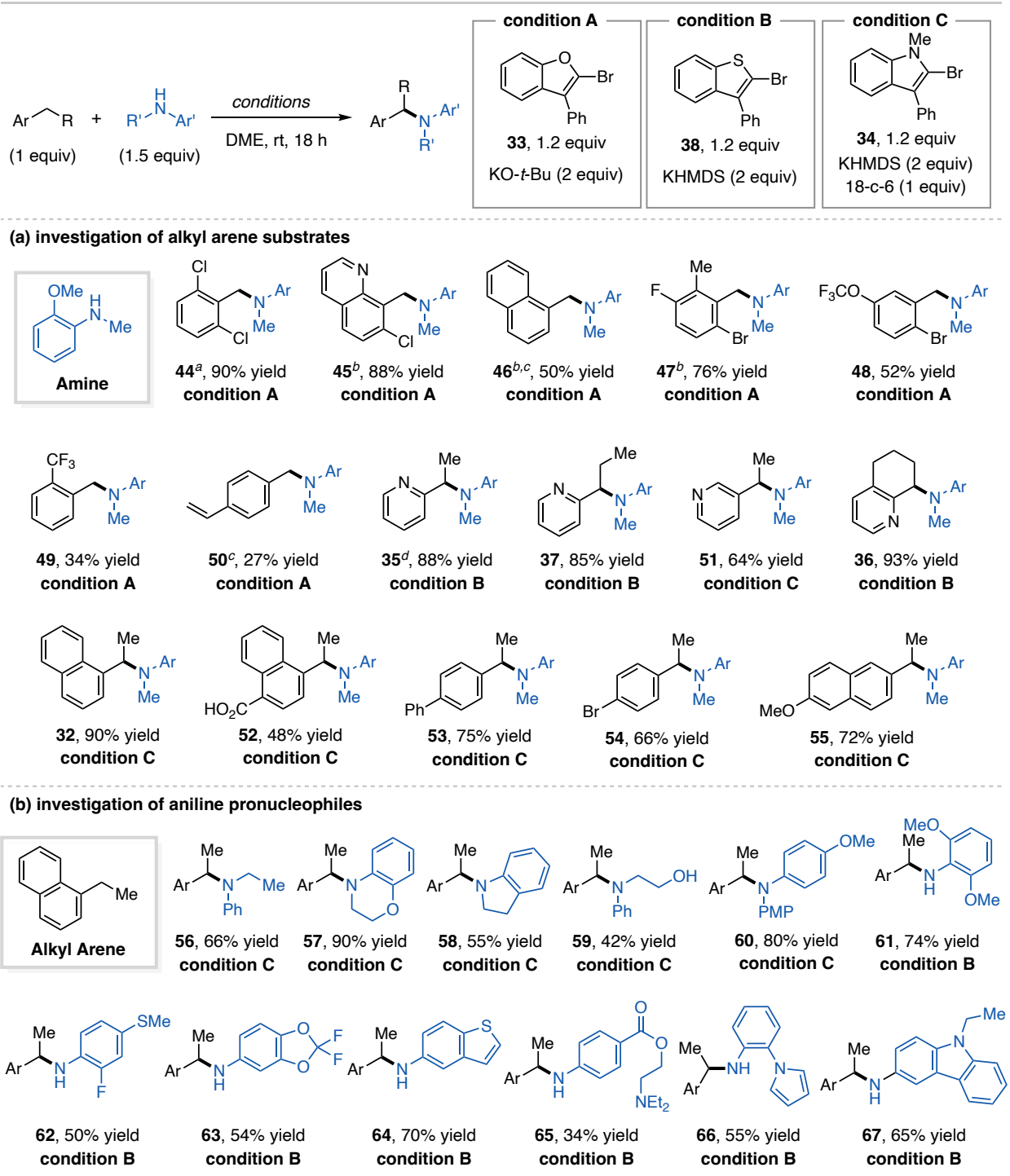

Figure 4.12: Substrate scope. [a] 1 equiv 18c6 used. [b] NaHMDS as base. [c] XTR 34 used. [d] XTR 20 and DMF solvent used. Yields determined by ^{1}H NMR spectroscopy.

Beginning with the alkyl arene scope, I investigated a series of substrates all while keeping the amine constant with aniline **31** (Figure 4.12a). This portion of the scope table is split between

methyl and longer-chain alkyl arenes and beginning with the methyl arenes, a variety of aryl halides are tolerated (**44**, **45**, **47**, **48**). Additionally, substrate **45** is SNAr active and no substitution product is observed under reaction conditions. Other electron withdrawing groups are tolerated including trifluoromethyl (**48**) and trifluoromethoxy (**49**) groups. Substrates **46** and **50** demonstrate this method is operable on unactivated substrates where the benzylic position does not need to be greatly acidified. Substrate 51 also does not undergo competing hydroamination under reaction conditions, selecting for only benzylic amination. Interestingly when a polymethyl arene is utilized, the reaction is selective for one methyl position over the other (**47**).

With longer alkyl chains, *N*-heterocycles are easily accessible (**35-37**, **51**), providing a complimentary approach to established benzylic amination methods where these substrates are incompatible (discussed in Chapter Three). Substrate **37** shows the ability to access longer aliphatic chains and substrate **36** shows the ability to access bicyclic substrates. This reaction is not restricted to 2-alkylpyridines, demonstrated with substrate **51**. The utility of this method is further demonstrated with **36**, which is selectivity for the position adjacent to the pyridine nitrogen and **52** which is selectivity for ethyl over methyl group functionalization. This reaction also tolerates less activated substrates including naphthalenes (**32**, **52**, **55**), biphenyl systems (**53**), and aryl halides (**54**). Substrate **52** features an unprotected carboxylic acid that is tolerated under reaction conditions provided an excess of base is used. Substrate **55** features an electron-rich naphthalene that is tolerated here as well.

The next section of the scope showcases the scope of amines that can be utilized in this reaction (Figure 4.12b). For this reaction, 1-ethylnaphthalene (**23**) was used as the alkyl arene while the amine coupling partner was varied. Beyond *N*-methyl anilines, other 2° anilines (**56-58**) are tolerated under reaction conditions. Amino alcohols (**59**) are tolerated and feature exclusive N-

selectivity with no benzylic etherification observed. Diaryl amines are also tolerated, shown with bis(4-methoxyphenyl)amine in **60**. With the use of X-transfer reagent **34**, I found that primary anilines are also tolerated (**61**-**67**). This is an important development as 1° anilines are far more available commercially than *N*-alkyl anilines, which greatly improves the utility of this reaction. Electron rich anilines function well under reaction conditions (**61**-**63**, **66, 67**). Substrate **62** features a thioether that would typically oxidize with established methods that is completely untouched here. Substrate **63** features a difluorobenzodioxole containing a that is not cleaved or functionalized under reaction conditions. Substrate **64** features a benzothiophene that is tolerated under reaction conditions and does not undergo X-transfer. Electron-deficient anilines are also compatible, as shown in substrate **65**, which features an ester that is untouched under reaction conditions. Anilines featuring other N-heterocycles such as pyrroles (**66**) and carbazoles (**67**) are represented here as well.

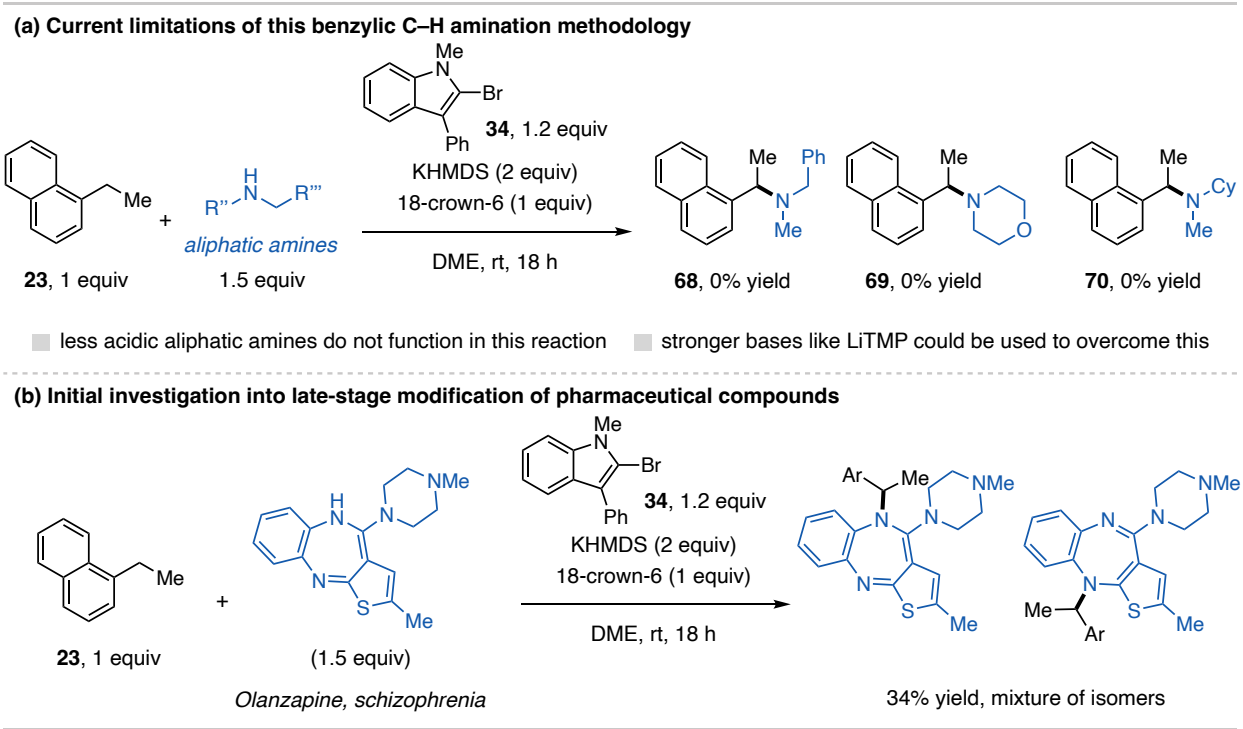

Figure 4.13: Limitations and outlook for alkyl arene benzylic C–H amination methodology

Not featured in this scope are aliphatic amines, which currently represent a limitation of this method. Under the current reaction conditions, I tested *N*-methylbenzylamine, morpholine, and *N*-methylcyclohexylamine, but observed no formation of product (**68**-**70**, Figre 4.13a). This is presumably due to the increased acidity of aliphatic amines as compared to anilines, making these substrates inaccessible using the bases developed for this reaction.[22] The use of stronger bases such as LiTMP is currently being investigated in our group as a solution to this challenge, which could provide access to aliphatic amines for benzylic C–H amination.

The development of this reaction as described in this chapter represents the current state of the project and where I will be leaving it off. A younger student in the group, Kayla, will be taking over to complete this project for publication. As it stands, the scope of the reaction is developed, with a few substrates potentially still to be investigated and replaced by Kayla. Another important area to explore this reaciotn in is the development and functionalization of complex pharmaceutical compounds. Figure 4.13b shows a preliminary result for this where I utilized olanzapine, utilized to treat schizophrenia and bipolar disorder, and obtained 35% yield of a mixture of isomers. Though I have not pursued this further, this method could be utilized to functionalize a series of amine and alkyl arenes in pharmaceutical compounds.

Conclusion

I have fully developed the direct benzylic C–H amination of alkyl (hetero)arenes and the work is currently being prepared towards publication. Although I am not able to complete this work, I am excited to see Kayla take over and completing this project and continuing pushing the boundaries of its capabilities. The successful development of this project establishes the first general method for direct benzylic amination between any alkyl arene and amine coupling partner.

In the development of this project, I found that alkyl arenes were prone to desaturation processes upon benzylic halogenation, and Chapter Five will discuss my further development of this area.

REFERENCES

[1] Puleo, T. R.; Bandar, J. S. Base-catalyzed aryl halide isomerization enables the 4-selective substitution of 3-bromopyridines. *Chem. Sci.* **2020**, *11*, 10517-10522.

[2] Puleo, T. R.; Klaus, D. R.; Bandar, J. S. Nucleophilic C–H Etherification of Heteroarenes Enabled by Base-Catalyzed Halogen Transfer. *J. Am. Chem. Soc.* **2021**, *143*, 12480–12486.

[3] Bone, K. I.; Puleo, T. R.; Bandar, J. S. Direct C–H Hydroxylation of N-Heteroarenes and Benzenes via Base-Catalyzed Halogen Transfer. *J. Am. Chem. Soc.* **2024**, *146*, 9755–9767.

[4] Bone, K. I.; Puleo, T. R.; Delost, M. D.; Shimizu, Y.; Bandar, J. S. Direct Benzylic C–H Etherification Enabled by Base-Promoted Halogen Transfer. *ChemRxiv preprint, DOI: 10.26434/chemrxiv-2024-fvrc1*.

[5] Lum, R. C.; Grabowski, J. J. The Intrinsic Competition between Elimination and Substitution Mechanisms Is Controlled by Nucleophile Structure. *J. Am. Chem. Soc.* **1992**, *114*, 9663-9665.

[6] Gronert, S. Gas Phase Studies of the Competition between Substitution and Elimination Reactions. *Acc*. *Chem*. *Res*. **2003**, *36*, 848-857.

[7] Liu, X.; Zhang, J.; Yang, L.; Hase, W. L. How a Solvent Molecule Affects Competing Elimination and Substitution Dynamics. Insight into Mechanism Evolution with Increased Solvation. *J. Am. Chem. Soc.* **2018**, *140*, 10995−11005.

[8] Bordwell, F.G.; Algrim, D.; Vanier, N. R. Acidities of Anilines and Toluenes. *J. Org. Chem.* **1977**, *42*, 1817-1819.

[9] Bordwell, F. G.; Algrim, D. J. Acidities of Anilines in Dimethyl Sulfoxide Solution. *J. Am. Chem. Soc.* **1988**, *110*, 2964-2968.

[10] Beller, M.; Seayad, J.; Tillack, A.; Jiao, H. Catalytic Markovnikov and anti-Markovnikov Functionalization of Alkenes and Alkynes: Recent Developments and Trends. *Angew. Chem. Int. Ed.* **2004**, *43*, 3368-3398.

[11] Yin, X.; Li, S.; Guo, K.; Wang, X. Palladium-Catalyzed Enantioselective Hydrofunctionalization of Alkenes: Recent Advances. *Eur. J. Org. Chem.* **2023**, *26*, e202300783.

[12] Zhu, Y.; Liao, Y.; Jin, S.; Ding, L.; Zhong, G.; Zhang, J. Functionality-Directed Regio- and Enantio-Selective Olefinic C–H Functionalization of Aryl Alkenes. *Chem. Rec.* **2023**, *23*, e202300012.

[13] Sadowsky, D.; McNeill, K.; Cramer, C. J. Thermochemical Factors Affecting the Dehalogenation of Aromatics. *Environ. Sci. Technol*. **2013**, *47*, 14194−14203.

[14] Dong, Y.; Lipschutz, M. I.; Tilley, T. D. Regioselective, Transition Metal-Free C−O Coupling Reactions Involving Aryne Intermediates. *Org. Lett*. **2016**, *18*, 1530−1533.

[15] Wetzel, D. M.; Brauman, J. I. Quantitative Measure of -Silyl Carbanion Stabilization. The Electron Affinity of (Trimethylsilyl)methyl Radical. *J. Am. Chem. Soc*. **1988**, *110*, 8333-8336.

[16] Streitwieser, A.; Facchetti, A.; Xie, L.; Zhang, X.; Wu, E. C. Ion Pair p*K*s of Some Amines: Extension of the Computed Lithium p*K* Scale. *J. Org. Chem*. **2012**, *77*, 985−990.

[17] Huang, M.; Wu, G. Organolithium Reagents in Pharmaceutical Asymmetric Processes. *Chem. Rev*. **2006**, *106*, 2596−2616.

[18] Mulvey, R. E.; Robertson, S. D. Synthetically Important Alkali-Metal Utility Amides: Lithium, Sodium, and Potassium Hexamethyldisilazides, Diisopropylamides, and Tetramethylpiperidides. *Angew. Chem. Int. Ed*. **2013**, *52*, 11470 – 11487.

[19] Ojeda-Amador, A. I.; Martínez-Martínez, A. J.; Kennedy, A. R.; O'Hara, C. T. Structural Studies of Cesium, Lithium/Cesium, and Sodium/Cesium Bis(trimethylsilyl)amide (HMDS) Complexes. *Inorg. Chem*. **2016**, *55*, 5719−5728.

[20] Ojeda-Amador, A. I.; Martínez-Martínez, A. J.; Robertson, G.; Robertson, S. D.; Kennedy, A. R.; O'Hara, C. T. Exploring the solid state and solution structural chemistry of the utility amide potassium hexamethyldisilazide (KHMDS). *Dalton Trans*. **2017**, *46*, 6392-6403.

[21] Ren, L.; Wang, M.; Fang, B.; Yu, W.; Chang, J. Iodine-mediated oxidative N–N coupling of secondary amines to hydrazines. *Org. Biomol. Chem.* **2019**, *17*, 3446-2450.

[22] Bordwell, F. G.; Drucker, G. E.; Fried, H. E. Acidities of Carbon and Nitrogen Acids: The Aromaticity of the Cyclopentadienyl Anion. *J. Org. Chem*. **1981**, *46*, 632-635.

CHAPTER FIVE

DIRECT ALKYL ARENE DESATURATION AND CASCADE FUNCTIONALIZATION ENABLED BY BASE-PROMOTED HALOGEN TRANSFER

5.1 Chapter Overview

When I began working in the area of halogen transfer (X-transfer) within our group, one of the major unmet challenges was engaging longer-chain alkyl arenes in benzylic substitution processes. The predominant reason for this limitation is due to elimination upon benzylic halogenation that competes with the desired substitution process (Figure 5.1).[1,2] Chapter Four describes my efforts in successfully favoring benzylic amination over elimination or other overoxidation side pathways. Instead of viewing the competitive elimination pathway as a problem and limitation, I instead considered it an opportunity to explore the desaturation of alkyl (hetero)arenes. Given the utility of vinyl arenes as described in Chapter Three, a general and simple approach to access them from abundantly available alkyl (hetero)arenes is highly desirable. This chapter describes my development of alkyl (hetero)arene desaturation *via* base-promoted X-transfer as well as my discovery of a one-pot cascade functionalization method with amines. The methods discussed here have led to two projects within our group that are being completed by younger graduate students.

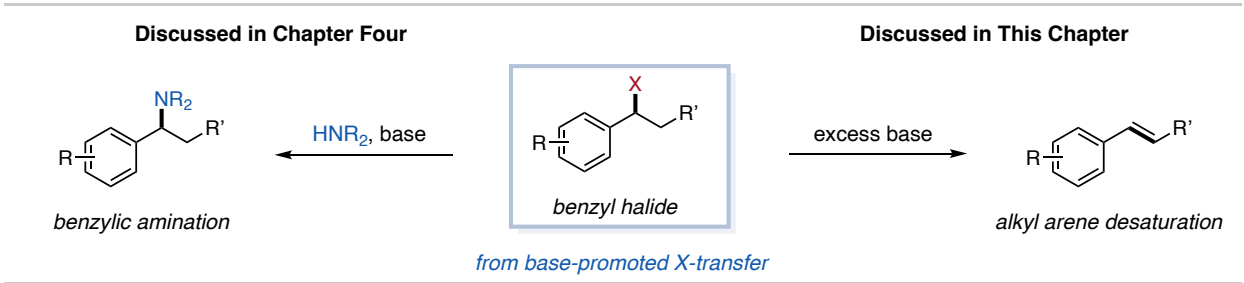

Figure 5.1: Competitive elimination with benzyl halides presents an opportunity for alkyl arene desaturation

5.2 Reaction Discovery and Development of Alkyl (Hetero)Arene Desaturation

Competitive elimination with substitution has been observed in our group's benzylic etherification protocol, ultimately precluding these substrates from being included in the manuscript, and in my investigation of benzylic C–H amination.[3] I reasoned that if the pronucleophile is removed from the reaction conditions, under basic conditions the benzyl halide should undergo efficient elimination. Vinyl arenes are prevalent and useful structural motifs that are frequently leveraged as building blocks for more complex molecule synthesis.[4-6] Alkyl arenes represent an abundant and ideal precursor to these motifs, however, few methods exist to reliably achieve this transformation (discussed extensively in Chapter Three). As such, the method described here offers the first general approach for the desaturation of alkyl (hetero)arenes.

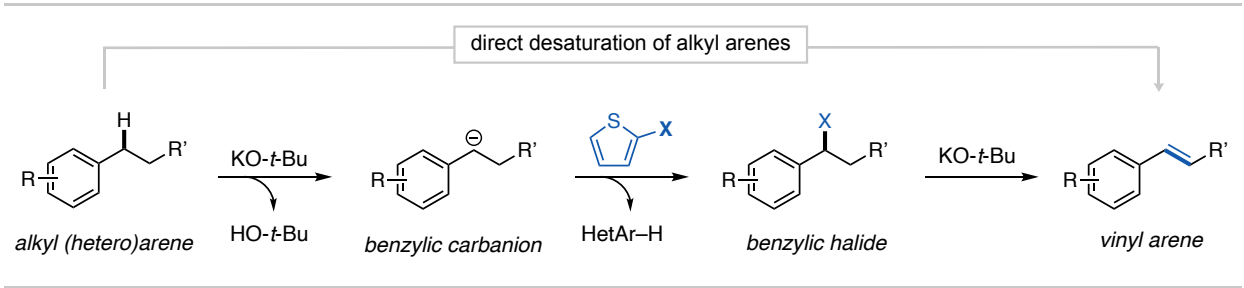

Figure 5.2: Proposed mechanism for alkyl arene desaturation *via* base-promoted X-transfer

Figure 5.2 shows the proposed mechanism for this transformation. Here, the alkyl arene is deprotonated in the benzylic position using KO-*t*-Bu or a base of similar strength. Given the difference in pK_a values, the benzyl halide is generated in low concentration, which is key to avoiding unproductive side reactions like substrate dimerization.[7-9] The benzylic carbanion then reacts with the X-transfer reagent to generate the benzyl halide, which undergoes E_2 elimination to provide the vinyl arene product.

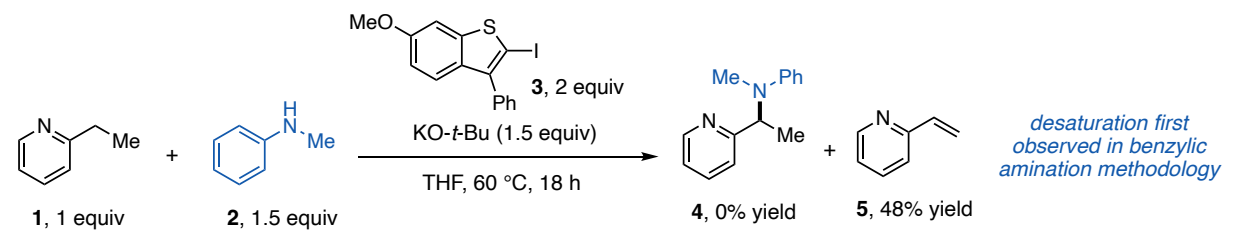

Figure 5.3: Initial observation of desaturation in benzylic amination investigation

My first observation of alkyl arene desaturation came when I was investigating the benzylic amination of 2-ethylpyridine (**1**) with N-methylaniline (**2**) using X-transfer reagent **3** (Figure 5.3). Under these conditions, elimination dominates over substitution (4% yield **4** *versus* 48% yield **5**). Based off of this result, I started with 2-ethylpyridine (**1**) as a model substrate using 1.5 equivalents of KO-*t*-Bu as the base and screened a variety of X-transfer reagents for desaturation (Figure 5.4). Overall, iodine X-transfer reagents provide higher yields than bromine X-transfer reagents. This could be due to the higher reactivity of iodine *versus* bromine for X-transfer as well as for elimination.[2,10] Commercial X-transfer reagents (**6**-**9**) provide good yield of **5**, but use of our group's designer X-transfer reagents (**10**-**13**) lead to high yield of **5**. Notably, benzofuran X-transfer reagent **13** leads to lower yield of **5**, indicating more reactive X-transfer reagents featuring the benzothiophene substructure are necessary for high reactivity in this protocol.

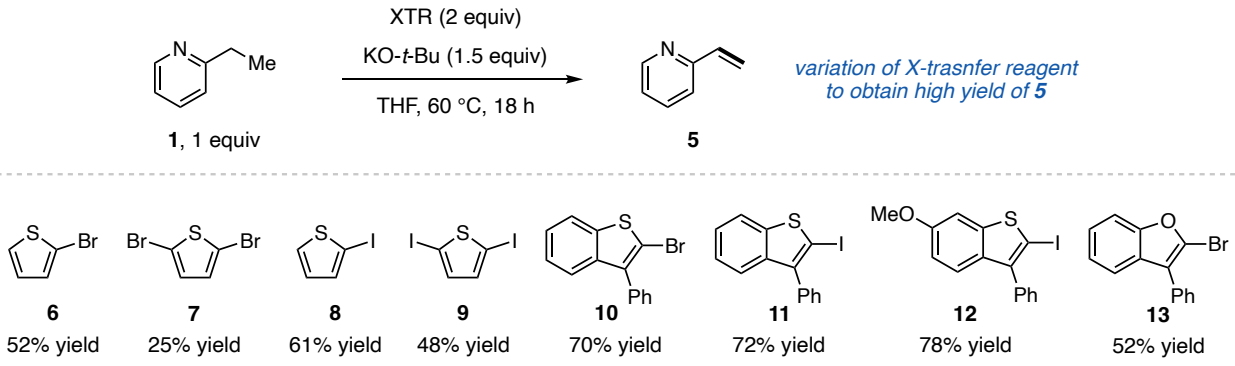

Figure 5.4: X-transfer reagent screen for alkyl arene desaturation

With effective conditions identified for the desaturation of model substrate **1**, I next moved on to explore the scope of alkyl arenes that are operable under these conditions. Figure 5.5 shows the scope with substrates featuring diverse substitution patterns and types of tolerated arenes. Along with **5**, this reaction tolerates 4-ethylpyridine (**14**) as well as β- and α-substituted 2-alkylpyridines (**15**, **16**). Moving away from alkylpyridines, 2-ethylbenzofuran (**17**) and 3,5-dibromoethylbenzene (**18**) can be desaturated with this method. By switching to more base-stable and less reactive X-transfer reagent **13** and use of KHMDS as the base, unactivated alkyl arenes can be incorporated, with 1-ethylnaphthalene as an example (**19**). I am currently mentoring a younger graduate student in the lab, Viet Ngo, who is exploring a broader scope for this transformation that will include substrates that feature broad functional group tolerance.

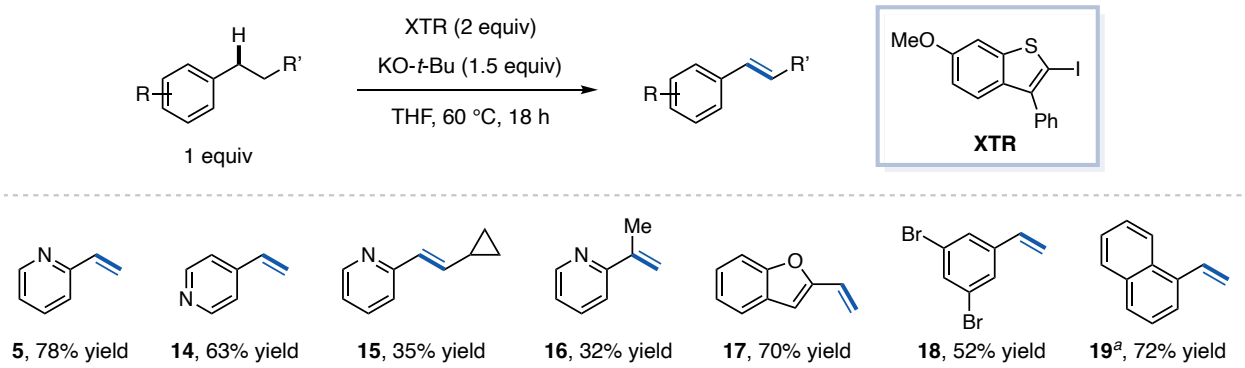

Figure 5.5: Initial substrate scope for alkyl arene desaturation. Yields determined by ^{1}H NMR spectroscopy.

One substrate class that I identified as a limitation in this protocol is the use of alkyl arenes with chains longer than ethyl groups (Figure 5.6a). Although **15** does feature a β-substituted alkyl arene, the reactivity is likely due to the incorporation of the cyclopropane as an activating group, thus making the reaction easier.[11] Substrates like 2-propylpyridine (**20**) and propyl- and butylbenzene derivatives (**21**-**23**) do not undergo desaturation with retention of the starting material mass balance, indicating these substrates are completely unreactive. Empirical

optimization of reaction conditions did not lead to desaturation of these substrates, indicating there is an incompatibility issue using longer-chain alkyl arenes. 2-Propylpyrine (**20**) undergoes efficient substitution with 2-methoxy-*N*-methylaniline (**24**) using X-transfer reagent **10**, indicating X-transfer to the benzylic position will occur under reaction conditions. This implies that the problematic step here is likely the elimination which does not occur upon benzylic halogenation. Since the X-transfer process is proposed to be reversible, with no functionalization reaction to influence this equilibrium the reaction results in complete retention of starting material.[12,13] Thus, more control reactions need to be run to elucidate the reason the elimination pathway is disfavored for longer-chain alkyl arenes.

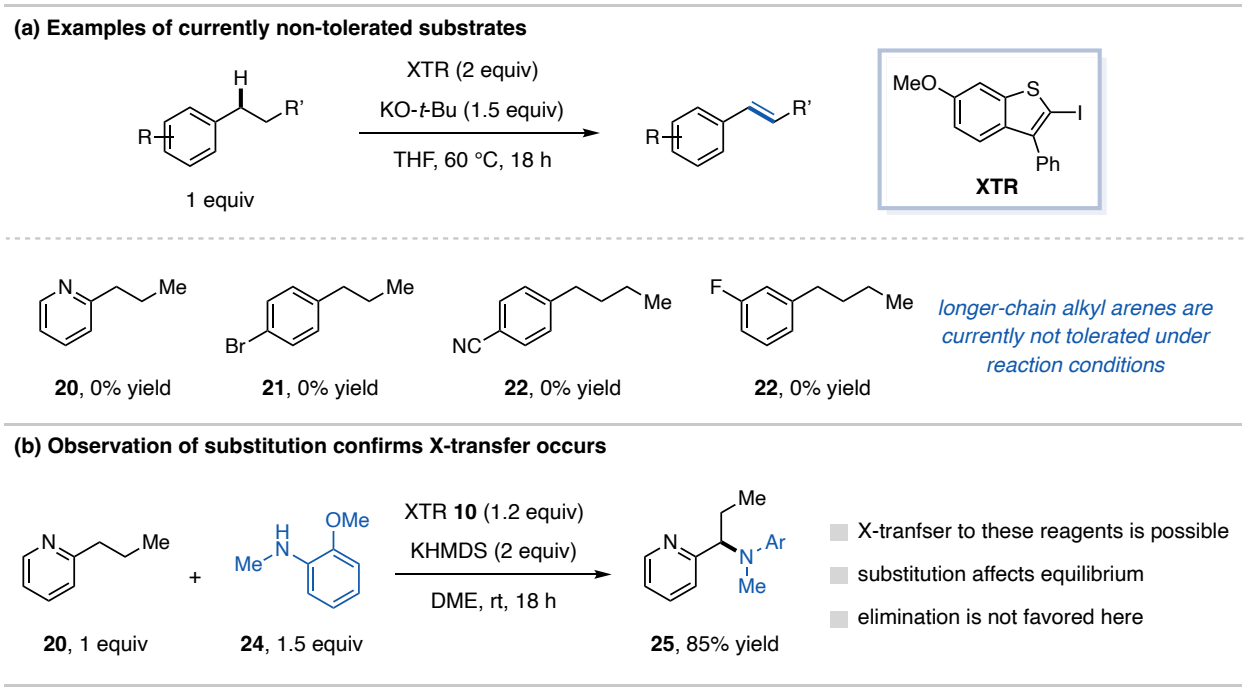

Figure 5.6: Current limitations with base-promoted alkyl arene desaturation *via* X-transfer

With an initial scope established for alkyl arene substrates, I next moved on to exploring other alkanes with activating groups for desaturation. Figure 5.7 shows examples of alternate activating groups as well as some substrates classes that do not undergo desaturation under current reaction conditions. Both amides and esters can be desaturated to the corresponding acrylamides

and acrylates (**26**, **27**). These products are useful in Michael-type reactions and as monomers in polymerizations, and this method could provide access to these substructures from their saturated counterparts.[14-16] Desaturation of saturated heterocycles is also possible under reaction conditions, shown with the ability to access quinoline (**28**) from 1,2,3,4-tetrahydroquinoline (), providing a facile route to access N-heterocycles. This approach can potentially provide access to with substitution patterns or functional groups that would be difficult to access *via* aromatic functionalization methods. This would also complement existing approaches to this technique, like the Stahl Group's aerobic dehydrogenation approach and the Oestreich Group's Pd-catalyzed aerobic dehydrogenation approach.[17-19] Beyond these activating groups, I also attempted desaturation of nitroalkanes and alkyl sulfone which would provide access to nitroalkenes and vinyl sulfones, which are useful functional groups in synthetic chemistry.[20-22] When I attempted these substrates, I was unable to observe formation of the desaturated products, however, there is still room to explore alternate activating groups for desaturation for the future of this project.

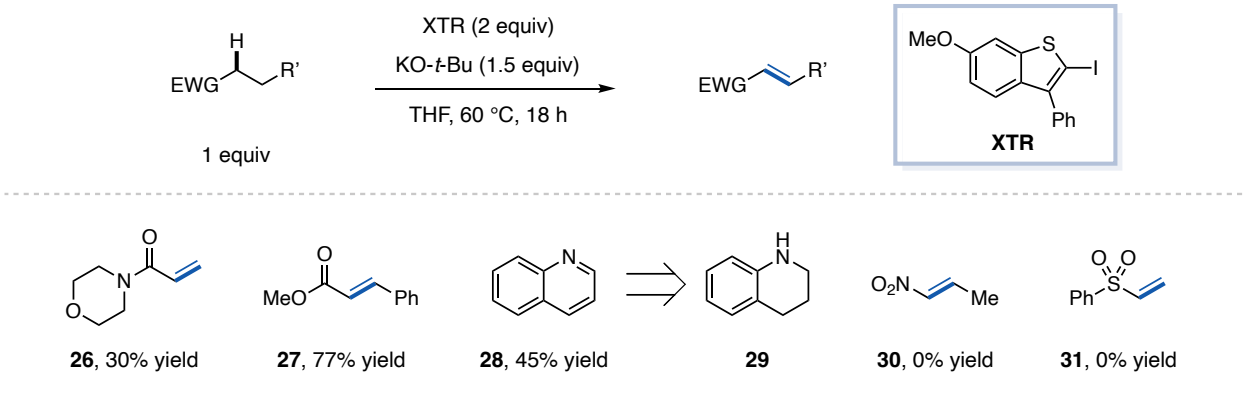

Figure 5.7: Investigation of other activating groups for base-promoted desaturation *via* X-transfer. Yields determined by ^{1}H NMR spectroscopy.

A final application that I tested was the desaturation of cyclohexanones for the synthesis of phenol derivatives. This area has been pioneered by the Stahl and Leonori Groups as a strategy to access phenols and anilines with diverse substitution patterns that would be challenging to

access *via* typical aromatic functionalization reactions (discussed in Chapter Three in more detail).[23-25] These approaches rely on transition-metal catalysts and, as such, the use of base-promoted X-transfer to achieve the same transformation would provide a practical and complementary approach. I attempted this reaction using 4-phenylcyclohexanone (**32**), which would result in 4-phenylphenol (**33**) upon desaturation (Figure 5.8). Unfortunately, I was unable to observe any formation of the phenol product and no other desaturation products were present. Due to the utility of synthesizing diverse substituted phenols with this method, I am currently mentoring Viet Ngo in our lab who is further investigating this transformation.

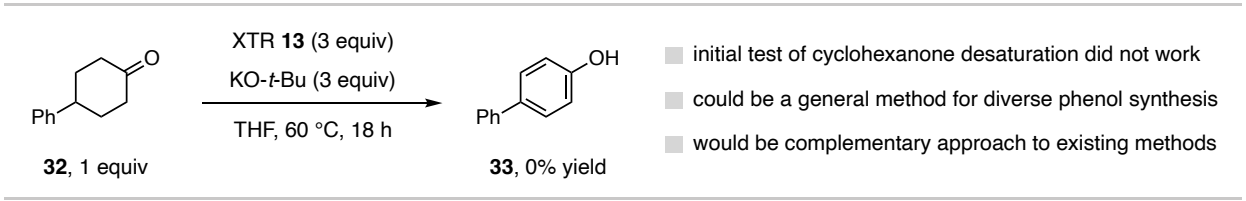

Figure 5.8: Initial investigation into phenol synthesis from cyclohexanone desaturation

5.3 Reaction Discovery and Development of Cascade Alkyl (Hetero)Arene Desaturation and Functionalization

The above-described alkyl (hetero)arene desaturation method provides access to a highly diversifiable vinyl arene functional handle. [4-6] Given the known compatibility of pronucleophiles with X-transfer processes, I reasoned that this desaturation method could be coupled with a subsequent functionalization reaction in a one-pot, cascade procedure. A well-known aryl alkene functionalization method is hydroamination, which would result in a homobenzylic amine, which is a useful and prevalent functional group.[26-28] Given the utility of this motif and my experience engaging amines in X-transfer transformations, I targeted this reaction to couple with the desaturation protocol I developed.

I first attempted this cascade transformation using 2-ethylpyridine (**1**) as the alkyl arene and *N*-methylaniline (**2**) as the pronucleophile. Under optimal conditions for desaturation with

excess of X-transfer reagent to promote rapid desaturation and excess of base to promote the hydroamination step, I unfortunately did not observe any formation of hydroaminated product **34**. Instead, I observed 40% yield of enamine product **35**, presumably formed from subsequent X-transfer and elimination of product **34** (Figure 5.9a). Further attempts to optimize this reaction were unsuccessful in obtaining product **34**, still only resulting in the formation of **35**.

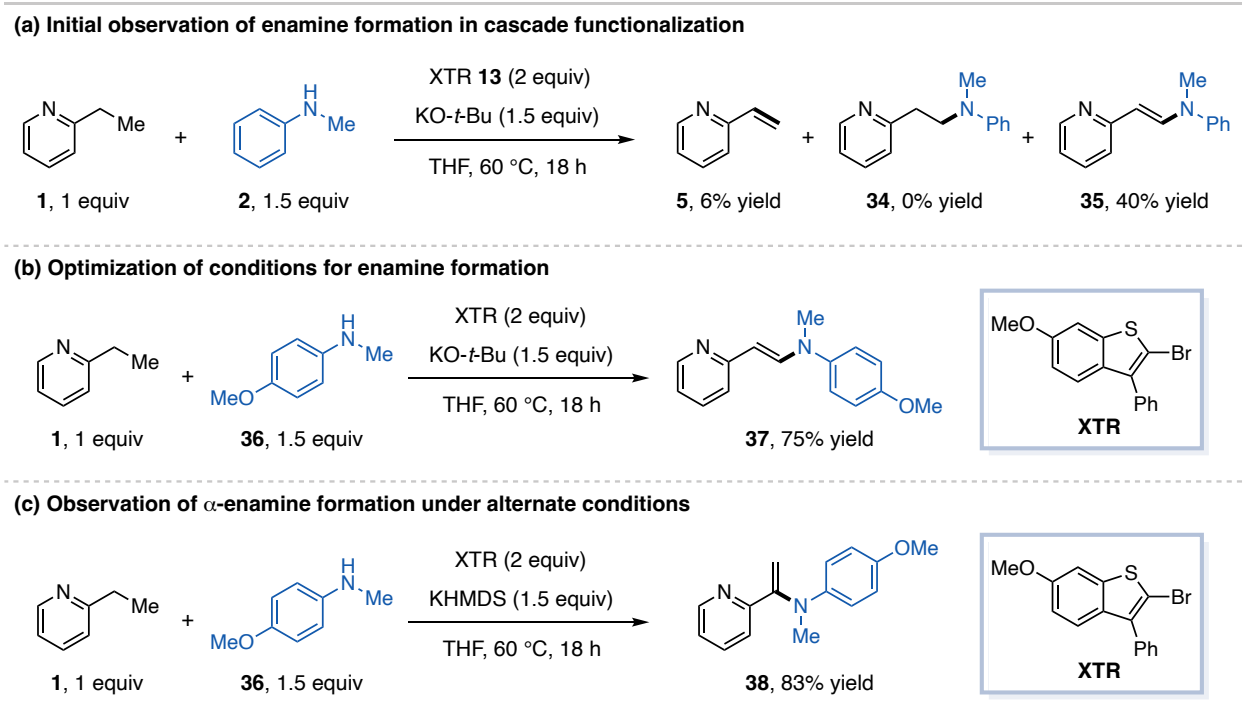

Figure 5.9: Observation and optimization of cascade desaturation and enamine formation

Much like with the initial development of the desaturation protocol, I viewed the formation of enamine **35** not as a limitation, but as an opportunity. Enamines are highly useful functional handles that can be easily diversified into a number of useful products.[29] In this regard, I reasoned this reaction could be optimized with the goal of forming the β-aryl enamine to be used in subsequent functionalization reactions. Figure 5.9b showcases optimized conditions utilizing *N*-methylaninline (**2**) and 4-methoxy-N-methylaniline (**36**) as pronucleophiles where use of bromine X-transfer reagent (**3**) is optimal for this reaction. When I was investigating reaction conditions

for the formation of the β-aryl enamine, I found that when KHMDS is used as a base in place of KO-*t*-Bu, the α-isomer of the enamine (**38**) is formed exclusively in 83% yield (Figure 5.9c). Thus, by simply altering the choice of base in this reaction, the regioselectivity of this reaction can be switched. This result was observed during empirical optimization and the nature of this selectivity switching is currently being investigated in our lab. The utilization of this result in the development of the benzylic amination of (hetero)arenes is discussed in Chapter Four.

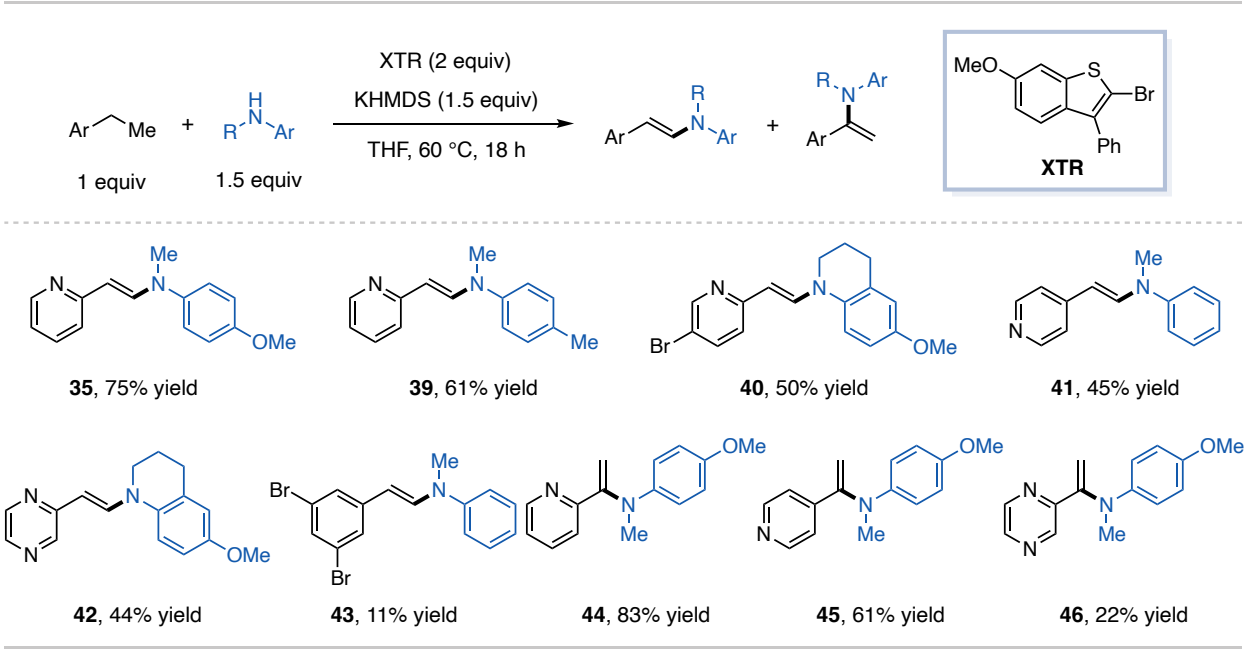

Figure 5.10: Scope of α- and β-enamines from cascade functionalization of alkyl arenes. Yields determined by ^{1}H NMR spectroscopy.

Figure 5.10 shows an initial scope investigation for this transformation featuring both α- and β-aryl enamines, depending on which base is utilized. This initial scope features mainly N-heterocycle alkyl arene substrates (**35, 39-42**, **44-46**) with one example of an ethylbenzene derivative that does function, albeit in low yield (**43**). Both 2- (**35, 39**, **40**, **44**) and 4-ethylpyridines (**41**, **45**) are incorporated here as well as pyrazine (**42**, **46**) alkyl heteroarenes. Various anilines also function in this reaction including activated (**35**, **36**, **44-46**) and unactivated (**41**, **43**) anilines as well as a 1,2,3,4-tetrahydroquinoline derivative (**40**, **42**). This represents an initial screen of

substrates for this reaction and this scope will be further investigated to incorporate more alkyl benzene derivatives as well as greater functional group tolerance.

As mentioned, these enamine products are diversifiable functional handles that can be leveraged for further reactivity. Figure 5.11 showcases two applications of this that I have demonstrated, the hydrolysis and reduction of the enamines. The hydrolysis protocol provides access to the α-aryl aldehyde and is achieved through reaction of the enamine with aqueous HCl. The reduction product provides access to the homobenzylic amine that I was originally targeting with this protocol and quantitative conversion can be achieved using $NaBH_4$ and AcOH. Therefore, using the same protocol under variable reaction conditions, I have developed protocols to access both the benzylic and homobenzylic amine starting from the same alkyl arene with high selectivity. Combined, this is a powerful method to selectively access a wide variety of useful products from a single, readily available starting material.

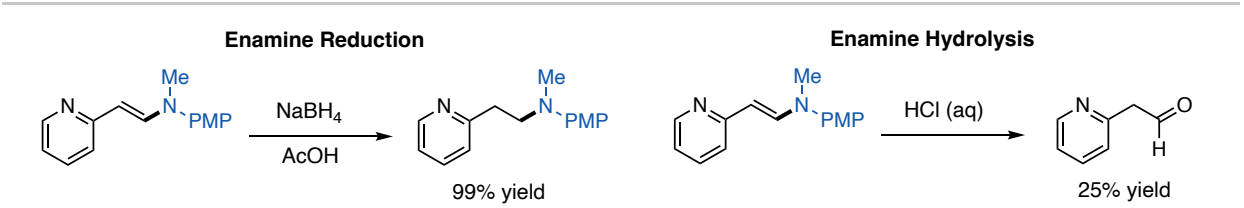

Figure 5.11: Initial examples of enamine product functionalization

A final application of this system involves the use of primary anilines for the cascade desaturation and aziridination of alkyl arenes. Aziridines are very useful class of *N*-heterocycle that serve as intermediates to a number of useful products.[30] A younger student in our lab, Cristian, is currently working on the aziridination of vinyl arenes using X-transfer methodology, which would be the second step of this cascade process (Figure 5.12a). In this reaction, upon hydroamination of the vinyl arene, subsequent X-transfer delivers a halogen to the benzylic position, followed by base-promoted intramolecular cyclization with the newly-bound aniline. A

cascade method starting with the alkyl arene could provide a complementary approach to starting with the vinyl arene, as alkyl arenes are more prevalent and available. I tested this reaction using 2-ethylpyridine (**1**) and aniline (**48**) and observed 27% yield of aziridine **49** (Figure 4.12b). This represents a good preliminary result for the direct aziridination of alkyl arenes, a transformation that is not currently possible. This cascade alkyl arene aziridination reaction has the potential to be further optimized and explored by our group in the future.

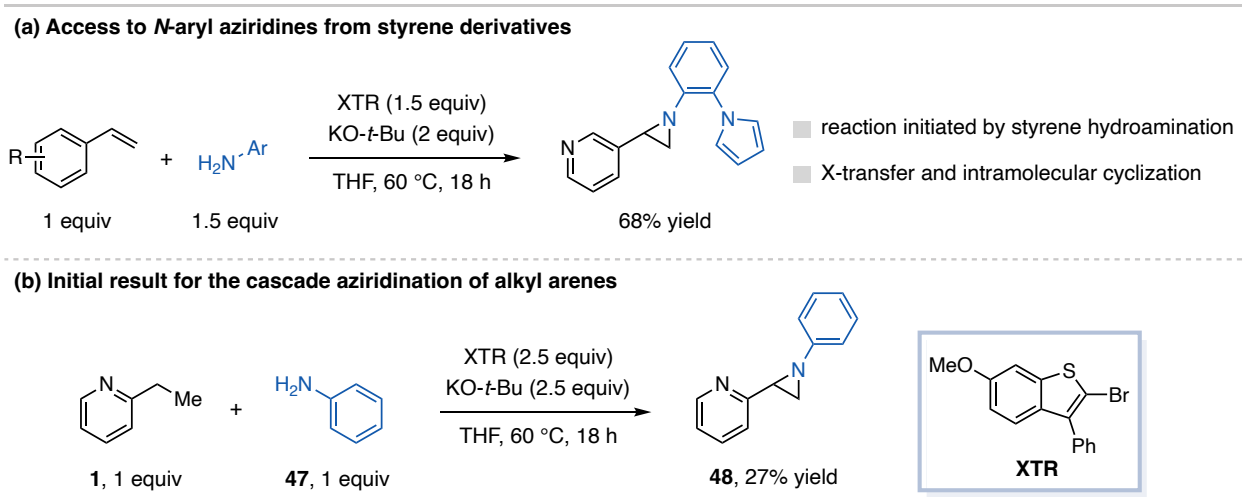

Figure 5.12: Development of cascade aziridination of alkyl arenes using primary anilines

5.4 Conclusion

I have developed the initial reactivity for the base-promoted desaturation of alkyl (hetero)arenes as well as the cascade desaturation-functionalization of alkyl (hetero)arenes. The discovery and development of these transformations were made possible by the exploitation of the completive elimination pathway when alkyl arenes are engaged in X-transfer methodology. Although I am not able to further develop and complete these projects, I am excited for Viet to take over and continue working on it and see where he is able to take the project. Successful realization of the desaturation protocol will provide the first general method for the oxidative dehydrogenation of alkyl arenes. Realization of the cascade functionalization methodology will

enable chemists to view alkyl arenes as diversifiable functional handles to rapidly build complexity in either the benzylic or homobenzylic position or, in the case of the aziridination method, in both positions in a single step. I am excited to see where the Bandar Group can take these projects I have laid the groundwork for in the future.

REFERENCES

[1] Lum, R. C.; Grabowski, J. J. The Intrinsic Competition between Elimination and Substitution Mechanisms Is Controlled by Nucleophile Structure. *J. Am. Chem. Soc.* **1992**, *114*, 9663-9665.

[2] Gronert, S. Gas Phase Studies of the Competition between Substitution and Elimination Reactions. *Acc*. *Chem*. *Res*. **2003**, *36*, 848-857.

[3] Bone, K. I.; Puleo, T. R.; Delost, M. D.; Shimizu, Y.; Bandar, J. S. Direct Benzylic C–H Etherification Enabled by Base-Promoted Halogen Transfer. *ChemRxiv preprint, DOI: 10.26434/chemrxiv-2024-fvrc1*.

[4] Beller, M.; Seayad, J.; Tillack, A.; Jiao, H. Catalytic Markovnikov and anti-Markovnikov Functionalization of Alkenes and Alkynes: Recent Developments and Trends. *Angew. Chem. Int. Ed.* **2004**, *43*, 3368-3398.

[5] Yin, X.; Li, S.; Guo, K.; Wang, X. Palladium-Catalyzed Enantioselective Hydrofunctionalization of Alkenes: Recent Advances. *Eur. J. Org. Chem.* **2023**, *26*, e202300783.

[6] Zhu, Y.; Liao, Y.; Jin, S.; Ding, L.; Zhong, G.; Zhang, J. Functionality-Directed Regio- and Enantio-Selective Olefinic C–H Functionalization of Aryl Alkenes. *Chem. Rec.* **2023**, *23*, e202300012.

[7] Bordwell, F.G.; Algrim, D.; Vanier, N. R. Acidities of Anilines and Toluenes. *J. Org. Chem.* **1977**, *42*, 1817-1819.

[8] Olmstead, W. N.; Margolin, Z.; Bordwell, F. G. Acidities of water and simple alcohols in dimethyl sulfoxide solution. *J. Org. Chem*. **1980**, *45*, 3295–3299.

[9] Ren, L.; Wang, M.; Fang, B.; Yu, W.; Chang, J. Iodine-mediated oxidative N–N coupling of secondary amines to hydrazines. *Org. Biomol. Chem.* **2019**, *17*, 3446-2450.

[10] The Chemistry of the Carbon-Halogen Bond; Patai, S., Ed.; John Wiley & Sons, London, 1973.

[11] Modern Physical Organic Chemistry; Anslyn, E. V., Dougherty, D. A., Ed.; University Science Books, Sausalito, CA, 2005.

[12] Bunnett, J. F. Base-catalyzed halogen dance, and other reactions of aryl halides. *Acc. Chem. Res.* **1972**, *5*, 139–147.

[13] Puleo, T. R.; Klaus, D. R.; Bandar, J. S. Nucleophilic C–H Etherification of Heteroarenes Enabled by Base-Catalyzed Halogen Transfer. *J. Am. Chem. Soc.* **2021**, *143*, 12480–12486.

[14] Kennemur, J. L.; Maji, R.; Scharf, M. J.; List, B. Catalytic Asymmetric Hydroalkoxylation of C−C Multiple Bonds. *Chem. Rev.* **2021**, *121*, 14649–14681.

[15] Corsaro, C.; Neri, G.; Santoro, A.; Fazio, E. Acrylate and Methacrylate Polymers' Applications: Second Life with Inexpensive and Sustainable Recycling Approaches. *Materials* **2022**, *15*, 282-311.

[16] Menter, P. Acrylamide Polymerization – A Practical Approach. *BioRad Tech Note* **2000**, ID: 97055792.

[17] Iosub, A. V.; Stahl, S. S. Palladium-Catalyzed Aerobic Oxidative Dehydrogenation of Cyclohexenes to Substituted Arene Derivatives. *J. Am. Chem. Soc*. **2015**, *137*, 3454−3457.

[18] Iosub, A. V.; Stahl, S. S. Catalytic Aerobic Dehydrogenation of Nitrogen Heterocycles Using Heterogeneous Cobalt Oxide Supported on Nitrogen-Doped Carbon. *Org. Lett*. **2015**, *17*, 4404−4407.

[19] Kandukuri, S. R.; Oestreich, M. Aerobic Palladium(II)-Catalyzed Dehydrogenation of Cyclohexene-1- carbonyl Indole Amides: An Indole-Directed Aromatization. *J. Org. Chem*. **2012**, *77*, 8750−8755.

[20] Ballini, R.; Castagnani, R.; Petrini, M. Chemoselective Synthesis of Functionalized Conjugated Nitroalkenes. *J. Org. Chem*. **1992**, *57*, 2160-2162.

[21] Chandrasekhar, S.; Shrinidhi, A. Useful Extensions of the Henry Reaction: Expeditious Routes to Nitroalkanes and Nitroalkenes in Aqueous Media. *Synthetic Commun.* **2014**, *44*, 3008-3018.
[22] Ahmadi, R.; Emami, S. Recent applications of vinyl sulfone motif in drug design and discovery. *Eur. J. Med. Chem.* **2022**, *234*, 114255.
[23] Iosub, A. V.; Stahl, S. S. Palladium-Catalyzed Aerobic Dehydrogenation of Cyclic Hydrocarbons for the Synthesis of Substituted Aromatics and Other Unsaturated Products. *ACS Catal.* **2016**, *6*, 8201−8213.
[24] Dighe, S. U.; Julia, F.; Luridiana, A.; Douglas, J. J.; Leonori, D. A photochemical dehydrogenative strategy for aniline synthesis. *Nature* **2020**, *584*, 75-81.
[25] Corpas, J.; Caldora, H. P.; Di Tommaso, E. M.; Hernandez-Perez, A. C.; Turner, O.; Azofra, L. M.; Ruffoni, A.; Leonori, D. A general strategy for the amination of electron-rich and electron-poor heteroaromatics by desaturative catalysis. *Nat. Catal.* **2024**, *24*.
[26] Müller, T. E.; Hultzsch, K. C; Yus, M.; Foubelo, F.; Tada, M. Hydroamination: Direct Addition of Amines to Alkenes and Alkynes. *Chem. Rev.* **2008**, *108*, 3795–3892.
[27] Trowbridge, A.; Walton, S. M.; Gaunt, M. J. New Strategies for the Transition-Metal Catalyzed Synthesis of Aliphatic Amines. *Chem. Rev*. **2020**, *120*, 2613−2692.
[28] Pozhydaiev, V.; Vayer, M.; Fave, C.; Moran, J.; Lebœuf, D. Synthesis of Unprotected β-Arylethylamines by Iron(II)-Catalyzed 1,2-Aminoarylation of Alkenes in Hexafluoroisopropanol. *Angew. Chem. Int. Ed*. **2023**, *62*, e202215257.
[29] Enamines, Synthesis: Structure, and Reactions, Second Edition; Cook G., Ed.; Marcel Dekker, Inc., New York, NY, 1988.
[30] Dank, C.; Ielo, L. Recent advances in the accessibility, synthetic utility, and biological applications of aziridines. *Org. Biomol. Chem*. **2023**, *21*, 4553–4573.

APPENDIX A

A STRATEGY FOR THE CONTROLLABLE GENERATION OF ORGANIC SUPERBASES FROM BENCHTOP-STABLE SALTS

I. General Information

General Reagent Information: *tert*-Butylimino-tri(pyrrolidino)phosphorane (BTPP), 1-*tert*-butyl-2,2,4,4,4-pentakis(dimethylamino)-2λ^5,4λ^5-catenadi(phosphazene) (P_2-*t*-Bu) and 1-ethyl-2,2,4,4,4-pentakis(dimethylamino)-2λ^5,4λ^5-catenadi(phosphazene) (P_2-Et) were purchased from Millipore Sigma (products #79432, #79416 and #79417, respectively) and were stored in a -30 °C freezer inside a nitrogen-filled glovebox. Before use, the superbases were allowed to warm to room temperature (rt) and homogenize if any solid was evident. Tetrahydrofuran and toluene were deoxygenated and dried by passage over packed columns of neutral alumina and copper (II) oxide under positive pressure of nitrogen. The following solvents were purchased anhydrous from Millipore Sigma and used as received: dimethyl sulfoxide (#276855), *N*,*N*-dimethylformamide (#227056), 1,4-dioxane (#296309), and acetonitrile (#271004). *t*-BuXPhosPdG3 (#762229) and *t*-BuBrettPhosPdG3 (#745979) were purchased from Millipore Sigma and used as received. Deoxybenzoin was purchased from Combi-Blocks (#QE-4078) and recrystallized from ethanol before use. *N*-(Diphenylmethylene)glycine *tert*-butyl ester was purchased from Oakwood Chemical (#050237) and recrystallized from hexanes before use. 4-Nitrobenzaldehyde was

purchased from Combi-Blocks (#AN-3207) and recrystallized from 1:1 EtOH/H_2O before use. 4-Ethoxycarbonylmethylphenylboronic acid, pinacol ester was purchased from Combi-Blocks (#PN-8932) and was purified by silica gel chromatography (5% EtOAc in hexanes) before use. 2-(4-Aminophenyl)acetonitrile was purchased from Ambeed (#A913458) and purified by silica gel chromatography (40% EtOAc in hexanes) before use. All other reagents were purchased from Millipore Sigma, Combi-Blocks, Ambeed, Oakwood Chemical, TCI, Acros Organics, Matrix, or Alfa Aesar and used as received. Flash Chromatography was performed on 40-63 μm silica gel (SiliaFlash® F60 from Silicycle).

General Analytical Information: All new compounds were characterized by ^{1}H, ^{13}C, ^{19}F and ^{31}P (as appropriate) NMR spectroscopy, FTIR spectroscopy, mass spectrometry, and melting point analysis (if solid). NMR spectra were obtained on a Bruker Advanced NEO or Varian Inova 400 MHz spectrometer. ^{1}H NMR data is reported as follows: chemical shift (δ ppm), multiplicity (s = singlet, d = doublet, t = triplet, q = quartet, dd = doublet of doublets, td = triplet of doublets, ddd = doublet of doublet of doublets, m = multiplet), coupling constant (Hz), and integration. ^{13}C NMR data is reported as follows: chemical shift (δ ppm), multiplicity (if applicable, d = doublet, q = quartet). All ^{1}H and ^{13}C NMR signals are reported as chemical shifts (δ ppm) relative to residual solvent peaks of the deuterated NMR solvents. ^{31}P NMR data is reported in reference to 85% phosphoric acid as an external standard with delay time of 2 s. For comparison between multiple ^{31}P NMR experiments, triphenylphosphine oxide internal standard (set to δ 23.2 ppm) was used. All ^{31}P NMR data is reported as follows: chemical shift (δ ppm), multiplicity (if applicable, s = singlet, d = doublet). All ^{19}F NMR signals are reported as chemical shifts (δ ppm) in reference to an internal standard (fluorobenzene set to -112.96 ppm) and are not proton decoupled. High

resolution mass spectra (HRMS) were recorded on an Agilent 6210 TOF interfaced to a DART 100 or APCI source provided by Colorado State University's Materials and Molecular Analysis Center. Infrared spectra were recorded using a Thermo Scientific Nicolet iS-50 FTIR Spectrometer and reported as frequency of absorption (cm^{-1}). Melting point analyses were conducted using a Mel-Temp capillary melting point apparatus. Thin-layer chromatography analysis was performed on silica gel 60Å F254 plates (250 μm, SiliaPlate from Silicycle, #TLGR10014B-323) and interpreted using UV light (254 nm) and/or potassium permanganate stain. Preparatory thin layer chromatography purification was performed on silica gel 60 Å F254 (1000 μm, SiliaPlate from Silicycle, #TLGR10011B-341) and interpreted using UV light (254 nm). Gel permeation chromatography (GPC) was used to analyze number (M_n) and weight (M_w) average molecular weights and dispersity index of polymers. GPC data was obtained using an Agilent 1260 II instrument equipped with an Agilent HPLC system one guard column and two PLgel 5 μm mixed-C gel permeation columns and coupled with a Wyatt DAWN HELEOS II multi (18)-angle light scattering detector, a Wyatt Optilab TrEX dRI detector, and a Wyatt Viscostar III viscometer.

Note on nomenclature: The names provided for the structures below were obtained from ChemDraw Professional 20.0.

Abbreviations: List of abbreviations used in this document.

BTPP salt **A** = 1-phenyl-1-cyclopropanecarboxylate *tert*-butylimino-tri(pyrrolidino)phosphorane

BTPP salt **B** = 2-cyclohexylphenylacetate *tert*-butylimino-tri(pyrrolidino)phosphorane

P_2-*t*-Bu salt **A** = 2-methyl-phenylpropionate 1-*tert*-butyl-2,2,4,4,4-pentakis(dimethylamino)-2λ^5,4λ^5-catenadi(phosphazene)

P_2-*t*-Bu salt **B** = 1-(4-fluorophenyl)cylohpentanecarboxylate 1-*tert*-butyl-2,2,4,4,4-pentakis(dimethylamino)-2λ^5,4λ^5-catenadi(phosphazene)

Me = methyl

Et = ethyl

t-Bu = *tert*-butyl

n-Bu = *n*-butyl

Ph = phenyl

Bn = benzyl

PMP = *para*-methoxyphenyl

Ar = aryl

Ts = *p*-toluenesulfonyl

h = hour

min = minute

s = second

rt = room temperature

II. Superbase Salt Synthesis

a. Identification of a crystalline carboxylate salt for BTPP

We investigated a series of carboxylic acids to identify one that forms a solid, shelf-stable salt with the BTPP superbase (representative examples shown in Figure S1). This led to identification of 1-phenyl-1-cyclopropanecarboxylic acid that forms a stable salt with BTPP, labeled as BTPP salt **A**.

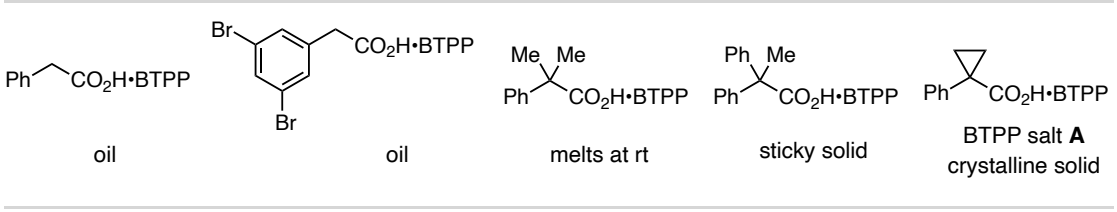

Figure S1: BTPP•carboxylic acid salts examined to identify a solid salt.

Carboxylate Salt Testing Procedure: An oven-dried 1-dram vial (ThermoFisher, C4015-1) was charged with a magnetic stir bar, carboxylic acid (0.25 mmol, 1.0 equiv) and brought into a nitrogen-filled glovebox. Diethyl ether (0.5 mL, 0.5 M) and BTPP (78.1 mg, 0.25 mmol, 1.0 equiv) were added to the vial. The vial was capped with a PTFE-lined cap (ThermoFisher, C4015-1A), removed from the glovebox, and stirred for 2 h at 25 °C. The solutions were concentrated *in vacuo*, then placed under high vacuum for drying. The physical state of each salt was then evaluated visually and with agitation using a spatula. Representative results are shown in Figure S1 above.

b. Synthesis of BTPP Salt A from commercial BTPP freebase

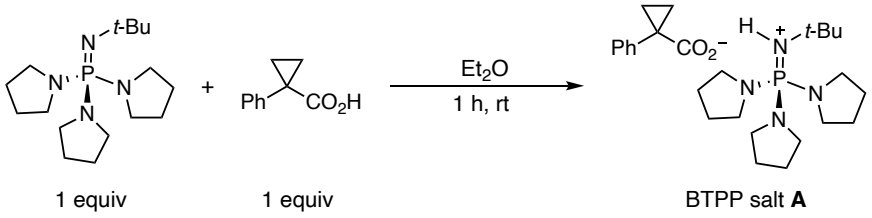

Procedure: An oven-dried 250 mL round bottom flask was charged with a magnetic stir bar, 1-phenyl-1-cyclopropanecarboxylic acid (811.0 mg, 5 mmol, 1.0 equiv) and diethyl ether (10 mL, 0.5 M). In a nitrogen-filled glovebox an oven-dried 20 mL scintillation vial (ThermoFisher, 03-341-25D) was charged with BTPP (1.56 g, 5 mmol, 1.0 equiv) and diluted with diethyl ether (10 mL). The vial was capped and removed from the glovebox. The vial containing BTPP was uncapped, and the solution was added *via* pipette to the stirring solution of 1-phenyl-1-cyclopropanecarboxylic acid. The reaction mixture was stirred for 1 hour at rt. The reaction solution was concentrated, and the resulting crystalline solid was washed with cold diethyl ether, dried *in vacuo*, and collected as a white powder (2.01 g, 4.24 mmol, 85% yield). **^{1}H NMR** (400 MHz, $CDCl_3$) δ 7.84 (d, *J* = 10.2 Hz, 1H), 7.33 (d, *J* = 7.5 Hz, 2H), 7.10 (t, *J* = 7.5 Hz, 2H), 6.99 (t, *J* = 7.5 Hz, 1H), 3.17 – 3.08 (m, 12H), 1.83 – 1.71 (m, 12H), 1.36 (q, *J* = 3.2 Hz, 2H), 1.23 (s, 9H), 0.74 (q, *J* = 3.2 Hz, 2H). **^{31}P NMR** (162 MHz, $CDCl_3$) δ 22.5 (s). **^{13}C NMR** (101 MHz, $CDCl_3$) δ 177.2, 146.1, 130.4, 127.1, 124.6, 52.0 (d, *J* = 2.0 Hz), 47.4 (d, *J* = 5.1 Hz), 31.7, 31.3 (d, *J* = 4.9 Hz), 26.0 (d, *J* = 8.0 Hz), 14.1. **IR (neat)** 2963, 2862, 2812, 1585, 1443, 1343, 1199, 1065, 984, 740 cm^{-1}. **HRMS (DART)** $[M]^+$ calcd. for $[C_{16}H_{34}N_4P]^+$ (for protonated phosphazene) = 313.2521, found 313.2533. **MP** 100 – 103 °C.

c. Synthesis of BTPP salt A from phosphorus pentachloride

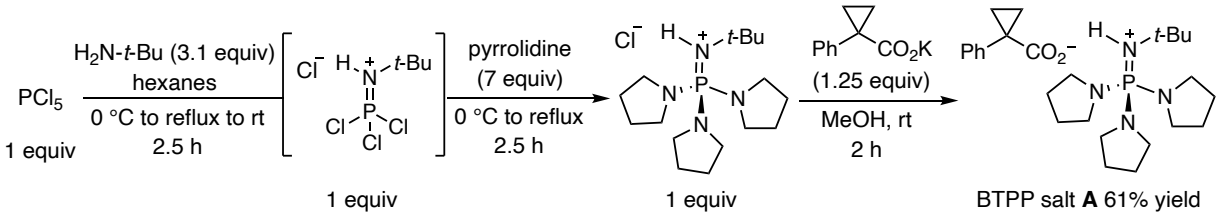

***tert*-Butyliminotri(pyrrolidino)phosphorane • hydrogen chloride**. Phosphorus pentachloride and *tert*-butylphosphorimidoyl trichloride are air and moisture sensitive; care was taken to exclude ambient air and moisture for the following procedure. In a nitrogen-filled glovebox, an oven-dried 1000 mL round bottom flask was charged with a magnetic stir bar and PCl_5 (15.6 g, 75 mmol, 1.0 equiv). The flask was capped with a rubber septum, removed from the glovebox, and connected to a nitrogen-flushed reflux condenser with a positive pressure of nitrogen. Hexanes (250 mL, 0.3 M) was added *via* nitrogen-flushed syringe. The solution was cooled to 0 °C in an ice bath with stirring and *tert*-butylamine (24.4 mL, 233 mmol, 3.1 equiv) was added dropwise *via* nitrogen-flushed syringe. The reaction solution was stirred for 30 min at 0 °C. The solution was warmed to rt, placed in an oil bath, and refluxed at 70 °C for 2 h. The reaction flask was removed from the oil bath, cooled to rt, and then cooled to 0 °C in an ice bath. Pyrrolidine (43.1 mL, 525 mmol, 7.0 equiv) was added *via* nitrogen-flushed syringe and stirred for 30 min at 0 °C. The solution was warmed to rt, placed in an oil bath, and refluxed at 70 °C for 2 h. The reaction flask was removed

from the oil bath and cooled to rt. Water (400 mL) was added and the resulting mixture was transferred to a separatory funnel, then washed with ethyl acetate (2 x 200 mL). The aqueous layer was then extracted with dichloromethane (3 x 150 mL). The combined dichloromethane layers were washed with brine (150 mL), dried over Na_2SO_4, then concentrated *in vacuo* to yield mostly pure BTPP•HCl. **^{1}H NMR** (400 MHz, $CDCl_3$) δ 6.51 (d, *J* = 9.5 Hz, 1H), 3.28 – 3.19 (m, 12H), 1.88 – 1.79 (m, 12H), 1.31 (s, 9H). **^{31}P NMR** (162 MHz, $CDCl_3$) δ 22.3 (s). **^{13}C NMR** (101 MHz, $CDCl_3$) δ 47.7 (d, *J* = 5.1 Hz), 31.5 (d, *J* = 4.6 Hz), 26.1 (d, *J* = 8.1 Hz).

BTPP salt A. An oven-dried 250 mL round bottom flask was charged with a magnetic stir bar, the crude BTPP•HCl salt (assumed to be 75 mmol) from above and MeOH (100 mL). Potassium 1-phenyl-1-cyclopropanecarboxylate (18.78 g, 93.75 mmol, 1.25 equiv) was added. The solution was stirred at rt for 2 h. The methanol was then removed *in vacuo*. The crude residue was placed in a filter and washed with EtOAc under vacuum to obtain a yellow solution. The filtrate was then concentrated and dried *in vacuo*. The yellow oil solidified under vacuum drying. The solid was then recrystallized from a minimal amount of hot ethyl acetate with hexanes layered over the solution to afford BTPP salt **A** as a colorless, crystalline solid (21.7 g, 45.6 mmol, 61% yield). **^{1}H NMR** (400 MHz, $CDCl_3$) δ 7.84 (d, *J* = 10.2 Hz, 1H), 7.33 (d, *J* = 7.5 Hz, 2H), 7.10 (t, *J* = 7.5 Hz, 2H), 6.99 (t, *J* = 7.5 Hz, 1H), 3.17 – 3.08 (m, 12H), 1.83 – 1.71 (m, 12H), 1.36 (q, *J* = 3.2 Hz, 2H), 1.23 (s, 9H), 0.74 (q, *J* = 3.2 Hz, 2H). **^{31}P NMR** (162 MHz, $CDCl_3$) δ 22.5 (s). **^{13}C NMR** (101 MHz, $CDCl_3$) δ 177.2, 146.1, 130.4, 127.1, 124.6, 52.0 (d, *J* = 2.0 Hz), 47.4 (d, *J* = 5.1 Hz), 31.7, 31.3 (d, *J* = 4.9 Hz), 26.0 (d, *J* = 8.0 Hz), 14.1. Characterization data matches BTPP salt **A** synthesized in Section IIb.

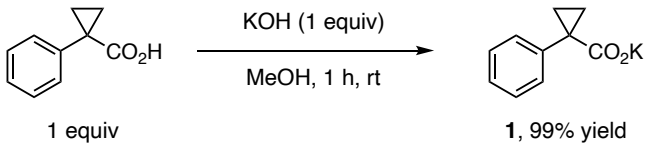

Potassium 1-phenyl-1-cyclopropanecarboxylate preparation (1). An oven-dried 500 mL round 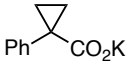 bottom flask was charged with a magnetic stir bar, 1-phenyl-1-cyclopropanecarboxylic acid (51.8 g, 319.3 mmol, 1.0 equiv) and MeOH (200 mL). An oven-dried 250 mL Erlenmeyer flask was charged with KOH (85%) (20.6 g, 319.3 mmol, 1.0 equiv) and solubilized with a minimal amount to MeOH (~50 mL). The KOH/MeOH solution was added dropwise to the stirring acid/MeOH solution. The round bottom flask was capped with a rubber septum and the combined solution was stirred for 1 h at rt. The MeOH was removed *in vacuo*, PhMe (150 mL) was added and removed *in vacuo* three times. The white solid was filtered and washed with ethyl acetate. The solid was collected and dried *in vacuo* to afford **1** as a white powder (63.2 g, 316.1 mmol, 99% yield). **^{1}H NMR** (400 MHz, DMSO-d_6) δ 7.21 (d, J = 8.1 Hz, 2H), 7.14 (t, J = 7.4 Hz, 2H), 7.03 (t, J = 7.1 Hz, 1H), 1.16 – 1.09 (m, 2H), 0.62 – 0.56 (m, 2H). **^{13}C NMR** (101 MHz, DMSO-d_6) δ 175.4, 146.6, 130.6, 127.4, 124.9, 31.7, 13.9. **IR (neat)** 3305, 3050, 1561, 1383, 700 cm^{-1}. **HRMS (DART)** $[RCO_2H+NH_4]^+$ calcd. for $[C_{10}H_{14}NO_2]^+$ = 180.1019, found 180.1027. **MP** 170 – 175 °C.

c. Identification of a crystalline carboxylate salt for P$_2$-*t*-Bu

We found that a solid salt does not form between 1-phenyl-1-cyclopropanecarboxylic acid and P_2-*t*-Bu, but with a slight modification to the carboxylate structure, 2-methyl-1-phenylpropanecarboxylic acid forms a solid salt with P_2-*t*-Bu to give P_2-*t*-Bu salt **A**.

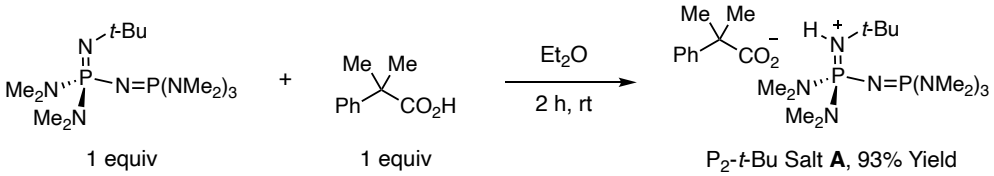

Procedure: An oven-dried 250 mL round bottom flask was charged with a magnetic stir bar, 2-methyl-2-phenylpropionic acid (1.6 g, 10 mmol, 1.0 equiv) and diethyl ether (50 mL, 0.2 M). In a nitrogen-filled glovebox, an oven-dried 20 mL scintillation vial (ThermoFisher, 03-341-25D) was charged with P_2-*t*-Bu (5 mL of a 2M THF solution, 10 mmol, 1.0 equiv) and diluted with diethyl ether (10 mL). The vial was capped and removed from the glovebox. The vial containing P_2-*t*-Bu dissolved in diethyl ether was uncapped and the solution was added slowly *via* pipette to the stirring solution of 2-methyl-2-phenylpropionic acid. The reaction solution was stirred for 2 h at rt. The reaction mixture was concentrated *in vacuo*, and the resulting crystalline solid was washed with 10 mL of cold diethyl ether, dried *in vacuo*, and collected as a white powder (4.9 g, 9.3 mmol, 93% yield). **^{1}H NMR** (400 MHz, $CDCl_3$) δ 7.56 (d, *J* = 7.7 Hz, 2H), 7.17 (t, *J* = 7.7 Hz, 2H), 7.02 (t, *J* = 7.7 Hz, 2H), 6.19 (d, *J* = 12.8 Hz, 1H)2.67 – 2.37 (m, 30H), 1.56 (s, 6H), 1.25 (s, 9H). **^{31}P NMR** (162 MHz, $CDCl_3$) δ 16.2 (d, *J* = 67.4 Hz, 1P), 12.2 (d, *J* = 67.4 Hz, 1P). **^{13}C NMR** (101 MHz, $CDCl_3$) δ 180.0, 150.9, 127.2, 126.6, 124.2, 48.2, 37.2 (d, *J* = 5.7 Hz), 37.0 (d, *J* = 5.0 Hz), 31.2, 28.5. **IR (neat)** 2910, 2850, 2812, 1592, 1572, 1456, 1331, 1292, 1182, 979 cm^{-1}. **HRMS**

(DART) $[M]^+$ calcd. for $[C_{14}H_{43}N_8P_2]^+$ (for protonated phosphazene) = 368.2854, found 368.2767.

MP 95 – 100 °C.

d. Discussion of the storage of superbase salts

The superbase salts were stored in 20 mL scintillation vials both in a benchtop desiccator and a freezer at -30 °C. The salts were regularly used and handled open-to-air for the studies described in the Article and detailed below, for both activation experiments and reaction applications. Additionally, once per week the salts were removed from the benchtop desiccator, uncapped, and mixed around with a metal spatula to mimic usage. No difference in the performance of the superbase salts stored in each of these environments was observed. See Section VIII for a more detailed description of the long-term stability of these superbases salts in a variety of environments and for development of less hygroscopic BTPP and P_2-*t*-Bu salts.

III. BTPP Salt A Activation Studies

In this section, we discuss the investigation of epoxide additives that, when added to solution with BTPP salt **A**, facilitate the generation of BTPP with formation of an alcohol activation byproduct. For these activation studies, we tested a series of aryl-substituted epoxides under various conditions and assessed the formation of BTPP and the tertiary alcohol byproduct by ^{31}P and ^{1}H NMR spectroscopy (Figure S3 and S4, respectively), measured in DMSO-d_6. When analyzing the protonation state of BTPP in an activation study by ^{31}P NMR spectroscopy, the proton exchange rate between the free and protonated BTPP is slower than the NMR timescale. This leads to the observation of two peaks, one at 20 ppm that corresponds to protonated BTPP and one at -10 ppm that corresponds to neutral BTPP. By comparing the ratio of the integrals of the two signals, we are able to estimate the percentage of the freebase; we note that this amount typically correlates

closely (□ 5%) with the amount of the alcohol activation byproduct formed, determined by ^{1}H NMR spectroscopy. Figure S2 below shows titration experiments of different ratios of BTPP freebase to protonated base both with and without the alcohol activation byproduct present. For each sample, we measured the relative integration between protonated and neutral BTPP peaks. In each case, this ratio matches the ratio of BTPP:BTPP salt **A** that was premixed for the experiment. At the end of this section, Figures S3 and S4 show example ^{31}P and ^{1}H NMR spectra (measured in DMSO-d_6) respectively, to demonstrate how we assess the amount of freebase and byproduct formed in an activation study.

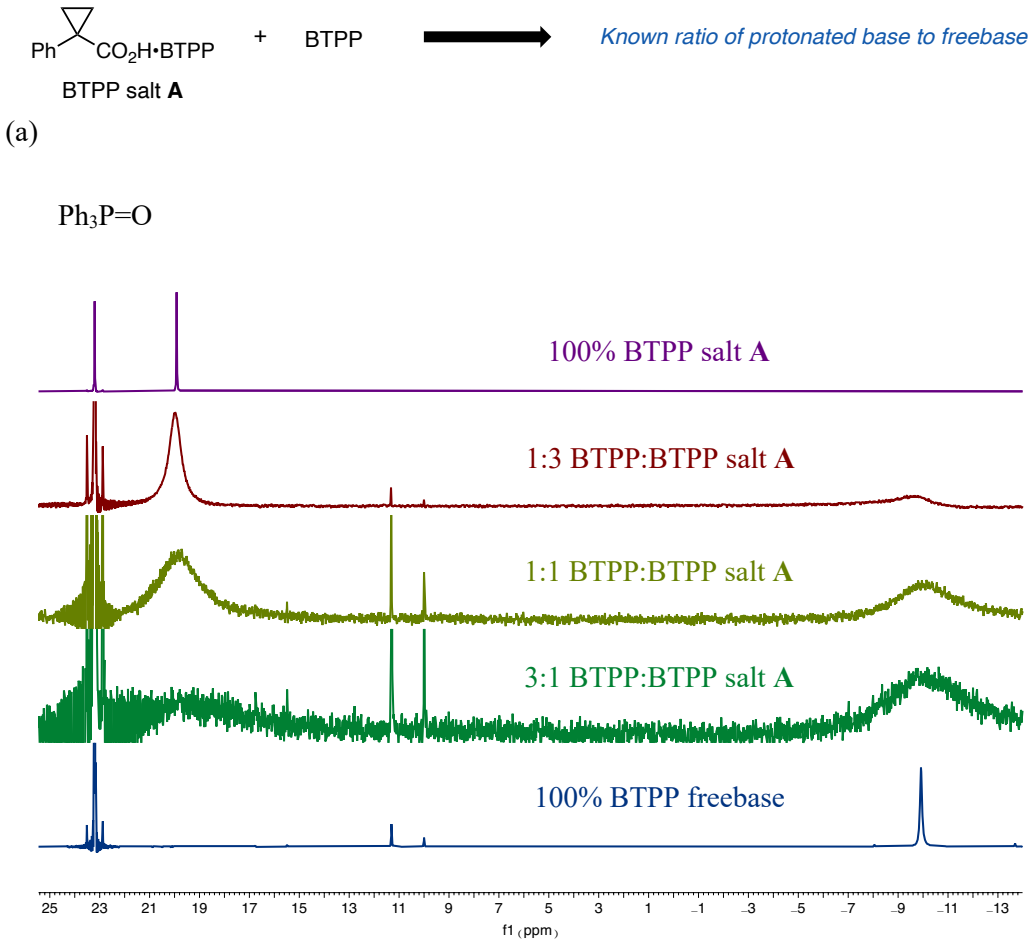

(b)

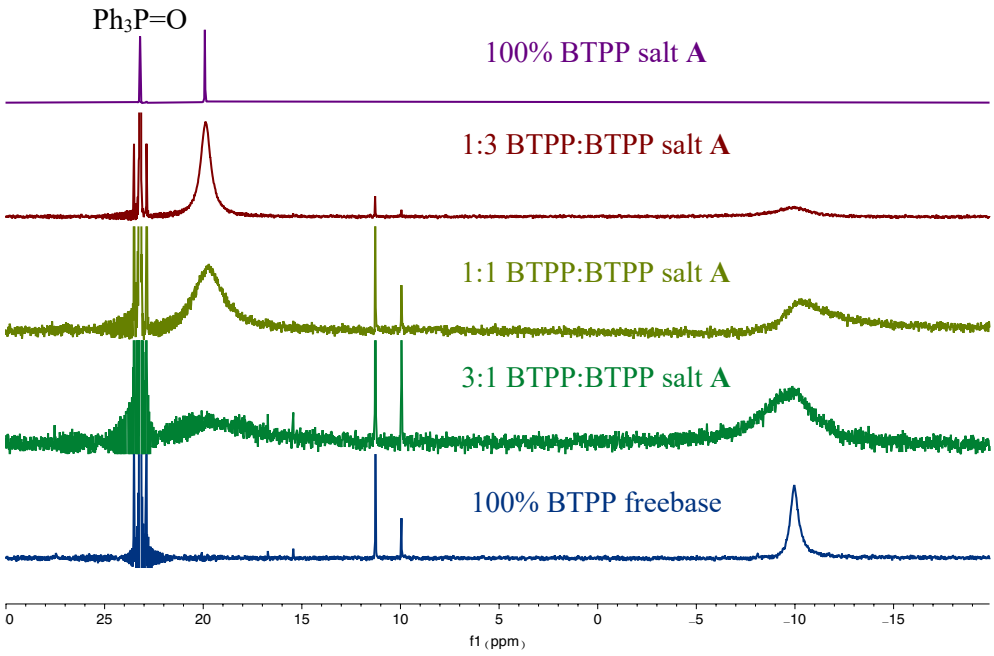

Figure S2: (a) ^{31}P NMR spectra of BTPP and BTPP salt **A** mixed in various ratios in DMSO-d_6. (b) ^{31}P NMR spectra of BTPP and BTPP salt **A** in various ratios with 1.0 equiv alcohol activation byproduct **62** present in DMSO-d_6. Signals at 10 to 12 ppm correspond to decomposed BTPP and the resulting phosphoramide. The peak at 23.2 ppm corresponds to triphenylphosphine oxide (Ph_3P=O) internal standard.

a. General activation procedure and analysis for BTPP salt A activation studies

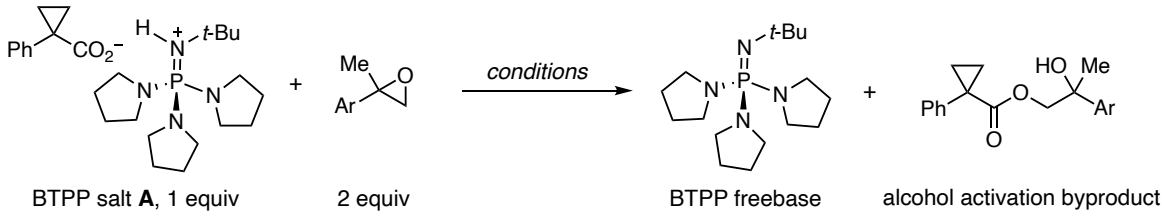

BTPP salt **A**, 1 equiv | 2 equiv | BTPP freebase | alcohol activation byproduct

General Procedure A: Activation studies for BTPP salt A. Note: these control activation studies were carried out under nitrogen atmosphere and in deuterated solvents. An oven-dried 1-dram vial (ThermoFisher, C4015-1) was charged with a magnetic stir bar and BTPP salt **A** (23.7 mg, 0.05 mmol, 1.0 equiv). The vial was brought into a nitrogen-filled glovebox where deuterated solvent (0.1 mL, 0.5 M) and epoxide additive (0.1 mmol, 2.0 equiv) were added. The reaction vial was capped with a PTFE-lined cap (ThermoFisher, C4015-1A), removed from the glovebox, and placed in a preheated aluminum reaction block with stirring for the indicated time. The vial was then taken into a nitrogen-filled glovebox where the solution was diluted with additional deuterated solvent (0.4 mL, total of 0.5 mL), transferred to an NMR tube, which was then capped and sealed with parafilm wax. ^{31}P NMR and ^{1}H NMR spectroscopy were used to assess each reaction and determine the percentage of freebase and alcohol activation byproduct, respectively.

Example of percent freebase assessment. Below is a representative example of an activation study using BTPP salt **A** and epoxide **2** in DMSO-d_6. The reaction was set up using General Procedure A and Figure S3 shows a ^{31}P NMR spectrum of a time point taken at 45 min. Based on the ratio of the protonated superbase to the freebase, we assess this activation reaction to be 53% generation of BTPP. We also analyze the results of the activation studies by ^{1}H NMR spectroscopy where we can observe the presence of the alcohol activation byproduct, which shows characteristic peaks (two doublets) at 4.0 – 4.5 ppm. In all cases, the amount of the activation byproduct (analyzed by ^{1}H NMR spectroscopy) correlates with the amount of freebase formed (analyzed by ^{31}P NMR spectroscopy). Therefore, we can also use ^{1}H NMR spectroscopy to reliably assess the amount of freebase produced in an activation study. In this study, we assessed the amount of the

activation byproduct in relation to the BTPP methylene peak at 3.12 ppm and determined a 52% yield, which correlates to the amount of freebase determined by ^{31}P NMR spectroscopy.

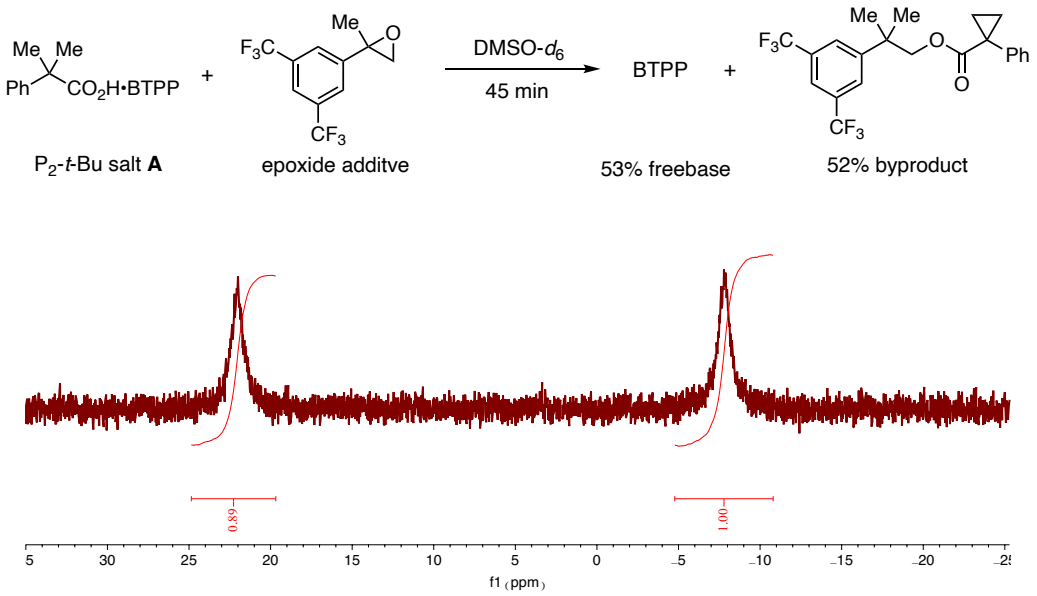

Figure S3: Example ^{31}P NMR spectrum from above activation reaction of BTPP salt A and epoxide **2** at 45 min in DMSO-d_6. The peak at 22 ppm corresponds to protonated BTPP and the peak at -7.8 ppm corresponds to BTPP freebase. Based on the integration values on the spectrum, we assess activation to be 53% generation of BTPP freebase.

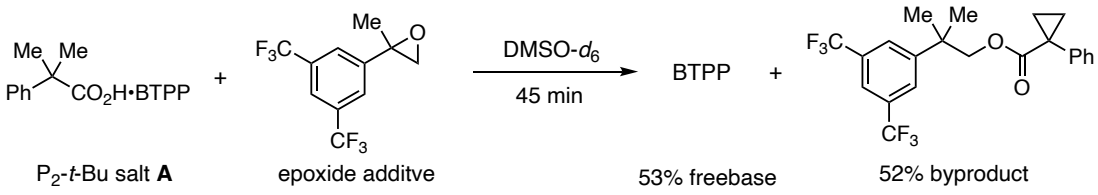

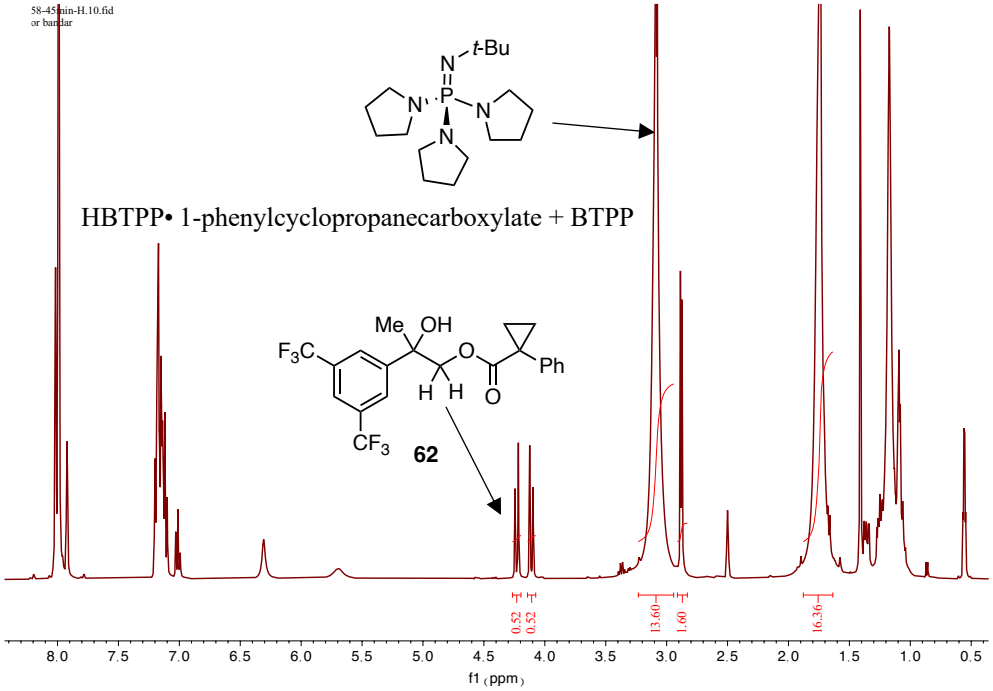

Figure S4: Example ^{1}H NMR spectrum from above activation reaction of BTPP salt A and epoxide **2** at 45 min in DMSO-d_6. The peaks at 4.1 and 4.25 ppm correspond to the methylene protons of alcohol activation byproduct **62**. Based on integration with respect to the BTPP signal at 3.12 ppm, we assess activation to be 52% generation of alcohol activation byproduct **62**.

b. Activation studies of BTPP salt A under various conditions

Epoxide effects on BTPP freebase generation. General Procedure A was followed using epoxides **2**-**4**. Each time point was obtained from an individual reaction set up and stopped at the indicated time *via* dilution with DMSO-d_6.

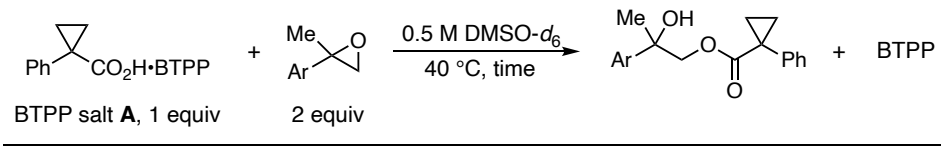

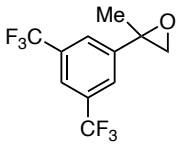

2

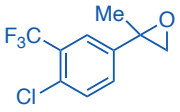

3

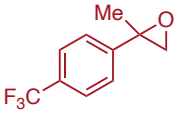

4

Table S1: Amount of BTPP freebase generated over time by epoxides **2**, **3** and **4**.

Entry	**Time (min)**	**Estimated % BTPP Freebase**		
		Epoxide 2	**Epoxide 3**	**Epoxide 4**
1	0	0	0	0
2	5	17	7	0
3	15	31	13	2.5
4	45	53	28	5
5	90	70	40	10
6	240	93	69	30

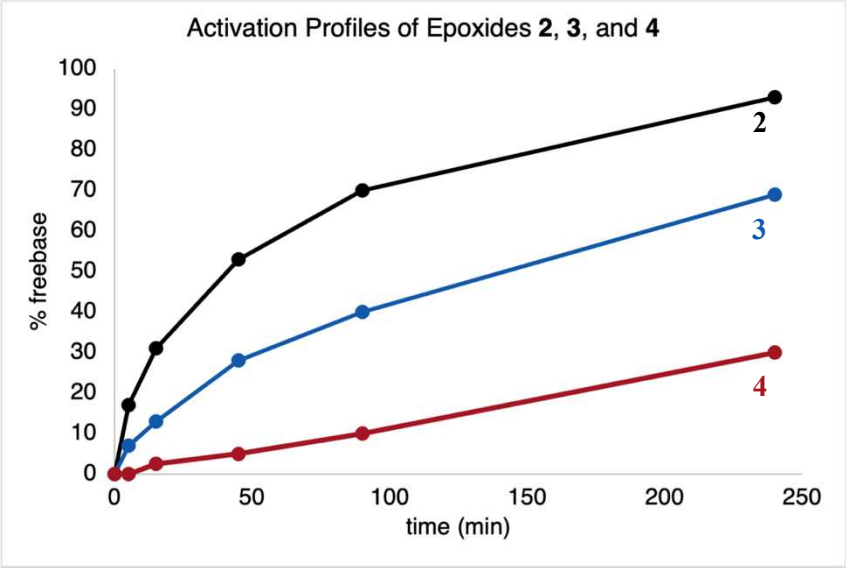

Figure S5: Activation curves for BTPP salt **A** using epoxides **2** (black curve), **3** (blue curve) and **4** (red curve).

Solvent-dependent BTPP freebase generation. General Procedure A was followed using BTPP salt **A** and epoxide **2**. Each time point was obtained from an individual reaction set up and stopped at the indicated time *via* dilution with deuterated solvent (DMSO-d_6, CD_3CN, THF-d_8 or PhMe-d_8). Note: for reactions run in CD_3CN, the ^{31}P NMR spectra have baselines with too much noise for reliable integration for percent freebase determination, likely due to low solubility of BTPP in MeCN. Therefore, in these cases, ^{1}H NMR spectroscopy was used to determine the amount of freebase by analyzing the amount of activation byproduct **62** formed in the reaction.

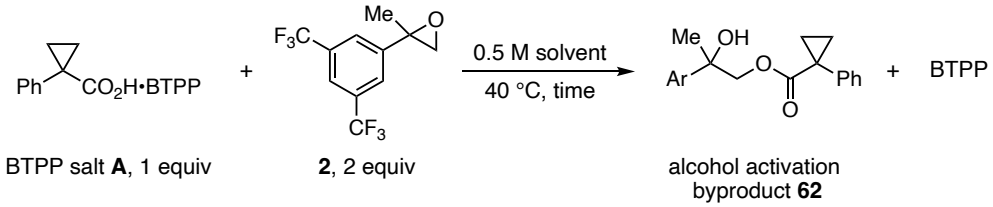

Table S2: Amount of BTPP freebase generated over time in DMSO-d_6, CD_3CN, THF-d_8 and PhMe-d_8 using BTPP salt **A** and epoxide **2**.

Entry	Time (min)	Estimated % BTPP Freebase			
		DMSO-d_6	CD_3CN	THF-d_8	PhMe-d_8
1	0	0	0	0	0
2	5	17	10	24	24
3	15	31	15	39	32
4	45	53	25	60	44
5	90	70	50	76	54
6	240	93	55	93	73

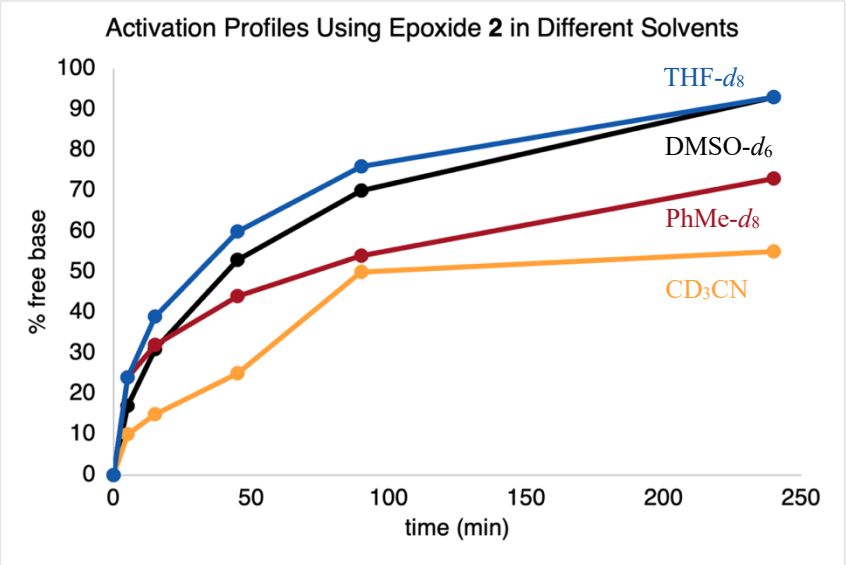

Figure S6: Activation curves in DMSO-d_6 (black curve), CD_3CN (orange curve), THF-d_8 (blue curve), and PhMe-d_8 (red curve) using BTPP salt **A** and epoxide **2**.

Temperature-dependent BTPP freebase generation. General Procedure A was followed using BTPP salt **A** and epoxide **2**. Each time point was obtained from an individual reaction set up and stopped at the indicated time *via* dilution with DMSO-d_6.

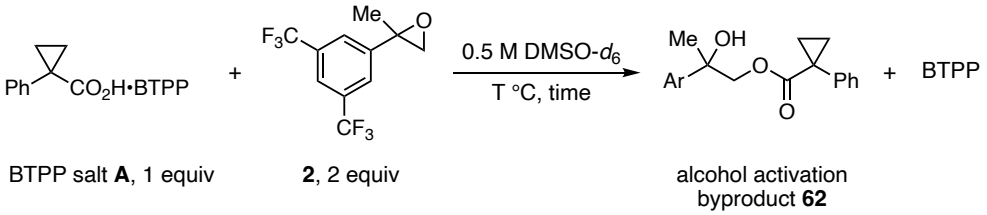

Table S3: Amount of BTPP freebase generated over time at 25, 40, 60, and 80 °C using BTPP salt **A** and epoxide **2**.

Entry	Time (min)	Estimated % BTPP Freebase			
		25 °C	40 °C	60 °C	80 °C
1	0	0	0	0	0
2	5	11	17	60	99
3	15	17	31	85	99
4	45	29	53	99	99
5	90	40	70	99	99
6	240	64	93	99	99

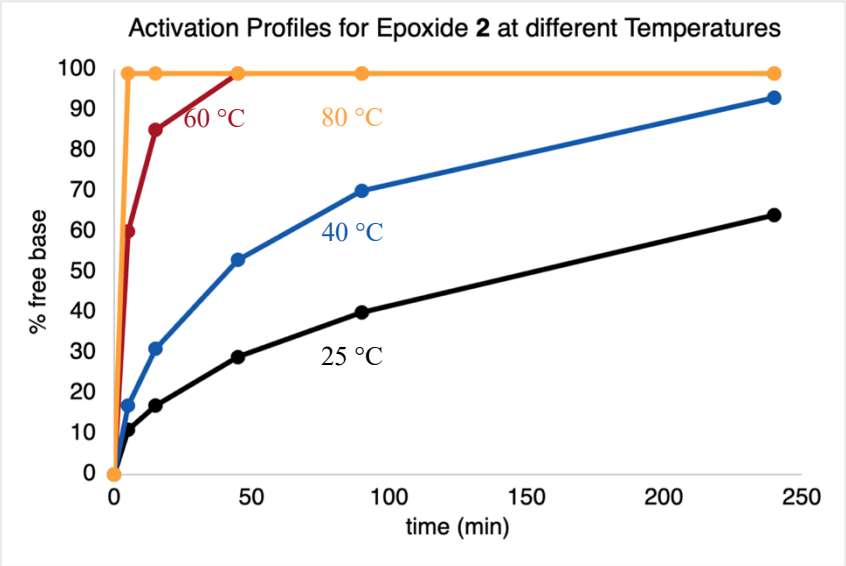

Figure S7: Activation curves at 25 (black curve), 40 (blue curve), 60 (red curve), and 80 °C (orange curve) using BTPP salt **A** and epoxide **2**.

IV. Applications of BTPP Salt A and Epoxides as Precatalyst Systems

a. Use of BTPP salt A as a precatalyst for Michael, aldol, and Mannich reactions

i. Reaction scheme and General Procedures

Table S4: Example substrates of addition reactions using BTPP salt **A** and epoxide **2**. General Procedure C was followed for BTPP freebase yields.

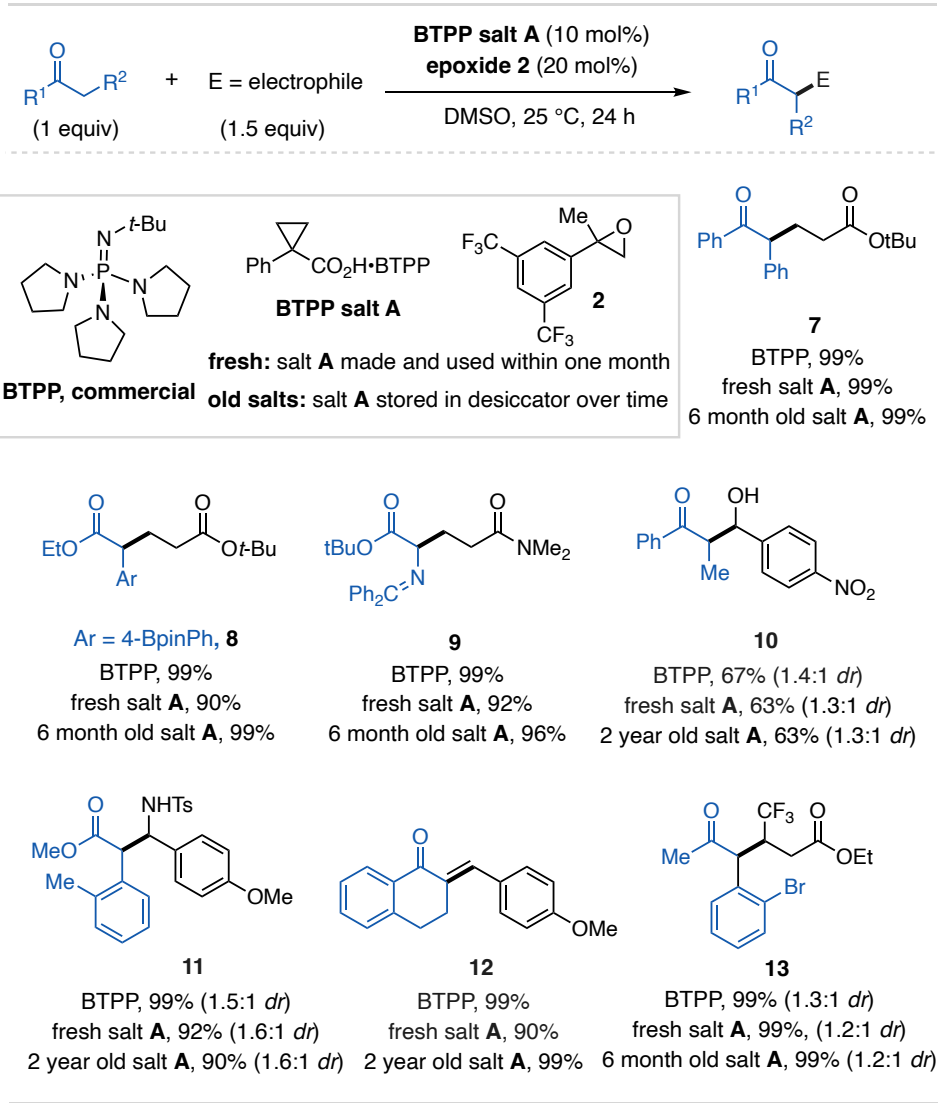

General Procedure B: BTPP salt A and epoxide 2 promoted reaction. An oven-dried 1-dram vial (ThermoFisher, C4015-1) was charged with a magnetic stir bar and BTPP salt **A** (47.5 mg, 0.1 mmol, 10 mol%). The vial was sealed with a PTFE lined screw cap (ThermoFisher, C4015-A) and evacuated then flushed with nitrogen three times *via* a nitrogen inlet tube on a Schlenk manifold line. DMSO (2 mL, 0.5M), pronucleophile (1 mmol, 1.0 equiv), electrophile (1.5 mmol, 1.5 equiv), and epoxide **2** (ρ = 1.39 g/mL, 38.8 μL, 0.2 mmol, 20 mol%) were added to the vial *via* nitrogen-flushed microsyringe. **Note**: the pronucleophile and/or electrophile were charged to the vial prior to capping and nitrogen flushing if they are solids at rt. The reaction vial was left under a positive pressure of nitrogen and placed into an aluminum reaction block preheated to 25 °C with stirring for 24 h. Dibromomethane (35.1 mL, 0.5 mmol, 0.5 equiv) or 1,3,5-trimethoxybenzene (84.1 mg, 0.5 mmol, 0.5 equiv) internal standard was then added to the reaction solution, a 50 □L aliquot was taken and added to an NMR tube, then diluted with $CDCl_3$ (0.5 mL). ^1H NMR spectroscopy was used to determine the yield of the reaction.

ii. Reaction results and characterization data

General description: For all of the substrates in this section, we use ^1H NMR yields to assess the efficacy of the precatalyst salt system. In each case, we benchmarked the success of the precatalyst against the use of commercial BTPP and BTPP salt **A** that has been handled regularly open to air and stored in a benchtop desiccator for six months to two years (see Section VIII for details). The reactions carried out with commercial BTPP were set up in a nitrogen-filled glovebox, described in General Procedure C, and the reactions carried out with aged BTPP salt **A** were set up using

General Procedure B. The substrates were subsequently isolated from General Procedure B with fresh BTPP salt **A** for characterization. To do this, the crude reactions mixtures were directly subjected to flash column chromatography to yield purified products. The results of these experiments are summarized in Table S4 above. We note that these reactions are sensitive to water and therefore anhydrous DMSO must be used.

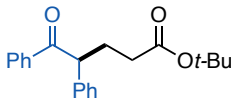

***tert*-butyl 5-oxo-4,5-diphenylpentanoate (7).** General Procedure B was followed using deoxybenzoin (196.2 mg, 1 mmol, 1.0 equiv), *tert*-butyl acrylate (219.7 µL, 1.5 mmol, 1.5 equiv), BTPP salt **A** (47.5 mg, 0.1 mmol, 10 mol%), and epoxide **2** (54.0 mg, 0.2 mmol, 20 mol%) in DMSO (2 mL) to provide 99% ^{1}H NMR yield. The reaction was repeated using commercial BTPP (99% ^{1}H NMR yield) and six-month-old BTPP salt **A** (99% ^{1}H NMR yield). Following General Procedure B, the product was purified *via* silica gel chromatography using 100% hexanes to 6% EtOAc/hexanes to afford **7** as a white solid (323.7 mg, 1 mmol, 100% yield). **^{1}H NMR** (400 MHz, $CDCl_3$) δ 7.95 (d, J = 8.3 Hz, 1H), 7.47 (t, J = 7.2 Hz, 1H), 7.38 (t, J = 7.6 Hz, 2H), 7.29 (d, J = 4.4 Hz, 4H), 7.24 – 7.18 (m, 2H), 4.68 (t, J = 7.2 Hz, 1H), 2.48 – 2.35 (m, 1H), 2.21 (t, J = 6.9 Hz, 2H), 2.18 – 2.07 (m, 1H), 1.43 (s, 9H). Characterization data matches literature reports.[1]

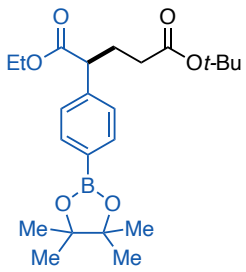

5-(*tert*-butyl) 1-ethyl 2-(4-(4,4,5,5-tetramethyl-1,3,2-dioxaborolan-2-yl)phenyl)pentanedioate (8). General Procedure B was followed using ethyl 2-(4-(4,4,5,5-tetramethyl-1,3,2-dioxaborolan-2-yl)phenyl)acetate (290.2 mg, 1 mmol, 1.0 equiv), *tert*-butyl acrylate (219.7 µL, 1.5 mmol, 1.5 equiv), BTPP

salt **A** (47.5 mg, 0.1 mmol, 10 mol%), and epoxide **2** (54.0 mg, 0.2 mmol, 20 mol%) in DMSO (2 mL) to provide 90% ^{1}H NMR yield. The reaction was repeated using commercial BTPP (99% ^{1}H NMR yield) and six-month-old BTPP salt **A** (99% ^{1}H NMR yield). Following General Procedure B, the reaction was purified *via* silica gel chromatography using 5% MeOH/DCM to afford **8** as a colorless oil (420.0 mg, 1 mmol, 100% yield). The silica gel used for this purification was dried in an oven (120 °C) for 24 hours before use; approximately 10% protodeboronation occurred during purification and we note this side product is not observed in ^{1}H NMR analysis of the crude reaction mixture. **^{1}H NMR** (400 MHz, $CDCl_3$) δ 7.76 (d, *J* = 7.5 Hz, 2H), 7.29 (d, *J* = 7.7 Hz, 2H), 4.20 – 4.01 (m, 2H), 3.66 – 3.54 (m, 1H), 2.38 – 2.23 (m, 1H), 2.15 (t, *J* = 7.6 Hz, 1H), 2.13 – 1.96 (m, 1H), 1.42 (s, 7H), 1.33 (s, 10H), 1.18 (t, *J* = 7.1 Hz, 2H). **^{13}C NMR** (101 MHz, $CDCl_3$) δ 173.4, 172.3, 135.3, 135.2, 128.8, 127.5, 83.9, 80.5, 61.0, 50.9, 33.2, 28.6, 28.2, 25.0, 14.2. **IR** (neat) 3061, 3026, 2971, 2932, 1926, 1677, 1367, 1158, 1142, 696 cm^{-1}. **HRMS (DART)** $[M+H]^+$ calcd. for $[C_{23}H_{36}BO_6]^+$ = 419.2599, found 419.2614. Note: peaks can be observed at 141.8 and 41.8 ppm in the ^{13}C NMR spectrum that correspond to protodeboronation of **8**.

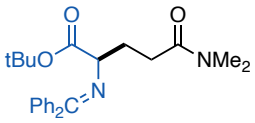

***tert*-butyl 5-(dimethylamino)-2-((diphenylmethylene)amino)-5-oxopentanoate (9).** General Procedure B was followed using *tert*-butyl 2-((diphenylmethylene)amino)acetate (295.4 mg, 1 mmol, 1.0 equiv), *N,N*-dimethylacrylamide (154.9 µL, 1.5 mmol, 1.5 equiv), BTPP salt **A** (47.5 mg, 0.1 mmol, 10 mol%), and epoxide **2** (54.0 mg, 0.2 mmol, 20 mol%) in DMSO (2 mL) to provide 92% ^{1}H NMR yield. The reaction was repeated using commercial BTPP (99% ^{1}H NMR yield) and six-month-old BTPP salt **A** (96% ^{1}H NMR yield). Following General Procedure B, the product was purified *via* silica gel chromatography using 50% EtOAc/hexanes to afford **9** as a white solid (318.0 mg, 0.81 mmol,

81% yield). **^{1}H NMR** (400 MHz, $CDCl_3$) δ 7.64 (d, *J* = 7.3 Hz, 2H), 7.47 – 7.40 (m, 3H), 7.37 (d, *J* = 7.1 Hz, 1H), 7.32 (t, *J* = 7.4 Hz, 3H), 7.16 (dd, *J* = 6.6, 2.9 Hz, 2H), 4.01 (t, *J* = 6.0 Hz, 1H), 3.00 (s, 3H), 2.90 (s, 3H), 2.50 – 2.27 (m, 2H), 2.21 (s, 2H), 1.43 (s, 9H). Characterization data matches literature reports.[2]

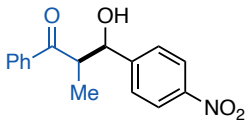

3-hydroxy-2-methyl-3-(4-nitrophenyl)-1-phenylpropan-1-one (10). General Procedure B was followed using propiophenone (132.9 µL, 1 mmol, 1.0 equiv), 4-nitrobenzaldehyde (227.0 mg, 1.5 mmol, 1.5 equiv), BTPP salt **A** (47.5 mg, 0.1 mmol, 10 mol%), and epoxide **2** (81.0 mg, 0.3 mmol, 30 mol%) in DMSO (2 mL) to provide 63% ^{1}H NMR yield and 1.3:1 dr (1,3,5-trimethoxybenzene internal standard used to avoid overlap with product peaks). The reaction was repeated using commercial BTPP (67% ^{1}H NMR yield, 1.4:1 dr) and two-year-old BTPP salt **A** (63% ^{1}H NMR yield, 1.3:1 dr). Following General Procedure B, the product was purified *via* silica gel chromatography using 20% EtOAc in hexanes to afford **10** as a mixture of diastereomers as a yellow oil (173.4 mg, 0.61 mmol, 61% yield, 1.3:1 dr). ^{1}H NMR shifts are reported with signals corresponding to major and minor isomers labeled. **^{1}H NMR** (400 MHz, $CDCl_3$) δ 8.27 – 8.17 (m, 2H, includes both isomers), 7.99-7.89 (m, 2H includes both isomers), 7.67-7.55 (m, 3H includes both isomers), 7.55-7.43 (m, 2H, includes both isomers), 5.36 (s, 1H, minor), 5.10 (t, *J* = 6.2 Hz, 1H, major), 4.01 (d, *J* = 1.9 Hz, 1H, minor), 3.82 (p, *J* = 7.2 Hz, 1H, major), 3.69 (qd, *J* = 7.3, 2.7 Hz, 1H, minor), 3.47 (d, *J* = 3.5 Hz, 1H, major), 1.19 (d, *J* = 7.3 Hz, 3H, major), 1.16 (d, *J* = 7.3 Hz, 3H, minor). Characterization data matches literature reports.[3]

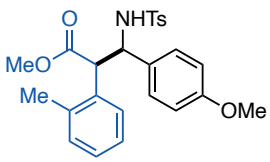

Methyl 3-((4-methylphenyl)sulfonamido)-3-(4-nitrophenyl)-2-(o-tolyl)propanoate (11). General Procedure B was followed using methyl 2-(*o*-tolyl)acetate (164.2 mg, 1 mmol, 1.0 equiv), *N*-(4-methoxybenzylidene)-4-methylbenzenesulfonamide[4] (434.0 mg, 1.5 mmol, 1.5 equiv), BTPP salt **A** (47.5 mg, 0.1 mmol, 10 mol%), and epoxide **2** (54.0 mg, 0.2 mmol, 20 mol%) in DMSO (2 mL) to provide 92% ^{1}H NMR yield and 1.6:1 dr (1,3,5-trimethoxybenzene internal standard used to avoid overlap with product peaks). The reaction was repeated using commercial BTPP (99% ^{1}H NMR yield, 1.5:1 dr) and six-month-old BTPP salt **A** (90% ^{1}H NMR yield, 1.6:1 dr). Following General Procedure B, the product was purified *via* silica gel chromatography using 20% EtOAc in hexanes to afford **11** as mixture of diastereomers as a white solid (363.5 mg, 0.80 mmol, 80% yield, 2.6:1 dr). ^{1}H NMR shifts are reported with signals corresponding to major and minor isomers labeled. **^{1}H NMR** (400 MHz, DMSO-d_6) δ 8.35 (d, J = 9.4 Hz, 1H, major), 8.02 (d, J = 10.4 Hz, 1H, minor), 7.70 (d, J = 9.1 Hz, 1H, minor), 7.43 (d, J = 8.0 Hz, 1H, major), 7.36 (d, J = 8.0 Hz, 1H, minor), 7.28 (d, J = 8.3 Hz, 2H, major), 7.22-7.12 (m, 3H, 1H from major, 2H from minor), 7.09-7.01 (m, 3H, 2H from major and 1H from minor), 7.03 (d, J = 8.1 Hz, 2H, major), 7.01-6.93 (m, 1H, both isomers), 6.90 (d, J = 7.5 Hz, 2H, minor), 6.82 (d, J = 9.0 Hz, 2H, major), 6.64 (d, J = 8.6 Hz, 2H, minor), 6.36 (d, J = 8.6 Hz, 2H, major), 4.97-4.87 (m, 1H, both isomers), 4.31 (d, J = 11.5 Hz, 1H, major), 4.19 (d, J = 11.5 Hz, 1H, minor), 3.67 (s, 3H, minor), 3.56 (s, 3H, major), 3.54 (s, 3H, major), 3.24 (s, 3H, minor), 2.41 (s, 3H, minor), 2.37 (s, 1H, both isomers), 2.25 (s, 3H, minor), 2.23 (s, 3H, major), 2.04 (s, 3H, major). **^{13}C NMR** (101 MHz, DMSO-d_6) δ 172.4, 171.4, 158.9, 158.4, 142.3, 142.0, 141.9, 139.1, 138.9, 137.5, 136.5, 134.3, 133.9, 131.7, 130.7, 130.5, 130.4, 139.8, 129.3, 129.2, 129.1, 129.0, 128.1, 127.8, 127.6, 126.7, 126.6, 126.6, 126.5, 126.1, 60.2, 58.5, 55.5, 55.3, 53.9,

52.6, 52.4, 52.2, 21.4, 21.3, 19.9, 19.7. **IR** (neat) 3389, 3241, 2959, 1746, 1516, 1157 cm^{-1}. **HRMS (DART)** $[M+H]^+$ calcd. for $[C_{25}H_{28}NO_5S]^+$ = 454.1683, found 454.1690. **MP** 125 – 130 °C.

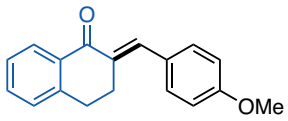

2-(4-methoxybenzylidene)-3,4-dihydronaphthalen-1(2H)-one (12). General Procedure B was followed using 3,4-dihydronaphthalen-1(2*H*)-one (133.0 µL, 1 mmol, 1.0 equiv), *N*-(4-methoxybenzylidene)-4-methylbenzenesulfonamide[4] (434.0 mg, 1.5 mmol, 1.5 equiv), BTPP salt **A** (47.5 mg, 0.1 mmol, 10 mol%), and epoxide **2** (54 mg, 0.2 mmol, 20 mol%) in DMSO (2 mL) to provide 90% ^{1}H NMR yield. The reaction was repeated using commercial BTPP (99% ^{1}H NMR yield) and two-year-old BTPP salt **A** (99% ^{1}H NMR yield). Following General Procedure B, the product was purified *via* silica gel chromatography using 10% EtOAc in hexanes to afford **12** as a yellow solid (248.5 mg, 0.94 mmol, 94% yield). **^{1}H NMR** (400 MHz, DMSO-d_6) δ 7.95 (d, J = 7.8 Hz, 1H), 7.69 (s, 1 H), 7.61-7.49 (m, 3H), 7.44-7.34 (m, 2H), 7.03 (d, J = 8.5 Hz, 2H), 3.81 (s, 3H), 3.10 (t, J = 5.5 Hz, 2 H), 2.94 (t, J = 5.5 Hz, 2 H). Characterization data matches literature reports.[5]

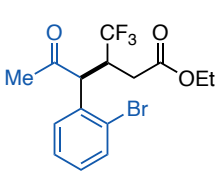

ethyl 4-(2-bromophenyl)-5-oxo-3-(trifluoromethyl)hexanoate (13). General Procedure B was followed using 1-(2-bromophenyl)propan-2-one (213.1 mg, 1 mmol, 1.0 equiv), ethyl (*E*)-4,4,4-trifluorobut-2-enoate (224.2 µL, 1.5 mmol, 1.5 equiv), BTPP salt **A** (47.5 mg, 0.1 mmol, 10 mol%), and epoxide **2** (54.0 mg, 0.2 mmol, 20 mol%) in DMSO (2 mL) to provide 99% ^{1}H NMR yield and 1.2:1 dr. The reaction was repeated using commercial BTPP (99% ^{1}H NMR yield, 1.3:1 dr) and six-month-old BTPP salt **A** (99% ^{1}H NMR yield, 1.2:1 dr). Following General Procedure B, the product was purified *via* silica gel

chromatography using 5% EtOAc to 25% EtOAc/hexanes to afford **13** as a mixture of diastereomers as a pale-yellow oil (348.6 mg, 0.91 mmol, 91% yield, 1.3:1 dr). ^{1}H NMR shifts are reported with signals corresponding major and minor isomers labeled. **^{1}H NMR** (400 MHz, $CDCl_3$) δ 7.64 (d, *J* = 8.0 Hz, 1H, both isomers), 7.33 – 7.12 (m, 3H, both isomers), 4.88 (d, *J* = 9.4 Hz, 1H, minor), 4.74 (d, *J* = 10.5 Hz, 1H, major), 4.15 (q, *J* = 7.1 Hz, 2H, major), 4.08 – 3.81 (m, 3H, 1 from major and 2 from minor), 3.61 – 3.45 (m, 1H, minor), 2.78 (dd, *J* = 16.6, 7.0 Hz, 1H, minor), 2.62 (dd, *J* = 16.6, 3.9 Hz, 1H, minor), 2.41 (dd, *J* = 16.7, 6.7 Hz, 1H, major), 2.14 (s, 3H, major), 2.11 (s, 3H, minor), 2.03 (dd, *J* = 16.7, 6.0 Hz, 1H, major), 1.26 (t, *J* = 7.1 Hz, 3H, minor), 1.13 (t, *J* = 7.1 Hz, 3H, major). **^{19}F NMR** (376 MHz, $CDCl_3$) δ -66.85 (d, *J* = 9.0 Hz), -69.97 (d, *J* = 8.3 Hz). **^{13}C NMR** (101 MHz, $CDCl_3$) δ 204.5, 203.7, 170.7, 170.4, 134.5, 133.9, 133.8, 133.1, 130.3, 130.1, 129.8, 129.6, 129.4 (q, J = 205.7 Hz), 128.8 (q, *J* = 190.6 Hz), 128.3, 128.1, 125.9, 125.8, 61.2, 61.1, 55.0, 54.5, 42.2 (q, *J* = 26.3 Hz), 40.9 (q, *J* = 26.0 Hz), 32 (q, *J* = 2.9 Hz), 31.5 (q, *J* = 2.5 Hz), 30.2, 30.0, 14.2, 14.1. **IR** (neat) 3026, 2970, 2922, 1726, 1676, 1367, 1280, 1158, 1142, 696 cm^{-1}. **HRMS (DART)** $[M+H]^+$ calcd. for $[C_{15}H_{17}BrF_3O_3]^+$ = 381.0308, found 381.0308.

iii. Control reactions for Michael, aldol, and Mannich reactions

In this section we describe a series of control reactions that support that the BTPP generated from the precatalyst salt is responsible for reaction catalysis and not background reactivity from any components or intermediates of the activation process. General Procedure C below was followed for each control reaction. We also tested to see if the carboxylate anion is capable of catalyzing

reactions by running reactions with only BTPP salt **A**, with a variety of 1-phenylcyclopropanecarboxylate salts. Here, we tested different countercations (e.g., potassium and ammoniums) to survey salt solubility trends. Additionally, we tested if using only epoxide **2** could promote the reaction. We also considered the possibility that a carboxylate anion can attack the epoxide to generate an alkoxide intermediate that could serve as an active basic catalyst. We tested this by mixing non-superbase carboxylate salts with epoxide **2** under reaction conditions. For each indicated system other than the commercial freebase or full precatalyst system, we observed either 0% or reduced yield of the product. Overall, these results are consistent with the active catalyst being BTPP generated from the precatalyst system, as the individual components and intermediates of the activation process do not provide high yields. We also conducted time studies for the synthesis of **7** using epoxides **2** and **3** to test the effect of the precatalyst activation rate on the reaction rate. Figure S8 shows an extended induction period when epoxide **3** is employed, indicative of slower precatalyst activation, further supporting that BTPP generated from the precatalyst system is the active catalyst *in situ*. Data for these experiments is provided in Tables S5 and S6 for substrates **7** and **8**, respectively. We note that for all substrates in Table S4, reactions cannot be promoted by BTPP salt **A** without the use of an epoxide.

General Procedure C: Control reactions run in a nitrogen-filled glovebox. In a nitrogen-filled glovebox, an oven-dried 1-dram vial (ThermoFisher, C4015-1) was charged with a magnetic stir bar, pronucleophile (0.1 mmol, 1.0 equiv), DMSO (0.2 mL, 0.5 M), epoxide **2** (5.4 mg, 0.2 mmol, 20 mol%, unless excluded), Michael acceptor (0.15 mmol, 1.5 equiv), and the indicated catalyst mixture in Table S5 or S6 (0.01 mmol, 10 mol%, unless excluded) in successive order. The vial was capped with a PTFE-lined cap (ThermoFisher, C4015-1A), removed from the glovebox, and

placed into an aluminum reaction block preheated to 25 °C with stirring for 24 h. Dibromomethane (0.1 mmol, 7 □L, 1.0 equiv) internal standard was added to the reaction solution, a 50 □L aliquot was taken and added to an NMR tube, then diluted with $CDCl_3$ (0.5 mL). Analysis of the ^{1}HNMR spectrum was used to determine the yield of product.

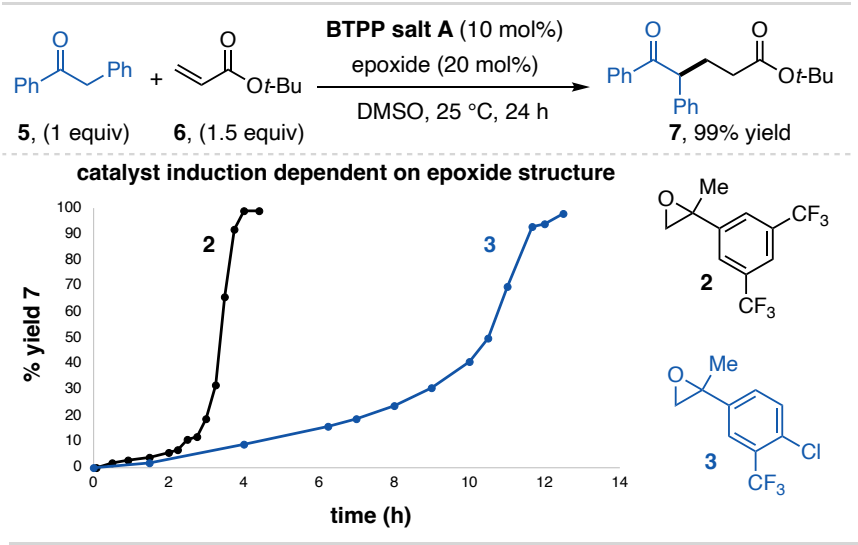

Figure S8. Michael addition reaction between deoxybenzoin (**5**) and *tert*-butylacrylate (**6**) using the BTPP precatalyst system with epoxides **2** and **3**.

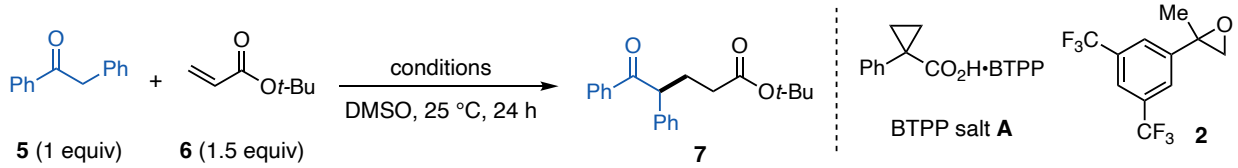

Table S5: Control reactions for the Michael addition between deoxybenzoin (**5**) and *tert*-butyl acrylate (**6**) with various potential catalyst systems. For the controls, all salts fully dissolve in the DMSO reaction solution. [a] Indicates the use of P_2-*t*-Bu salt **A** that has been recovered after water absorption *via* azeotrope with PhMe, see Section VIIIb for details.

Entry	Conditions	Results
1	10% BTPP	99%

2	10% BTPP salt **A** + 20% epoxide **2**	99%
3	5% BTPP salt **A** + 10% epoxide **2**	6%
4	2.5% BTPP salt **A** + 5% epoxide **2**	2%
5	10% BTPP salt **B** + 20% epoxide **2**	99%
6	10% BTPP salt **B** (aged 2 h in 84% humidity) + 20% epoxide **2**	99%
7[a]	10% BTPP salt **A** (from moisture recovery) + 20% epoxide **2**	99%
8	10% BTPP salt **A**	5%
9	10% potassium 1-phenylcyclopropanecarboxylate	0%
10	10% triethylammonium 1-phenylcyclopropanecarboxylate	0%
11	10% NEt_3	0%
12	10% pyridinium 1-phenylcyclopropanecarboxylate + 20% epoxide **2**	0%
13	10% pyridine	0%
14	10% tetrabutylammonium acetate + 20% epoxide **2**	10%
15	20% epoxide **2**	0%
16	10% potassium 1-phenylcyclopropanecarboxylate + 20% epoxide **2**	0%
17	10% H^+NEt_3 1-phenylcyclopropanecarboxylate + epoxide **2**	0%

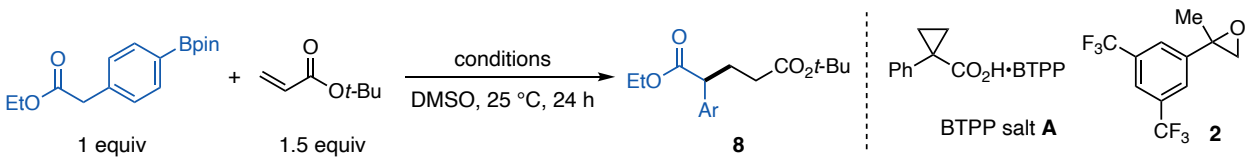

Table S6: Control reactions for the Michael addition between ethyl 2-(4-(4,4,5,5-tetramethyl-1,3,2-dioxaborolan-2-yl)phenyl)acetate and *tert*-butyl acrylate with various potential catalyst systems. For the controls, all salts fully dissolve in the DMSO reaction solution.

Entry	Conditions	Results
1	10% BTPP	86%
2	10% BTPP salt **A** + 20% epoxide **2**	90%
3	5% BTPP salt **A** + 10% epoxide **2**	46%
4	2.5% BTPP salt **A** + 5% epoxide **2**	0%
5	10% BTPP salt **B** + epoxide **2**	93%
6	10% BTPP salt **B** (aged 2h in 84% humidity) + epoxide **2**	93%
7	10% BTPP salt **A**	0%
8	10% triethylammonium 1-phenylcyclopropanecarboxylate	0%
9	10% NEt_3	0%
10	10% tetrabutylammonium acetate	0%
11	20% epoxide **2**	0%
12	10% potassium 1-phenylcyclopropanecarboxylate + 20% epoxide **2**	78%
13	10% H^+NEt_3 1-phenylcyclopropanecarboxylate + epoxide **2**	0%

We note that for Table S6 Entry 12, the combination of potassium 1-phenylcyclopropanecarboxylate and epoxide **2** is capable of promoting the Michael addition reaction; here, we speculate a potassium alkoxide intermediate is generated that promotes the reaction. However, the corresponding alkoxide intermediate in the use of the precatalyst system likely neutralizes the BTPP immediately to generate the freebase as the active catalyst. We supported this by stirring BTPP salt **A** with epoxide **2** at 80 °C for 30 min to allow preformation of the base (100% freebase observed by ^{31}P NMR), followed by addition of starting materials. Here, the Michael addition rate using the precatalyst system is very similar to use of BTPP freebase (reaction complete in 1h). Direct use of BTPP salt **A** and epoxide **2** shows a slower reaction rate (reaction complete in 6 h), consistent with precatalyst activation. When potassium 1-phenylcyclopropanecarboxylate and epoxide **2** are used, we observe an even slower reaction rate (0% yield at 1h, 12% yield in 6 h). These results are consistent with the BTPP generated from the precatalyst system being the active catalyst for the reaction.

b. Use of BTPP salt A as a precatalyst for ester amidation reactions

i. Reaction scheme and General Procedures

This application is inspired by prior reports on the use of phosphazenes, especially BEMP, to catalyze ester amidation reactions.[6] The results presented in this section are therefore benchmarked

against this work and as such we compared the utility of BTPP salt **A** with epoxide **2** against the use of BEMP, as described below.

Table S7: Example substrates of ester amidation using BTPP salt **A** and epoxide **2**. General Procedure E followed for BEMP freebase yields.

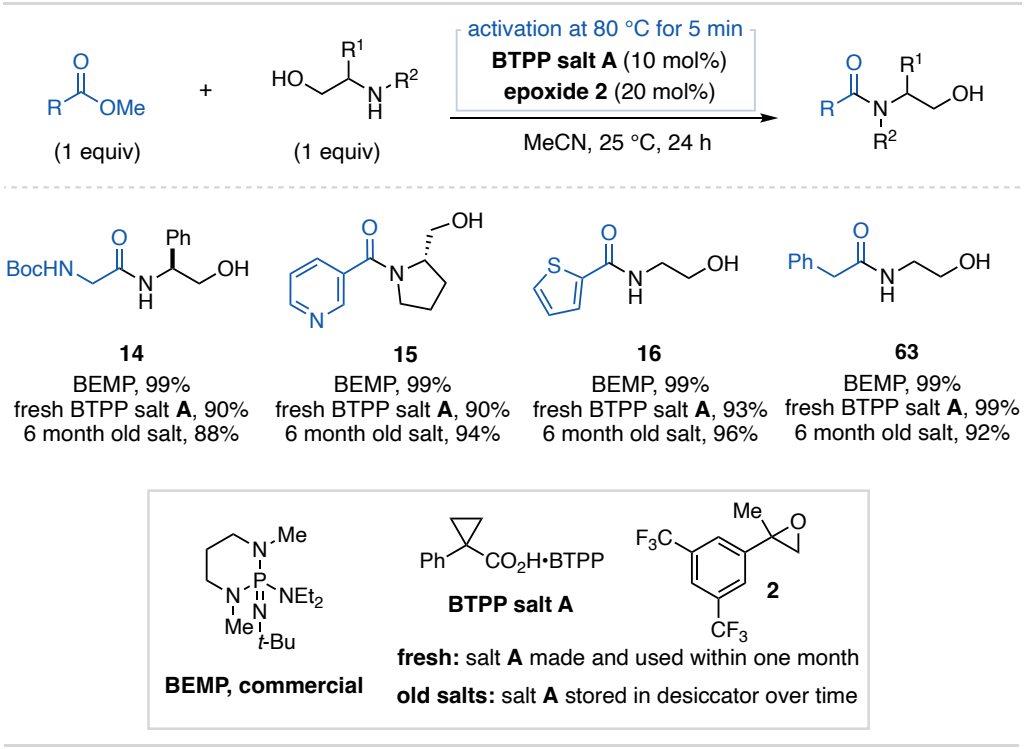

General Procedure D: BTPP salt A and epoxide 2 promoted reaction. For these reactions, we found the aminoalcohol substrate reacts with epoxide **2**, preventing the BTPP activation process. To address this, we developed a preactivation procedure where an oven-dried 1-dram vial (ThermoFisher, C4015-1) was charged with a magnetic stir bar and BTPP salt **A** (47.5 mg, 0.1 mmol, 10 mol%). The vial was capped with a PTFE-lined cap (ThermoFisher, C4015-1A) and evacuated then back filled with nitrogen three times *via* a nitrogen inlet tube on a Schlenk manifold line. While attached to the inlet tube to maintain positive pressure of nitrogen, DMSO (0.2 mL, 0.5 M in BTPP salt A) and epoxide **2** (54.0 mg, 0.2 mmol, 20 mol%) were added *via* nitrogen-

flushed syringe. The pre-activation solution vial was placed in a preheated aluminum reaction block at 80 °C for 5 minutes while attached to the nitrogen inlet tube.

Reagent solution: a separate oven-dried 1-dram vial (ThermoFisher, C4015-1) was charged with a magnetic stir bar and capped (ThermoFisher, C4015-1A) and evacuated then back filled with nitrogen three times *via* a nitrogen inlet tube on a Schlenk manifold line. While attached to the nitrogen inlet tube, MeCN (0.8 mL, 1 M with respect to total reaction volume), ester (1 mmol, 1.0 equiv), and aminoalcohol (1 mmol, 1.0 equiv) were added *via* nitrogen-flushed syringe. The pre-activation solution was allowed to cool to rt, at which point the reagent solution was transferred to the pre-activation solution *via* nitrogen-flushed syringe. The combined reaction solution was stirred at rt for 24 h. Dibromomethane (35.0 μL, 0.5 mmol, 0.5 equiv) internal standard was added to the reaction solution, a 50 □L aliquot was taken and added to an NMR tube, then diluted with $CDCl_3$ (0.5 mL). ^1H NMR spectroscopy was used to determine the yield of the reaction.

ii. Reaction and characterization data

General description: For all of the substrates in this section, we use ^1H NMR yields to determine the efficacy of the precatalyst salt system. In each case, we benchmarked the success of the precatalyst against the use of commercial BEMP and BTPP salt **A** that has been aged in a benchtop desiccator for six months (see Section VIII for details). The reactions carried out with BEMP were set up with the use of a nitrogen-filled glovebox, described in General Procedure E, and the reactions carried out with BTPP salt **A** that has been aged for six months were set up using General Procedure D. The products were subsequently isolated using General Procedure D and BTPP salt **A** for characterization. To do this, the crude reactions mixtures were directly subjected to flash

column chromatography to yield purified products. The purification conditions and characterization data are given below. The results are summarized in Table S7 above.

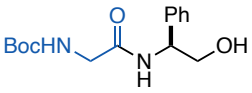

***tert*-butyl (*S*)-(2-((2-hydroxy-1-phenylethyl)amino)-2-oxoethyl)carbamate (14).** General Procedure D was followed using BTPP salt **A** (47.5 mg, 0.1 mmol, 10 mol%), epoxide **2** (54.0 mg, 0.2 mmol, 20 mol%), DMSO (0.2 mL), methyl (*tert*-butoxycarbonyl)glycinate (189.2 mg, 1.0 mmol, 1.0 equiv), (*S*)-2-amino-2-phenylethan-1-ol (137.2 mg, 1.0 mmol, 1.0 equiv), and MeCN (0.8 mL) to provide 90% ^{1}H NMR yield. The reaction was repeated using commercial BEMP (99% ^{1}H NMR yield) and six-month-old BTPP salt **A** (88% ^{1}H NMR yield). The product was isolated *via* silica gel chromatography using 100% DCM to 6% MeOH/DCM to afford **14** as a white solid (296.8 mg, 1 mmol, 100% yield). **^{1}H NMR** (400 MHz, $CDCl_3$) δ 7.37 – 7.25 (m, 5H), 7.11 (d, *J* = 7.8 Hz, 1H), 5.44 (s, 1H), 5.11 – 5.02 (m, 1H), 3.89 – 3.75 (m, 4H), 3.20 (s, 1H), 1.43 (s, 9H). Characterization data matches literature reports.[7]

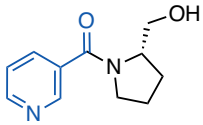

(*S*)-(2-(hydroxymethyl)pyrrolidin-1-yl)(pyridin-3-yl)methanone (15). General Procedure D was followed using BTPP salt **A** (47.5 mg, 0.1 mmol, 10 mol%), epoxide **2** (54.0 mg, 0.2 mmol, 20 mol%), DMSO (0.2 mL), methyl nicotinate (137.1 mg, 1.0 mmol, 1.0 equiv), (*S*)-pyrrolidin-2-ylmethanol (98.7 µL, 1.0 mmol, 1.0 equiv), and MeCN (0.8 mL) to provide 90% ^{1}H NMR yield. The reaction was repeated using commercial BEMP (99% ^{1}H NMR yield) and six-month-old BTPP salt **A** (94% ^{1}H NMR yield). The product was isolated *via* silica gel chromatography using 100% DCM to 6% MeOH/DCM to afford **15** as a colorless oil

(197.6 mg, 0.96 mmol, 96% yield). **^{1}H NMR** (400 MHz, $CDCl_3$) δ 8.76 (s, 1H), 8.66 (d, *J* = 4.9 Hz, 1H), 7.84 (d, *J* = 7.9 Hz, 1H), 7.35 (dd, *J* = 7.9, 4.9 Hz, 1H), 4.56 (s, 1H), 4.46 – 4.34 (m, 1H), 3.86 – 3.78 (m, 1H), 3.78 – 3.69 (m, 1H), 3.56 – 3.46 (m, 2H), 2.22 – 2.11 (m, 1H), 1.98 – 1.87 (m, 1H), 1.89 – 1.64 (m, 2H). Characterization data matches literature reports.[6]

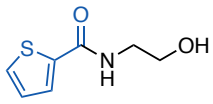

***N*-(2-hydroxyethyl)thiophene-2-carboxamide (16).** General Procedure D was followed using BTPP salt **A** (47.5 mg, 0.1 mmol, 10 mol%), epoxide **2** (54.0 mg, 0.2 mmol, 20 mol%), DMSO (0.2 mL), ethyl thiophene-2-carboxylate (134.4 µL, 1.0 mmol, 1.0 equiv), 2-aminoethan-1-ol (60.4 µL, 1.0 mmol, 1.0 equiv), and MeCN (0.8 mL) to provide 93% ^{1}H NMR yield. The reaction was repeated using commercial BEMP (99% ^{1}H NMR yield) and six-month-old BTPP salt **A** (96% ^{1}H NMR yield). The product was isolated *via* silica gel chromatography using 100% DCM to 5% MeOH/DCM to afford **16** as a white solid (167.2 mg, 0.98 mmol, 98% yield). **^{1}H NMR** (400 MHz, $CDCl_3$) δ 7.54 (d, *J* = 3.7 Hz, 1H), 7.42 (d, *J* = 4.9 Hz, 1H), 7.13 (t, *J* = 5.7 Hz, 1H), 7.00 (t, *J* = 4.4 Hz, 1H), 3.75 (t, *J* = 5.1 Hz, 2H), 3.63 (s, 1H), 3.54 (q, *J* = 5.3 Hz, 2H). Characterization data matches literature reports.[6]

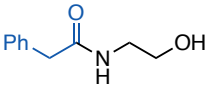

***N*-(2-hydroxyethyl)-2-phenylacetamide (63).** General Procedure D was followed using BTPP salt **A** (47.5 mg, 0.1 mmol, 10 mol%), epoxide **2** (54.0 mg, 0.2 mmol, 20 mol%), DMSO (0.2 mL), methyl phenylacetate (140.9 µL, 1.0 mmol, 1.0 equiv), 2-aminoethan-1-ol (60.4 µL, 1.0 mmol, 1.0 equiv), and MeCN (0.8 mL) to provide 99% ^{1}H NMR yield. The reaction was repeated using commercial BEMP (99% ^{1}H NMR yield) and six-month-old BTPP salt **A** (92% ^{1}H NMR yield). The product was isolated *via* silica gel chromatography

using 100% DCM to 6% MeOH/DCM to afford **63** as a white solid (169.2 mg, 0.94 mmol, 94% yield). **^{1}H NMR** (400 MHz, $CDCl_3$) δ 7.38 – 7.31 (m, 2H), 7.30 – 7.24 (m, 3H), 6.10 (s, 1H), 3.63 (t, *J* = 5.0 Hz, 2H), 3.56 (s, 2H), 3.34 (q, *J* = 5.3 Hz, 2H), 2.97 (s, 1H). Characterization data matches literature reports.[6]

iii. Control Reactions

In this section we describe control reactions that support BTPP generated from the precatalyst salt is responsible for catalyzing the amidation reaction and not background reactivity from any components or intermediates of the activation process. General Procedure E was followed for each control reaction. We also tested to see if the carboxylate anion is capable of catalyzing reactions by running reactions with only BTPP salt **A**, with a variety of 1-phenylcyclopropanecarboxylate salts. Here, we tested different countercations (e.g., potassium and ammoniums) to survey salt solubility trends. Additionally, we tested if using only epoxide **2** could promote the reaction. We also considered the possibility that a carboxylate anion can attack the epoxide to generate an alkoxide intermediate that could serve as an active basic promoter. We tested this by mixing non-superbase carboxylate salts with epoxide **2** under reaction conditions. For each indicated catalyst system other than the commercial freebase or precatalyst system, we observed either 0% or reduced yield of the product. In certain cases, a limited amount of reactivity is observed, but does not account for the significant product yield observed when the precatalyst system is used. Overall, these results are consistent with the active catalyst being BTPP generated from the precatalyst

system. Data for these experiments is provided in Tables S8 and S9 for substrates **16** and **63**, respectively.

General Procedure E: Control reactions run in a nitrogen-filled glovebox. Since a pre-activation procedure was required for amidation reactions with the BTPP salt **A** precatalyst, a pre-activation procedure was used for control reactions that employ epoxide **2**. If epoxide was excluded from the control reaction, all reagents were added sequentially inside a nitrogen-filled glovebox.

Pre-activation procedure: in a nitrogen-filled glovebox an oven-dried 1-dram vial (ThermoFisher, C4015-1) was charged with a magnetic stir bar, indicated catalyst mixture in Table S8 or S9 (0.01 mmol, 10 mol%), DMSO (0.1 mL, 0.1 M in indicated catalyst mixture) and epoxide **2** (0.02 mmol, 20 mol%). The vial was capped with a PTFE-lined cap (ThermoFisher, C4015-1A), removed from the glovebox, and placed in a preheated aluminum reaction block at 80 °C for 5 minutes.

Reagent solution: in a nitrogen-filled glovebox, a separate oven-dried 1-dram vial (ThermoFisher, C4015-1) was charged with a magnetic stir bar. If epoxide was excluded, the indicated potential catalyst (0.01 mmol, 10 mol%) was added, followed by ester (0.1 mmol, 1.0 equiv), MeCN (0.1 mL, 1 M) and aminoalcohol (0.1 mmol, 1.0 equiv). The vial was capped (ThermoFisher, C4015-1A), removed from the glovebox, and connected to a Schlenk manifold line *via* an inlet tube and placed under positive pressure of nitrogen. The pre-activation solution was allowed to cool to rt. The pre-activated solution (20 □L, 0.01 mmol, 10 mol% indicated catalyst mixture) was transferred *via* nitrogen-flushed syringe to the reagent solution. The combined reaction solution was stirred for 24 h in a preheated aluminum reaction block at 25 °C.

Dibromomethane (1.0 equiv, 0.1 mmol 7 □L) internal standard was added to the reaction solution, a 50 □L aliquot was taken and added to an NMR tube, then diluted with $CDCl_3$ (0.5 mL). ^1H NMR spectroscopy was used to determine the yield of product.

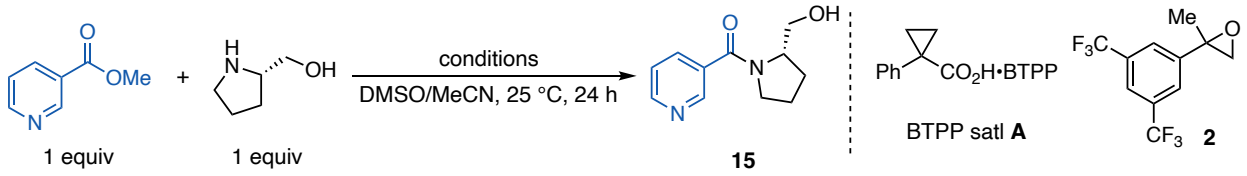

Table S8: Control reactions for the ester amidation reaction between methyl nicotinate and (*S*)-pyrrolidin-2-ylmethanol with various potential catalyst systems. [a] A preactivation procedure was not followed as noted in General Procedure E.

Entry	Conditions	Results
1[a]	10% BEMP	99%
2	10% BTPP salt **A** + 20% epoxide **2**	99%
3	5% BTPP salt **A** + 10% epoxide **2**	82%
4	2.5% BTPP salt **A** + 5% epoxide **2**	68%
5[a]	10% BTPP salt **A**	44%
6	10% BTPP salt **A** + 20% epoxide **2** (5 h reaction time)	99%
7	10% BTPP salt **A** (5 h reaction time)	0%
8[a]	10% triethylammonium 1-phenylcyclopropanecarboxylate salt	0%
9[a]	10% NEt_3	35%

10[a]	10% tetrabutylammonium acetate	0%
11[a]	20% epoxide **2**	0%
12	10% potassium 1-phenylcyclopropanecarboxylate + 20% epoxide **2**	30%
13	10% potassium 1-phenylcyclopropanecarboxylate + 20% epoxide **2** (5 h reaction time)	0%
14	10% H^+NEt_3 1-phenylcyclopropanecarboxylate + 20% epoxide **2**	35%

We note that for substrate **15** above, BTPP salt **A** on its own and potassium 1-phenylcyclopropanecarboxylate with epoxide **2** are capable of promoting the reaction. Here, we speculate that either the carboxylate or potassium alkoxide intermediate is promoting the reaction. However, the ester amidation rate utilizing the precatalyst system is very similar to use of BTPP freebase (reaction complete in 5 h). Conversely, when just BTPP salt A or potassium 1-phenylcyclopropanecarboxylate with epoxide **2** are used, we observe a much slower rate (0% yield in 5 h). These results are consistent with the BTPP generated from the precatalyst system being the active catalyst for the reaction. Additionally, we note that the ester amidation reaction for substrate **63** below is more challenging, which illustrates that only BTPP freebase works to catalyze the reaction in high yield.

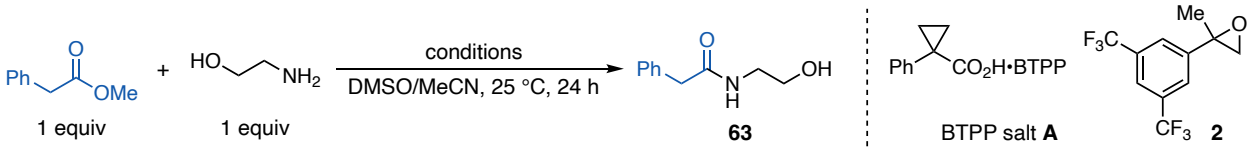

Table S9: Control reactions for the ester amidation reaction between methyl phenylacetate and 2-aminoethan-1-ol with various potential catalyst systems. [a] A preactivation procedure was not followed as noted in General Procedure E.

Entry	Conditions	Results
1[a]	10% BEMP	99%
2	10% BTPP salt **A** + 20% epoxide **2**	94%
3	5% BTPP salt **A** + 10% epoxide **2**	8%
4	2.5% BTPP salt **A** + epoxide **2**	8%
5[a]	10% BTPP salt **A**	8%
6[a]	10% triethylammonium 1-phenylcyclopropanecarboxylate salt	0%
7[a]	10% NEt_3	4%
8[a]	10% tetrabutylammonium acetate	0%
9[a]	20% epoxide **2**	0%
10	10% potassium 1-phenylcyclopropanecarboxylate + 20% epoxide **2**	4%
11	10% H^+NEt_3 1-phenylcyclopropanecarboxylate + 20% epoxide **2**	8%

c. Use of BTPP salt A as a stoichiometric prereagent for alcohol deoxyfluorination

i. Reaction scheme and General Procedures

Table S10: Example substrates of deoxyfluorination using BTPP salt **A** and epoxide **2**. General Procedure G was followed for BTPP freebase yields.

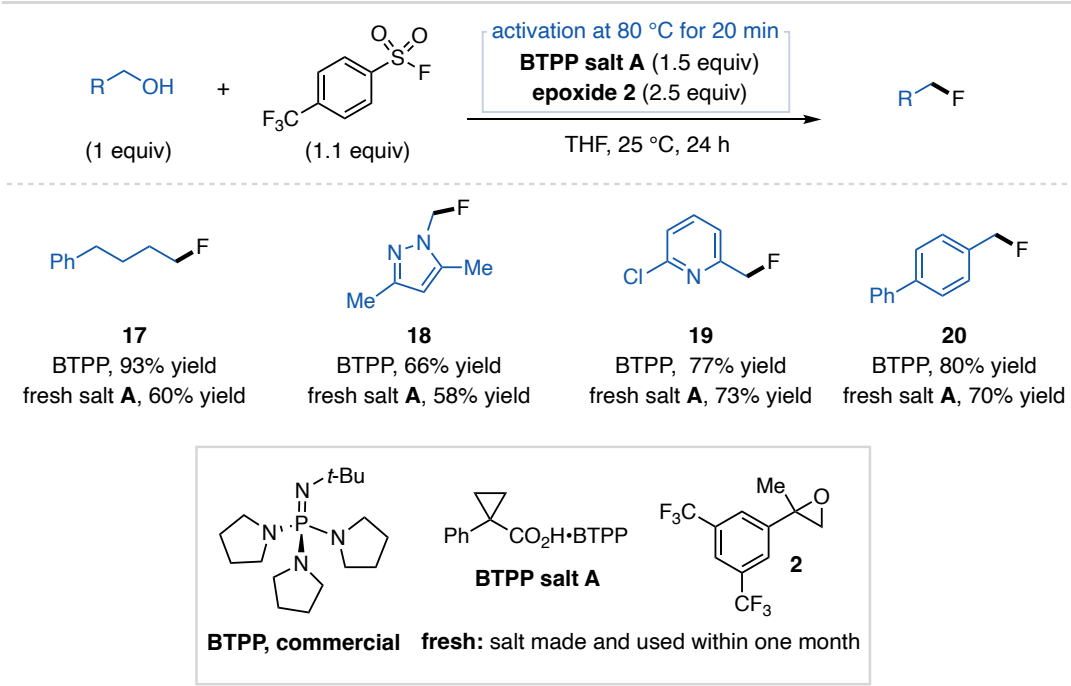

General Procedure F: BTPP salt A and epoxide 2 promoted reaction. For these reactions, we found the alcohol substrate reacts with epoxide **2**, which interrupts the BTPP activation process. To address this, we developed a preactivation procedure where an oven-dried 1-dram vial (ThermoFisher, C4015-1) was charged with a magnetic stir bar and BTPP salt **A** (336.0 mg, 0.75 mmol, 1.5 equiv). The vial was capped with a PTFE-lined cap (ThermoFisher, C4015-1A) and evacuated then back filled with nitrogen three times *via* a nitrogen inlet tube on a Schlenk manifold line. While attached to the nitrogen inlet tube, THF (0.25 mL, 3 M in BTPP salt A) and epoxide **2**

(337.7 mg, 1.25 mmol, 2.5 equiv) were then added *via* nitrogen-flushed syringe. The pre-activation solution was placed in a preheated aluminum reaction block at 80 °C for 20 min with stirring while attached to the nitrogen inlet.

Reagent solution: a separate oven-dried 1-dram vial (ThermoFisher, C4015-1) was charged with 4-(trifluoromethyl)benzenesulfonyl fluoride[8] (125.5 mg, 0.55 mmol, 1.1 equiv). The vial was capped with a PTFE-lined cap (ThermoFisher, C4015-1A) and evacuated then back filled with nitrogen three times *via* a nitrogen inlet tube on a Schlenk manifold line. While attached to the nitrogen inlet tube, THF (0.5 mL, 1.0 M) and alcohol (1.0 equiv, 0.5 mmol) were added *via* nitrogen-flushed syringes. The pre-activation solution was allowed to cool to rt and the reagent solution was transferred to the pre-activation solution *via* nitrogen-flushed syringe. The combined reaction solution was stirred at 25 °C for 24 h. Dibromomethane (35.1 μL, 0.5 mmol, 1.0 equiv) internal standard was added to the reaction solution, a 50 □L aliquot was taken and added to an NMR tube, then diluted with $CDCl_3$ (0.5 mL). ^1H NMR spectroscopy was used to determine the yield of the crude reaction. The crude reaction material was directly subjected to flash chromatography to yield pure product for characterization.

ii. Reaction and characterization data

General description: For all of the substrates in this section, we use ^1H NMR yields to determine the efficacy of the precatalyst salt system. In each case, we benchmarked the success of the precatalyst against the use of commercial BTPP. The reactions carried out with BTPP were set up with the use of a nitrogen-filled glovebox, as described below. The substrates were subsequently

isolated using General Procedure F and BTPP salt **A** for characterization. To do this, the crude reactions mixtures were directly subjected to flash column chromatography to yield purified products. The purification conditions and characterization data are given below.

(4-fluorobutyl)benzene (17). General Procedure F was followed using BTPP salt **A** (336.0 mg, 0.75 mmol, 1.5 equiv), epoxide **2** (337.7 mg mg, 1.25 mmol, 2.5 equiv), THF (0.25 mL for preactivation), 4-phenylbutan-1-ol (76.3 µL, 0.5 mmol, 1.0 equiv), 4-(trifluoromethyl)benzenesulfonyl fluoride[8] (125.5 mg, 0.55 mmol, 1.1 equiv), and THF (0.5 mL) to provide 60% ^{1}H NMR yield. The reaction was repeated using commercial BTPP (93% ^{1}H NMR yield). Following General Procedure F, the product was purified *via* preparatory thin layer chromatography using 1% EtOAc/hexanes to afford **17** as a colorless oil (12.2 mg, 0.08 mmol, 16% yield). **^{1}H NMR** (400 MHz, $CDCl_3$) δ 7.36 – 7.26 (m, 2H), 7.26 – 7.17 (m, 3H), 4.60 – 4.50 (m, 1H), 4.43 (t, *J* = 5.8 Hz, 1H), 2.69 (t, *J* = 7.2 Hz, 2H), 1.87 – 1.67 (m, 4H). Characterization data matches literature reports.[8]

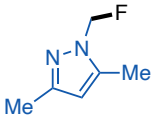

1-(fluoromethyl)-3,5-dimethyl-1H-pyrazole (18). General Procedure F was followed using BTPP salt **A** (336.0 mg, 0.75 mmol, 1.5 equiv), epoxide **2** (337.7 mg mg, 1.25 mmol, 2.5 equiv), THF (0.25 mL for preactivation), (3,5-dimethyl-1*H*-pyrazol-1-yl)methanol (63.1 mg, 0.5 mmol, 1.0 equiv), 4-(trifluoromethyl)benzenesulfonyl fluoride[8] (125.5 mg, 0.55 mmol, 1.1 equiv), and THF (0.5 mL) to provide 58% ^{1}H NMR yield. The reaction was repeated using commercial BTPP (66% ^{1}H NMR yield). Substrate **18** has been previously reported to be unstable to silica gel chromatography.[8] Therefore, for identification, the crude material was

extracted with saturated aqueous sodium chloride (10 mL), dried over sodium sulfate, and concentrated *in vacuo* to afford crude **18** as a brown-yellow oil that also contains BTPP, byproduct **62**, epoxide **2**, 4-(trifluoromethyl)benzenesulfonate side products and other minor species. **^{1}H NMR** (400 MHz, $CDCl_3$) δ 5.92 (d, J = 54.4 Hz, 2H), 5.92 (s, 1H), 2.32 (s, 3H), 2.25 – 2.21 (m, 3H). Characterization data matches literature reports.[8]

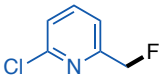

2-chloro-6-(fluoromethyl)pyridine (19). General Procedure F was followed using BTPP salt **A** (336.0 mg, 0.75 mmol, 1.5 equiv), epoxide **2** (337.7 mg mg, 1.25 mmol, 2.5 equiv), THF (0.25 mL for preactivation), (6-chloropyridin-2-yl)methanol (71.8 mg, 0.5 mmol, 1 equiv), 4-(trifluoromethyl)benzenesulfonyl fluoride[8] (125.5 mg, 0.55 mmol, 1.1 equiv), and THF (0.5 mL) to provide 73% ^{1}H NMR yield. The reaction was repeated using commercial BTPP (77% ^{1}H NMR yield). Under these deoxyfluorination conditions, substrate **19** could not be separated from ether dimer using normal phase chromatography. Therefore, for characterization purposes, the product was prepared *via* deoxyfluorination using DAST, described below.

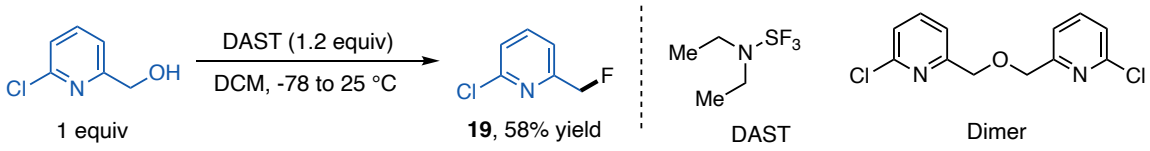

Deoxyfluorination with DAST procedure. An oven-dried 50 mL round bottom flask was charged with a magnetic stir bar, (6-chloropyridin-2-yl)methanol (718.0 mg, 5.0 mmol, 1.0 equiv) and DCM (20 mL). The flask was sealed with a rubber septum, connected to a Schlenk manifold line

under a positive pressure of nitrogen, and cooled to -78 °C in an acetone and dry ice bath. Diethylaminosulfur trifluoride (DAST) (967.1 mg, 6 mmol, 1.2 equiv) was solubilized in DCM (5 mL). The DAST solution was added dropwise to the reaction flask *via* syringe. The reaction solution was allowed to warm to rt then stirred for 12 h. The reaction solution was transferred to a separatory funnel with water (25 mL), followed by slow addition of a saturated $NaHCO_3$ solution (25 mL). The mixture was extracted with Et_2O (3 x 25 mL). The combined organic layers were washed with brine (25 mL), dried over sodium sulfate, filtered, and concentrated *in vacuo*. Silica gel column chromatography using 100% hexanes to 5% EtOAc/hexanes afforded **19** as a white solid (430.2 mg, 2.9 mmol, 58% yield). **^{1}H NMR** (400 MHz, $CDCl_3$) δ 7.71 (t, *J* = 7.8 Hz, 1H), 7.38 (d, *J* = 7.6 Hz, 1H), 7.27 (d, *J* = 8.1 Hz, 1H), 5.43 (d, *J* = 46.6 Hz, 2H). **^{19}F NMR** (376 MHz, $CDCl_3$) δ 18.99 (t, *J* = 46.6 Hz). **^{13}C NMR** (101 MHz, $CDCl_3$) δ 157.4 (d, *J* = 22.5 Hz), 150.9 (d, *J* = 2.8 Hz), 139.5, 123.6, 118.7 (d, *J* = 6.2 Hz), 83.5 (d, *J* = 171.5 Hz). **IR** (neat) 3082, 2946, 1581.94, 1436, 1155, 1035, 987, 855, 788, 701, 608 cm^{-1}. **HRMS (DART)** $[M+H]^+$ calcd. for $[C_6H_6ClFN]^+$ = 146.0167, found 146.0173. **MP** 32 – 38 °C.

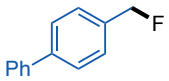

4-(fluoromethyl)-1,1'-biphenyl (20). General Procedure F was followed using BTPP salt **A** (336.0 mg, 0.75 mmol, 1.5 equiv), epoxide **2** (337.7 mg mg, 1.25 mmol, 2.5 equiv), THF (0.25 mL for preactivation), 4-(hydroxymethyl)biphenyl (92.1 mg, 0.5 mmol, 1.0 equiv), 4-(trifluoromethyl)benzenesulfonyl fluoride[8] (125.5 mg, 0.55 mmol, 1.1 equiv), and THF (0.5 mL) to provide 70% ^{1}H NMR yield. The reaction was repeated using commercial BTPP (80% ^{1}H NMR yield). Following General Procedure F, the product was purified *via* preparatory thin layer chromatography using 20% DCM/hexanes to afford **20** as a white solid (37.5 mg, 0.20 mmol, 40% yield). **^{1}H NMR** (400 MHz, $CDCl_3$) δ 7.62 (dd, *J* = 10.6, 7.8 Hz, 4H), 7.50

– 7.42 (m, 4H), 7.42 – 7.33 (m, 1H), 5.44 (d, J = 46.9 Hz, 2H). Characterization data matches literature reports.[8]

iii. Control Reactions

In this section we describe control reactions that support the BTPP generated from the prereagent salt is responsible for promoting deoxyfluorination and not background reactivity from any components or intermediates of the activation process. General Procedure G was followed for each of the controls. We also tested to see if the carboxylate anion is capable of catalyzing reactions by running reactions with only BTPP salt **A**, with a variety of 1-phenylcyclopropanecarboxylate salts. Here, we tested different countercations (e.g., potassium and ammoniums) to survey salt solubility trends. Additionally, we tested if using only epoxide **2** could promote the reaction. We also considered the possibility that a carboxylate anion could attack the epoxide to generate an alkoxide intermediate that could serve as an active basic promoter. We tested this by mixing non-superbase carboxylate salts with epoxide **2** under reaction conditions. For each indicated potential promotor other than the commercial freebase or precatalyst system, we observed either 0% or significantly reduced yield of the product. Overall, these results are consistent with the active promoter being BTPP generated from the prereagent system. Data for these experiments is provided in Tables S11 and S12 for substrates **17** and **20**, respectively.

General Procedure G: Control reactions run in a nitrogen-filled glovebox. Since a pre-activation procedure was required for deoxyfluorination reactions with BTPP salt A, a pre-

activation procedure was used for control reactions that employed epoxide **2**. If epoxide was excluded from the reaction, all reagents were added sequentially inside a nitrogen-filled glovebox.

Pre-activation procedure: in a nitrogen-filled glovebox, an oven-dried 1-dram vial was charged with a magnetic stir bar, indicated basic additive (0.075 mmol, 1.5 equiv), THF (0.125 mL, 0.5 M) and epoxide **2** (0.125 mmol, 2.5 equiv relative to basic "reagent"). The vial was capped with a PTFE-lined cap (ThermoFisher, C4015-1A), removed from the glovebox, and placed in a preheated aluminum reaction block at 80 °C for 20 minutes. The pre-activation solution was then allowed to cool to rt and taken into a nitrogen-filled glovebox. Alcohol (0.05 mmol, 1.0 equiv) and sulfonyl fluoride (0.055 mmol, 1.1 equiv) were added, the vial was recapped, removed from the glovebox and placed in an aluminum reaction block at 25 °C with stirring for 24 h. Dibromomethane (2.0 equiv, 0.1 mmol 7 □L) internal standard was added to the reaction solution, a 50 □L aliquot was taken and added to an NMR tube, then diluted with $CDCl_3$ (0.5 mL). ^1H NMR spectroscopy was used to determine product yield.

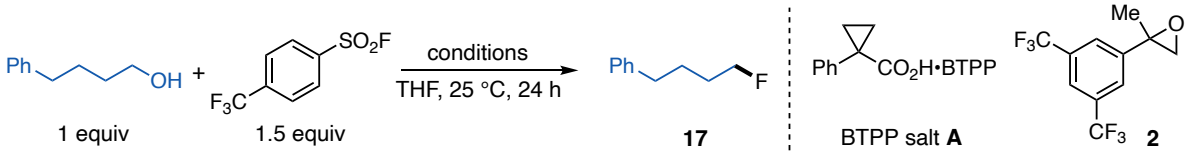

Table S11: Control reactions for the deoxyfluorination reaction of 4-phenylbutan-1-ol with various potential promoters. [a] A preactivation procedure was not followed as noted in General Procedure G.

Entry	Conditions	Results
1[a]	1.5 equiv BTPP	93%
2	1.5 equiv BTPP salt **A** + 2.5 equiv epoxide **2**	60%

3[a]	1.5 equiv BTPP salt **A**	0%
4[a]	1.5 equiv triethylammonium 1-phenylcyclopropanecarboxylate salt	0%
5[a]	NEt_3	0%
6[a]	1.5 equiv tetrabutylammonium acetate	0%
7	1.5 equiv H^+NEt_3 1-phenylcyclopropanecarboxylate + 2.5 equiv epoxide **2**	0%
8	1.5 equiv tetrabutylammonium acetate + 2.5 equiv epoxide **2**	0%
9[a]	2.5 equiv epoxide **2**	0%

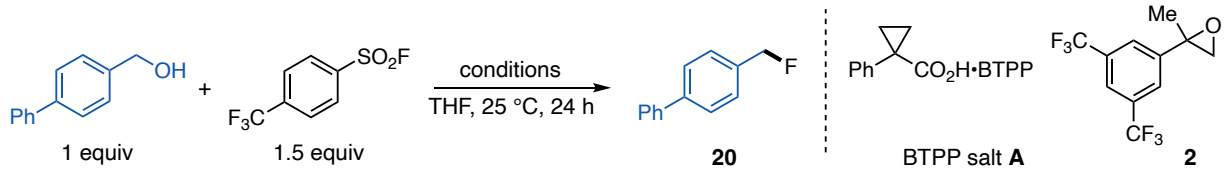

Table S12: Control reactions for the deoxyfluorination reaction of [1,1'-biphenyl]-4-ylmethanol with various potential promoters. [a] A preactivation procedure was not followed as noted in General Procedure G.

Entry	**Conditions**	**Results**
1[a]	1.5 equiv BTPP	80%
2	1.5 equiv BTPP salt **A** + 2.5 equiv epoxide **2**	70%
3[a]	1.5 equiv BTPP salt **A**	0%
4	1.5 equiv triethylammonium 1-phenylcyclopropanecarboxylate[a]	0%
5[a]	NEt_3	0%

6[a]	1.5 equiv tetrabutylammonium acetate	0%
7	1.5 equiv H^+NEt_3 1-phenylcyclopropanecarboxylate + 2.5 equiv epoxide **2**	0%
8	1.5 equiv tetrabutylammonium acetate + 2.5 equiv epoxide **2**	0%
9[a]	2.5 equiv epoxide **2**	0%

V. P_2-*t*-Bu Salt A Activation Studies

i. Procedure for evaluating the generation of P_2-*t*-Bu from P_2-*t*-Bu salt A

In this section we discuss investigation of epoxide additives that, when added to solution with P_2-*t*-Bu salt **A**, facilitate the generation of P_2-*t*-Bu along with an alcohol activation byproduct. For these studies, we tested epoxides under various conditions and assessed the formation of P_2-*t*-Bu and the tertiary alcohol byproduct by ^{31}P and ^{1}H NMR spectroscopy, respectively. When analyzing the protonation state of P_2-*t*-Bu in an activation study by ^{31}P NMR spectroscopy, the proton exchange between free and protonated P_2-*t*-Bu is relatively fast, and as such, we do not observe distinct peaks for the protonated and freebase. Therefore, we developed a process for estimating the quantity of P_2-*t*-Bu based on known ratios of the protonated and freebase, described below. For reference, protonated P_2-*t*-Bu displays two doublets at 16.2 and 13.6 ppm and the freebase displays two doublets at 14.8 and -6.7 ppm.

The amount of freebase can be estimated using ^{31}P NMR spectroscopy by evaluating the chemical shift of the two phosphorus signals. To determine the characteristic spectra of various

ratios of freebase to P_2-*t*-Bu carboxylate salt, we conducted titration experiments where we prepared a series of solutions by mixing commercial P_2-*t*-Bu with P_2-*t*-Bu salt **A** at various ratios on a 0.1 mmol scale. Figure S9 shows ratios ranging from 10:1 to 1:10 P_2-*t*-Bu salt **A**:P_2-*t*-Bu freebase. Here, we utilized a 2 s delay time as well as increased number of scans in order to improve baseline resolution for observation of broad spectral features. The ^{31}P NMR spectra of activation studies were compared to these spectra and an estimated range of percent freebase was assigned. The amount of the alcohol activation byproduct formed in the reaction was determined using ^{1}H NMR spectroscopy with 1,3,5-trimethoxybenzene as an internal standard. The amount of the alcohol byproduct matches well (□ 10%) with the estimated amount of P_2-*t*-Bu generated from the activation reaction.

The ^{31}P NMR spectra for high ratios of the freebase to protonated base (Figure S9, 4:1 P_2-*t*-Bu:P_2-*t*-Bu salt **A** and 10:1 P_2-*t*-Bu:P_2-*t*-Bu salt **A**) are broader than commercial P_2-*t*-Bu. We reasoned that under the activation reaction conditions, this peak broadening could be due to interactions between the freebase and the activation byproduct (e.g., H-bonding). To support this, we subjected commercial P_2-*t*-Bu mixed with 1 equivalent of alcohol activation byproduct **64** and 1 equivalent of epoxide **22** to ^{31}P NMR spectroscopy (Figure S10) and found that the peaks broaden in its presence.

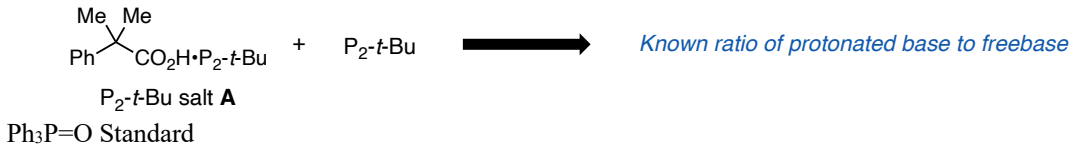

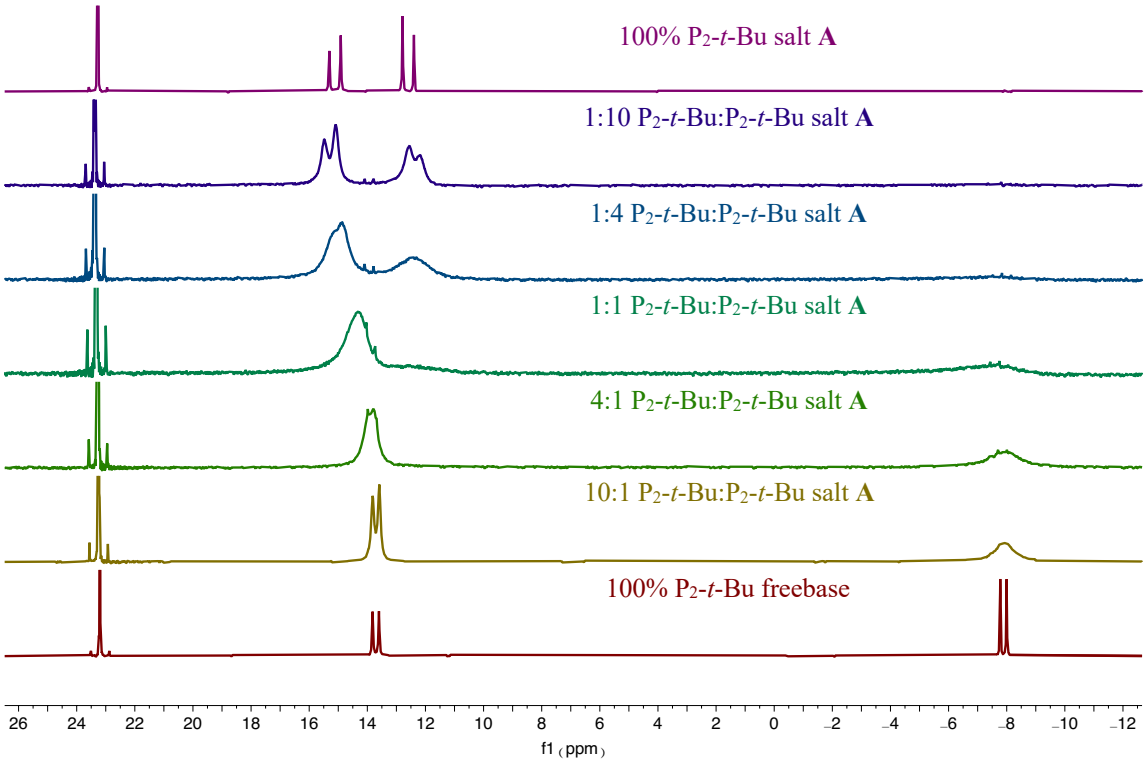

Figure S9: ^{31}P NMR spectra of various ratios of P_2-*t*-Bu freebase and salt **A** in PhMe-d_8.

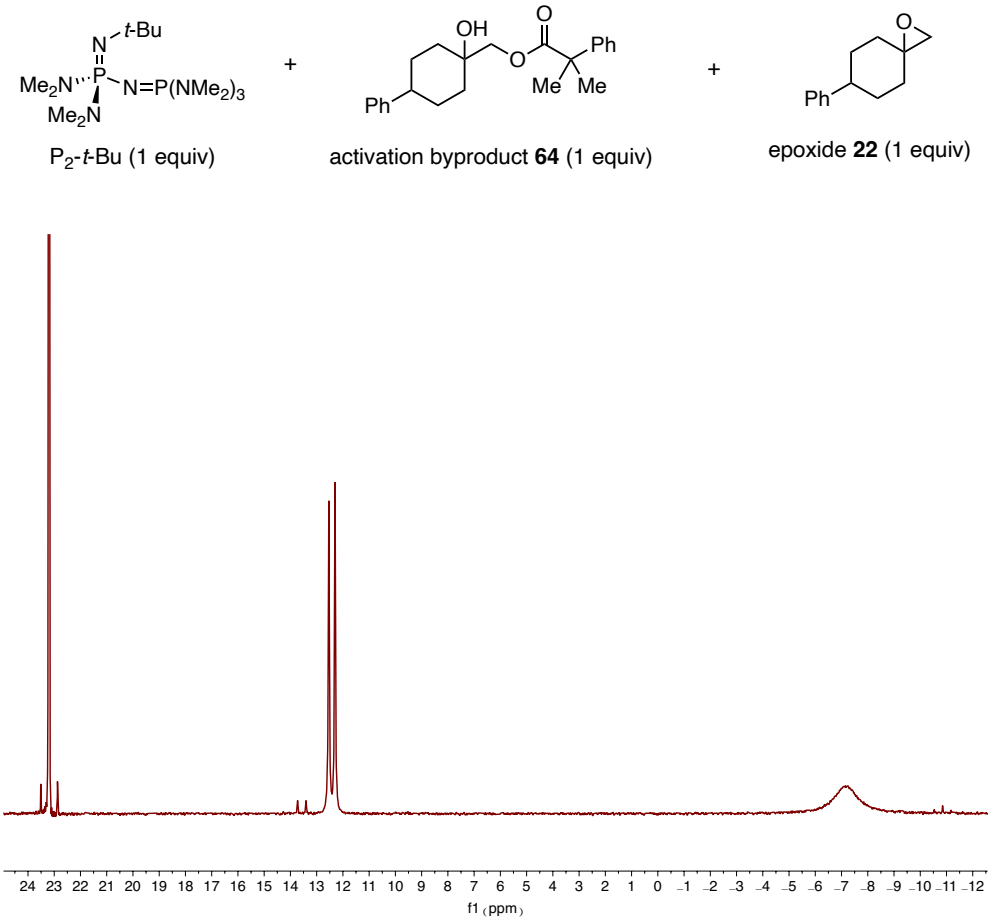

Figure S10. ^{31}P NMR spectrum of commercial P$_2$-*t*-Bu mixed with 1 equivalent of activation byproduct **64** and epoxide **22** that shows broadened spectral features in PhMe-d_8.

b. Examination of epoxide additives for the activation of P$_2$-*t*-Bu salt A

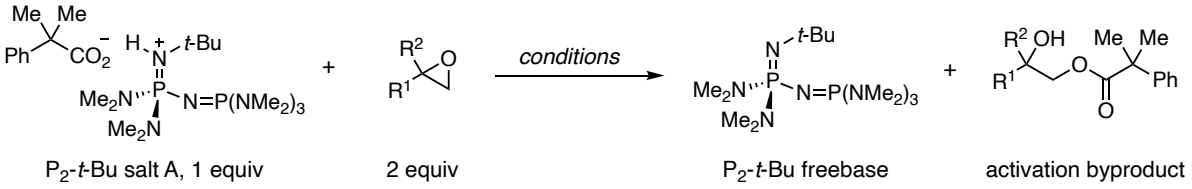

General Procedure H: Activation studies for P_2-*t*-Bu salt A. An oven-dried 1-dram vial (ThermoFisher, C4015-1) was charged with a magnetic stir bar and P_2-*t*-Bu salt **A** (26.6 mg, 0.05 mmol, 1.0 equiv). The vial was brought into a nitrogen-filled glovebox where solvent (0.1 mL, 0.5 M) and epoxide additive (0.1 mmol, 2.0 equiv) were added successively. The vial was sealed with a PTFE-lined cap (ThermoFisher, C4015-1A), removed from the glovebox, and placed in a preheated aluminum reaction block with stirring for the indicated time. The vial was then brought into a nitrogen-filled glovebox where the reaction solution was diluted with deuterated solvent (0.5 mL), transferred to an NMR tube that was capped and sealed with parafilm wax. ^{31}P and ^{1}H NMR spectroscopy were used to assess each reaction to determine the amount of freebase produced and yield of the activation byproduct according to the process described above.

Table S13. Epoxide additives tested for the activation of P_2-*t*-Bu salt **A**. Shown are the estimated ranges for percent freebase generated and the yield of the alcohol activation byproduct.

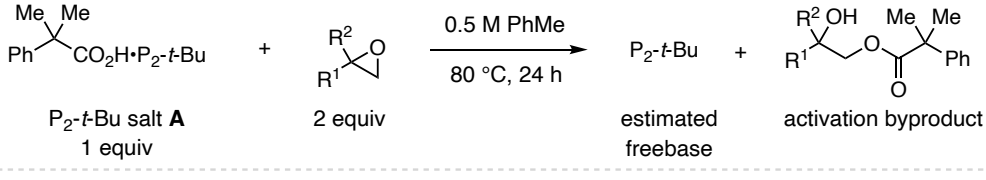

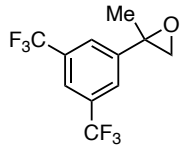

2
40-50% freebase
44% byproduct

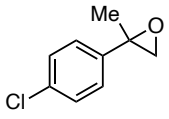

21
40-50% freebase
57% byproduct

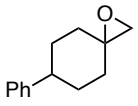

22
80-90% freebase
90% byproduct

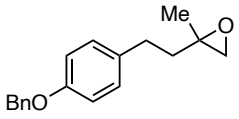

23
75-85% freebase
75% byproduct

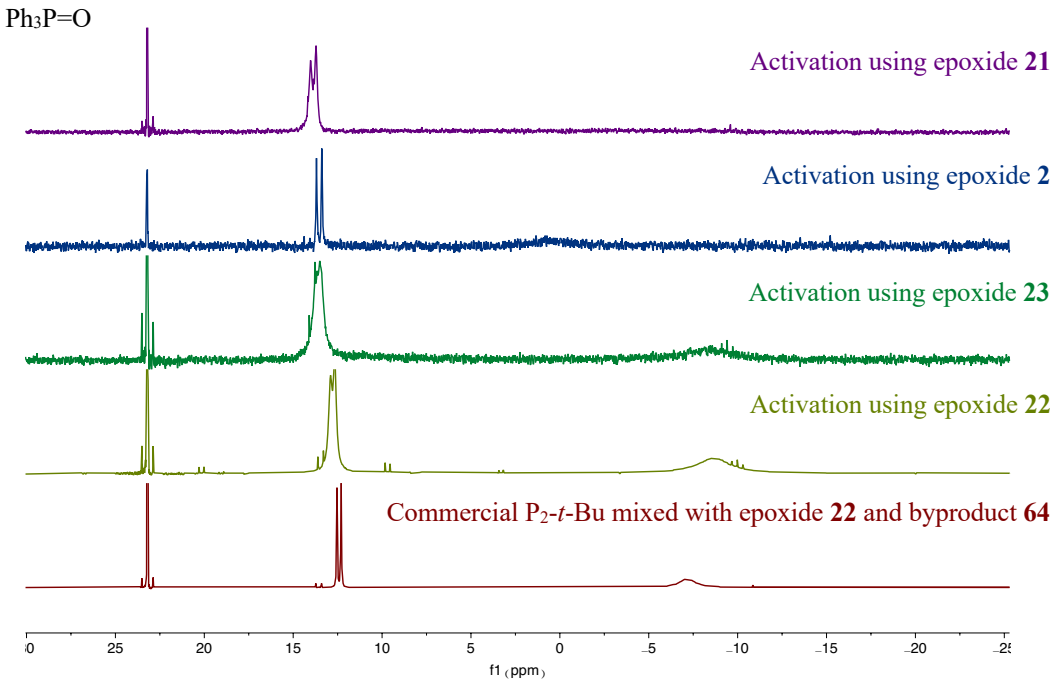

Figure S11. Stacked ^{31}P NMR spectra for the activation of P_2-*t*-Bu salt **A** using various epoxides in PhMe-d_8, with commercial P_2-*t*-Bu mixed with epoxide **22** and byproduct **64**, for comparison.

Description of initial findings: Using General Procedure H in PhMe at 80 °C we first tried aryl substituted epoxides (epoxides **2** and **21** in Table S13 as representative examples), as these epoxides allow rapid and facile activation of BTPP salt **A**. We observed that epoxides **2** and **21** result in 40-50% freebase. Aliphatic epoxides lead to an increased amount of freebase generated, with epoxides **22** and **23** as representative examples leading to 80-90% and 75-85% freebase, respectively. Figure S11 above shows the ^{31}P NMR spectra for use of epoxides in Table S13 in the activation reaction of P_2-*t*-Bu salt **A**. With more freebase generated, a characteristic upfield shift of the peak at 14-16 ppm is observed as well as the appearance of the peak at approximately -6 ppm. Figure S12 below shows the ^{1}H NMR spectra for the activation with epoxides **2** and **22** showing the amount of activation byproduct formed in each case.

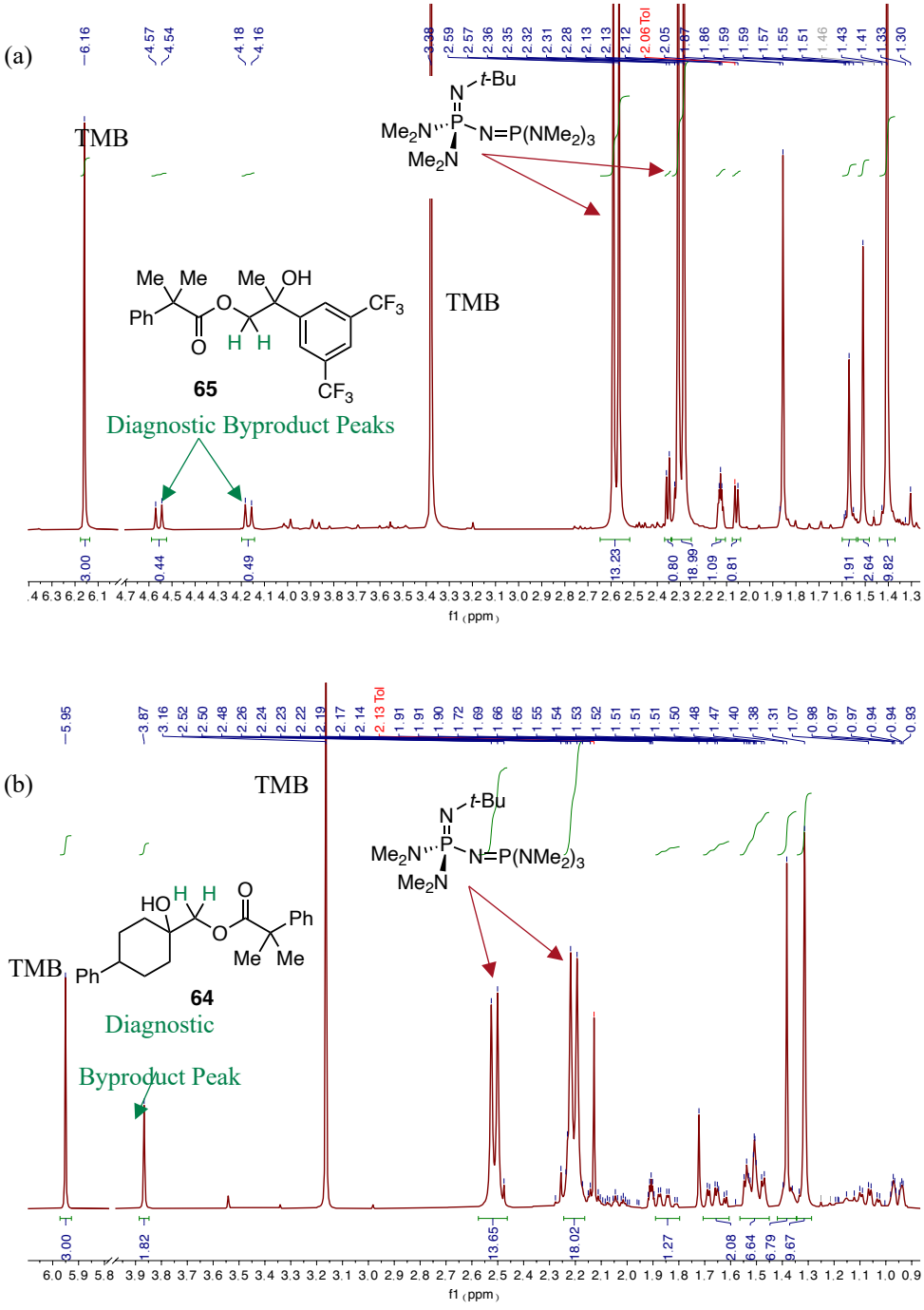

Figure S12: (a) ^{1}H NMR spectrum of epoxide **2** activation reaction with byproduct **65** peaks labeled and integrated compared to 1,3,5-trimethoxybenzene internal standard. (b) ^{1}H NMR spectrum of epoxide **22** activation reaction with byproduct **64** peaks labeled and integrated compared to 1,3,5-trimethoxybenzene (TMB) internal standard.

While we were investigating epoxides for P_2-*t*-Bu salt **A** activation, we found that when aryl-substituted epoxides are used, activation never exceeds 50% generation of the freebase. Our hypothesis for this observation is that activation reaches an equilibrium point at approximately 50% freebase when aryl-substituted epoxides are used. To test this proposal, we studied both the forward and reverse reactions of P_2-*t*-Bu salt **A** activation, using epoxide **21** at 40 °C, as this temperature allowed us to monitor the reaction rate. The forward reaction was set up following General Procedure H and the reverse reaction was setup using General Procedure I (below). The amount of epoxide **21** and byproduct **66** in the crude reaction mixture were evaluated *via* ^{1}H NMR spectroscopy. The results show that the forward and reverse reactions converge at 50% conversion (Figure S13), indicating that the activation of P_2-*t*-Bu salt **A** using aryl-substituted epoxides is reversible and limited by the reaction equilibrium. This limitation was overcome by using aliphatic epoxides like **22** and **23**, which shift the equilibrium towards P_2-*t*-Bu freebase.

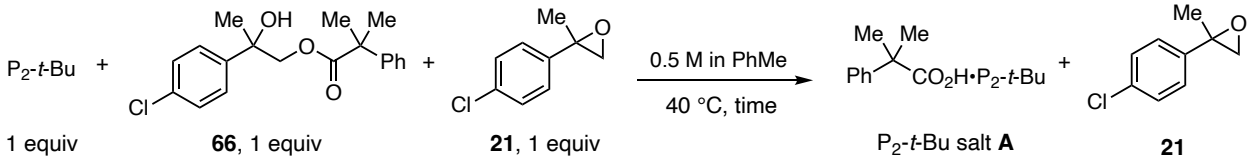

General Procedure I: Reverse activation process for P_2-*t*-Bu salt A. An oven-dried 1-dram vial (ThermoFisher, C4015-1) was charged with a magnetic stir bar and 2-(4-chlorophenyl)-2-hydroxypropyl 2-methyl-2-phenylpropanoate (**66**) (33.3 mg, 0.1 mmol, 1 equiv) open to air. The vial was brought into a nitrogen-filled glovebox where PhMe-d_8 (0.2 mL, 0.5M), epoxide **21** (16.9 mg, 0.1 mmol, 1 equiv), and P_2-*t*-Bu (50 µL of a 2 M THF solution, 0.1 mmol, 1 equiv) were added

successively. The vial was sealed with a PTFE-lined cap (ThermoFisher, C4015-1A), removed from the glovebox, placed in a preheated aluminum reaction block at 40 °C with stirring for the indicated time. The vial was brought into a nitrogen-filled glovebox where the reaction solution was diluted with deuterated PhMe (0.4 mL, total of 0.5 mL), transferred to an NMR tube that was capped and sealed with parafilm wax. ^{31}P NMR and ^{1}H NMR spectroscopic analyses were used to assess each reaction to determine the amount of freebase and alcohol activation byproduct.

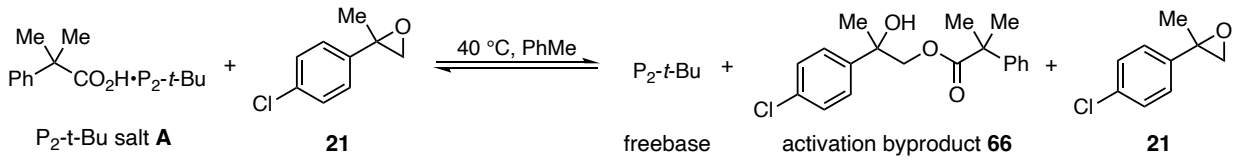

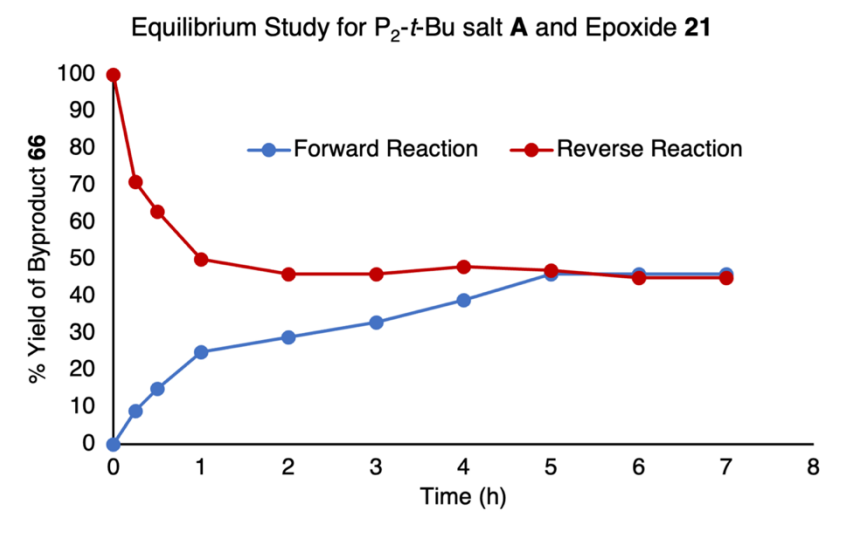

Figure S13: Equilibrium study showing forward and reverse activation reaction for P_2-*t*-Bu salt **A** and epoxide **21**.

b. P_2-*t*-Bu A activation with epoxide 22 under various conditions

This section describes condition variation using epoxide **22** to activate P_2-*t*-Bu salt **A** in a variety of solvents, temperatures, concentrations, and reaction times (Table S14). These experiments were setup using General Procedure H. Entry 1 shows the initial conditions that were used to evaluate the epoxide structure.

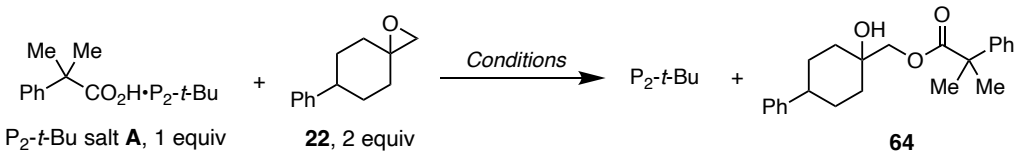

Table S14: Data for the activation of P_2-*t*-Bu salt **A** with epoxide **22** under various conditions.

Entry	Conditions	Estimated Free Base Yield	Byproduct 64 Yield
1	80 °C, 24 h, 0.5 M in PhMe	80-90%	90%
2	80 °C, 3 h, 0.5 M in PhMe	60-70%	75%
3	80 °C, 3 h, 0.5 M in PhMe (open air)	25-35%	38%
4	80 °C, 3 h, 0.5 M in THF	65-75%	73%
5	40 °C, 24 h, 1.0 M in PhMe	50-60%	51%
6	40 °C, 24 h, 1.0 M in THF	50-60%	58%
7	60 °C, 3 h, 1.0 M in THF	65-75%	70%
8	60 °C, 3 h, 1.0 M in DME	65-75%	71%

9	40 °C, 24 h, 1.0 M in *n*-Bu_2O	50-60%	74%
10	80 °C, 24 h, 1.0 M in NMP	40-50%	53%
11	80 °C, 24 h, 0.5 M in DMSO	25-35%	40%
12	80 °C, 24 h, 0.5 M in DMF	65-75%	69%
13	100 °C, 0.5 h, 0.6 M in 1,4-Dioxane	75-85%	92%

c. All-in-one activation system combining P_2-*t*-Bu salt A with epoxide 23

For the activation studies described thus far, the superbase salt and epoxide additive have been stored separately and combined *in situ* for base activation. We identified solid epoxide **23** that can be stored in the same vial as P_2-*t*-Bu salt **A** as a stable mixture. We made this by combining P_2-*t*-Bu salt **A** with epoxide **23** in a 1:2 ratio in a vial and mixing them together with a spatula for even distribution. This mixture was stored in a benchtop desiccator with no physical or spectral changes over 1 month of storage. Stored in a freezer, we observe no physical changes for 1 year of storage. We note that in ^{1}H NMR spectra in Figure S14, the ratio of P_2-*t*-Bu salt **A** to epoxide **23** changes depending on the sample taken, observable at 1–1.5 ppm. Due to manual mixing of the components, the ratio can vary by 1-10% based on the sample that is taken from the vial, resulting in relative peak intensity differences. See Table S16 for data on application of the all-in-one precatalyst in the oxa-Michael addition where it functions just as well as P_2-*t*-Bu salt **A** stored separate from the epoxide.

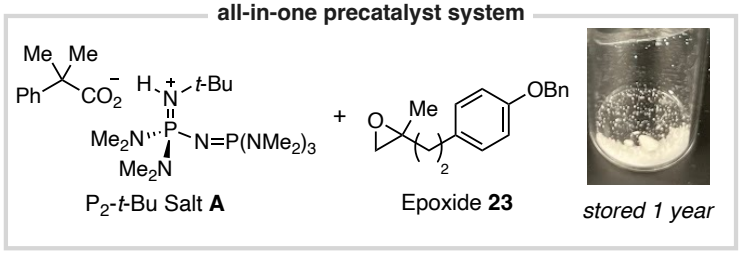
all-in-one precatalyst system
Me Me
Ph
CO2
H
t-Bu
Me2N
P
N=P(NMe2)3
Me2N
P2-t-Bu Salt A
+
O
Me
OBn
2
Epoxide 23
stored 1 year

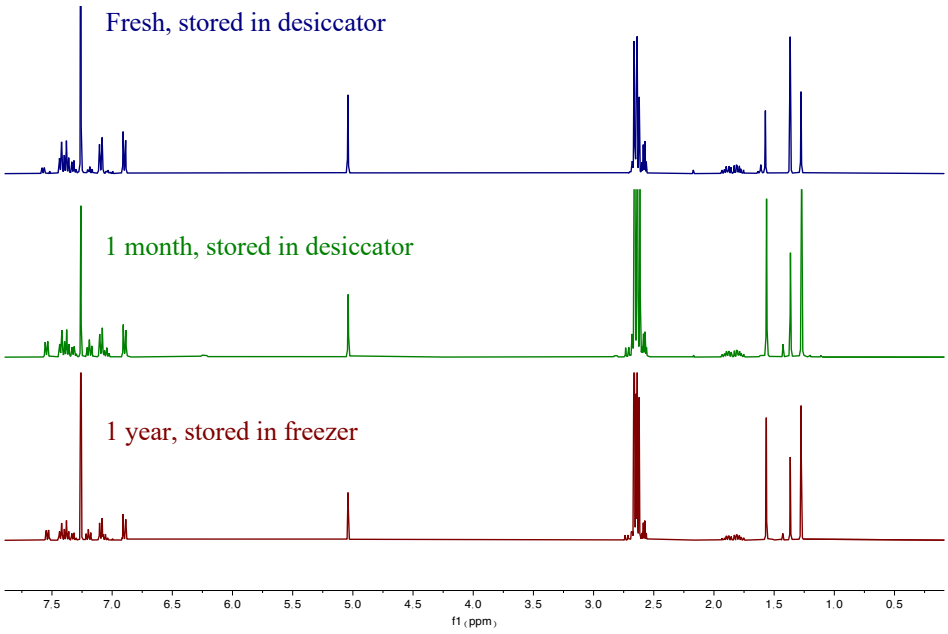
Fresh, stored in desiccator
1 month, stored in desiccator
1 year, stored in freezer
7.5 7.0 6.5 6.0 5.5 5.0 4.5 4.0 3.5 3.0 2.5 2.0 1.5 1.0 0.5
f1 (ppm)

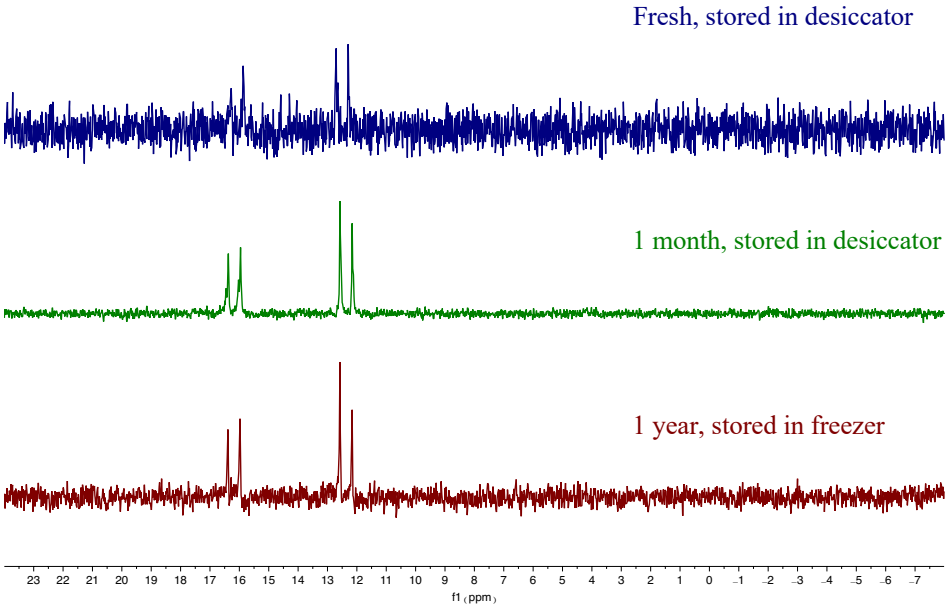
Fresh, stored in desiccator
1 month, stored in desiccator
1 year, stored in freezer
23 22 21 20 19 18 17 16 15 14 13 12 11 10 9 8 7 6 5 4 3 2 1 0 -1 -2 -3 -4 -5 -6 -7
f1 (ppm)

Figure S14. Top: ^{1}H NMR spectra for "all-in-one" precatalyst aged over time with only minor changes in spectral features. Bottom: ^{31}P NMR spectra for "all-in-one" precatalyst aged over time with minimal changes in spectral features.

VI. Applications of P_2-*t*-Bu Salt A and Epoxides as Precatalyst Systems

a. Use of P_2-*t*-Bu salt A as a precatalyst for oxa- and aza-Michael reactions

i. Reaction scheme and General Procedures

Table S15: Substrate table of oxa/aza-Michael addition reactions run using P_2-*t*-Bu catalyst systems stored in various environments. [a] Reaction run in DMSO.

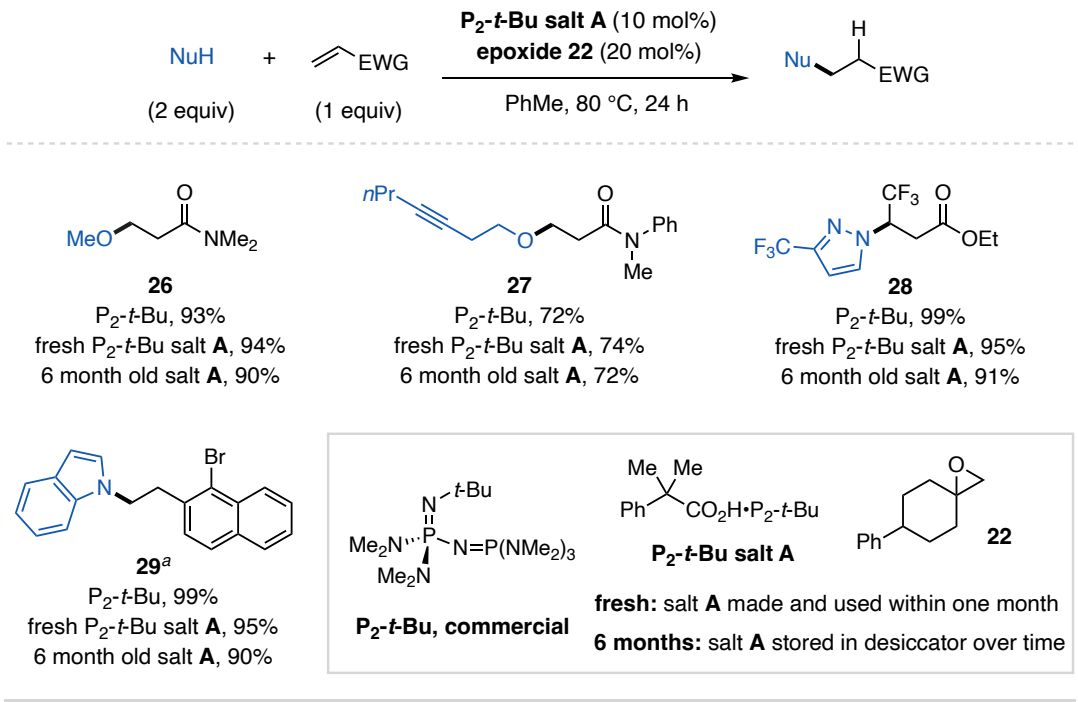

General Procedure J: P_2-*t*-Bu salt A and epoxide 22 promoted reaction. An oven-dried 1-dram vial (ThermoFisher, C4015-1) was charged with a magnetic stir bar, P_2-*t*-Bu salt **A** (53.2 mg, 0.10 mmol, 10 mol%), and epoxide **22** (37.6 mg, 0.20 mmol, 20 mol%). The vial was sealed with a PTFE lined screw cap (ThermoFisher, C4015-A) and evacuated then flushed with nitrogen three times *via* a nitrogen inlet tube on a Schlenk manifold line. PhMe (2.0 mL, 0.5 M), alkene (1.0 mmol, 1.0 equiv), and pronucleophile (2.0 mmol, 2.0 equiv) were added to the vial *via* nitrogen-flushed syringe. **Note**: alkene and/or pronucleophile were charged to the vial prior to capping and nitrogen flushing if they are solids at rt. The inlet tube was removed from the vial and the cap was wrapped in parafilm and PVC tape. The vial was placed into a preheated aluminum reaction block at 80 °C with stirring for 24 h. The reaction solution was cooled to rt and dibromomethane (70 µL, 1.0 mmol, 1.0 equiv) was added to the solution, a 50 µL aliquot was taken and added to an NMR tube, then diluted with $CDCl_3$ (0.5 mL). ^{1}H NMR spectroscopy was used to determine the yield of the reaction. The crude reaction material was directly subjected to flash chromatography to yield purified product for characterization.

ii. Reaction and characterization data

General description: For all of the substrates in this section, we use ^{1}H NMR yields to assess the efficacy of the precatalyst salt system. In each case, we benchmarked the success of the precatalyst against the use of commercial P_2-*t*-Bu and P_2-*t*-Bu salt **A** that has been handled regularly open to air and stored in a benchtop desiccator for six months (see Section VIII for details). The reactions carried out with P_2-*t*-Bu were set up using General Procedure K below, and the reactions carried out with aged P_2-*t*-Bu salt **A** were set up using General Procedure J. The substrates were

subsequently isolated using General Procedure J and P_2-*t*-Bu salt **A** for characterization. The purification conditions and characterization data are given below.

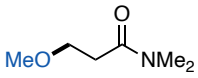

3-Methoxy-*N*,*N*-dimethylpropanamide (26). General Procedure J was followed using *N*,*N*-dimethylacrylamide (99.1 mg, 1 mmol, 1.0 equiv), methanol (81 µL, 2.0 mmol, 2.0 equiv), P_2-*t*-Bu salt **A** (53.2 mg, 0.1 mmol, 10 mol%), epoxide **22** (37.6 mg, 0.2 mmol, 20 mol%) and PhMe (2 mL) to provide 94% ^{1}H NMR yield. The reaction was repeated using commercial P_2-*t*-Bu (93% ^{1}H NMR yield) and six-month-old P_2-*t*-Bu salt **A** (90% ^{1}H NMR yield). Following General Procedure J, the product was purified *via* silica gel chromatography (TLC visualized with PMA stain) using 10% EtOAc in hexanes to afford **26** as a colorless oil (98.1 mg, 0.75 mmol, 75% yield). **^{1}H NMR** (400 MHz, $CDCl_3$) δ 3.65 (t, *J* = 6.6 Hz, 2H), 3.31 (s, 3H), 2.97 (s, 3H), 2.90 (s, 3H), 2.55 (t, *J* = 6.6 Hz, 2H). Characterization data matches literature reports.[9]

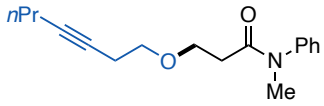

3-(Hept-3-yn-1-yloxy)-*N*-methyl-*N*-phenylpropanamide (27). General Procedure J was followed using *N*-methyl-*N*-phenylprop-2-enamide[10] (161.0 mg, 1.0 mmol, 1.0 equiv), 3-heptyn-1-ol (250.0 µL, 2.0 mmol, 2.0 equiv), P_2-*t*-Bu salt **A** (53.2 mg, 0.1 mmol, 10 mol%), epoxide **22** (37.6 mg, 0.2 mmol, 20 mol%) and PhMe (2 mL) to provide 74% ^{1}H NMR yield. The reaction was repeated using commercial P_2-*t*-Bu (72% ^{1}H NMR yield) and six-month-old P_2-*t*-Bu salt **A** (72% ^{1}H NMR yield). Following General Procedure J, the product was purified *via* silica gel chromatography using 20% EtOAc in hexanes to afford **27** as a colorless oil (167.6 mg, 0.61 mmol, 61% yield). **^{1}H NMR** (400 MHz, $CDCl_3$) δ 7.42-7.35 (m, 2H), 7.34-7.27 (m, 1H), 7.22-7.16 (m, 2H), 3.69 (t, *J* = 6.8 Hz, 2H), 3.45 (t, *J* = 7.1

Hz, 2H), 3.25 (s, 3H), 2.41-2.30 (m, 4H), 2.07 (tt, J = 7.0, 2.4 Hz, 2H), 1.45 (h, J = 7.3 Hz, 2H), 0.92 (t, J = 7.4 Hz, 3H). **^{13}C NMR** (101 MHz, $CDCl_3$) δ 170.9, 144.0, 129.8, 127.9, 127.5, 81.3, 76.8, 69.9, 67.2, 37.3, 34.6, 22.4, 20.8, 20.1, 13.5. **IR** (neat) 2961, 2931, 2870, 1654, 1595, 1496, 1382, 1110, 773, 700 cm^{-1}. **HRMS (DART)** $[M+H]^+$ calcd. for $[C_{17}H_{24}NO_2]^+$ = 274.1807, found 274.1802.

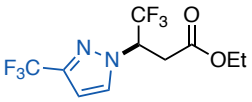

Ethyl-4,4,4-trifluoro-3-(3-(trifluoromethyl)-1*H*-pyrazol-1-yl)-butanoate (28). General Procedure J was followed using ethyl (*E*)-4,4,4-trifluorobut-2-enoate (149.4 μL, 1.0 mmol, 1.0 equiv), 3-(trifluoromethyl)pyrazole (272.2 mg, 2.0 mmol, 2.0 equiv), P_2-*t*-Bu salt **A** (53.2 mg, 0.1 mmol, 10 mol%), epoxide **22** (37.6 mg, 0.2 mmol, 20 mol%), and PhMe (2 mL) to provide 95% ^{1}H NMR yield. The reaction was repeated using commercial P_2-*t*-Bu (99% ^{1}H NMR yield) and six-month-old P_2-*t*-Bu salt **A** (91% ^{1}H NMR yield). Following General Procedure J, the product was purified *via* silica gel chromatography using 20% EtOAc in hexanes to afford **28** as a colorless oil (152.1 mg, 0.50 mmol, 50% yield). **^{1}H NMR** (400 MHz, $CDCl_3$) δ 7.60 (d, J = 2.5 Hz, 2H), 6.59 (d, J = 2.5 Hz, 2H), 5.25 (dqd, J = 10.6, 6.9, 3.6 Hz, 1H), 4.19 – 4.04 (m, 2H), 3.54 (dd J = 17.2, 10.5 Hz, 1H), 3.07 (dd, J = 17.2, 3.6 Hz, 1H), 1.18 (t, J = 7.1 Hz, 3H). **^{19}F NMR** (376 MHz, $CDCl_3$) δ -62.22 (s, 3F), -74.55 (d, J = 6.9 Hz, 3F). **^{13}C NMR** (101 MHz, $CDCl_3$) δ 168.5, 144.1 (q, J = 38.8 Hz), 132.8, 123.0 (q, J = 286.9 Hz), 121.3 (q, J = 271.6 Hz), 105.5, 61.8, 60.0 (q, J = 32.4 Hz), 32.7, 14.0. **IR** (neat) 3134, 2989, 1738, 1487, 1388, 1315, 1241, 1167, 1126 cm^{-1}. **HRMS (ESI)** $[M+H]^+$ clacd. for $[C_{10}H_{11}F_6N_2O_2]^+$ = 305.0725, found 305.0720.

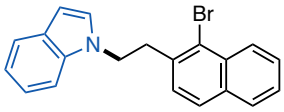

1-(2-(1-bromonaphthalen-2-yl)ethyl)-1*H*-indole (29). General Procedure J was followed using 1-bromo-2-vinylnaphthalene[11] (233.1 mg, 1.0 mmol, 1.0 equiv), 1*H*-indole (234.3 mg, 2.0 mmol, 2.0 equiv), P_2-*t*-Bu salt **A** (53.2 mg, 0.1 mmol, 10 mol%), epoxide **22** (37.6 mg, 0.2 mmol, 20 mol%), and DMSO (2 mL) to provide 95% ^{1}H NMR yield. The reaction was repeated using commercial P_2-*t*-Bu (99% ^{1}H NMR yield) and six-month-old P_2-*t*-Bu salt **A** (90% ^{1}H NMR yield). Following General Procedure J, the product was purified *via* silica gel chromatography using 5% EtOAc in hexanes with 2% NEt_3 to afford **29** as a white solid (295.0 mg, 0.84 mmol, 90% yield). **^{1}H NMR** (400 MHz, $CDCl_3$) δ 8.36 (dd, *J* = 8.5, 1.2 Hz, 1H), 7.80 (dd, *J* = 8.1, 1.3 Hz, 1H), 7.70 – 7.58 (m, 3H), 7.56 – 7.45 (m, 2H), 7.23 (t, *J* = 7.5 Hz, 1H), 7.13 (t, *J* = 7.4 Hz, 1H), 7.07 (d, *J* = 8.3 Hz, 1H), 6.97 (d, *J* = 3.1 Hz, 1H), 6.46 (dd, *J* = 3.1, 0.9 Hz, 1H), 4.47 (t, *J* = 7.7 Hz, 2H), 3.50 (t, *J* = 7.7 Hz, 2H). **^{13}C NMR** (101 MHz, $CDCl_3$) δ 136.1, 136.0, 133.7, 132.7, 128.9, 128.4, 128.3, 128.0, 128.0, 127.7, 127.4, 126.4, 124.2, 121.7, 121.2, 119.5, 109.5, 101.4, 46.3, 38.6. **IR** (neat) 3052, 2933, 1555, 1513, 1462, 1359, 1319, 1173, 1019, 732 cm^{-1}. **HRMS (DART)** $[M+H]^+$ calcd. for $[C_{20}H_{16}BrN]^+$ = 350.0539, found 350.0547. **MP** 72 – 76 °C.

iii. Control Reactions

In this section we describe control reactions to support that P_2-*t*-Bu generated from the precatalyst salt is responsible for catalyzing the reaction and not background reactivity from any components or intermediates of the activation process. General Procedure K below was followed for each of the controls. We also tested to see if the carboxylate anion is capable of catalyzing reactions by

running reactions with only P_2-*t*-Bu salt **A**, with a variety of 1-phenylcyclopropanecarboxylate salts. Here, we tested different countercations (e.g., potassium and ammoniums) to survey salt solubility trends. Additionally, we tested if using only epoxide **22** could promote the reaction. We also considered the possibility that a carboxylate anion can attack the epoxide to generate an alkoxide intermediate that could serve as an active basic catalyst. We tested this by mixing non-superbase carboxylate salts with epoxide **22** under reaction conditions. For each indicated catalyst system other than the commercial freebase or precatalyst system, we observed either 0% or reduced yield of the product. Overall, these results are consistent with the active catalyst being P_2-*t*-Bu generated from the precatalyst system. Data for these experiments is provided in Tables S16 and S17 for substrates **26** and **29**, respectively.

General Procedure K: Control reactions run in a nitrogen-filled glovebox. In a nitrogen-filled glovebox, an oven-dried 1-dram vial (ThermoFisher, C4015-1) was charged with a magnetic stir bar, pronucleophile (0.2 mmol, 2.0 equiv), PhMe (0.2 mL, 0.5 M), epoxide **22** (0.02 mmol, 20 mol%, unless excluded), alkene (0.1 mmol, 1.0 equiv), and the indicated catalyst (0.01 mmol, 10 mol%) in successive order. The vial was sealed with a PTFE-lined cap (ThermoFisher, C4015-1A), removed from the glovebox, placed in a preheated aluminum reaction block at 80 °C with stirring for 24 h. The reaction solution was cooled to rt and dibromomethane (7 μL, 0.1 mmol, 1.0 equiv) internal standard was added to the reaction solution. A 50 μL aliquot was taken and added to an NMR tube, then diluted with 0.5 mL of $CDCl_3$. Analysis of the ^1H NMR spectrum was used to determine the yield of the product.

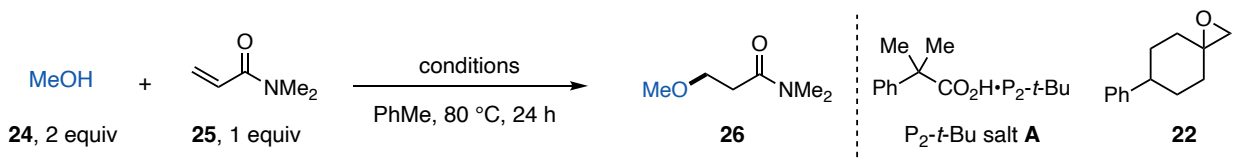

Table S16. Control reactions for methanol addition to *N,N*-dimethylacrylamide. [a] Indicates reaction was set up following General Procedure J . [b] Indicates use of the combined P_2-*t*-Bu salt **A** and epoxide **23** all-in-one system, see Section Vc for details. [c] Indicates the use of the all-in-one system after it had been aged for 1 month in a benchtop desiccator. [d] Indicates the use of P_2-*t*-Bu salt **A** that has been recovered after water absorption *via* azeotrope with PhMe, see Section VIIIb for details.

Entry	Conditions	Results
1	10% P_2-*t*-Bu	93%
2 [a]	10% P_2-*t*-Bu salt **A** + 20% epoxide **22**	94%
3	5% P_2-*t*-Bu salt **A** + 10% epoxide **22**	95%
4	2.5% P_2-*t*-Bu salt **A** + 5% epoxide **22**	33%
5	1% P_2-*t*-Bu salt **A** + 2% epoxide **22**	22%
6 [a]	10% P_2-*t*-Bu salt **A** + epoxide **23**	89%
7	10% P_2-*t*-Bu salt **B** + 20% epoxide **22**	87%
8	10% P_2-*t*-Bu salt **B** (aged 2h in 84% humidity) + 20% epoxide **22**	89%
9 [b]	10% P_2-*t*-Bu salt **A** + 20% epoxide **23** (all-in-one precatalyst)	96%
10 [a,c]	10% P_2-*t*-Bu salt **A** + 20% epoxide **23** (all-in-one precatalyst), 1-month old	91%
11 [d]	10% P_2-*t*-Bu salt **A** (from moisture recovery) + 20% epoxide **22**	90%
12	10% P_2-*t*-Bu salt **A**	0%

13	10% potassium 2-methyl-2-phenylpropionate	0%
14	10% triethylammonium 2-methyl-2-phenylpropionate	0%
15	10% NEt_3	0%
16	10% tetrabutylammonium acetate	0%
17	20% epoxide **22**	0%
18	10% potassium 2-methyl-2-phenylpropionate + 20% epoxide **22**	0%
19	10% $HNEt_3^+$ 2-methyl-2-phenylpropionate + 20% epoxide **22**	0%
20	10% tetrabutylammonium acetate + 20% epoxide **22**	0%

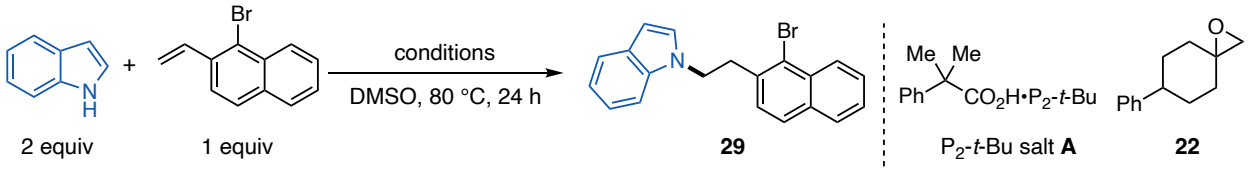

Table S17: Control reactions for addition of indole to 1-bromo-2-vinylnaphthalene. [a] Indicates the use of P_2-*t*-Bu salt **A** that has been recovered after water absorption *via* azeotrope with PhMe, see Section VIIIb for details.

Entry	**Conditions**	**Results**
1	10% P_2-*t*-Bu	99%
2	10% P_2-*t*-Bu salt **A** + 20% epoxide **22**	93%
3 [a]	10% P_2-*t*-Bu salt **A** (from moisture recovery) + 20% epoxide **22**	94%
4	10% P_2-*t*-Bu salt **B** + 20% epoxide **22**	91%

5	10% P_2-*t*-Bu salt **A**	19%
6	10% potassium 2-methyl-2-phenylpropionate	0%
7	10% triethylammonium 2-methyl-2-phenylpropionate	0%
8	10% NEt_3	0%
9	10% tetrabutylammonium acetate	0%
10	20% epoxide **22**	0%
11	10% potassium 2-methyl-2-phenylpropionate + 20% epoxide **22**	66%
12	10% $HNEt_3^+$ 2-methyl-2-phenylpropionate + 20% epoxide **22**	0%
13	10% tetrabutylammonium acetate + 20% epoxide **22**	0%
14	No Base	0%

We note that for Table S17 Entry 11, the combination of potassium 2-methyl-2-phenylpropionate and epoxide **22** is capable of promoting the hydroamination reaction; we speculate a potassium alkoxide intermediate is generated that promotes the reaction. However, the corresponding alkoxide intermediate of the precatalyst system likely neutralizes P_2-*t*-Bu immediately to generate the freebase as the active catalyst. We supported this by premixing P_2-*t*-Bu salt **A** with epoxide **22** for 1 h at 100 °C in PhMe that showed complete formation of the freebase (observed by ^{31}P and ^{1}H NMR spectroscopy), followed by addition of starting materials. Here, the hydroamination rate is very similar to the use of P_2-*t*-Bu freebase (reaction complete in 2 h). Direct use of the preacatlyst system shows a slower rate (60% yield in 6 h), consistent with precatalyst activation. When

potassium 2-methyl-2-phenylpropionate with epoxide **22** is used, we observe a slower reaction rate (40% yield at 6 h). Additionally, we repeated Entries 5 and 11 from Table S17 for substrates **27** and **28** to assess whether any background processes could be responsible for catalyzing these reactions and found that all gave 0% or very low yield as compared to the use of the precatalyst. Collectively, these results are consistent with the P_2-*t*-Bu generated from the precatalyst system being the active catalyst in these reactions.

b. Use of P_2-*t*-Bu salt A as a precatalyst for the polymerization of ε-caprolactone

i. Reaction scheme and General Procedures

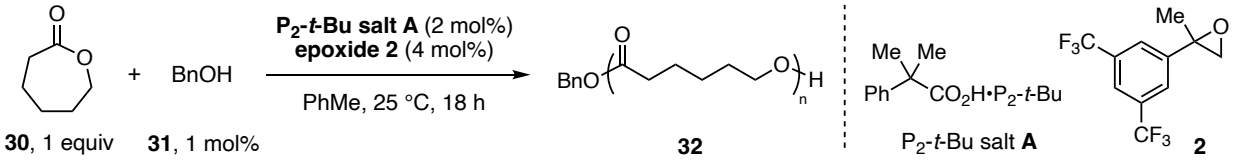

General Procedure L: P_2-*t*-Bu salt A and epoxide 2 promoted reaction. Note: this reaction is run at 25 °C and as such epoxide **2**, which can activate P_2-*t*-Bu salt **A** to 50% conversion at low temperatures, was used in place of epoxide **22**, which requires high temperature for activation. An oven-dried 1-dram vial (ThermoFisher, C4015-1) was charged with a magnetic stir bar and P_2-*t*-Bu salt **A** (31.9 mg, 0.06 mmol, 2.0 mol%). The vial was sealed with a PTFE lined screw cap (ThermoFisher, C4015-A) and evacuated then flushed with nitrogen three times on a Schlenk

manifold line. Toluene (1.2 mL, 2.5 M), ε-caprolactone (**30**, 332.2 μL, 3.0 mol, 1.0 equiv), benzyl alcohol (**31**, 3.1 μL, 0.03 mol, 1.0 mol%) were added to the vial *via* nitrogen-flushed syringe. Epoxide **2** (32.4 mg, 0.12 mmol, 4.0 mol%) was weighed into a 50 μL microsyringe and added to the vial. The vial was wrapped in parafilm and PVC tape and placed into a preheated aluminum reaction block at 25 °C with stirring for 24 h. Benzoic acid (100 μL) was used to quench the reaction and a 50 μL aliquot was taken and added to an NMR tube, then diluted with $CDCl_3$ (0.5 mL). ^{1}H NMR analysis showed 90% polymerization of the ε-caprolactone monomer initiated by BnOH, characterized by the diagnostic triplet at 4.15 ppm against the diagnostic multiplet of the monomer at 4.30 ppm. Representative spectra are shown below in Figure S15 for the analysis of the degree of polymerization for various time points. We note that when P_2-*t*-Bu salt **A** and epoxide **2** are used, 5-10% of an oligomer side product is also formed. The crude reaction mixture was added dropwise to 10 mL of MeOH in an ice bath at 0 °C and to precipitate the polymeric material. The solid material was isolated using vacuum filtration and redissolved in $CHCl_3$ and then precipitated again in cold MeOH. The white solid was collected by vacuum filtration (130.4 mg material collected) and GPC analysis showed approximate M_n = 14.9 kDa with Đ = 1.07. **^{1}H NMR** (400 MHz, $CDCl_3$) δ 5.12 (s, 2H, end group), 4.06 (t, *J* = 6.7 Hz, 2 H, repeat unit), 2.31 (t, *J* = 7.5 Hz, 2 H, repeat unit), 1.66 (m, 4 H, repeat unit), 1.38 (m, 2 H, repeat unit). Characterization matches literature reports.[12]

For comparison to the use of the precatalyst system, we isolated material from a polymerization reaction using the P_2-*t*-Bu freebase using the same protocol as described in General Procedure L, set up in a N_2-filled glovebox (no oligomer side product is observed). The isolated material shows

the same spectral features as the material isolated from the precatalyst procedure. This material was analyzed by GPC and showed approximate M_n = 12.0 kDa with Đ = 1.14.

ii. Polymerization of ε-Caprolactone Reaction Analysis

To assess polymerization, the total integration of diagnostic polymer **32** peak (triplet, 4.15 ppm) was divided by the total integration of both the polymer peak and monomer **30** peak (triplet, 4.30 ppm). We note that for reactions run with P_2-*t*-Bu salt **A** and epoxide **2**, a peak at 4.25 ppm appears, corresponding to an oligomer side product that is may be initiated by the alcohol activation byproduct. We do not observe the formation of the oligomer side product when P_2-*t*-Bu is used as the catalyst. In these cases, the percent conversion to polymer **32** was assessed by dividing the integration of diagnostic polymer **32** peak by the sum of polymer peak, monomer **30** peak, and oligomer side product peak. After undergoing the precipitation procedures to purify these materials (described in General Procedure L), the oligomer side product is not present in isolated materials. Ongoing work is being conducted to eliminate the formation of this side product in polymerization applications.

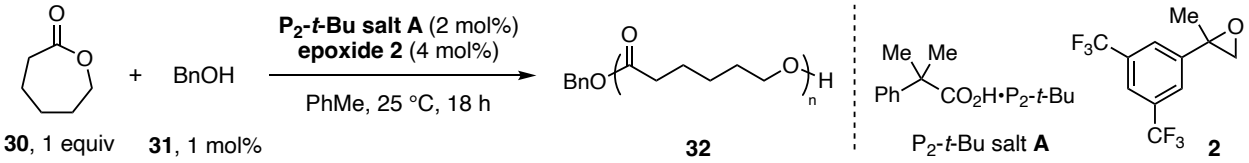

30, 1 equiv **31**, 1 mol% **32** P_2-*t*-Bu salt **A** **2**

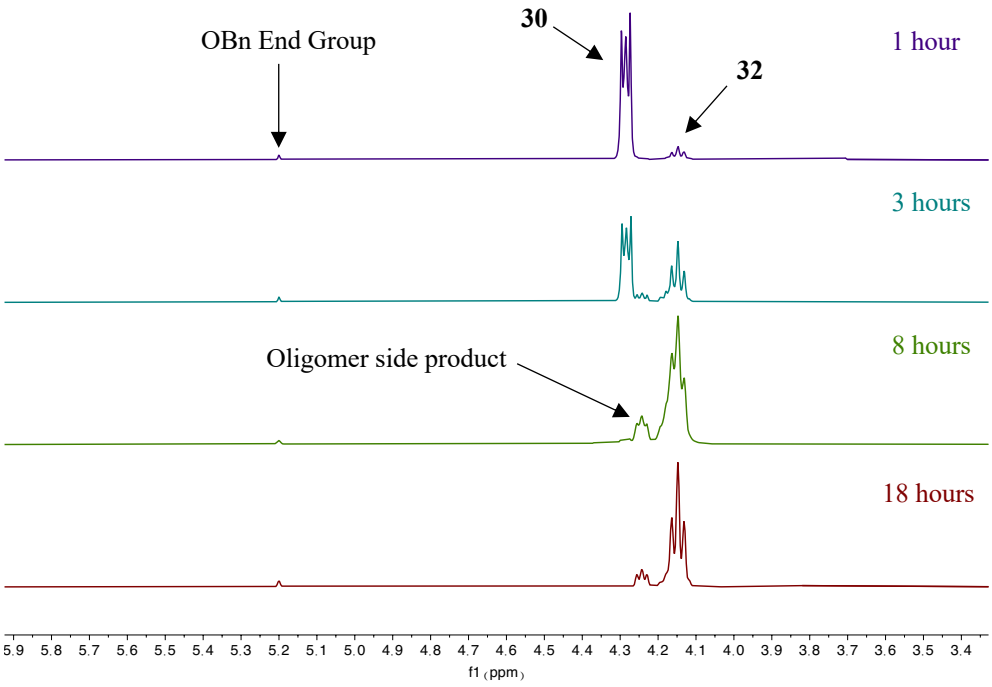

Figure S15. Overlayed ^{1}H NMR spectra of ε-caprolactone polymerization reaction demonstrating the growth of polymer **32** and consumption of monomer **30** over time. The signal at 4.25 ppm corresponds to an oligomer side product.

iii. Control Reactions

In this section we describe control reactions that support the P_2-*t*-Bu generated from the precatalyst salt is responsible for catalyzing polymerization and not background reactivity from any components or intermediates of the activation process. General Procedure M below was followed for each of the controls. We also considered the possibility that a carboxylate can attack the epoxide to generate an alkoxide intermediate that could serve as an active basic catalyst. We tested this by mixing non-superbase carboxylate salts with epoxide **2** under reaction conditions. We also tested if the presence of epoxide or activation byproduct with commercial P_2-*t*-Bu have any

inhibitory effect on the polymerization. We investigated if a carboxylate-opened epoxide intermediate could catalyze polymerization by using tetrabutylammonium acetate with epoxide **2**. For each potential system other than the commercial freebase or precatalyst system, we observed 0% conversion to polymer. Overall, these results are consistent with the active catalyst as P_2-*t*-Bu generated from the precatalyst system. Data for these experiments is provided in Table S18.

General Procedure M: Control reactions run in a nitrogen-filled glovebox. In a nitrogen-filled glovebox, an oven-dried 1-dram vial (ThermoFisher, C4015-1) was charged with a magnetic stir bar, PhMe (1.2 mL, 2.5 M), ε-caprolactone (332.2 μL, 3.0 mol, 1.0 equiv), benzyl alcohol (3.1 μL, 0.03 mol, 1.0 mol%), and the potential control catalyst (0.06 mmol, 2.0 mol%). The vial was sealed with a PTFE-lined cap (ThermoFisher, C4015-1A), removed from the glovebox, placed in a preheated aluminum reaction block at 25 °C with stirring for 24 h. Benzoic acid (100 μL) was used to quench the reaction and a 50 μL aliquot was taken and added to an NMR tube, then diluted with $CDCl_3$ (0.5 mL). ^{1}H NMR analysis was utilized to determine the percent conversion.

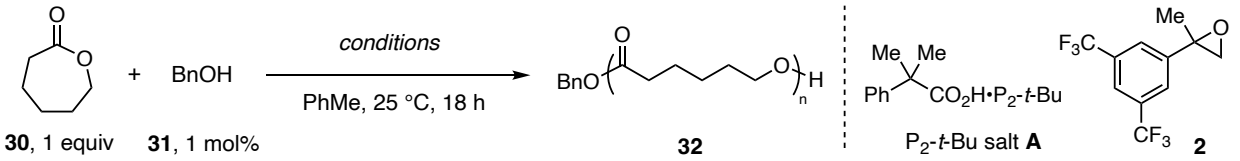

Table S18: Control reactions for the polymerization of ε-caprolactone. For all control reactions, all components are fully soluble in PhMe. [a]Activation byproduct **62** was used in this case as it was previously synthesized for BTPP salt **A** activation studies and is structurally similar to **65**.

Entry	Conditions	% Conversion to 32	% Oligomer
1	2% P_2-*t*-Bu	97%	0%
2	2% P_2-*t*-Bu salt **A** + 4% epoxide **2**	90%	10%
3	1% P_2-*t*-Bu salt **A** + 2% epoxide **2**	92%	8%
4	2% P_2-*t*-Bu + 2% activation byproduct **62** + 2% epoxide **2**	90%	9%
5	2% P_2-*t*-Bu salt **A**	0%	0%
6	2% Bu_4NOAc	0%	0%
7	2% Bu_4NOAc + 4% Epoxide **2**	0%	0%
8 [a]	2% activation byproduct **62**	0%	0%

c. Use of P_2-*t*-Bu salt A as a prereagent for nucleophilic aromatic substitution (S_NAr) reactions

i. Reaction scheme and General Procedures

Table S19: Substrate table for S_NAr reactions run using the P_2-*t*-Bu prereagent system compared to P_2-*t*-Bu freebase. [a] Reaction using prereagent system run in THF. [b] Reaction run in DMSO. [c] Reaction requires preactivation for 1 h in PhMe at 100 °C.

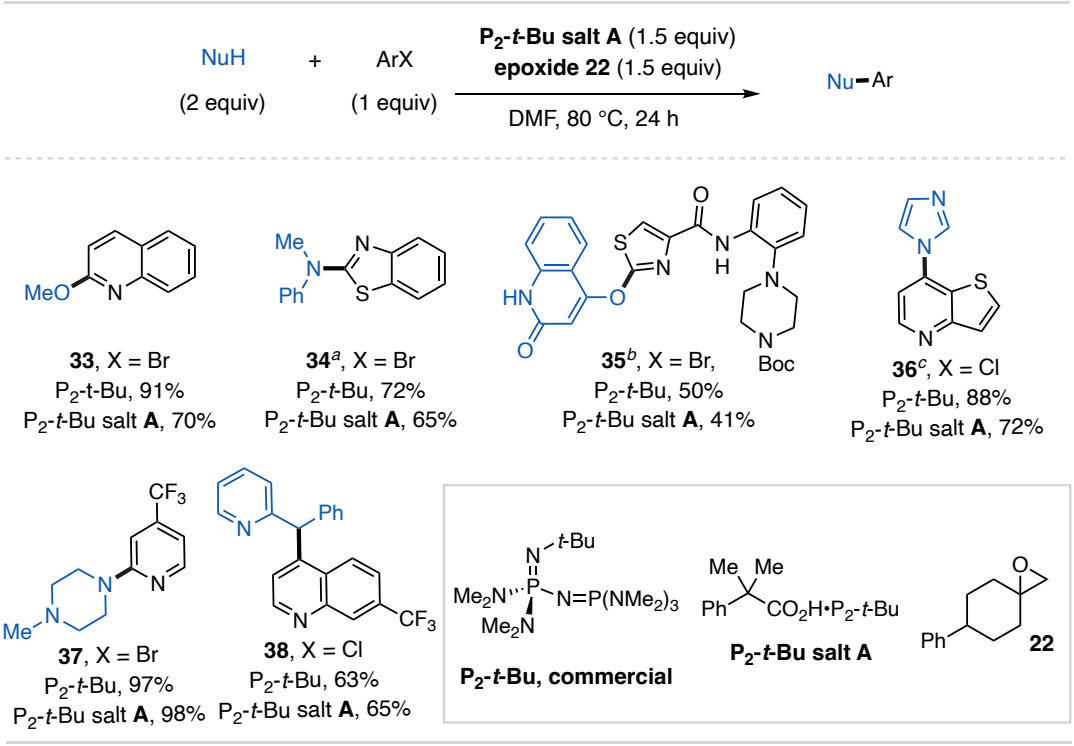

General Procedure N: P_2-*t*-Bu salt A and epoxide 22 promoted reaction. An oven-dried 1-dram vial (ThermoFisher, C4015-1) was charged with a magnetic stir bar, P_2-*t*-Bu salt **A** (398.7 mg, 0.75 mmol, 1.5 equiv), and epoxide **22** (141.2 mg, 0.75 mmol, 1.5 equiv). The vial was sealed with a PTFE-lined cap (ThermoFisher, C4015-1A) and evacuated then backfilled with nitrogen

three times *via* a nitrogen inlet tube on a Schlenk manifold line. To the vial, solvent (1 mL, 0.75M with respect to P_2-*t*-Bu salt **A**) was added *via* nitrogen-flushed syringe and the vial was evacuated then backfilled with nitrogen three times under vigorous stirring *via* a nitrogen inlet tube on a Schlenk manifold line. To a separate oven-dried 1-dram vial (ThermoFisher, C4015-1), solid electrophile (0.5 mmol, 1.0 equiv) and solid pronucleophile (1.0 mmol, 2.0 equiv) were added. The vial was sealed with a PTFE-lined cap (ThermoFisher, C4015-1A) and evacuated then backfilled with nitrogen three times. To the vial, solvent (1 mL, 0.25M for total volume), and, if liquid, electrophile (0.5 mmol, 1.0 equiv) and pronucleophile (1.0 mmol, 2.0 equiv) were added to the vial *via* nitrogen-flushed syringe and the vial was evacuated then backfilled with nitrogen three times under vigorous stirring *via* a nitrogen inlet tube on a Schlenk manifold line. The prereagent solution was transferred to the reagent vial *via* nitrogen-flushed syringe. The inlet tube was removed from the vial and the cap was wrapped in parafilm and PVC tape. The vial was placed in a preheated aluminum reaction block at 80 °C for 24 h with stirring. The reaction solution was cooled to rt and dibenzyl ether (95.0 μL, 0.5 mmol, 1.0 equiv) was added to the reaction solution, a 50 μL aliquot was taken and added to an NMR tube, then diluted with $CDCl_3$ (0.5 mL). ^{1}H NMR spectroscopic analysis was used to determine the yield of the reaction.

General Procedure O: Preactivation for P_2-*t*-Bu salt A and epoxide 22 promoted reaction. Note: this procedure was used for substrate **36** because imidazole reacts with epoxide **22**, preventing the P_2-*t*-Bu activation process. An oven-dried 1-dram vial (ThermoFisher, C4015-1) was charged with a magnetic stir bar, P_2-*t*-Bu salt **A** (398.7 mg, 0.15 mmol, 1.5 equiv), and epoxide **22** (141.2 mg, 0.15 mmol, 1.5 equiv). The vial was sealed with a PTFE-lined cap (ThermoFisher, C4015-1A) and evacuated then back filled with nitrogen three times *via* a nitrogen inlet tube on a

Schlenk manifold line. PhMe (1 mL, 0.75 M with respect to P_2-*t*-Bu salt **A**) was added as the activation solvent to the vial *via* nitrogen-flushed syringe and the vial was evacuated and backfilled with nitrogen three times under vigorous stirring *via* a nitrogen inlet tube on a Schlenk manifold line to degas the solution. The inlet tube was removed from the vial and the cap was wrapped in parafilm and PVC tape. The vial was placed in a preheated aluminum reaction block at 100 °C for 1 h with stirring.

Reagent solution: a separate oven-dried 1-dram vial (ThermoFisher, C4015-1) was charged with a magnetic stir bar, solid pronucleophile (0.5 mmol, 1.0 equiv), and solid electrophile (1.0 mmol, 2.0 equiv). The vial was sealed with a PTFE-lined cap (ThermoFisher, C4014-1A) and evacuated and backfilled with nitrogen three times *via* a nitrogen inlet tube on a Schlenk manifold line. While attached to the inlet tube to maintain positive pressure of nitrogen, solvent (1 mL, 0.25 M total volume) was added to the vial *via* nitrogen-flushed syringe and the vial was evacuated and backfilled with nitrogen three times under vigorous stirring *via* a nitrogen inlet tube on a Schlenk manifold line. The preactivation solution was allowed to cool to rt, placed under a nitrogen atmosphere *via* a nitrogen inlet tube from the Schlenk manifold, and was transferred to the reagent solution *via* nitrogen-flushed syringe. The inlet tube was removed from the reagent solution and the cap was wrapped in parafilm and PVC tape. The vial was placed in a preheated aluminum reaction block at 80 °C for 24 h with stirring. The reaction solution was cooled to rt and dibenzyl ether (95.0 µL, 0.5 mmol, 1.0 equiv) was added to the reaction solution, a 50 µL aliquot was taken and added to an NMR tube, then diluted with $CDCl_3$ (0.5 mL). ^{1}H NMR spectroscopy was used to determine the yield of the reaction.

General Procedure P: P_2-*t*-Bu freebase promoted control reactions. An oven-dried 1-dram vial (ThermoFisher, C4015-1) was charged with a magnetic stir bar. For solid electrophiles and pronucleophiles, the electrophile (1.0 mmol, 2.0 equiv) and the pronucleophile (0.5 mmol, 1.0 equiv) were added to the vial. The vial was brought into a nitrogen-filled glovebox where solvent (2 mL, 0.25M) was added *via* syringe. For liquid electrophiles and pronucleophiles, the electrophile (1.0 mmol, 2.0 equiv) and the pronucleophile (0.5 mmol, 1.0 equiv) were added to the vial. P_2-*t*-Bu (2.0 M solution in THF, 0.375 mL, 0.75 mmol, 1.5 equiv) was added to the vial *via* syringe. The vial was sealed with a PTFE-lined cap (ThermoFisher, C4015-1A), removed from the glovebox and placed into a preheated aluminum reaction block at 80 °C with stirring for 24 h. The reaction solution was cooled to rt and dibenzyl ether (95.3 µL, 0.5 mmol, 1.0 equiv) was added to the reaction solution, a 50 µL aliquot was taken and added to an NMR tube, then diluted with $CDCl_3$ (0.5 mL). ^1H NMR spectroscopy was used to determine the yield of the reaction. The product was purified *via* silica gel chromatography for characterization.

ii. Reaction and characterization data

General description: For all of the substrates in this section, we use ^1H NMR yields to determine the efficacy of the prereagent salt system. In each case, we benchmarked the success of the prereagent against the use of commercial P_2-*t*-Bu setup using General Procedure P above. The substrates were subsequently isolated using General Procedure P to be characterized and confirm the product identity. The purification conditions and characterization data are given below.

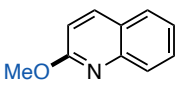

2-Methoxyquinoline (33). General Procedure N was followed using 2-bromoquinoline (104.1 mg, 0.5 mmol, 1.0 equiv), methanol (60.7 µL, 1.5 mmol, 3.0 equiv), P_2-*t*-Bu salt **A** (398.7 mg, 0.75 mmol, 1.5 equiv), epoxide **22** (141.2 mg, 0.75 mmol, 1.5 equiv) and DMF (2 mL) to provide 70% ^{1}H NMR yield. The reaction was repeated using commercial P_2-*t*-Bu (91% ^{1}H NMR yield). Following General Procedure P, for characterization purposes, the product was purified *via* silica gel chromatography using 10% EtOAc in hexanes to afford **33** as a yellow oil (68.4 mg, 0.40 mmol, 80% yield). **^{1}H NMR** (400 MHz, $CDCl_3$) δ 7.97 (d, *J* = 9.4 Hz, 1H), 7.87 (dd, *J* = 8.4, 1.5 Hz, 1H), 7.71 (dd, *J* = 8.0, 1.5 Hz, 1H), 7.63 (ddd, *J* = 8.5, 7.0, 1.5 Hz, 1H), 7.38 (ddd, *J* = 8.1, 7.0, 1.2 Hz, 1H), 6.91 (d, *J* = 8.8 Hz, 1H), 4.09 (s, 3H). Characterization data matches literature reports.[13]

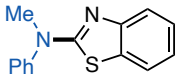

***N*-methyl-*N*-phenylbenzo[d]thiazol-2-amine (34).** General Procedure N was followed using 2-bromobenzothiazole (107.0 mg, 0.5 mmol, 1.0 equiv), *N*-methylaniline (108.3 µL, 1.0 mmol, 2.0 equiv), P_2-*t*-Bu salt **A** (398.7 mg, 0.75 mmol, 1.5 equiv), epoxide **22** (141.2 mg, 0.75 mmol, 1.5 equiv), and DMF (2 mL) to provide 65% ^{1}H NMR yield. The reaction was repeated using commercial P_2-*t*-Bu (72% ^{1}H NMR yield). Following General Procedure P, for characterization purposes, the product was purified *via* silica gel chromatography using 5% EtOAc in hexanes to afford **34** as a yellow oil (84.1 mg, 0.35 mmol, 70% yield). **^{1}H NMR** (400 MHz, $CDCl_3$) δ 7.62 (d, *J* = 7.5 Hz, 1H), 7.53 – 7.40 (m, 5H), 7.39 – 7.27 (m, 2H), 7.07 (t, *J* = 7.5 Hz, 1H), 3.65 (s, 3H). Characterization data matches literature reports.[14]

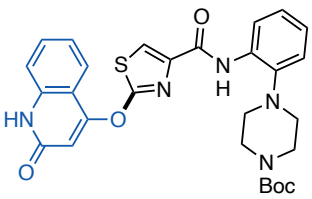

***tert*-Butyl 4-(2-(2-((2-oxo-1,2-dihydroquinolin-4-yl)oxy)thiazole-4-carboxamido)phenyl)piperazine-1-carboxyalte (35).** General Procedure N was followed on a 0.25 mmol scale using *tert*-butyl 4-(2-(2-bromothiazole-4-carboxamido)phenyl)piperazine-1-carboxylate[15] (116.8 mg, 0.25 mmol, 1.0 equiv), 4-hydroxyquinolin-2(1*H*)-one (80.6 mg, 0.5 mmol, 2.0 equiv), P_2-*t*-Bu salt **A** (199.4 mg, 0.375 mmol, 1.5 equiv), epoxide **22** (70.6 mg, 0.375 mmol, 1.5 equiv), and DMSO (1 mL) to provide 41% ^{1}H NMR yield. The reaction was repeated using commercial P_2-*t*-Bu (50% ^{1}H NMR yield). Following General Procedure P, for characterization purposes, the product was purified *via* silica gel chromatography using 100% EtOAc to afford **35** as a pale-yellow solid (72.9 mg, 0.13 mmol, 50% yield). **^{1}H NMR** (400 MHz, $CDCl_3$) δ 11.31 (s, 1H), 10.02 (s, 1H), 8.53 (d, *J* = 7.8 Hz, 1H), 8.00 (s, 1H), 7.94 (dd, *J* = 8.1, 1.4 Hz, 1H), 7.61 (ddd, *J* = 8.5, 7.3, 1.4 Hz, 1H), 7.41 (d, *J* = 8.2 Hz, 1H), 7.32 (ddd, *J* = 8.2, 7.2, 1.0 Hz, 1 H), 7.25 – 7.17 (m, 1H), 7.15 – 7.06 (m, 2H), 6.63 (s, 1H), 3.52 – 3.24 (m, 4H), 2.77 (t, 4.9 Hz, 4H), 1.44 (s, 9H). **^{13}C NMR** (101 MHz, $CDCl_3$) δ 168.7, 164.1, 161.3, 157.9, 154.5, 145.2, 141.5, 138.7, 132.8, 132.3, 125.6, 124.3, 123.1, 122.6, 120.4, 120.1, 119.8, 116.2, 114.5, 106.3, 79.8, 77.2, 52.1, 28.4. **IR** (neat) 3042, 1661, 1510, 1412, 1213, 756 cm^{-1}. **HRMS (DART)** $[M+H]^+$ calcd. for $[C_{28}H_{30}N_5O_5S]^+$ = 548.1968, found 548.1974. **MP** 239 – 244 °C.

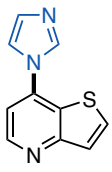

7-(1*H*-Imidazol-1-yl)thieno[3,2-*b*]pyridine (36). General Procedure O was followed using P_2-*t*-Bu salt **A** (398.7 mg, 0.75 mmol, 1.5 equiv), epoxide **22** (141.2 mg, 0.75 mmol, 1.5 equiv), 7-chlorothieno[3,2-*b*]pyridine (84.8 mg, 0.5 mmol, 1.0 equiv), 1*H*-imidazole (68.1 mg, 1.0 mmol, 2.0 equiv), and DMF (2 mL) to provide 72% ^{1}H NMR yield. The reaction was repeated using commercial P_2-*t*-Bu (88% ^{1}H NMR yield). Following General

Procedure P, for characterization purposes, the product was purified *via* silica gel chromatography using 5% MeOH in DCM to afford **36** as a pale-yellow solid (67.5 mg, 0.34 mmol, 68% yield). **^{1}H NMR** (400 MHz, $CDCl_3$) δ 8.80 (d, *J* = 5.1 Hz, 1H), 8.15 (s, 1H), 7.87 (d, *J* = 5.6 Hz, 1H), 7.69 (d, *J* = 5.5 Hz, 1H), 7.58 (s, 1H), 7.35 (s, 1H), 7.28 (d, *J* = 5.1 Hz, 2H). **^{13}C NMR** (101 Hz, $CDCl_3$) δ 159.1, 148.9, 139.6, 136.1, 131.5, 131.3, 126.2, 125.7, 118.2, 111.6. **IR** (neat) 3159, 3071, 1554, 1516, 1478, 1311, 1250, 1168, 1107, 1062, 1022, 812, 666 cm^{-1}. **HRMS (DART)** $[M+H]^+$ calcd. for $[C_{10}H_8N_3S]^+$ = 202.0467, found 202.0441. **MP** 153 – 159 °C.

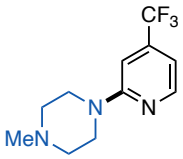

1-Methyl-4-(4-(trifluoromethyl)pyridine-2-yl)piperazine (37). General Procedure N was followed using 2-chloro-4-(trifluoromethyl)pyridine (64.3 µL, 0.5 mmol, 1.0 equiv), *N*-methylpiperazine (110.9 µL, 1.0 mmol, 2.0 equiv), P_2-*t*-Bu salt **A** (398.7 mg, 0.75 mmol, 1.5 equiv), epoxide **22** (141.2 mg, 0.75 mmol, 1.5 equiv), and DMF (2 mL) to provide 98% ^{1}H NMR yield. The reaction was repeated using commercial P_2-*t*-Bu (97% ^{1}H NMR yield). Following General Procedure P, for characterization purposes, the product was purified *via* silica gel chromatography using 5% MeOH in DCM to afford **37** as a yellow solid (93.0 mg, 0.38 mmol, 76% yield). **^{1}H NMR** (400 MHz, $CDCl_3$) δ 8.32 (d, *J* = 5.1 Hz, 1H), 6.82 (s, 1H), 6.80 (d, *J* = 5.1 Hz, 1H), 3.65 (t, *J* = 5.1 Hz, 4H), 2.55 (t, *J* = 5.1 Hz, 4H), 2.38 (s, 3H). Characterization data matches literature reports.[16]

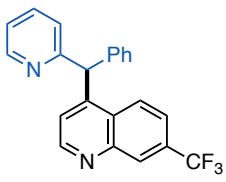

4-(Phenyl(pyridine-2-yl)methyl)-7-(trifluoromethyl)quinoline (38). General Procedure N was followed using 4-chloro-7-(trifluoromethyl)quinoline (115.8 mg, 0.5 mmol, 1.0 equiv), 2-benzylpyridine

(169.2 mg, 1.0 mmol, 2.0 equiv), P_2-*t*-Bu salt **A** (398.7 mg, 0.75 mmol, 1.5 equiv), epoxide **22** (141.2 mg, 0.75 mmol, 1.5 equiv), and DMF (2 mL) to provide 65% ^{1}H NMR yield. The reaction was repeated using commercial P_2-*t*-Bu (63% ^{1}H NMR yield). Following General Procedure P, for characterization purposes, the product was purified *via* silica gel chromatography using 40% EtOAc in hexanes to afford **38** as a yellow solid (106.8 mg, 0.29 mmol, 58% yield). **^{1}H NMR** (400 MHz, $CDCl_3$) δ 8.91 (d, *J* = 4.5 Hz, 1H), 8.62 (d, *J* = 4.9 Hz, 1H), 8.42 (s, 1H), 8.08 (d, *J* = 8.8 Hz, 1H), 7.69 – 7.58 (m, 2H), 7.39-7.27 (m, 3H), 7.21 (ddd, *J* = 7.5, 4.9, 1.2 Hz, 1H), 7.18 – 7.13 (m, 2H), 7.08 – 6.99 (m, 2H), 6.39 (s, 1H). **^{19}F NMR** (376 MHz, $CDCl_3$) δ -62.64. **^{13}C NMR** (101 MHz, $CDCl_3$) δ 161.2, 151.6, 150.1, 148.8, 147.7, 140.3, 136.9, 130.8 (q, *J* = 32.9 Hz), 129.4, 129.0, 128.1 (q, *J* = 4.4 Hz), 127.4, 125.6, 124.0, 123.8 (q, *J* = 272.6 Hz), 123.5, 122.3 (q, *J* = 3.1 Hz), 122.1, 77.2, 55.5. **IR** (neat) 3052, 2925, 1598, 1433, 1335, 1123, 841, 738 cm^{-1}. **HRMS (DART)** $[M+H]^+$ calcd. for $[C_{22}H_{16}F_3N_2]^+$ = 365.1261, found 365.1280. **MP** 144 – 148 °C.

iii. Control Reactions

In this section we describe control reactions that support the P_2-*t*-Bu generated from the prereagent system is responsible for promoting the reaction and not background reactivity from any components or intermediates of the activation process. General Procedure Q below was followed for each of the controls. We also tested to see if the carboxylate anion is capable of catalyzing reactions by running reactions with only P_2-*t*-Bu salt **A**, with a variety of 1-phenylcyclopropanecarboxylate salts. Here, we tested different countercations (e.g., potassium and ammoniums) to survey salt solubility trends. Additionally, we tested if using only epoxide **22** could

promote the reaction. We also considered the possibility that a carboxylate anion can attack the epoxide to generate an alkoxide intermediate that could serve as an active basic promoter. We tested this by mixing non-superbase carboxylate salts with epoxide **22** under reaction conditions. Overall, the results of the below control reactions are consistent with the active catalyst as P_2-*t*-Bu generated from the precatalyst system, as described below. Data for these experiments is provided in Tables S20 and S21 for substrates **33** and **34**, respectively.

General Procedure Q: Control reactions. In a nitrogen-filled glovebox, an oven-dried 1-dram vial (ThermoFisher, C4015-1) was charged with a magnetic stir bar, pronucleophile (0.10 mmol, 2.0 equiv), electrophile (0.05 mmol, 1.0 equiv), epoxide (0.075 mmol, 1.5 equiv), solvent (0.2 mL, 0.25 M), and the indicated basic additive (0.075 mmol, 1.5 equiv) in successive order. The vial was sealed with a PTFE-lined cap (ThermoFisher, C4015-1A), removed from the glovebox, and placed in a preheated aluminum reaction block at 80 °C with stirring for 24 h. The reaction solution was cooled to rt and dibenzyl ether (9.5 µL, 0.05 mmol, 1.0 equiv) internal standard was added to the reaction solution. A 50 µL aliquot was taken and added to an NMR tube, then diluted with 0.5 mL of $CDCl_3$. ^1H NMR spectroscopy was used to determine the yield of the product.

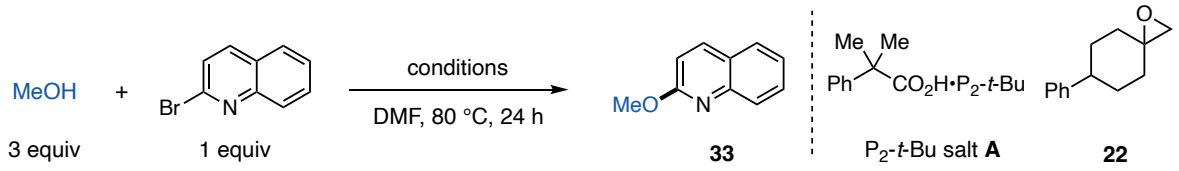

Table S20: Control reactions for the S_NAr reaction between 2-bromoquinoline and methanol. [a] Reaction utilizing P_2-*t*-Bu salt **B** that had been stored in a humidity chamber with set 84% humidity, see Section VIIIb for more details.

Entry	Conditions	Results

1	1.5 equiv P_2-*t*-Bu	91%
2	1.5 equiv P_2-*t*-Bu salt **A** + 1.5 equiv epoxide **22**	70%
3	1.5 equiv P_2-*t*-Bu salt **B** + 1.5 equiv epoxide **22**	65%
4[a]	1.5 equiv P_2-*t*-Bu salt **B** (aged 2h in 84% humidity) + 1.5 equiv epoxide **22**	62%
5	1.5 equiv P_2-*t*-Bu salt **A**	2%
6	1.5 equiv potassium 2-methyl-2-phenylpropionate	0%
7	1.5 equiv tetrabutylammonium acetate	5%
8	1.5 equiv epoxide **22**	0%
9	1.5 equiv potassium 2-methyl-2-phenylpropionate + 1.5 equiv epoxide **22**	52%
10	1.5 equiv tetrabutylammonium acetate + 1.5 eqiuv epoxide **22**	23%
11	No Base	0%

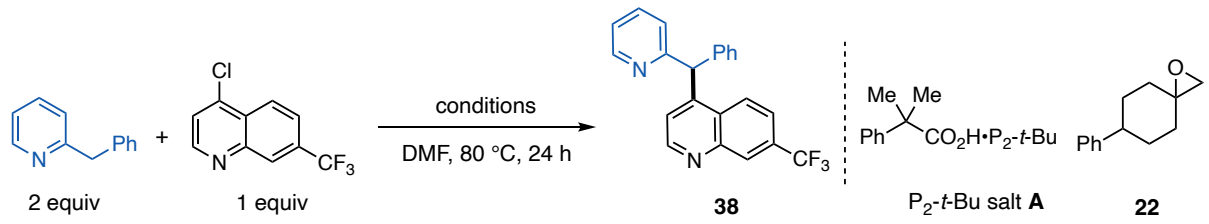

Table S21: Control reactions for the S_NAr reaction between 4-chloro-7-(trifluoromethyl)quinoline and 2-benzylpyridine.

Entry	**Conditions**	**Results**
1	1.5 equiv P_2-*t*-Bu	63%

2	1.5 equiv P_2-*t*-Bu salt **A** + 1.5 equiv epoxide **22**	65%
3	1.5 equiv P_2-*t*-Bu salt **A**	0%
4	1.5 equiv potassium 2-methyl-2-phenylpropionate	0%
5	1.5 equiv tetrabutylammonium acetate	0%
6	1.5 equiv epoxide **22**	0%
7	1.5 equiv potassium 2-methyl-2-phenylpropionate + 1.5 equiv epoxide **22**	61%
8	1.5 equiv tetrabutylammonium acetate + 1.5 eqiuv epoxide **22**	0%
9	No Base	0%

We note that for Table S20, Entry 9 and Table S21, Entry 7 the combination of potassium 2-methyl-2-phenylpropionate and epoxide **22** is capable of promoting the respective S_NAr reaction; we speculate a potassium alkoxide intermediate is generated that promotes the reaction. However, the corresponding alkoxide intermediate of the prereagent system likely neutralizes the P_2-*t*-Bu to generate the freebase as the active catalyst. We supported this by conducting a control experiment where we preactivated P_2-*t*-Bu salt **A** with epoxide **22** in the presence of the pronucleophile (Step 1 in scheme below, MeOH for **33** and 2-benzylpyridine for **38**).

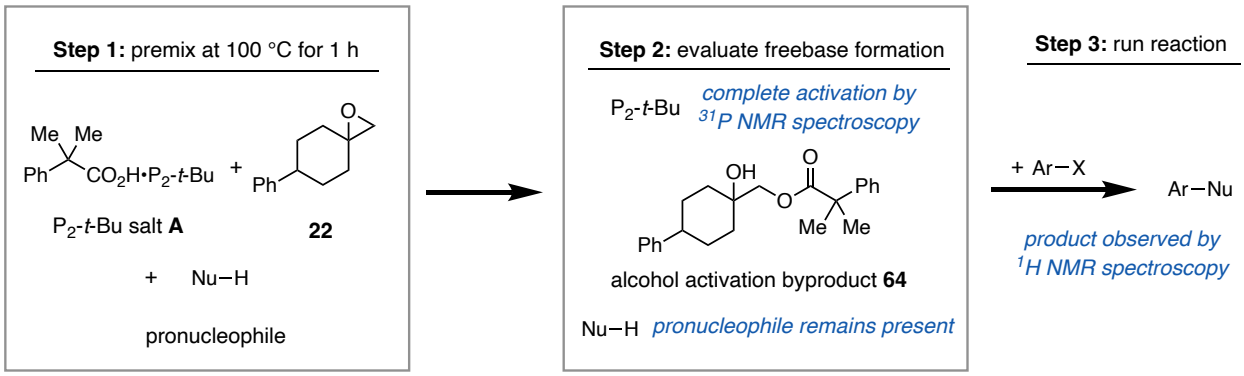

In each case, we observed complete generation of P_2-*t*-Bu from the prereagent system by ^{31}P NMR and ^{1}H NMR spectroscopy, indicating P_2-*t*-Bu is the base that forms in the mixture of these reagents. We then add the aryl electrophile to these activation solutions and observed 53% yield of **33** and 50% yield of **38**. These results are consistent with the P_2-*t*-Bu generated from prereagent activation being the active basic promoter in solution. Entries 5 and 9 from Table S20 were repeated for the rest of the substrates in Table S19 and we found that substrate **37** can be promoted by these conditions, albeit in reduced yield (65% and 53%, respectively).

c. Use of P_2-*t*-Bu salt A as a prereagent for enolate-type alkylation reaction

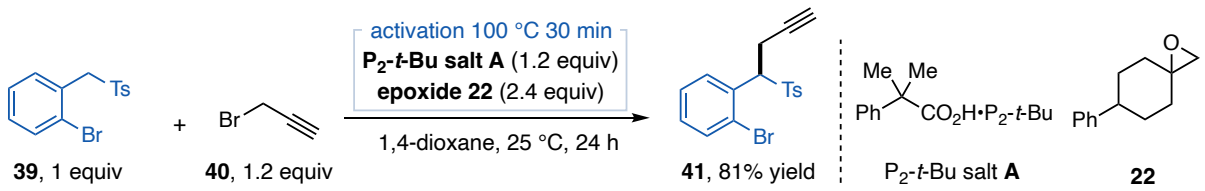

General Procedure R: Use of P_2-*t*-Bu salt A and epoxide 22. Note: A preactivation procedure is required as the alkylation reaction takes place at 25°C while P_2-*t*-Bu salt **A** with epoxide **22** does not activate quickly at 25°C. An oven-dried 1-dram vial (ThermoFisher, C4015-1) was charged with a magnetic stir bar, P_2-*t*-Bu salt **A** (63.8 mg, 0.12 mmol, 1.2 equiv), and epoxide **22** (45.2 mg, 0.24 mmol, 2.4 equiv). The vial was sealed with a PTFE-lined cap (ThermoFisher, C4015-1A) and evacuated then back filled with nitrogen three times *via* a nitrogen inlet tube on a Schlenk manifold line. 1,4-Dioxane (0.2 mL, 0.6 M with respect to P_2-*t*-Bu salt **A**) was added to the vial *via* nitrogen-flushed syringe. The manifold line was removed from the vial and the cap was wrapped in parafilm and PVC tape. The vial was placed in a preheated aluminum reaction block at 100 °C for 1 h with stirring.

Reaction Solution: a separate oven-dried 1-dram vial (ThermoFisher, C4015-1) was charged with a magnetic stir bar and 1-bromo-2-(tosylmethyl)benzene (32.5 mg, 0.1 mmol, 1.0 equiv). The vial was sealed with a PTFE-lined cap (ThermoFisher, C4015-1A) and evacuated then back filled with nitrogen three times *via* a nitrogen inlet tube on a Schlenk manifold line. 1,4-Dioxane (0.2 mL, 0.5 M with respect to limiting reagent) and propargyl bromide (80 wt. % in PhMe, contains 0.3% magnesium oxide as stabilizer, 21.2 µL, 0.12 mmol, 1.2 equiv) were added *via* nitrogen-flushed syringe. The vial containing the preactivation solution was removed from the reaction block, allowed to cool to rt and placed under a nitrogen atmosphere *via* a nitrogen inlet tube on a Schlenk manifold line. The preactivation solution was transferred to the starting material solution *via* nitrogen-flushed syringe. The preactivation vial was washed with an additional 0.1 mL (0.2 M total volume) of 1,4-dioxane and this was transferred to the reaction vial. The inlet tube was removed from the reaction vial and the cap was wrapped in parafilm and PVC tape. The vial was placed in a preheated aluminum reaction block at 25 °C with stirring for 24 h. The reaction solution

was removed from the reaction block and 1,3,5-trimethoxybenzene (16.8 mg, 0.1 mmol, 1.0 equiv) was added to the reaction solution, a 50 µL aliquot was taken and added to an NMR tube, then diluted with $CDCl_3$ (0.5 mL). ^1H NMR spectroscopic analysis was used to determine the yield of the reaction (81% yield).

General Procedure S: Use of P_2-*t*-Bu freebase. Note: this procedure was adapted from a report using P_2-Et to promote this transformation and serves as a control for the prereagent method.[17] This procedure was also used to isolate the pure material for characterization purposes. An oven-dried 2-dram vial (ThermoFisher, C4015-2) was charged with a magnetic stir bar and 1-bromo-2-(tosylmethyl)benzene (162.6 mg, 0.5 mmol, 1.0 equiv). The vial was brought into a nitrogen-filled glovebox where 1,4-dioxane (2.5 mL, 0.2 M), propargyl bromide (80 wt. % in PhMe, contains 0.3% magnesium oxide as stabilizer, 106.2 µL, 0.6 mmol, 1.2 equiv), and P_2-*t*-Bu (2.0 M solution in THF, 0.3 mL, 0.6 mmol, 1.2.0 equiv) were added to the solution. The vial was sealed with a PTFE-lined cap (ThermoFisher, C4015-1A), removed from the glovebox, and placed into a preheated aluminum reaction block at 25 °C with stirring for 24 h. The reaction vial was removed from the reaction block, 1,3,5-trimethoxybenzene (84.1 mg, 0.5 mmol, 1.0 equiv) was added to the solution and a 50 µL aliquot was taken and added to an NMR tube, then diluted with $CDCl_3$ (0.5 mL). For characterization purposes, the product was purified *via* silica gel chromatography using 10% EtOAc in hexanes to afford **41** as a yellow solid (157.1 mg, 0.43 mmol, 86% yield). **^{1}H NMR** (400 MHz, $CDCl_3$) δ 7.71 (d, J = 7.9 Hz, 1H), 7.56 – 7.37 (m, 4H), 7.26 – 7.16 (m, 3H), 5.13 (dd, J = 11.2 Hz, 4.2 Hz, 1H), 3.37 – 3.27 (m, 1H), 3.18 – 3.05 (m, 1H), 2.43 (s, 3H), 1.87 (t, J = 2.6 Hz, 1H). Characterization data matches literature reports.[17]

ii. Control Reactions

In this section we describe control reactions that support P_2-*t*-Bu generated from the prereagent salt is responsible for promoting the reaction and not background reactivity from any components or intermediates of the activation process. General Procedure T below was followed for each of the controls. We also tested to see if the carboxylate anion is capable of catalyzing reactions by running reactions with only P_2-*t*-Bu salt **A**, with a variety of 1-phenylcyclopropanecarboxylate salts. Here, we tested different countercations (e.g., potassium and ammoniums) to survey salt solubility trends. Additionally, we tested if using only epoxide **22** or byproduct **64** could promote the reaction. We also considered the possibility that a carboxylate anion can attack the epoxide to generate an alkoxide intermediate that could serve as an active base. We tested this by mixing non-superbase carboxylate salts with epoxide **22** under reaction conditions. For each indicated basic system other than the commercial freebase or precatalyst system, we observed 0% yield of the product. These results are consistent with the active basic promoter as P_2-*t*-Bu generated from the prereagent system. Data for these experiments is provided in Tables S20 for substrate **41**.

General Procedure T: Control reactions. In a nitrogen-filled glovebox, an oven-dried 1-dram vial (ThermoFisher, C4015-1) was charged with a magnetic stir bar, 1,4-dioxane (0.5 mL, 0.2 M), 1-bromo-2-(tosylmethyl)benzene (32.5 mg, 0.1 mmol, 1.0 equiv), propargyl bromide (80 wt. % in PhMe, contains 0.3% magnesium oxide as stabilizer, 21.2 μL, 0.12 mmol, 1.2.0 equiv), indicated basic additive (0.12 mmol, 1.2 equiv), and epoxide **22** (0.24 mmol, 2.4 equiv (unless excluded)) in successive order. The vial was sealed with a PTFE lined cap (ThermoFisher, C4015-1A),

removed from the glovebox, and placed in a preheated aluminum reaction block at 25 °C with stirring for 24 h. 1,3,5-Trimethoxybenzene (16.8 mg, 0.1 mmol, 1.0 equiv) internal standard was added to the reaction solution and a 50 μL aliquot was taken and added to an NMR tube, then diluted with $CDCl_3$ (0.5 mL). ^1H NMR spectroscopy was used to determine the reaction yield.

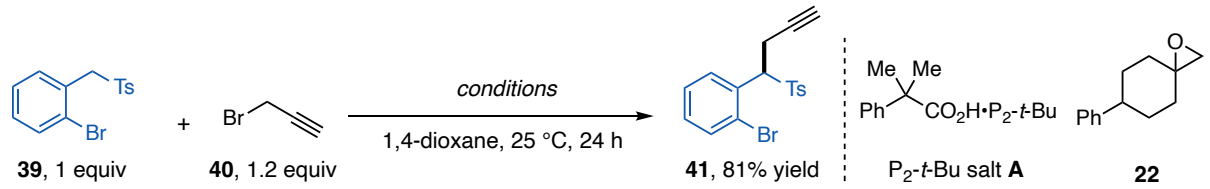

Table S22: Control reactions for the substitution reaction between 1-bromo-2-(tosylmethyl)benzene (**39**) and propargyl bromide (**40**). [a] A preactivation procedure was followed by stirring potassium 2-methyl-2-phenylpropionate and epoxide **22** for 1 h at 100 °C in 1,4-dioxane.

Entry	Conditions	Results
1	1.2 equiv P_2-*t*-Bu	88%
2	1.2 equiv P_2-*t*-Bu salt **A** + 2.4 equiv epoxide **22** with preactivation	81%
3	1.2 equiv P_2-*t*-Bu salt **A**	0%
4	1.2 equiv potassium 2-methyl-2-phenylpropionate	0%
5	1.2 equiv tetrabutylammomnium acetate	0%
6	2.4 equiv epoxide **22**	0%
7	1.2 equiv byproduct **64**	0%
8	1.2 equiv potassium 2-methyl-2-phenylpropionate + 2.4 equiv epoxide **22**	0%
9[a]	1.2 equiv potassium 2-methyl-2-phenylpropionate + 2.4 equiv epoxide **22**	0%

10	1.2 equiv tetrabutylammonium acetate + 2.4 equiv epoxide **22**	0%

VII. Prereagent Application in Pd-Catalyzed Cross-Coupling Reactions

a) Reaction Scheme and General Procedures

Table S23: Substrate table for Pd-catalyzed cross coupling using either BTPP salt **A** or P_2-*t*-Bu salt **A** with comparison to their corresponding freebases. All reactions that do not use a preactivation procedure use epoxide **2**. [a] THF used as solvent. [b] *tert*-Amyl alcohol used as solvent. [c] DMSO used as solvent. [d] *t*-BuBrettPhos Pd G3 (5 mol%) used as catalyst. [e] Pre-activation with equimolar P_2-*t*-Bu salt **A** and epoxide **22** at 100 °C for 3 h in PhMe.

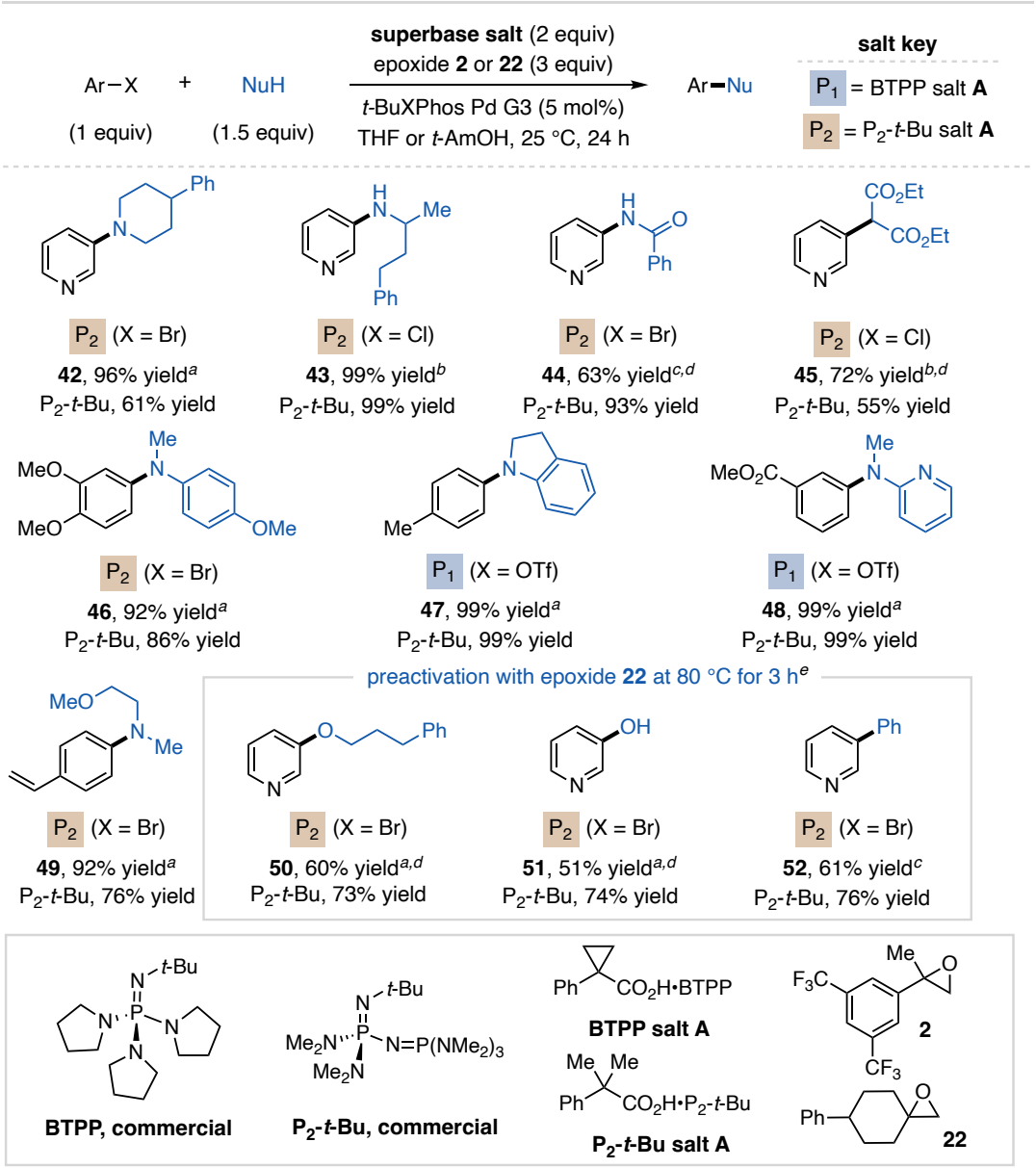

General Procedure U: Prereagent salt and epoxide promoted reaction. An oven-dried 1-dram vial (ThermoFisher, C4015-1) was charged with a magnetic stir bar, prereagent salt (531.7 mg, 1.0 mmol, 2.0 equiv) and Pd precatalyst (0.025 mmol, 5 mol%). The vial was sealed with a PTFE-lined cap (ThermoFisher, C4015-1A), and evacuated then backfilled with nitrogen three times *via* a nitrogen inlet tube on a Schlenk manifold line. Solvent (2.5 mL, 0.2 M) was then added to the vial *via* nitrogen-flushed syringe. Aryl halide (0.5 mmol, 1.0 equiv), nucleophile (0.75 mmol, 1.5 equiv), then epoxide (1.5 mmol, 3 equiv) were added *via* nitrogen-flushed syringes. Note: aryl halide and/or nucleophile were charged to the vial prior to capping and nitrogen flushing if they are solids at rt. The reaction vial was then disconnected from the Schlenk line, sealed with parafilm wax, and placed in a preheated aluminum reaction block at 25 °C with stirring for 24 h. Dibromomethane (35 μL, 0.5 mmol, 1.0 equiv) was added to the reaction solution, a 50 μL aliquot was taken and added to an NMR tube, then diluted with $CDCl_3$ (0.5 mL). ^1H NMR spectroscopy was used to determine the yield of the reaction.

General Procedure V: Prereagent salt and epoxide promoted reaction with preactivation. An oven-dried 1-dram vial (ThermoFisher, C4015-1) was charged with a magnetic stir bar, prereagent salt (1.0 mmol, 2.0 equiv) and epoxide (1.5 mmol, 3 equiv). The vial was sealed with a PTFE-lined cap (ThermoFisher, C4015-1A) and evacuated then backfilled with nitrogen three times *via* a nitrogen inlet tube on a Schlenk manifold line. PhMe (2 mL, 0.5 M with respect to P_2-*t*-Bu salt **A**) was added *via* nitrogen-flushed syringe. The inlet tube was removed from the vial and the cap was wrapped in parafilm and PVC tape. The vial was placed in a preheated aluminum reaction block at 80 °C for 3 h with stirring.

Reagent solution. A separate oven-dried 1-dram vial (ThermoFisher, C4015-1) was charged with Pd precatalyst (0.025 mmol, 5 mol%). The vial was sealed with a PTFE-lined cap (ThermoFisher, C4015-1A), and evacuated then backfilled with nitrogen three times *via* a nitrogen inlet tube on a Schlenk manifold line. Solvent (0.5 mL, 0.2M total volume), aryl halide (0.5 mmol, 1.0 equiv), and nucleophile (0.75 mmol, 1.5 equiv) were added *via* nitrogen-flushed syringes and the solution was mixed thoroughly. Note: aryl halide and/or nucleophile were charged to the vial prior to capping and nitrogen flushing if they are solids at rt. The preactivation solution was allowed to cool to rt and was placed under a positive pressure of nitrogen *via* a nitrogen inlet tube from the Schlenk manifold. The reagent solution was transferred to the preactivation vial *via* nitrogen-flushed syringe. The inlet tube was removed from the reaction vial and the cap was wrapped in parafilm and PVC tape. The vial was placed into a preheated aluminum reaction block at 25 °C for 24 h with stirring. Dibromomethane (35 μL, 0.5 mmol, 1.0 equiv) was added to the reaction solution, a 50 μL aliquot was taken and added to an NMR tube, then diluted with $CDCl_3$ (0.5 mL). ^1H NMR spectroscopy was used to determine the yield of the reaction.

b) Reaction and characterization data

General description: For all of the substrates in this section, we use ^1H NMR yields to assess the efficacy of the precatalyst salt system. In each case, we benchmarked the success of the prereagent against the use of commercial BTPP or P_2-*t*-Bu using ^1H NMR yields. The reactions carried out with BTPP or P_2-*t*-Bu were set up using General Procedure W below. The substrates were subsequently isolated using General Procedures U and V, depending on if preactivation was

necessary, for characterization. To do this, the crude reactions mixtures were directly subjected to flash column chromatography to yield purified products. The purification conditions and characterization data are given below.

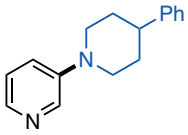

3-(4-phenylpiperidin-1-yl)pyridine (42). General Procedure U was followed using P_2-*t*-Bu salt **A** (531.6 mg, 1.0 mmol, 2.0 equiv), *t*-BuXPhos Pd G3 (19.9 mg, 0.025 mmol, 5 mol%), epoxide **2** (405.2 mg, 1.5 mmol, 3.0 equiv), 3-bromopyridine (48.2 µL, 0.5 mmol, 1.0 equiv), 4-phenylpiperidine (120.9 mg, 0.75 mmol, 1.5 equiv), and THF (2.5 mL, 0.2 M) to provide 96% ^{1}H NMR yield. The reaction was repeated using commercial P_2-*t*-Bu (61% ^{1}H NMR yield). Following General Procedure U, the product was purified *via* silica gel chromatography using 100% DCM to 5% MeOH/DCM to afford **42** as a pale-yellow solid (81.5 mg, 0.34 mmol, 68% yield). **^{1}H NMR** (400 MHz, $CDCl_3$) δ 8.42 (d, *J* = 2.9 Hz, 1H), 8.15 (d, *J* = 4.5 Hz, 1H), 7.38 (t, *J* = 7.5 Hz, 2H), 7.33 – 7.18 (m, 4H), 7.22 (dd, *J* = 8.5, 4.6 Hz, 1H), 3.88 (d, *J* = 11.9 Hz, 2H), 2.93 (td, *J* = 12.2, 2.9 Hz, 2H), 2.73 (tt, *J* = 11.9, 3.9 Hz, 1H), 2.08 – 1.87 (m, 4H). Characterization data matches literature reports.[18]

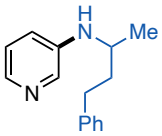

***N*-(4-phenylbutan-2-yl)pyridin-3-amine (43).** General Procedure U was followed using P_2-*t*-Bu salt **A** (531.6 mg, 1.0 mmol, 2.0 equiv), *t*-BuXPhos Pd G3 (19.9 mg, 0.025 mmol, 5 mol%), epoxide **2** (405.2 mg, 1.5 mmol, 3.0 equiv), 3-chloropyridine (47.5 µL, 0.5 mmol, 1.0 equiv), 4-phenylbutan-2-amine (121.6 µL, 0.75 mmol, 1.5 equiv), and *tert*-amyl alcohol (2.5 mL, 0.2 M) to provide 99% ^{1}H NMR yield. The reaction was repeated using commercial P_2-*t*-Bu (99% ^{1}H NMR yield). Following General Procedure U, the product was

purified *via* silica gel chromatography using 1% NEt_3/DCM to 8% MeOH/1% NEt_3 in DCM to afford **43** as a brown oil (94.3 mg, 0.42 mmol, 84% yield). **^{1}H NMR** (400 MHz, $CDCl_3$) δ 8.00 (d, *J* = 2.9 Hz, 1H), 7.96 (d, *J* = 4.7 Hz, 1H), 7.33 (t, *J* = 7.4 Hz, 2H), 7.28 – 1.18 (m, 3H), 7.08 (dd, *J* = 8.3, 4.6 Hz, 1H), 6.83 – 6.76 (m, 1H), 3.57 – 3.44 (m, 2H), 2.77 (t, *J* = 7.8 Hz, 2H), 2.00 – 1.78 (m, 2H), 1.32 – 1.24 (m, 4H). Characterization data matches literature reports.[18]

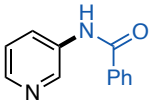

***N*-(pyridin-3-yl)benzamide (44).** General Procedure U was followed using P_2-*t*-Bu salt **A** (531.6 mg, 1.0 mmol, 2.0 equiv), *t*-BuBrettPhos Pd G3 (21.4 mg, 0.025 mmol, 5 mol%), epoxide **2** (405.2 mg, 1.5 mmol, 3.0 equiv), 3-bromopyridine (48.2 µL, 0.5 mmol, 1.0 equiv), benzamide (90.9 mg, 0.75 mmol, 1.5 equiv), and DMSO (2.5 mL, 0.2 M) to provide 63% ^{1}H NMR yield. The reaction was repeated using commercial P_2-*t*-Bu (93% ^{1}H NMR yield). Following General Procedure U, the product was purified *via* silica gel chromatography using 100% hexanes to 75% EtOAc in hexanes to afford **44** as a yellow solid (58.2 mg, 0.29 mmol, 58% yield). **^{1}H NMR** (400 MHz, $CDCl_3$) δ 8.48 (d, *J* = 2.6 Hz, 1H), 8.35 (s, 1H), 8.13 (d, *J* = 4.8 Hz, 1H), 8.09 (d, *J* = 8.5 Hz, 1H), 7.69 (d, *J* = 7.4 Hz, 2H), 7.39 – 7.31 (m, 1H), 7.26 (t, *J* = 7.6 Hz, 2H), 7.13 – 7.05 (m, 1H). Characterization data matches literature reports.[18]

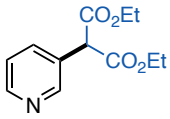

diethyl 2-(pyridin-3-yl)malonate (45). General Procedure U was followed using P_2-*t*-Bu salt **A** (531.6 mg, 1.0 mmol, 2.0 equiv), *t*-BuBrettPhos Pd G3 (21.4 mg, 0.025 mmol, 5 mol%), epoxide **2** (405.2 mg, 1.5 mmol, 3.0 equiv), 3-chloropyridine (47.5 µL, 0.5 mmol, 1.0 equiv), diethyl malonate (113.9 µL, 0.75 mmol, 1.5 equiv), and *tert*-amyl alcohol (2.5 mL, 0.2 M) to provide 72% ^{1}H NMR yield. The reaction was repeated using commercial P_2-*t*-Bu

(55% ^{1}H NMR yield). Following General Procedure U, the product was purified *via* silica gel chromatography using 100% hexanes to 40% EtOAc in hexanes to afford **45** as a yellow oil (50.3 mg, 0.21 mmol, 42% yield). **^{1}H NMR** (400 MHz, $CDCl_3$) δ 8.60 – 8.53 (m, 2H), 7.83 (dd, *J* = 8.1, 2.2 Hz, 1H), 7.30 (dd, *J* = 8.0, 4.8 Hz, 1H), 4.61 (s, 1H), 4.26 – 4.15 (m, 4H), 1.25 (t, *J* = 7.1 Hz, 6H). Characterization data matches literature reports.[18]

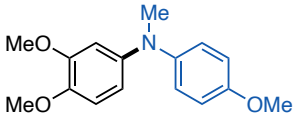

3,4-dimethoxy-*N*-(4-methoxyphenyl)-*N*-methylaniline (46). General Procedure U was followed using P_2-*t*-Bu salt **A** (531.6 mg, 1.0 mmol, 2.0 equiv), *t*-BuXPhos Pd G3 (19.9 mg, 0.025 mmol, 5 mol%), epoxide **2** (405.2 mg, 1.5 mmol, 3.0 equiv), 4-bromo-1,2-dimethoxybenzene (71.9 µL, 0.5 mmol, 1.0 equiv), 4-methoxy-*N*-methylaniline (102.9 mg, 0.75 mmol, 1.5 equiv), and THF (2.5 mL, 0.2 M) to provide 92% ^{1}H NMR yield. The reaction was repeated using commercial P_2-*t*-Bu (86% ^{1}H NMR yield). Following General Procedure U, the product was purified *via* silica gel chromatography using 40% EtOAc in hexanes to afford **46** as a brown solid (15.6 mg, 0.06 mmol, 12% yield). **^{1}H NMR** (400 MHz, $CDCl_3$) δ 6.95 (d, *J* = 8.9 Hz, 2H), 6.84 (d, *J* = 9.0 Hz, 2H), 6.79 (d, *J* = 8.5 Hz, 2H), 6.56 – 6.45 (m, 2H), 3.85 (s, 3H), 3.79 (s, 3H), 3.77 (s, 3H), 3.23 (s, 3H). **^{13}C NMR** (101 MHz, $CDCl_3$) δ 154.8, 149.6, 144.3, 143.9, 143.6, 122.3, 114.7, 112.3, 111.4, 105.1, 56.5, 55.9, 55.7, 41.2. **IR** (neat) 2922, 1598, 1505, 1460, 1231, 1131, 1024, 947, 839, 770 cm^{-1}. **HRMS (DART)** $[M+H]^+$ *m/z* calcd. for $[C_{16}H_{20}NO_3]^+$ = 274.1438, found 274.1451. **MP** 90 – 94 °C.

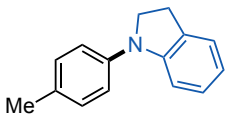

1-(*p*-tolyl)indoline (47). General Procedure U was followed using BTPP salt **A** (118.7 mg, 0.5 mmol, 2.0 equiv), *t*-BuXPhos Pd G3 (9.9 mg, 0.0125 mmol,

5 mol%), epoxide **2** (202.6 mg, 0.75 mmol, 3.0 equiv), *p*-tolyl trifluoromethanesulfonate (44.7 µL, 0.25 mmol, 1.0 equiv), indoline (42.0 µL, 0.375 mmol, 1.5 equiv), and THF (1.3 mL, 0.2 M) to provide 99% ^{1}H NMR yield. The reaction was repeated using commercial BTPP (99% ^{1}H NMR yield). Following General Procedure U, the product was purified *via* silica gel chromatography using 10% EtOAc in hexanes to afford **47** as a white solid (41.5 mg, 0.20 mmol, 80% yield). **^{1}H NMR** (400 MHz, $CDCl_3$) δ 7.21 – 7.13 (m, 5H), 7.08 (d, *J* = 4.2 Hz, 2H), 6.79 – 6.71 (m, 1H), 3.94 (t, *J* = 8.4 Hz, 2H), 3.14 (t, *J* = 8.4 Hz, 2H), 2.36 (s, 3H). Characterization data matches literature reports.[19]

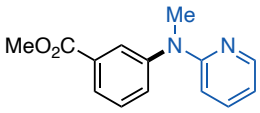

methyl 3-(methyl(pyridin-2-yl)amino)benzoate (48). General Procedure U was followed using BTPP salt **A** (118.7 mg, 0.5 mmol, 2.0 equiv), *t*-BuXPhos Pd G3 (9.9 mg, 0.0125 mmol, 5 mol%), epoxide **2** (202.6 mg, 0.75 mmol, 3.0 equiv), methyl 3-(((trifluoromethyl)sulfonyl)oxy)benzoate (71.1 mg, 0.25 mmol, 1.0 equiv), *N*-methylpyridin-2-amine (38.5 µL, 0.375 mmol, 1.5 equiv), and THF (1.3 mL, 0.2 M) to provide 99% ^{1}H NMR yield. The reaction was repeated using commercial BTPP (99% ^{1}H NMR yield). Following General Procedure U, the product was purified *via* silica gel chromatography using 50% EtOAc in hexanes to afford **48** as a yellow oil (51.1 mg, 0.21 mmol, 84% yield). **^{1}H NMR** (400 MHz, $CDCl_3$) δ 8.24 (d, *J* = 4.9 Hz, 1H), 7.94 (s, 1H), 7.89 – 7.80 (m, 1H), 7.49 – 7.42 (m, 2H), 7.38 – 7.32 (m, 1H), 6.66 (dd, *J* = 7.2, 5.0 Hz, 1H), 6.57 (d, *J* = 8.7, 1H), 3.91 (s, 3H), 3.49 (s, 3H). Characterization data matches literature reports.[19]

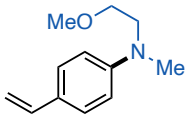

***N*-(2-methoxyethyl)-*N*-methyl-4-vinylaniline (49).** General Procedure U was followed using P_2-*t*-Bu salt **A** (531.6 mg, 1.0 mmol, 2.0 equiv), *t*-BuXPhos Pd G3 (19.9 mg mg, 0.025 mmol, 5 mol%), epoxide **2** (405.2 mg, 1.5 mmol, 3.0 equiv), 4-bromostyrene (65.4 µL, 0.5 mmol, 1.0 equiv), 2-methoxy-*N*-methylethan-1-amine (81.6 µL, 0.75 mmol, 1.5 equiv), and THF (2.5 mL, 0.2 M) to provide 92% ^{1}H NMR yield. The reaction was repeated using commercial P_2-*t*-Bu (76% ^{1}H NMR yield). Following General Procedure U, the product was purified *via* silica gel chromatography using 20% EtOAc in hexanes to afford **49** as a yellow oil (36.1 mg, 0.19 mmol, 38% yield). **^{1}H NMR** (400 MHz, $CDCl_3$) δ 7.31 (d, *J* = 8.6 Hz, 2H), 6.75 – 6.59 (m, 3H), 5.55 (d, *J* = 17.6 Hz, 1H), 5.03 (d, *J* = 11.0 Hz, 1H), 3.61 – 3.47 (m, 4H), 3.37 (s, 3H), 3.01 (s, 3H). **^{13}C NMR** (101 MHz, $CDCl_3$) δ 149.1, 136.7, 127.4, 126.1, 112.1, 109.3, 70.3, 59.2, 52.5, 39.1. **IR** (neat) 2883, 1616, 1518, 1367, 1192, 1115, 817 cm^{-1}. **HRMS (DART)** $[M+H]^+$ calcd. for $[C_{12}H_{18}NO]^+$ = 192.1383, found 192.1386.

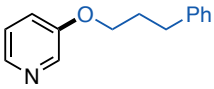

3-(3-phenylpropoxy)pyridine (50). General Procedure V was followed using P_2-*t*-Bu salt **A** (531.6 mg, 1.0 mmol, 2.0 equiv), epoxide **22** (282.4 mg, 1.5 mmol, 3.0 equiv), THF (2 mL), *t*-BuBrettPhos Pd G3 (21.4 mg, 0.025 mmol, 5 mol%), 3-bromopyridine (48.2 µL, 0.5 mmol, 1.0 equiv), 3-phenylpropan-1-ol (102.0 µL, 0.75 mmol, 1.5 equiv), and THF (0.5 mL, 0.2 M total volume) to provide 60% ^{1}H NMR yield. The reaction was repeated without a preactivation protocol using commercial P_2-*t*-Bu (73% ^{1}H NMR yield). Following General Procedure V, the product was purified *via* silica gel chromatography using 100% hexanes to 40% EtOAc in hexanes to afford **50** as a yellow oil (30.0 mg, 0.14 mmol, 28% yield). **^{1}H NMR** (400 MHz, $CDCl_3$) δ 8.32 (d, *J* = 2.6 Hz, 1H), 8.21 (d, *J* = 4.4 Hz, 1H), 7.39 –

7.29 (m, 2H), 7.29 – 7.17 (m, 5H), 4.00 (t, J = 6.2 Hz, 2H), 2.82 (t, J = 7.6 Hz, 2H), 2.13 (p, J = 6.6 Hz, 3H). Characterization data matches literature reports.[18]

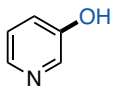

pyridin-3-ol (51). General Procedure V was followed using P_2-*t*-Bu salt **A** (531.6 mg, 1.0 mmol, 2.0 equiv), epoxide **22** (282.4 mg, 1.5 mmol, 3.0 equiv), THF (2 mL), *t*-BuBrettPhos Pd G3 (21.4 mg, 0.025 mmol, 5 mol%), 3-bromopyridine (48.2 µL, 0.5 mmol, 1.0 equiv), water (13.5 µL, 0.75 mmol, 1.5 equiv), and THF (0.5 mL, 0.2 M total volume) to provide 51% ^{1}H NMR yield. The reaction was repeated without a preactivation protocol using commercial P_2-*t*-Bu (74% ^{1}H NMR yield). The crude ^{1}H NMR spectrum matches with commercial pyridin-3-ol, and therefore this product was not isolated from reaction conditions. The characteristic peak at 8.29 ppm (d, 1H) was used to assess ^{1}H NMR yields of this product (see Figure S16 below).

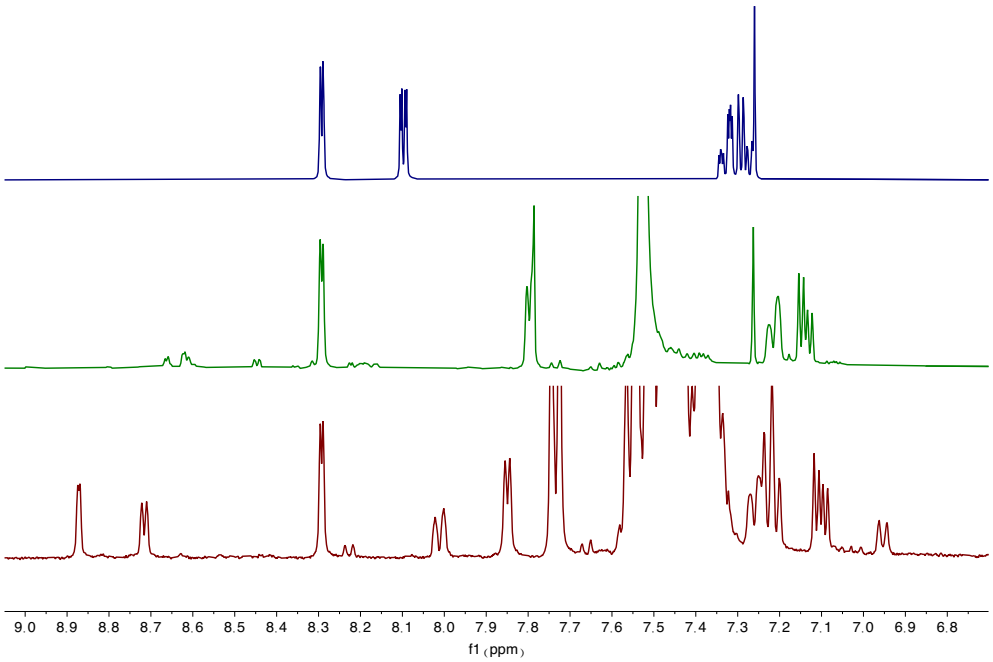

Figure S16. Stacked ^{1}H NMR spectrum of commercial 3-hydroxypyridine (top) compared to crude reaction mixtures using P_2-*t*-Bu freebase (middle) and prereagent system (bottom). The peak at

8.29 ppm was used to assess the yield of the reaction. For the freebase and prereagent system spectra, the peak at 8.10 ppm shifts due to a different protonation state of the product in the presence of differing amounts of base.

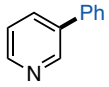

3-phenylpyridine (52). General Procedure V was followed using P_2-*t*-Bu salt **A** (531.6 mg, 1.0 mmol, 2.0 equiv), epoxide **22** (282.4 mg, 1.5 mmol, 3.0 equiv), THF (2 mL), *t*-BuXPhos Pd G3 (19.9 mg, 0.025 mmol, 5 mol%), 3-bromopyridine (48.2 µL, 0.5 mmol, 1.0 equiv), 4,4,5,5-tetramethyl-2-phenyl-1,3,2-dioxaborolane (153.1 mg, 0.75 mmol, 1.5 equiv), water (18.0 µL, 1.0 mmol, 2.0 equiv), and DMSO (0.5 mL, 0.2 M total volume) to provide 61% ^{1}H NMR yield. The reaction was repeated without a preactivation protocol using commercial P_2-*t*-Bu (76% ^{1}H NMR yield). The crude ^{1}H NMR spectrum matches with commercial 3-phenylpyridine, and therefore this product was not isolated from reaction conditions. The characteristic peak at 8.86 ppm (s, 1H) was used to assess ^{1}H NMR yields of this product (see Figure S17 below)

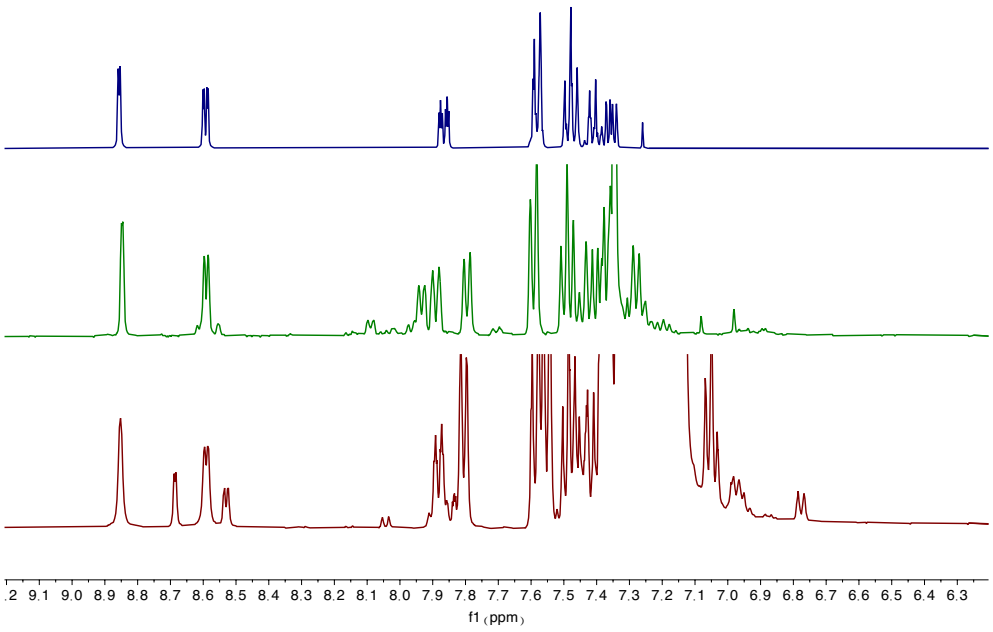

Figure S17. Stacked ^{1}H NMR spectrum of commercial 3-phenylpyridine (top) compared to crude reaction mixtures using P_2-*t*-Bu freebase (middle) and prereagent system (bottom). The peak at 8.86 ppm was used to assess the yield of the reaction.

c) Control Reactions

In this section we describe control reactions that support P_2-*t*-Bu generated from the prereagent salt is responsible for promoting the reactions and not background reactivity from any components or intermediates of the activation process. General Procedure W below was followed for each of the controls. We also tested to see if the carboxylate anion is capable of catalyzing reactions by running reactions with only P_2-*t*-Bu salt **A**, with a variety of 1-phenylcyclopropanecarboxylate salts. Here, we tested different countercations (e.g., potassium and ammoniums) to survey salt solubility trends. Additionally, we tested if using only epoxide **2** could promote the reaction. We also considered the possibility that a carboxylate anion can attack the epoxide to generate an alkoxide intermediate that could serve as an active basic catalyst. We tested this by mixing non-superbase carboxylate salts with epoxide **2** under reaction conditions. For each indicated basic system other than the commercial freebase or precatalyst system, we observed 0% yield of the product. These results are consistent with the active basic promoter being P_2-*t*-Bu generated from the prereagent system. Data for these experiments is provided in Table S24 for substrate **42**.

General Procedure W: Control reactions. In a nitrogen-filled glovebox, an oven-dried 1-dram vial (ThermoFisher, C4015-1) was charged with a magnetic stir bar, indicated basic additive (0.2 mmol, 2.0 equiv), epoxide **2** (if applicable) (0.3 mmol, 3 equiv), *t*-BuXPhos Pd G3 (4.0 mg, 0.005

mmol, 5 mol%), 3-bromopyridine (9.6 µL, 0.1 mmol, 1.0 equiv), 4-phenylpiperidine (24.2 mg, 0.15 mmol, 1.5 equiv), and THF (0.5 mL, 0.2 M). The vial was sealed with a PTFE-lined cap (ThermoFisher, C4015-1A) and removed from the glovebox. The reaction vial was then placed in a preheated aluminum reaction block at 25 °C for 24 h with stirring. Dibromomethane (7 µL, 0.1 mmol, 1.0 equiv) was added to the reaction solution, a 50 µL aliquot was taken and added to an NMR tube, then diluted with $CDCl_3$ (0.5 mL). ^1H NMR spectroscopy was used to determine the yield of the reaction.

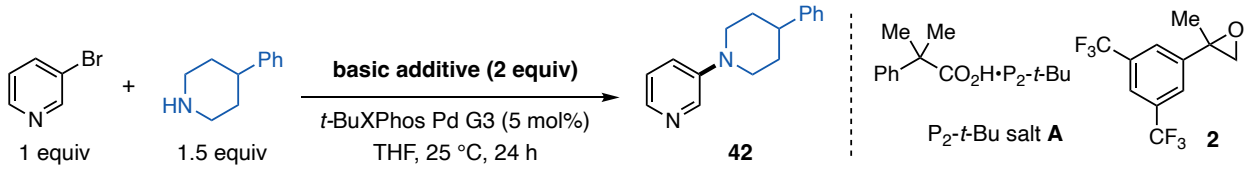

Table S24: Control reactions for the Pd-catalyzed C–N coupling reaction of 3-bromopyridine and 4-phenylpiperidine with various basic promoters. [a] General Procedure V was followed for preactivation protocol. [b] This work is follows a previous literature report[18] where P_2-Et was used and this base is included here for comparison.

Entry	Conditions	Results
1	2 equiv P_2-*t*-Bu	61%
2	2 equiv P_2-*t*-Bu salt **A** + 3 equiv epoxide **2**	96%
3	2 equiv P_2-*t*-Bu salt **A** + 3 equiv epoxide **22**	2%
4[a]	2 equiv P_2-*t*-Bu salt **A** + 3 equiv epoxide **22** with preactivation	99%
5[b]	2 equiv P_2-Et	83%
6	2 equiv P_2-*t*-Bu salt **A**	0%
7	2 equiv potassium 2-methyl-2-phenylpropionate	0%

8	2 equiv tetrabutylammonium acetate	0%
9	3 equiv epoxide **2**	0%
10	2 equiv potassium 2-methyl-2-phenylpropionate + 3 equiv epoxide **2**	0%
11	2 equiv tetrabutylammonium acetate + 3 equiv epoxide **2**	0%
12	No Base	0%

Next, conditions from Entries 6 and 10 were repeated for substrates **43**-**52** to assess whether or not background processes can promote other amination reactions. For Entry 6, only substrate **47** can be promoted by this condition to 41% yield, which is significantly lower than the yield with the prereagent system (99% yield). For entry 10, substrates **44** and **47** can be promoted by potassium 2-methyl-2-phenylpropionate plus epoxide **2** to 79% and 62%, respectively; we speculate a potassium alkoxide intermediate is generated that promotes the reaction. However, the corresponding alkoxide intermediate of the precatalyst system likely neutralizes the P_2-*t*-Bu immediately to generate the freebase as the active basic promoter as previously described and studied for P_2-*t*-Bu salt **A** promoted addition and S_NAr reactions. Overall, the results for substrates **42**-**52** are consistent with the P_2-*t*-Bu generated from the precatalyst system being the active basic promoter for these reactions.

d) Scaled-up Pd-catalyzed cross-coupling for the recovery and regeneration P_2-*t*-Bu salt A

i. Isolation and recovery of P_2-*t*-Bu salt A from a reaction mixture

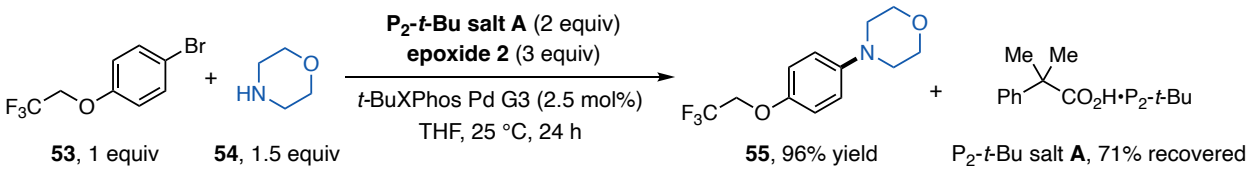

Isolation of 4-(4-(2,2,2-trifluoroethoxy)phenyl)morpholine and P_2-*t*-Bu•HCl: An oven-dried 25 mL round bottom flask was charged with a magnetic stir bar, *t*-BuXPhos Pd G3 (19.9 mg, 0.025 mmol, 2.5 mol%), P_2-*t*-Bu salt **A** (1.063 g, 2.0 mmol, 2.0 equiv), and 1-bromo-4-(2,2,2-trifluoroethoxy)benzene (255.0 mg, 1.0 mmol, 1.0 equiv). The flask was sealed with a rubber septum (Chemglass, CG-3022-06) and evacuated then backfilled with nitrogen three times *via* a nitrogen inlet tube on a Schlenk manifold line. To the flask, THF (5.0 mL, 0.2 M), morpholine (131.2 µL, 1.5 mmol, 1.5 equiv), and epoxide **2** (810.4 mg, 3.0 mmol, 3.0 equiv) were added *via* nitrogen-flushed syringes. The inlet tube was removed, and the flask was placed in a 25 °C oil bath with stirring for 24 h. THF was then removed *in vacuo* and the crude material was transferred to a separatory funnel using 10 mL of diethyl ether. The solution was washed with 0.25M aqueous HCl (3 x 5 mL), water (5 mL) and brine (5 mL) and was dried over Na_2SO_4. The combined organic layer was then concentrated *in vacuo*. The crude organic material was purified by column chromatography (100% hexanes to 20% EtOAc/hexanes to yield pure 4-(4-(2,2,2-trifluoroethoxy)phenyl)morpholine (**55**) as a pale-orange solid (250.0 mg, 0.96 mmol, 96% isolated yield). **^{1}H NMR** (400 MHz, $CDCl_3$) δ 6.94– 6.84 (m, 4H), 4.30 (q, J = 8.2 Hz, 2H), 3.89 – 3.83 (m, 4H), 3.11 – 3.04 (m, 4H). Characterization data matches literature reports.[20]

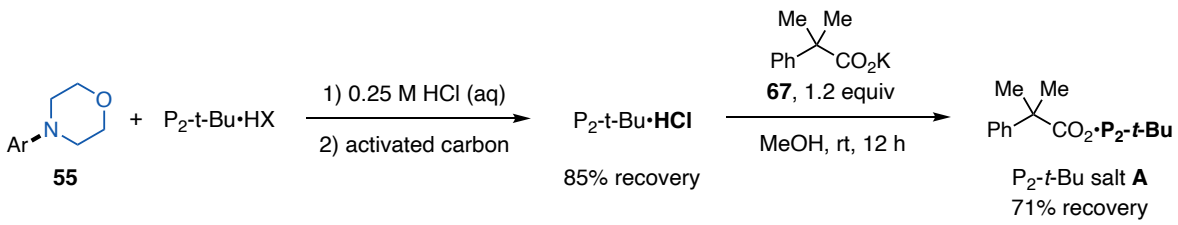

Recovery of P_2-*t*-Bu salt A through anion metathesis: The combined aqueous layers from the above workup were added to a round bottom flask containing a magnetic stir bar and activated carbon (~3 g) then stirred for 12 h at rt. The aqueous solution was filtered through a bed of celite then concentrated *in vacuo* (aq $NaHCO_3$ was added to the receiving flask to neutralize the condensed solution) to collect P_2-*t*-Bu•HCl (686.8 mg, 1.70 mmol, 85% recovery). The collected material was added to a 25 mL round bottom flask with MeOH (10 mL) and a magnetic stir bar. Potassium 2-methyl-2-phenylpropanoate (**68**, 404.4 mg, 2.0 mmol, 1.2 equiv) was added and the mixture was stirred for 12 h at rt. The MeOH was removed *in vacuo* and the crude salt mixture was suspended in ethyl acetate and filtered through a fine fritted funnel. The ethyl acetate solution was concentrated *in vacuo* and dried under vacuum. The pale-yellow oil was placed in a -30 °C freezer overnight to crystallize. The resulting P_2-*t*-Bu salt **A** crystals were collected *via* vacuum filtration with a fine fritted funnel and cold diethyl ether. The crystallization and filtration process were repeated to yield white powdery crystals of P_2-*t*-Bu salt **A** (754.9 mg, 1.42 mmol, 71% regeneration). Characterization data matches P_2-*t*-Bu salt **A** synthesized in Section IId.

ii. Use of recovered P_2-*t*-Bu salt A in a Pd-catalyzed cross-coupling reaction

In this section, we use the recovered P_2-*t*-Bu salt **A** from above in the Pd-catalyzed cross-coupling of 1-bromo-4-(2,2,2-trifluoroethoxy)benzene (**53**) and morpholine (**54**) (Figure S18) following General Procedure U. The results demonstrate there is no difference in reactivity between P_2-*t*-Bu salt **A** synthesized from the commercial freebase and P_2-*t*-Bu salt **A** recovered using the anion metathesis procedure above.

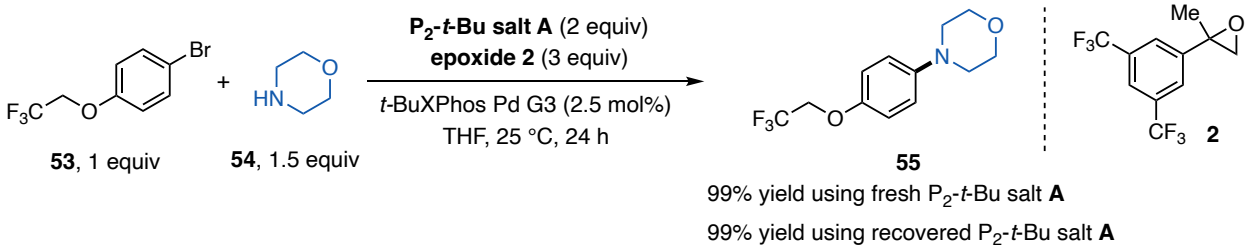

Figure S18. Use of fresh and recovered P_2-*t*-Bu salt **A** in the Pd-catalyzed cross-coupling of 1-bromo-4-(2,2,2-trifluoroethoxy)benzene (**53**) and morpholine (**54**).

e) Pd-Catalyzed Cross-Coupling of Bromobenzene and Morpholine Using Various Epoxides

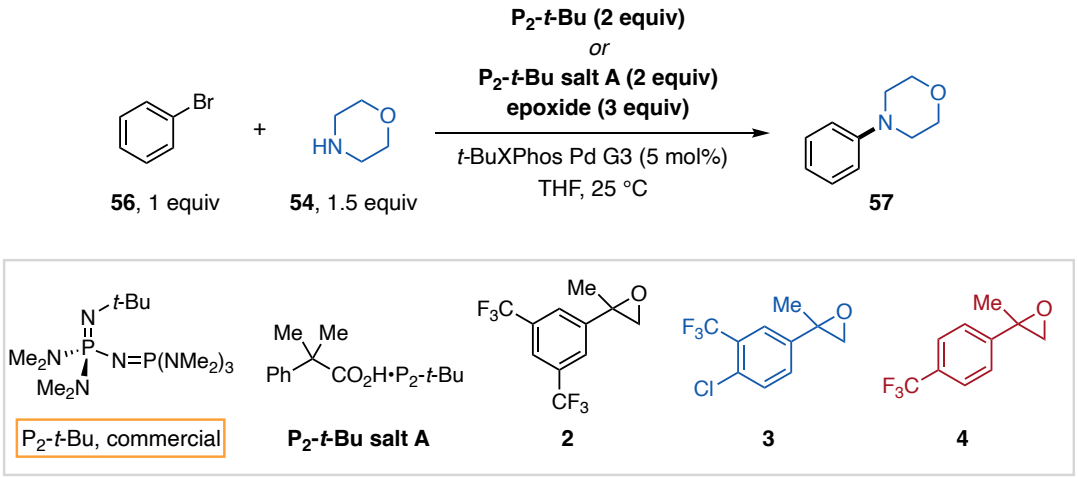

General Procedure X: reaction profiles for the coupling of bromobenzene and morpholine. In a nitrogen-filled glovebox, an oven-dried 1-dram vial (ThermoFisher, C4015-1) was charged with a magnetic stir bar, *t*-BuXPhos Pd G3 (4.0 mg, 0.005 mmol, 5 mol%), 1,3,5-trimethoxybenzene (16.8 mg, 0.1 mmol, 1.0 equiv, used as an internal NMR standard), THF (0.5 mL, 0.2 M), bromobenzene (16.8 mg, 0.1 mmol, 1.0 equiv), morpholine (13.1 µL, 0.15 mmol, 1.5 equiv), then P_2-*t*-Bu (2.0 M THF solution, 50 µL, 0.2 mmol, 2.0 equiv) or P_2-*t*-Bu salt **A** (106.3 mg, 0.2 mmol, 2.0 equiv) and epoxide (0.3 mmol, 3 equiv). The vial was capped with a PTFE-lined cap (ThermoFisher, C4015-1A) and homogenized. Immediately after, a 50 µL aliquot was taken and added to an NMR tube, then diluted with $CDCl_3$ (0.5 mL) and recorded as time point 0 min. The reaction vial was then removed from the glovebox and placed in a preheated reaction block at 25 °C with stirring. Aliquots (50 µL) were taken at various time points; each aliquot was added to an NMR tube, then diluted with $CDCl_3$ (0.5 mL). ^{1}H NMR spectroscopy was used to determine the amount of product at each time point. The amount of product versus time is graphed below. The ^{1}H NMR peaks for the product are consistent with commercial *N*-phenylmorpholine (**57**) and therefore the product was not isolated for these studies. To determine ^{1}H NMR yields for the below studies, the characteristic peak at 4.13 ppm (t, 4H) was used.

Table S25: ^{1}H NMR yields over time using P_2-*t*-Bu salt **A** with epoxides **2**, **3**, and **4** as compared to using commercial P_2-*t*-Bu. [a] This reaction reaches 86% yield after 7 h.

Entry	Time (min)	Base system (% yield of 57)			
		P_2-*t*-Bu	P_2-*t*-Bu salt A + 2	P_2-*t*-Bu salt A + 3	P_2-*t*-Bu salt A + 4[a]
1	0	11	0	0	0
2	5	41	22	6	2

3	10	64	49	16	2
4	15	94	71	25	3
5	20	100	85	37	6
6	40	-	-	62	11
7	60	100	100	80	20
8	120	-	-	100	39

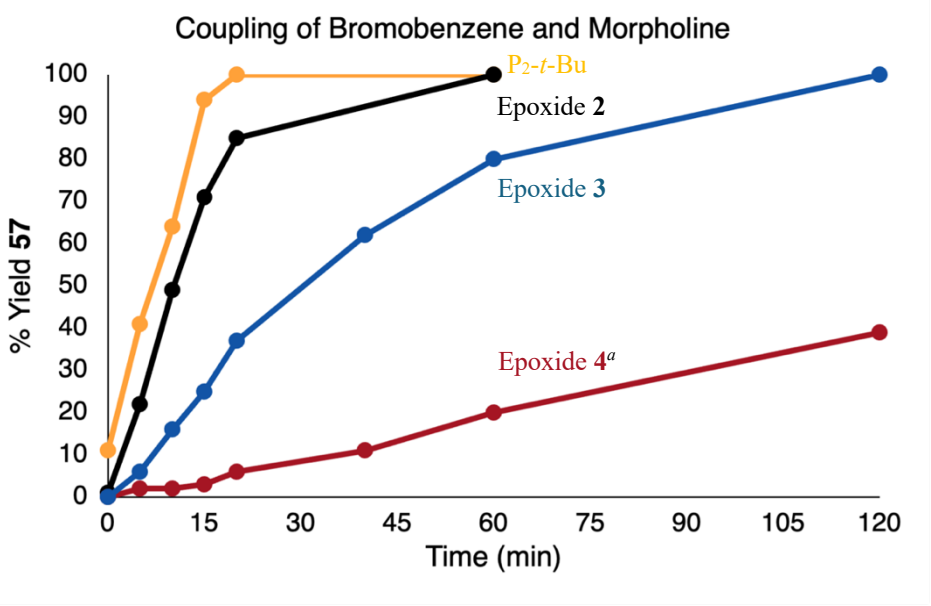

Figure S19. Reaction profiles for the coupling of bromobenzene and morpholine using P_2-*t*-Bu (yellow) and epoxides **2** (black curve), **3** (blue curve), and **4** (red curve) with P_2-*t*-Bu salt **A**. [a] This reaction reaches 86% yield after 24 h.

f) Base-sensitive amine coupling enabled by epoxide-controlled base release

During our studies on Pd-catalyzed cross-coupling reactions using the P_2-*t*-Bu prereagent system, we noticed numerous cases where use of the prereagent gives a higher yield than use of the commercial freebase. Table S26 shows examples of this trend with substrates **58**-**61**. For each substrate, epoxides **2**-**4** were examined and the best yield is shown in Table S26 below. The ^{1}H NMR yields for substrates in Table S24 are the average of two runs. Additionally, we lowered the Pd catalyst loading from 5 mol% to 2.5 mol% and observed a more pronounced effect. We hypothesize that as the concentration of Pd is lowered, the reaction becomes more sensitive to the amount of base present. To elucidate the nature of this effect, we selected substrate **61** to investigate further, discussed below. For each substrate shown in this section, Entries 6 and 10 from Table S24 were repeated to support that P_2-*t*-Bu generated from the prereagent is the active base promoter in solution.

i. Reaction scheme and General Procedures

Table S26. Examples of yield improvements by using the P_2-*t*-Bu prereagent salt system over commercial P_2-*t*-Bu in Pd-catalyzed cross-coupling reactions. [a] Reaction uses 5 mol% Pd.

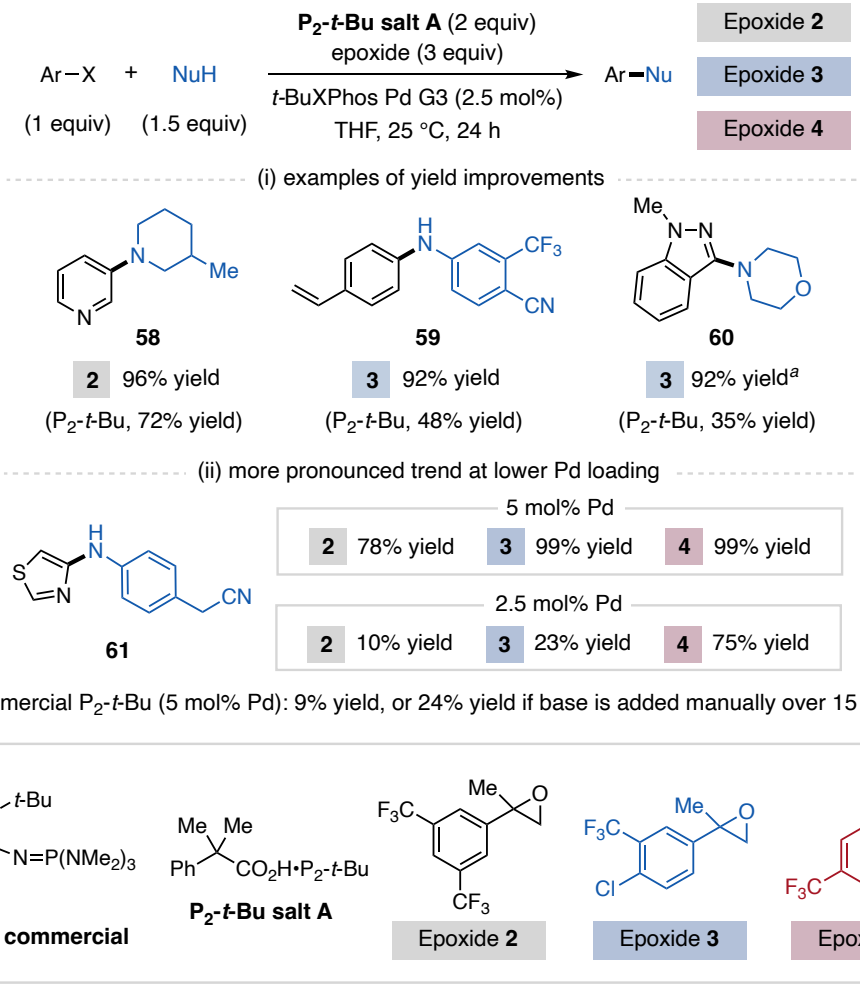

ii. Reaction and characterization data

General description: For all of the substrates in this section, we use ^{1}H NMR yields. In each case, we benchmarked the success of the prereagent against the use of commercial P_2-*t*-Bu. All reactions were carried out using General Procedure W in a nitrogen-filled glovebox and the crude reaction

mixtures were subsequently directly subjected to flash column chromatography to yield purified products. Each substrate in Table S26 was reproduced on a 0.5 mmol scale using a Schlenk line procedure described in General Procedure U.

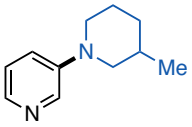

3-(3-methypiperidin-1-yl)pyridine (58). General Procedure W was followed using P_2-*t*-Bu salt **A** (531.7 mg, 1.0 mmol, 2.0 equiv), *t*-BuXPhos Pd G3 (9.9 mg, 0.0125 mmol, 2.5 mol%), epoxide **2** (405.3 mg, 1.5 mmol, 3.0 equiv), 3-bromopyridine (48.2 µL, 0.5 mmol, 1.0 equiv), 3-methylpiperidine (88.0 µL, 0.75 mmol, 1.5 equiv), and THF (2 mL, 0.25 M) to provide 96% ^{1}H NMR yield. The reaction was repeated using commercial P_2-*t*-Bu (72% ^{1}H NMR yield) and on a 0.5 mmol scale using P_2-*t*-Bu Salt **A** with General Procedure U (99% ^{1}H NMR yield). Following General Procedure W, the product was purified *via* silica gel chromatography using 20% EtOAc in hexanes to afford **58** as a yellow oil (76.6 mg, 0.43 mmol, 86% yield). **^{1}H NMR** (400 MHz, $CDCl_3$) δ 8.30 (s, 1H), 8.03 (d, *J* = 4.4 Hz, 1H), 7.22 – 7.08 (m, 2H), 3.66 – 3.51 (m, 2H), 2.68 (t, *J* = 11.8 Hz, 1H), 2.37 (t, *J* = 10.3 Hz, 1H), 1.92 – 1.59 (m, 4H), 1.13 – 0.98 (m, 1H), 0.95 (d, *J* = 6.8 Hz, 3H). **^{13}C NMR** (101 MHz, $CDCl_3$) δ 147.7, 140.0, 139.0, 123.5, 122.7, 57.0, 49.3, 32.8, 30.8, 25.2, 19.6. **IR** (neat) 2926, 2864, 1586, 1494, 1420, 1249, 1138 796, 712 cm^{-1}. **HRMS (ESI)** $[M+H]^+$ calcd. for $[C_{11}H_{17}N_2]^+$ = 177.1392, found 177.1386.

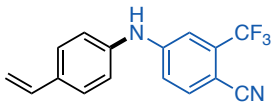

2-(trifluoromethyl)-4-((4-vinylphenyl)amino)benzonitrile (59). General Procedure W was followed using P_2-*t*-Bu salt **A** (531.7 mg, 1.0 mmol, 2.0 equiv), *t*-BuXPhos Pd G3 (9.9 mg, 0.0125 mmol, 2.5 mol%), epoxide **3** (354.9 mg, 1.5 mmol, 3.0 equiv), 4-bromostyrene (65.4 µL, 0.5 mmol, 1.0 equiv), 4-(methylamino)-2-

(trifluoromethyl)benzonitrile (139.6 mg, 0.75 mmol, 1.5 equiv), and THF (2 mL, 0.25 M) to provide 93% ^{1}H NMR yield. The reaction was repeated using commercial P$_2$-*t*-Bu (48% ^{1}H NMR yield) and on a 0.5 mmol scale using P$_2$-*t*-Bu Salt **A** with General Procedure U (91% ^{1}H NMR yield). Following General Procedure W, the product was purified *via* silica gel chromatography using 20% EtOAc in hexanes to afford **59** as a yellow solid (60.5 mg, 0.21 mmol, 42% yield). **^{1}H NMR** (400 MHz, $CDCl_3$) δ 7.61 (d, *J* = 8.5 Hz, 1H), 7.44 (d, *J* = 8.1 Hz, 2H), 7.23 (d, *J* = 2.2 Hz, 1H), 7.14 (d, *J* = 8.1 Hz, 2H), 7.09 (dd, *J* = 8.5, 2.2 Hz), 6.71 (dd, *J* = 17.6, 10.8 Hz, 6.26 (bs, 1H), 5.73 (d, *J* = 17.6 Hz, 1H), 5.26 (d, *J* = 10.9 Hz, 1H). **^{13}C NMR** (101 MHz, $CDCl_3$) δ 148.0, 138.3, 136.3, 135.8, 134.7, 134.6, 127.7, 122.4 (q, *J* = 273.2 Hz), 121.9, 116.5, 116.4, 113.8, 112.6 (q, *J* = 4.9 Hz), 98.5. **^{19}F NMR** (376 MHz, $CDCl_3$) δ -62.37. **IR** (neat) 3319, 2926, 2226, 1591, 1529, 1350, 1176, 1130, 1040, 827 cm^{-1}. **HRMS (ESI)** $[M+H]^+$ calcd. for $[C_{16}H_{12}F_3N_2]^+$ = 289.0953, found 289.0947. MP 151 – 154 °C.

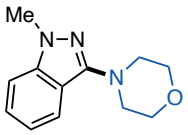

4-(1-methyl-1*H*-indazol-3-yl)morpholine (60). General Procedure W was followed using P$_2$-*t*-Bu salt **A** (531.7 mg, 1.0 mmol, 2.0 equiv), *t*-BuXPhos Pd G3 (19.9 mg, 0.025 mmol, 5 mol%), epoxide **3** (354.9 mg, 1.5 mmol, 3.0 equiv), 3-bromo-1-methyl-1*H*-indazole (105.5 mg, 0.5 mmol, 1.0 equiv), morpholine (65.3 µL, 0.75 mmol, 1.5 equiv), and THF (2 mL, 0.25 M) to provide 92% ^{1}H NMR yield. The reaction was repeated using commercial P$_2$-*t*-Bu (35% ^{1}H NMR yield) and on a 0.5 mmol scale using P$_2$-*t*-Bu Salt **A** with General Procedure U (99% ^{1}H NMR yield). Following General Procedure W, the product was purified *via* silica gel chromatography using 20% EtOAc in hexanes to afford **60** as a yellow oil (22.6 mg, 0.11 mmol, 22% yield). **^{1}H NMR** (400 MHz, $CDCl_3$) δ 7.71 (d, *J* = 8.2 Hz, 1H), 7.37 (t, *J* = 7.8 Hz, 1H), 7.30 – 7.25 (m, 1H), 7.05 (t, *J* = 8.5 Hz, 1H), 3.98 – 3.93 (m, 4H), 3.93 (s, 3H), 3.49 – 3.41 (m, 4H).

^{13}C NMR (101 MHz, $CDCl_3$) δ 151.4, 142.1, 126.7, 121.2, 118.8, 115.2, 109.1, 66.9, 50.5, 35.1. **IR** (neat) 2964, 2915, 2855, 1740, 1616, 1523, 1447, 1249, 1122, 750 cm^{-1}. **HRMS (ESI)** $[M+H]^+$ calcd. for $[C_{12}H_{16}N_3O]^+$ = 218.1293, found 218.1288.

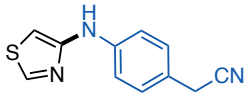

2-(4-(thiazol-4-ylamino)phenyl)acetonitrile (61). General Procedure U was followed using P_2-*t*-Bu salt **A** (265.8 mg, 0.5 mmol, 2.0 equiv), *t*-BuXPhos Pd G3 (9.9 mg, 0.0125 mmol, 5 mol%), epoxide **4** (151.6 mg, 0.75 mmol, 3.0 equiv), 4-bromothiazole (22.3 μL, 0.25 mmol, 1.0 equiv), 2-(4-aminophenyl)acetonitrile (49.6 mg, 0.375 mmol, 1.5 equiv), and THF (1.25 mL, 0.2 M) to provide **61** in 99% yield. The reaction was repeated using commercial P_2-*t*-Bu (9% ^{1}H NMR yield) and on a 0.5 mmol scale using P_2-*t*-Bu Salt **A** with General Procedure U (92% ^{1}H NMR yield). Following General Procedure U, the product was purified *via* preparatory thin layer chromatography using 5% EtOAc in DCM to afford **61** as a grey solid (21.4 mg, 0.1 mmol, 40% yield). **^{1}H NMR** (400 MHz, $CDCl_3$) δ 8.64 (s, 1H), 7.25 (d, *J* = 9.3 Hz, 2H), 7.14 (d, *J* = 8.4 Hz, 2H), 6.68 (bs, 1H), 6.51 (s, 1H), 3.70 (s, 2H). Characterization data matches literature reports.[21]

iii. Additional investigation with substrate 61

We selected substrate **61** to investigate further to elucidate the nature of the yield improvements using the prereagent system over commercial P_2-*t*-Bu. Direct use of commercial P_2-*t*-Bu results in 9% yield of **61** with observation of a black precipitate form inside of the vial, suggesting the Pd catalyst may not be stable towards excess base under these conditions. For comparison, we

conducted the model reaction with manual slow addition of commercial P_2-*t*-Bu over 15 minutes, resulting in an increased yield of 24% **61**, suggesting the reaction is sensitive to the initial concentration of base. We next investigated use of P_2-*t*-Bu salt **A** with epoxides **2-4** at 5 mol% and 2.5 mol% Pd loading (Table S26ii). Here, we observe that slower activating epoxides result in higher yield of **61**, a trend that is amplified at lower catalyst loading. These results suggest that the ability to slowly generate base in solution, enabled by the prereagent system, is key to obtain high yield. To understand the effect of high concentration of base on the reaction, we conducted further control studies, described below.

iv. Control studies for the effect of base on the individual reaction components

Here, we tested to see if P_2-*t*-Bu engages in undesired background processes with any of the reaction components that could lead to reaction inhibition. We tested for this by subjecting 4-bromothiazole and 2-(4-aminophenyl)acetonitrile to P_2-*t*-Bu to observe their stability over time.

General Procedure Y: Mixing starting materials with excess P_2-*t*-Bu. In a nitrogen-filled glovebox, an oven-dried 1-dram vial (ThermoFisher, C4015-1) was charged with a magnetic stir bar, 4-bromothiazole (4.5 µL, 0.05 mmol, 1.0 equiv) and/or 2-(4-aminophenyl)acetonitrile (9.9 mg, 0.075 mmol, 1.5 equiv), P_2-*t*-Bu (2.0 M THF solution, 50 µL, 0.2 mmol, 2.0 equiv), and THF (0.25 mL, 0.2 M). The vial was sealed with a PTFE-lined cap (ThermoFisher, C4015-1A) and removed from the glovebox. The reaction vial was then placed in a preheated aluminum reaction block at 25 °C with magnetic stirring for 24 h. A 1 M solution of aqueous HCl (100 µL, 1.0 mmol)

and dibenzyl ether (9.5 µL, 0.05 mmol, 1.0 equiv) were added to the reaction solution, a 50 µL aliquot was taken and added to an NMR tube, then diluted with $CDCl_3$ (0.5 mL). ^1H NMR spectroscopy was used to determine the mass balance of the starting materials and yield of potential products.

Stability 4-bromothiazole in the presence of P_2-*t*-Bu:

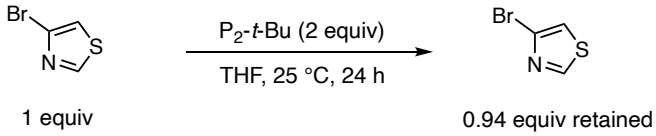

Figure S20. Treatment of 4-bromothiazole with P_2-*t*-Bu under pseudo-reaction conditions.

Results: Stirring 4-bromothiazole with P_2-*t*-Bu over the course of 24 h results in near complete retention of the starting material. This indicates this aryl halide is not sensitive to P_2-*t*-Bu alone.

Stability of 2-(4-aminophenyl)acetonitrile in the presence of P_2-*t*-Bu:

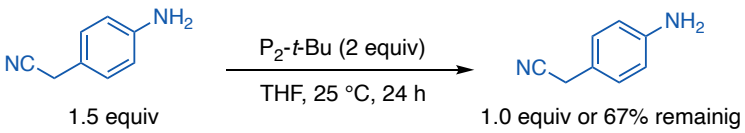

Figure S21. Treatment of 2-(4-aminophenyl)acetonitrile with P_2-*t*-Bu under pseudo-reaction conditions.

Results: Stirring 2-(4-aminophenyl)acetonitrile with P_2-*t*-Bu over the course of 24 h results in the loss of 33% of the aniline mass balance. This indicates this aniline is sensitive to the presence of P_2-*t*-Bu in solution.

Stability 4-bromothiazole + 2-(4-aminophenyl)acetonitrile in the presence of P_2-*t*-Bu:

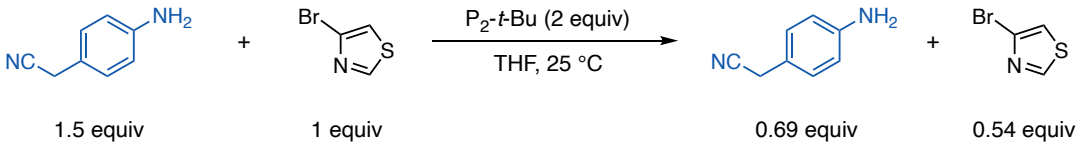

Figure S22. Treatment of 4-bromothiazole and 2-(4-aminophenyl)acetonitrile with P_2-*t*-Bu under pseudo-reaction conditions.

Results: Stirring both 4-bromothiazole and 2-(4-aminophenyl)acetonitrile together with P_2-*t*-Bu over the course of 24 h resulted in loss of mass balance of both substrates. This indicates the substrate combination of this reaction is sensitive to the presence of P_2-*t*-Bu in solution.

v. Reaction profile of the coupling reaction using P_2-*t*-Bu salt A and epoxide 4

Here, we provide a reaction profile for the formation of **61** using P_2-*t*-Bu salt **A** and epoxide **4**, also tracking the amount of activation byproduct **65** that is formed (Table S27, Figure S23). We

observe similar rates of formation of **61** and the of alcohol activation byproduct **65**, aside from a short induction period in the beginning for the formation of **65**.

General Procedure Z: Reaction profile using P_2-*t*-Bu salt A and epoxide 4. In a nitrogen-filled glovebox, an oven-dried 1-dram vial (ThermoFisher, C4015-1) was charged with a magnetic stir bar, *t*-BuXPhos Pd G3 (4.0 mg, 0.005 mmol, 5 mol%), 1,3,5-trimethoxybenzene (16.8 mg, 0.1 mmol, 1.0 equiv, to serve as an internal NMR standard), THF (0.5 mL, 0.2 M), 4-bromothiazole (8.9 µL, 0.1 mmol, 1.0 equiv), 2-(4-aminophenyl)acetonitrile (19.8 mg, 0.15 mmol, 1.5 equiv), P_2-*t*-Bu salt **A** (106.3 mg, 0.2 mmol, 2.0 equiv) and epoxide **4** (60.7 mg, 0.3 mmol, 3 equiv) in successive order. The vial was capped with a PTFE-lined cap (ThermoFisher, C4015-1A) and homogenized. Immediately after, a 50 µL aliquot was taken and added to an NMR tube, then diluted with $CDCl_3$ (0.5 mL) as time point 0 min. The reaction vial was then placed in a preheated aluminum reaction block at 25 °C for 24 h with stirring. Aliquots (50 µL) were taken at various time points and each aliquot was added to an NMR tube, then diluted with $CDCl_3$ (0.5 mL). ^1H NMR spectroscopy was used to determine the amount of product and alcohol activation byproduct at each time point. The amount of these products versus time is graphed below.

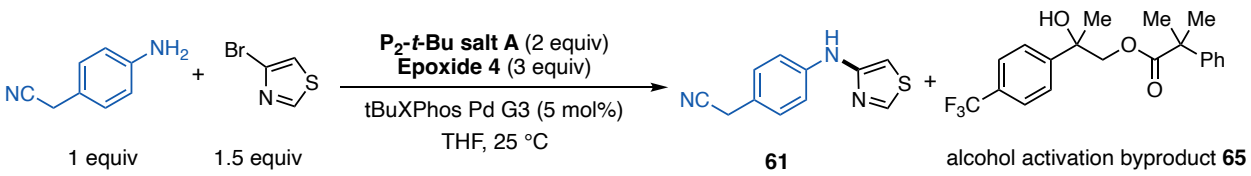

Time (h)	% yield **61**	% yield **65**
0	0	0
0.15	2	3
0.5	3	13
1	11	26
2	29	46
3	44	64
4.5	60	81
6	75	97
7.5	88	109

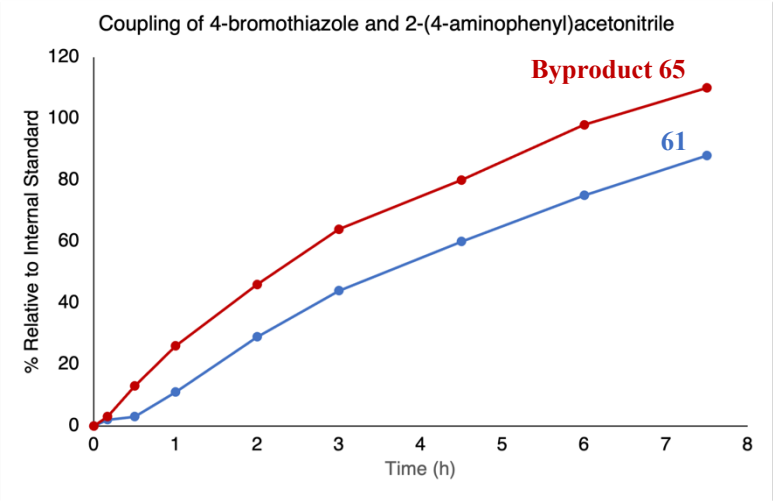

Table S27 and Figure S23: Reaction profile for the Pd-catalyzed coupling reaction of 4-bromothiazole and 2-(4-aminophenyl)acetonitrile with P_2-*t*-Bu salt **A** and epoxide **4**. Blue profile corresponds to the yield of **61** and red corresponds to the yield of byproduct **65**, relative to 1,3,5-trimethoxybenzene internal standard. The product yield was observed to be 95% at 23 h with 1.20 equiv byproduct generated.

Summary discussion: Based on the studies described here, we found that the amine, aryl halide and Pd catalyst all possess base sensitivity which may lead to low yield. The results of the above time study show a direct correlation between the rate of epoxide opening and the reaction yield. This suggests that with the prereagent system using epoxide **4**, P_2-*t*-Bu is consumed as it is generated. Collectively, the results described in Sections ii-v provide support for the hypothesis that the prereagent system can controllably introduce base into solution to facilitate coupling reactions that are sensitive to high concentration of base.

VIII. Long-Term Stability of Superbase Carboxylate Salts

This section describes experiments and studies performed to test the long-term stability of the superbase carboxylate salts under various environments. In order to confirm that the salts do not lose their reactivity benchmark use of them are shown in Tables S5, S6, S16, S17, and S20.

a) Longevity studies with BTPP salt A and P_2-*t*-Bu salt A

In order to test the long-term stability of the phosphazene carboxylate salts, we prepared two 20 mL scintillation vials containing 2 g of either BTPP salt **A** or P_2-*t*-Bu salt **A**. These vials were stored in a benchtop desiccator for six months, and three times per week the vials were uncapped and the salts were mixed around open to air with a spatula to mimic heavy usage. After six months,

no change was observed in the physical properties of these salts or their performance in reactions. Use of these aged salts in reaction applications are shown in throughout Sections IV and VI.

b) Observation of moisture sensitivity of superbase carboxylate salts

During our studies, the superbase carboxylate salts have been stable over long periods of time in a benchtop desiccator. However, upon exposure to high humidity (greater than 60%), we observe the formation of droplets when the salts are on weigh paper as the salts began absorbing water. When stored over long periods of time open-to-air in this environment, the salts became wet semi-solids. It is important to note that this work was conducted in Fort Collins, Colorado, where the atmosphere is typically under 50% humidity. We therefore investigated the salt sensitivity to greater humidity levels, detailed here. In order to accomplish this, we used humidity control packets that can maintain 72% (Boveda 72% RH size 8) and 84% (Boveda 84% RH size 8) humidity and placed them in a glass chamber sealed with high-vacuum grease and kept on the benchtop (see images below).

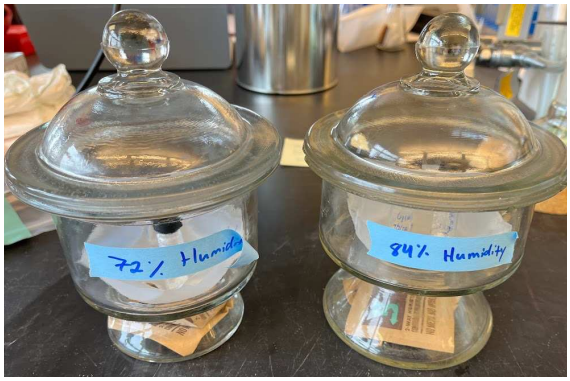

We placed a hygrometer inside each of these chambers to confirm the humidity levels. To test how long a salt can maintain its physical properties as a free-flowing powder in the humid environment, it was placed into the humidity chamber on a piece of weigh paper. Every five minutes, the chamber was opened, and the salt was mixed around with a metal spatula to mimic use in the humid environment. When BTPP salt **A** and P_2-*t*-Bu salt **A** were tested in this fashion, we found that they each lasted for fifteen minutes before they became sticky and clumped together and formed droplets on the weigh paper, becoming challenging to handle. We note that the absorption of water by the salts is exacerbated on weigh paper and as such we recommend storage in glass containers while not in use. These findings motivated us to develop solutions to overcome humidity sensitivity. For reference, we stored commercial P_2-*t*-Bu (in its crystalline form) in the 84% humidity chamber and after five minutes the base clumped together and formed droplets on the weigh paper, indicative of moisture absorption. ^{31}P and ^{1}H NMR spectra of this material are shown in Figure S24. Additionally, we stored BTPP open-to-air for two weeks and observed significant formation of the phosphoramide through reaction with CO_2 in the air, the primary decomposition pathway of BTPP (Figure S25).

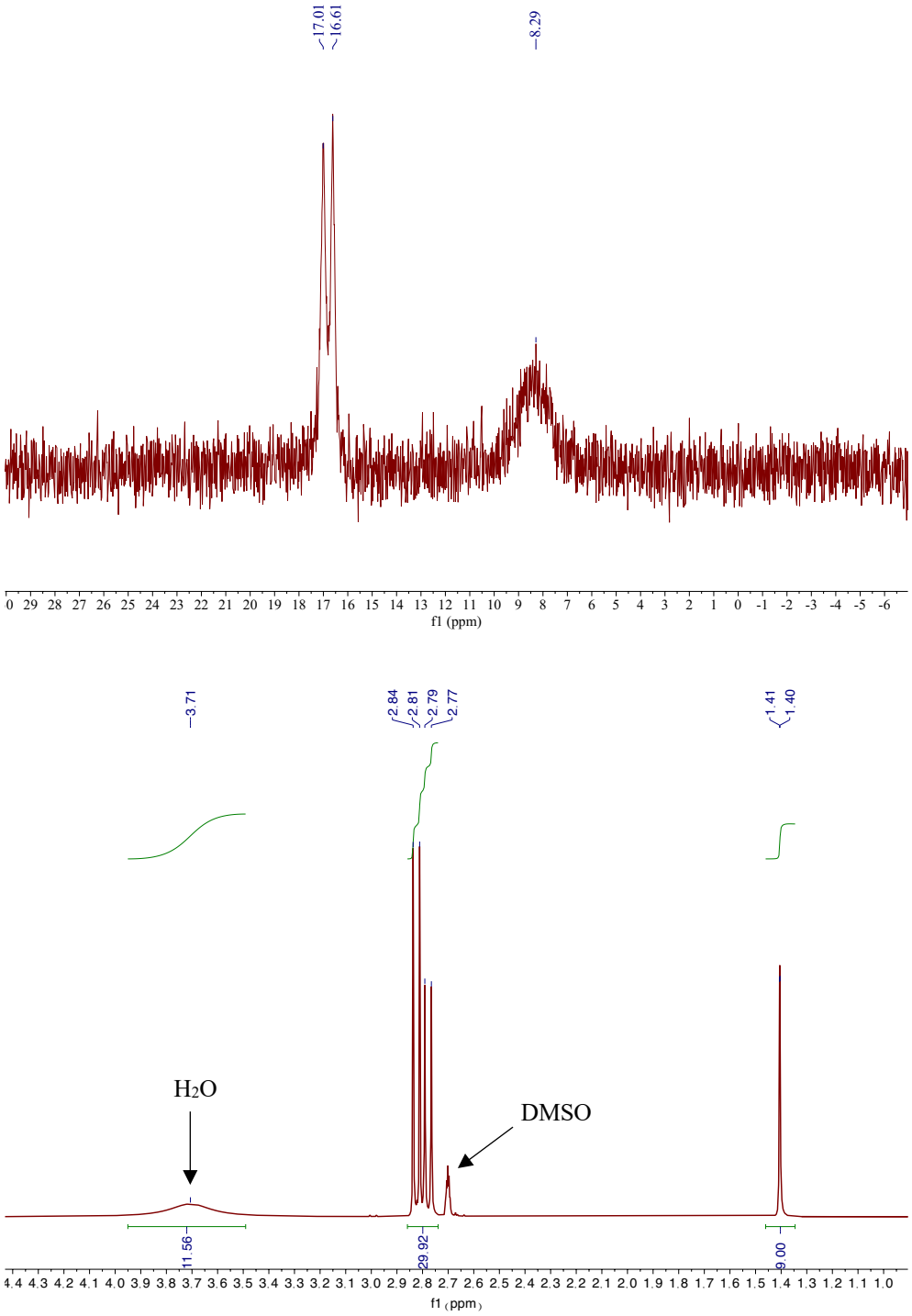

Figure S24. ^{31}P (top) and ^{1}H NMR (bottom) spectra for commercial P_2-*t*-Bu that has been in 84% humidity for 8 h. The ^{31}P NMR spectrum shows peaks at 16 and 7.5 ppm which are similar to protonated P_2-*t*-Bu, indicating that it has absorbed water. The broad singlet at 3.71 ppm on the ^{1}H NMR spectrum corresponds to the absorbed water.

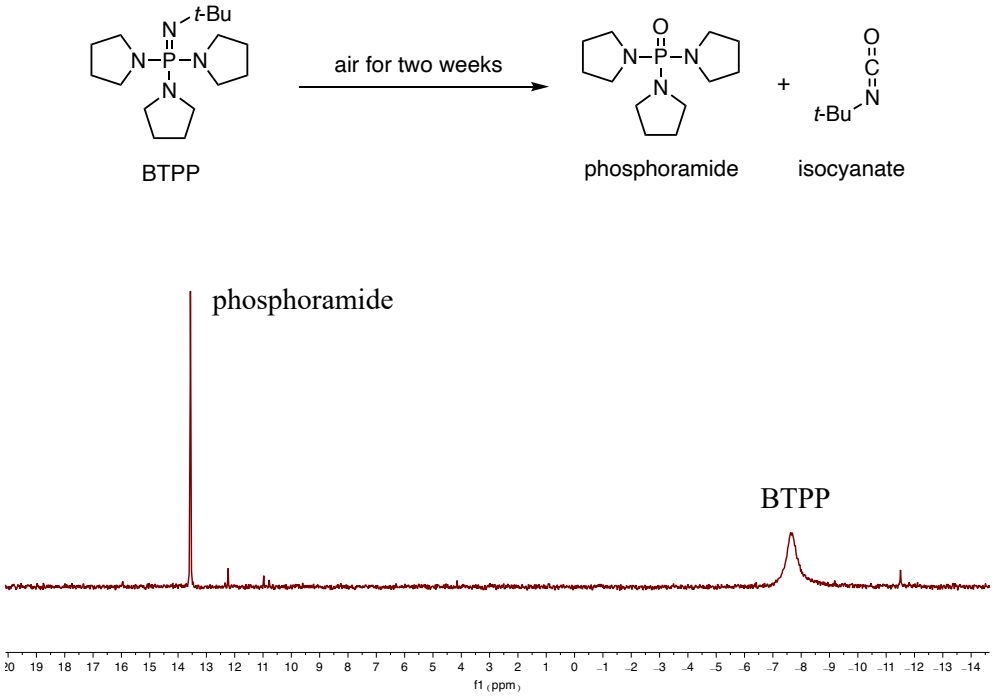

Figure S25. ^{31}P NMR spectrum of commercial BTPP left open-to-air for two weeks. Peak at -8 ppm corresponds to the freebase and the peak at 13.5 ppm corresponds to the phosphoramide resulting from reaction with CO_2.

c) Solutions to moisture sensitivity of superbase carboxylate salts

To address this limitation, we developed two solutions to enable the use of superbase carboxylate salts in more humid environments. First, we developed a restoration process that allows for the facile removal of the absorbed water to re-obtain the crystalline solid *via* an azeotrope with PhMe where the water is removed by rotary evaporation (Figure S26). For the second solution, changes in the carboxylate structure led to superbase salts that are far less hygroscopic and last for longer periods of time in the humidity chambers (Figure S29). These salts are shown to be equally effective as the freshly synthesized salts, as seen in Sections IVaiii and VIaiii. Ultimately, we

recommend storage of the superbase salts in a benchtop desiccator or freezer when not in use to ensure their long-term stability.

i. Regeneration of crystalline solid superbase salts *via* azeotrope with PhMe

General Procedure AA: Azeotrope with PhMe to remove water from carboxylate salts. We placed the superbase salts uncapped into an 84% humidity chamber after which we subjected them to the following procedure. To the vial containing the water-absorbed carboxylate salt, PhMe (~5 mL/g) was added, then the solution was concentrated using a rotary evaporator. This procedure was repeated three times, and the sample was dried on a Schlenk line under high vacuum for 12 h, providing dry, crystalline powder. The regenerated crystalline superbase salts were stored in a benchtop desiccator for further use (see Entry 6 in Table S7 for use of recovered BTPP salt **A** in the Michael addition reaction and Entry 11 in Table S16 for use of the recovered P_2-*t*-Bu salt **A** salts in the oxa-Michael addition reaction, where they perform similarly to freshly prepared salts). An illustration of this procedure is shown in Figure S26 below, where BTPP salt **A** and P_2-*t*-Bu salt **A** were placed into an 84% humidity chamber. Both salts absorbed enough water (41.4 mg and 32.4 mg of water, respectively) to turn from crystalline solids to oils in the vial. After the restoration process, the salts regained their crystallinity and showed removal of all of the added mass of water. Figures S27 and S28 show the ^{1}H NMR spectra of this process and the appearance and removal of water for both BTPP salt **A** and P_2-*t*-Bu salt **A**.

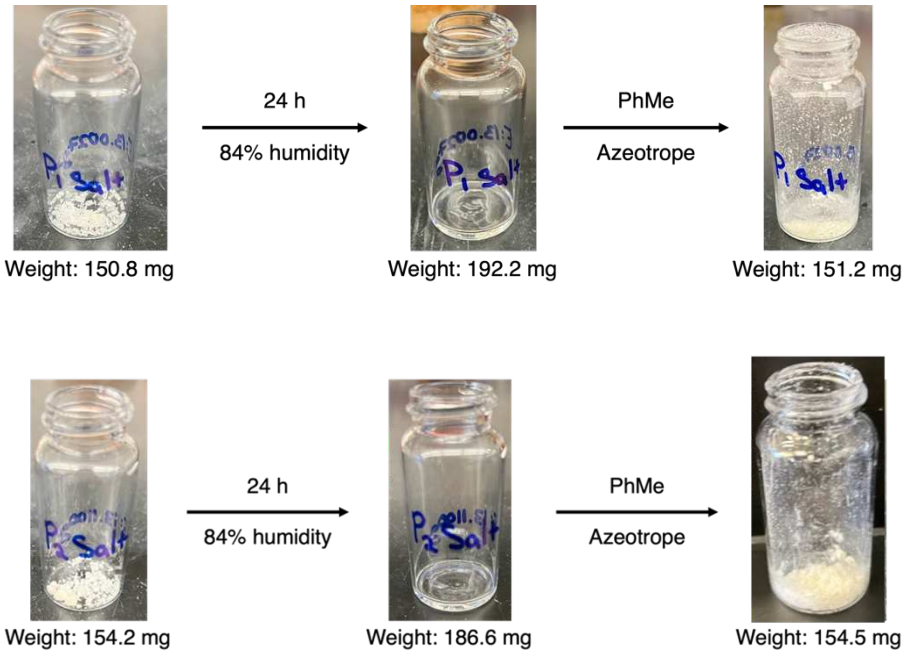

Figure S26. Images of BTPP Salt **A** (top) and P_2-*t*-Bu Salt **A** (bottom) stored for 24 h in 84% humidity and recovery using the regeneration procedure through azeotrope with toluene.

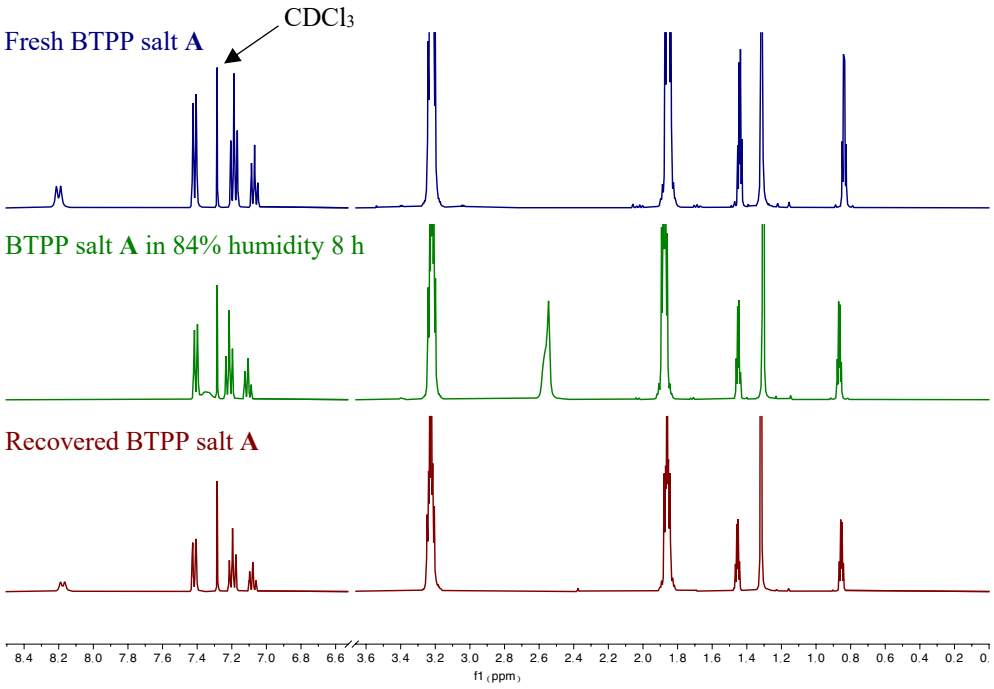

Figure S27. ^{1}H NMR spectra comparing fresh BTPP salt **A** (top), BTPP salt **A** exposed to 84% humidity (middle), and BTPP salt **A** recovered *via* the azeotrope procedure (bottom).

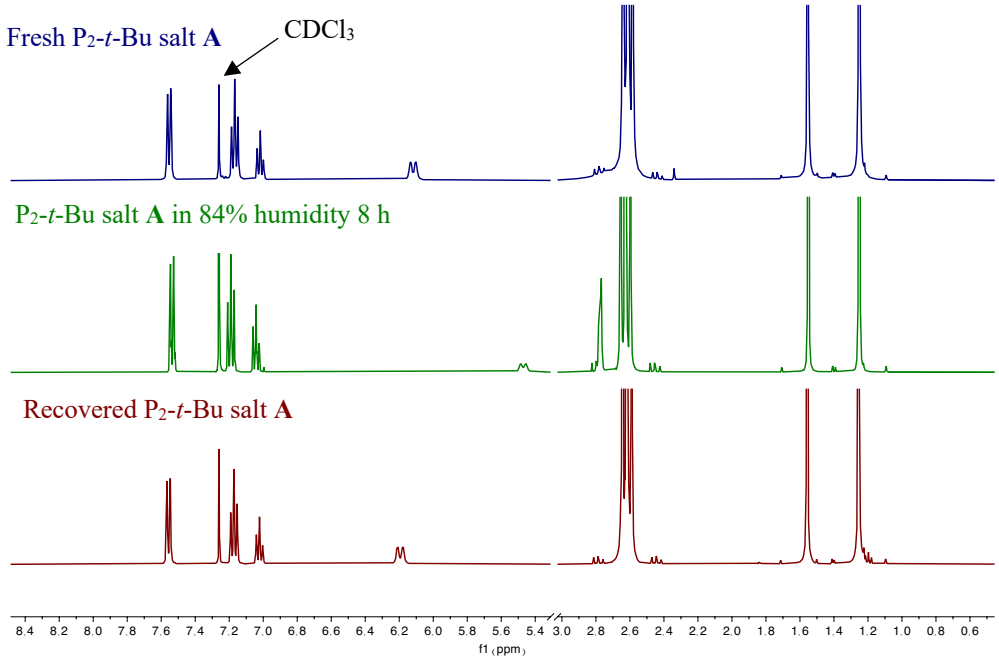

Figure S28. ^{1}H NMR spectra comparing fresh P_2-*t*-Bu salt **A** (top), P_2-*t*-Bu salt **A** exposed to 84% humidity (middle), and P_2-*t*-Bu salt **A** recovered *via* the azeotrope procedure (bottom).

ii. Preparation of less hygroscopic superbase carboxylate salts.

Superbase salts with alternate carboxylate anions were synthesized for both BTPP and P_2-*t*-Bu from the commercial superbase and a carboxylic acid using the procedures described below. From this investigation, we found BTPP salt **B** and P_2-*t*-Bu salt **B** form solid, crystalline salts. These salts retain their crystallinity and ease-of-use without any changes in physical appearance or formation of droplets on the weighing paper for 8 and 24 hours, respectively, when stored in an

84% humidity chamber. Additionally, these salts show no change in physical characteristics over 24 h in 84% humidity while stored in an open vial. The syntheses of these salts are shown below and their use in reaction applications are shown in Sections IV and VI where they work just as well as BTPP salt **A** and P_2-*t*-Bu salt **A**.

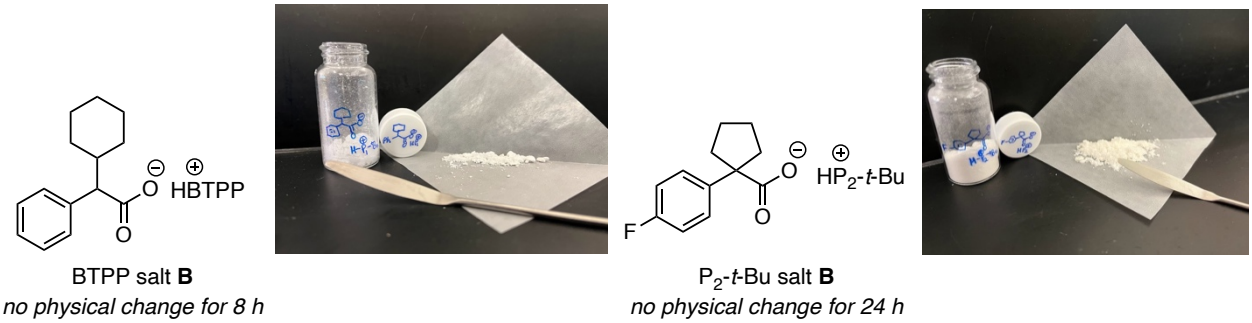

BTPP salt **B**
no physical change for 8 h

P_2-*t*-Bu salt **B**
no physical change for 24 h

Figure S29. Structures and images of BTPP salt **B** and P_2-*t*-Bu salt **B** that show improved stability in highly humid environments. Shown with the salts is the length of time they remain crystalline in 84% humidity without any changes to their physical properties or droplets forming on the weigh paper.

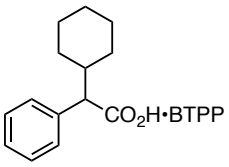

***tert*-butylimino-tri(pyrrolidino)phosphorane 2-cyclohexyl-2-phenylacetate (BTPP Salt B).** An oven-dried 20 mL scintillation vial (ThermoFisher, 03-341-25D) was charged with a magnetic stir bar, 2-cyclohexyl-2-phenylacetic acid (436.6 mg, 2.0 mmol, 1.0 equiv), and Et_2O (5 mL, 0.1 M). In a nitrogen-filled glovebox, an oven-dried 20 mL scintillation vial (ThermoFisher, 03-341-25D) was charged with BTPP (611.4 µL, 2.0 mmol, 1.0 equiv) and Et_2O (1 mL, 2 M). The vial was capped and removed from the glovebox. The vial containing BTPP dissolved in Et_2O was opened to air and added dropwise *via* glass pipette to the stirring solution of the acid. The reaction mixture was stirred at rt for 1 hr, during which time a white precipitate formed. The precipitated solid was

filtered and washed with cold Et_2O, providing the product as a white solid (1.99 g, 3.8 mmol, 75% yield). **^{1}H NMR** (400 MHz, $CDCl_3$) δ 8.51 (d, *J* = 10.4 Hz, 1H), 7.46 (d, *J* = 7.3 Hz, 2 H), 7.16 (t, *J* = 7.5 Hz, 2 H), 7.10 – 7.01 (m, 1H), 3.20 (h, *J* = 3.6 Hz, 12H), 3.05 (d, *J* = 10.7 Hz, 1 H), 2.13 (d, *J* = 12.9 Hz, 1 H), 2.03 (dt, 11.1, 3.1 Hz, 1H), 1.83 – 1.72 (m, 12H), 1.69 (d, *J* = 12.8 Hz, 1H), 1.62 – 1.51 (m, 2 H), 1.40 – 1.30 (m, 1H), 1.28 (s, 9H), 1.17-1.04 (m, 3 H), 0.79-0.59 (m, 1H). **^{31}P NMR** (162 MHz, $CDCl_3$) δ 22.82 (s, 1P). **^{13}C NMR** (101 MHz, $CDCl_3$) δ 177.4, 143.8, 129.0, 127.2, 124.8, 64.6, 51.9 (d, *J* = 2.2 Hz), 47.5 (d, *J* = 5.1 Hz), 41.4, 32.6, 31.3 (d, *J* = 4.8 Hz), 31.1, 26.9, 26.6, 26.5, 26.1 (d, *J* = 8.0 Hz). **IR** (neat) 3058, 2925, 2683, 1598, 1486, 1364, 1205, 1077, 1022, 709 cm^{-1}. **HRMS (DART)** $[M]^+$ calcd. for $[C_{16}H_{34}N_4P]^+$ (for protonated phosphazene) = 313.2516, found 313.2558. **MP** 110 – 115 °C.

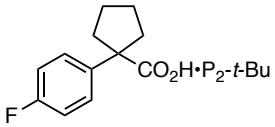

***tert*-butylimino-tri(pyrrolidino)phosphorane 1-(4-fluorophenyl)cyclopentane-1-carboxylate (P_2-*t*-Bu Salt B).** An oven-dried 20 mL scintillation vial (ThermoFisher, 03-341-25D) was charged with a magnetic stir bar, 1-(4-fluorophenyl)cyclopentanecarboxylic acid (1.11 g, 5.0 mmol, 1.0 equiv), and Et_2O (5 mL, 0.1 M). In a nitrogen-filled glovebox, an oven-dried 20 mL scintillation vial (ThermoFisher, 03-341-25D) was charged with P_2-*t*-Bu (0.2 M solution in THF, 2.5 mL, 5.0 mmol, 1.0 equiv) and Et_2O (1 mL, 2M). The vial was capped and removed from the glovebox. The vial containing P_2-*t*-Bu dissolved in Et_2O was opened to air and added dropwise *via* glass pipette to the stirring solution of the acid. The reaction mixture was stirred at rt open-to-air for 1 hr, during which time a white precipitate formed. The precipitated solid was filtered and washed with cold Et_2O, providing the product as a white solid (2.01 g, 3.4 mmol, 68% yield). **^{1}H NMR** (400 MHz, $CDCl_3$) δ 7.48 (dd, *J* = 8.5, 5.8 Hz, 2 H), 6.84 (t, *J* = 8.8 Hz, 2H), 6.09 (d, 12.4 Hz, 1H), 2.85 – 2.78 (m, 2H), 2.67 –

2.54 (m, 30 H), 1.84 – 1.76 (m, 2H), 1.75 – 1.64 (m, 2H), 1.64 – 1.55 (m, 2H), 1.25 (s, 9H). **^{31}P NMR** (162 MHz, $CDCl_3$) δ 16.23 (d, *J* = 67.8 Hz, 1P), 12.25 (d, *J* = 67.2 Hz, 1P). **^{19}F NMR** (376 MHz, $CDCl_3$) δ -121.03. **^{13}C NMR** (101 MHz, $CDCl_3$) δ 178.7, 161.8 (d, *J* = 242.6 Hz), 145.4 (d, *J* = 3.0 Hz), 128.7 (d, *J* = 7.5 Hz), 113.5 (d, *J* = 20.6 Hz), 61.1, 50.8 (d, *J* = 2.6 Hz), 37.4, 37.1 (d, *J* = 5.5 Hz), 37.0 (d *J* = 5.1 Hz), 31.1 (d, *J* = 4.7 Hz), 24.3. **IR** (neat) 3060, 2928, 2681, 1592, 1473, 1351, 1213, 1067, 1014, 703 cm^{-1}. **HRMS (DART)** $[M]^+$ calcd. for $[C_{14}H_{40}N_7P_2]^+$ (for protonated phosphazene)= 368.2815, found 368.2866. **MP** 95 – 100 °C.

iv. Identification of a crystalline solid spirocyclic epoxide

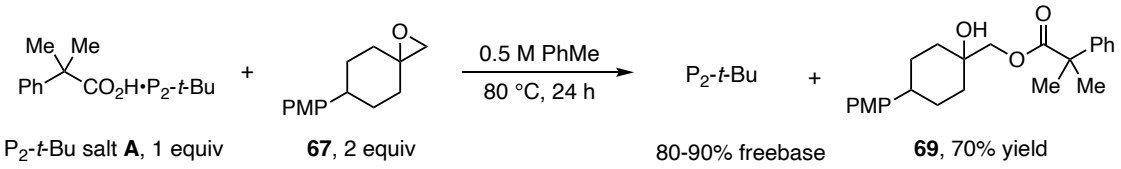

P_2-*t*-Bu salt **A**, 1 equiv | **67**, 2 equiv | 80-90% freebase | **69**, 70% yield

In our studies with superbase salt activation using epoxide additives, we found that epoxide **22** is a semisolid that melts near rt, so we identified a new epoxide that remains solid at rt. Epoxide **67** is a crystalline solid alternative to epoxide **22**, with the ability to generate 80-90% freebase along with 70% of the activation byproduct at equilibrium in an activation reaction setup according to General Procedure H. Provided below is the synthesis and characterization of this epoxide. See Table S16 for use of this epoxide in the oxa-Michael addition reaction.

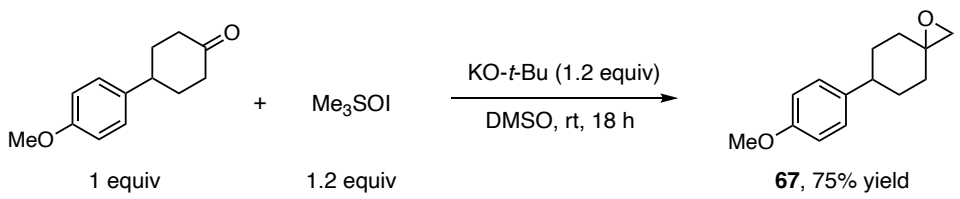

6-(4-methoxyphenyl)-1-oxaspiro[2.5]octane (67). An oven-dried 250 mL round bottom flask was charged with a magnetic stir bar, trimethylsulfoxonium iodide (6.61 g, 30.0 mmol, 1.2 equiv), and DMSO (125 mL, 0.2 M) open to air. To the stirring mixture, KO-*t*-Bu (3.37 g, 30.0 mmol, 1.2 equiv) was added slowly, in portions, and the solution was stirred for 1 h. To the stirring mixture, 4-(4-methoxyphenyl)cyclohexan-1-one[22] (5.11 g, 25.0 mmol, 1.0 equiv) was added and the reaction was allowed to stir at rt for a further 18 h. Water (150 mL) was added to the reaction flask and the mixture was extracted with EtOAc (3 x 100 mL). The combined organic layers were washed with brine (100 mL), dried over Na_2SO_4, and concentrated *in vacuo*. The crude material was purified *via* silica gel chromatography using 7% EtOAc in hexanes to afford **67** as a white solid (4.09 g, 18.8 mmol, 75% yield). **^{1}H NMR** (400 MHz, $CDCl_3$) δ 7.17 (d, J = 8.7 Hz, 2H), 6.86 (d, J = 8.8 Hz, 2H), 3.79 (s, 3H), 2.69 (s, 2H), 2.57 (tt, J = 11.5, 3.9 Hz, 2H), 2.12 – 1.99 (m, 1H), 1.95 – 1.76 (m, 4H), 1.37 (d, J = 14.2 Hz, 2H). **^{13}C NMR** (101 MHz, $CDCl_3$) δ 157.9, 138.9, 127.7, 113.8, 57.8, 55.3, 54.0, 42.4, 33.3, 31.8. **IR (neat)** 3018, 2944, 2856, 1611, 1516, 1441, 1178, 1038, 982, 918, 817. **HRMS (DART)** $[M+H]^+$ calcd. for $[C_{14}H_{19}O_2]^+$ = 219.1385, found 219.1377. **MP** 53 – 57 °C.

IX. Reagent Synthesis

a. Synthesis of potassium carboxylate salts and epoxide activation byproducts

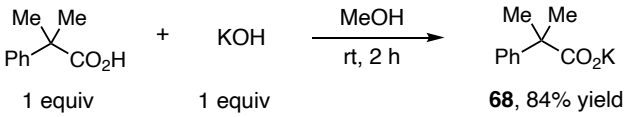

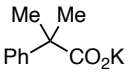

Potassium 2-methyl-2-phenylpropionate (68). An oven-dried 250 mL round bottom flask was charged with a magnetic stir bar, 2-methyl-2-phenylpropionic acid (20.0 g, 121.8 mmol, 1.0 equiv), and MeOH (75 mL, 1.6 M). A 125 mL Erlenmeyer flask was charged with KOH (85%) (7.859 g, 121.8 mmol, 1.0 equiv) and solubilized with a minimal amount to MeOH (50 mL). The KOH/MeOH solution was added dropwise to the stirring carboxylic acid/MeOH solution. The round bottom flask was capped with a rubber septum and the combined solution was stirred for 2 h at rt. The solution was concentrated *in vacuo*, PhMe (40 mL) was added and removed *in vacuo* three times. The white solid was filtered and washed with ethyl acetate (15 mL). The solid was collected and dried *in vacuo* to yield **68** (20.83 g, 102.9 mmol, 84% yield) as a white powder. **^{1}H NMR** (400 MHz, DMSO-d_6) δ 7.35 (d, J = 7.7 Hz, 2H), 7.17 (t, J = 7.5 Hz, 2H), 7.04 (t, J = 7.4 Hz, 1H), 1.31 (s, 6H). **^{13}C NMR** (101 MHz, DMSO-d_6) 178.0, 151.1, 127.5, 126.5, 124.7, 47.5, 28.9 δ . **IR (neat)** 3350, 3050, 2957, 1577, 1468, 1399, 1356, 703 cm^{-1}. **HRMS (DART)** $[RCO_2H+K]^+$ calcd. for $[C_{10}H_{12}O_2K]^+$ = 203.0474, found 203.0468. **MP** 205 – 210 °C.

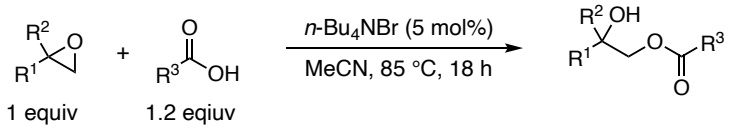

General Procedure AB: alcohol activation byproduct synthesis. An oven-dried 250 mL round bottom flask was charged with a magnetic stir bar, epoxide (10.0 mmol, 1.0 equiv) and MeCN (35 mL, 0.25 M). To the stirring solution, carboxylic acid (12.0 mmol, 1.2 equiv) and tetrabutylammonium bromide (161.2 mg, 0.5 mmol, 5.0 mol%) were added. The round bottom flask was fitted with a reflux condenser and the reaction solution was refluxed for 18 h in an oil bath with stirring. The reaction mixture was allowed to cool to rt, and water (35 mL) was added to the flask and the mixture was extracted with EtOAc (3 x 20 mL). The combined organic layers were washed with brine (25 mL), dried over Na_2SO_4, and concentrated *in vacuo*. The crude material was purified *via* silica gel chromatography. To confirm which isomer of the byproduct is present, we collected DEPT 135 ^{13}C NMR and HMBC spectra of **62** to determine the identities of key carbon atoms and to which hydrogen atoms they correlate. Figure S30 below shows this analysis where we support the structure to be as drawn for substrates **62**, **66**, and **64**. Highlighted on the HMBC spectrum is the O–H proton at 2.60 ppm, which correlates to carbons A, D, and E, leading to our structural assignment.

(a)

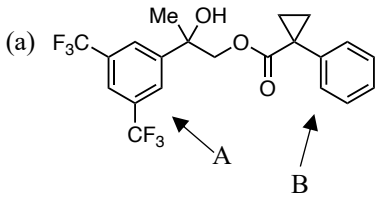
Me
OH
F3C
O
O
CF3
A
B

62

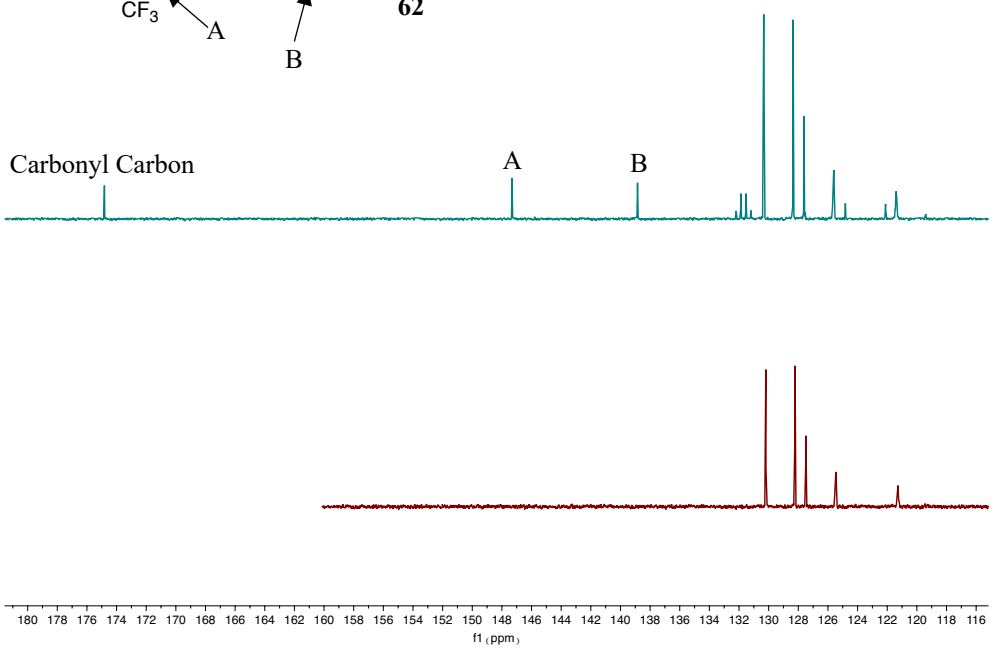
Carbonyl Carbon
A
B
180 178 176 174 172 170 168 166 164 162 160 158 156 154 152 150 148 146 144 142 140 138 136 134 132 130 128 126 124 122 120 118 116
f1 (ppm)

(b)

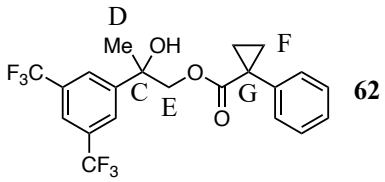
D
Me
OH
F
F3C
C
E
O
G
CF3

62

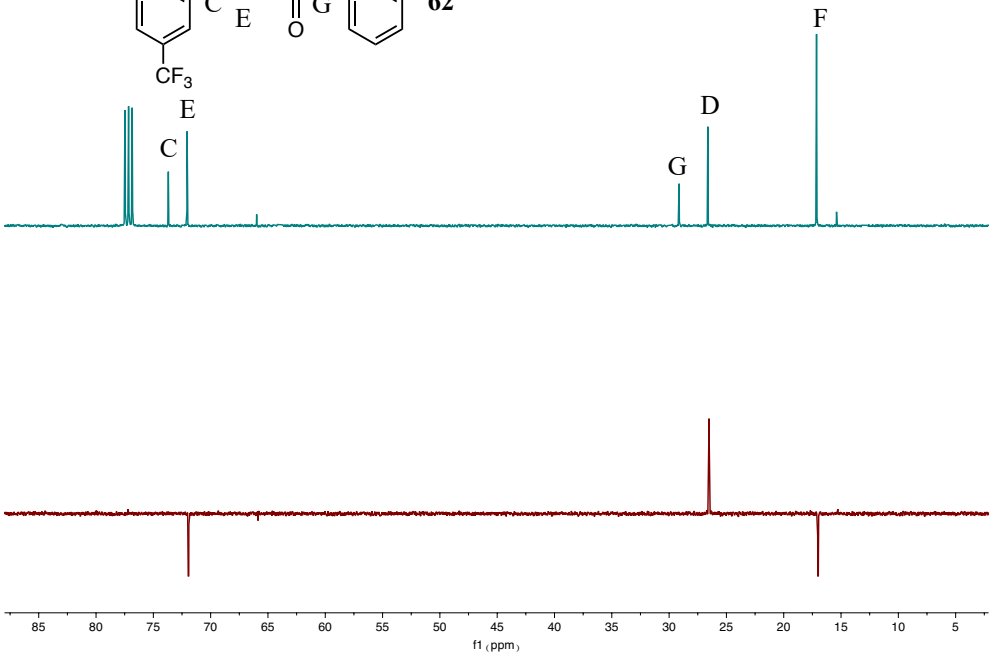
E
C
G
D
F
85 80 75 70 65 60 55 50 45 40 35 30 25 20 15 10 5
f1 (ppm)

(c)

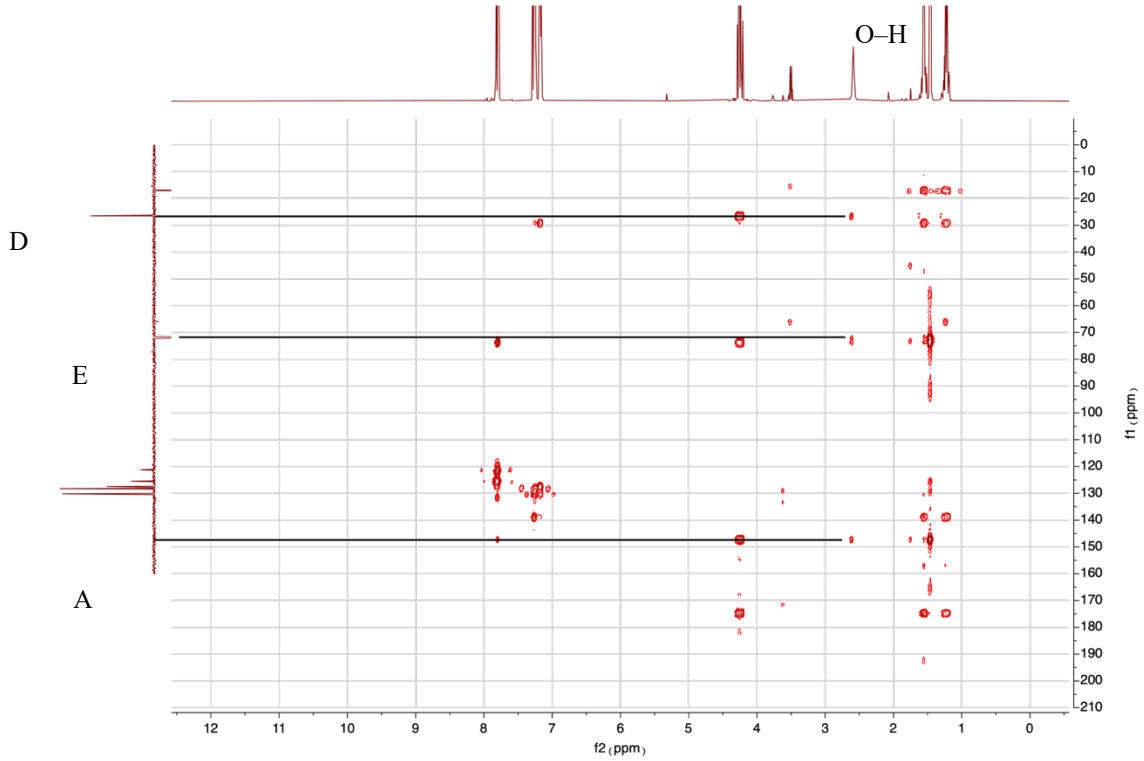

Figure S30. (a) Stacked ^{13}C NMR and DEPT spectra in the aromatic region. (b) Stacked ^{13}C NMR and DEPT spectra in the aliphatic region. (c) HMBC between ^{13}C and ^{1}H NMR spectra.

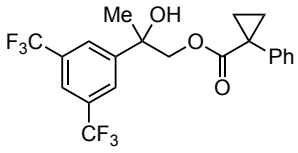

2-(3,5-bis(trifluoromethyl)phenyl)-2-hydroxypropyl 1-phenylcyclopropane-1-carboxylate (62). General Procedure AB was followed using 2-(3,5-bis(trifluoromethyl)phenyl)-2-methyloxirane (2.7 g, 10.0 mmol, 1.0 equiv), 1-phenylcyclopropanecarboxylic acid (1.6 g, 12.0 mmol, 1.2 equiv), tetrabutylammonium bromide (161.2 mg, 0.5 mmol, 5.0 mol%), and MeCN (35 mL, 0.25 M). The crude material was purified *via* silica gel chromatography using 30% EtOAc in hexanes to afford **62** as a pale-yellow oil (1.86 g, 4.3 mmol, 43% yield). **^{1}H NMR** (400 MHz, $CDCl_3$) δ 7.79 (d, *J* = 10.2 Hz, 3H), 7.27 – 7.19 (m, 3H), 7.15 (dd, *J* = 6.8, 3.0 Hz, 2H), 4.29 – 4.17 (m, 2H), 2.61 (bs, 1H), 1.59 – 1.47 (m, 2H), 1.44 (s, 3H), 1.29 – 1.14 (m, 2H). **^{19}F NMR** (376 MHz, $CDCl_3$) δ -62.59.

^{13}C NMR (101 MHz, $CDCl_3$) δ 174.8, 147.3, 138.8, 131.7 (q, *J* = 33.2 Hz), 130.3, 128.5, 127.6, 125.6 (m), 123.3 (q, *J* = 272.7 Hz), 121.38 (m), 73.7, 72.0, 29.1, 26.6, 17.1. **IR** (neat) 3473.01, 2984, 1708, 1372, 1275, 1167, 1126, 899 cm^{-1}. **HRMS (DART)** $[M+H]^+$ calcd. for $[C_{21}H_{19}F_6O_3]^+$ = 432.1160, found 432.1145.

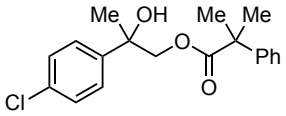

2-(4-chlorophenyl)-2-hydroxypropyl 2-methyl-2-phenylpropanoate (66). General Procedure AB was followed using 2-(4-chlorophenyl)-2-methyloxirane (1.7 g, 10.0 mmol, 1.0 equiv), 2-methyl-2-phenylpropionic acid (2.0 g, 12.0 mmol, 1.2.0 equiv), tetrabutylammonium bromide (161.2 mg, 0.5 mmol, 5.0 mol%), and MeCN (35 mL, 0.25 M). The crude material was purified *via* silica gel chromatography using 20% EtOAc in hexanes to afford **66** as a colorless oil (2.03 g, 5.4 mmol, 30% yield). **^{1}H NMR** (400 MHz, $CDCl_3$) δ 7.45 – 7.17 (m, 9H), 4.31 (d, *J* = 11.3 Hz, 1H), 4.15, (d, *J* = 11.3 Hz, 1H), 2.31 (bs, 1H), 1.54 (s, 3H), 1.51 (s, 3H), 1.41 (s, 3H). **^{13}C NMR** (101 MHz, $CDCl_3$) δ 176.6, 144.1, 142.7, 133.1, 128.5, 128.3, 126.9, 126.5, 125.7, 125.6, 71.9, 46.6, 26.5, 26.2. **IR** (neat) 3552, 2981, 1717, 1494, 1253, 1157, 1101, 1016, 820, 703 cm^{-1}. **HRMS (DART)** $[M+NH_4]^+$ calcd. for $[C_{19}H_{25}ClNO_3]^+$ = 350.1517, found 350.1534. **MP** 35 – 37 °C.

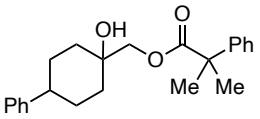

(1-hydroxy-4-phenylcyclohexyl)methyl 2-methyl-2-phenylpropanoate (64). General Procedure AB was followed using 6-phenyl-1-oxaspiro[2,5]octane (1.9 g, 10.0 mmol, 1.0 equiv), 2-methyl-2-phenylpropionic acid (2.0 g, 12.0 mmol, 1.2.0 equiv), tetrabutylammonium bromide (161.2 mg, 0.5 mmol, 5.0 mol%), and MeCN (35 mL, 0.25 M). The crude material was purified *via* silica gel chromatography using 20% EtOAc

in hexanes to afford **64** as a colorless solid (1.8 g, 5.0 mmol, 50% yield).). **^{1}H NMR** (400 MHz, DMSO-d_6) δ 7.40 – 7.32 (m, 4H), 7.31 – 7.23 (m, 3H), 7.22 – 7.12 (m, 3H), 4.43 (s, 1H), 3.82 (s, 2H), 2.29 (tt, J = 12.4 Hz, 2.8 Hz, 1H), 1.82 – 1.67 (m, 2H), 1.54 – 1.46 (m, 4H), 1.30 (td, 13.4, 4.1 Hz, 2H). **^{13}C NMR** (101 MHz, $CDCl_3$) δ 176.7, 146.9, 144.5, 128.4, 128.3, 126.9, 126.8, 126.1, 125.7, 72.8, 69.8, 46.7, 44.0, 34.1, 28.6, 26.4. **IR** (neat) 3538, 2941, 1712, 1492, 1255, 1149, 1107, 977, 701 cm^{-1}. **HRMS (DART)** $[M+NH_4]^+$ calcd. for $[C_{23}H_{32}NO_3]^+$ = 370.2377, found 370.2386. **MP**: 46 – 51 °C.

b. Epoxide Synthesis

i. General Procedures

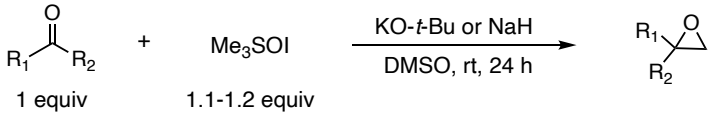

General Procedure AC: Epoxidation *via* the Corey-Chaykovsky reaction. An oven-dried 500 mL round bottom flask was charged with a magnetic stir bar, trimethylsulfoxonium iodide (1.1 – 1.2 equiv), and DMSO (0.2 M). To the stirring mixture, base (KO-*t*-Bu or NaH, 1.1 – 1.2 equiv) was added slowly, in portions, and the solution was stirred for 1 h. To the stirring mixture, the ketone (1.0 equiv) was added, and the reaction mixture was stirred for 18 h at rt. Water (150 mL) was added to the reaction flask and the mixture was extracted with EtOAc (3 x 100 mL). The

combined organic layers were washed with brine (100 mL), dried over Na_2SO_4, and concentrated *in vacuo*. The crude material was purified *via* silica gel chromatography.

ii. Substrate Characterization

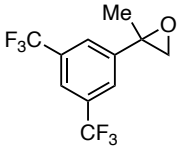

2-(3,5-bis(trifluoromethyl)phenyl)-2-methyloxirane (2). General Procedure AC was followed using 3',5'-bis(trifluoromethyl)acetophenone (15.0 g, 58.6 mmol, 1.0 equiv), trimethylsulfoxonium iodide (14.17 g, 64.4 mmol, 1.1 equiv), KO-*t*-Bu (7.23 g, 64.4 mmol, 1.1.0 equiv), and DMSO (250 mL, 0.2 M). The crude material was purified *via* silica gel chromatography using 100% hexanes to 5% EtOAc in hexanes to afford **2** as a colorless oil (10.01 g, 37.1 mmol, 63% yield). **^{1}H NMR** (400 MHz, $CDCl_3$) δ 7.84 (s, 2H), 7.82 (s, 1H), 3.08 (d, *J* = 5.2 Hz, 1H), 2.81 (d, *J* = 5.2 Hz, 1H), 1.81 (s, 3H). **^{19}F NMR** (376 MHz, $CDCl_3$) δ -62.76. **^{13}C NMR** (101 MHz, $CDCl_3$) δ 144.3, 132.0 (q, 33.3 Hz), 125.8 (m),123.2 (q, *J* = 272.8 Hz), 121.7 (dt, 7.8 Hz, 3.9 Hz), 57.2, 56.2, 21.4. **IR** (neat) 2973, 2876, 1574, 1384, 1277, 1131, 682 cm^{-1}. **HRMS (ESI)** $[M+H]^+$ calcd. for $[C_{11}H_9F_6O]^+$ = 271.0552, found 271.0552.

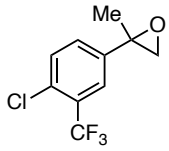

2-(4-chloro-3-(trifluoromethyl)phenyl)-2-methyloxirane (3). General Procedure AC was followed using 4'-chloro-3'-(trifluoromethyl)acetophenone (10.0 g, 44.9 mmol, 1.0 equiv), trimethylsulfoxonium iodide (11.86 g, 53.9 mmol, 1.2 equiv), KO-*t*-Bu (6.05 g, 53.9 mmol, 1.2.0 equiv), and DMSO (220 mL, 0.2 M). The crude material was purified *via* silica gel chromatography using 100% hexanes to 5% EtOAc in hexanes to afford **3** as a colorless oil (6.91 g, 29.2 mmol, 65% yield). **^{1}H NMR** (400 MHz, $CDCl_3$) δ 7.67 (s, 1H), 7.47

(s, 1H), 3.01 (d, J = 5.2 Hz, 1H), 2.75 (d, J = 5.3 Hz, 1H), 1.72 (s, 3H). **^{19}F NMR** (376 MHz, $CDCl_3$) δ -62.51. **^{13}C NMR** (101 MHz, $CDCl_3$) δ 140.8, 131.6, 130.0, 128.7, 124.8 (q, J = 5.3 Hz), 122.8 (q, J = 173.2 Hz), 57.1, 56.0, 21.5. **IR** (neat) 3051, 2990, 1580, 1319, 1128, 1069, 682 cm^{-1}. **HRMS (ESI)** $[M+H]^+$ calcd. for $[C_{10}H_9ClF_3O]^+$ = 237.0289, found 237.0296.

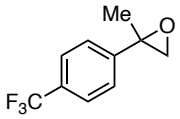

2-methyl-2-(4-(trifluoromethyl)phenyl)oxirane (4). General Procedure AC was followed using 4'-(trifluoromethyl)acetophenone (5.0 g, 26.6 mmol, 1.0 equiv) trimethylsulfoxonium iodide (7.02 g, 31.9 mmol, 1.2.0 equiv), KO-*t*-Bu (3.58 g, 31.9 mmol, 1.2.0 equiv), and DMSO (140 mL, 0.2 M). The crude material was purified *via* silica gel chromatography using 100% hexanes to 5% EtOAc in hexanes to afford **4** as a colorless oil (4.29 g, 21.2 mmol, 80% yield). **^{1}H NMR** (400 MHz, $CDCl_3$) δ 7.60 (d, J = 8.1 Hz, 2H), 7.48 (d, J = 8.1 Hz, 2H), 3.01 (d, J = 5.3 Hz, 1H), 2.77 (d, J = 5.4 Hz, 1H), 1.74 (s, 3H). Characterization data matches literature reports.[23]

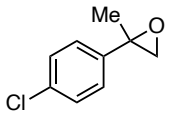

2-(4-chlorophenyl)-2-methyloxirane (21). General Procedure AC was followed using 4'-chloroacetophenone (3.09 g, 20.0 mmol, 1.0 equiv), trimethylsulfoxonium iodide (5.29 g, 24.0 mmol, 1.2.0 equiv), KO-*t*-Bu (2.69 g, 24.0 mmol, 1.2.0 equiv), and DMSO (100 mL, 0.2 M). The crude material was purified *via* silica gel chromatography using 100% hexanes to 5% EtOAc in hexanes to afford **21** as a colorless oil (2.42 g, 14.3 mmol, 72% yield). **^{1}H NMR** (400 MHz, $CDCl_3$) δ 7.28 – 7.24 (m, 4H), 2.93 (d, J = 5.4 Hz, 1H), 2.71 (d, J = 5.4 Hz, 1H), 1.66 (s, 3H). Characterization data matches literature reports.[24]

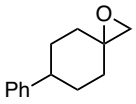

6-phenyl-1-oxaspiro[2.5]octane (22). General Procedure AC was followed using 4-phenylcyclohexanone (6.97 g, 40.0 mmol, 1.0 equiv), trimethylsulfoxonium iodide (10.57 g, 48.0 mmol, 1.2.0 equiv), KO-*t*-Bu (5.39 g, 48.0 mmol, 1.2.0 equiv), and DMSO (200 mL, 0.2 M). The crude material was purified *via* silica gel chromatography using 5% EtOAc in hexanes to afford **22** as a colorless, low melting point solid (5.96 g, 31.6 mmol, 79%). **^{1}H NMR** (400 MHz, $CDCl_3$) δ 7.38 – 7.28 (m, 4H), 7.24 (tt, *J* = 6.9, 1.6 Hz, 1H), 2.73 (s, 2H), 2.71 – 2.69 (m, 1 H), 2.10 (td, *J* = 13.2, 5.1 Hz, 2H), 2.00-1.85 (m, 4H) 1.46 – 1.38 (m, 2H). Characterization data matches literature reports.[25]

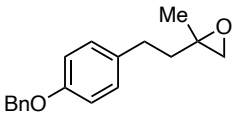

2-(4-(benzyloxy)phenethyl)-2-methyloxirane (23). General Procedure AC was followed using 4-(4-(benzyloxy)phenyl)butan-2-one[26] (3.81 g, 15.0 mmol, 1.0 equiv), trimethylsulfoxonium iodide (3.96 g, 18.0 mmol, 1.2.0 equiv), NaH (60 wt% dispersion in mineral oil, 0.75 g, 18.0 mmol, 1.2.0 equiv), and DMSO (75 mL, 0.2 M). The crude material was purified *via* silica gel chromatography using 5% EtOAc in hexanes to afford **23** as a white solid (3.31 g, 11.60 mmol, 77% yield). **^{1}H NMR** (400 MHz, $CDCl_3$) δ 7.48 – 7.32 (m, 5H), 7.12 (d, *J* = 8.4 Hz, 2H), 6.92 (d, *J* = 8.6 Hz, 2H), 5.07 (s, 2H), 2.72 – 2.65 (m, 2H), 2.61 (q, *J* = 4.9 Hz), 1.97 – 1.87 (m, 1H), 1.86 – 1.77 (m, 1H), 1.39 (s, 3H). **^{13}C NMR** (101 MHz, $CDCl_3$) δ 157.1, 137.2, 134.0, 129.2, 128.6, 127.9, 127.5, 114.8, 70.1, 56.7, 54.0, 38.8, 30.6, 21.1. **IR** (neat) 3042, 2930, 1600, 1518, 1383, 1237, 1181, 1016, 823, 748,– 59 °C. **HRMS (DART)** $[M+H]^+$ calcd. for $[C_{18}H_{21}O_2]^+$ = 269.1537, found 269.1544.

X. References

[1] Chu, X.-Q.; Meng, H.; Zi, Y.; Xu, X.-P.; Ji, S.-J. Metal-Free Oxidative Radical Addition of Carbonyl Compounds to α,α-Diaryl Allylic Alcohols: Synthesis of Highly Functionalized Ketones. *Chem. Eur. J.* **2014**, *20*, 17198-17206.

[2] Tiffner, M.; Novacek, J.; Busillo, A.; Gratzer, K.; Massa, A.; Waser, M. Design of chiral urea-quaternary ammonium salt hybrid catalysts for asymmetric reactions of glycine Schiff bases. *RSC Adv.* **2015**, *5*, 78941-78949.

[3] (a) Ollevier, T.; Plancq, B. Highly enantioselective Mukiyama aldol reaction in aqueous conditions using a chiral iron(II) bipyridine catalyst. *Chem. Commun.* **2012**, *48*, 2289-2291. (b) Xu, W.; Ollevier, T.; Kleitz, F. Iron-Modified Mesoporous Silica as an Effective Solid Lewis Acid Catalyst for the Mukiyama Aldol Reaction. *ACS Catal.* **2018**, *8*, 1932-1944.

[4] Cai, H.; Zhou, Y.; Zhang, D.; Xu, J.; Liu, H. A Mannich/cyclization cascade process for the asymmetric synthesis of spirocyclic thioimidazolidineoxindoles. *Chem. Commun.* **2014**, *50*, 14771-14774.

[5] (a) Jin, J.; Xie, J.; Pan, C.; Zhu, Z.; Cheng, Y.; Zhu, C. Rhenium-Catalyzed Acceptorless Dehydrogenative Coupling via Dual Activation of Alcohols and Carbonyl Compounds. *ACS Catal.* **2013**, *3*, 2195-2198. (b) Zong, X.; Cai, J.; Chen, J.; Li, L.; Ji, M. Discovery of 3,3a,4,5-tetrahydro-2H-benzo[g]indazole containing quinoxaline derivatives as novel EGFR/HER-2 dual inhibitors. *RSC Adv.* **2015**, *5*, 24814-24823.

[6] (a) Caldwell, N.; Jamieson, C.; Simpson, I.; Tuttle, T. Organobase-Catalyzed Amidation of Esters with Amino Alcohols. *Org. Lett.* **2013**, *15*, 2506-2509. (b) Horn, H. W.; Jones, G. O.; Wei, D. S.; Fukushima, K.; Lecuyer, J. M.; Coady, D. J.; Hedrick, J. L.; Rice, J. E. Mechanisms of Organocatalytic Amidation and Trans-Esterification of Aromatic Esters as a Model for the Depolymerization of Poly(ethylene) Terephthalate. *J. Phys. Chem. A* **2012**, *116*, 12389-12398.

[7] Pastor, I. M.; Västilä, P.; Adolfsson, H. Employing the Structural Diversity of Nature: Development of Modular Dipeptide-Analogue Ligands for Ruthenium-Catalyzed Enantioselective Transfer Hydrogenation of Ketones. *Chem. Eur. J.* **2003**, *9*, 4031-4045.

[8] Nielsen, M. K.; Ahneman, D. T.; Riera, O.; Doyle, A. G. Deoxyfluorination with Sulfonyl Fluorides: Navigating Reaction Space with Machine Learning. *J. Am. Chem. Soc.* **2018**, *140*, 5004-5008.

[9] Giller, S. A.; Eremeev, A. V.; Kalvin'sh, I. Y.; Liepins, E.; Semenikhina, V. G. Derivatives of 1-H-Aziridine-2-carboxylic acid. *Chem. Heterocycl. Compd.* **1975**, *11*, 1625-1631.

[10] Procedure adapted from: Allen, C. E.; Curran, P. R.; Brearley, A. S.; Boissel, V.; Sviridenko, L.; Press, N. J.; Stonehouse, J. P.; Armstrong, A. Efficient and Facile Synthesis of Acrylamide Libraries for Protein-Guided Tethering. *Org. Lett.* **2015**, *17*, 458-460.

[11] Procedure adapted from: Yang, Y.; Buchwald, S. L. Copper-Catalyzed Regioselective ortho C–H Cyanation of Vinylarenes. *Angew. Chem. Int. Ed.* **2014**, *53*, 8677-8681.

[12] (a) Alamri, H.; Zhao, J.; Pahovnik, D.; Hadjichristidis, N. Phosphazene-catalyzed ring-opening polymerization of ε-caprolactone: influence of solvents and initiators. *Polym. Chem.* **2014**, *5*, 5471-5478. (b) Hao, J.; Granowski, P. C.; Stefan, M. C. Zinc Undecylenate Catalyst for Ring-Opening Polymerization of Caprolactone Monomers. *Macromol. Rapid Commun.* **2012**, *33*, 1294-1299.

[13] Broch, S.; Aboab, B.; Anizon, F.; Moreau, P. Synthesis and in vivo antiproliferative activities of quinoline derivatives. *Eur. J. Med. Chem.* **2010**, *45*, 1657-1662.

[14] Hooper, M. W.; Utsunomiya, M.; Hartwig, J. F. Scope and Mechanism of Palladium-Catalyzed Amination of Five-Memberd Heterocyclic Halides. *J. Org. Chem.* **2003**, *68*, 2861-2873.

[15] Gesmundo, N. J.; Sauvagnat, B.; Curran, P. J.; Richards, M. P.; Andrews, C. L.; Dandliker P. J.; Cernak, T. Nanoscale Synthesis and Affinity Ranking. *Nature* **2018**, *557*, 228-232.

[16] Dunn, A. D. Nucleophilic displacement in 2-chloro(trifluoromethyl)pyridines with amines and ammonia. *J. Fluorine Chem.* **1998**, *93*, 153-157.

[17] Costa, A.; Nájera, C.; Sansano, J. M. Synthetic Applications of *o*- and *p*-Halobenzyl Sulfones as Zwitterionic Synthons: Preparation of Ortho-Substituted Cinnamates and Biarylacetic Acids. *J. Org. Chem.* **2002**, *67*, 5216-5225.

[18] Buitrago Santanilla, A.; Christensen, M.; Campeau, L.-C.; Davies, I. W.; Dreher, S. D. P_2Et Phosphazene: A Mild, Functional Group Tolerant Base for Soluble, Room Temperature Pd-Catalyzed C–N, C–O, and C–C Cross-Coupling Reactions. *Org. Lett.* **2015**, *17*, 3370-3373.

[19] Dennis, J. M.; White, N. A.; Liu, R. Y.; Buchwald S. L. Pd-Catalyzed C–N Coupling Reactions Facilitated by Organic Bases: Mechanistic Investigation Leads to Enhanced Reactivity in the Arylation of Weakly Binding Amines. *ACS Catal.* **2019**, *9*, 3822-3830.

[20] Szpera, R.; Isenegger, P. G.; Ghosez, M.; Straathof, N. J. W.; Cookson, R.; Blakemore, D. C.; Richardson, P.; Gouverneur, V. Synthesis of Fluorinated Alkyl Aryl Ethers by Palladium-Catalyzed C–O Cross Coupling. *Org. Lett.* **2020**, *22*, 6573-6577.

[21] Reichert, E. C.; Feng K.; Sather, A. C.; Buchwald, S. L. Pd-Catalyzed Amination of Base-Sensitive Five-Membered Heteroaryl Halides with Aliphatic Amines. *J. Am. Chem. Soc.* **2023**, *145*, 3323-3329.

[22] Xu, B.; Su, W. A Tandem Dehydrogenation-Driven Cross-Coupling between Cyclohexanones and Primary Amines for Construction of Benzoxazoles. *Angew. Chem. Int. Ed.* **2022**, *25*, e202203365.

[23] Deregnaucourt, J.; Archelas, A.; Barbirato, F.; Paris, J.-P.; Furstoss, R. Enzymatic Transformations 63. High-Concentration Two Liquid-Liquid Phase *Aspergillus niger* Epoxide Hydrolase-Catalysed Resolution: Application to Trifluoromethyl-Substituted Aromatic Epoxides. *Adv. Synth. Catal.* **2007**, *349*, 1405-1417.

[24] Sone, T.; Yamaguchi, A.; Matsunaga, S.; Shibasaki, M. Catalytic Asymmetric Synthesis of 2,2-Disubstituted Terminal Epoxides via Dimethyloxosulfonium Methylide Addition to Ketones. *J. Am. Chem. Soc.* **2008**, *130*, 10078-10079.

[25] Peng, Y.; Yang, J.-H.; Li, W.-D. Z. Revisiting the Corey-Chaykovsky reaction: the solvent effect and the formation of α-hydroxy methylthioethers. *Tetrahedron* **2006**, *62*, 1209-1215.
[26] Ramachandra, M. S.; Subbaraju, G. V.; Synthesis and Bioactivity of Novel Caffeic Acid Esters from *Zuccagnia punctata*. *J. Asian Nat. Prod. Res.* **2006**, *8*, 683-688.

XI. NMR Spectra

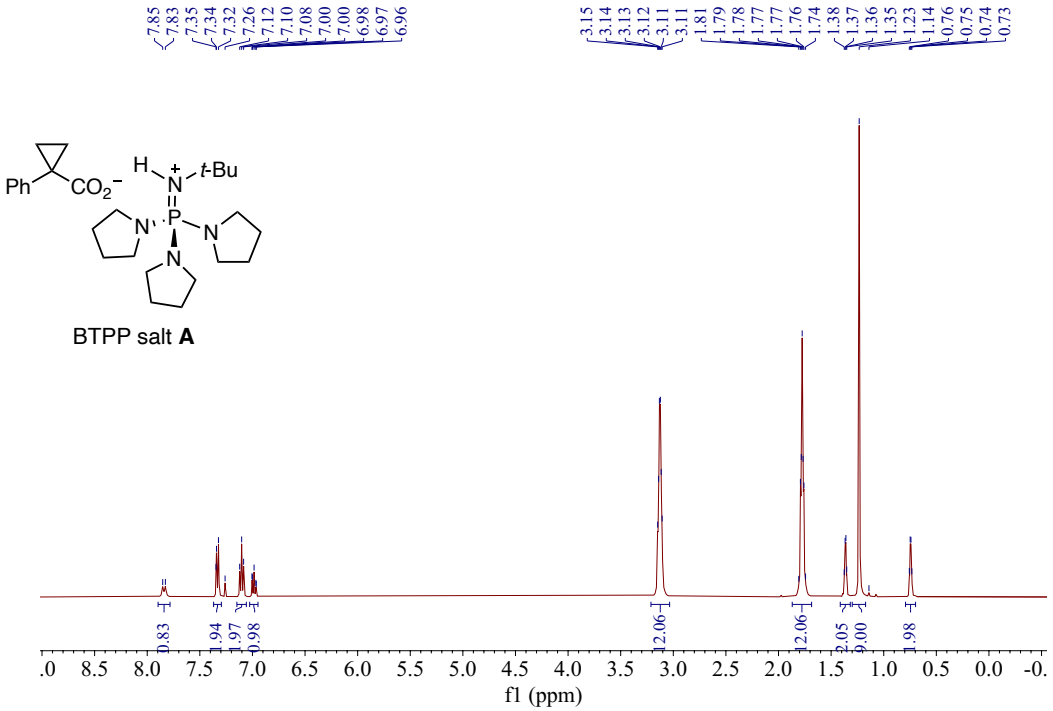

^{1}H NMR of BTPP salt **A** (400 MHz, $CDCl_3$)

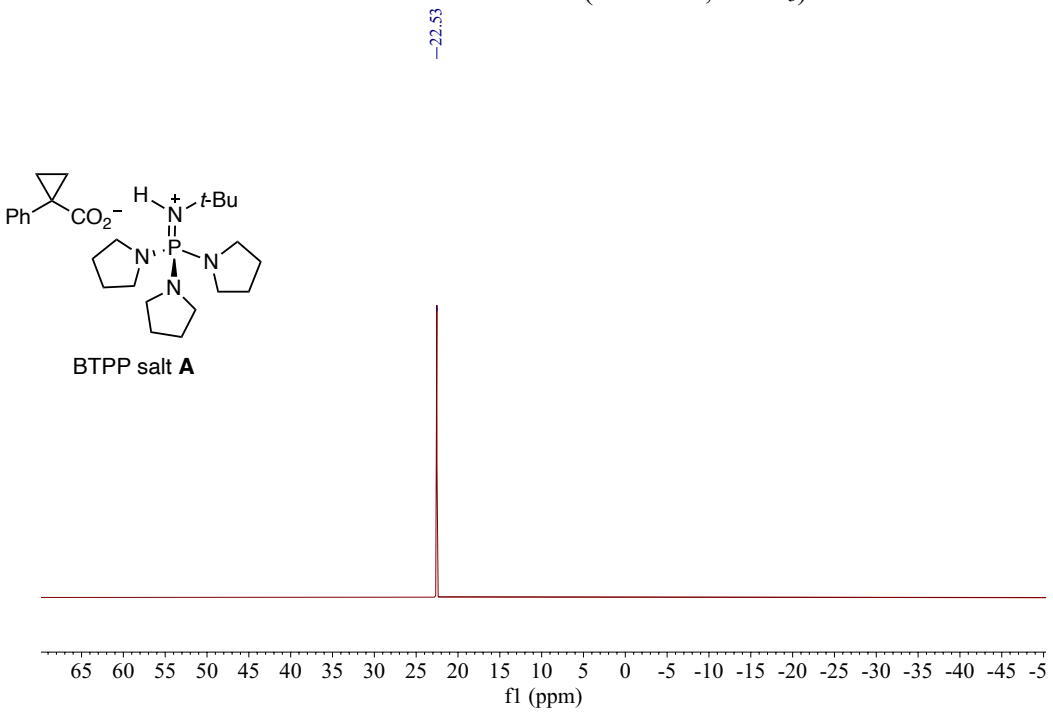

^{31}P NMR of BTPP Salt **A** (162 MHz, $CDCl_3$)

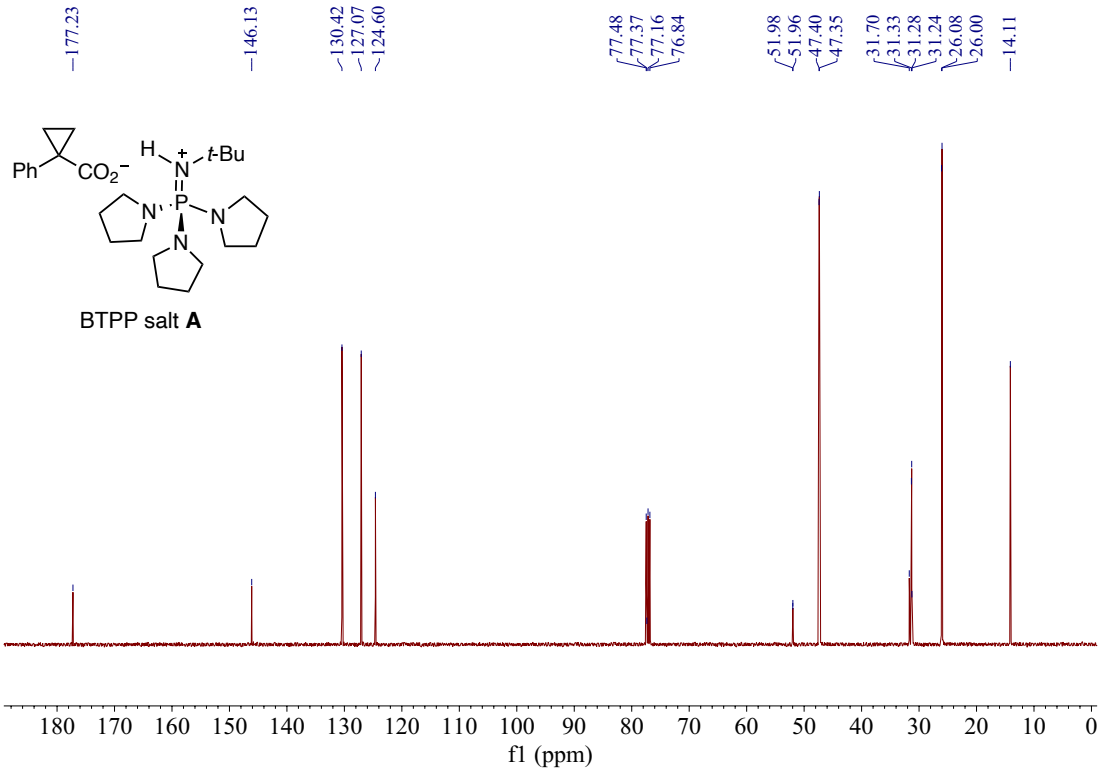

^{13}C NMR of BTPP Salt **A** (101 MHz, $CDCl_3$)

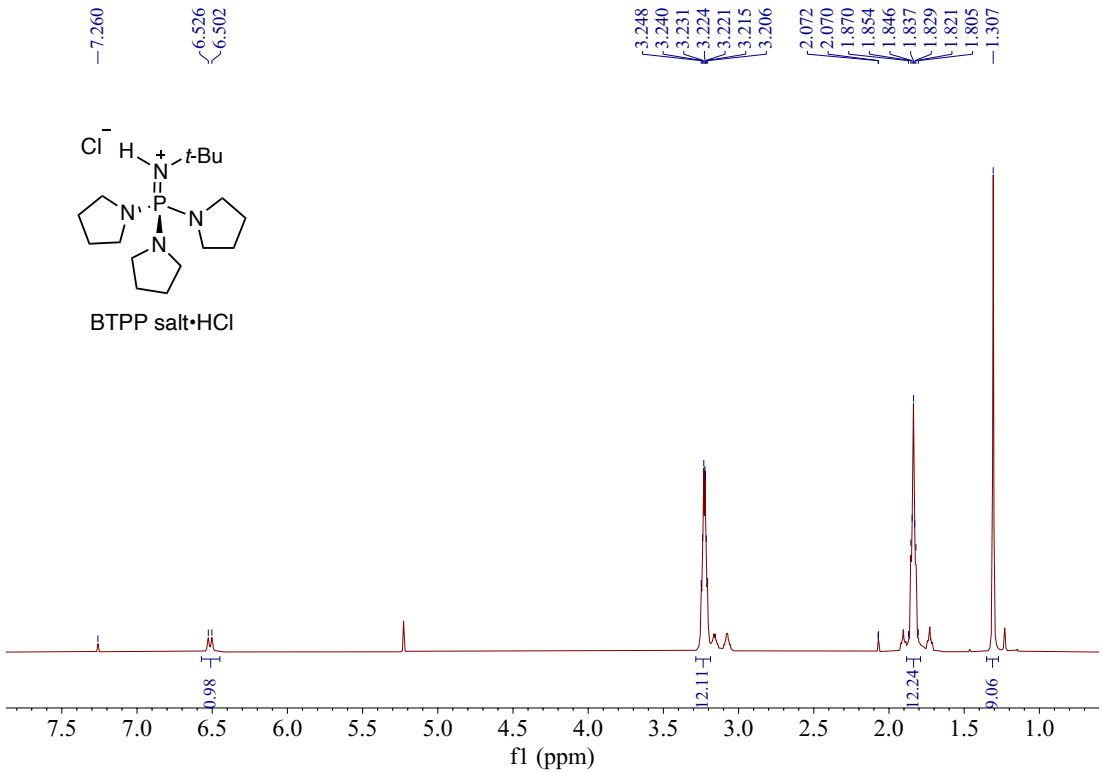

^{1}H NMR of BTPP•HCl (400 MHz, $CDCl_3$)

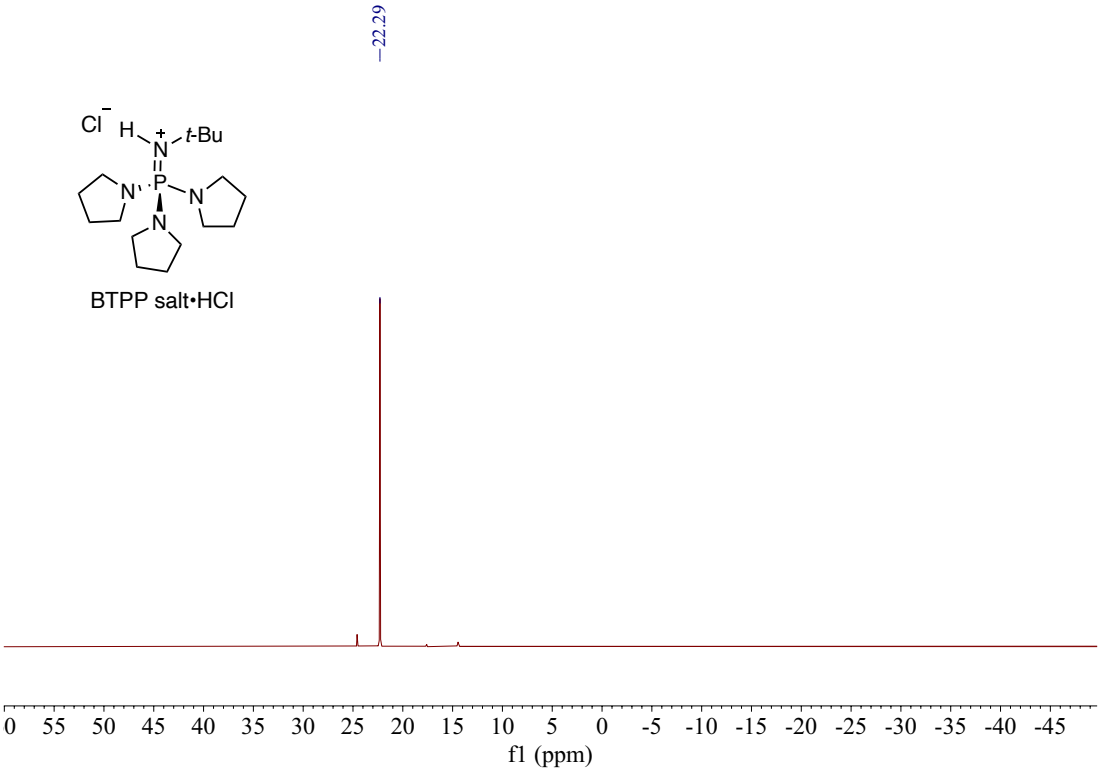

^{31}P NMR of BTPP•HCl (162 MHz, $CDCl_3$)

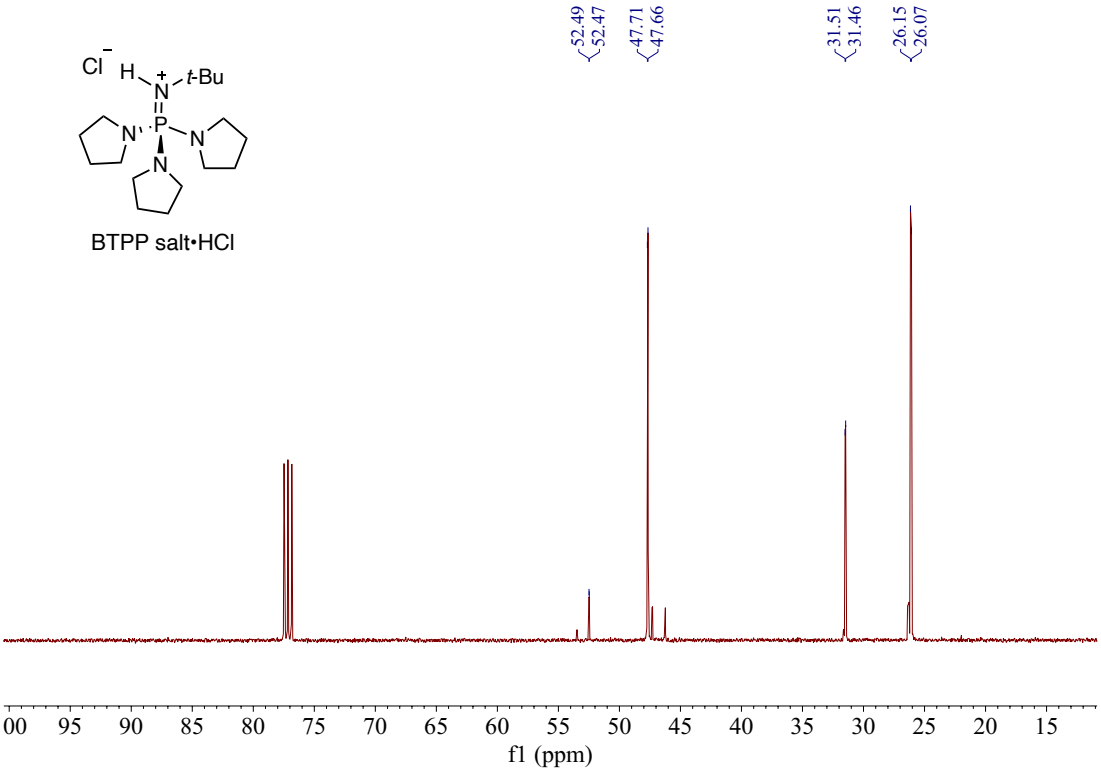

^{13}C NMR of BTPP•HCl (101 MHz, $CDCl_3$)

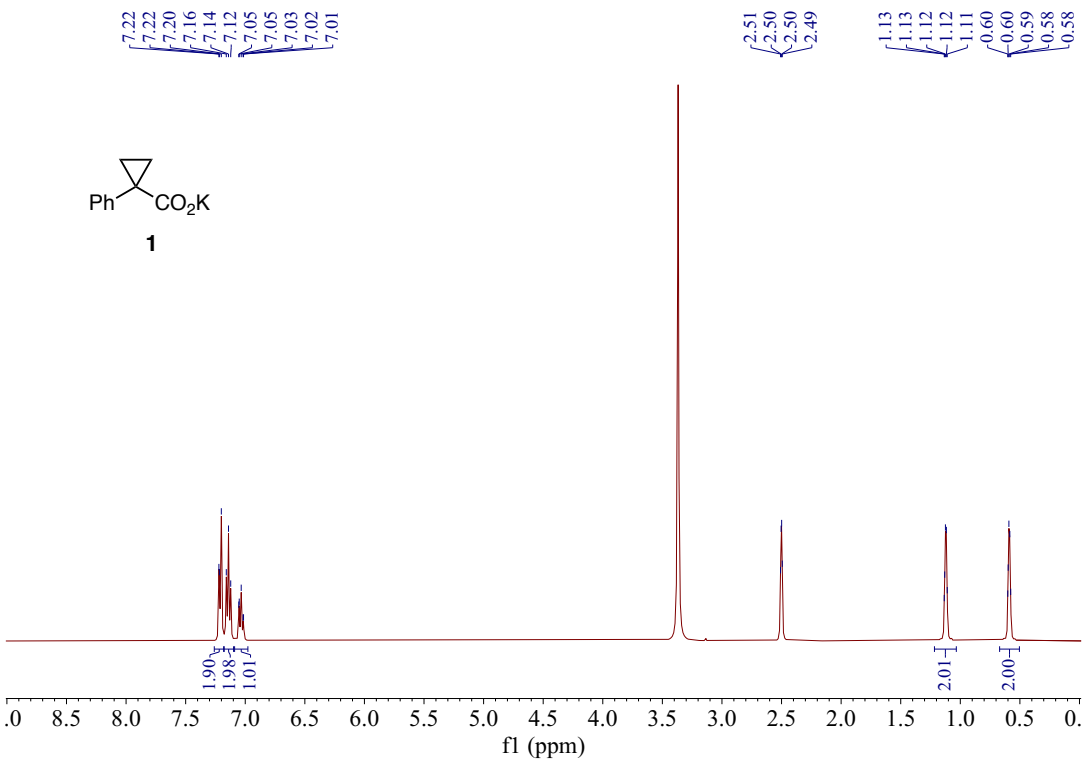

^{1}H NMR of Compound **1** (400 MHz, $CDCl_3$)

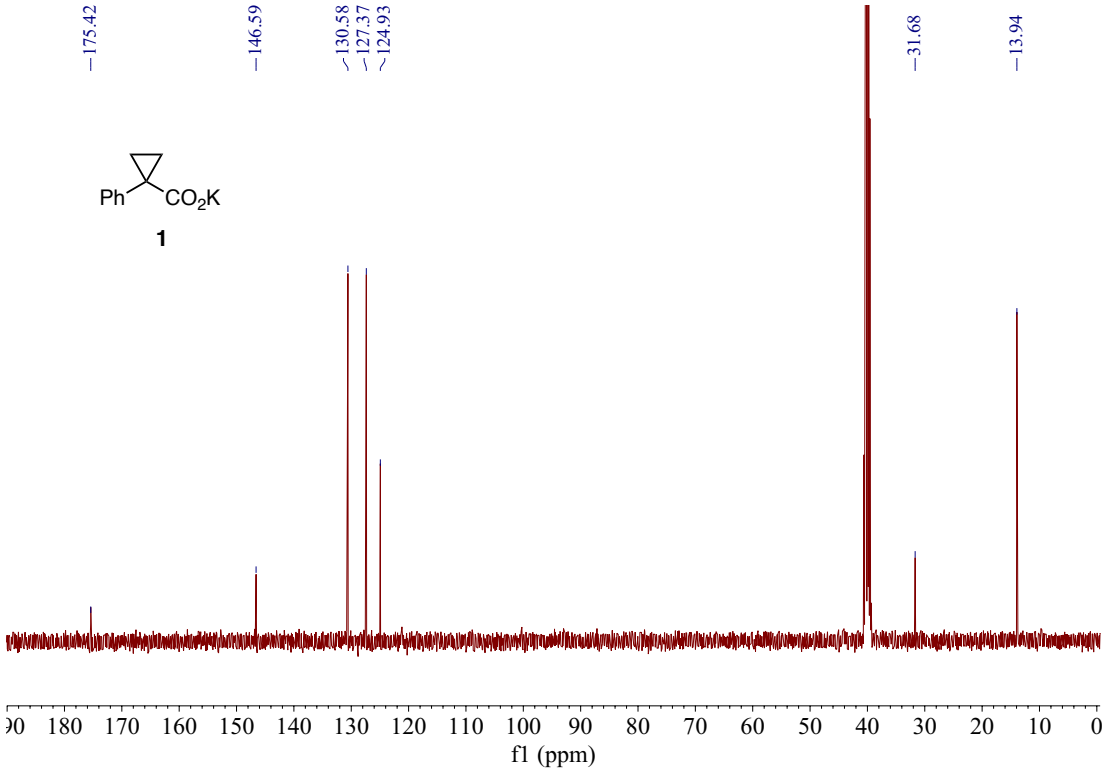

^{13}C NMR of Compound **1** (101 MHz, $CDCl_3$)

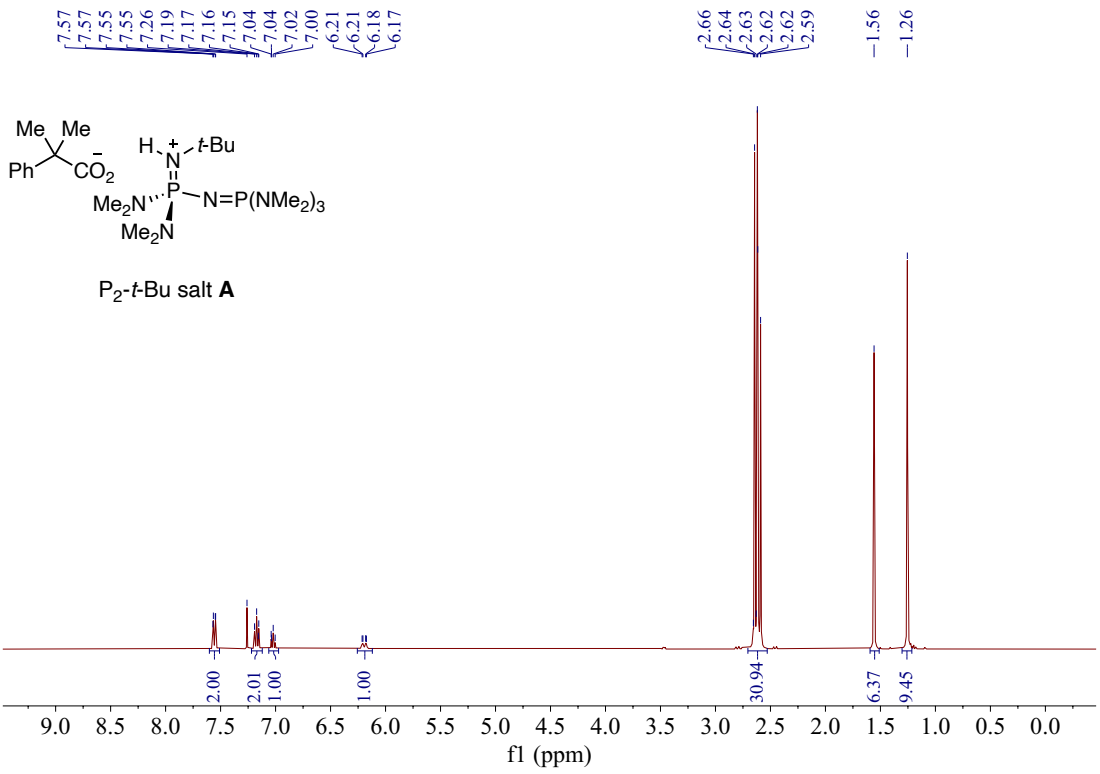

^{1}H NMR of P_2-*t*-Bu salt **A** (400 MHz, $CDCl_3$)

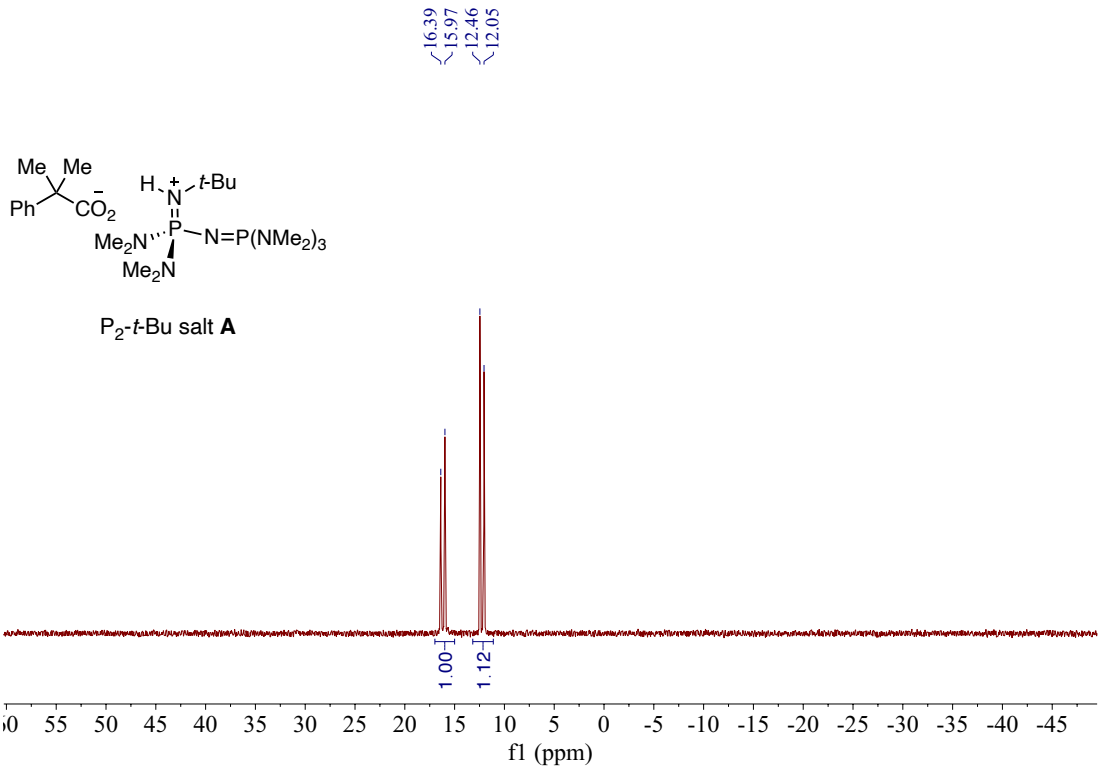

^{31}P NMR of P_2-*t*-Bu salt **A** (162 MHz, $CDCl_3$)

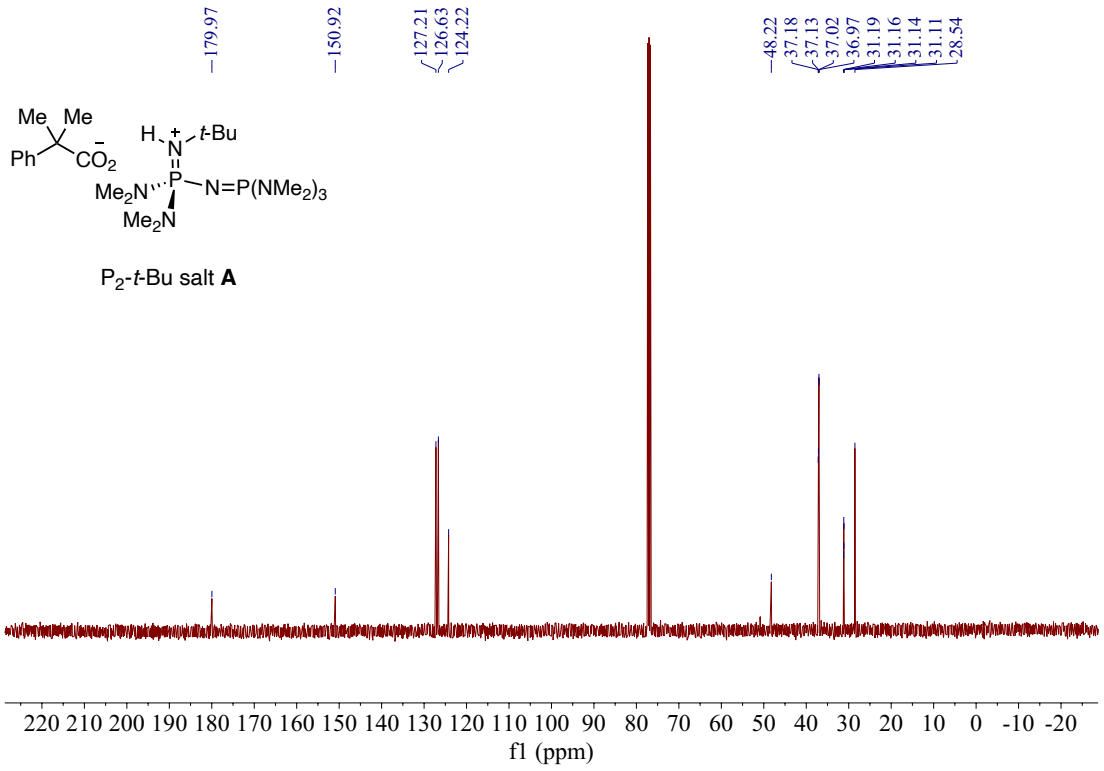

P$_2$-*t*-Bu salt **A**

^{13}C NMR of P$_2$-*t*-Bu salt **A** (101 MHz, $CDCl_3$)

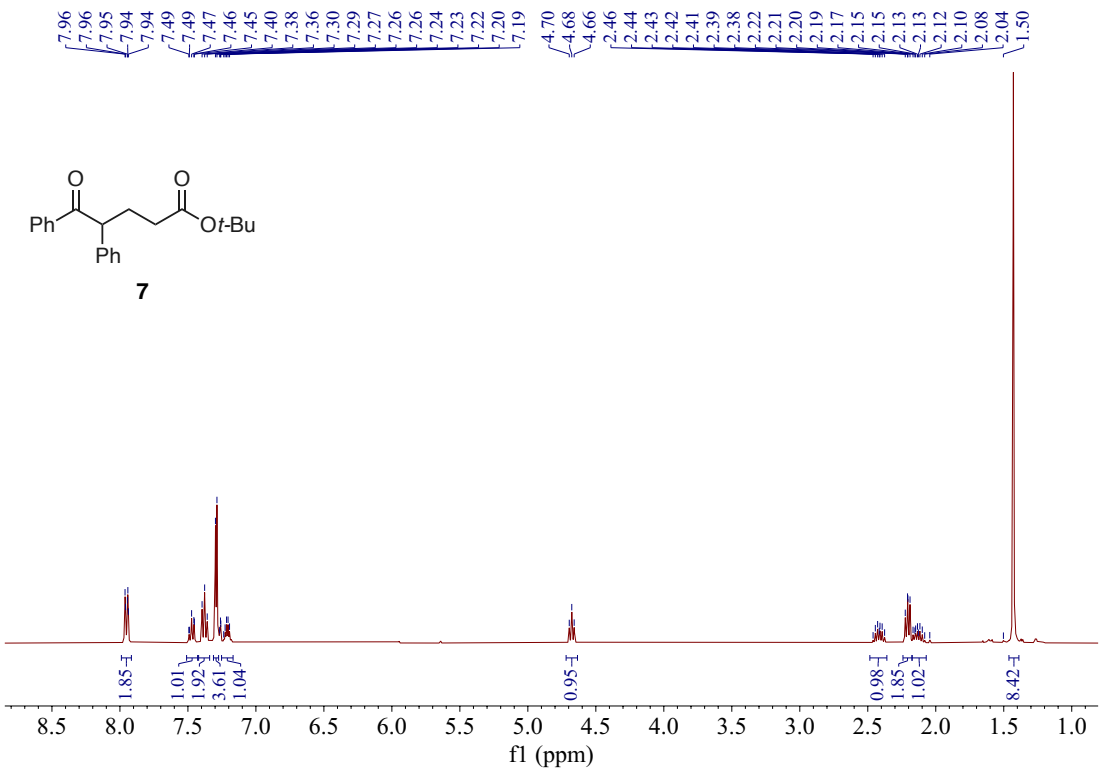

7

^{1}H NMR of Compound **7** (400 MHz, $CDCl_3$)

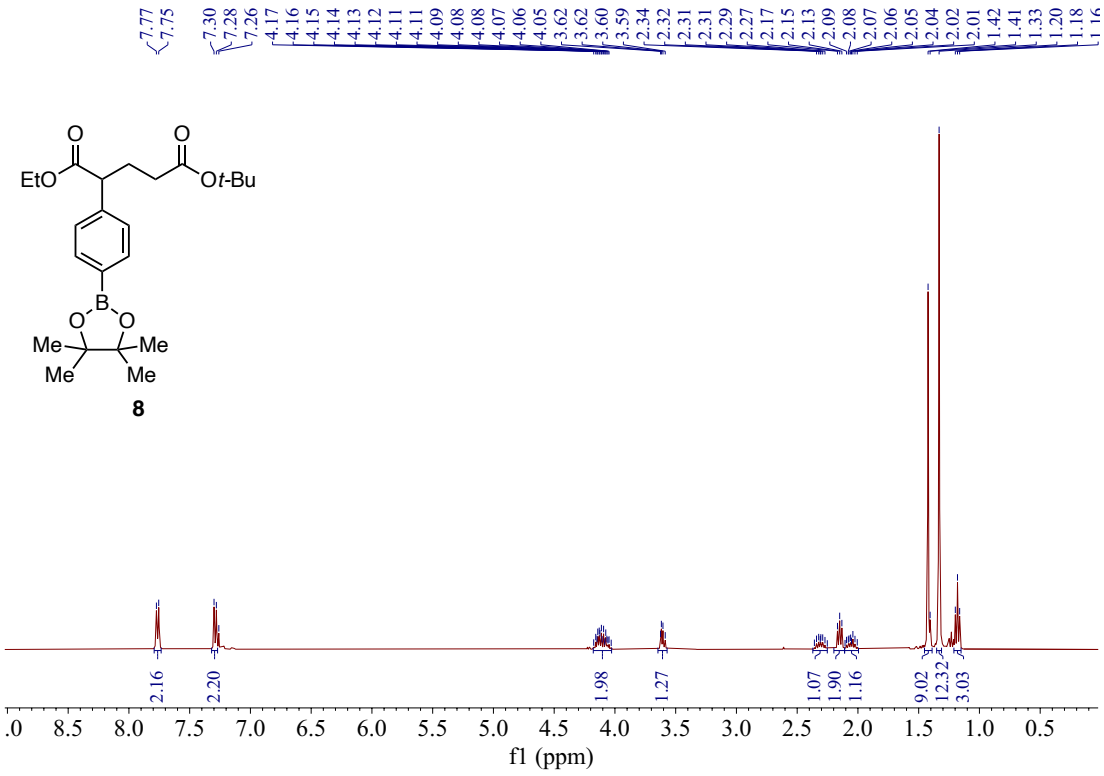

^{1}H NMR of Compound **8** (400 MHz, $CDCl_3$)

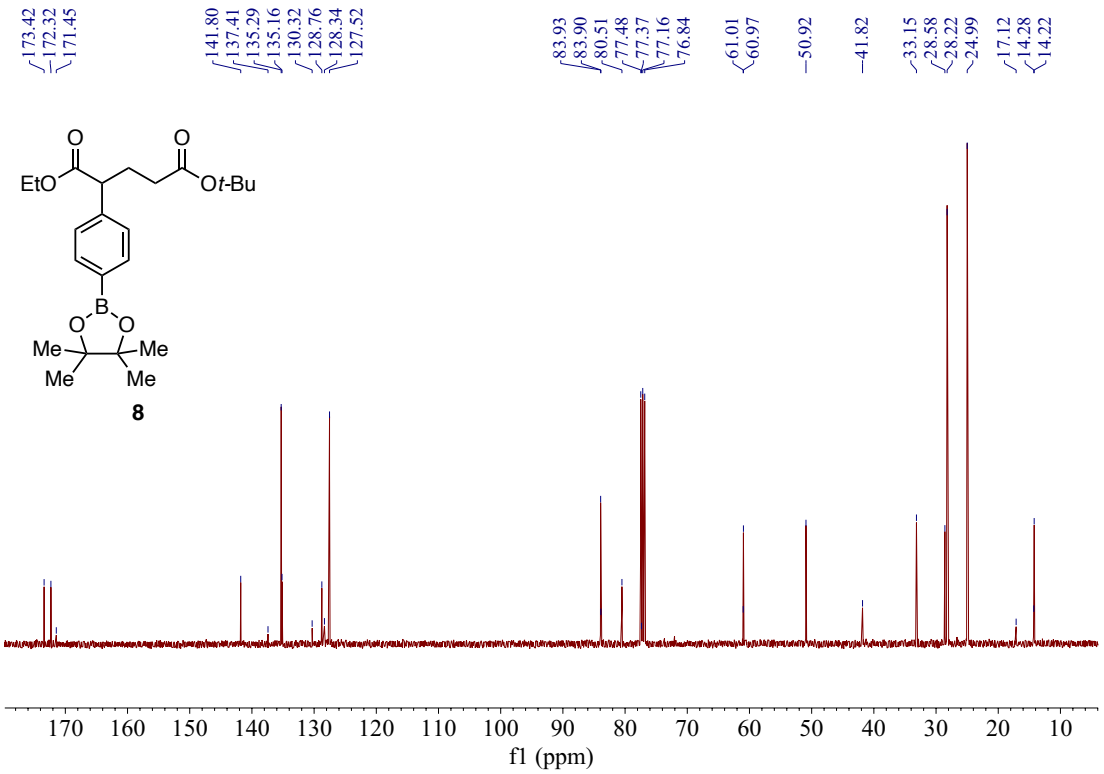

^{13}C NMR of Compound **8** (101 MHz, $CDCl_3$)

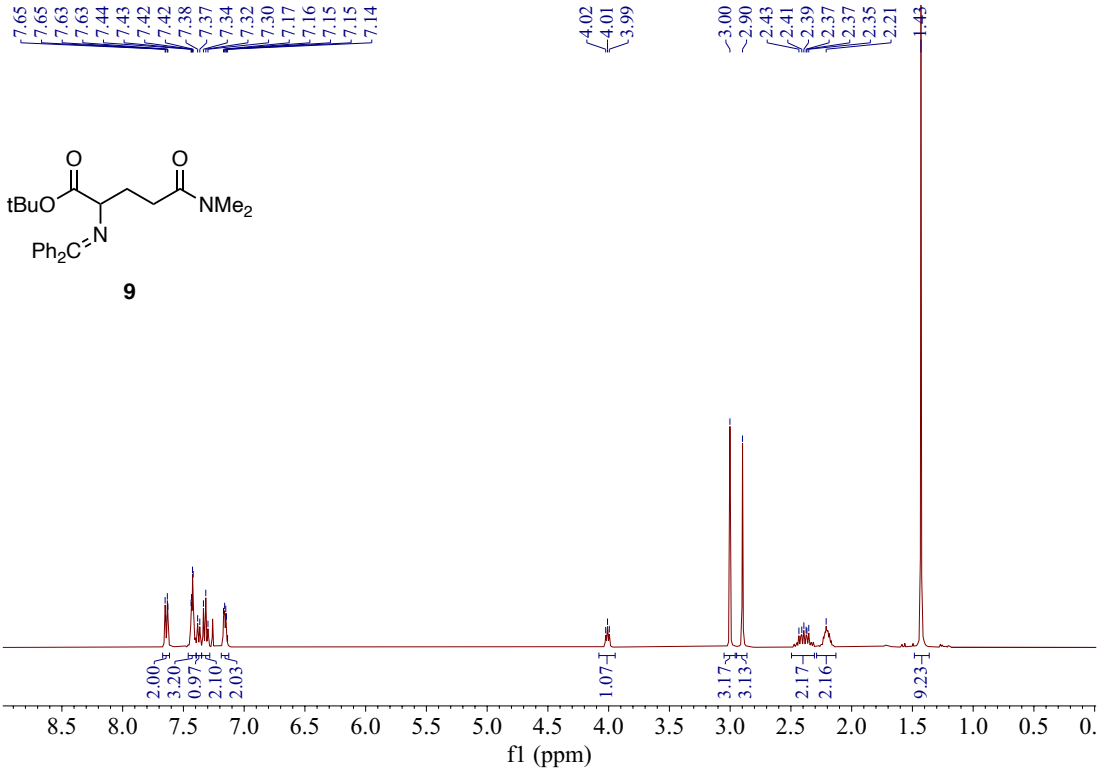

^{1}H NMR of Compound **9** (400 MHz, $CDCl_3$)

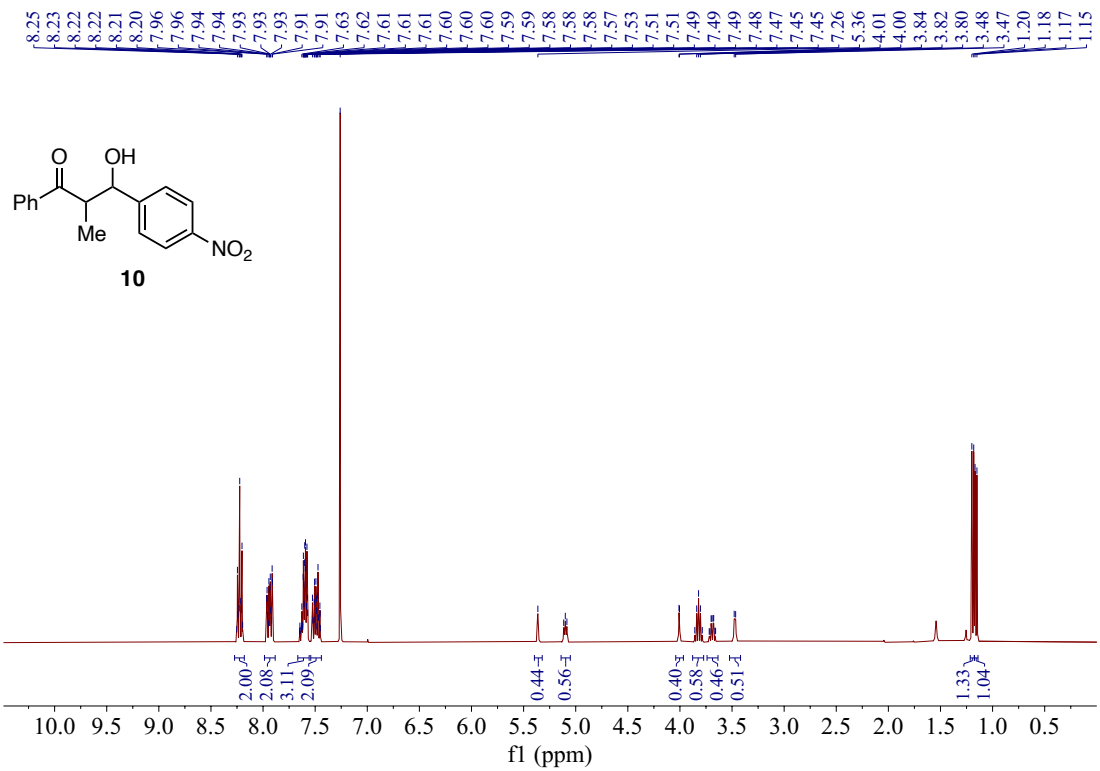

^{1}H NMR of Compound **10** as a mixture of diastereomers (400 MHz, $CDCl_3$)

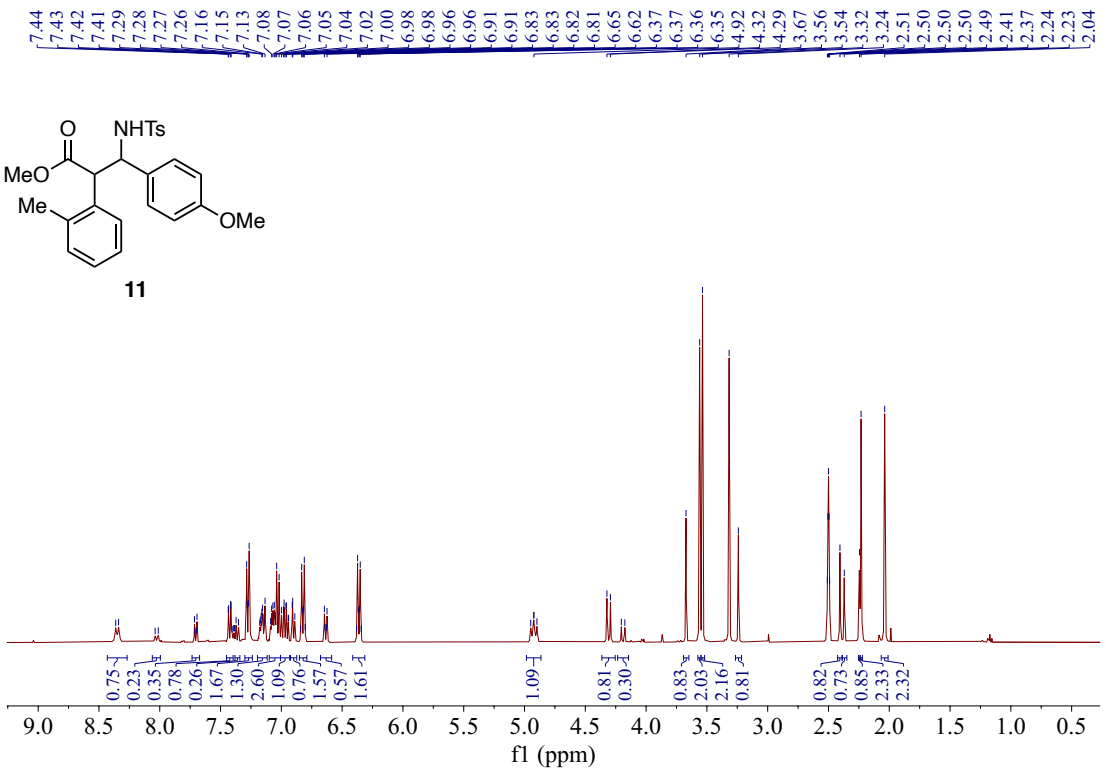

^{1}H NMR of Compound **11** as a mixture of diastereomers (400 MHz, DMSO-d_6)

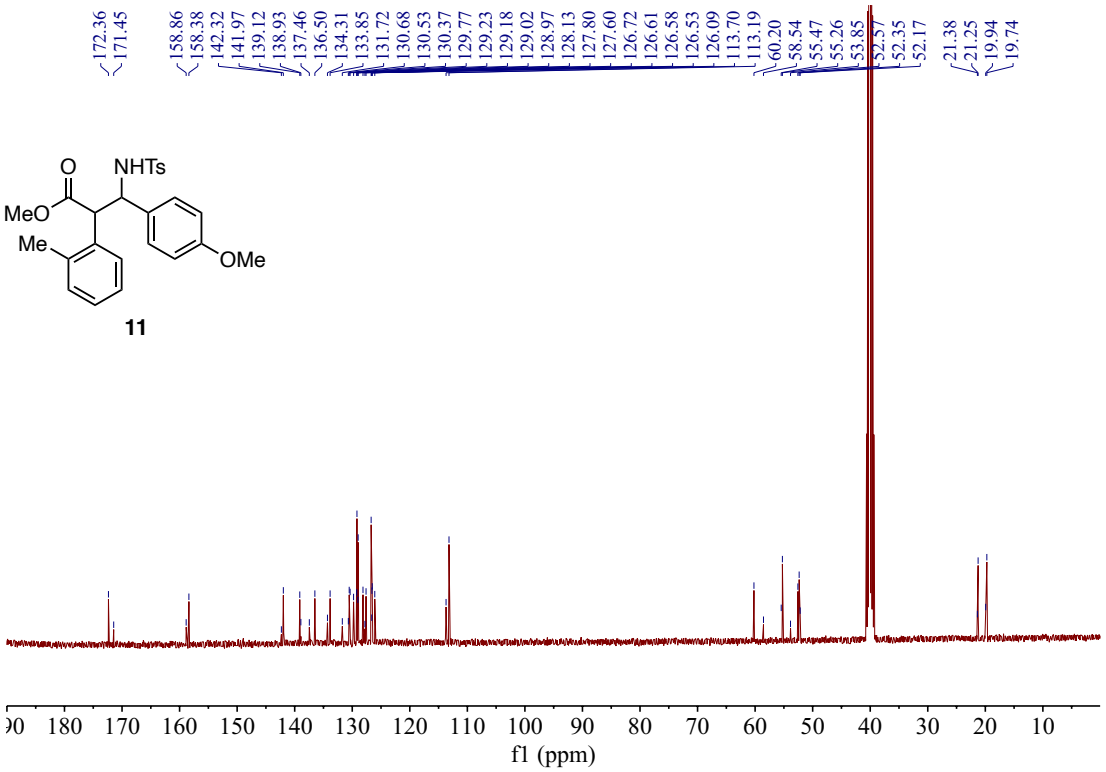

^{13}C NMR of Compound **11** as a mixture of diastereomers (101 MHz, DMSO-d_6)

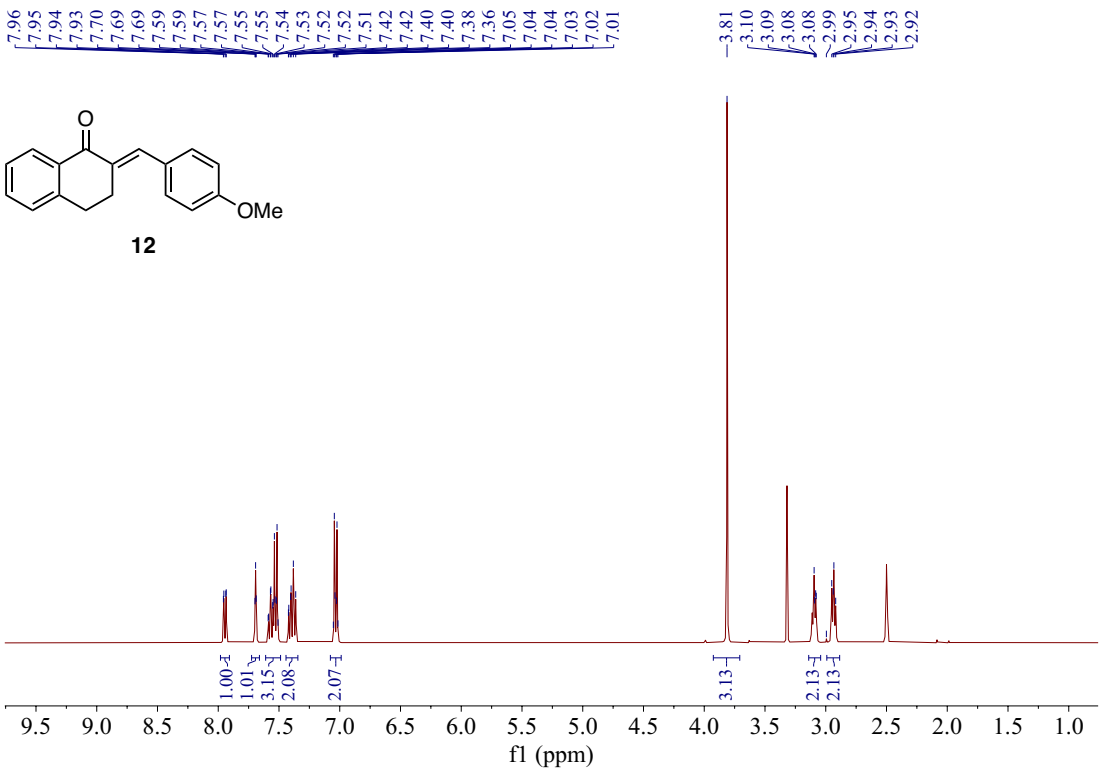

^{1}H NMR of Compound **12** (400 MHz, DMSO-d_6)

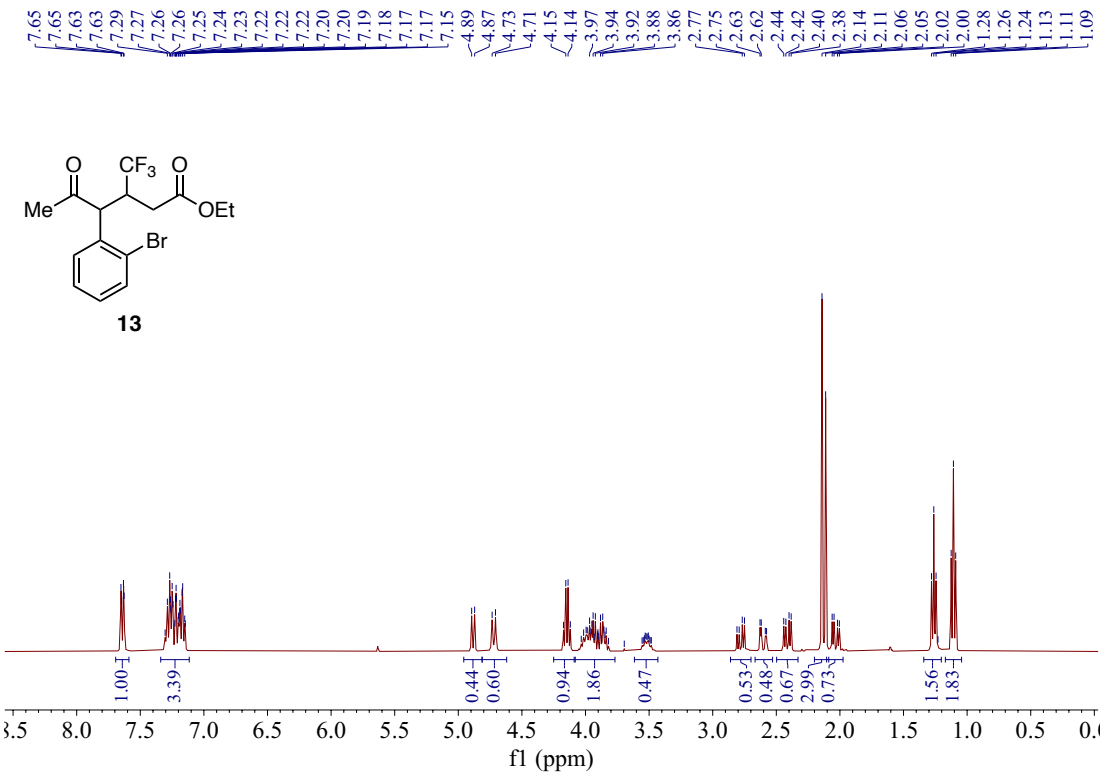

^{1}H NMR of Compound **13** as a mixture of diastereomers (400 MHz, $CDCl_3$)

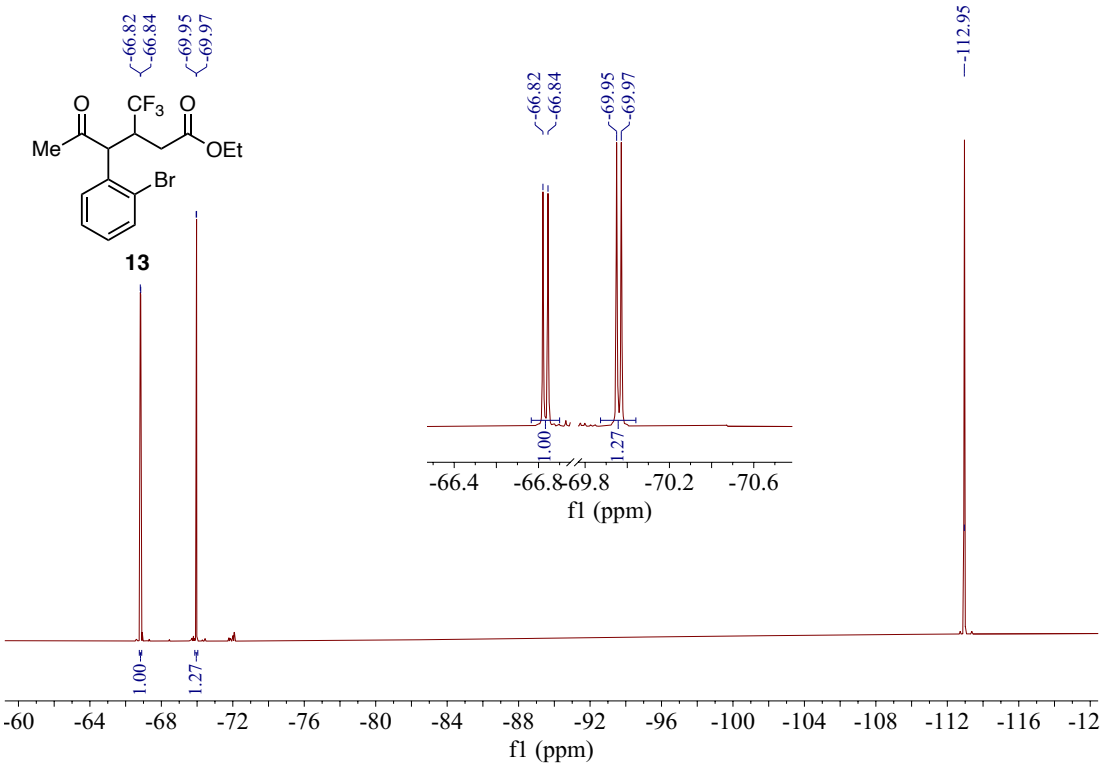

^{19}F NMR of Compound **13** as a mixture of diastereomers (376 MHz, $CDCl_3$)

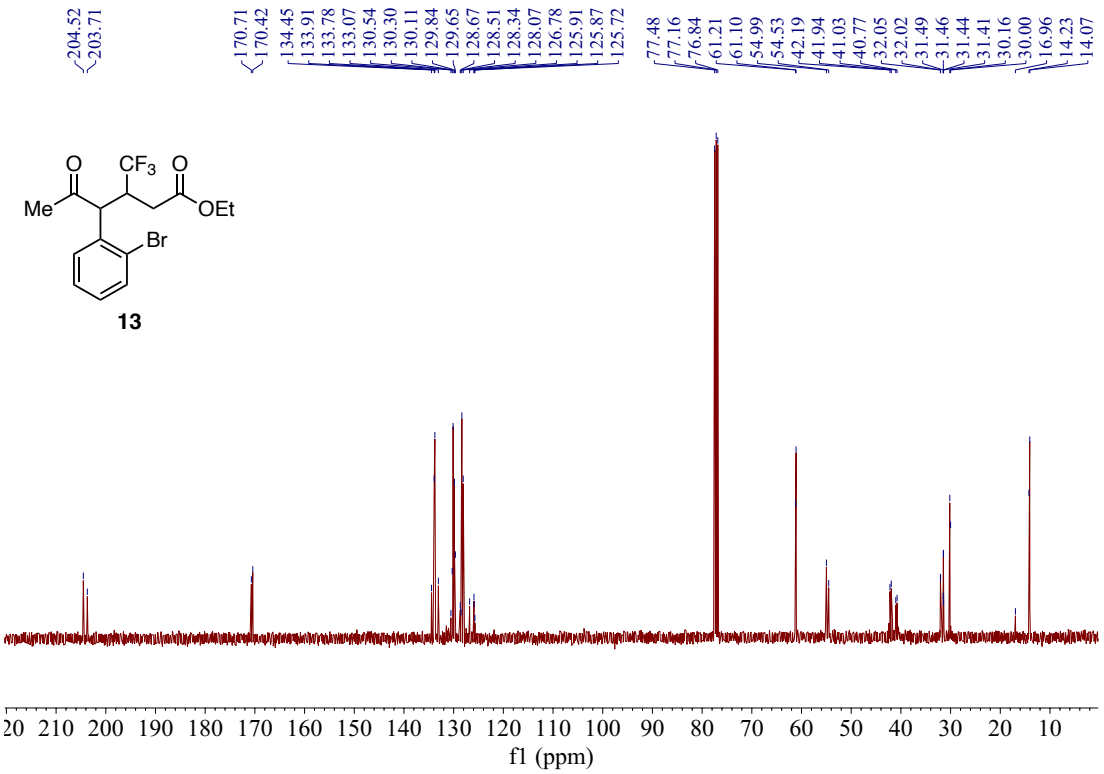

^{13}C NMR of Compound **13** as a mixture of diastereomers (101 MHz, $CDCl_3$)

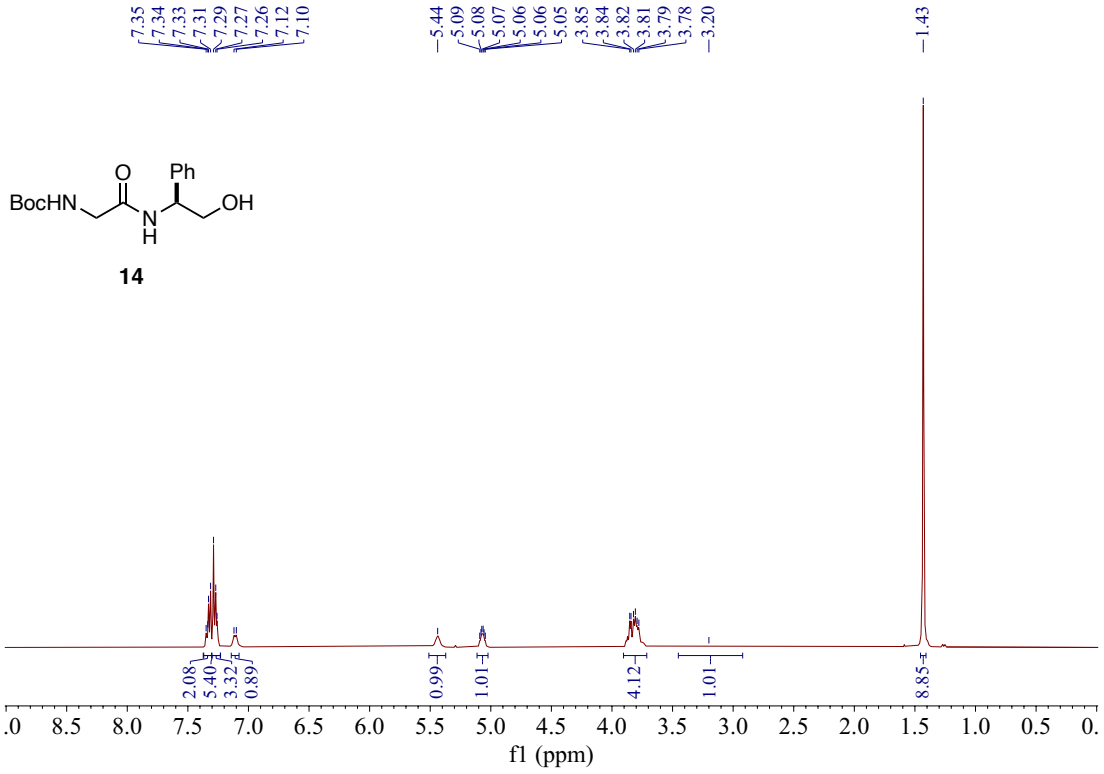

^{1}H NMR of Compound **14** (400 MHz, $CDCl_3$)

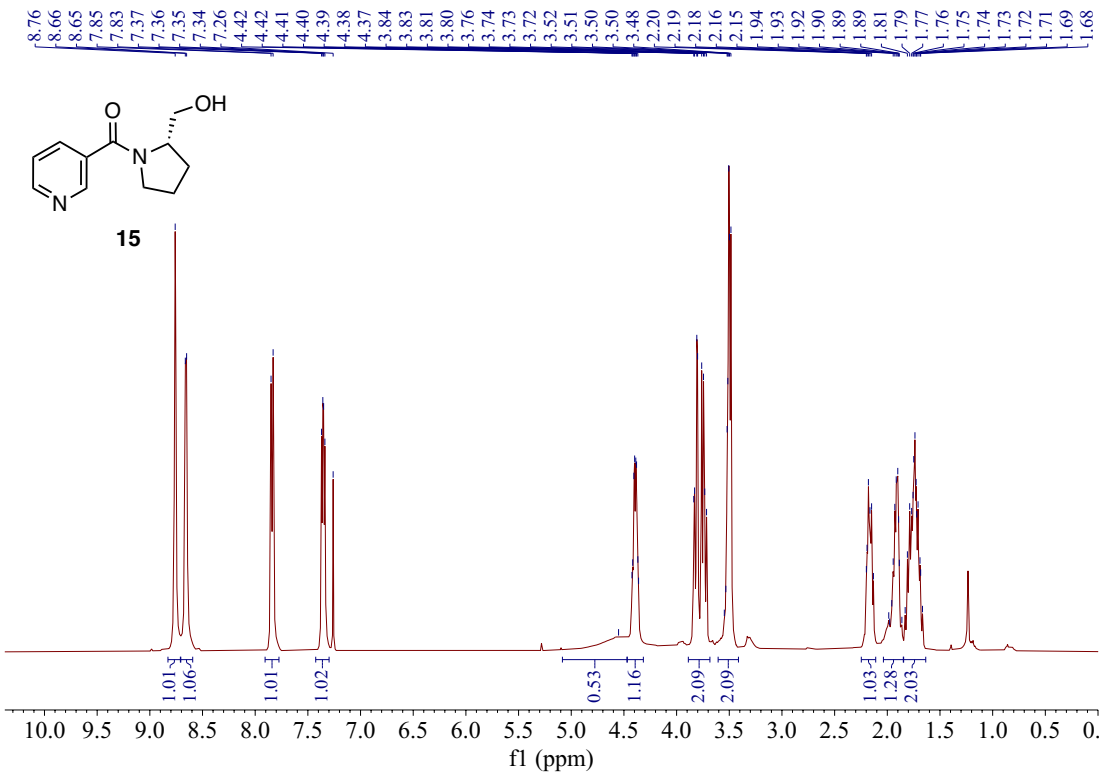

^{1}H NMR of Compound **15** (400 MHz, $CDCl_3$)

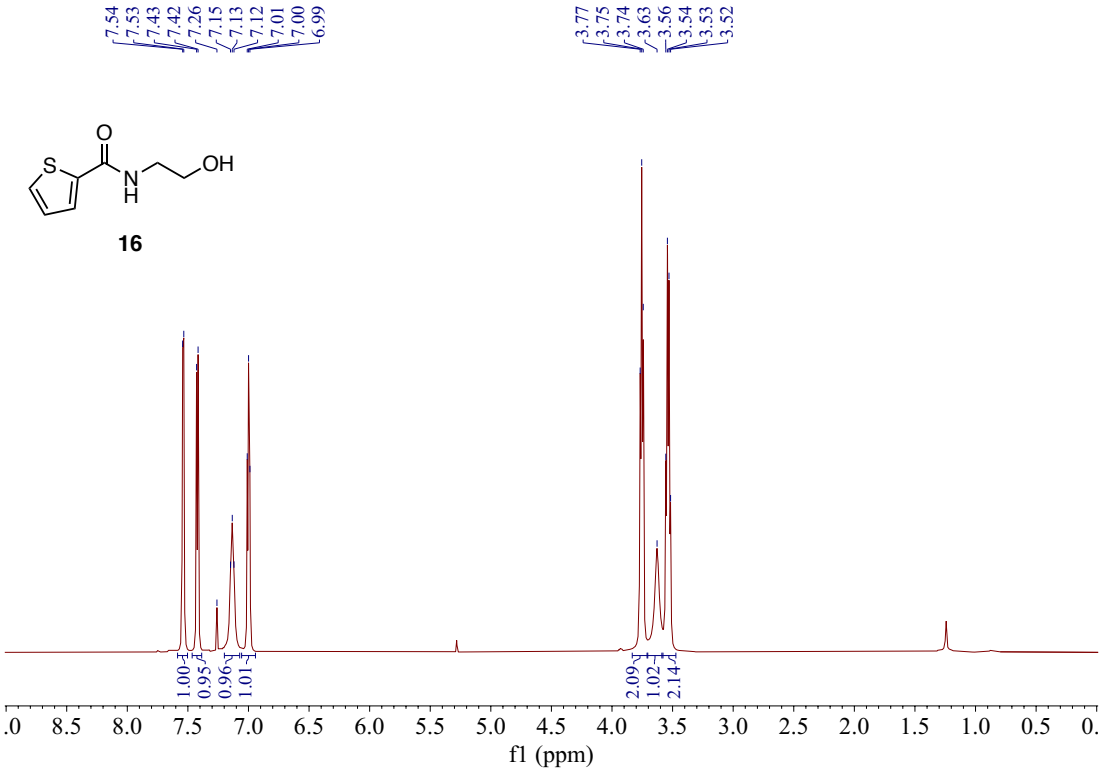

^{1}H NMR of Compound **16** (400 MHz, $CDCl_3$)

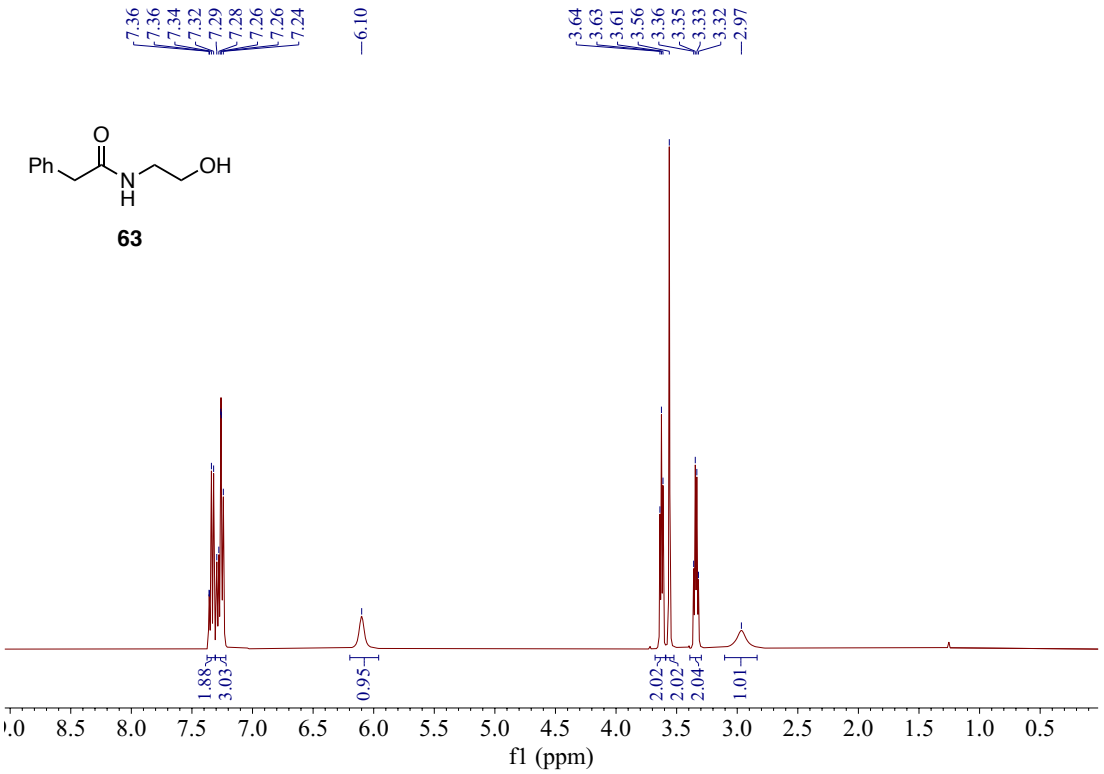

^{1}H NMR of Compound **63** (400 MHz, $CDCl_3$)

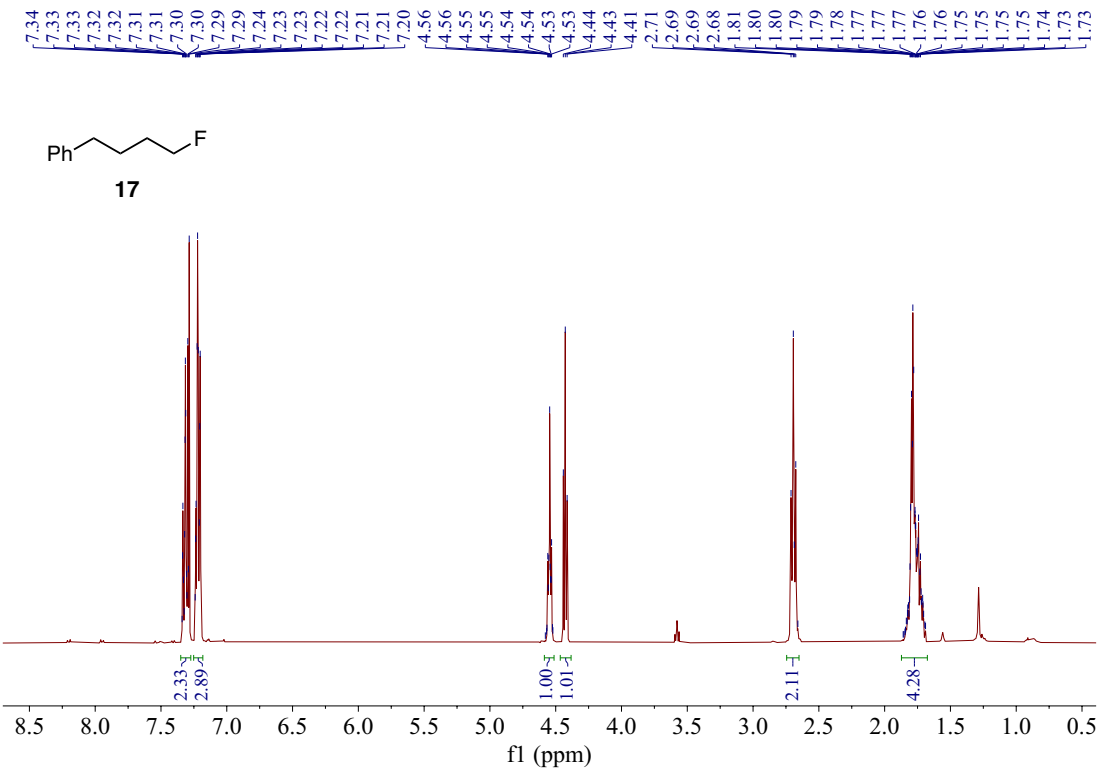

^{1}H NMR of Compound **17** (400 MHz, $CDCl_3$)

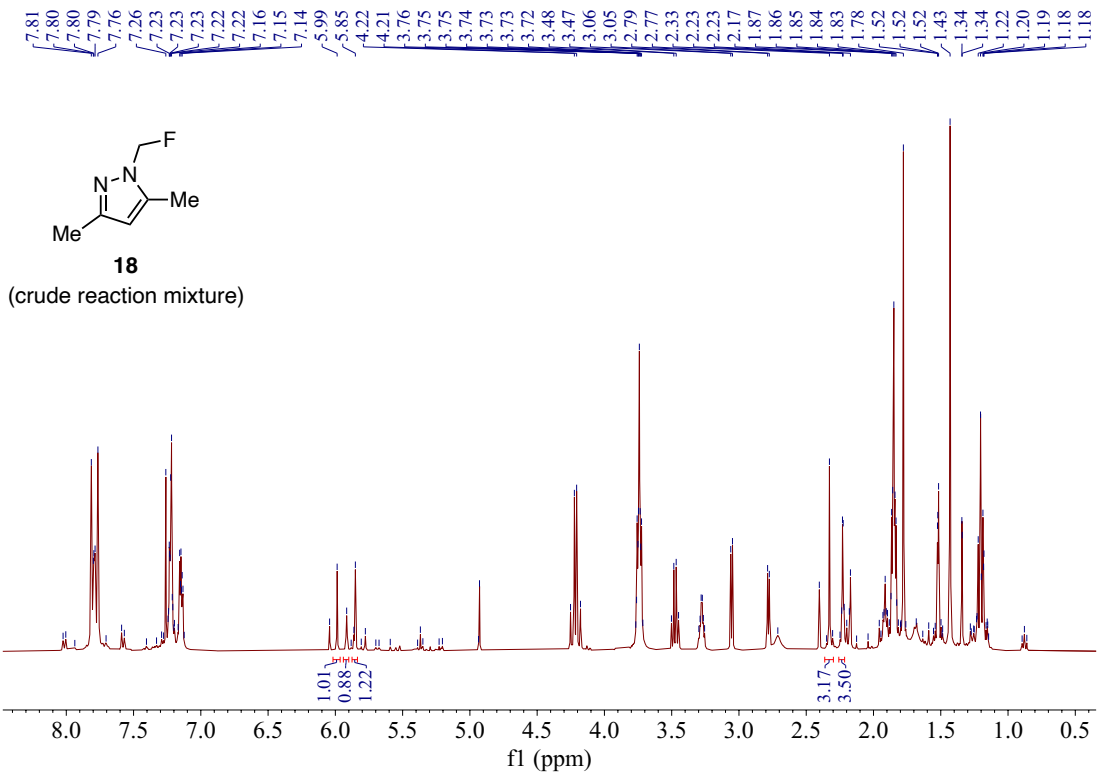

^{1}H NMR of Compound **18** crude reaction mixture (400 MHz, $CDCl_3$)

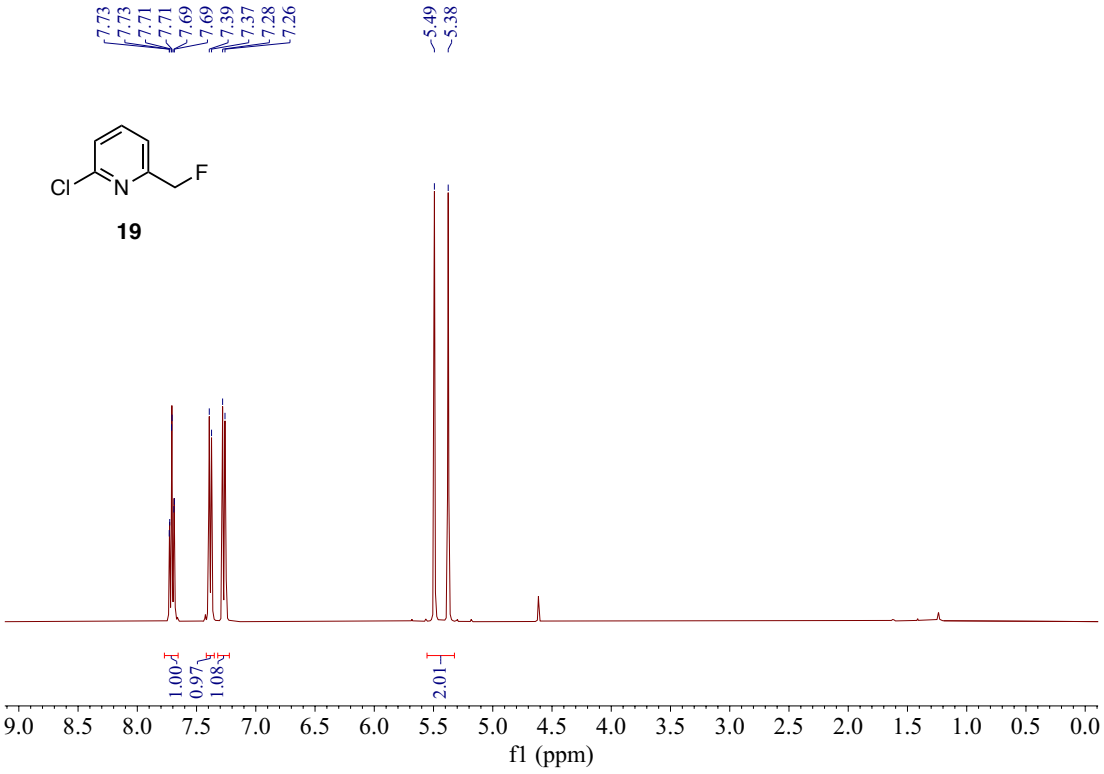

^{1}H NMR of Compound **19** (400 MHz, $CDCl_3$)

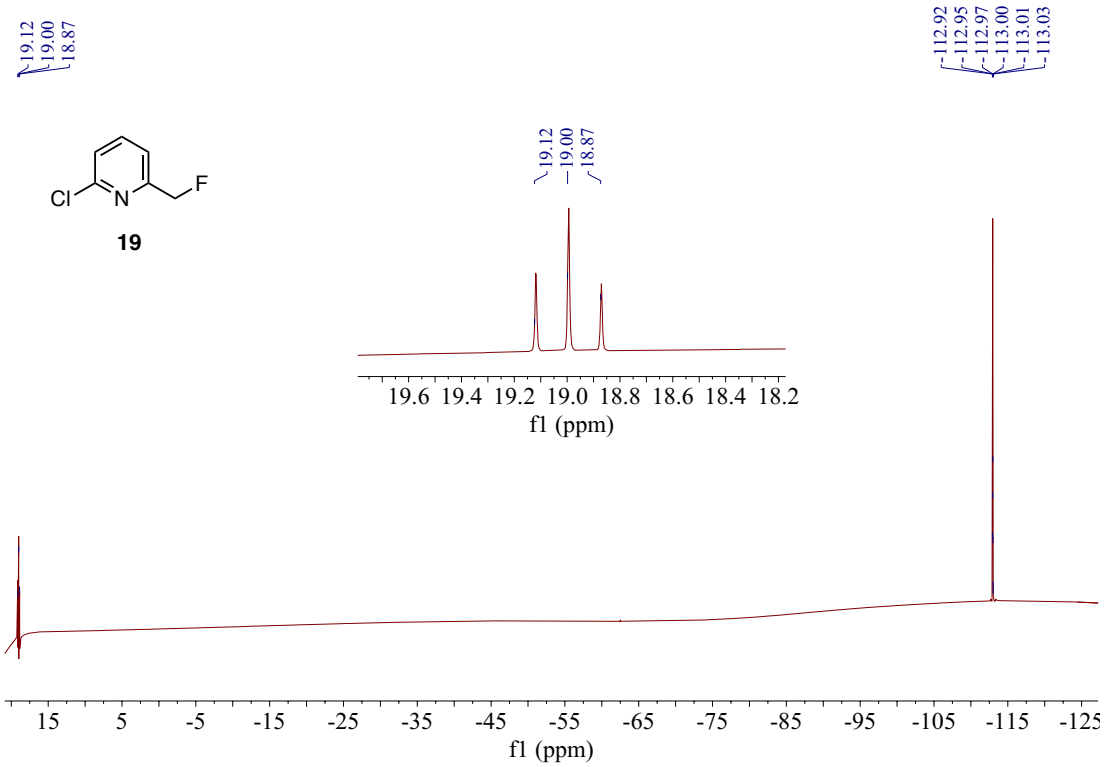

^{19}F NMR of Compound **19** (376 MHz, $CDCl_3$)

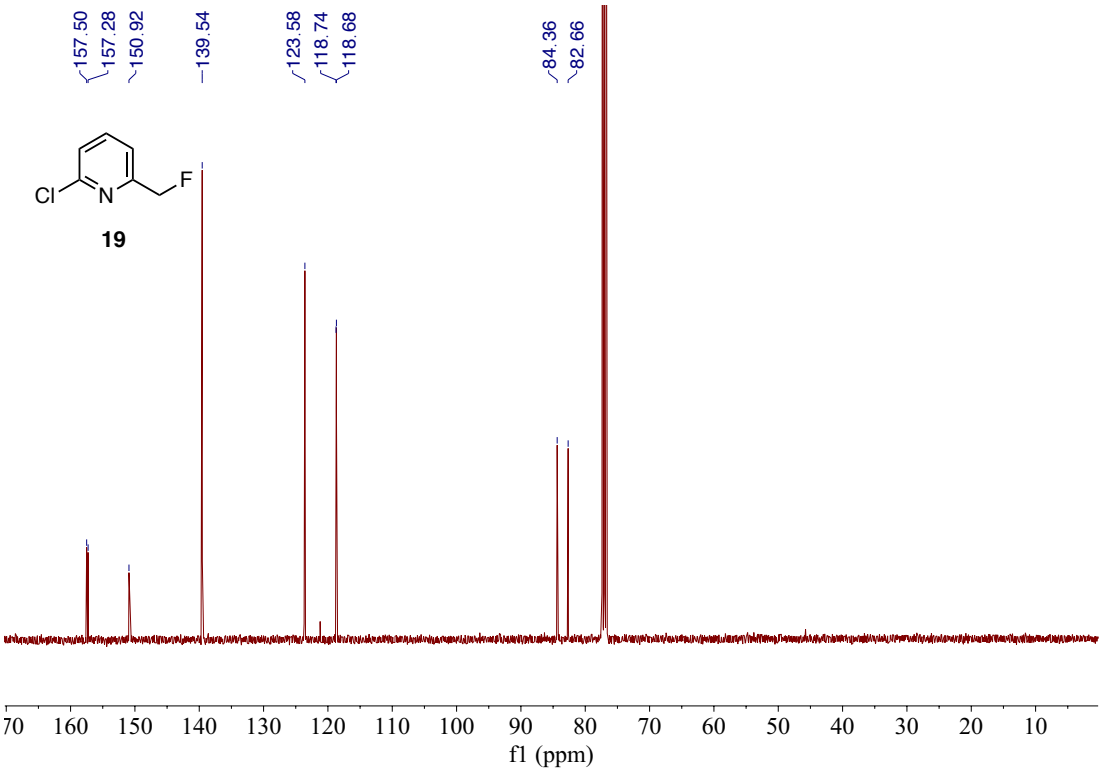

^{13}C NMR of Compound **19** (101 MHz, $CDCl_3$)

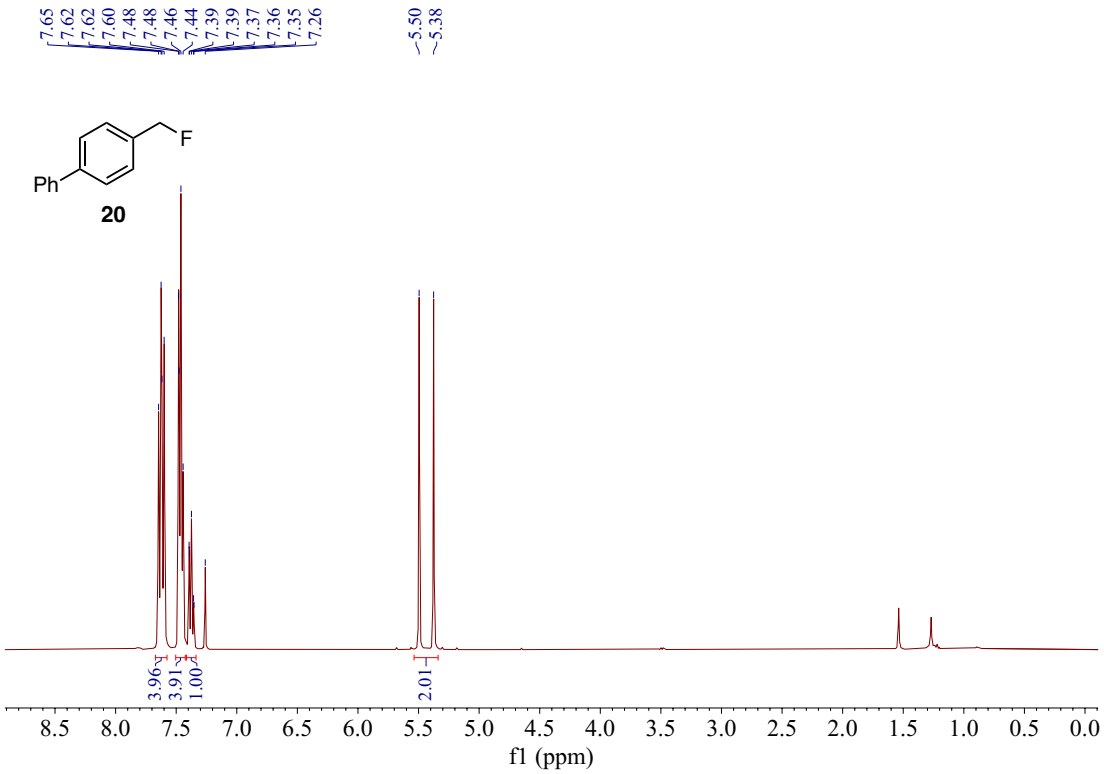

^{1}H NMR of Compound **20** (400 MHz, $CDCl_3$)

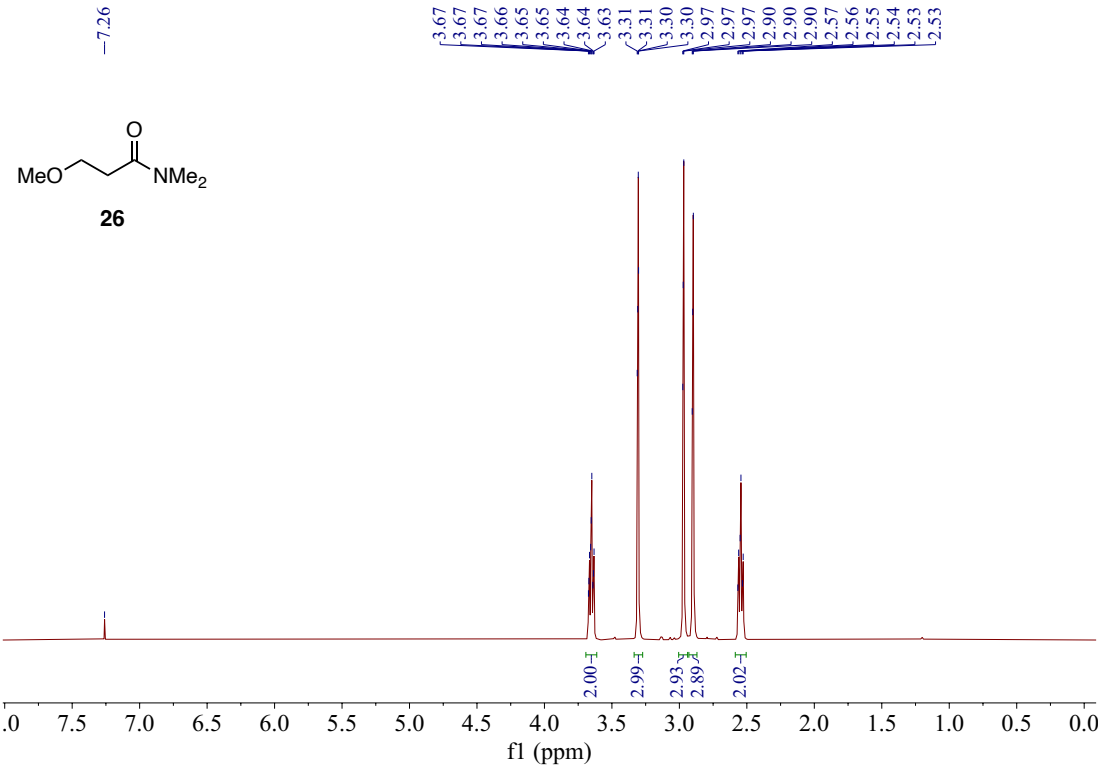

^{1}H NMR of Compound **26** (400 MHz, $CDCl_3$)

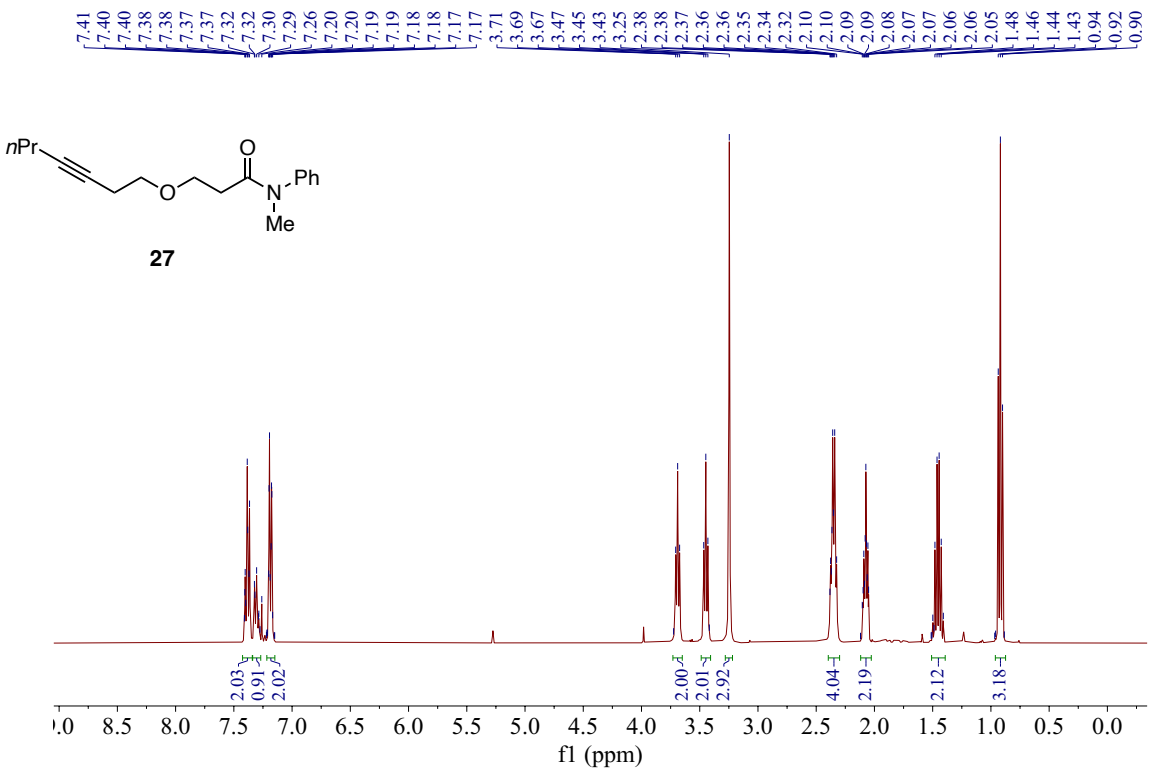

^{1}H NMR of Compound **27** (400 MHz, $CDCl_3$)

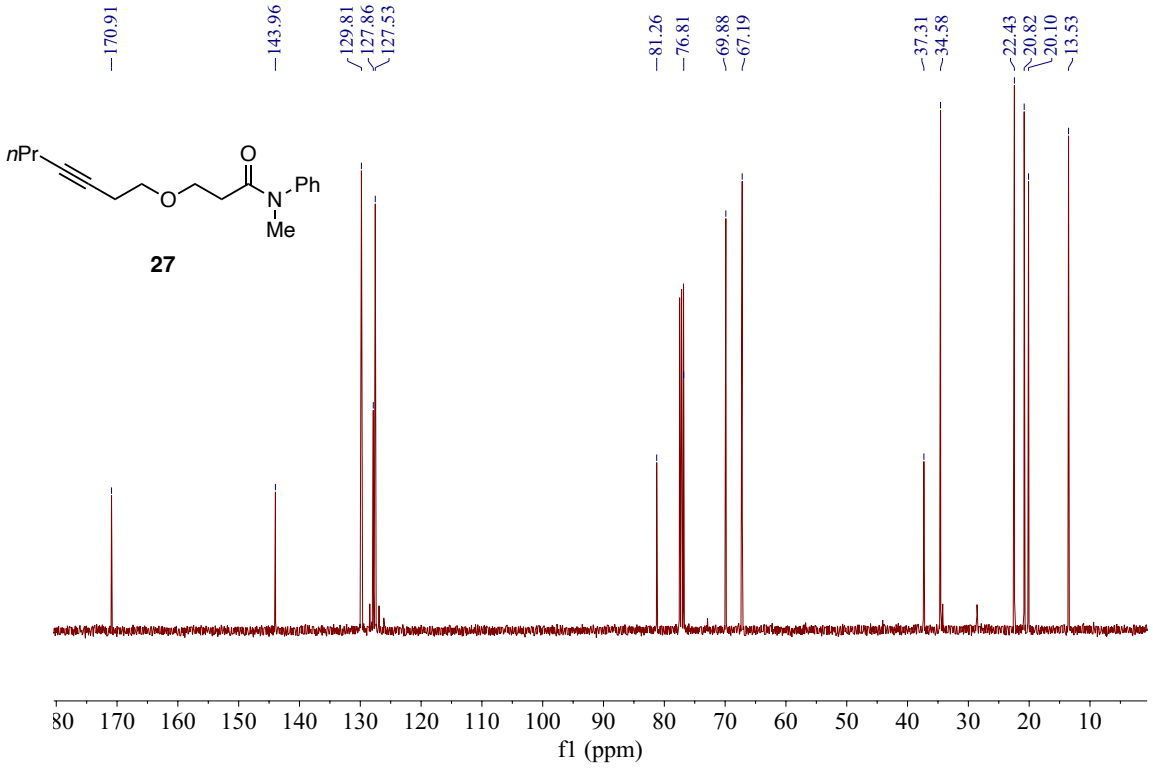

^{13}C NMR of Compound **27** (101 MHz, $CDCl_3$)

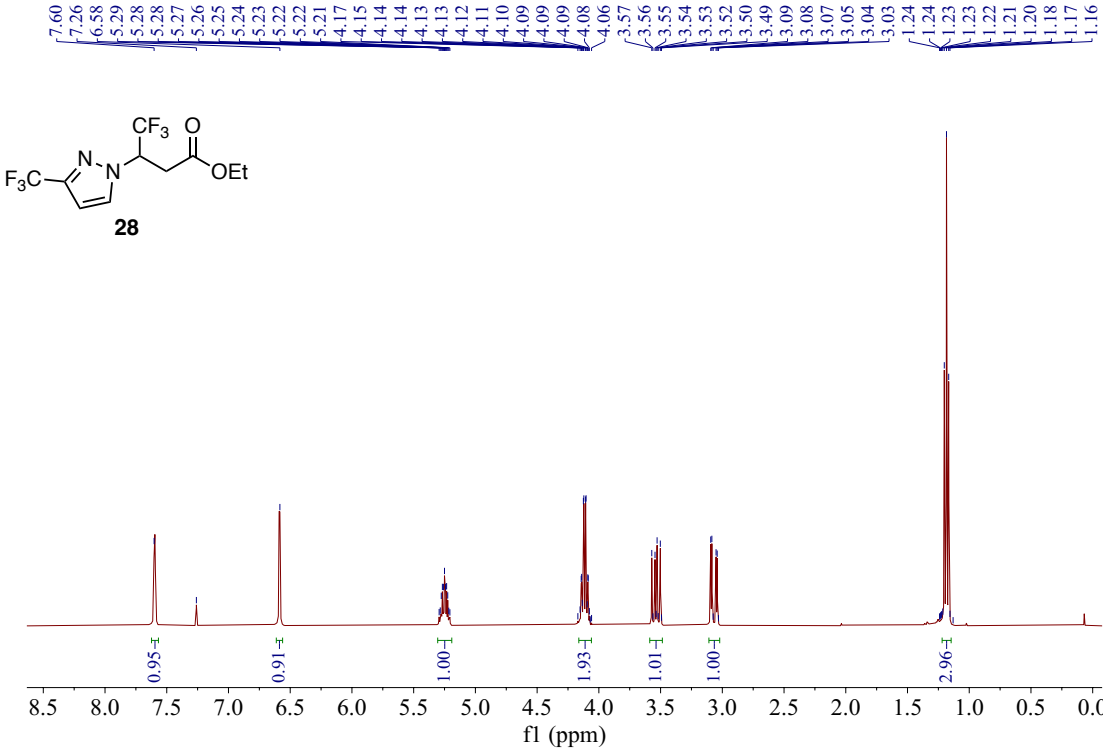

^{1}H NMR of Compound **28** (400 MHz, $CDCl_3$)

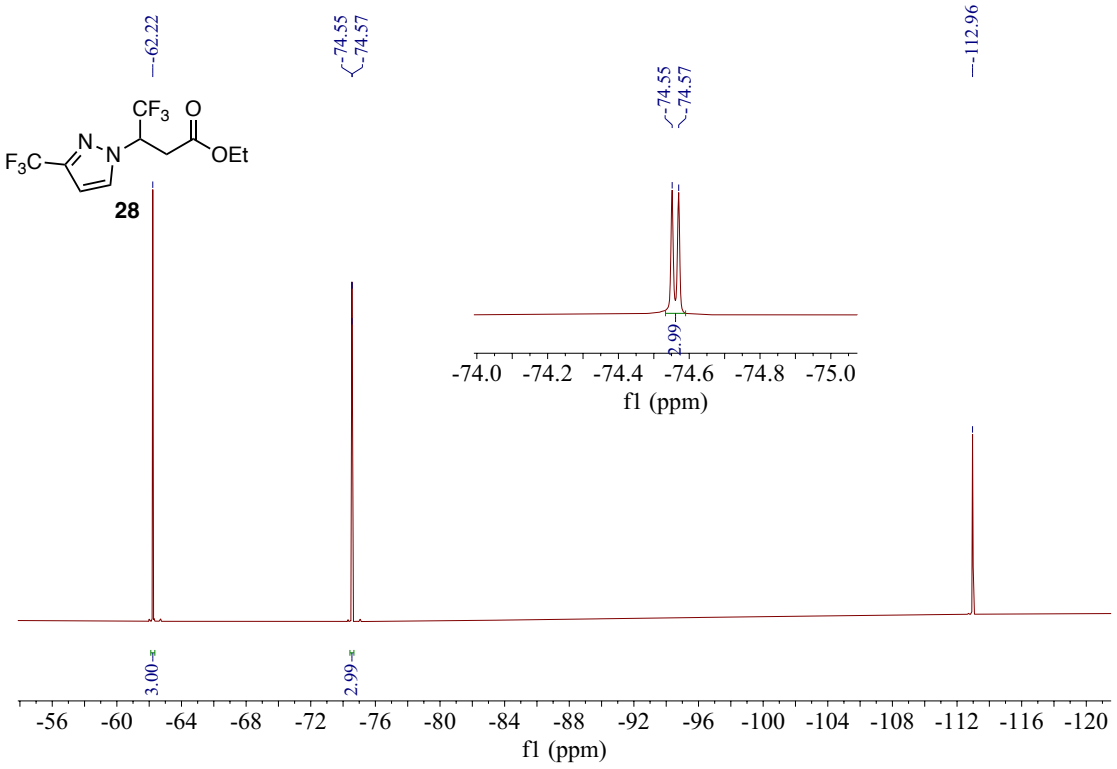

^{19}F NMR of Compound **28** (376 MHz, $CDCl_3$)

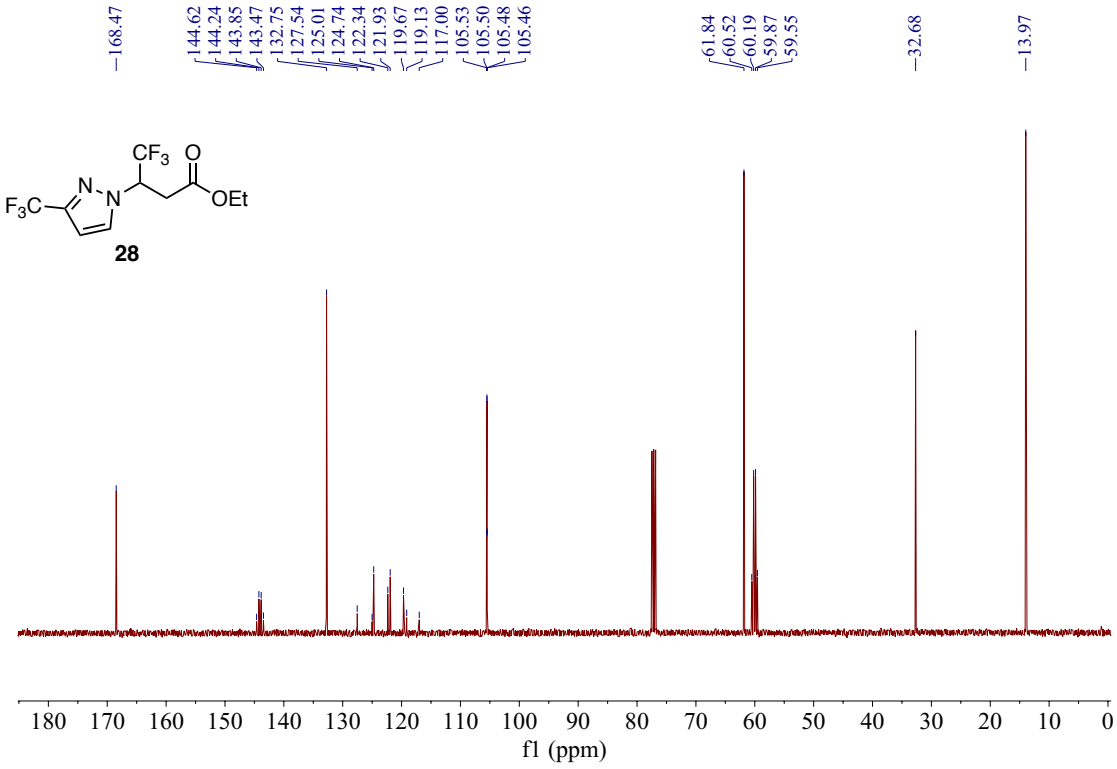

^{13}C NMR of Compound **28** (101 MHz, $CDCl_3$)

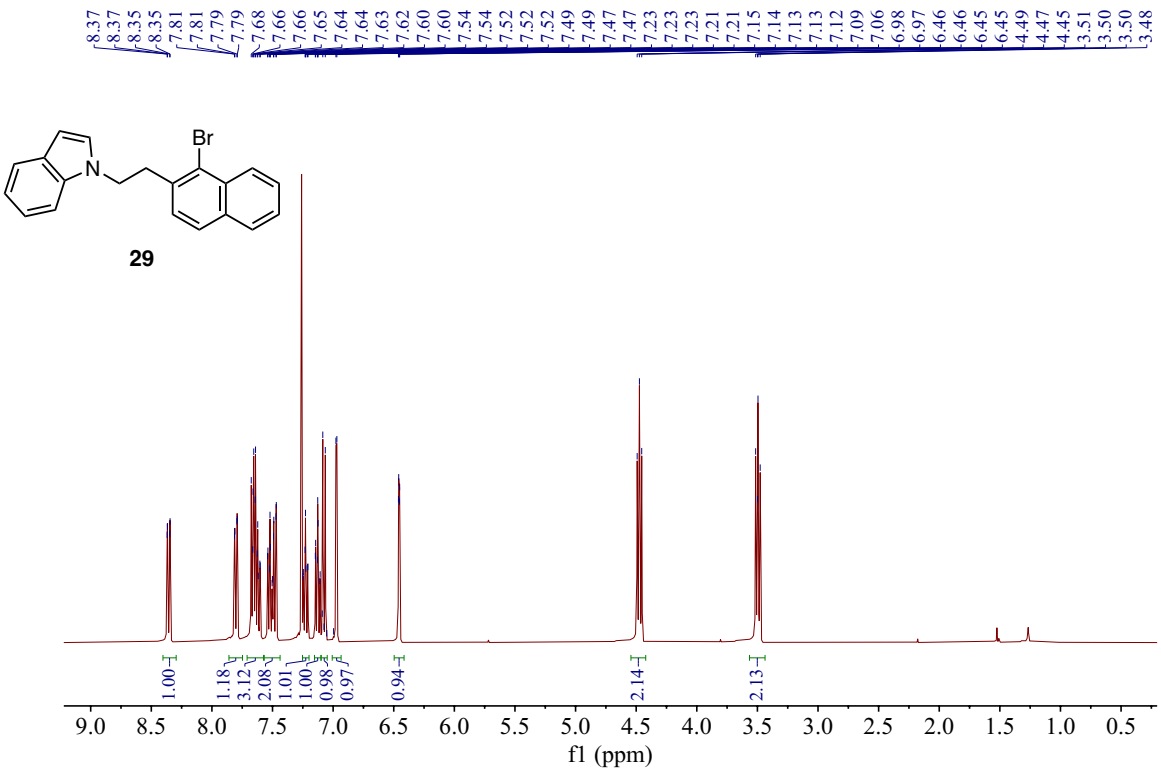

^{1}H NMR of Compound **29** (400 MHz, $CDCl_3$)

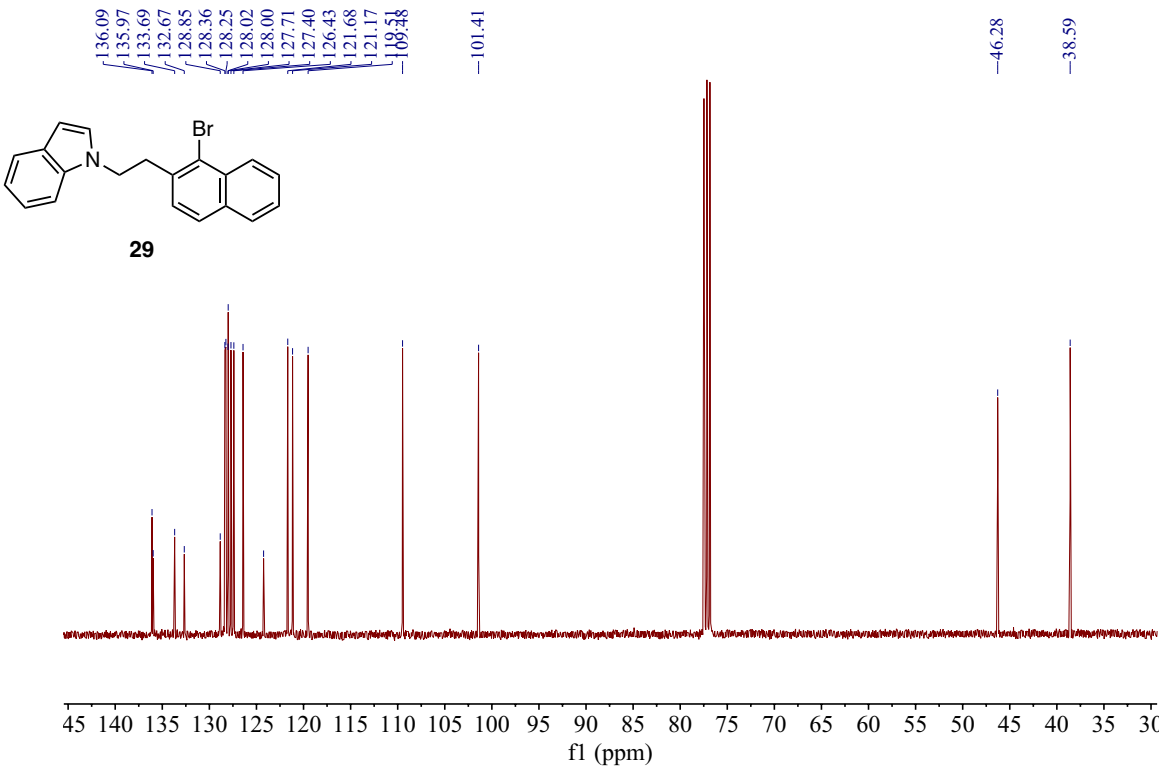

^{13}C NMR of Compound **29** (101 MHz, $CDCl_3$)

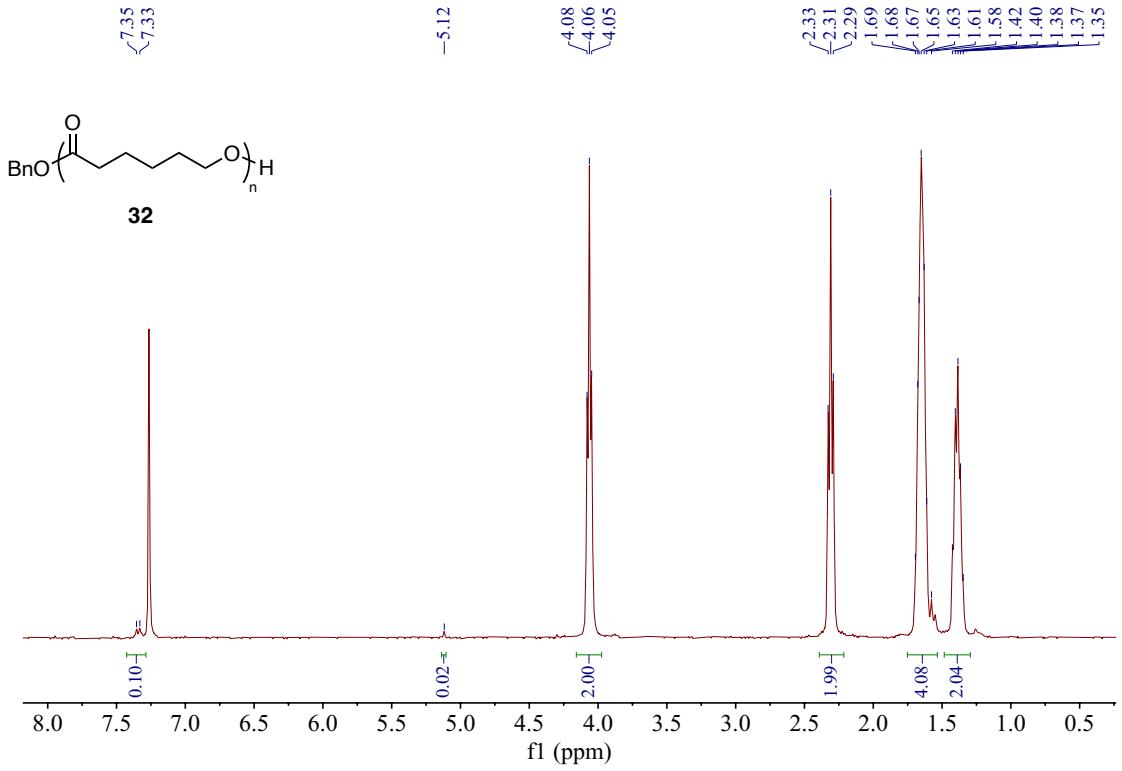

^{1}H NMR of Polymer **32** (400 MHz, $CDCl_3$)

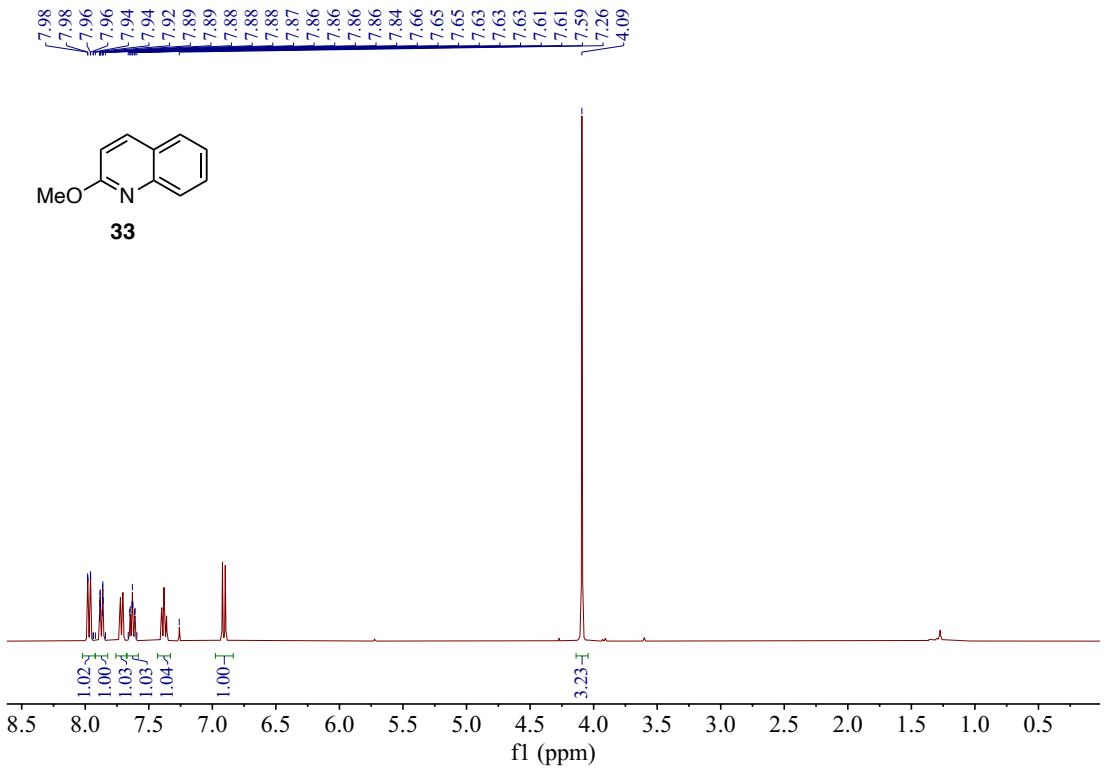

^{1}H NMR of Compound **33** (400 MHz, $CDCl_3$)

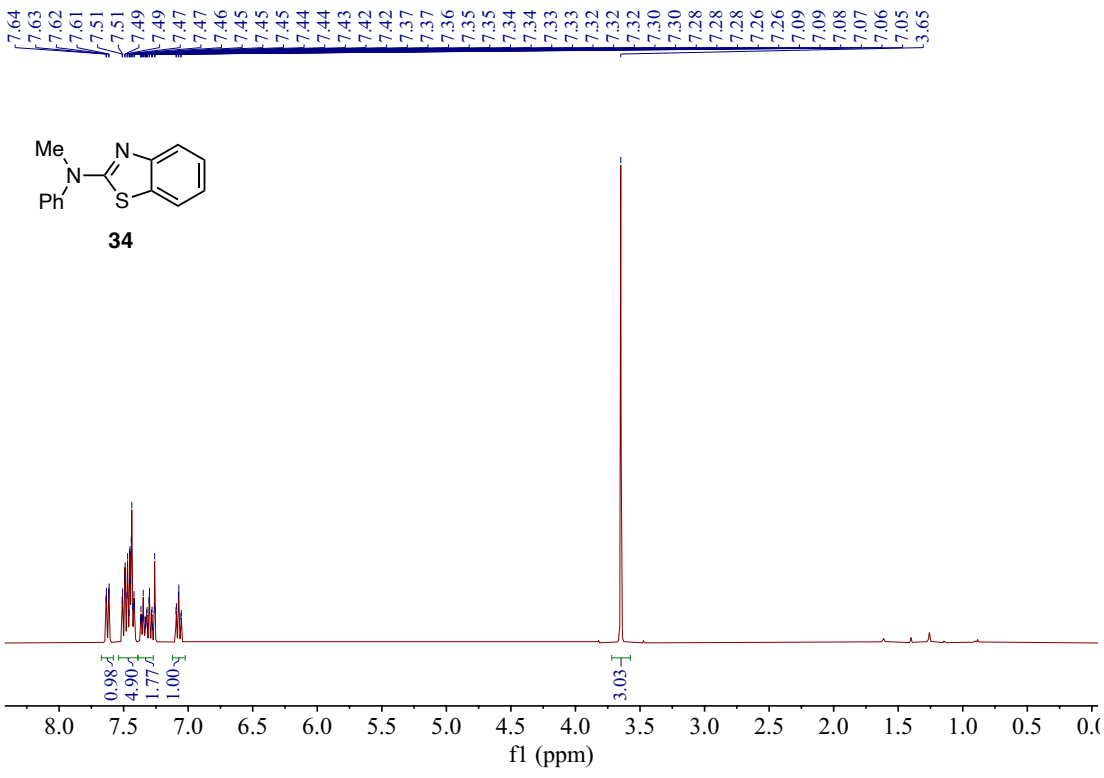

^{1}H NMR of Compound **34** (400 MHz, $CDCl_3$)

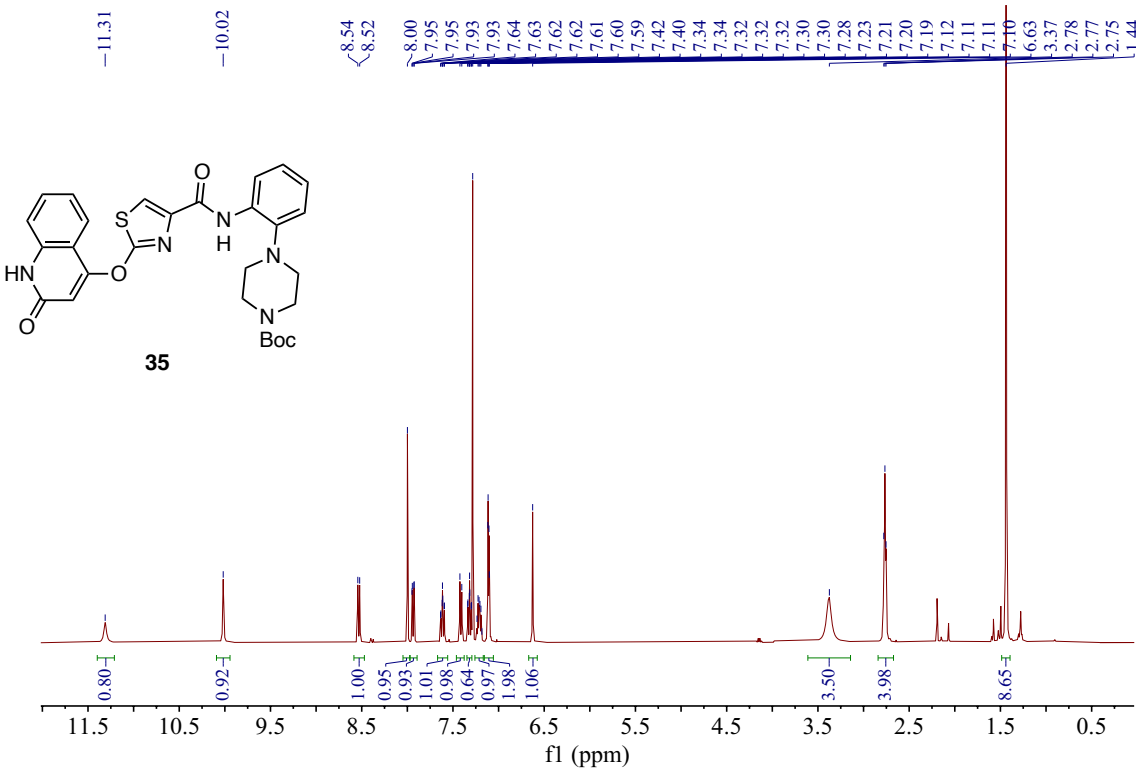

^{1}H NMR of Compound **35** (400 MHz, $CDCl_3$)

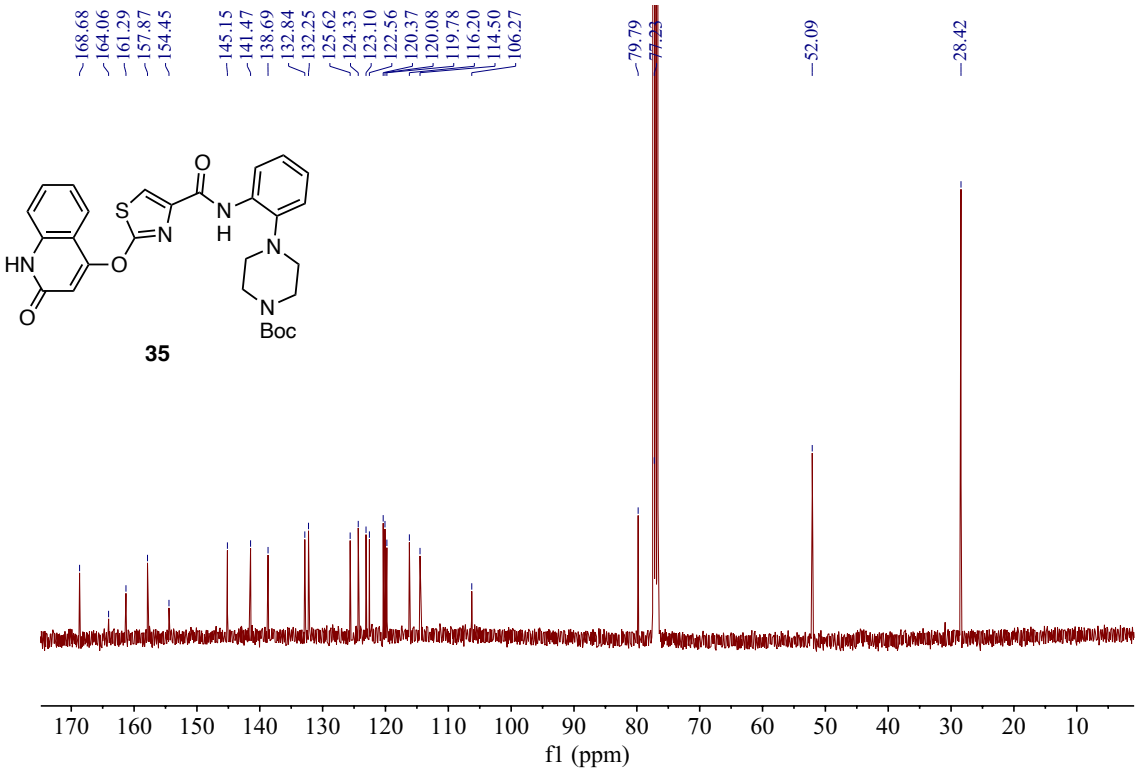

^{13}C NMR of Compound **35** (101 MHz, $CDCl_3$)

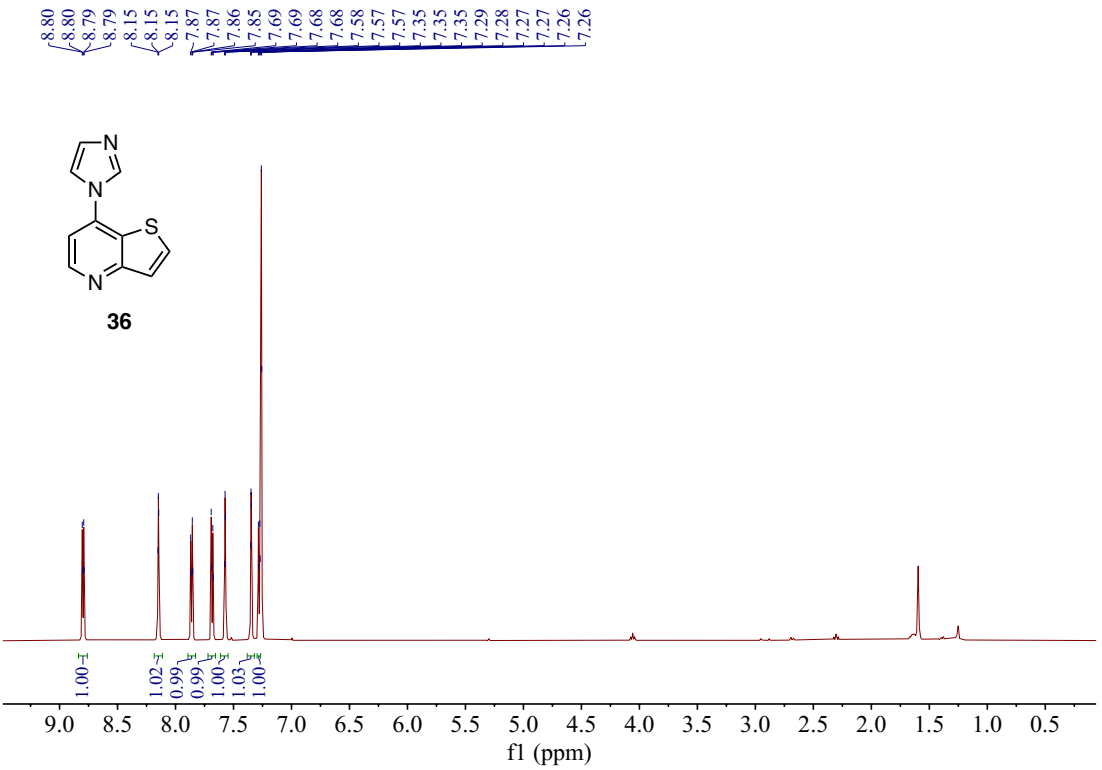

^{1}H NMR of Compound **36** (400 MHz, $CDCl_3$)

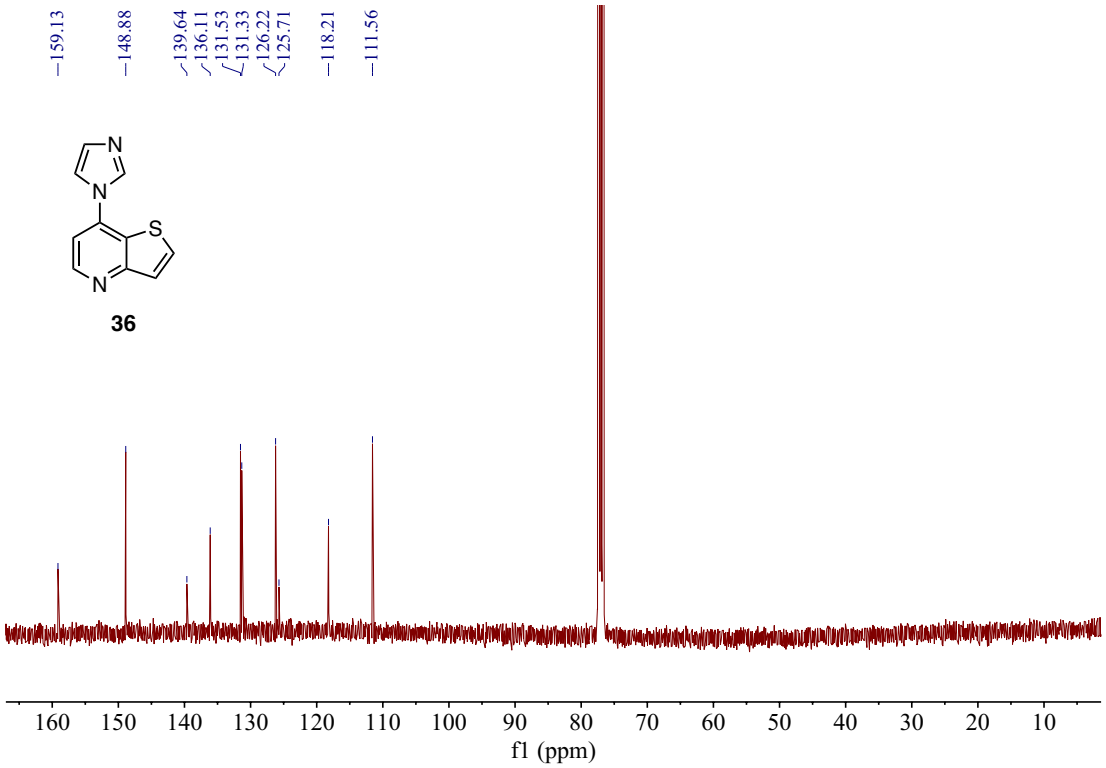

36

^{13}C NMR of Compound **36** (101 MHz, $CDCl_3$)

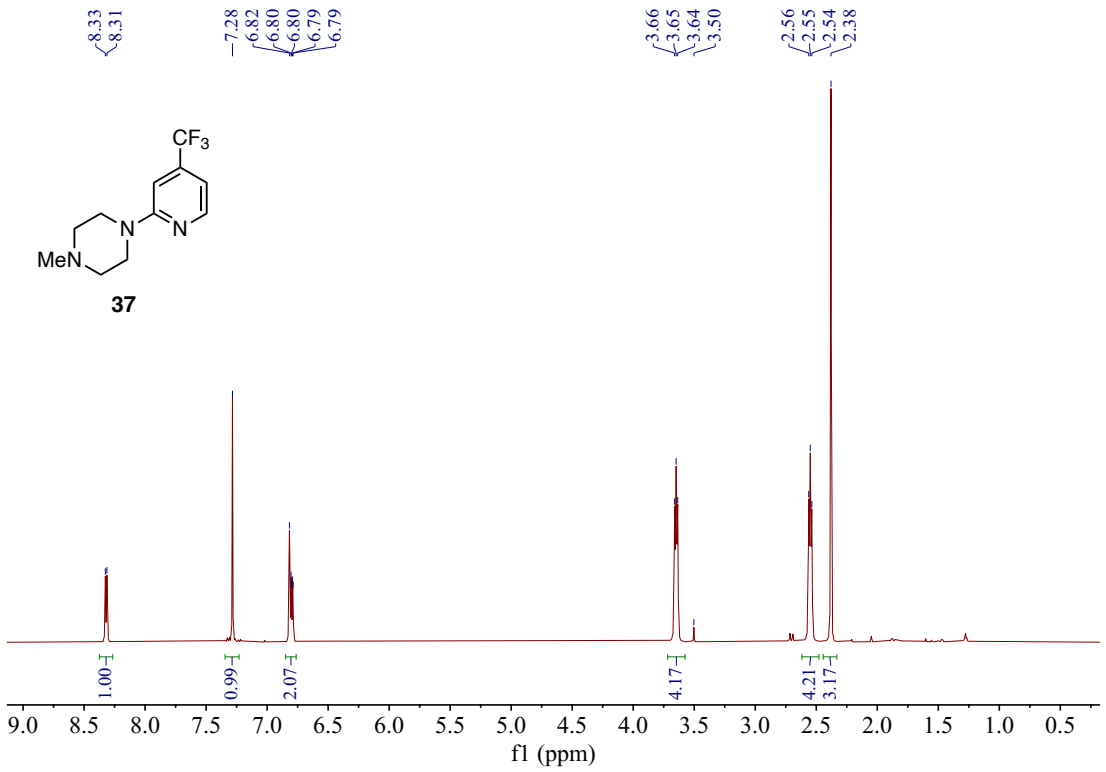

37

^{1}H NMR of Compound **37** (400 MHz, $CDCl_3$)

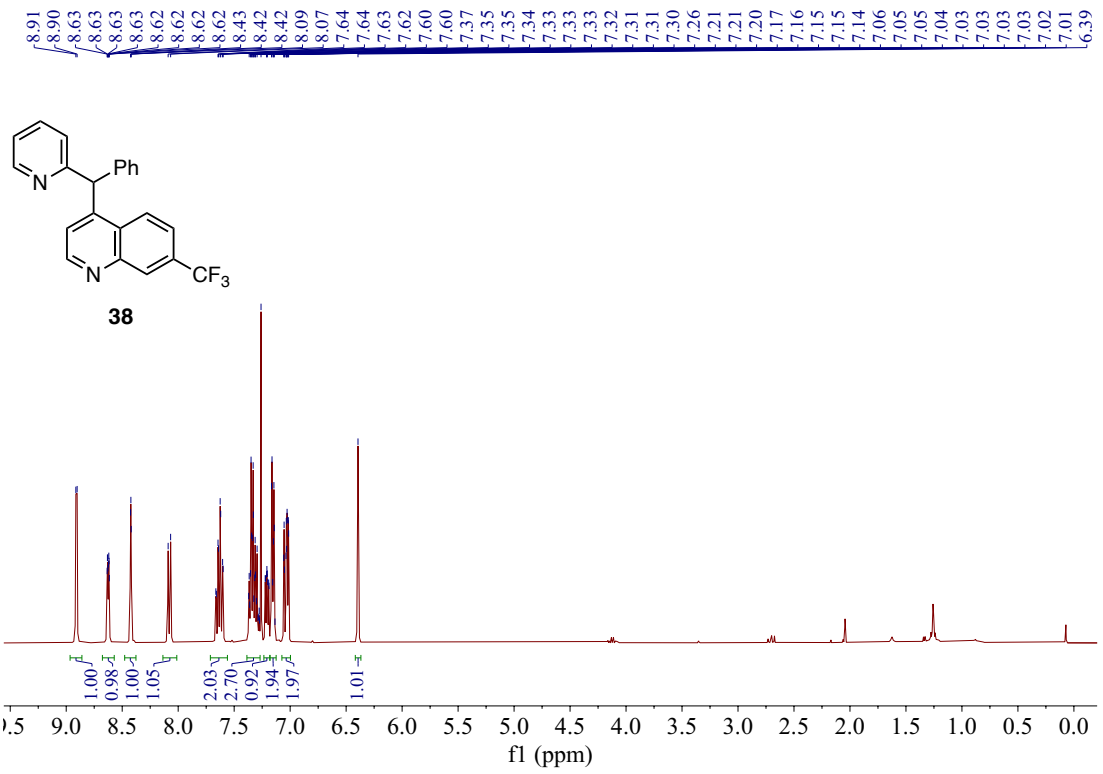

^{1}H NMR of Compound **38** (400 MHz, $CDCl_3$)

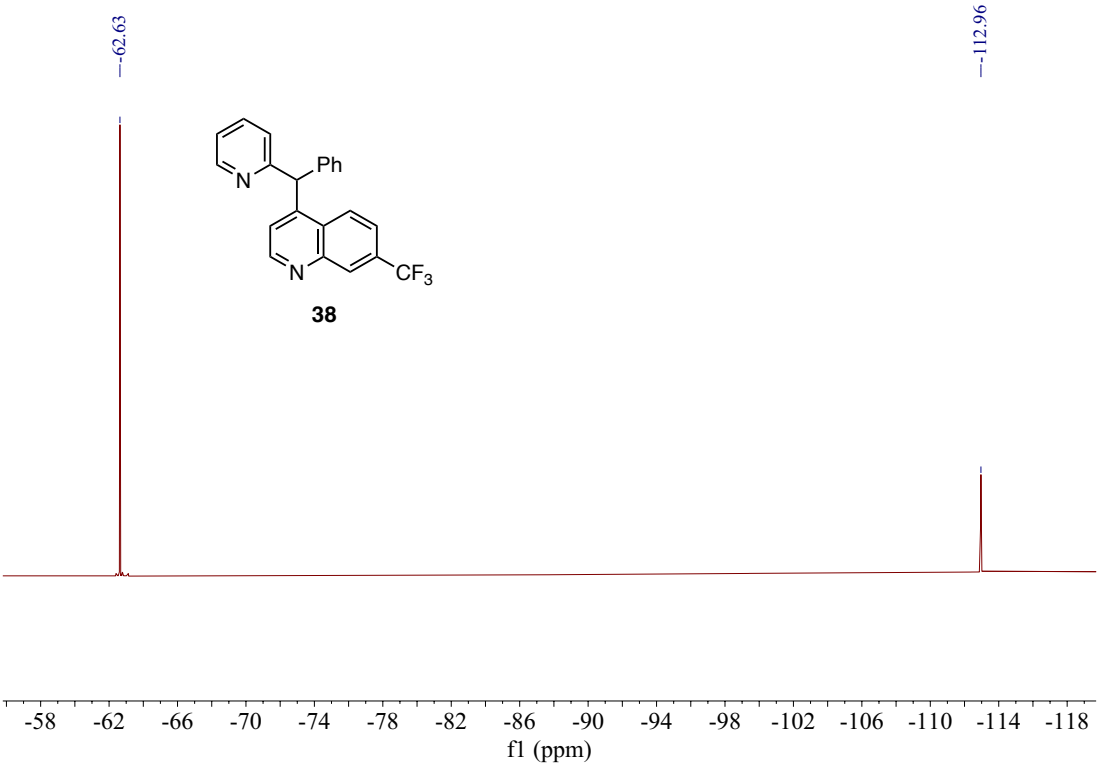

^{19}F NMR of Compound **38** (376 MHz, $CDCl_3$)

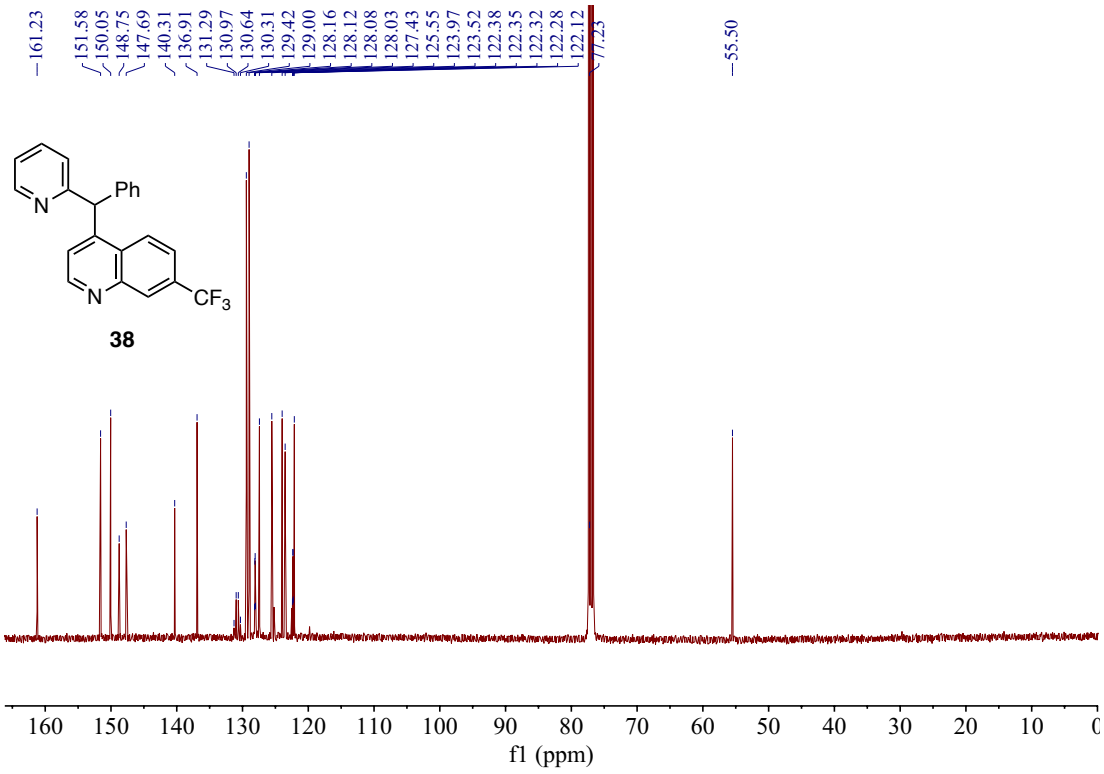

^{13}C NMR of Compound **38** (101 MHz, $CDCl_3$)

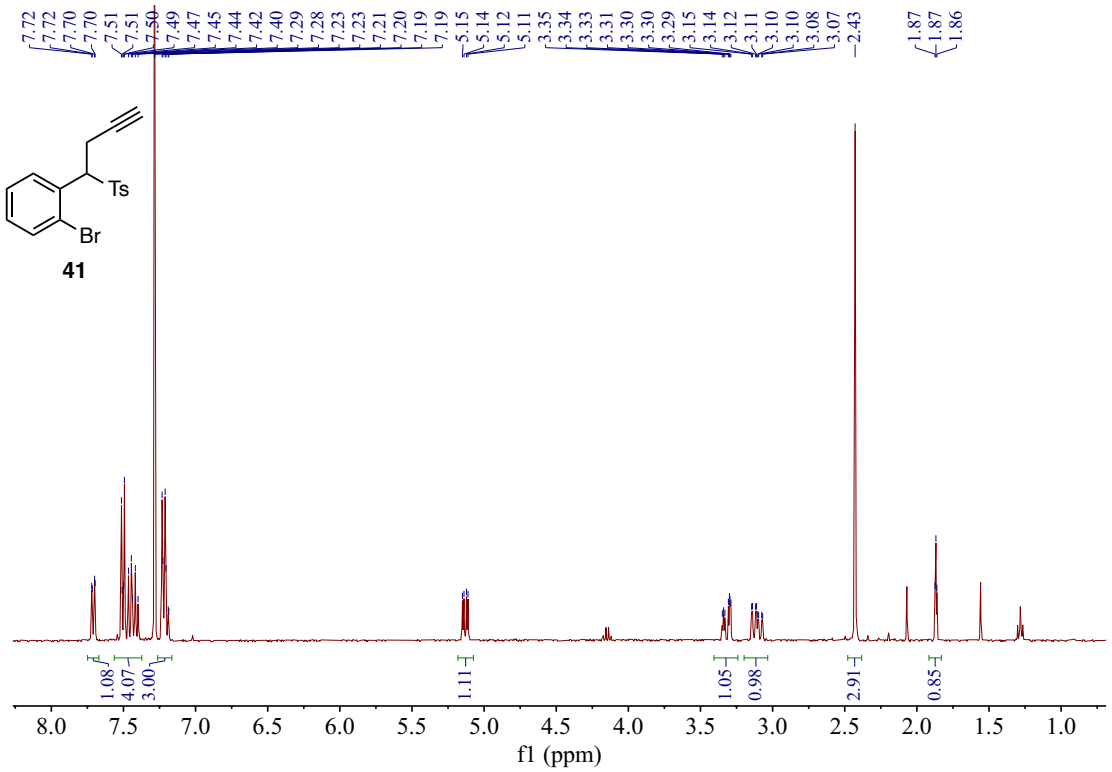

^{1}H NMR of Compound **41** (400 MHz, $CDCl_3$)

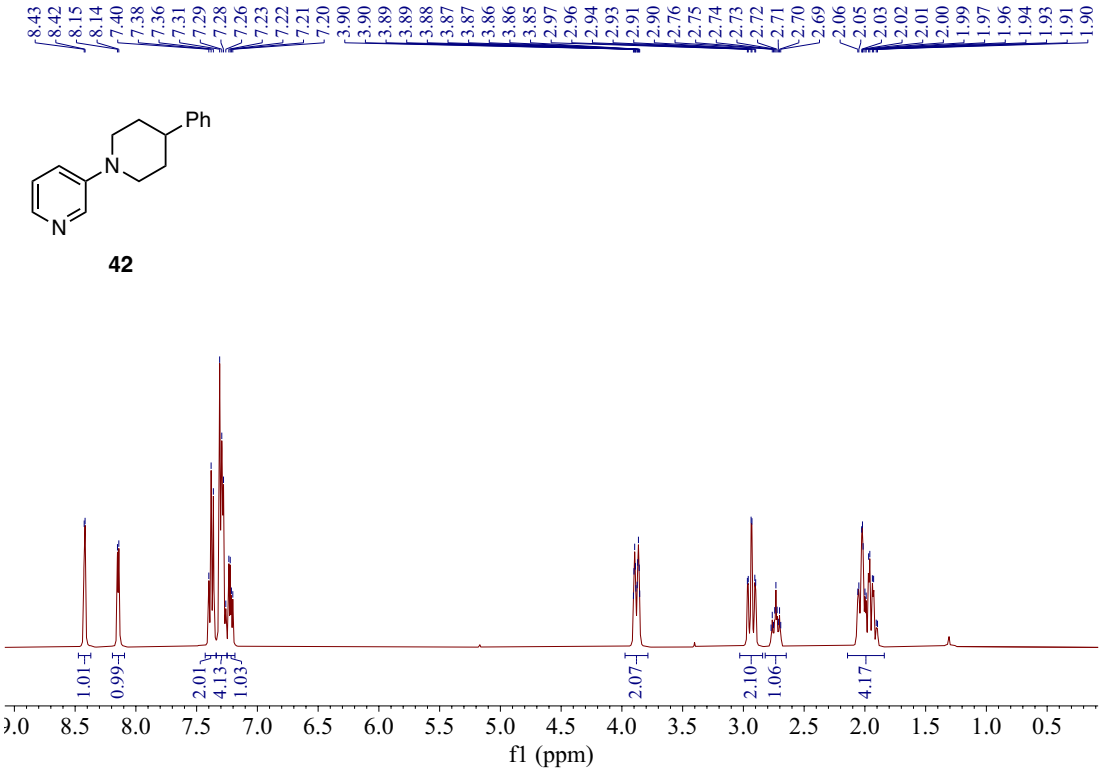

^{1}H NMR of Compound **42** (400 MHz, $CDCl_3$)

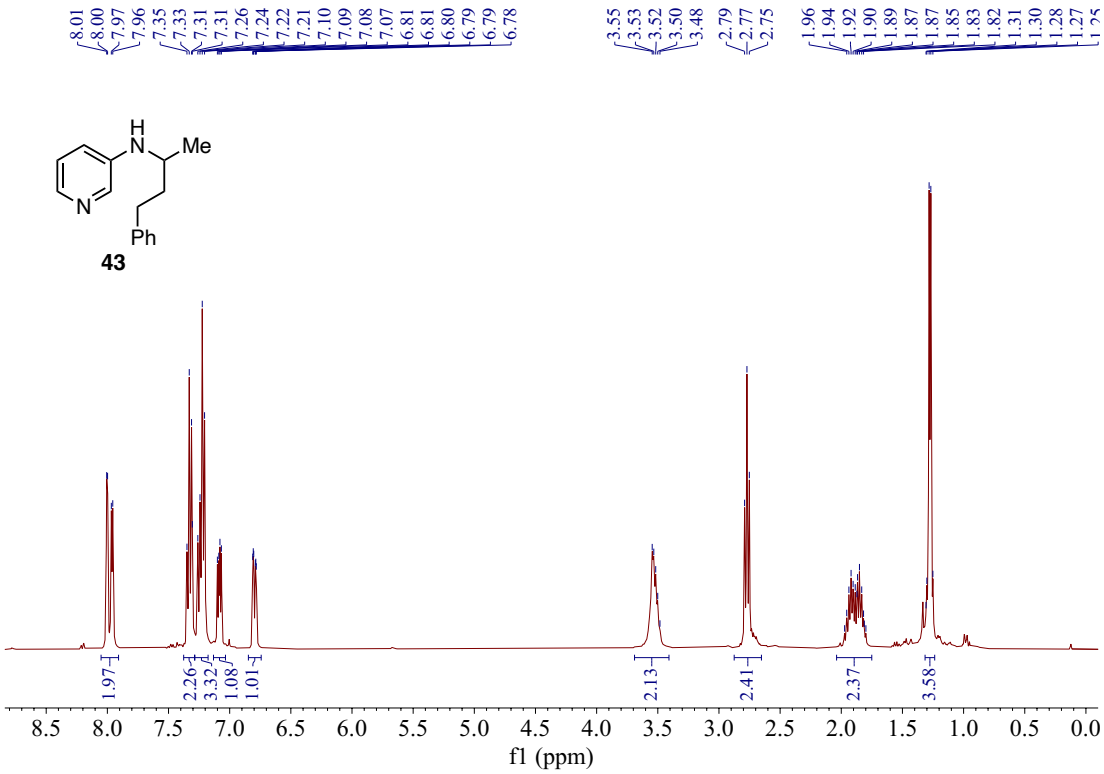

^{1}H NMR of Compound **43** (400 MHz, $CDCl_3$)

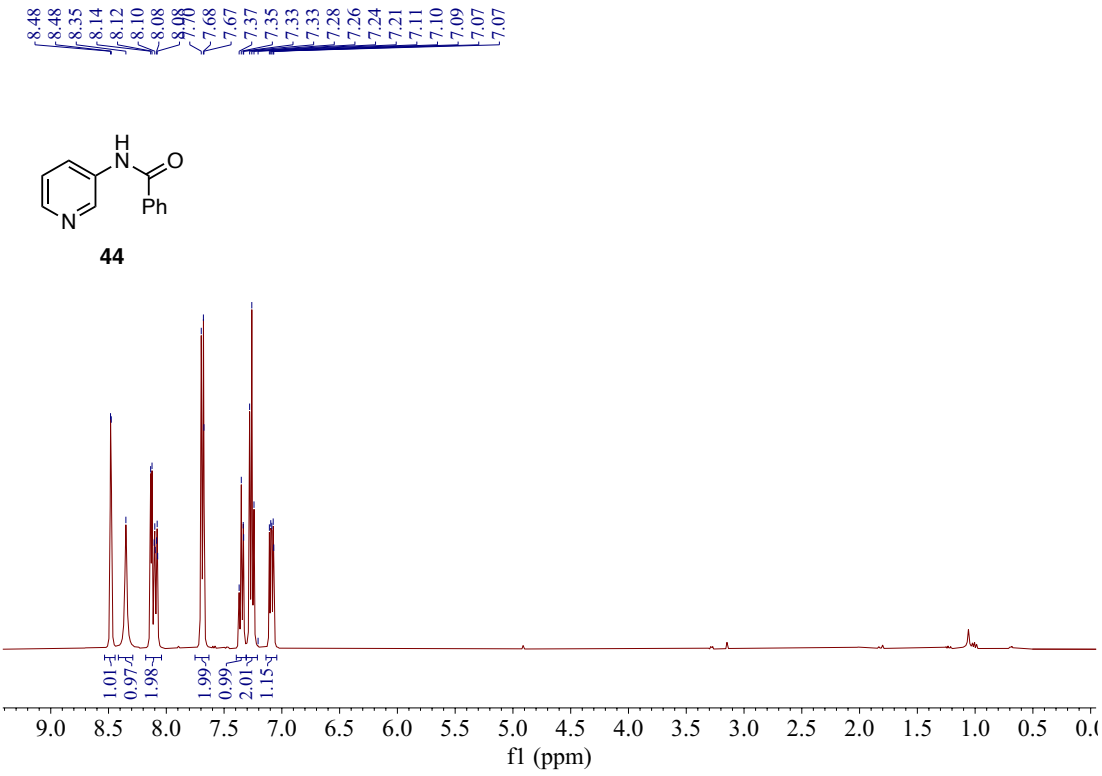

44

^{1}H NMR of Compound **44** (400 MHz, $CDCl_3$)

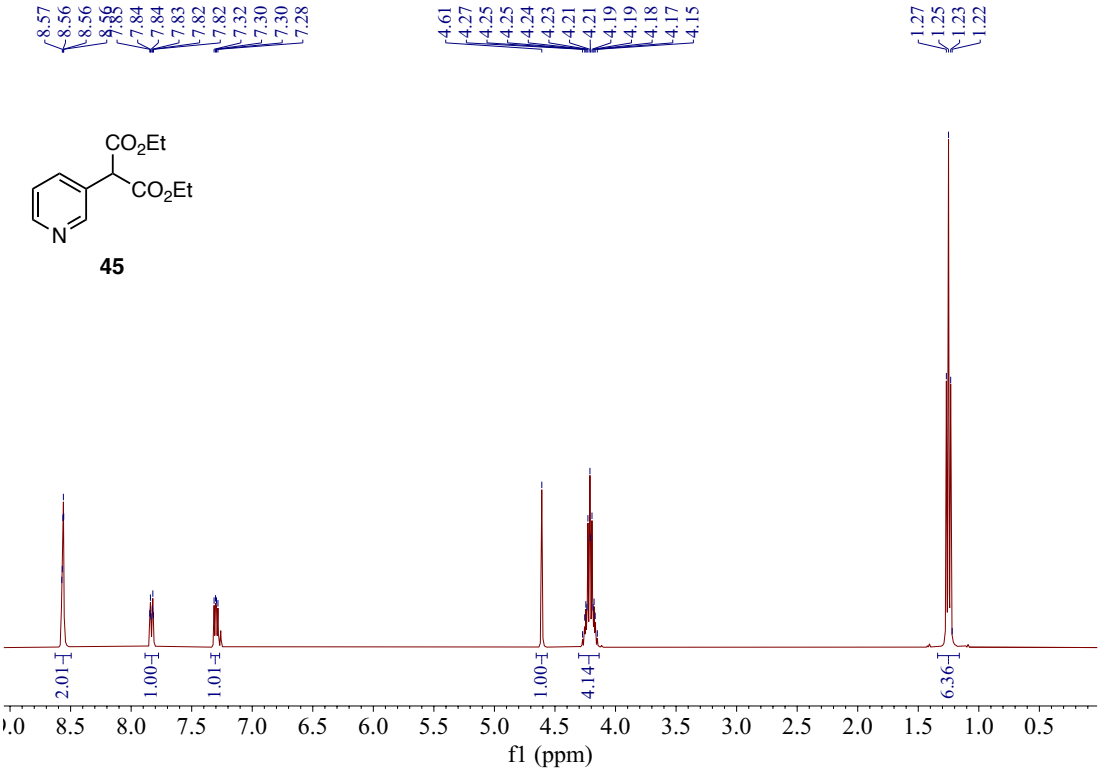

45

^{1}H NMR of Compound **45** (400 MHz, $CDCl_3$)

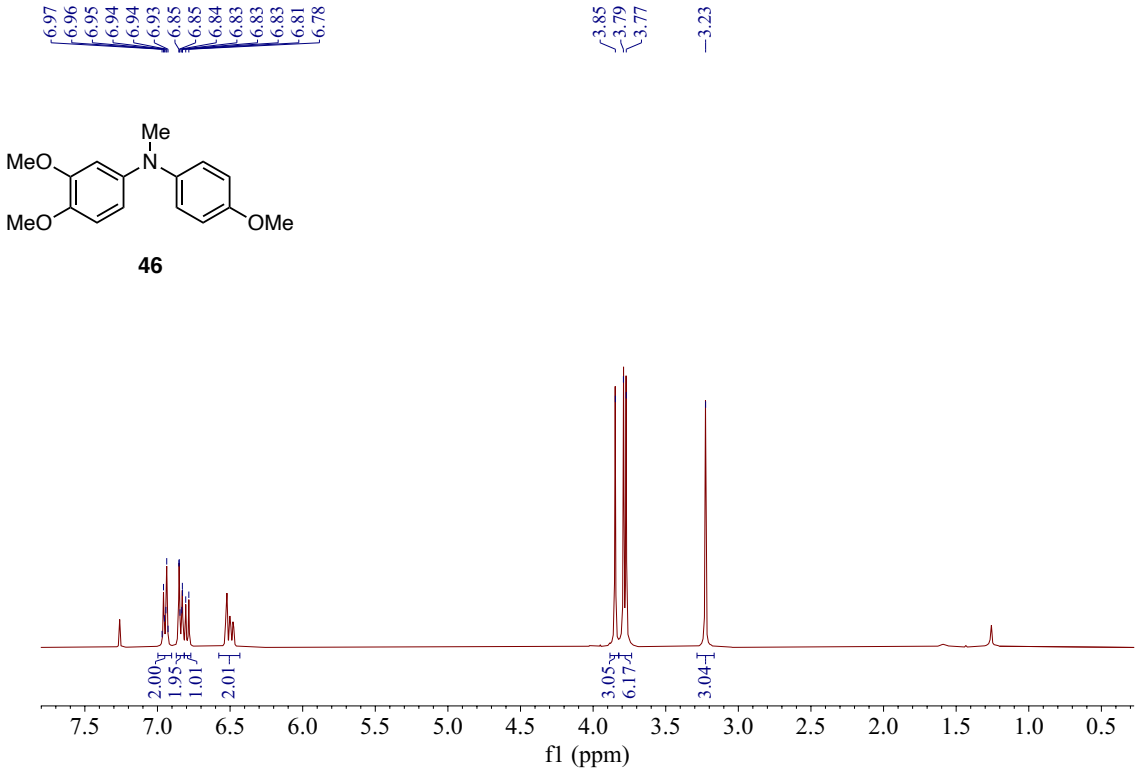

^{1}H NMR of Compound **46** (400 MHz, $CDCl_3$)

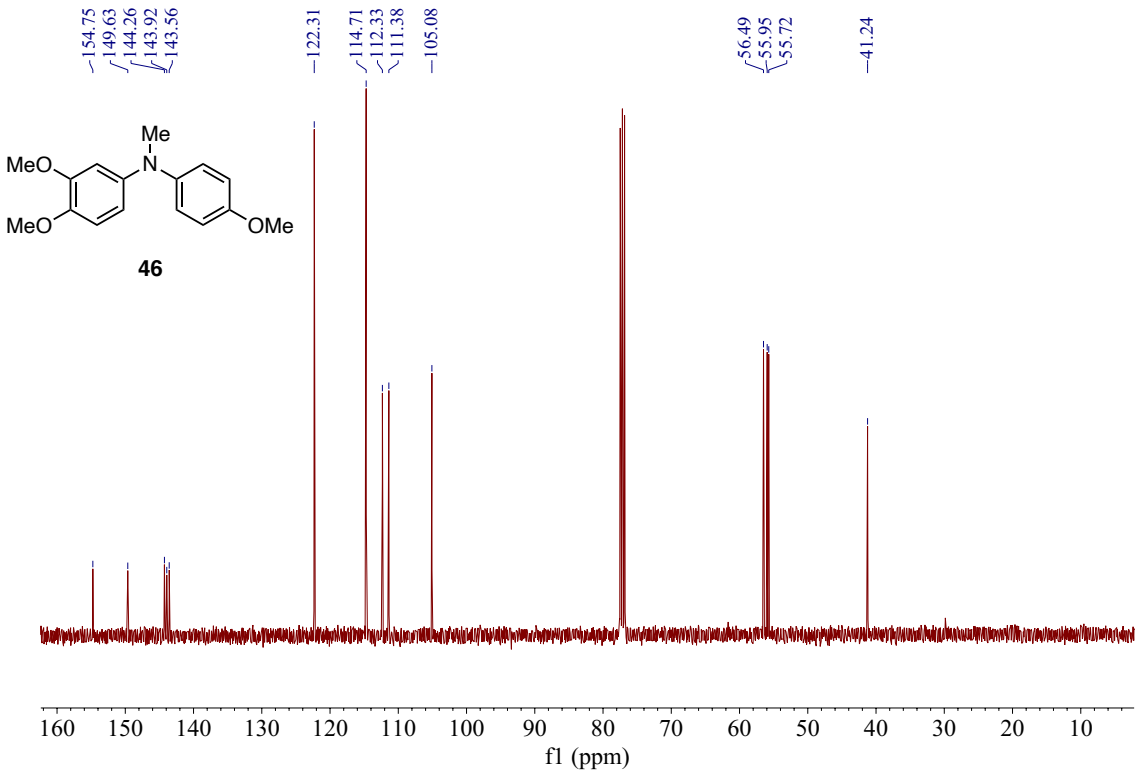

^{13}C NMR of Compound **46** (101 MHz, $CDCl_3$)

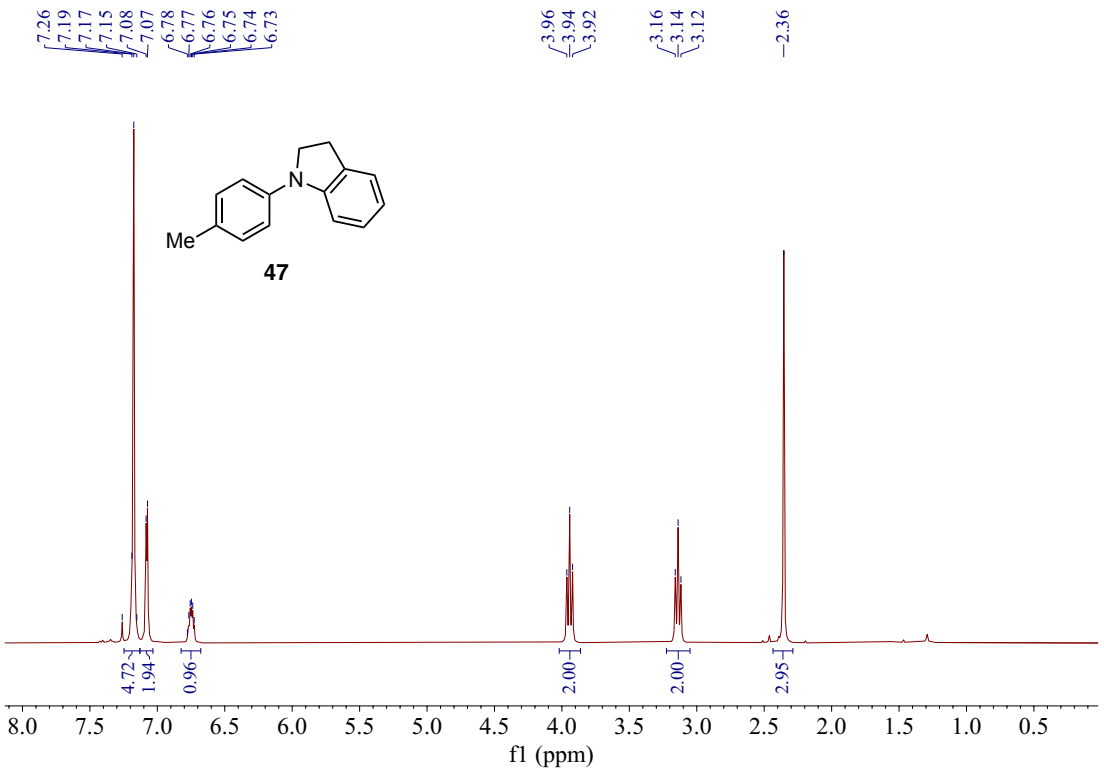

^{1}H NMR of Compound **47** (400 MHz, $CDCl_3$)

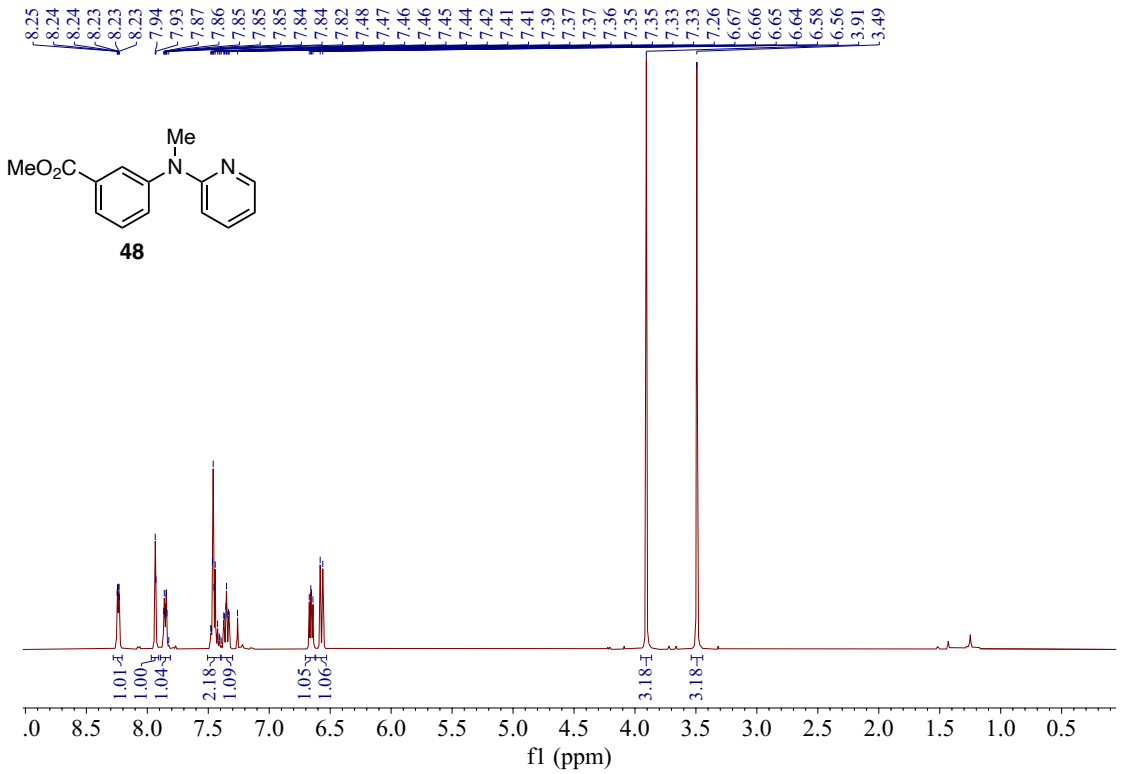

^{1}H NMR of Compound **48** (400 MHz, $CDCl_3$)

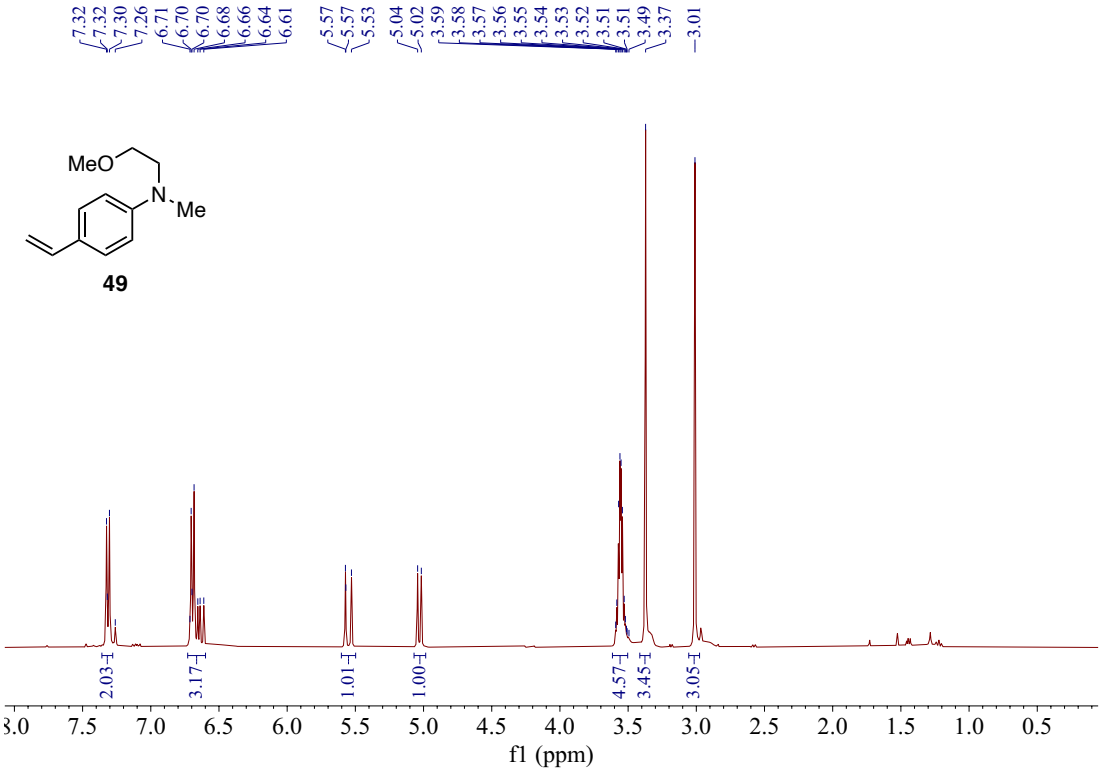

^{1}H NMR of Compound **49** (400 MHz, $CDCl_3$)

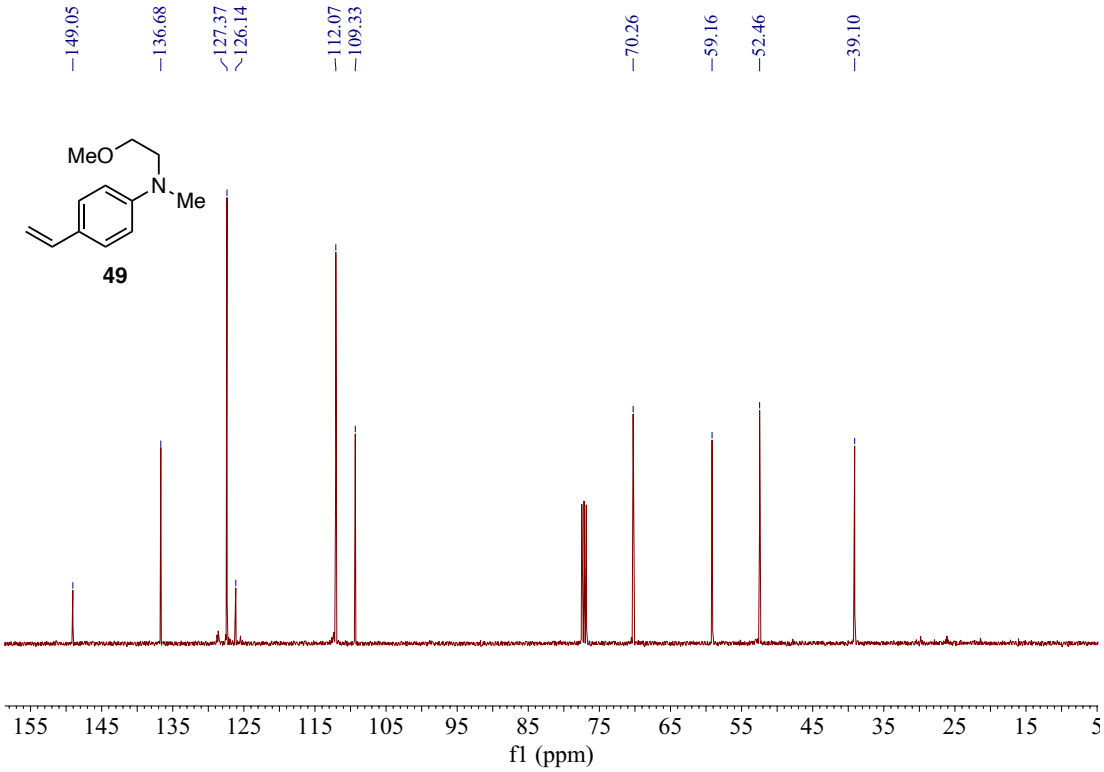

^{13}C NMR of Compound **49** (101 MHz, $CDCl_3$)

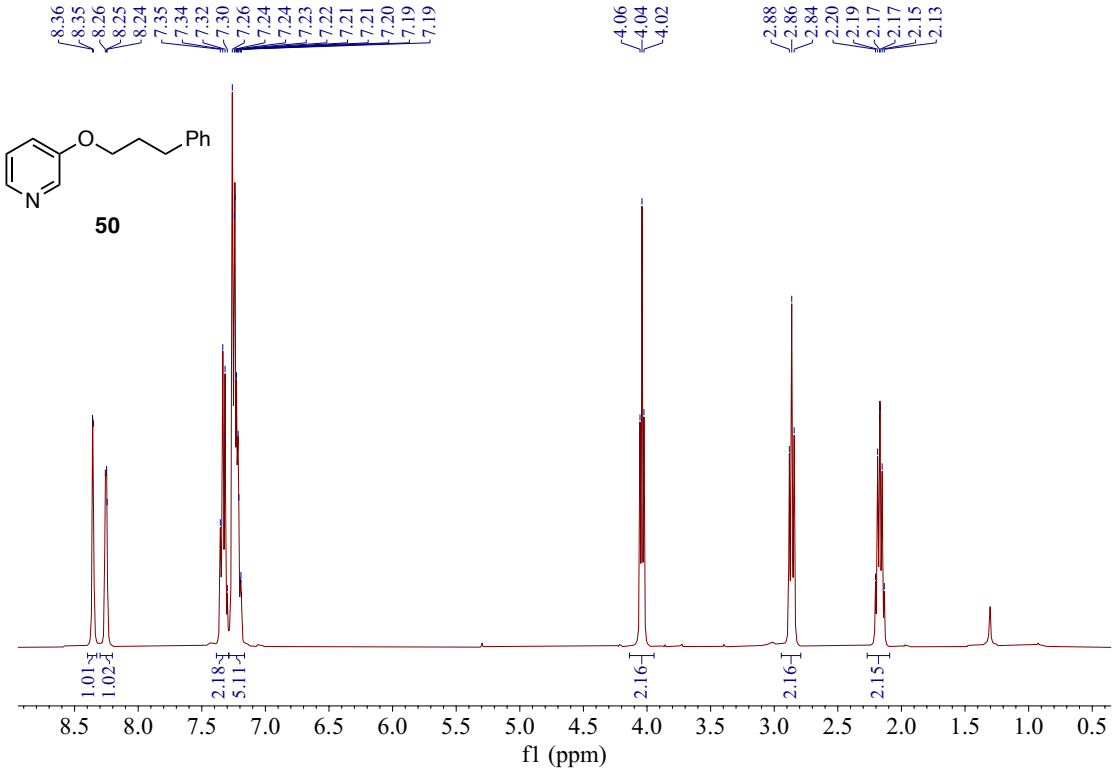

^{1}H NMR of Compound **50** (400 MHz, $CDCl_3$)

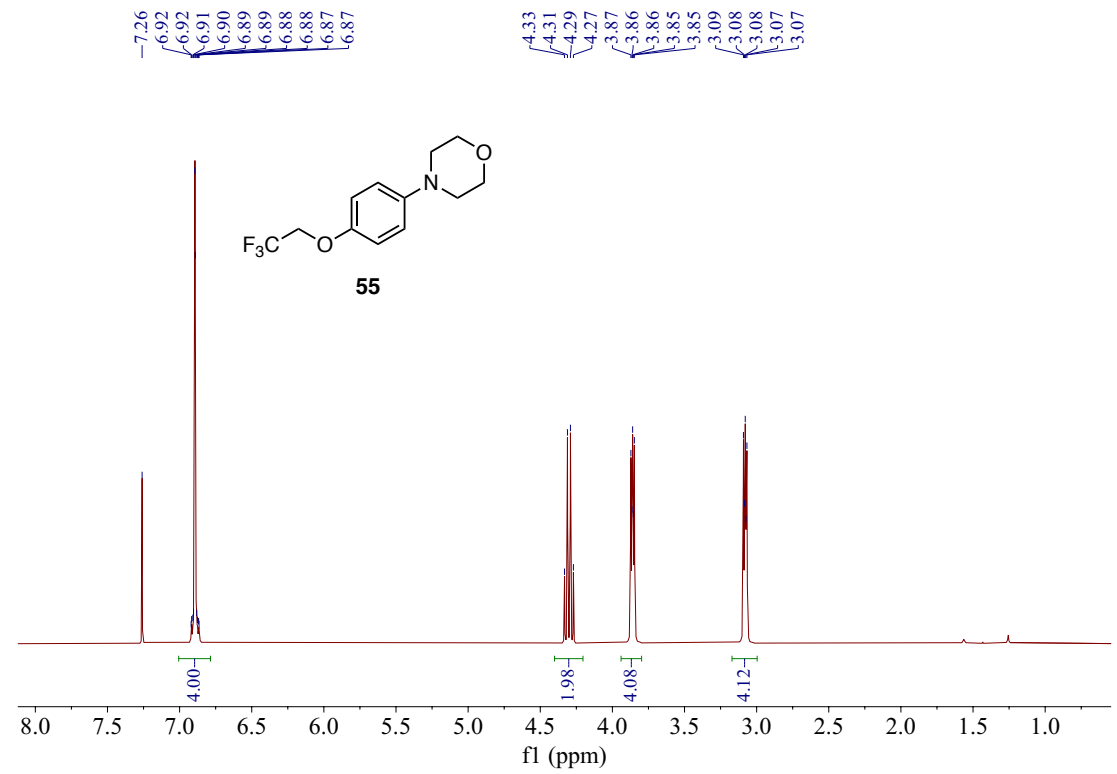

^{1}H NMR of Compound **55** (400 MHz, $CDCl_3$)

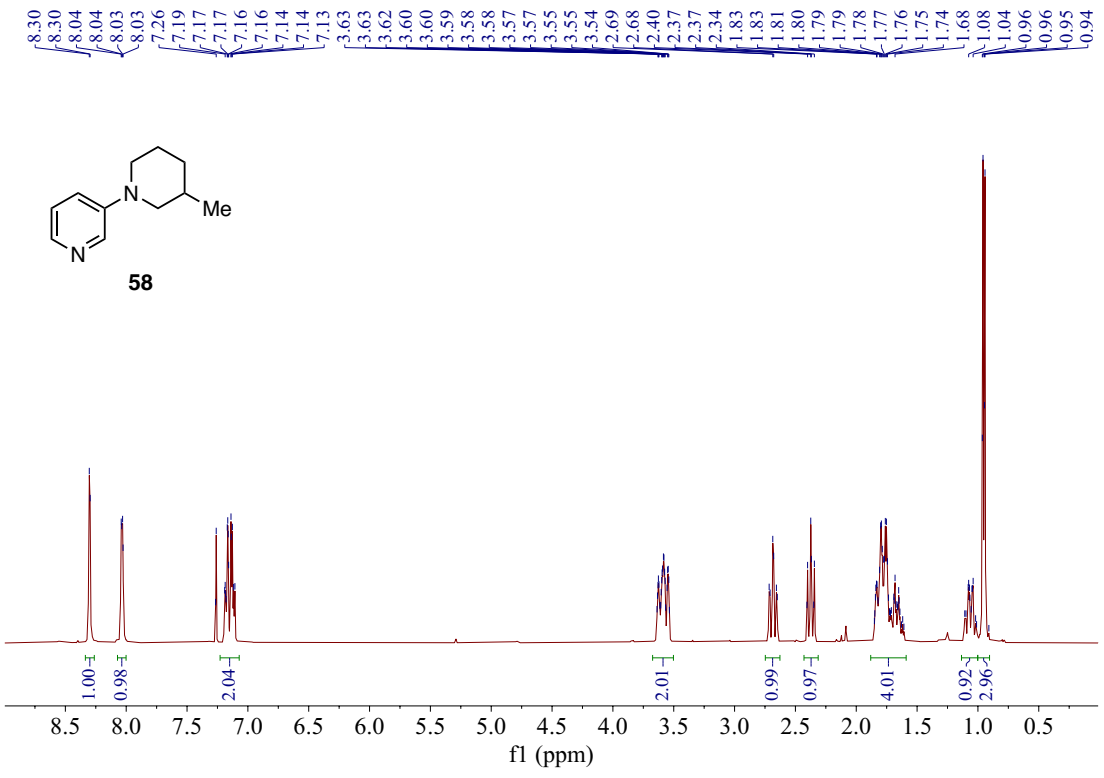

^{1}H NMR of Compound **58** (400 MHz, $CDCl_3$)

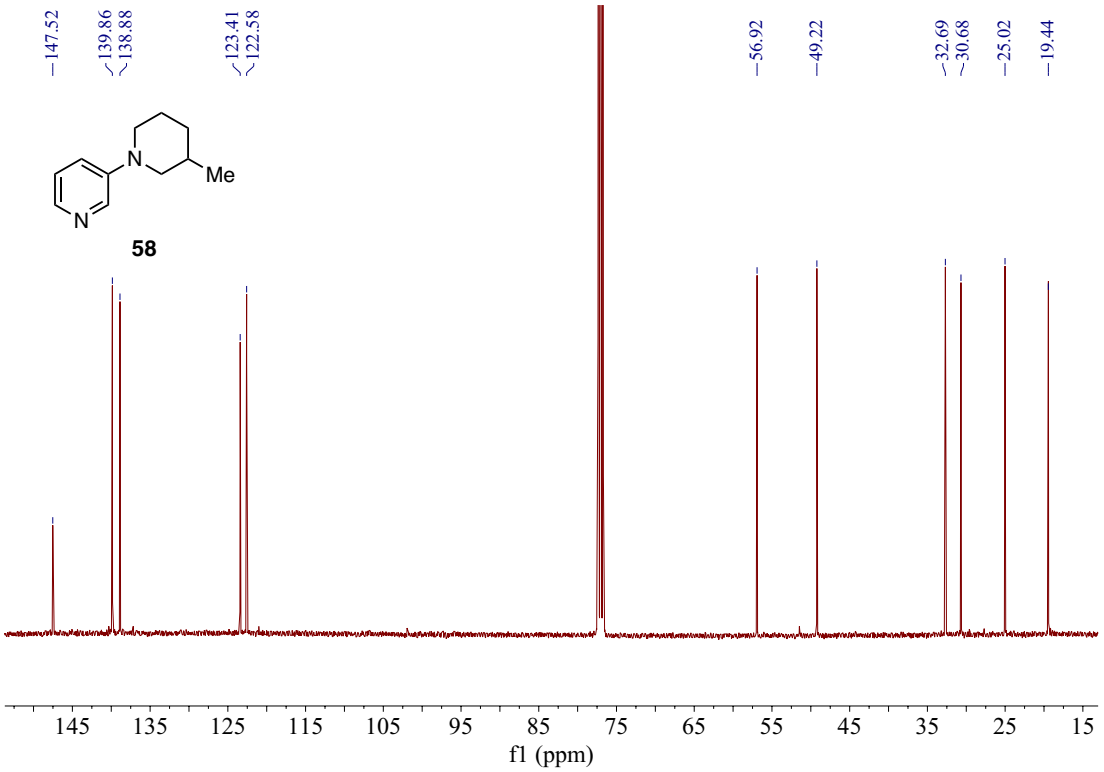

^{13}C NMR of Compound **58** (101 MHz, $CDCl_3$)

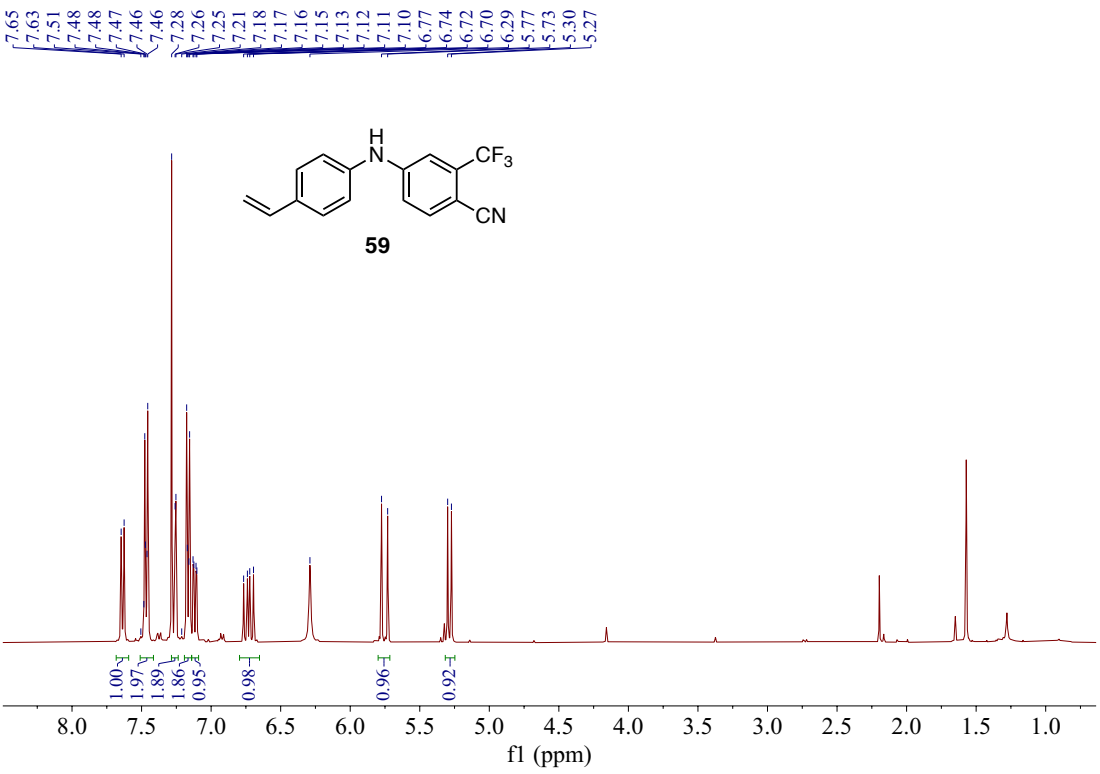

^{1}H NMR of Compound **59** (400 MHz, $CDCl_3$)

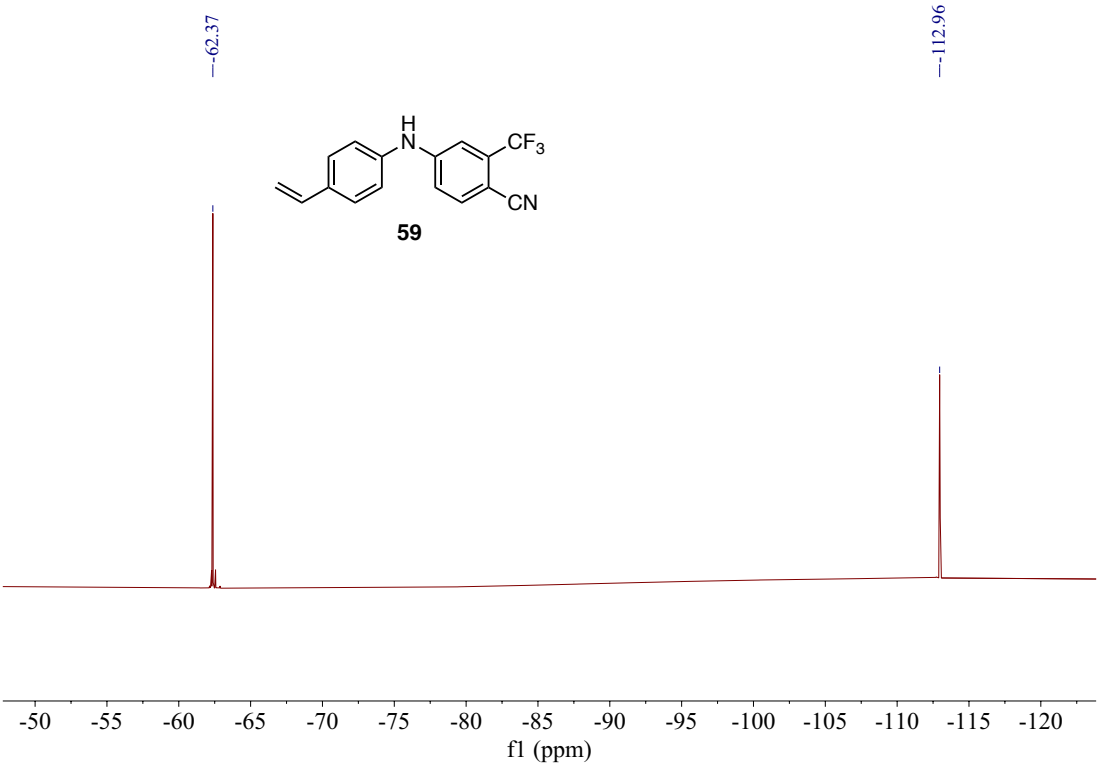

^{19}F NMR of Compound **59** (376 MHz, $CDCl_3$)

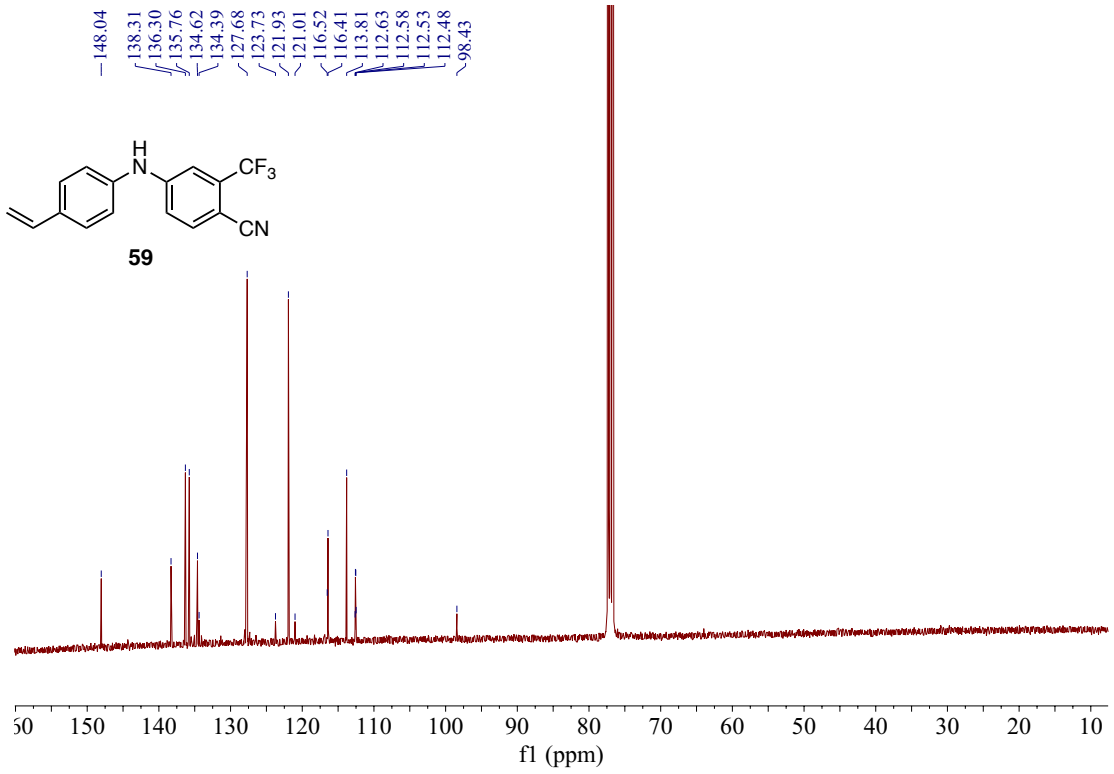

^{13}C NMR of Compound **59** (101 MHz, $CDCl_3$)

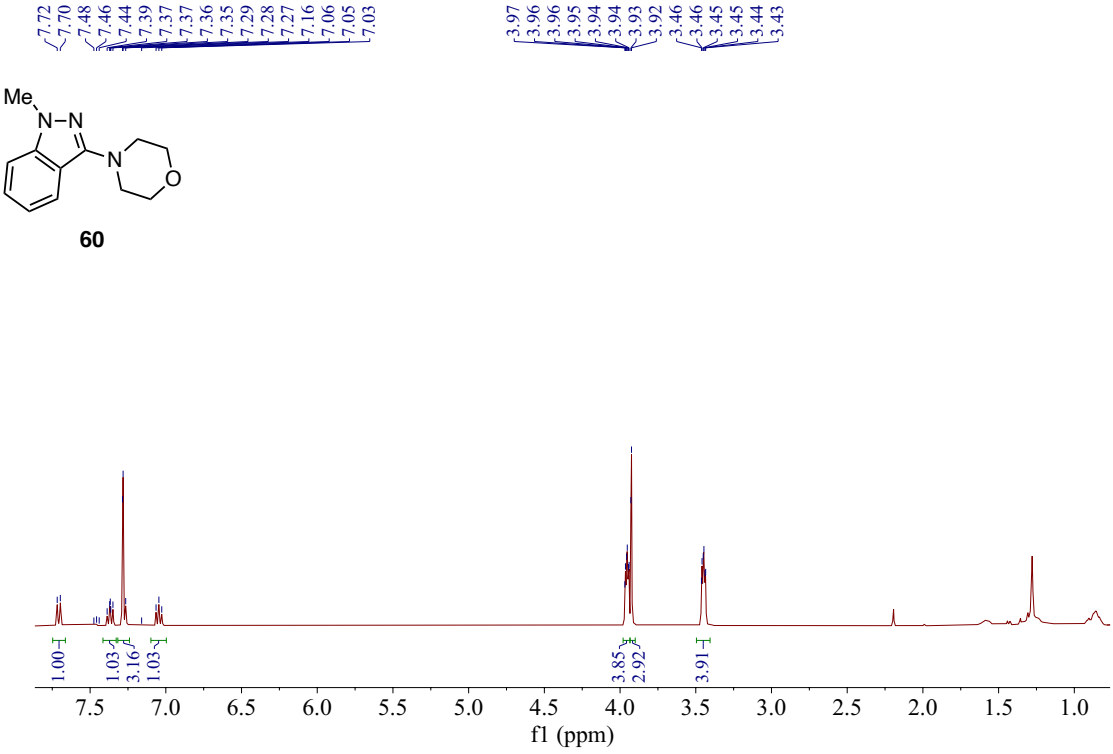

^{1}H NMR of Compound **60** (400 MHz, $CDCl_3$)

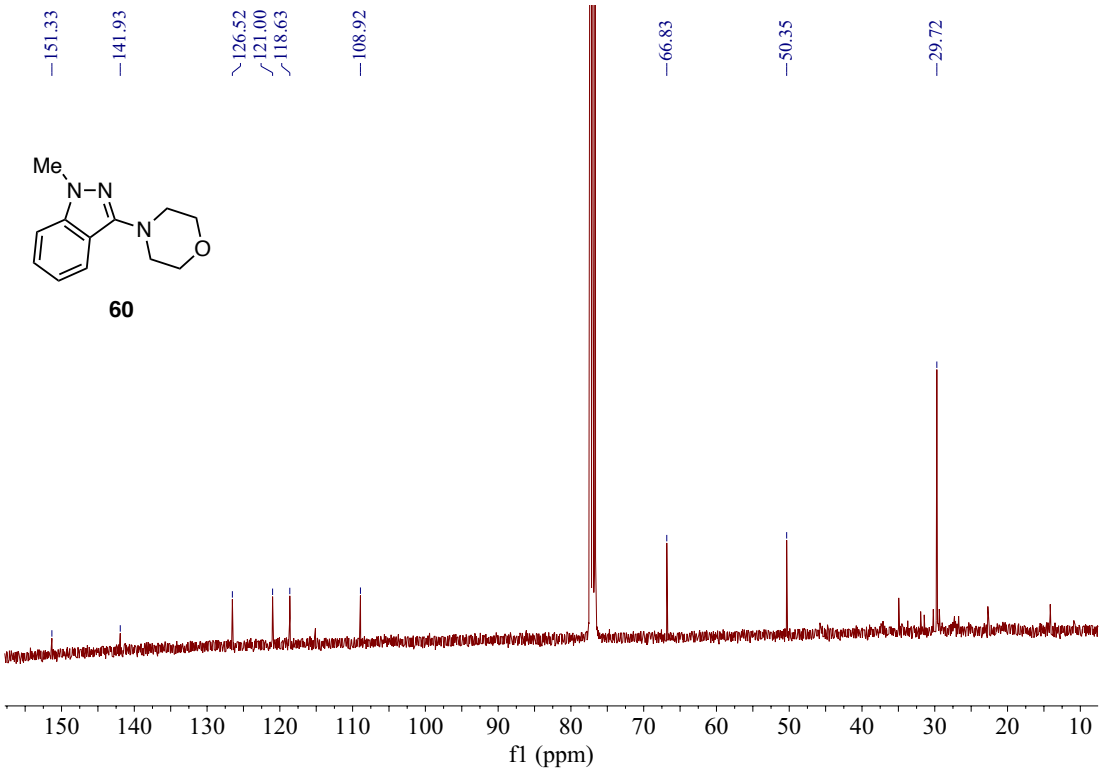

^{13}C NMR of Compound **60** (101 MHz, $CDCl_3$)

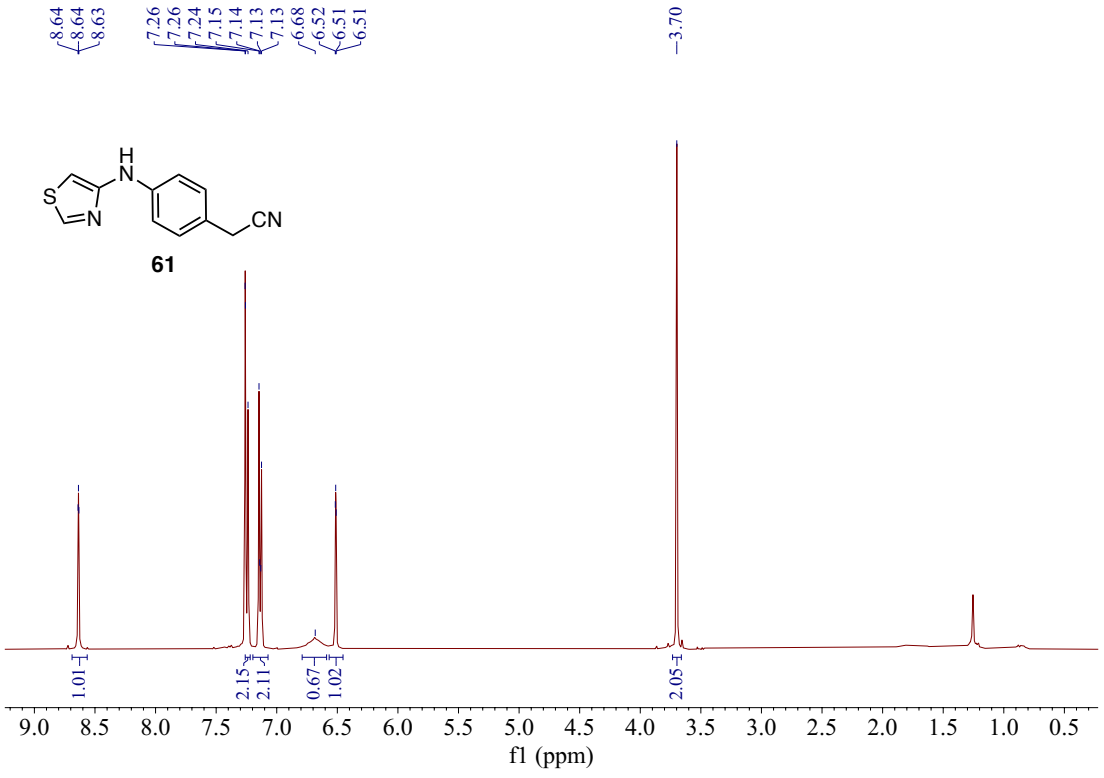

^{1}H NMR of Compound **61** (400 MHz, $CDCl_3$)

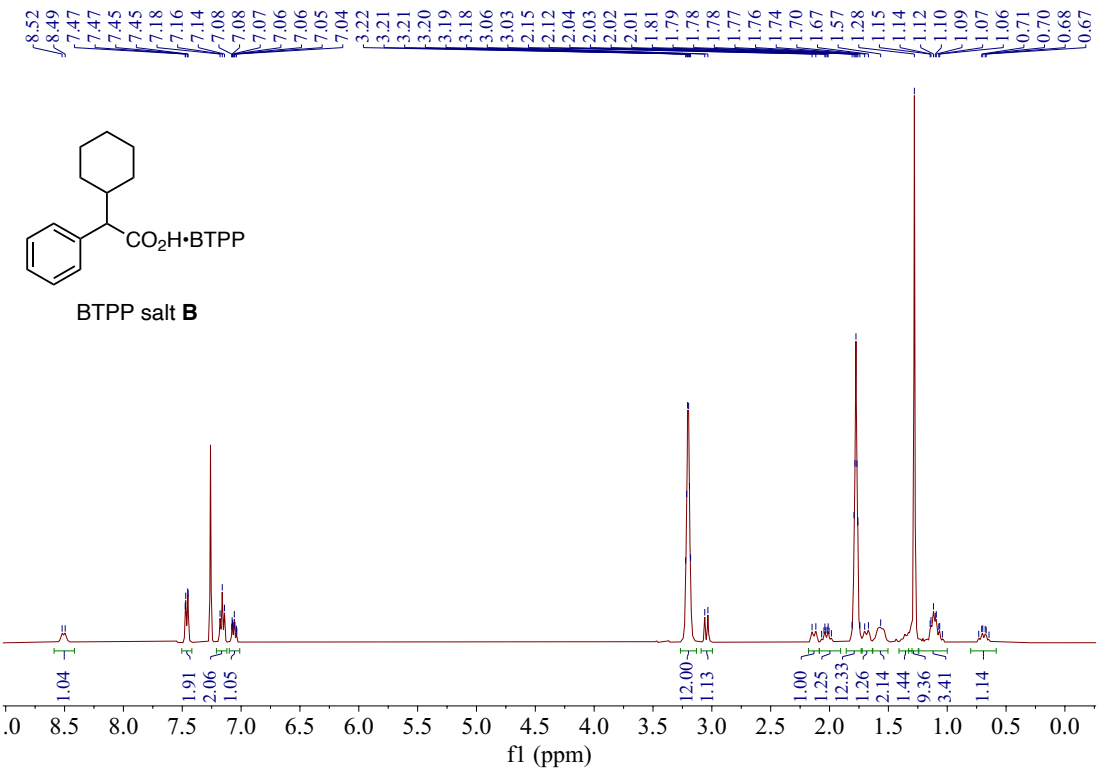

^{1}H NMR of BTPP salt **B** (400 MHz, $CDCl_3$)

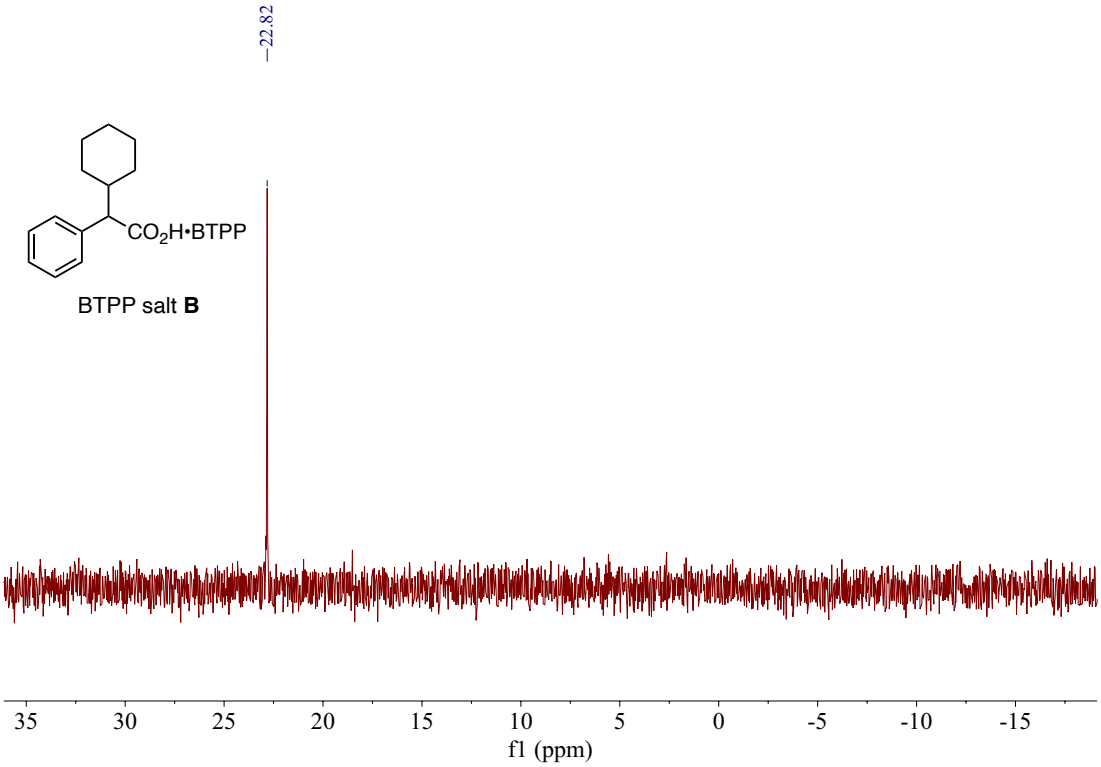

^{31}P NMR of BTPP Salt **B** (162 MHz, $CDCl_3$)

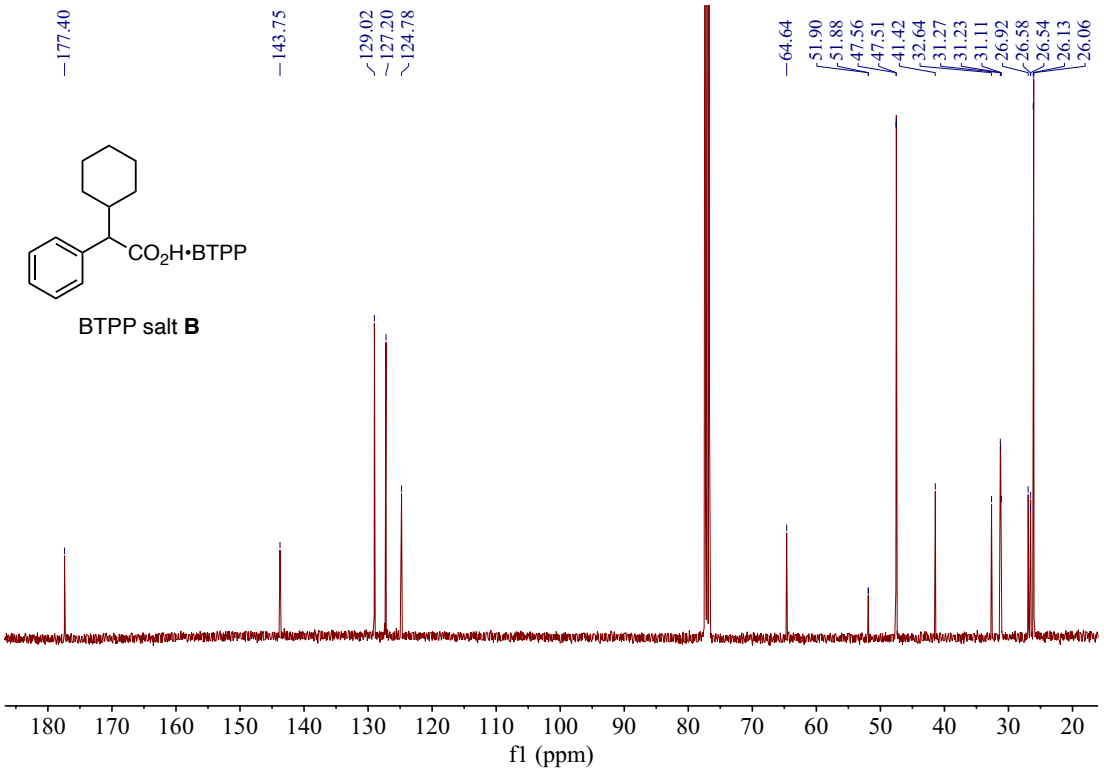

^{13}C NMR of BTPP salt **B** (101 MHz, $CDCl_3$)

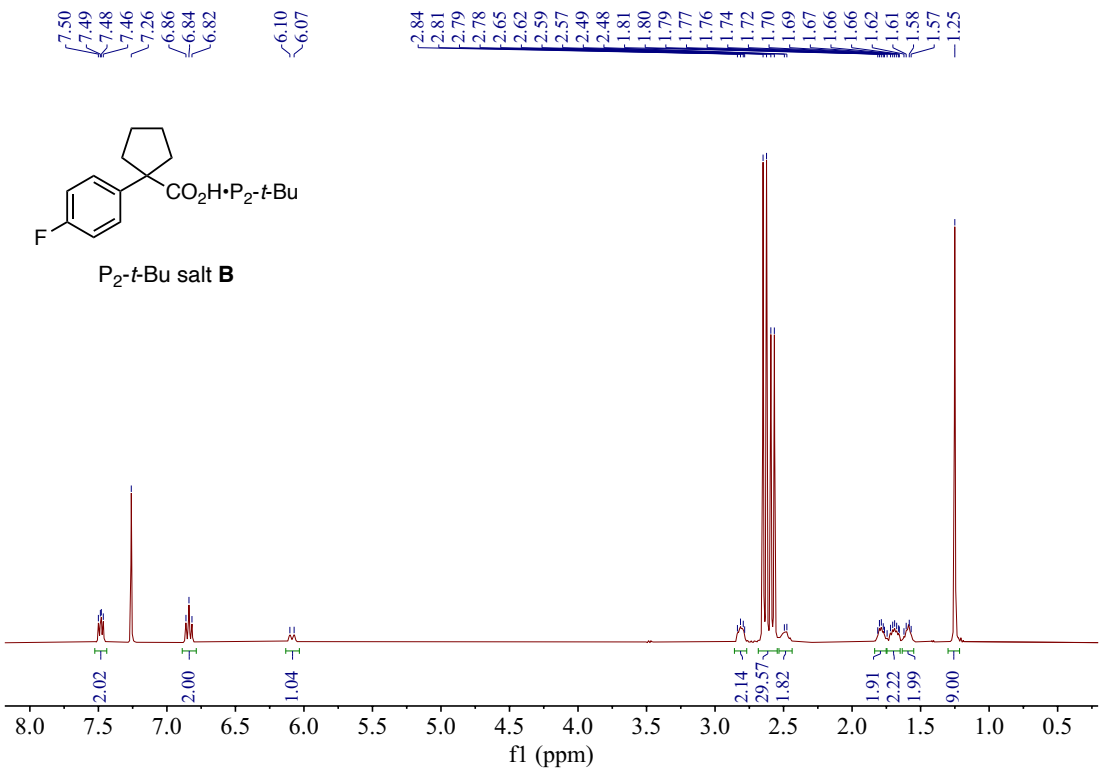

^{1}H NMR of P_2-*t*-Bu salt **B** (400 MHz, $CDCl_3$)

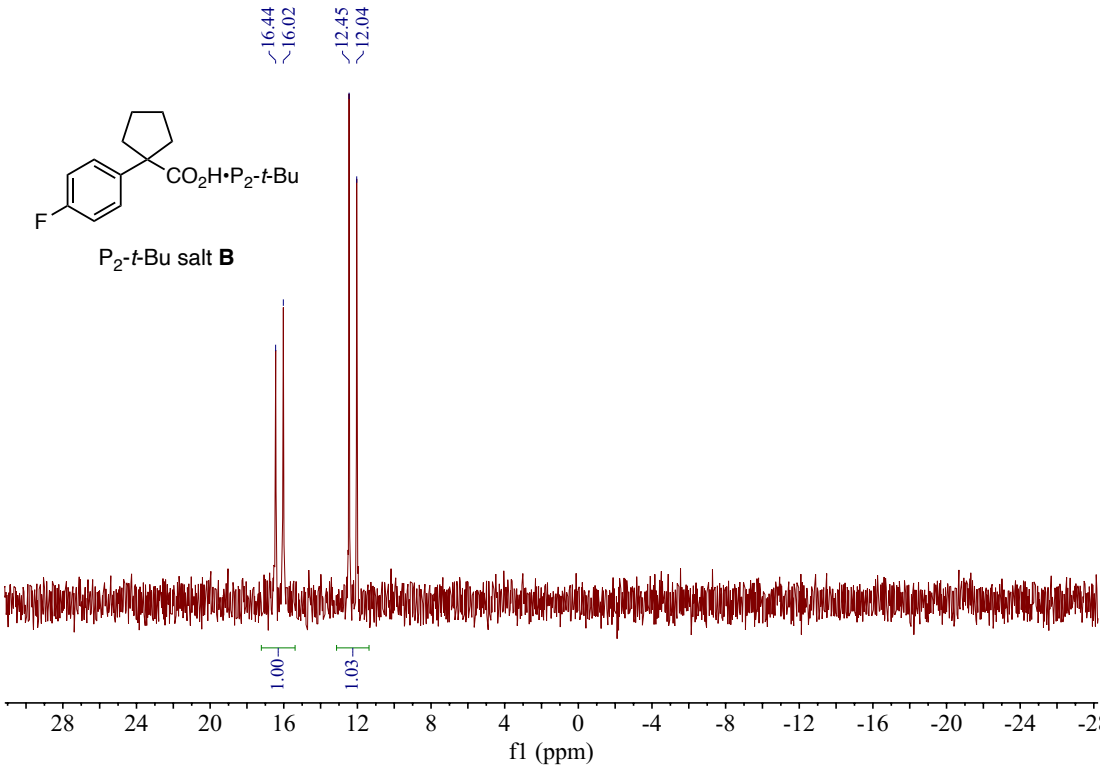

^{31}P NMR of P_2-*t*-Bu Salt **B** (162 MHz, $CDCl_3$)

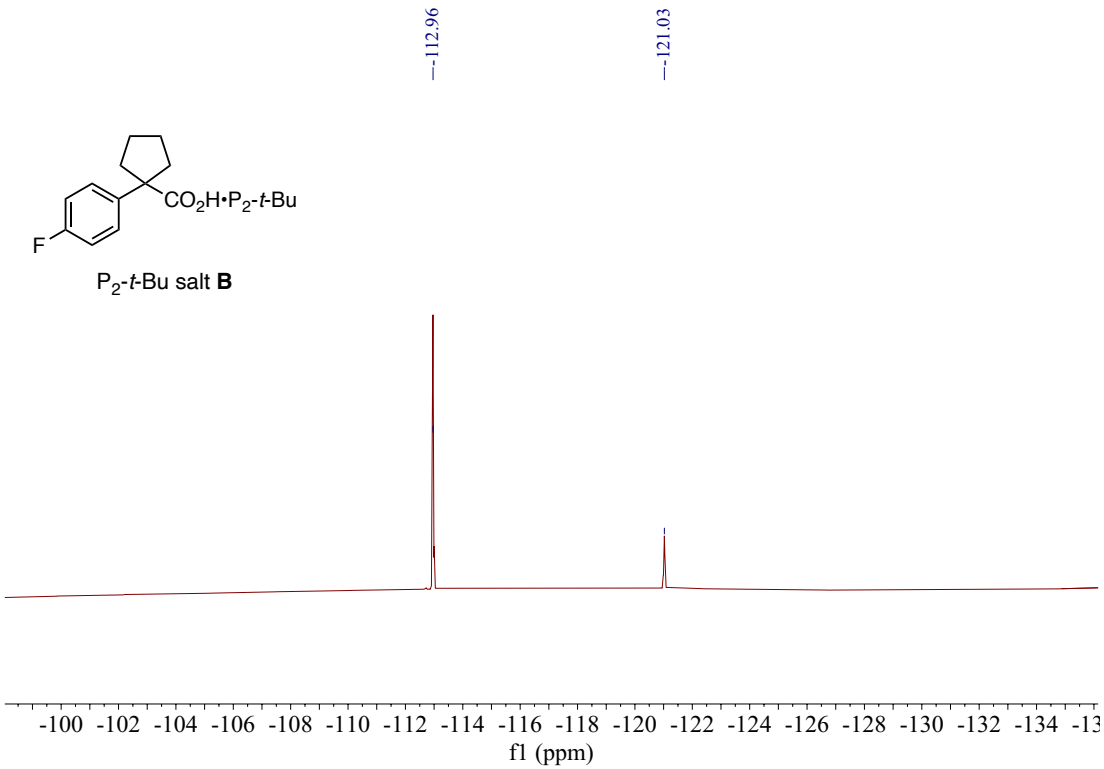

^{19}F NMR of P_2-*t*-Bu Salt **B** (376 MHz, $CDCl_3$)

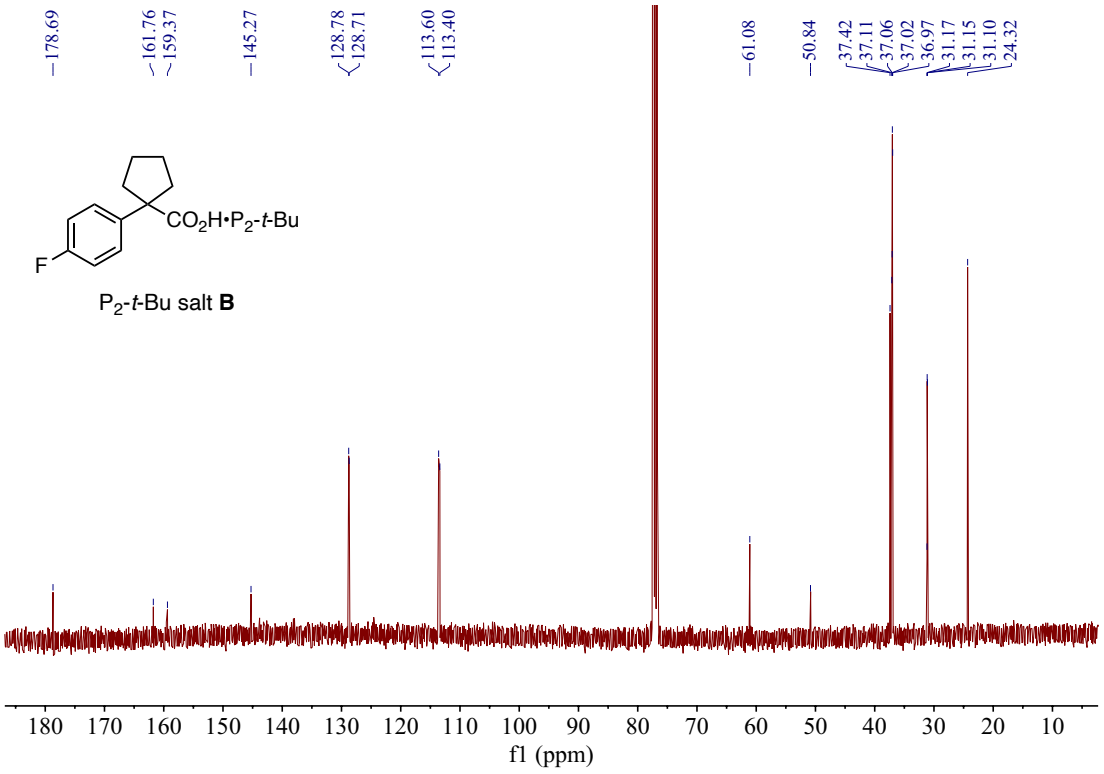

^{13}C NMR of P_2-*t*-Bu salt **B** (101 MHz, $CDCl_3$)

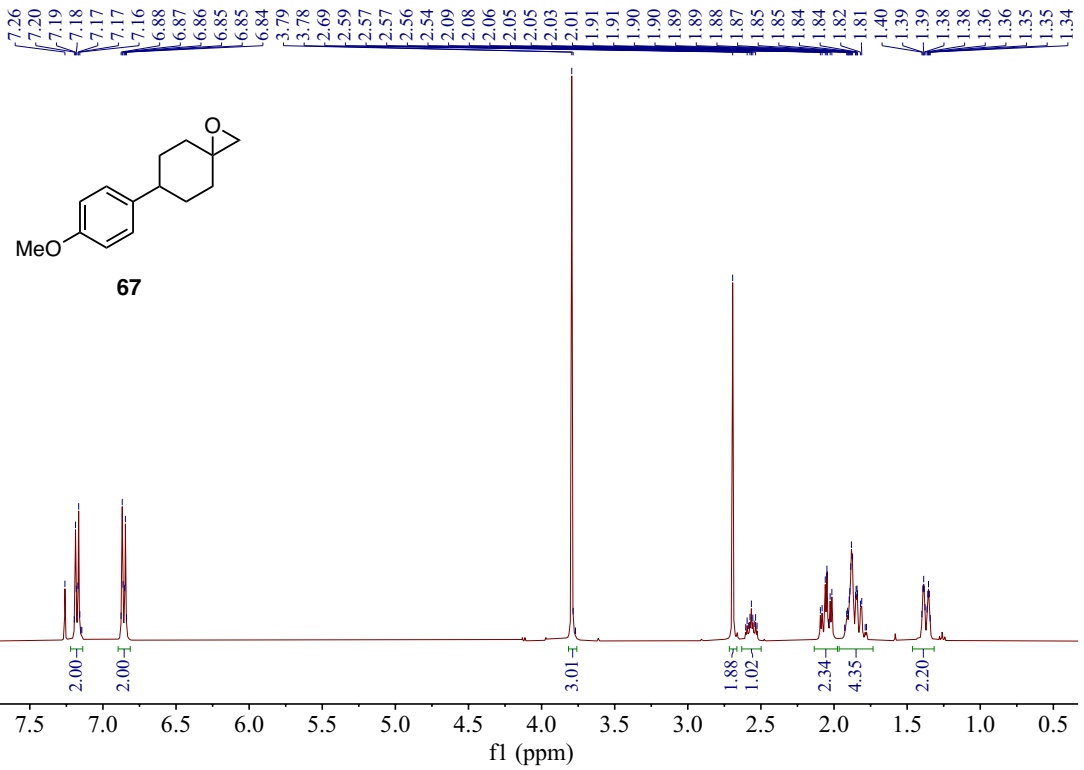

^{1}H NMR of Compound **67** (400 MHz, $CDCl_3$)

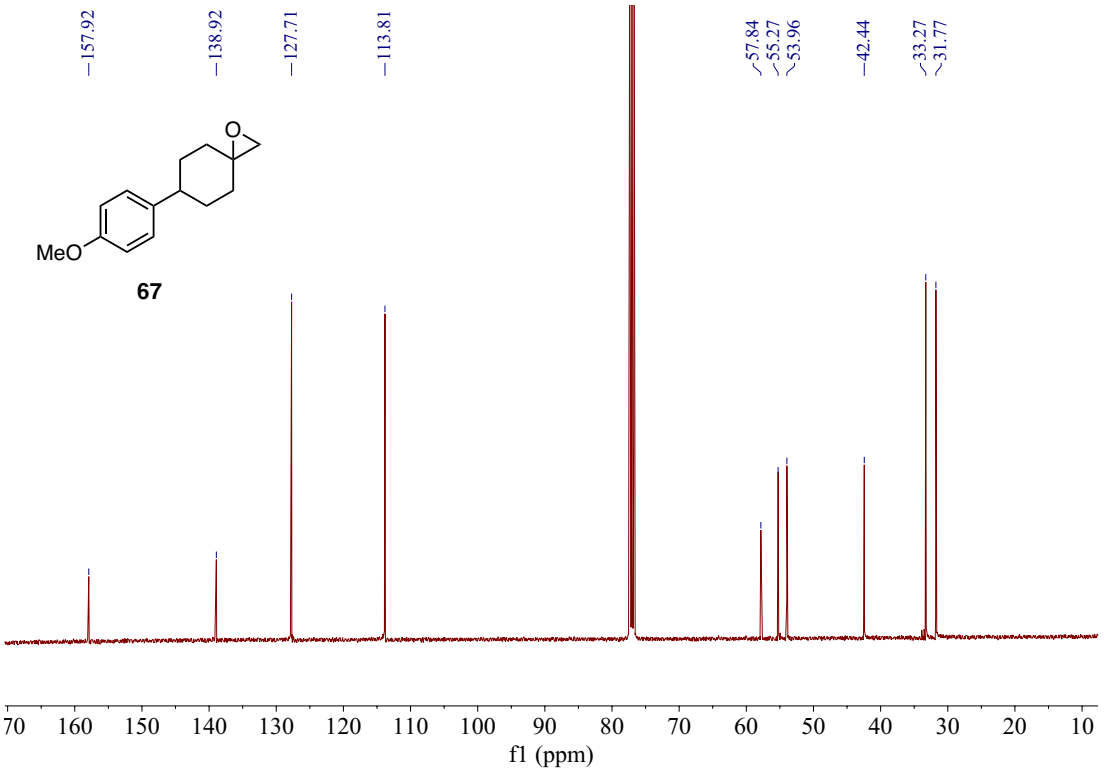

^{13}C NMR of Compound **67** (101 MHz, $CDCl_3$)

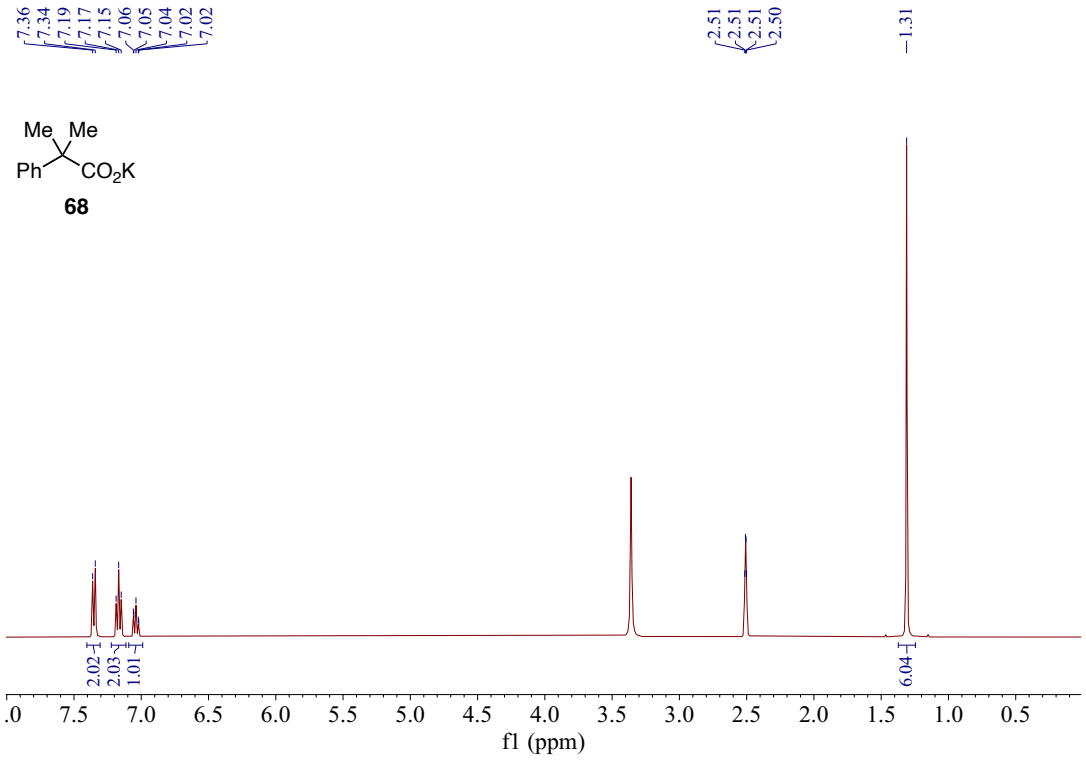

^{1}H NMR of Compound **68** (400 MHz, DMSO-d_6)

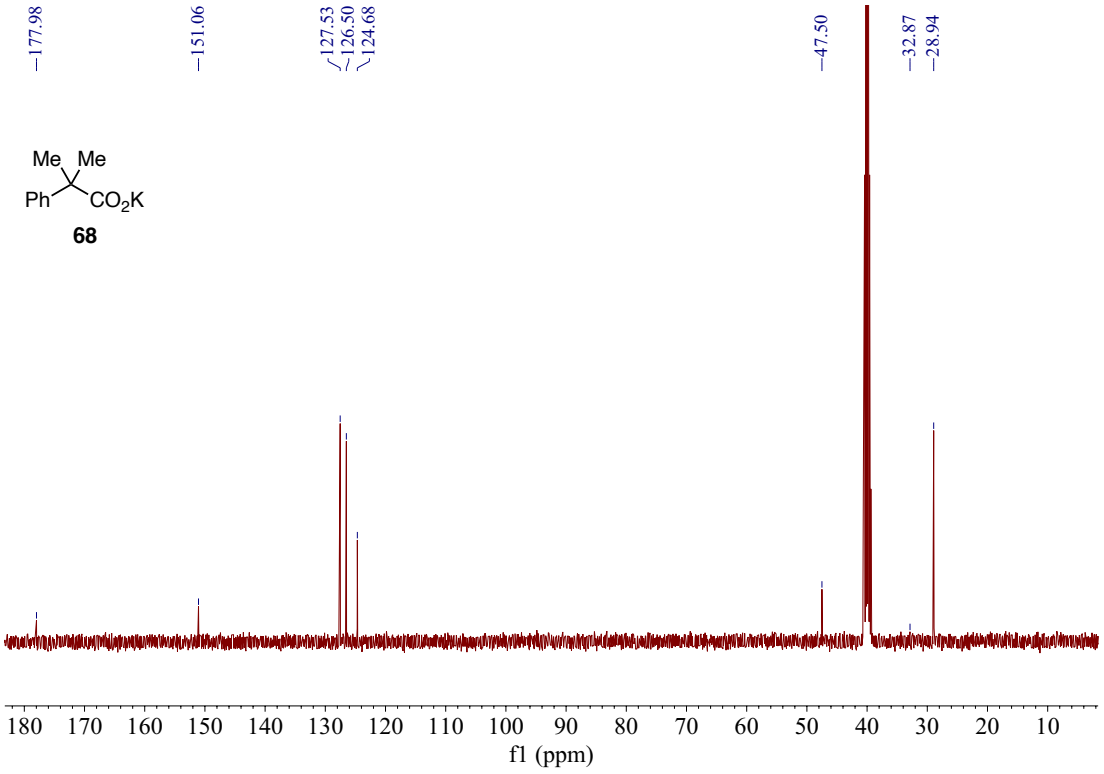

^{13}C NMR of Compound **68** (101 MHz, DMSO-d_6)

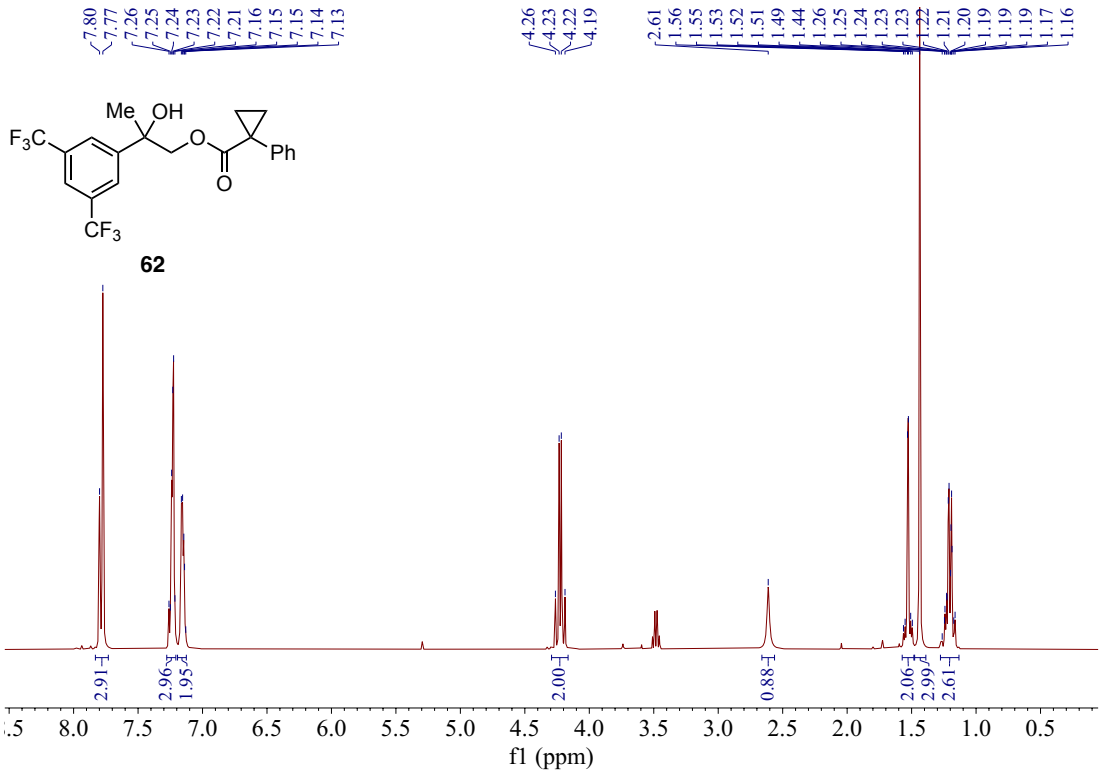

^{1}H NMR of Compound **62** (400 MHz, $CDCl_3$)

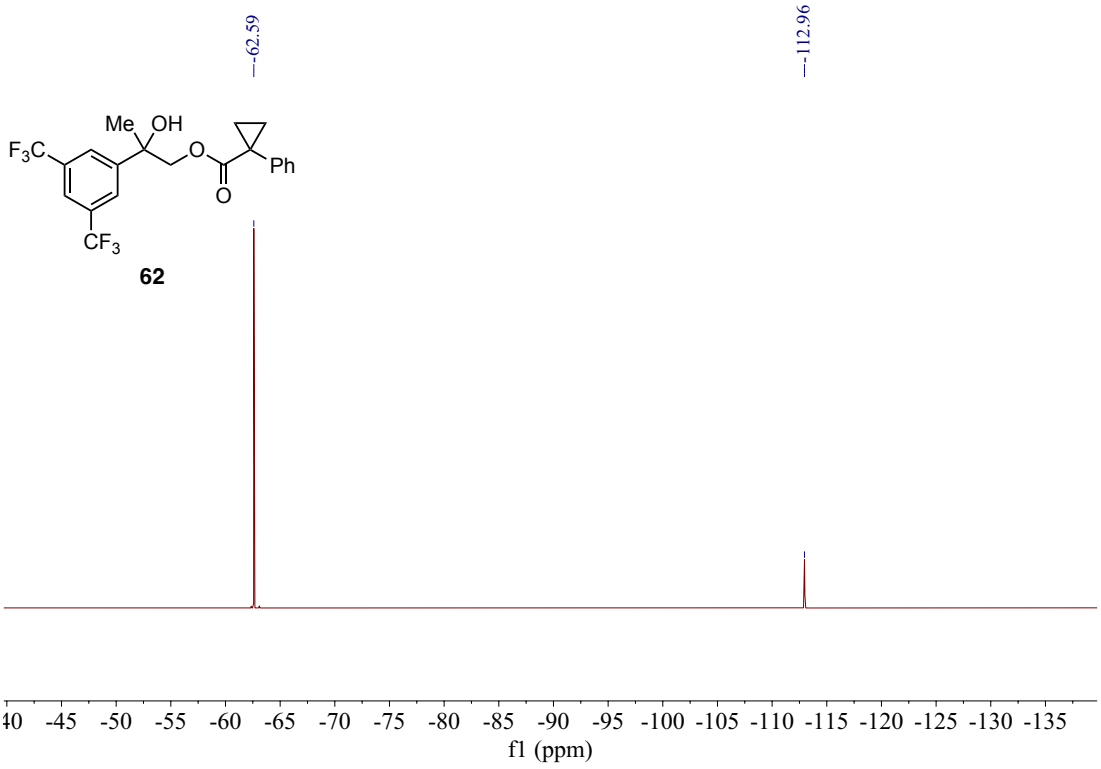

^{19}F NMR of Compound **62** (376 MHz, $CDCl_3$)

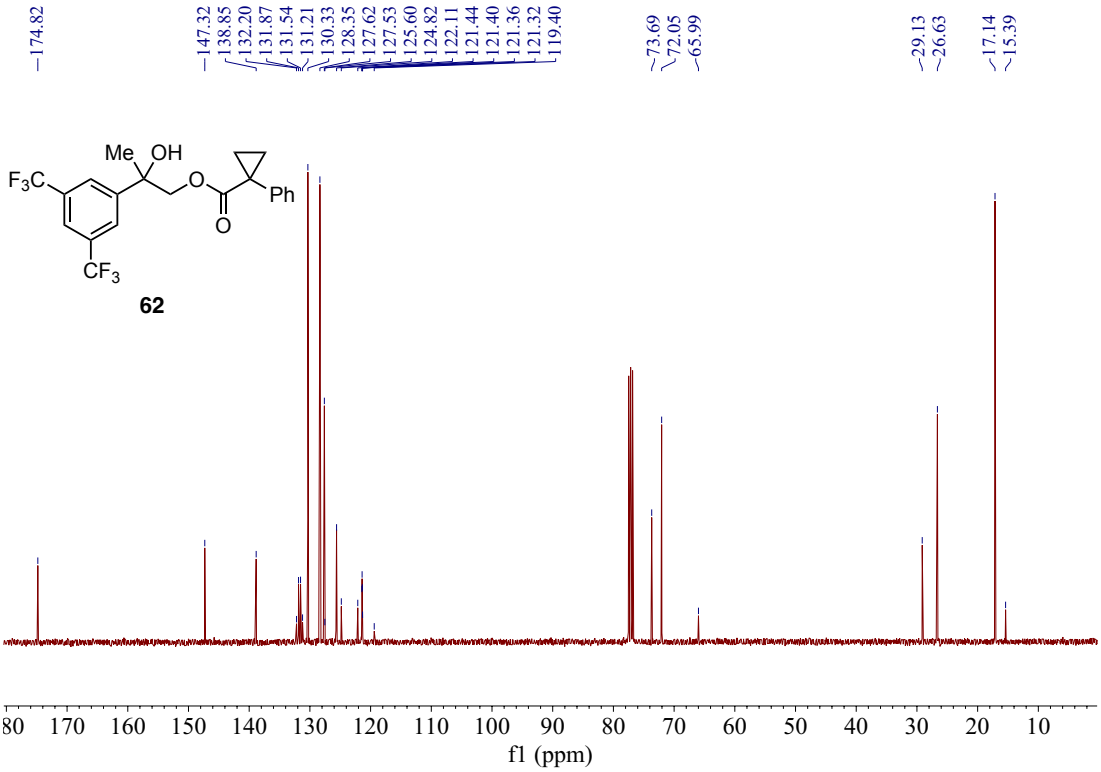

^{13}C NMR of Compound **62** (101 MHz, $CDCl_3$)

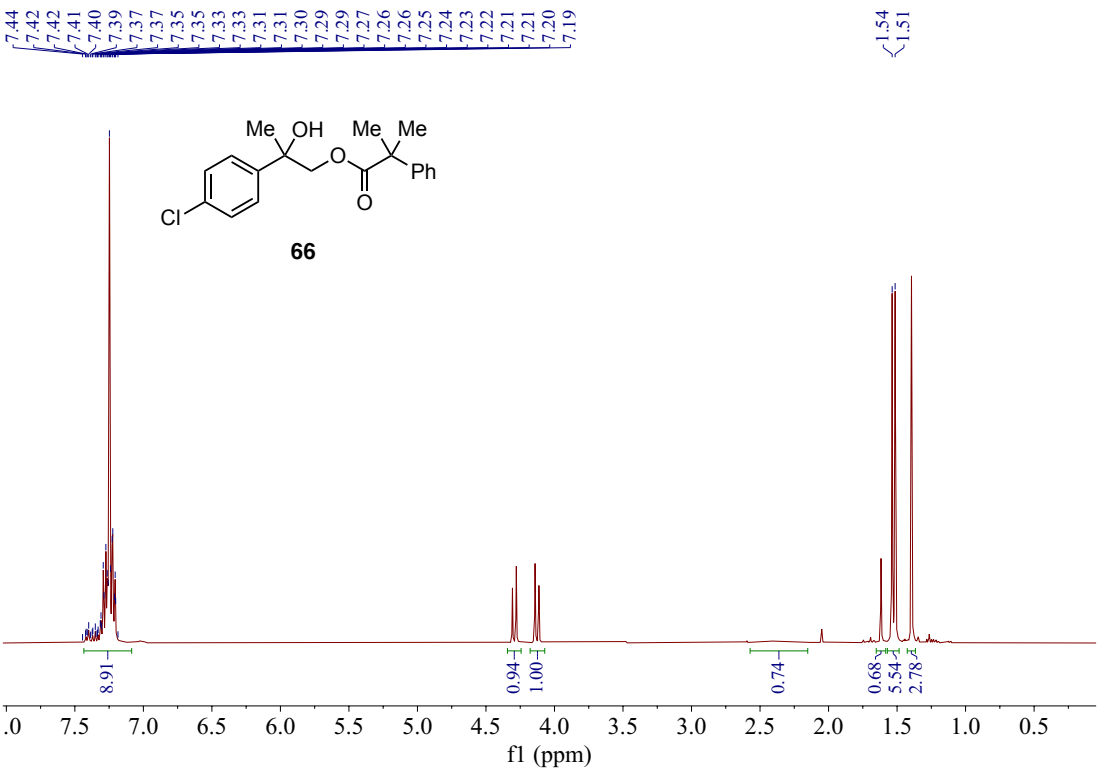

^{1}H NMR of Compound **66** (400 MHz, $CDCl_3$)

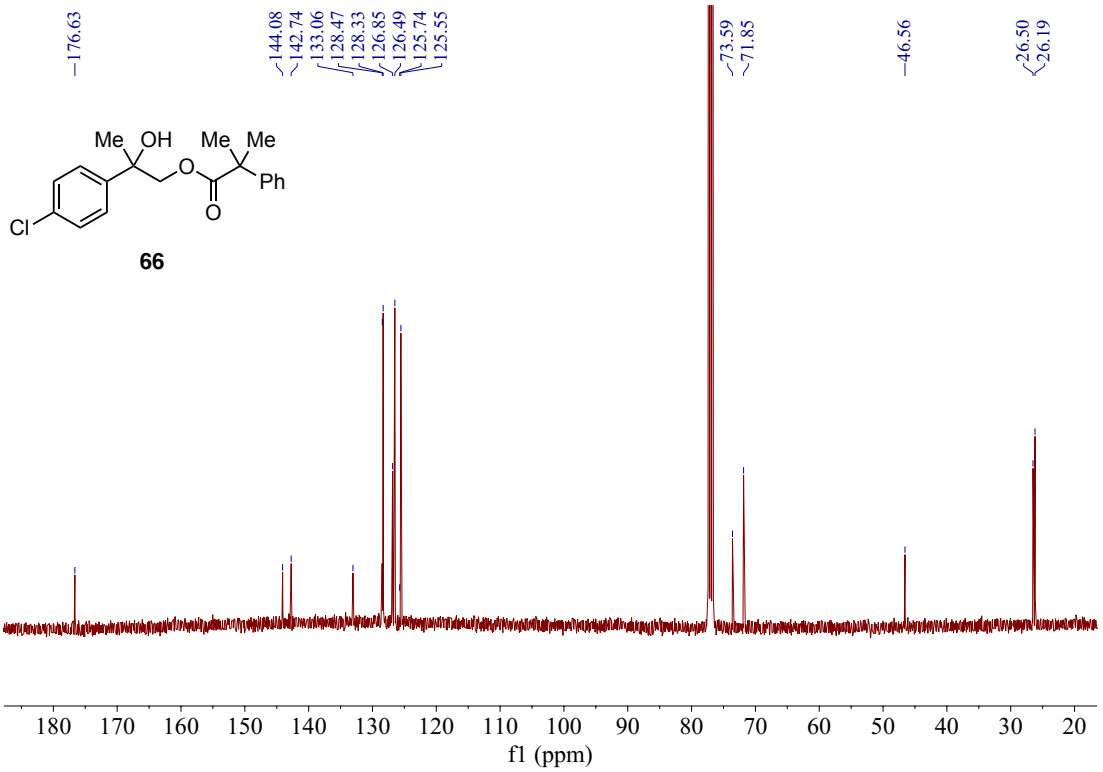

^{13}C NMR of Compound **66** (101 MHz, $CDCl_3$)

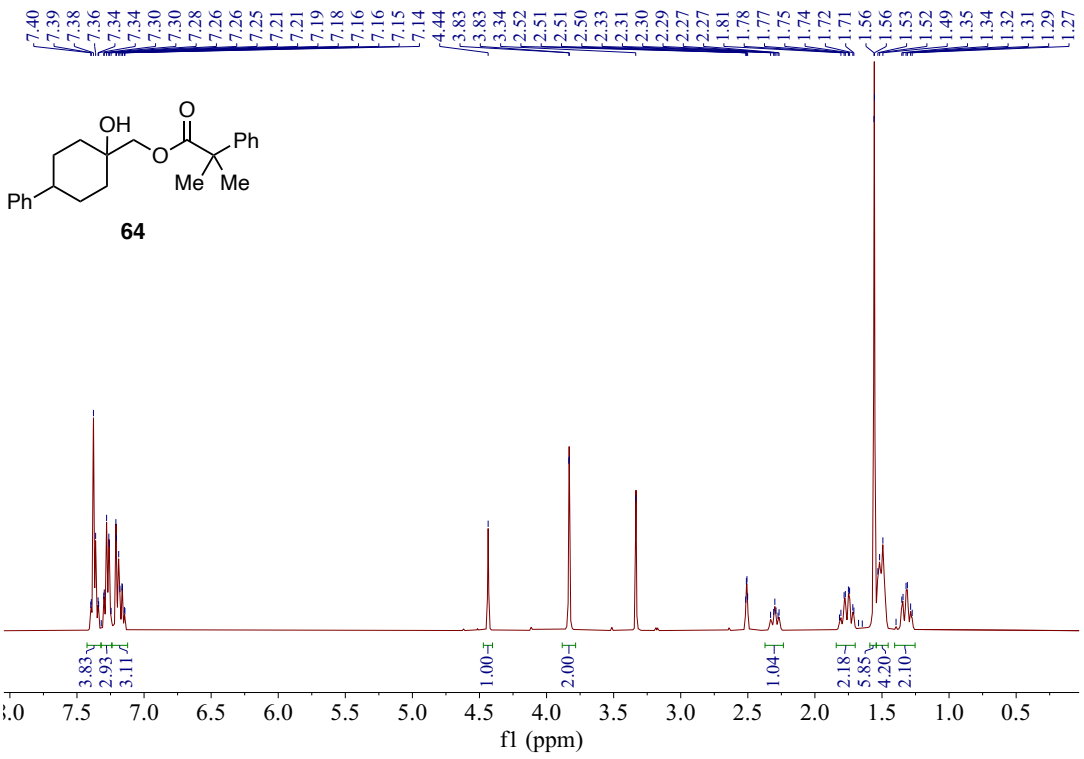

^{1}H NMR of Compound **64** (400 MHz, DMSO-d_6)

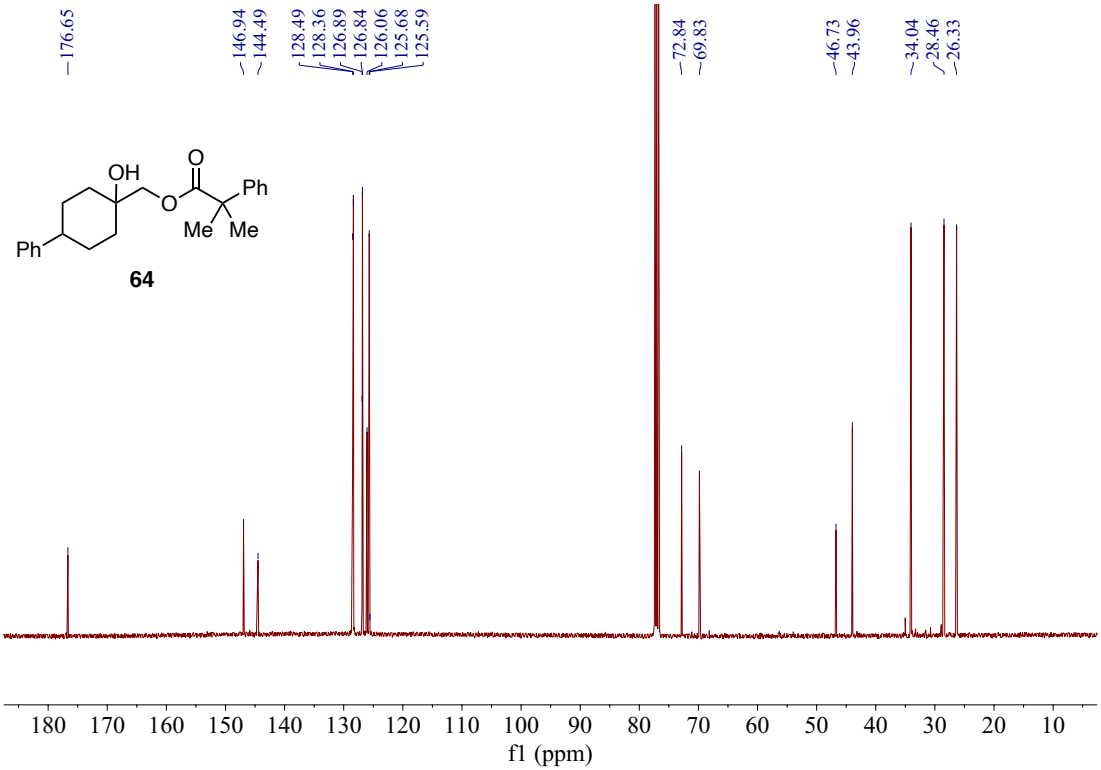

^{13}C NMR of Compound **64** (101 MHz, $CDCl_3$)

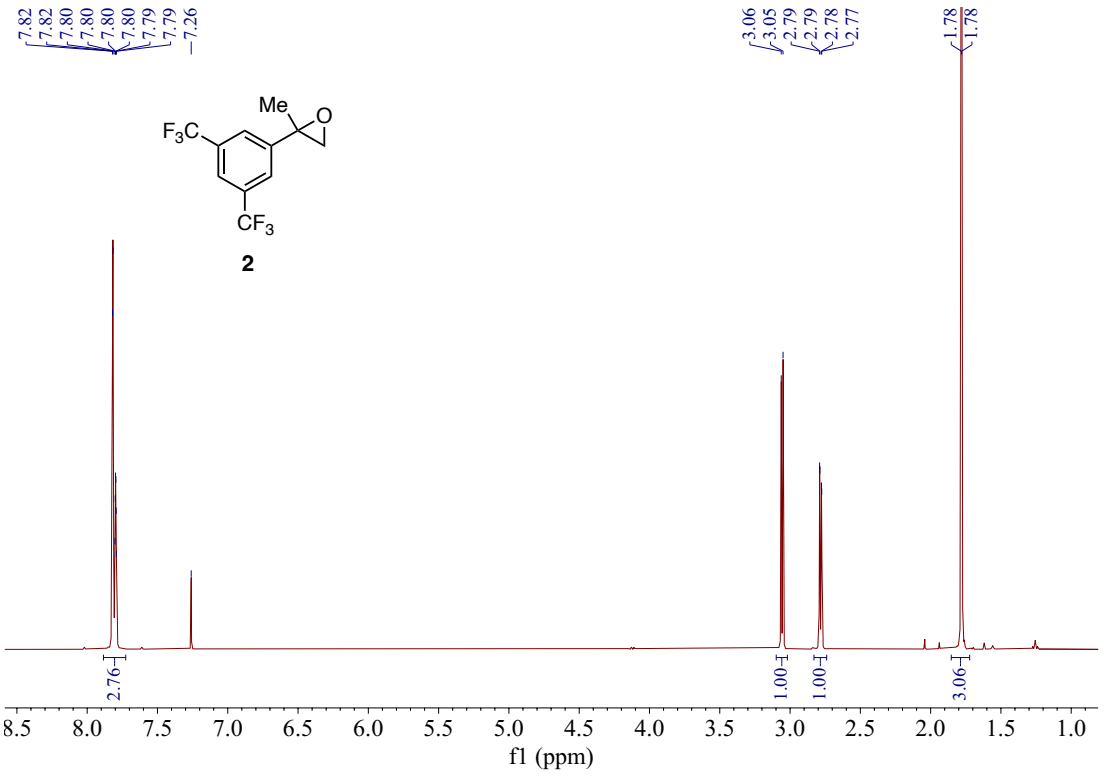

^{1}H NMR of Compound **2** (400 MHz, $CDCl_3$)

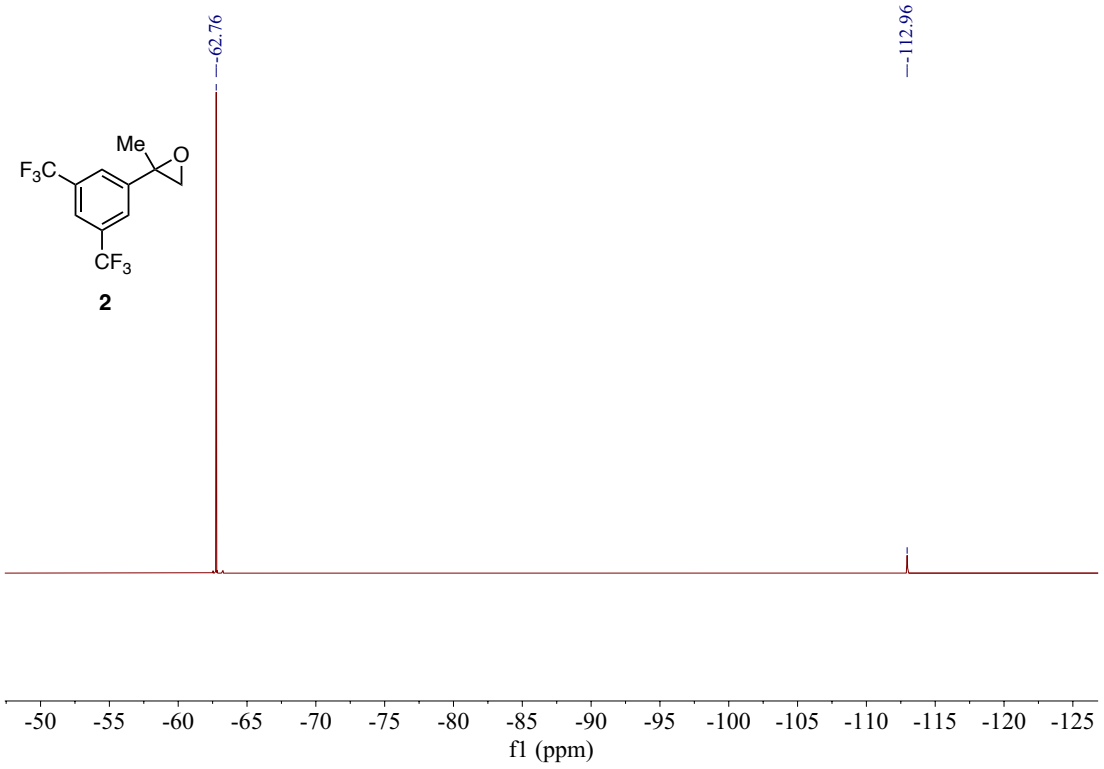

^{19}F NMR of Compound **2** (376 MHz, $CDCl_3$)

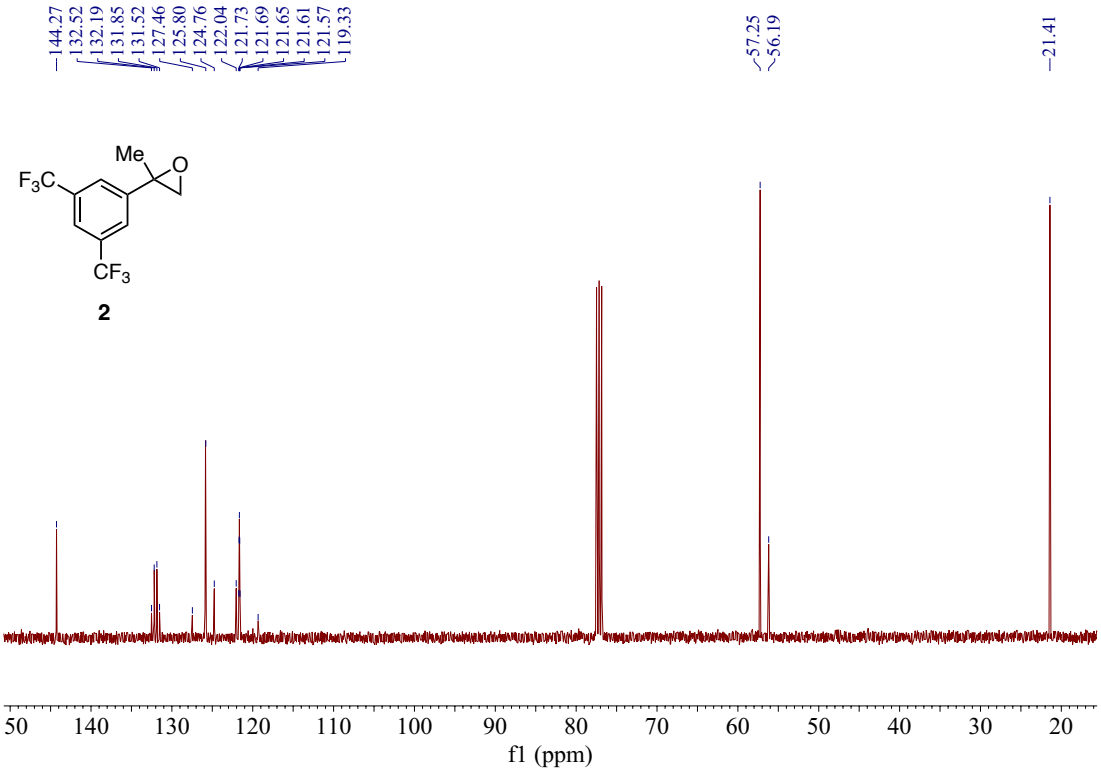

^{13}C NMR of Compound **2** (101 MHz, $CDCl_3$)

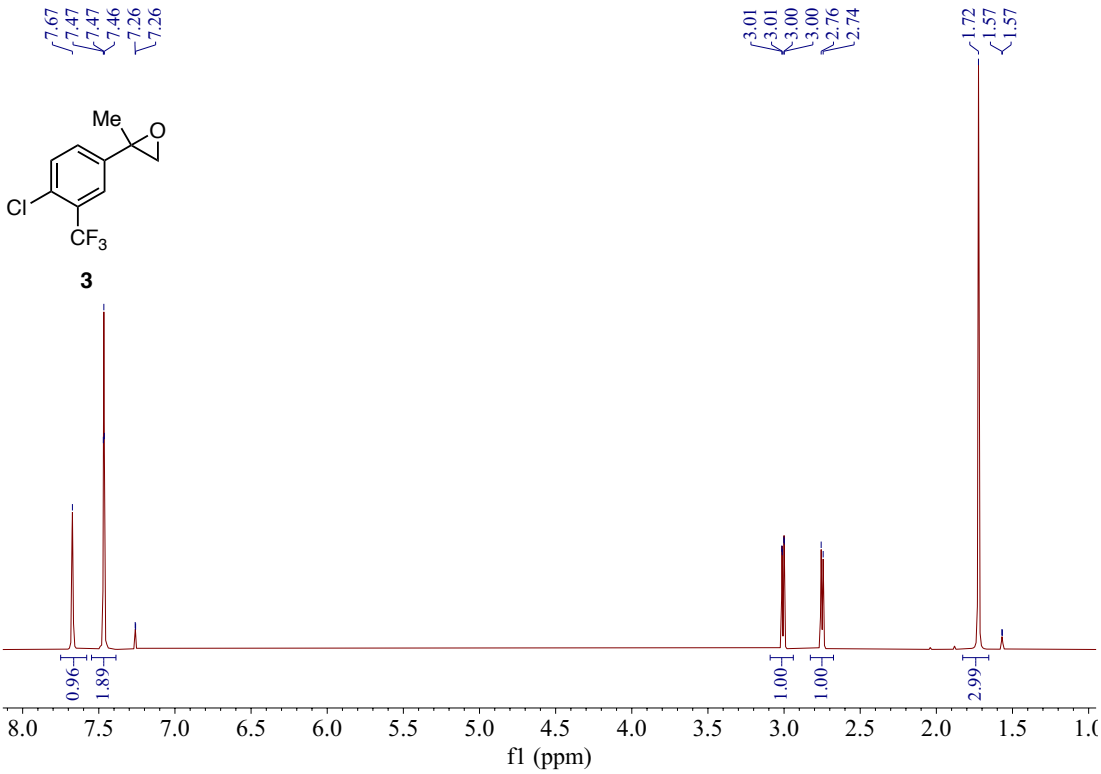

^{1}H NMR of Compound **3** (400 MHz, $CDCl_3$)

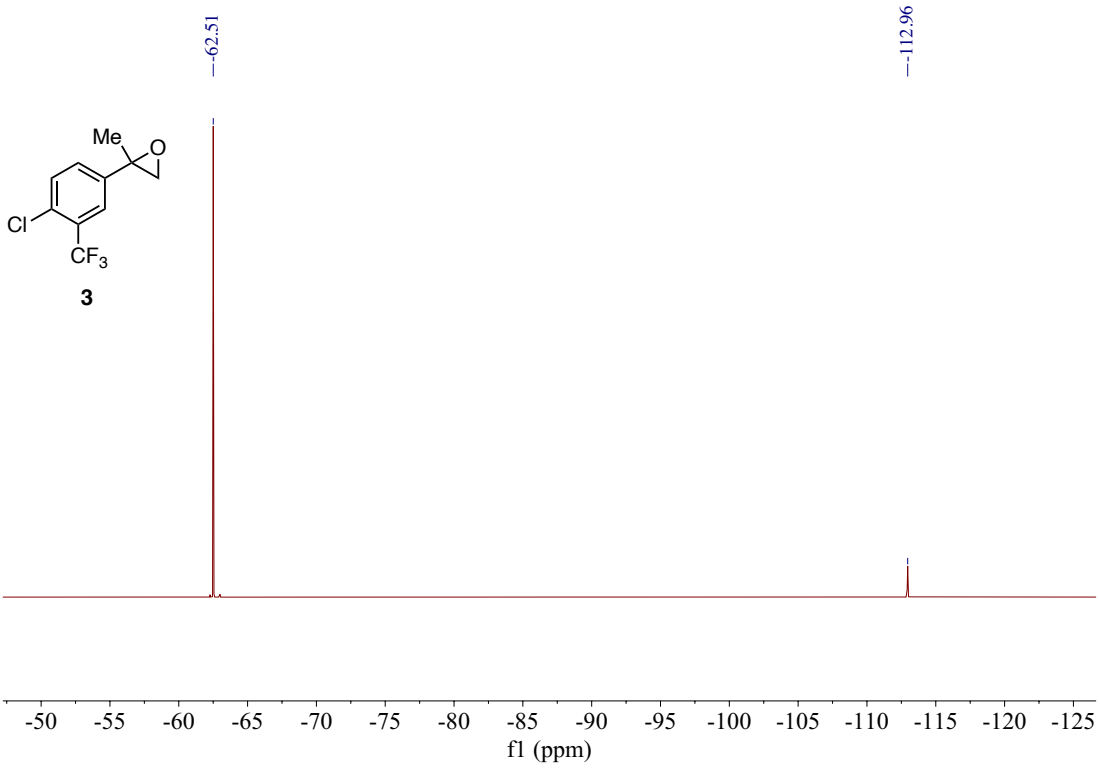

^{19}F NMR of Compound **3** (376 MHz, $CDCl_3$)

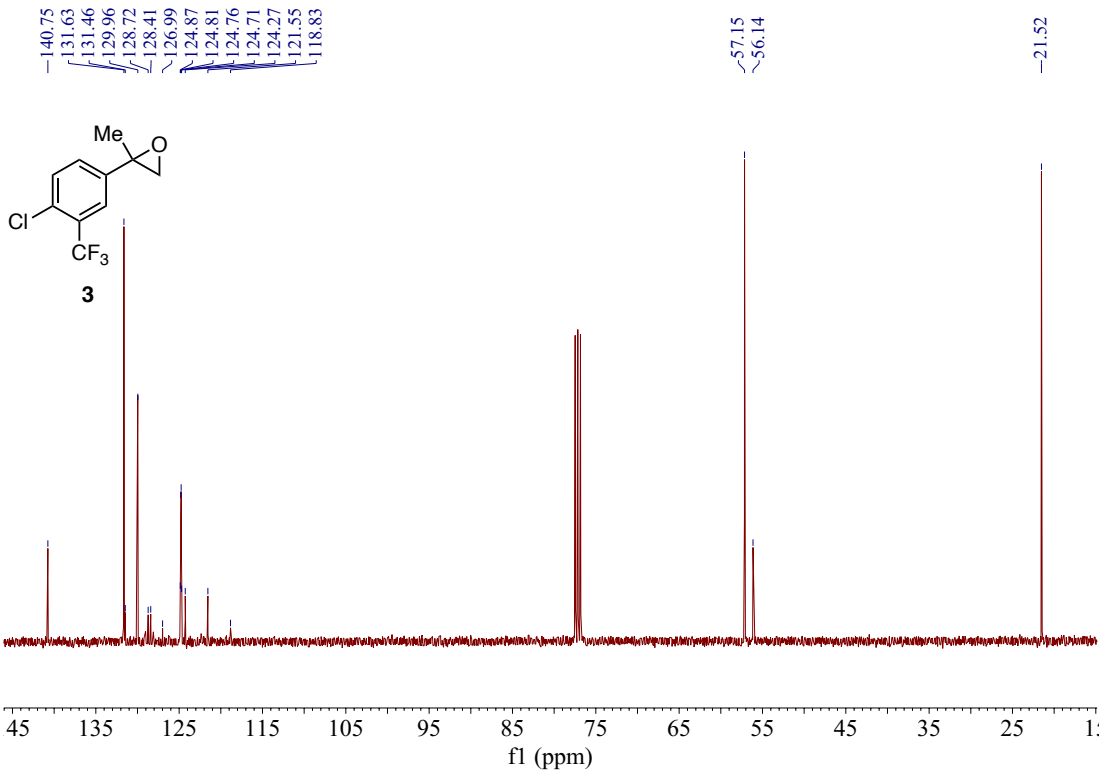

^{13}C NMR of Compound **3** (101 MHz, $CDCl_3$)

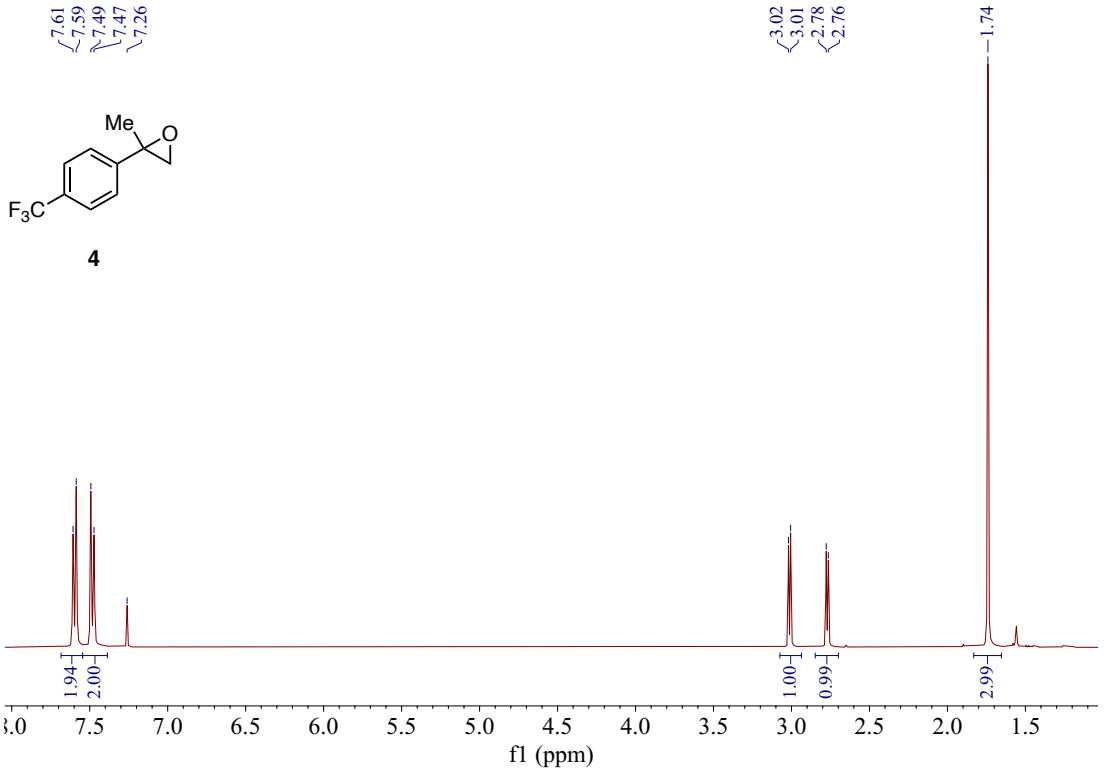

^{1}H NMR of Compound **4** (400 MHz, $CDCl_3$)

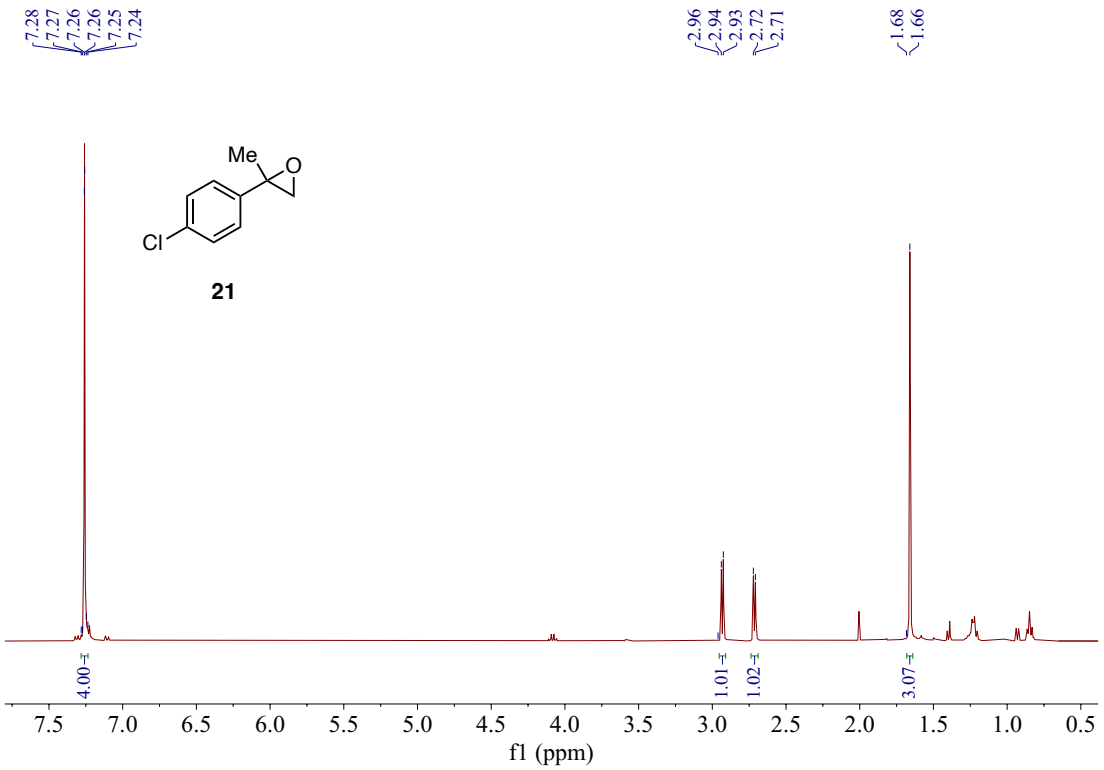

^{1}H NMR of Compound **21** (400 MHz, $CDCl_3$)

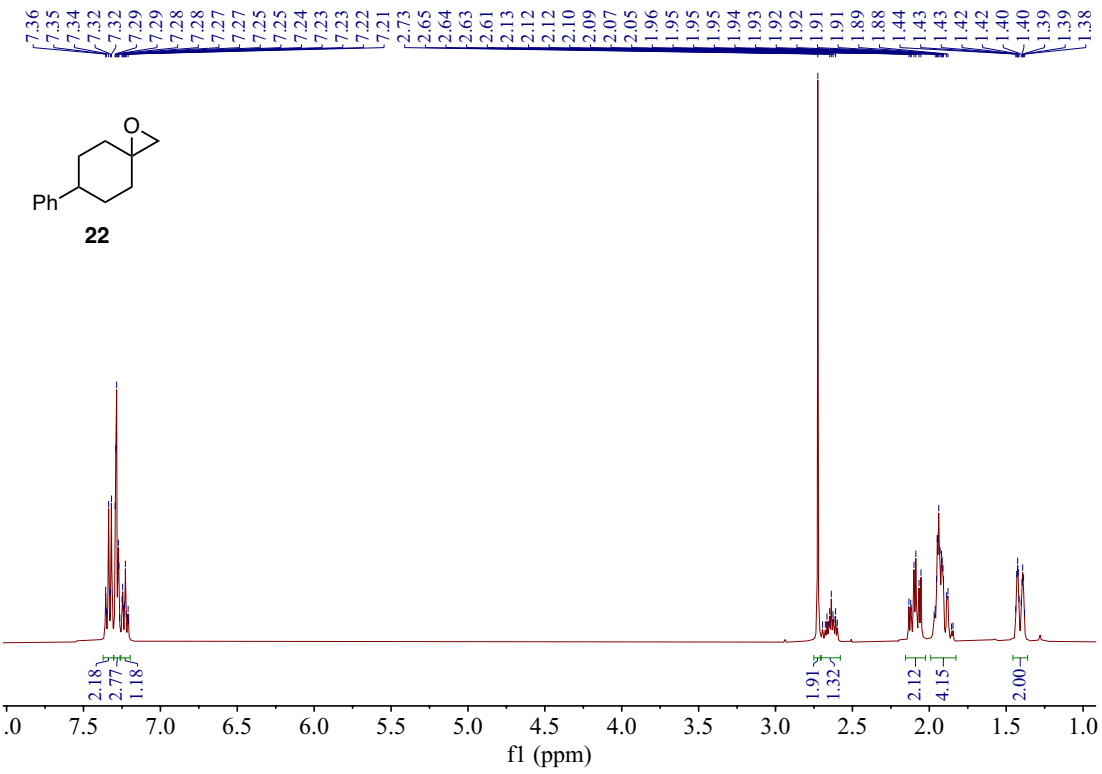

^{1}H NMR of Compound **22** (400 MHz, $CDCl_3$)

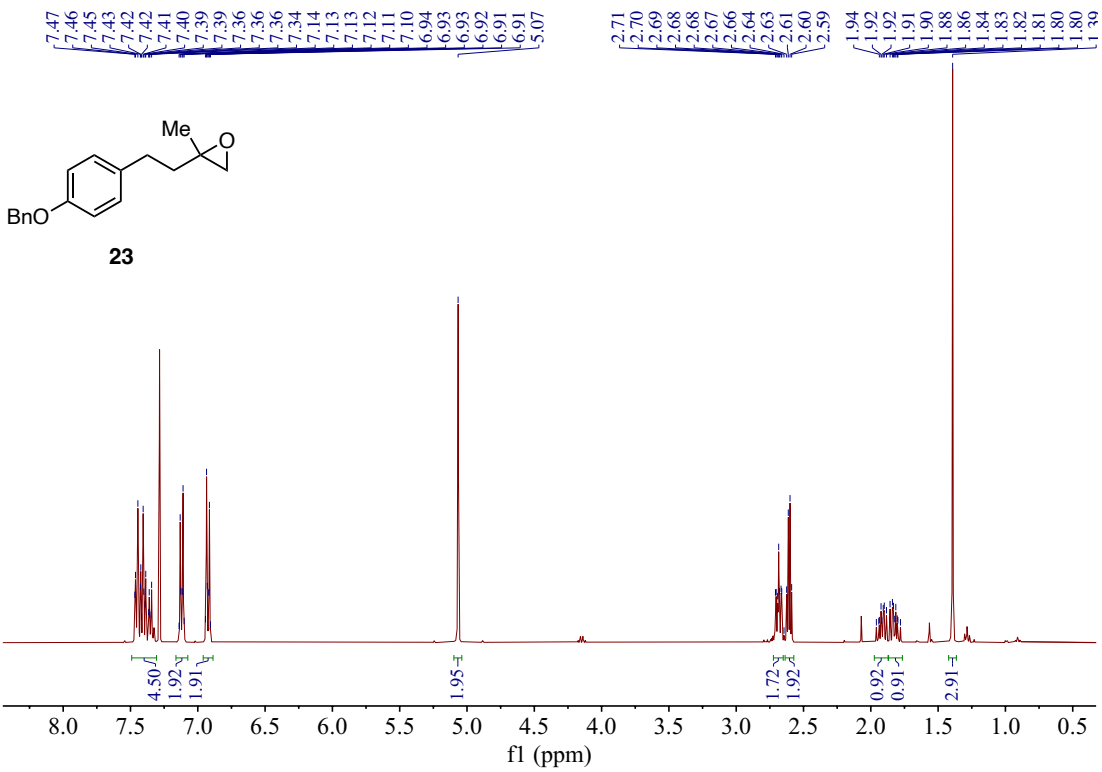

^{1}H NMR of Compound **23** (400 MHz, $CDCl_3$)

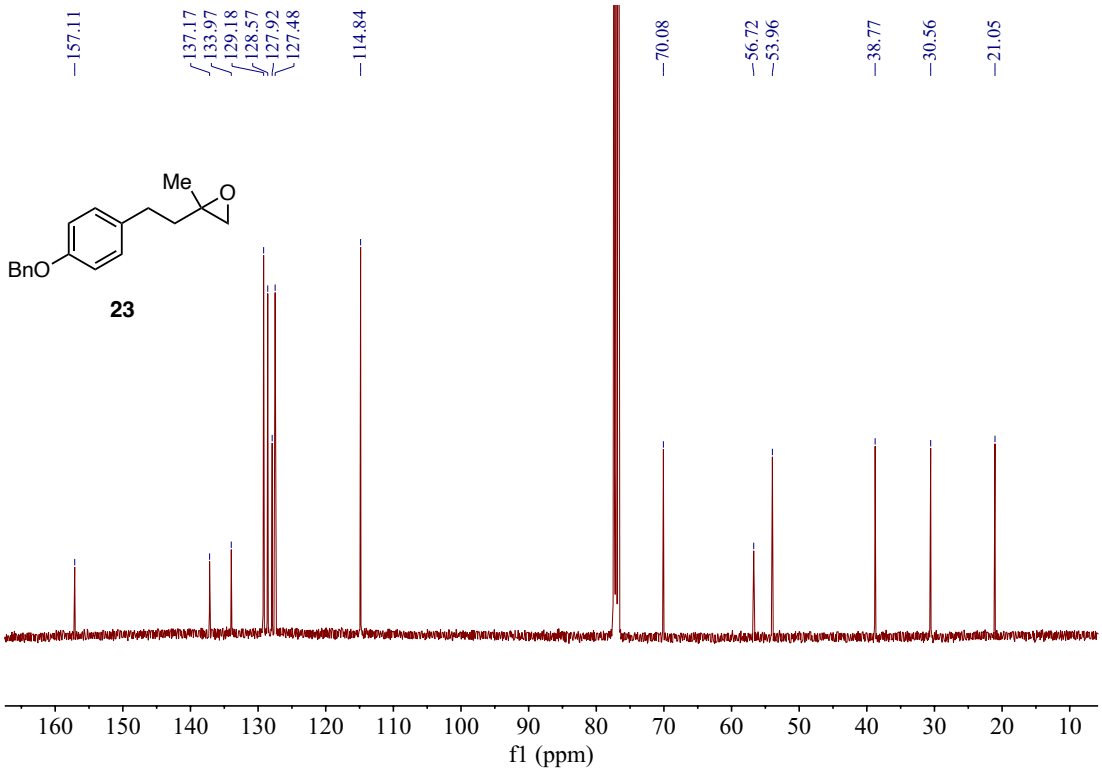

^{13}C NMR of Compound **23** (101 MHz, $CDCl_3$)

APPENDIX B

DIRECT BENZYLIC C–H AMINATION OF ALKYL ARENES ENABLED BY BASE-PROMOTED HALOGEN TRANSFER

I. General Information

General Reagent Information: All reactions were performed under a nitrogen (N_2) atmosphere unless otherwise noted. Potassium tert-butoxide (KO-t-Bu) was purchased from Oakwood Chemical (Catalog #075285) as a 99.8% pure powder and used as received. Potassium bis(trimethylsilyl)amide (KHMDS) was purchased from Millipore Sigma (Catalog # 324671) as a 95% pure powder or from Oakwood Chemical (Catalog #104258) as a 1M solution in THF and was used as received. Sodium bis(trimethylsilyl)amide (NaHMDS) was purchased from from Millipore Sigma (Catalog # 235083) as a 95% pure powder or from Oakwood Chemical (Catalog #S14980) as a 2M solution in THF and was used as received. 1,4,7,10,13,16-Hexaoxacyclooctadecane (18-crown-6) was purchased from Chem-Impex (Catalog #03901) and used as received. KO-t-Bu, KHMDS, NaHMDS, and 18-crown-6 were stored at room temperature (rt) inside a N2 filled glovebox and used immediately if brought outside the glovebox. 2-Ethylpyridine was purchased from Combi-Blocks (Catalog #QF-1149) as a 98% pure liquid and was used as received. 4-Methoxy-*N*-methylaniline was purchased from Ambeed (Catalog # A154384) as a 95% pure solid that was subsequently purified by flash column chromatography (40% EtOAc in Hexanes as mobile phase). 2-Methoxy-*N*-methylaniline was purchased from

Ambeed (Catalog # A253323) as a 95% pure solid that was subsequently purified by flash column chromatography (40% EtOAc in Hexanes as mobile phase). Anhydrous 1,2-dimethoxyethane (99.5%, inhibitor free, Millipore Sigma, Catalog # 259527) and *N*,*N*-dimethylformamide (99.8%, Millipore Sigma, Catalog # 227056). Tetrahydrofuran (THF) was deoxygenated and dried by passage over packed columns of neutral alumina and copper (II) oxide under positive pressure of N_2. All other solvents and reagents were purchased from Millipore Sigma, Ambeed, Combi-Blocks, TCI, Thermo Scientific Chemicals, Matrix Scientific, Alfa Aesar, or Oakwood Chemical, and used as received. Flash chromatography was performed on 40-63 μm silica gel (SiliaFlash® F60 from Silicycle). Preparative thin-layer chromatography (PTLC) was performed on silica gel 60 Å F254 plates (20 x 20 cm, 1000 μm, SiliaPlate from Silicycle, #TLG-R10011B-341) and visualized with UV light (254 nm) or KMnO4. Celite® 545 (Product #CX0574-3) was purchased from Millipore Sigma.

General Analytical Information: All new compounds were characterized by ^{1}H, ^{13}C, and All ^{19}F NMR signals are reported as chemical shifts (δ ppm) in reference to an internal standard (fluorobenzene set to -112.96 ppm) and are not proton decoupled. High resolution mass spectra (HRMS) were recorded on an Agilent 6210 TOF interfaced to a DART 100 or APCI source provided by Colorado State University's Materials and Molecular Analysis Center. Infrared spectra were recorded using a Thermo Scientific Nicolet iS-50 FTIR Spectrometer and reported as frequency of absorption (cm^{-1}). Melting point analyses were conducted using a Mel-Temp capillary melting point apparatus. ^{19}F (as appropriate) NMR spectroscopy, FTIR spectroscopy, mass spectrometry, and melting point analysis (if solid). NMR spectra were obtained on a Bruker Advanced NEO or Varian Inova 400 MHz spectrometer. ^{1}H NMR data is reported as follows:

chemical shift (δ ppm), multiplicity (s = singlet, d = doublet, t = triplet, q = quartet, dd = doublet of doublets, td = triplet of doublets, ddd = doublet of doublet of doublets, m = multiplet), coupling constant (Hz), and integration. ^{13}C NMR data is reported as follows: chemical shift (δ ppm), multiplicity (if applicable, d = doublet, q = quartet). All ^{1}H and ^{13}C NMR signals are reported as chemical shifts (δ ppm) relative to residual solvent peaks of the deuterated NMR solvents.

Note on nomenclature: The names provided for the structures below were obtained from ChemDraw Professional 20.0.

Abbreviations: List of abbreviations used in this document.

Me = methyl

Et = ethyl

t-Bu = *tert*-butyl

n-Bu = *n*-butyl

Ph = phenyl

PMP = *para*-methoxyphenyl

Ar = aryl

h = hour

min = minute

s = second

rt = room temperature

II. Synthesis of Designer Halogen Transfer Reagents

a. Synthesis of 2-bromo-4,6-dimethoxy-3-phenylbenzo[*b*]thiophene (20)

Step 1: Synthesis of 3,5-dimethoxybenzenethiol

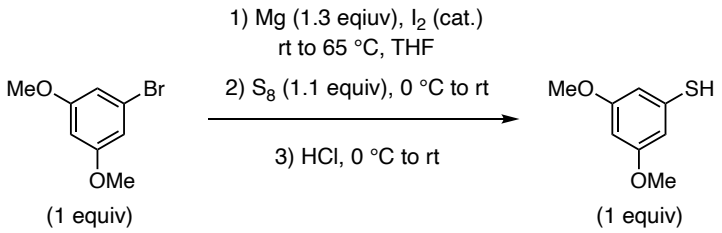

Figure S1: Synthesis of 3,5-dimethoxybenzenethiol

Procedure: An oven-dried 500mL round bottom flask was charged with a magnetic stir bar, magnesium (3.6g, 149.8 mmol, 1.3 equiv), iodine (5.8 mg, 23 mmol, 20 mol%), and THF (10 mL). The reaction flask was sealed with a rubber septum (ThermoFisher, CG302208) and evacuated then flushed with nitrogen three times *via* a nitrogen inlet tube on a Schlenk manifold line. The reaction was stirred at rt for 5 min followed by addition of 3 mL of a 1.2 M solution of 3,5-dimethoxybromobenzene (25g, 115.2 mmol, 96 mL THF total) via N_2-flushed syringe to initiate the reaction. The reaction was stirred for 5 min followed by the dropwise addition of the rest of the 1.2 M solution of 3,5-dimethoxybromobenzene *via* N_2-flushed syringe. The reaction flask was placed in a preheated oil bath at 65 °C and was stirred for 2 h. The reaction was cooled to 0 °C and

sulfur (4.1g, 126.7 mmol, 1 equiv) was added slowly in portions *via* N_2-flushed syringe. The reaction was warmed gradually to rt and stirred overnight. The reaction was quenched with 1M HCl (50 mL) and diluted with diethyl ether. The solution washed three times with diethyl ether (50 mL) and the combined organic layers were washed with brine and dried over $MgSO_4$, then dried *in vacuo* to afford 3,5-dimethoxybenzenethiol as a light-yellow liquid with no purification (17 g, 99.1 mmol, 86% yield). **^{1}H NMR** (400 MHz, CDCl3) δ 6.41 (d, *J* = 2.0 Hz, 2H), 6.25 (d, *J* = 2.1 Hz, 1H), 3.75 (s, 6H), 3.47 – 3.45 (s, 1H). Characterization data matches literature reports.[1]

Step 2: Synthesis of 2-((3,5-dimethoxyphenyl)thio)-1-phenylethan-1-one

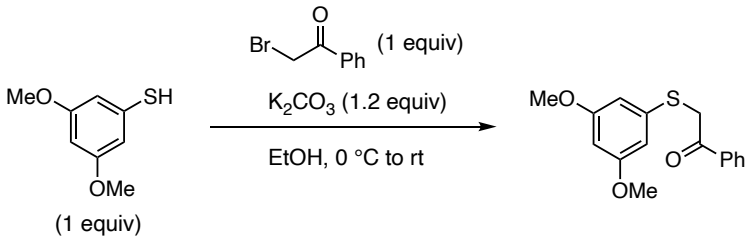

Figure S2: Synthesis of 2-((3,5-dimethoxyphenyl)thio)-1-phenylethan-1-one

Procedure: An oven-dried 500 mL round bottom flask was charged with a magnetic stir bar, anhydrous K_2CO_3 (14.6 g, 105.7 mmol, 1.2 equiv), and absolute ethanol (220 mL, 0.4 M). The flask was placed in an ice bath and the reaction mixture was cooled to 0 °C followed by addition of 3-methoxythiophenol (14 g, 88.1 mmol, 1 equiv). The reaction was stirred for 10 min followed by addition of 2-bromoacetophenone (17.5 g, 88.1 mmol, 1 equiv) slowly in portions. The reaction was gradually warmed to rt and stirred for 3 h. Ice was added to the stirring reaction mixture and the product precipitated from solution. The solid was collected by filtration and dried *in vacuo* to

afford 2-((3,5-dimethoxyphenyl)thio)-1-phenylethan-1-one as a yellow solid (19.5 mg, 67.6 mmol, 82% yield). **^{1}H NMR** (400 MHz, CDCl3) δ 7.91 – 7.86 (m, 2H), 7.55 – 7.49 (m, 1H), 7.40 (dd, J = 8.4, 7.0 Hz, 2H), 6.47 (d, *J* = 2.2 Hz, 2H), 6.24 (t, *J* = 2.3 Hz, 1H), 4.23 (s, 2H), 3.68 (s, 6H). Characterization data matches literature reports.[2]

Step 3: Synthesis of 4,6-dimethoxy-3-phenylbenzo[b]thiophene

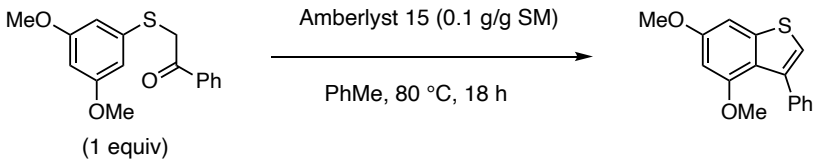

Figure S3: Synthesis of 4,6-dimethoxy-3-phenylbenzo[*b*]thiophene.

Procedure: An oven-dried 250 mL round bottom flask was charged with a magnetic stir bar, 2-((3,5-dimethoxyphenyl)thio)-1-phenylethan-1-one (14.0 g, 48.5 mmol, 1 equiv), dry amberlyst 15 (14 g), and PhMe (97 mL, 0.5 M). The flask was placed in a preheated oil bath at 80 °C and the reaction was stirred overnight. The reaction was cooled to rt and filtered through celite. The solid filtrate was washed with additional PhMe until clear of color. The reaction mixture was concentrated *in vacuo* and the solid residue was recrystallized from hexanes and chloroform to afford 4,6-dimethoxy-3-phenylbenzo[*b*]thiophene as a white solid (11.0 g, 40.7 mmol, 84% yield). **^{1}H NMR** (400 MHz, CDCl3) δ 7.52 – 7.47 (m, 2H), 7.43 – 7.34 (m, 3H), 7.01 (s, 1H), 6.98 (d, *J* = 2.1 Hz, 1H), 6.44 (d, *J* = 2.1 Hz, 1H), 3.91 (s, 3H), 3.68 (s, 3H).

*Step 4: Synthesis of 2-bromo-4,6-dimethoxy-3-phenylbenzo[b]thiophene (**20**)*

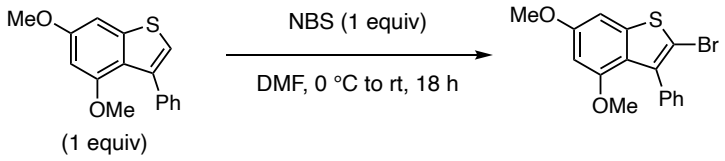

Figure S4: Synthesis of 2-bromo-4,6-dimethoxy-3-phenylbenzo[b]thiophene (**20**)

Procedure: An oven-dried 250 mL round bottom flask was charged with a magnetic stir bar, 4,6-dimethoxy-3-phenylbenzo[*b*]thiophene (11.0 g, 40.7 mmol, 1 equiv), and DMF (100 mL, 0.4 M). The flask was placed in an ice bath and the reaction mixture was cooled to 0 °C. *N*-Bromosuccinimide (8.4 g, 40.7 mmol, 1 equiv) was added to the stirring reaction mixture slowly in portions over 5 min. The reaction was gradually warmed to rt and stirred for 18 h. Ice was added to the stirring reaction mixture and the product precipitated from solution. The precipitate was collected by vacuum filtration and washed with additional water (50 mL). The solid residue was recrystallized from hexanes to afford 2-bromo-4,6-dimethoxy-3-phenylbenzo[b]thiophene (**20**) as a white solid (11.5 g, 33.0 mmol, 81% yield). **^{1}H NMR** (400 MHz, CDCl3) δ 7.49 – 7.42 (m, 2H), 7.41 – 7.33 (m, 3H), 7.06 (s, 1H), 6.51 (s, 1H), 3.99 (s, 3H), 3.69 (s, 3H).

b. Synthesis of 2-bromo-3-phenylbenzo[b]thiophene (38)

Step 1: Synthesis of 1-phenyl-2-(phenylthio)ethan-1-one

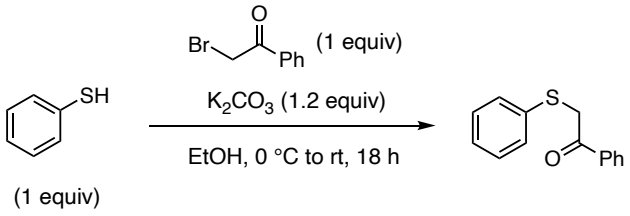

Figure S5: Synthesis of 1-phenyl-2-(phenylthio)ethan-1-one

Procedure: An oven-dried 2 L Erlenmeyer flask was charged with a magnetic stir bar, anhydrous K_2CO_3 (75.3 g, 544.6 mmol, 1.2 equiv), and absolute ethanol (1.5 L, ~0.3 M). The flask was placed in an ice bath and the reaction mixture was cooled to 0 °C, followed by addition of thiophenol (50.0 g, 453.8 mmol, 1 equiv). The reaction was stirred for 10 min, followed by addition of 2-bromoacetophenone (90.3 g, 453.8 mmol, 1 equiv) slowly in portions. The reaction was gradually warmed to rt and stirred for 18 h. Ice was added to the stirring reaction mixture and the product precipitated from solution. The precipitate was collected by vacuum filtration and washed with additional water (300 mL) to afford 1-phenyl-2-(phenylthio)ethan-1-one as a white solid (102.0 g, 446.8 mmol, 98% yield). **^{1}H NMR** (400 MHz, CDCl3) δ 7.97 (d, *J* = 8.2 Hz, 2H), 7.61 (td, *J* = 7.4, 1.6 Hz, 1H), 7.49 (td, *J* = 7.8, 1.6 Hz, 2H), 7.44 – 7.40 (m, 2H), 7.35 – 7.19 (m, 3H), 4.30 (s, 2H). Characterization data matches literature reports.[3]

Step 2: Synthesis of 3-phenylbenzo[b]thiophene

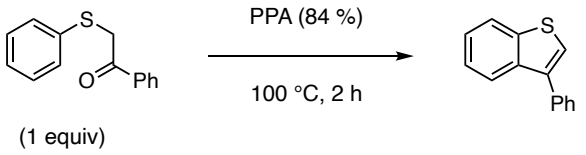

Figure S6: Synthesis of 3-phenylbenzo[b]thiophene.

Procedure: An oven-dried 500 mL Erlenmeyer flask was charged with a magnetic stir bar and 84% polyphosphoric acid (PPA, 125 g, 62.5 mL). The flask was placed in a preheated oil bath at 100 °C. 1-Phenyl-2-(phenylthio)ethan-1-one (25 g, 109.6 mmol, 1 equiv) was added to the stirring solution slowly in portions and the reaction mixture turned orange. We note that the stir bar must be smoothly stirring PPA before adding 1-Phenyl-2-(phenylthio)ethan-1-one to obtain the cleanest and highest yielding reaction. The reaction was stirred for 2 h. The reaction mixture was cooled to rt and then poured into a 1 L Erlenmeyer flask containing a magnetic stir bar with equal parts ice (~ 300 g) and EtOAc (300 mL). The resulting mixture was stirred vigorously until PPA dissolved and two layers were clearly formed. This mixture was transferred to a separatory funnel after which the aqueous layer was washed with EtOAc (3 x 200 mL). The combined organic layers were washed with brine, dried over Na_2SO_4, and concentrated *in vacuo*. The product was purified via silica gel flash chromatography using 100% hexanes to afford 3-phenylbenzo[b]thiophene as a colorless oil (18.0 g, 85.6 mmol, 78% yield). **^{1}H NMR** (400 MHz, CDCl3) δ 8.16 – 8.04 (m, 1H), 7.80 – 7.72 (m, 1H), 7.69 – 7.61 (m, 1H), 7.59 – 7.46 (m, 2H). Characterization data matches literature reports.[3]

*Step 3: Synthesis of 2-bromo-3-phenylbenzo[b]thiophene (**38**)*

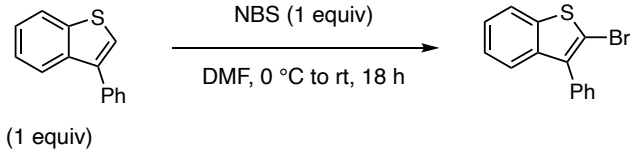

Figure S7: Synthesis of 2-bromo-3-phenylbenzo[b]thiophene (**38**)

Procedure: An oven-dried 500 mL round bottom flask was charged with a magnetic stir bar, 4,6-dimethoxy-3-phenylbenzo[b]thiophene (18.0 g, 85.6 mmol, 1 equiv), and DMF (214 mL, 0.4 M). The flask was placed in an ice bath and the reaction mixture was cooled to 0 °C. *N*-Bromosuccinimide (15.2 g, 85.6 mmol, 1 equiv) was added to the stirring reaction mixture slowly in portions over 5 min. The reaction was gradually warmed to rt and stirred for 18 h. Ice was added to the stirring reaction mixture and the product precipitated from solution. The precipitate was collected by vacuum filtration and washed with additional water (100 mL). The solid residue was recrystallized from hexanes to afford 2-bromo-3-phenylbenzo[b]thiophene (**38**) as a white solid (21.1 g, 72.8 mmol, 85% yield). **^{1}H NMR** (400 MHz, CDCl3) δ 7.80 (d, *J* = 7.8 Hz, 1H), 7.61 – 7.43 (m, 6H), 7.42 – 7.30 (m, 2H).[4]

c. Synthesis of 2-bromo-1-methyl-3-phenyl-1H-indole (34)

Step 1: Synthesis of 3-phenyl-1H-indole

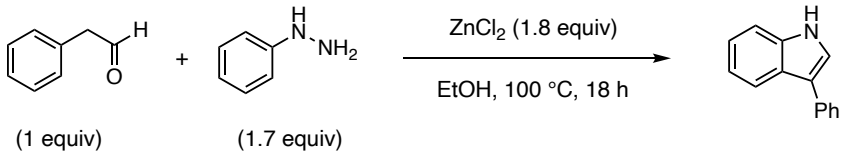

Figure S8: Synthesis of 3-phenyl-1H-indole

Procedure: An oven-dried 3-neck 500 mL round bottom flask was charged with a magnetic stir bar, 2-phenylacetaldehyde (30.0 g, 250 mmol, 1 equiv), and phenylhydrazine (45.0 g, 416.1 mmol, 1.7 mmol). The reaction mixture was stirred neat for 1 h at rt. The reaction flask was equipped with a reflux condenser and the additional necks were sealed with rubber septa (ThermoFisher, CG302208) and the reaction mixture and placed in a preheated oil bath at 100 °C and stirred for 30 min. Zinc chloride (61.3 g, 450.0 mmol, 1.8 equiv) was dissolved in absolute ethanol (312 mL, 0.8 M with respect to phenylacetaldehyde), and added dropwise to the stirring reaction solution, after which a color change is observed. The reaction was stirred for 18 h at 100 °C. The reaction was cooled to rt, filtered through celite, and washed with EtOH (100 mL). 1 M Aqueous HCl was added to the reaction solution and the mixture was extracted with DCM (3 x 100 mL). The combined organic layers were washed with brine (100 mL), dried over Na_2SO_4, and concentrated *in vacuo*. The residue was recrystallized using hexanes to afford 3-phenyl-1H-indole as a light orange solid (28.6 g, 148.0 mmol, 59% yield). **^{1}H NMR** (400 MHz, CDCl3) δ 8.23 (bs, 1H), 7.96 (d, *J* = 7.8 Hz, 1H), 7.72 – 7.61 (m, 2H), 7.51 – 7.42 (m, 3H), 7.38 (d, *J* = 2.5 Hz, 1H), 7.34 – 7.16 (m, 3H). Characterization data matches literature reports.[5]

Step 2: Synthesis of 1-methyl-3-phenyl-1H-indole

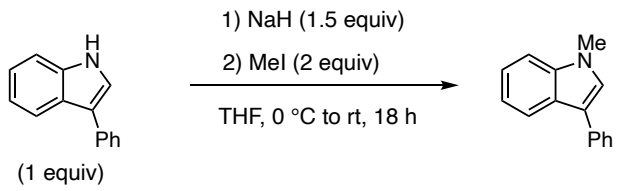

Figure S9: Synthesis of 1-methyl-3-phenyl-1H-indole

Procedure: An oven-dried 500 mL round bottom flask was charged with a magnetic stir bar, 3-phenyl-1H-indole (21.0 g, 108.0 mmol, 1 equiv), and THF (360 mL, 0.3 M). The flask was sealed with a rubber septum (ThermoFisher, CG302208) and evacuated then flushed with nitrogen three times *via* a nitrogen inlet tube on a Schlenk manifold line. The reaction flask was placed into an ice bath and cooled to 0 °C, after which sodium hydride (60% dispersion in mineral oil dissolved in 25 mL THF, 6.5 g, 162 mmol, 1.5 equiv) was added dropwise *via* a N_2-flushed syringe to the stirring solution. The reaction was stirred for 20 min at 0 °C. Methyl iodide (13.4 mL, 216 mmol, 2 equiv) was added dropwise *via* a N_2-flushed syringe to the stirring solution. The reaction was gradually warmed to rt and stirred for 18 h. The reaction was quenched by addition of saturated ammonium chloride (100 mL). This reaction mixture was extracted using EtOAc (3 x 100 mL) and the combined organic layers were washed with brine (100 mL), dried over Na_2SO_4, and concentrated *in vacuo*. The residue was recrystallized using hexanes to afford 1-methyl-3-phenyl-1H-indole as a light orange low melting point solid (18.0 g, 86.8 mmol, 80% yield). **^{1}H NMR** (400 MHz, CDCl3) δ 7.95 (d, *J* = 8.0 Hz, 1H), 7.66 (d, *J* = 7.8 Hz, 2H), 7.44 (t, *J* = 7.8 Hz, 2H), 7.37 (d, *J* = 8.2 Hz, 1H), 7.32 – 7.23 (m, 3H), 7.20 (t, *J* = 7.6 Hz, 1H). Characterization data matches literature reports.[6]

Step 3: Synthesis of 2-bromo-1-methyl-3-phenyl-1H-indole (34)

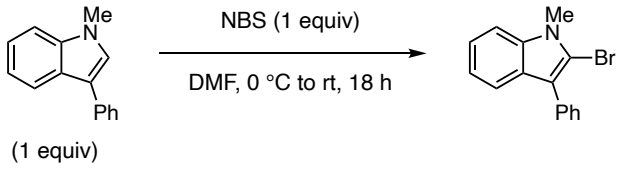

Figure S10: Synthesis of 2-bromo-1-methyl-3-phenyl-1H-indole (34)

Procedure: An oven-dried 500 mL round bottom flask was charged with a magnetic stir bar, 1-methyl-3-phenyl-1H-indole (19.5 g, 94.2 mmol, 1 equiv), and DMF (236 mL, 0.4 M). The flask was placed in an ice bath and the reaction mixture was cooled to 0 °C. *N*-Bromosuccinimide (16.8 g, 94.2 mmol, 1 equiv) was added to the stirring reaction mixture slowly in portions over 5 min. The reaction was gradually warmed to rt and stirred for 18 h. The reaction was quenched with saturated sodium thiosulfate and worked up with EtOAc (3 x 100 mL). The combined organic layers were washed with brine (100 mL), dried over Na_2SO_4, and concentrated *in vacuo*. The product was purified via silica gel flash chromatography using 5% EtOAc in hexanes to afford 2-bromo-1-methyl-3-phenyl-1H-indole (**34**) as a white solid (21.1 g, 71.5 mmol, 76% yield). **^{1}H NMR** (400 MHz, CDCl3) δ 7.69 (d, J = 8.0 Hz, 1H), 7.64 (d, J = 7.9 Hz, 2H), 7.49 (t, J = 7.9 Hz, 2H), 7.40 – 7.32 (m, 2H), 7.31 – 7.23 (m, 1H), 7.15 (t, J = 7.5 Hz, 1H), 3.85 (s, 3H). Characterization data matches literature reports.[6]

c. Synthesis of 2-bromo-3-phenylbenzofuran (33)

Step 1: Synthesis of phenyl benzoate

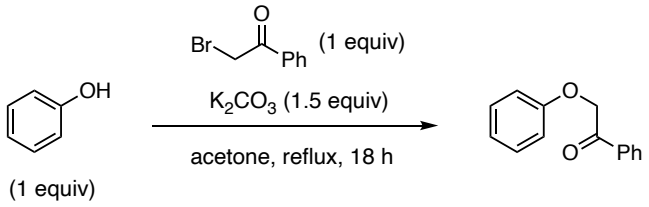

Figure S11: Synthesis of phenyl benzoate

Procedure: An oven-dried 1000 mL round bottom flask was charged with a magnetic stir bar, potassium carbonate (52.1 g, 377 mmol, 1.5 equiv), and acetone (500 mL, 0.5 M). Phenol (23.6 g, 251 mmol, 1 equiv) was added to the stirring solution and the reaction was stirred for 5 min. 2-Bromoacetophenone (50 g, 251 mmol, 1 equiv) was added to the stirring solution slowly in portions. The reaction flask was placed in a preheated oil bath at 55 °C and was fitted with a reflux condenser. The reaction was run for 18 h where it was observed the reaction solution turns an orange color. The reaction was cooled to rt and diluted with water (200 mL) and worked up with EtOAc (3 x 200 mL). The combined organic layers were washed with sodium thiosulfate (200 mL), brine (200 mL), dried over dried over Na_2SO_4, and concentrated *in vacuo*. The crude product was suspended in hexanes and collected *via* vacuum filtration to afford phenyl benzoate as an off-white solid (37.0 g, 186.6 mmol, 74% yield). **^{1}H NMR** (400 MHz, CDCl3) δ 8.01 (d, *J* = 7.74,

2H), 7.62 (t, *J* = 7.5 Hz, 1H), 7.51 (t, *J* = 7.6 Hz, 2H), 7.34 – 7.25 (m, 2H), 7.03 – 6.95 (m, 3H), 5.28 (s, 2H). Characterization data matches literature reports.[7]

Step 2: Synthesis of 3-phenylbenzofuran

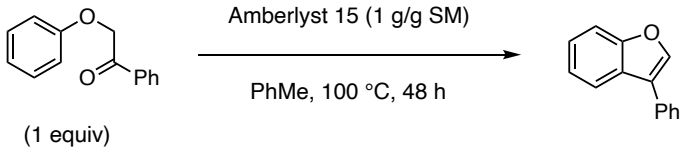

Figure S12: Synthesis of 3-phenylbenzofuran

Procedure: An oven-dried 500 mL round bottom flask was charged with a magnetic stir bar, phenyl benzoate (50 g, 235.6 mmol, 1 equiv), dry amberlyst 15 (50 g), and PhMe (236 mL, 1 M). The reaction flask was placed in a preheated oil bat at 100 °C and the flask was fitted with a reflux condenser. The reaction was stirred at 100 °C for 48 h. The reaction was cooled to rt and was filtered through celite and washed with additional PhMe until the residue was clear of color. The reaction mixture was concentrated *in vacuo* and placed in the freezer to afford the crude solid material. This residue was recrystallized from hexanes to afford 3-phenylbenzofuran as a white solid (39.0 g, 200.8 mmol, 86% yield). **^{1}H NMR** (400 MHz, CDCl3) δ 7.96 – 7.89 (m, 1H), 7.85 (s, 1H), 7.76 – 7.69 (m, 2H), 7.63 (dt, *J* = 8.3, 0.8 Hz, 1H), 7.60 – 7.50 (m, 2H), 7.49 – 7.33 (m, 3H). Characterization data matches literature reports.[8]

*Step 2: Synthesis of 2-bromo-3-phenylbenzofuran (**33**)*

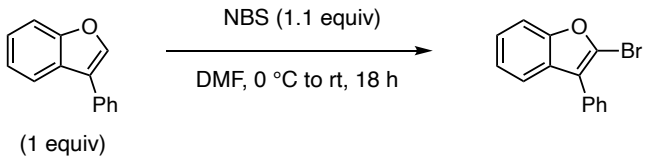

Figure S13: Synthesis of 2-bromo-3-phenylbenzofuran (**33**)

Procedure: An oven-dried 1000 mL round bottom flask was charged with a magnetic stir bar, 3-phenylbenzofuran (35.0 g, 175.7 mmol, 1 equiv), and DMF (440 mL, 0.4 M). The flask was placed in an ice bath and the reaction mixture was cooled to 0 °C. *N*-Bromosuccinimide (34.4 g, 193.2 mmol, 1.1 equiv) was added to the stirring reaction mixture slowly in portions over 5 min. The reaction was gradually warmed to rt and stirred for 18 h. The reaction was diluted with water (250 mL) and worked up with EtOAc (3 x 250 mL). The combined organic layers were washed with water (3 x 250 mL), brine (250 mL), dried over Na_2SO_4, and concentrated *in vacuo* to afford 2-bromo-3-phenylbenzofuran (**33**) as an orange liquid (46.0 g, 168.4 mmol, 96% yield). **^{1}H NMR** (400 MHz, CDCl3) δ 7.61 – 7.51 (m, 3H), 7.49 – 7.38 (m, 3H), 7.36 – 7.29 (m, 1H), 7.26 – 7.11 (m, 2H).

III. Optimization of Benzylic C–H Amination of Alkyl (Hetero)Arenes

a. Evaluation of changes in optimal base, halogenating agent, solvent, reaction time, and temperature for direct amination of 1-ethylnaphthalene.

The purpose of this section is to present the variation of reaction conditions that lead to high yielding benzylic amination of 1-ethylnaphthalene using 2-methoxy-*N*-methylaniline as a model reaction. Table S1 shows the optimal conditions for this reaction as well as the effect of making specific variations to the conditions on the yield of the reaction.

General Procedure for Condition Variation: Inside a N_2-filled glovebox, an oven-dried 1-dram vial (ThermoFisher, C4015-1) was charged with a magnetic stir bar, 1-ethylnaphthalene (15.6 mg, 0.1 mmol, 1 equiv), 2-Methoxy-*N*-methylaniline (20.6 mg, 0.15 mmol, 1.5 equiv), X-transfer reagent (0.12 mmol, 1.2 equiv), anhydrous solvent (0.4 mL, 0.25M), and base (0.2 mmol, 2 equiv) in successive order. The vial was sealed with a PTFE lined screw cap (ThermoFisher, C4015-A) and removed from the glovebox. The reaction was stirred at rt for 18 h. 1,3,5-trimethoxybenzene (mass weighed into the vial was recorded) internal standard was then added to the reaction solution, a 50 μL aliquot was taken and added to an NMR tube, then diluted with $CDCl_3$ (0.5 mL). ^{1}H NMR spectroscopy was used to determine the yield of the reaction. The aromatic C–H signal of 1,3,5-trimethoxybenzene at 6.09 ppm (s, 3H) was integrated against the benzylic methylene C–H signal of the product at 5.56 ppm (q, 1H) to assess the yield. The results of this investigation are summarized in Table S1 below. A representative example ^{1}H NMR spectrum for the crude reaction solution using the optimized conditions is shown in Figure S14 below to show how the yield was determined.

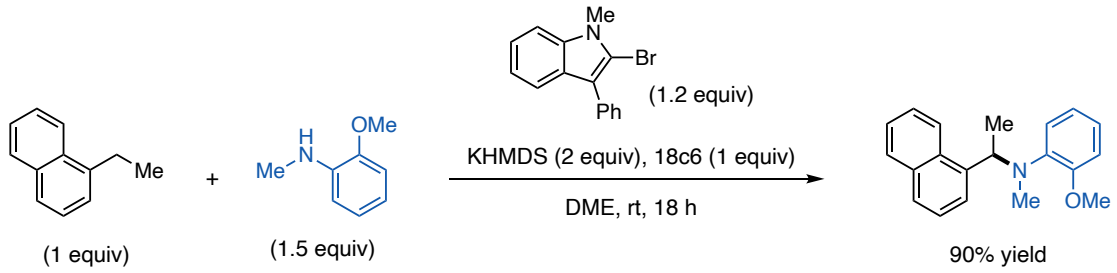

Table S1: Condition variation for the benzylic amination of 1-ethylnaphthalene.

Entry	Changes from Optimized Conditions	Yield
1	No Changes	90%
2	2-bromothiophene used as XTR	16%
3	NaHMDS instead of KHMDS	53%
4	KO-*t*-Bu instead of KHMDS	40%
5	DMF instead of DME	73%
6	THF instead of DME	90%
7	DMPU instead of DME	73%
8	PhMe instead of DME	27%
9	XTR **33** instead of XTR **34**	35%
10	XTR **20** instead of XTR **34**	68%
11	XTR **20** in DMF, no 18c6	28%
12	XTR **20**, 3 h reaction time	60%
13	1.5 equiv XTR **20**, 1.5 equiv KHMDS	49%

14	1.5 equiv XTR **20**, 1.5 equiv KHMDS, 85 °C	58%
15	2.5 equiv XTR **20**, 2.5 equiv KHMDS, 85 °C	44%

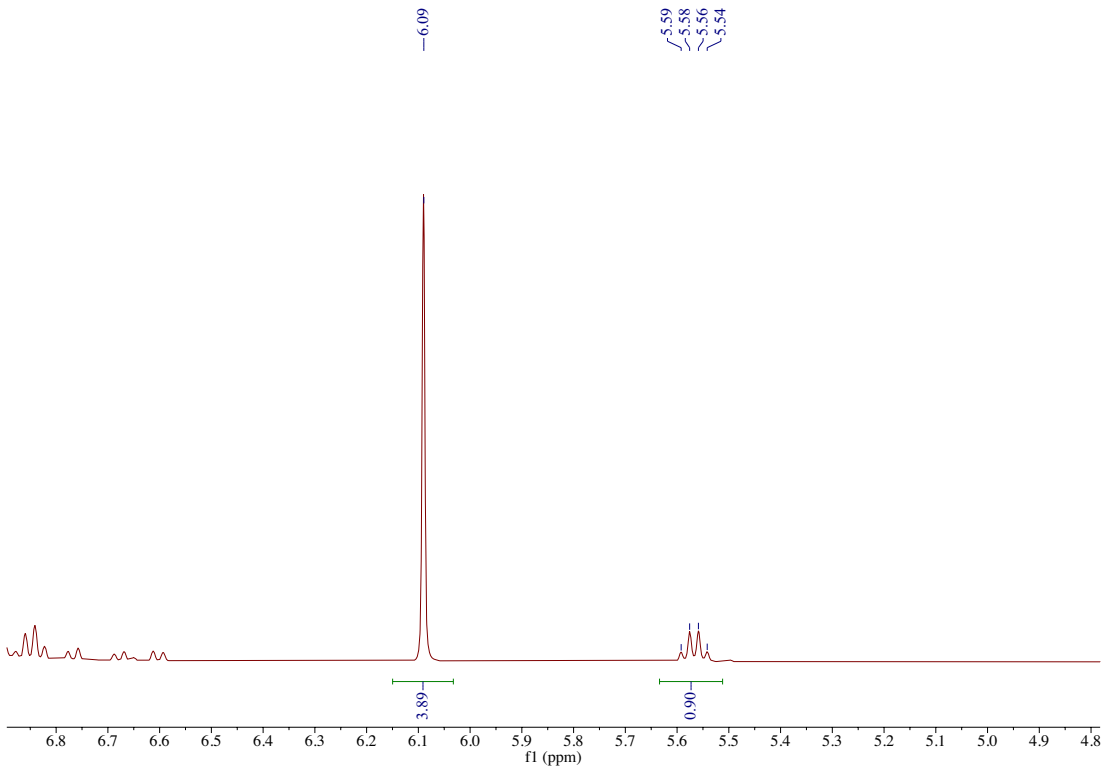

Figure S14: ^{1}H NMR spectral window of the crude reaction solution of reaction 1-ethylnaphthalene from Table S1 above. 1,3,5-Trimethoxybenzene internal standard (21.8 mg, 0.13 mmol, signal at 6.09 ppm calibrated to 3.89 for 0.1 mmol scale reaction) was used to determine the yield of 2-methoxy-N-methyl-N-(1-(naphthalen-1-yl)ethyl)aniline (90% yield).

b. Evaluation of changes in optimal base, halogenating agent, solvent, reaction time, and temperature for direct amination of 5,6,7,8-tetrahydroquinoline.

The purpose of this section is to present the variation of reaction conditions that lead to high yielding benzylic amination of 5,6,7,8-tetrahydroquinoline using 2-methoxy-*N*-methylaniline as a model reaction. Table S2 shows the optimal conditions for this reaction as well as the effect of making specific variations to the conditions on the yield of the reaction.

General Procedure for Condition Variation: Inside a N_2-filled glovebox, an oven-dried 1-dram vial (ThermoFisher, C4015-1) was charged with a magnetic stir bar, 5,6,7,8-tetrahydroquinoline (13.3 mg, 0.1 mmol, 1 equiv), 2-Methoxy-*N*-methylaniline (20.6 mg, 0.15 mmol, 1.5 equiv), X-transfer reagent (0.12 mmol, 1.2 equiv), anhydrous solvent (0.4 mL, 0.25M), and base (0.2 mmol, 2 equiv) in successive order. The vial was sealed with a PTFE lined screw cap (ThermoFisher, C4015-A) and removed from the glovebox. The reaction was stirred at rt for 18 h. 1,3,5-trimethoxybenzene (mass weighed into the vial was recorded) internal standard was then added to the reaction solution, a 50 μL aliquot was taken and added to an NMR tube, then diluted with $CDCl_3$ (0.5 mL). ^1H NMR spectroscopy was used to determine the yield of the reaction. The aromatic C–H signal of 1,3,5-trimethoxybenzene at 6.09 ppm (s, 3H) was integrated against the benzylic methylene C–H signal of the product at 4.96 ppm (t, 1H) to assess the yield. The results of this investigation are summarized in Table S2 below. A representative example ^1H NMR spectrum for the crude reaction solution using the optimized conditions is shown in Figure S15 below to show how the yield was determined.

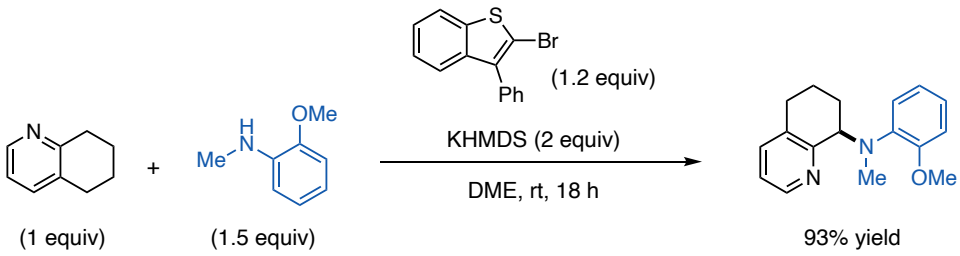

Table S2: Condition variation for the benzylic amination of 5,6,7,8-tetrahydroquinoline.

Entry	Changes from Optimized Conditions	Yield
1	No Changes	93%
2	2-bromothiophene as XTR	38%
3	3 h reaction time	65%
4	NaHMDS instead of KHMDS	59%
5	KO-*t*-Bu instead of KHMDS	10%
6	DMF instead of DME	45%
7	THF instead of DME	68%
8	DMPU instead of DME	33%
9	PhMe instead of DME	41%
10	XTR **34** instead of XTR **38**	32%
11	XTR **20** instead of XTR **38**	46%
12	XTR **20** instead of XTR **38**, 40 °C	64%
13	XTR **20** instead of XTR **38**, 40 °C, DMF	33%

14	1.5 equiv XTR **20**, 1.5 equiv KHMDS, 40 °C	85%

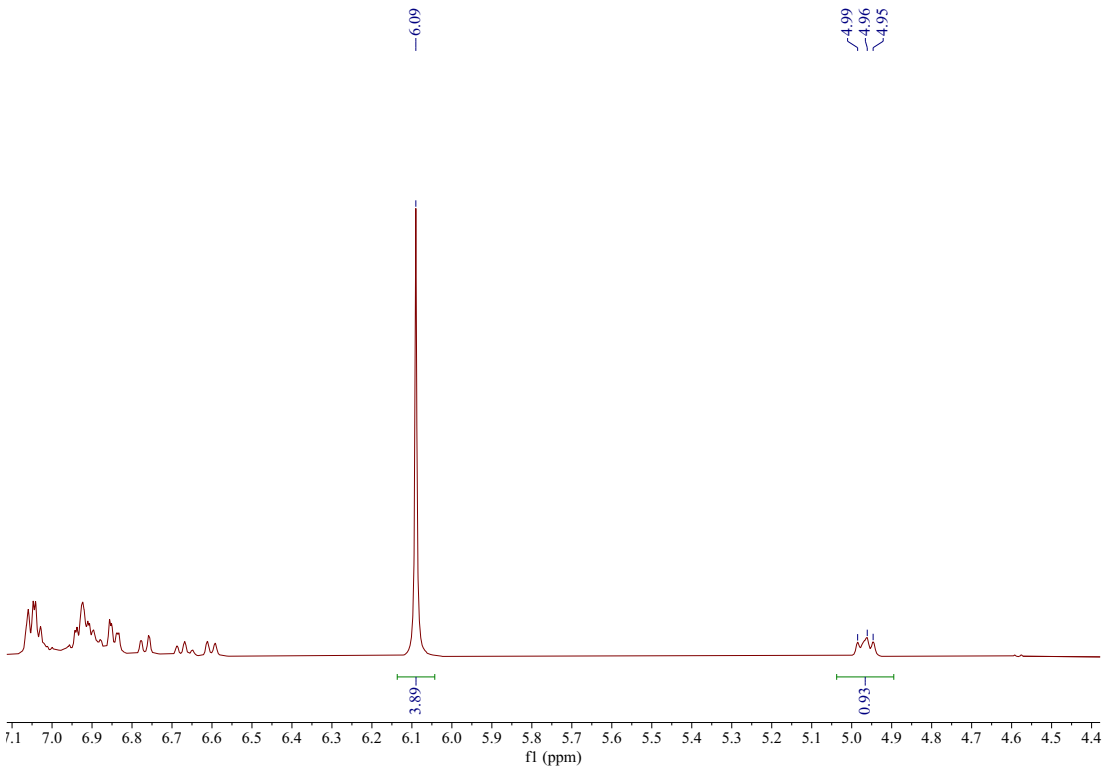

Figure S15: ^{1}H NMR spectral window of the crude reaction solution of reaction 5,6,7,8-tetrahydroquinoline from Table S2 above. 1,3,5-Trimethoxybenzene internal standard (21.8 mg, 0.13 mmol, signal at 6.09 ppm calibrated to 3.89 for 0.1 mmol scale reaction) was used to determine the yield of *N*-(2-methoxyphenyl)-*N*-methyl-5,6,7,8-tetrahydroquinolin-8-amine (93% yield).

c. Evaluation of changes in optimal base, halogenating agent, solvent, reaction time, and temperature for direct amination of 7-chloro-8-methylquinoline.

The purpose of this section is to present the variation of reaction conditions that lead to high yielding benzylic amination of 7-chloro-8-methylquinoline using 2-methoxy-*N*-methylaniline as a model reaction. Table S3 shows the optimal conditions for this reaction as well as the effect of making specific variations to the conditions on the yield of the reaction.

General Procedure for Condition Variation: Inside a N_2-filled glovebox, an oven-dried 1-dram vial (ThermoFisher, C4015-1) was charged with a magnetic stir bar, 7-chloro-8-methylquinoline (17.8 mg, 0.1 mmol, 1 equiv), 2-Methoxy-*N*-methylaniline (20.6 mg, 0.15 mmol, 1.5 equiv), X-transfer reagent (0.12 mmol, 1.2 equiv), anhydrous solvent (0.4 mL, 0.25M), and base (0.2 mmol, 2 equiv) in successive order. The vial was sealed with a PTFE lined screw cap (ThermoFisher, C4015-A) and removed from the glovebox. The reaction was stirred at rt for 18 h. 1,3,5-trimethoxybenzene (mass weighed into the vial was recorded) internal standard was then added to the reaction solution, a 50 μL aliquot was taken and added to an NMR tube, then diluted with $CDCl_3$ (0.5 mL). ^1H NMR spectroscopy was used to determine the yield of the reaction. The aromatic C–H signal of 1,3,5-trimethoxybenzene at 6.09 ppm (s, 3H) was integrated against the benzylic methylene C–H signal of the product at 5.19 ppm (s, 2H) to assess the yield. The results of this investigation are summarized in Table S3 below. A representative example ^1H NMR spectrum for the crude reaction solution using the optimized conditions is shown in Figure S16 below to show how the yield was determined.

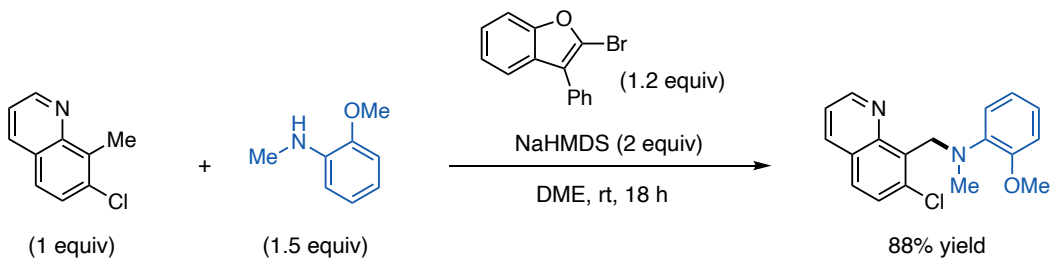

Table S3: Condition variation for the benzylic amination of 7-chloro-8-methylquinoline.

Entry	Changes from Optimized Conditions	Yield
1	No Changes	88%
2	2 equiv 15-crown-5 additive	86%
3	KO-*t*-Bu instead of NaHMDS	68%
4	KHMDS instead of NaHMDS	95%
5	2-bromothiophene as XTR	38%
6	DMF instead of DME	91%
7	THF instead of DME	38%
8	DMPU instead of DME	95%
9	PhMe instead of DME	0%
10	XTR **34** instead of XTR **33**	6%
11	XTR **34** instead of XTR **33** with 2 equiv 15-crown-5	40%
12	XTR **38** instead of XTR **33**	64%
13	1.1 equiv KO-*t*-Bu used	36%

14	KO-*t*-Bu instead of NaHMDS at 85 °C, 2 equiv 18-crown-6	64%

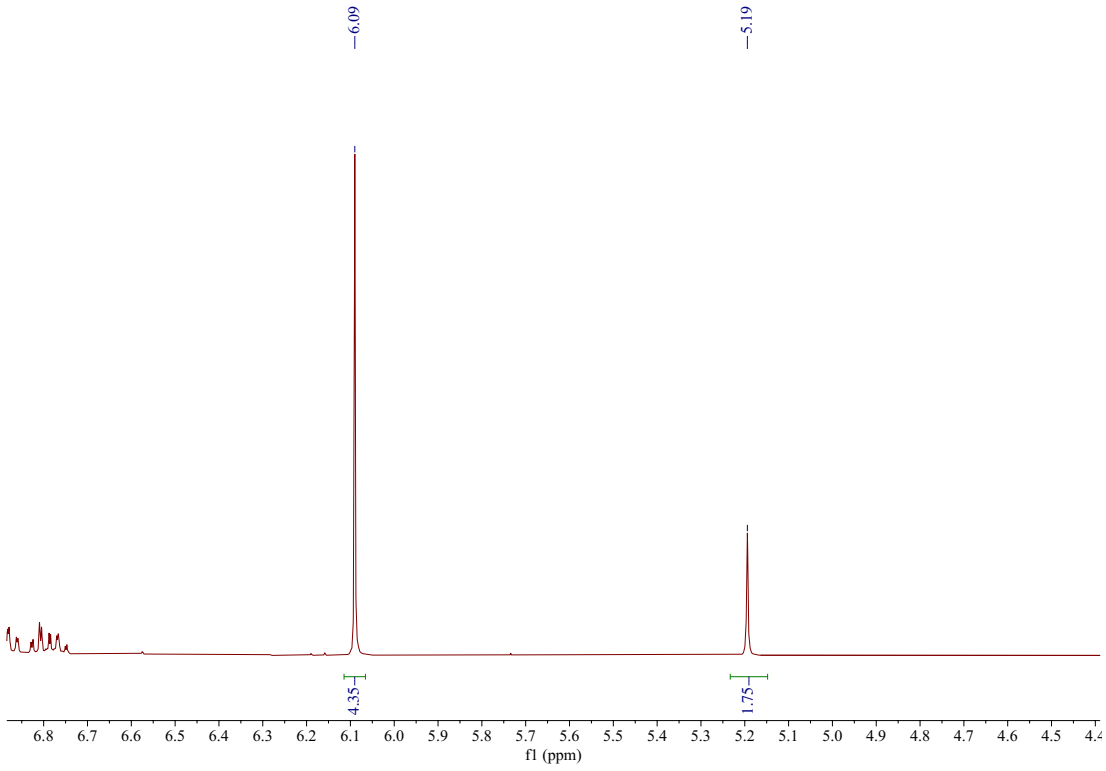

Figure S15: ^{1}H NMR spectral window of the crude reaction solution of reaction 7-chloro-8-methylquinoline from Table S3 above. 1,3,5-Trimethoxybenzene internal standard (24.4 mg, 0.15 mmol, signal at 6.09 ppm calibrated to 4.35 for 0.1 mmol scale reaction) was used to determine the yield of *N*-((7-chloroquinolin-8-yl)methyl)-2-methoxy-*N*-methylaniline (88% yield).

IV. General Procedures for Direct Benzylic C–H Amination

The substrates included in the scope of this reaction were isolated using General Procedures A or B below using a standard Schlenk manifold line outside of a glovebox. The reactions were set up

on a 1 mmol scale with respect to the alkyl arene substrate. The isolated yields of the materials are comparable to the ^{1}H NMR yields observed before isolation, unless otherwise noted. The compounds compiled here represent current isolated compounds with full isolation of the scope being undertaken by Kayla in our lab after I leave. Below are the general conditions (A-C) that have been utilized for most substrates in the scope. Any variation from conditions A-C are noted with the corresponding substrate.

General Procedure A (use of a solution of the base): An oven-dried 2-dram vial (ThermoFisher, 14-955-326) was charged with a magnetic stir bar, alkyl arene substrate (if solid, 1 mmol, 1 equiv), amine substrate (if solid, 1.5 mmol, 1.5 equiv), X-transfer reagent (1.2 mmol, 1.2 equiv), and 18-crown-6 (if used, 1 mmol, 1 equiv). The vial was sealed with a PTFE lined screw cap (ThermoFisher, C4015-A) and evacuated then flushed with nitrogen three times via a N_2 inlet tube on a Schlenk manifold line. Anhydrous DME (2 mL, 0.25 M total volume), alkyl arene substrate (if liquid, 1 mmol, 1 equiv), amine substrate (if liquid, 1.5 mmol, 1.5 equiv), and KHMDS or NaHMDS (1 M solution in THF, 2 mmol, 2 equiv, 0.25 M total volume) were added to the vial *via* N_2-flushed syringe. The N_2 inlet tube was removed from the vial and the cap was wrapped in parafilm and PVC tape and stirred at rt for 18 h. The reaction mixture was diluted with EtOAc (30 mL) and transferred to a separatory funnel and washed with H_2O (3 x 30 mL). The combined aqueous layers were washed with EtOAc (2 x 30 mL). The combined organic layers were washed with brine, dried over Na_2SO_4, and concentrated *in vacuo*. The crude reaction material was subsequently purified *via* silica gel chromatography.

General Procedure B (use of a solid base): An oven-dried 2-dram vial (ThermoFisher, 14-955-326) was charged with a magnetic stir bar, alkyl arene substrate (if solid, 1 mmol, 1 equiv), amine substrate (if solid, 1.5 mmol, 1.5 equiv), X-transfer reagent (1.2 mmol, 1.2 equiv), and 18-crown-6 (if used, 1 mmol, 1 equiv). The vial was sealed with a PTFE lined screw cap (ThermoFisher, C4015-A) and evacuated then flushed with nitrogen three times via a N_2 inlet tube on a Schlenk manifold line. A separate oven-dried 2-dram vial (ThermoFisher, 14-955-326) was charged with base (2 mmol, 2 equiv). The vial was sealed with a PTFE lined screw cap (ThermoFisher, C4015-A) and evacuated then flushed with nitrogen three times via a N_2 inlet tube on a Schlenk manifold line. Anhydrous DME (4 mL, 0.25 M), alkyl arene substrate (if liquid, 1 mmol, 1 equiv), and amine substrate (if liquid, 1.5 mmol, 1.5 equiv) were added to the vial containing the reagents *via* N_2-flushed syringe. The contents of the reagent vial were transferred to the vial containing the base *via* N_2-flushed syringe. . The N_2 inlet tube was removed from the vial and the cap was wrapped in parafilm and PVC tape and stirred at rt for 18 h. The reaction mixture was diluted with EtOAc (30 mL) and transferred to a separatory funnel and washed with H_2O (3 x 30 mL). The combined aqueous layers were washed with EtOAc (2 x 30 mL). The combined organic layers were washed with brine, dried over Na_2SO_4, and concentrated *in vacuo*. The crude reaction material was subsequently purified *via* silica gel chromatography.

V. Isolation and Characterization of Benzylic Amine Products

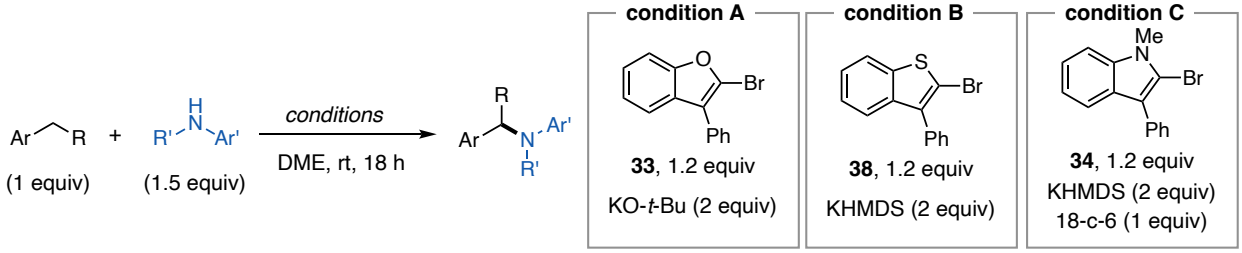

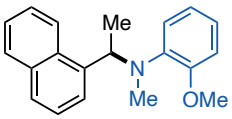

2-methoxy-*N*-methyl-*N*-(1-(naphthalen-1-yl)ethyl)aniline. *Due to challenges with coelution with the aniline and protodehalogenated X-transfer reagent byproduct, this material was run on a 0.3 mmol scale and isolated via prep TLC* The compound was prepared using General Procedure A in Section IV using 1-ethylnaphthalene (45.6 µL, 0.3 mmol, 1 equiv), 2-methoxy-*N*-methylaniline (61.7 mg, 0.45 mmol, 1.5 equiv), 2-bromo-1-methyl-3-phenyl-1H-indole (103.0 mg, 0.36 mmol, 1.2 equiv), 18-crown-6 (73.8 mg, 0.3 mmol, 1 equiv), KHMDS (1M solution in THF, 0.6 mL, 0.6 mmol, 2 equiv), and anhydrous DME (0.2 mL, 0.25 M overall). The product was purified *via* silica gel chromatography using 5% Et_2O in hexanes to afford 2-methoxy-*N*-methyl-*N*-(1-(naphthalen-1-yl)ethyl)aniline as a white solid (27.4 mg, 0.09 mmol, 31% yield). **^{1}H NMR** (400 MHz, $CDCl_3$) δ 8.55 (d, *J* = 8.7 Hz, 1H), 7.83 (d, *J* = 7.6 Hz, 1H), 7.75 (d, 8.1 Hz), 7.62 (d, *J* = 7.1 Hz, 1H), 7.50 – 7.37 (m, 3H), 7.05 – 6.97 (m, 1H), 6.97 – 6.91 (m, 2H), 6.88 – 6.78 (m, 1H), 5.57 (q, *J* = 6.8 Hz, 1H), 3.98 (s, 3H), 2.50 (s, 3H), 1.48 (d, *J* = 6.8 Hz, 3H). **^{13}C NMR** (101 MHz, $CDCl_3$) δ 153.9, 141.2, 139.1, 133.9, 132.4, 128.4, 127.5, 125.5, 125.3, 125.1, 124.9, 124.8, 122.9, 122.5, 120.8, 111.5, 55.8, 55.4, 36.0, 16.8.

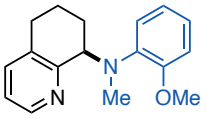

***N*-(2-methoxyphenyl)-*N*-methyl-5,6,7,8-tetrahydroquinolin-8-amine.** *This material coelutes with and is inseparable from the desaturated byproduct (quinoline) and is therefore reported here with this impurity present.* The compound was prepared using General Procedure A in Section IV using 5,6,7,8-tetrahydroquinoline (39 µL, 0.3 mmol, 1 equiv), 2-methoxy-*N*-methylaniline (61.7 mg, 0.45 mmol, 1.5 equiv), 2-bromo-3-phenylbenzo[b]thiophene (121.0 mg, 0.36 mmol, 1.2 equiv), KHMDS (1M solution in THF, 0.6 mL, 0.6 mmol, 2 equiv), and anhydrous DME (0.2 mL, 0.25 M overall). The product was purified *via* prep TLC using 20% EtOAc in hexanes to afford *N*-(2-methoxyphenyl)-*N*-methyl-5,6,7,8-tetrahydroquinolin-8-amine as an orange solid (22.1 mg, 0.08 mmol, 27% yield) with quinoline byproduct (shown below in ^{1}H NMR spectrum). **^{1}H NMR** (400 MHz, $CDCl_3$) δ 8.56 (d, J = 4.7 Hz, 1H), 7.42 (d, J = 6.9 Hz, 1H), 7.15 – 7.05 (m, 2H), 7.01 – 6.82 (m, 3H), 4.95 (dd, J = 9.6, 5.4 Hz, 1H), 3.85 (s, 3H), 2.92 – 2.79 (m, 1H), 2.78 – 2.68 (m, 1H), 2.61 (s, 3H), 2.07 – 1.88 (m, 3H), 1.79 – 1.62 (m, 1H).

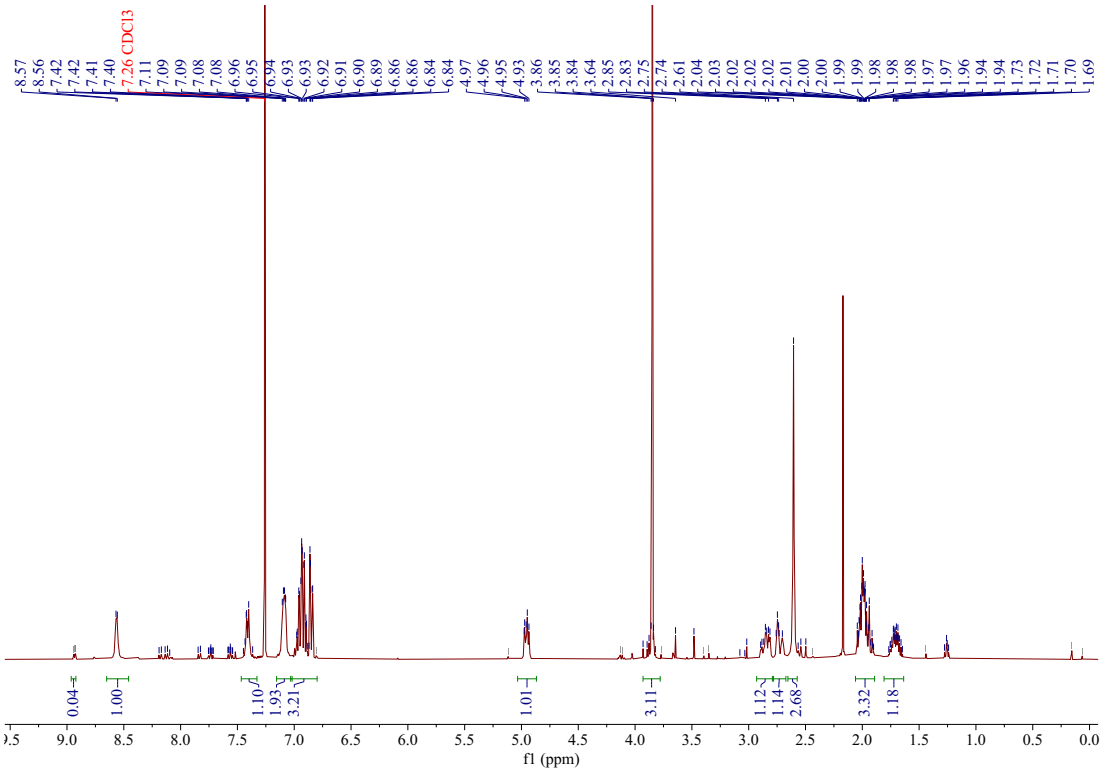

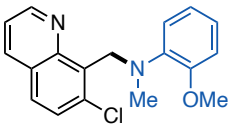

***N*-((7-chloroquinolin-8-yl)methyl)-2-methoxy-*N*-methylaniline.** The compound was prepared using General Procedure A in Section IV using 7-chloro-8-methylquinoline (177.6 mg, 1 mmol, 1 equiv), 2-methoxy-*N*-methylaniline (205.8 mg, 1.5 mmol, 1.5 equiv), 2-bromo-3-phenylbenzo[b]thiophene (347.0 mg, 1.2 mmol, 1.2 equiv), NaHMDS (1 M solution in THF, 2 mL, 2 mmol, 2 equiv), and anhydrous DME (2 mL, 0.25 M overall). The product was purified *via* silica gel chromatography using 20% EtOAc in hexanes to afford *N*-(2-methoxyphenyl)-*N*-methyl-5,6,7,8-tetrahydroquinolin-8-amine as an orange-brown solid (233.0 mg, 0.74 mmol, 74% yield). **^{1}H NMR** (400 MHz, $CDCl_3$) δ 8.76 (d, *J* = 4.3 Hz, 1H), 8.07 (dd, *J* = 8.2, 1.8 Hz, 1H), 7.65 (d, *J* = 8.7 Hz, 1H), 7.50 (d, *J* = 8.7 Hz, 1H), 7.32 (dd, *J* = 8.2 Hz, 4.2 Hz, 1H), 6.96 (t, *J* = 7.2 Hz, 1H), 6.91 – 6.77 (m, 3H), 5.20 (s, 2H), 3.90 (s, 3H), 2.71 (s, 3H).

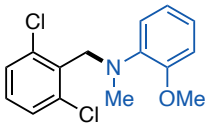

***N*-(2,6-dichlorobenzyl)-2-methoxy-*N*-methylaniline.** The compound was prepared using General Procedure B in Section IV using 2,6-dichlorotoluene (128.4 µL, 1 mmol, 1 equiv), 2-methoxy-*N*-methylaniline (205.8 mg, 1.5 mmol, 1.5 equiv), 2-bromo-3-phenylbenzofuran (327.8 mg, 1.2 mmol, 1.2 equiv), KO-*t*-Bu (224.4 mg, 2 mmol, 2 equiv), and anhydrous DME (4 mL, 0.25 M). The product was purified *via* silica gel chromatography using 5% Et_2O in hexanes to afford *N*-(2,6-dichlorobenzyl)-2-methoxy-*N*-methylaniline as a green-yellow oil (105.3 mg, 0.36 mmol, 36% yield). **^{1}H NMR** (400 MHz, $CDCl_3$) δ 7.29 (d, *J* = 8.0 Hz, 2H), 7.12 (t, *J* = 7.5 Hz, 1H), 7.06 – 6.96 (m, 1H), 6.94 – 6.84 (m, 2H), 4.58 (s, 2H), 3.87 (s, 3H), 2.75 (s, 3H). **^{13}C NMR** (101 MHz, $CDCl_3$) δ 153.8, 137.2, 134.1, 128.8, 128.4, 123.3, 121.5, 120.9, 111.9, 55.6, 53.1, 39.8.

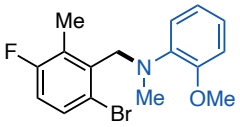

***N*-(6-bromo-3-fluoro-2-methylbenzyl)-2-methoxy-*N*-methylaniline.** The compound was prepared using General Procedure A in Section IV using 1-bromo-4-fluoro-2,3-dimethylbenzene (133.0 µL, 1 mmol, 1 equiv), 2-methoxy-*N*-methylaniline (205.8 mg, 1.5 mmol, 1.5 equiv), 2-bromo-3-phenylbenzo[b]thiophene (347.0 mg, 1.2 mmol, 1.2 equiv), NaHMDS (1 M solution in THF, 2 mL, 2 mmol, 2 equiv), and anhydrous DME (2 mL, 0.25 M overall). The product was purified *via* silica gel chromatography using 5% Et_2O in hexanes to afford *N*-(6-bromo-3-fluoro-2-methylbenzyl)-2-methoxy-*N*-methylaniline as a yellow oil (79.6 mg, 0.24 mmol, 24% yield). **^{1}H NMR** (400 MHz, $CDCl_3$) δ 7.38 (dd, *J* = 8.8, 5.3 Hz, 1H), 7.11 – 6.99 (m, 2H), 6.98 – 6.79 (m, 3H), 4.42 (s, 2H), 3.86 (s, 3H), 2.65 (s, 3H), 2.30 d, *J* = 2.6 Hz, 3H). **^{19}F NMR** (376 MHz, $CDCl_3$) δ -116.56. **^{13}C NMR** (101 MHz, $CDCl_3$) δ 160.7 (d, *J* = 243.9 Hz),

153.6, 142.1, 137.9, 130.7 (d, J = 8.5 Hz), 128.7, 128.4 (d, J = 16.8 Hz), 123.4, 121.0, 120.7 (d, J = 3.18 Hz), 115.5 (d, J = 24.5 Hz), 111.7, 55.8, 55.4, 39.4, 11.4 (d, J = 5.4 Hz).

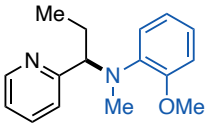

2-methoxy-*N*-methyl-*N*-(1-(pyridin-2-yl)propyl)aniline. The compound was prepared using General Procedure A in Section IV using 2-propylpyridine (133.0 µL, 1 mmol, 1 equiv), 2-methoxy-*N*-methylaniline (205.8 mg, 1.5 mmol, 1.5 equiv), 2-bromo-3-phenylbenzo[b]thiophene (347.0 mg, 1.2 mmol, 1.2 equiv), KHMDS (1 M solution in THF, 2 mL, 2 mmol, 2 equiv), and anhydrous DME (2 mL, 0.25 M overall). The product was purified *via* silica gel chromatography using 10% EtOAc in hexanes to afford 2-methoxy-*N*-methyl-*N*-(1-(pyridin-2-yl)propyl)aniline as a yellow oil (188.9 mg, 0.74 mmol, 74% yield). **^{1}H NMR** (400 MHz, $CDCl_3$) δ 8.58 (dd, J = 4.9, 1.9 Hz, 1H), 7.57 (td, J = 7.7, 1.2 Hz, 1H), 7.23 (d, J = 7.9 Hz, 1H), 7.13 (dd, J = 7.5, 4.9 Hz, 1H), 7.00 – 6.93 (m, 1H), 6.92 – 6.78 (m, 3H), 4.58 (dd, J = 8.6, 6.2 Hz, 1H), 3.89 (s, 3H), 2.64 (s, 3H), 2.32 – 2.17 (m, 1H), 2.00 – 1.85 (m, 1H), 0.85 (t, J = 7.4 Hz, 3H). **^{13}C NMR** (101 MHz, $CDCl_3$) δ 161.0, 153.0, 148.6, 141.7, 136.0, 124.1, 122.4, 121.9, 121.3, 120.9, 111.5, 67.7, 55.5, 34.4, 22.8, 11.6.

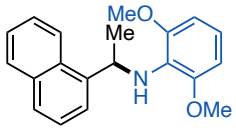

2,6-dimethoxy-*N*-(1-(naphthalen-1-yl)ethyl)aniline. The compound was prepared using General Procedure A in Section IV using 1-ethylnaphthalene (153.0 µL, 1 mmol, 1 equiv), 2,6-dimethoxyaniline (230.0 mg, 1.5 mmol, 1.5 equiv), 2-bromo-1-methyl-3-phenyl-1H-indole (343.4 mg, 1.2 mmol, 1.2 equiv), 18-crown-6 (246.1 mg, 1 mmol, 1 equiv), KHMDS (1 M solution in THF, 2 mL, 2 mmol, 2 equiv), and anhydrous DME (2 mL, 0.25

M overall). The product was purified *via* silica gel chromatography using a gradient from 5% to 10% EtOAc in hexanes to afford 2,6-dimethoxy-*N*-(1-(naphthalen-1-yl)ethyl)aniline as a yellow oil (278.9 mg, 0.91 mmol, 91% yield). **^{1}H NMR** (400 MHz, $CDCl_3$) δ 8.34 (d, *J* = 8.5 Hz, 1H), 7.83 (d, *J* = 8.1 Hz, 1H), 7.68 (d, *J* = 8.1 Hz, 1H), 7.58 – 7.36 (m, 4H), 6.71 (t, *J* = 8.2 Hz, 1H), 6.47 (d, *J* = 8.3 Hz, 2H), 5.96 (q, *J* = 6.7 Hz, 1H), 3.75 (s, 6H), 1.59 (d, 6.7 Hz, 3H). **^{13}C NMR** (101 MHz, $CDCl_3$) δ 150.6, 142.2, 134.0, 131.5, 128.8, 127.0, 126.3, 125.8, 125.6, 125.3, 123.6, 122.0, 119.3, 56.1, 50.4, 23.7.

V. References

[1] Wolfers, H.; Kraatz, U.; Korte, F. New route to 1-alkylthio-3,5-dihydroxybenzenes (monothiophlorglucinol-S-alkyl ethers). *Synthesis* **1975**, *1* 43-44.

[2] Hirota, T.; Tashima, Y.; Sasaki, K.; Namba, T.; Hayakawa, S. A novel synthesis of benzofuran and related compounds. IV. Vilsmeier reaction of 3,5-dimethoxyphenylthiomethyl compounds. *Heterocycles* **1987**, *26*, 2717-2725.

[3] Bone, K. I.; Puleo, T. R.; Delost, M. D.; Shimizu, Y.; Bandar, J. S. Direct Benzylic C–H Etherification Enabled by Base-Promoted Halogen Transfer. *ChemRxiv preprint, DOI: 10.26434/chemrxiv-2024-fvrc1.*

[4] Wang, C.-X.; Sheng, F.-F.; Liu, K.-H.; Gu, J.-G.; Shen, K.; Sun, Z.-Y.; Hong, K.; Zhang, H.-H. Bromide as the Directing Group for β-Arylation of Thiophenes. *Synthesis* **2022**, *54*, 4025-4032.

[5] Chen, S.; Liao, Y.; Zhao, F.; Qi, H.; Liu, S.; Deng, G.-J. Palladium-Catalyzed Direct Arylation of Indoles with Cyclohexanones. *Org*. *Lett*. **2014**, *16*, 1618−1621.

[6] Bedford, R. B.; Fey, N.; Haddow, M. F.; Sankey R. F. Remarkably reactive dihydroindoloindoles via palladium-catalysed dearomatisation. *Chem. Commun*. **2011**, *47*, 3649–3651.

[7] Luo, N.; Wang, M.; Li, H.; Zhang, J.; Liu, H.; Wang, F. Photocatalytic Oxidation−Hydrogenolysis of Lignin β-O-4 Models via a Dual Light Wavelength Switching Strategy. *ACS Catal.* **2016**, *6*, 7716−7721.

[8] Abarghooei, M. A.; Mohebat, R.; Karimi-Jaberi, Z.; Mosslemin, M. H. Synthesis of 3-aryl-benzo[*b*]furans and 3-aryl-naphtho[*b*]furans using *n*-propyl-4-aza-1-azoniabicyclo[2.2.2]octane chloride immobilised on SiO_2 as an efficient and reusable catalyst. *J. Chem. Res*. **2018**, *42*, 86-89.

VI. NMR Spectra

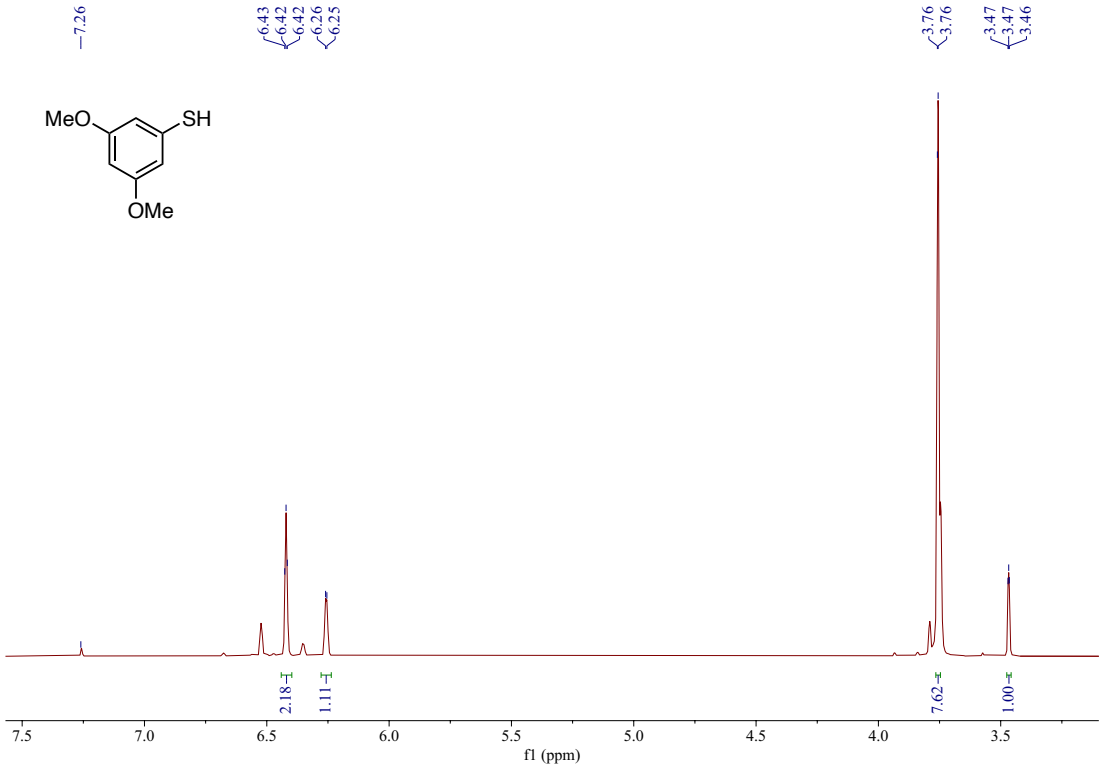

^{1}H NMR of 3,5-dimethoxybenzenethiol (400 MHz, $CDCl_3$)

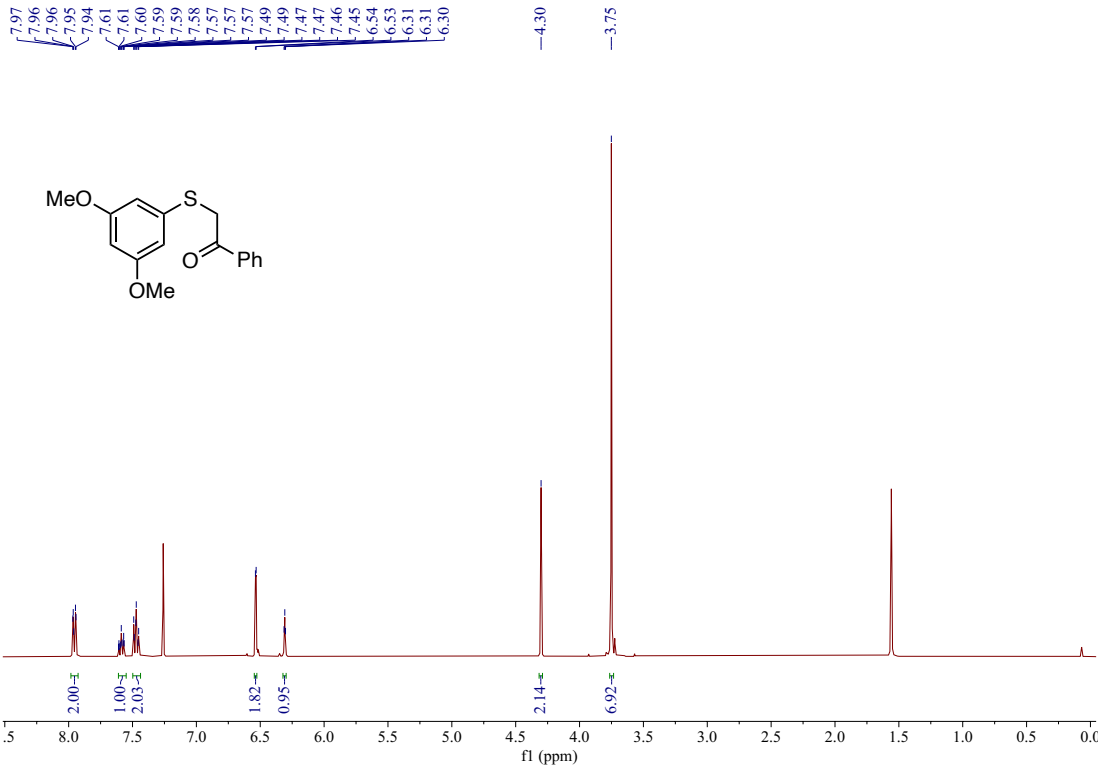

^{1}H NMR of 2-((3,5-dimethoxyphenyl)thio)-1-phenylethan-1-one (400 MHz, $CDCl_3$)

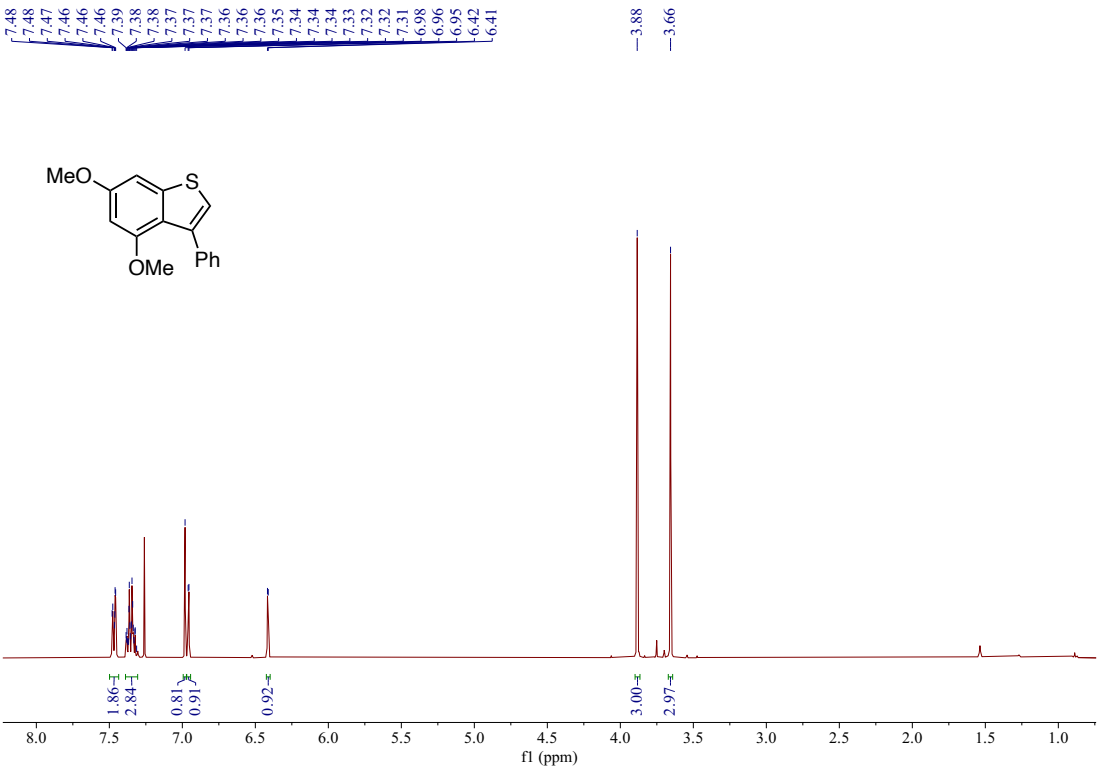

^{1}H NMR of 4,6-dimethoxy-3-phenylbenzo[*b*]thiophene (400 MHz, $CDCl_3$)

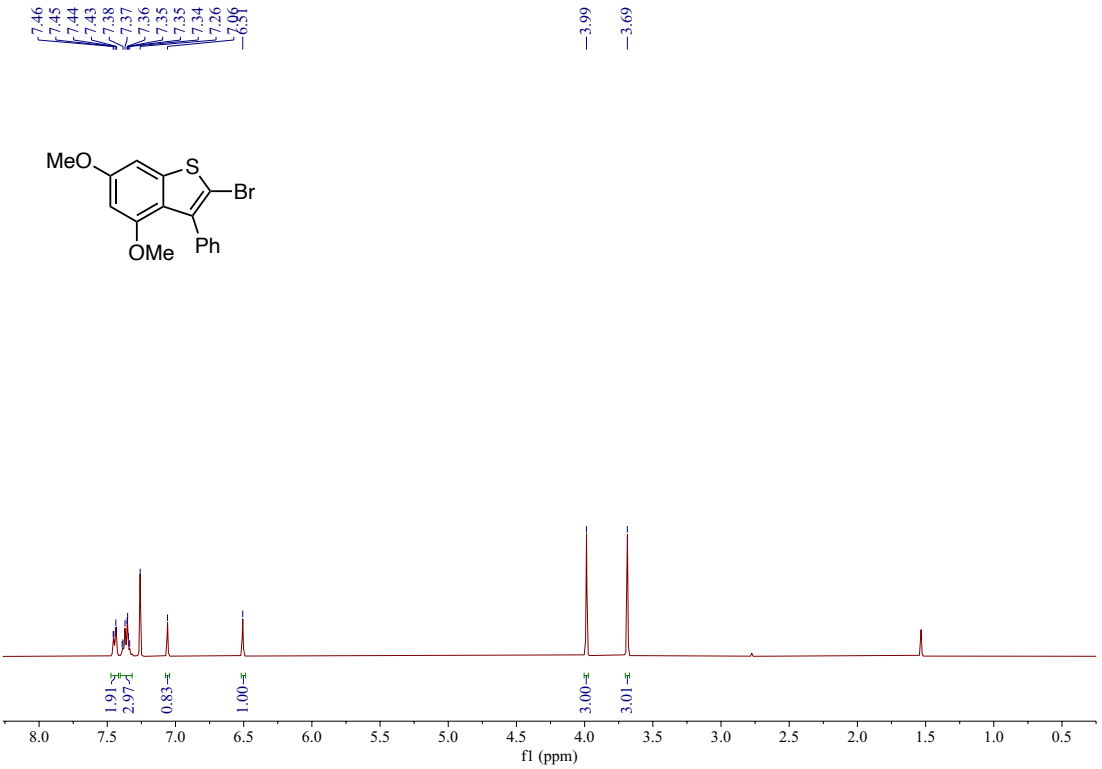

^{1}H NMR of 2-bromo-4,6-dimethoxy-3-phenylbenzo[b]thiophene (**20**) (400 MHz, $CDCl_3$)

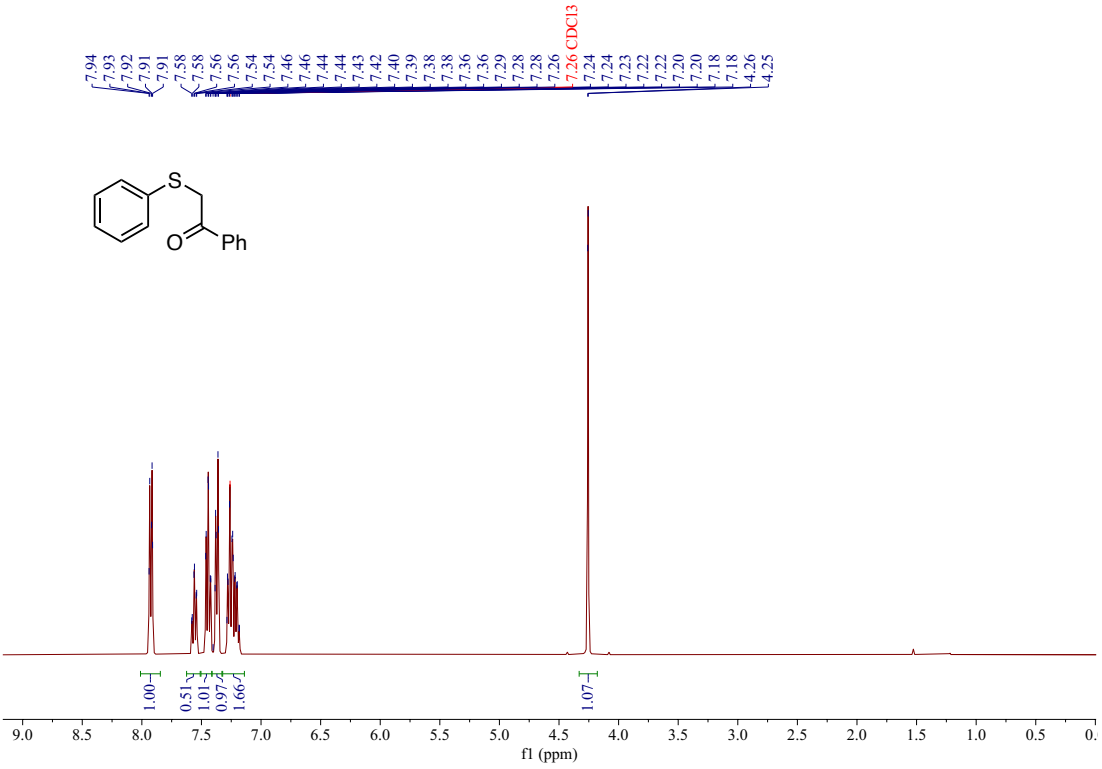

^{1}H NMR of 1-phenyl-2-(phenylthio)ethan-1-one (400 MHz, $CDCl_3$)

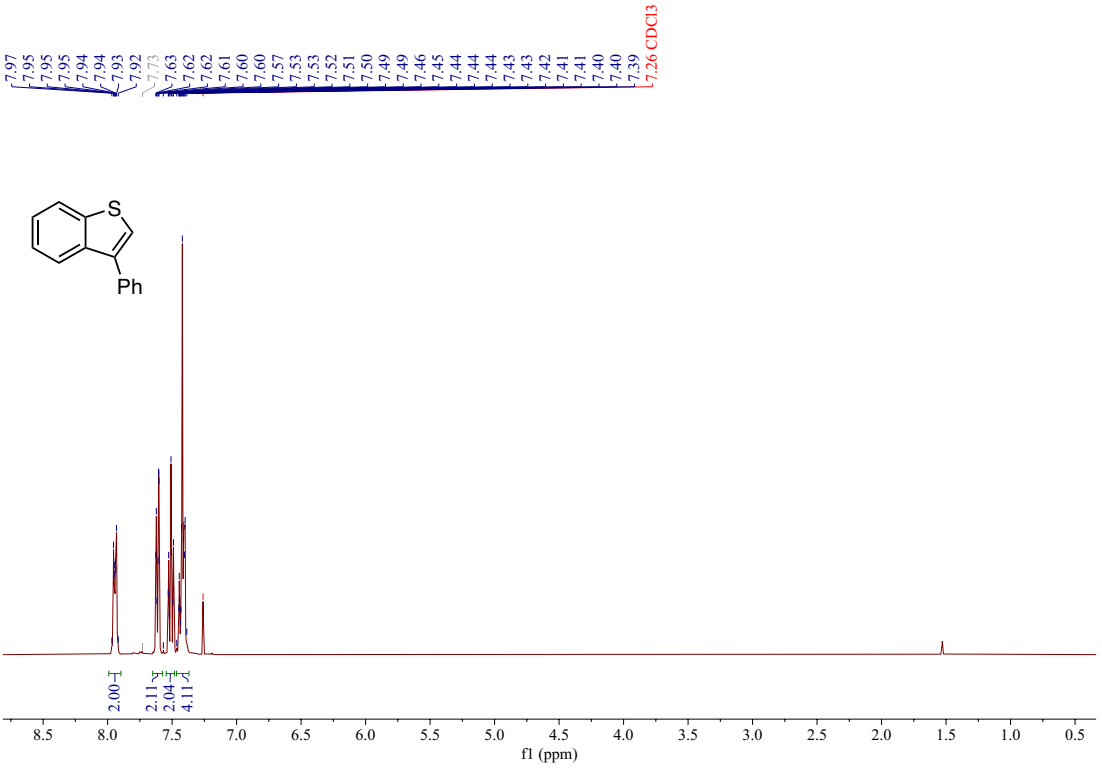

^{1}H NMR of 3-phenylbenzo[b]thiophene (400 MHz, $CDCl_3$)

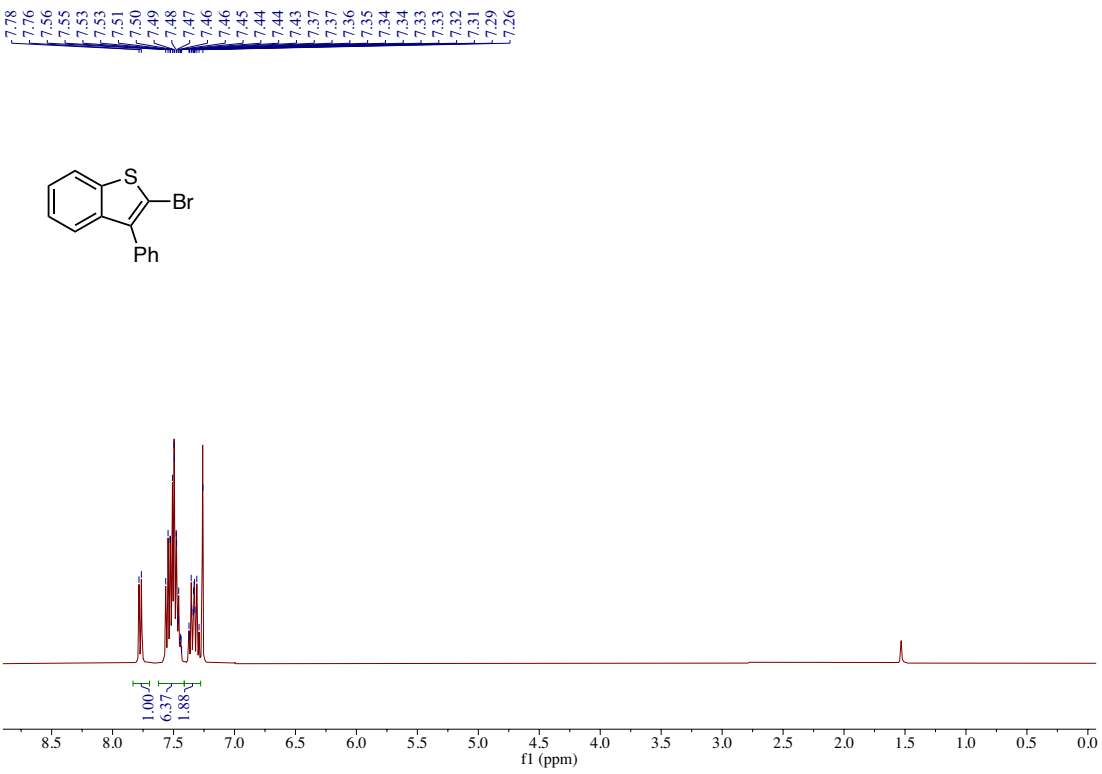

^{1}H NMR of 2-bromo-3-phenylbenzo[b]thiophene (**38**) (400 MHz, $CDCl_3$)

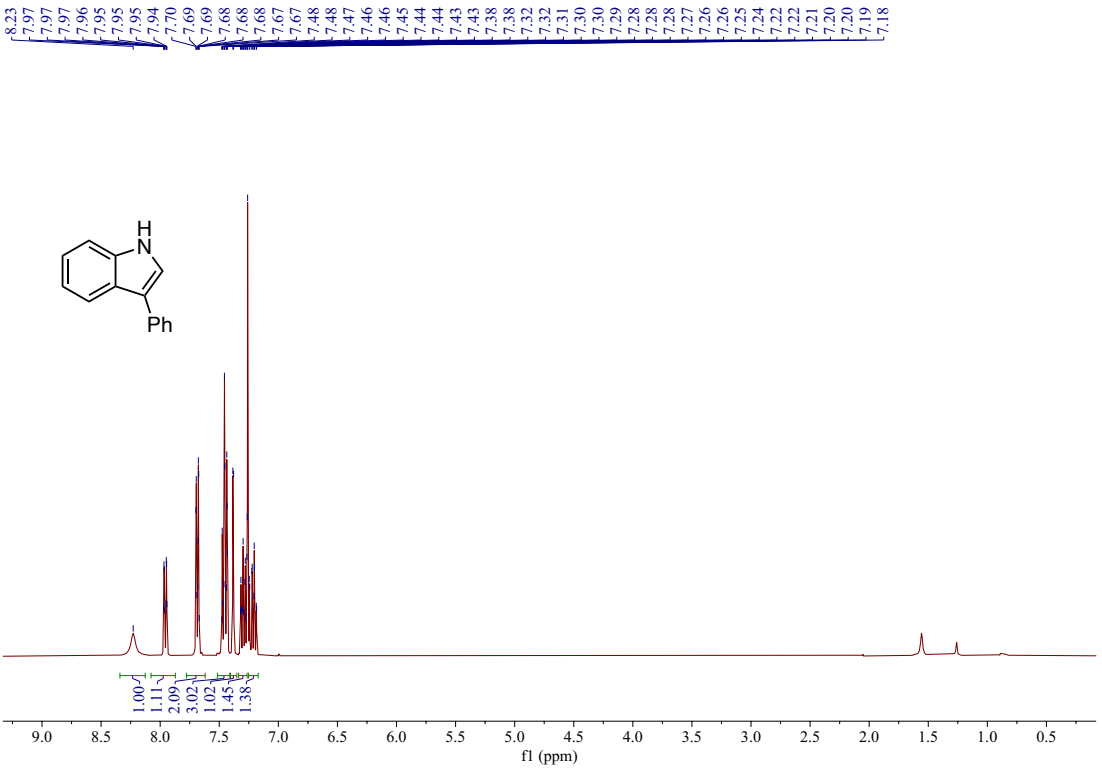

^{1}H NMR of 3-phenyl-1H-indole (400 MHz, $CDCl_3$)

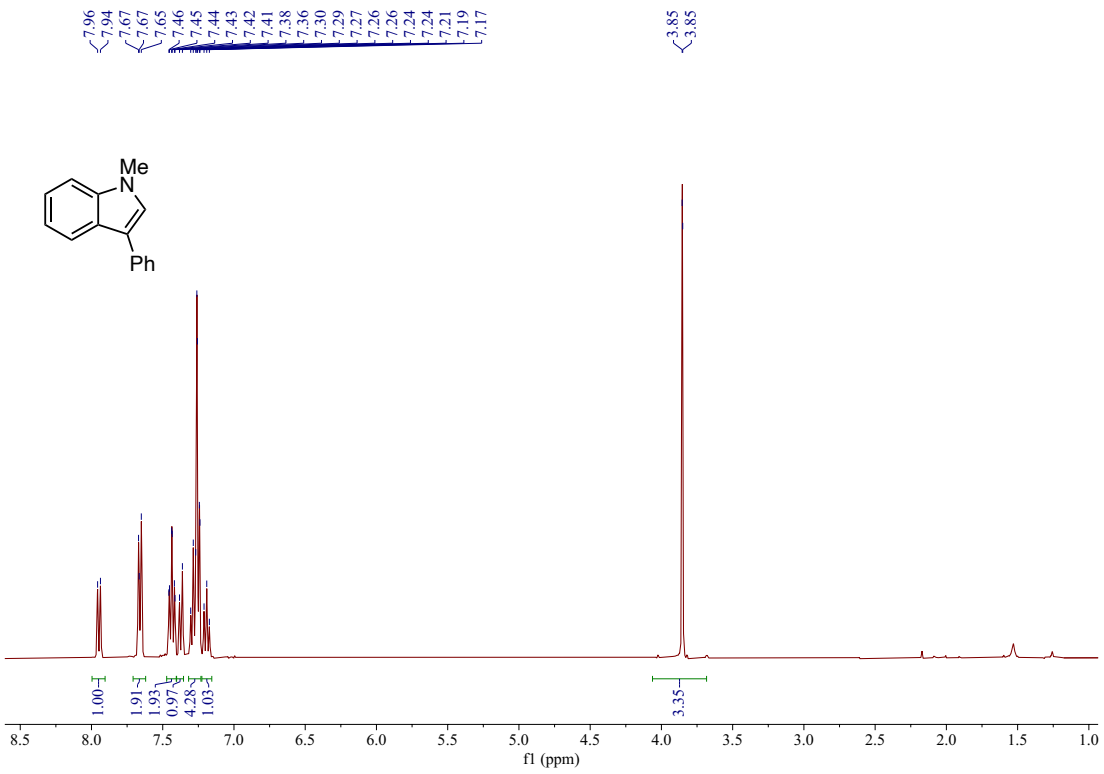

^{1}H NMR of 1-methyl-3-phenyl-1H-indole (400 MHz, $CDCl_3$)

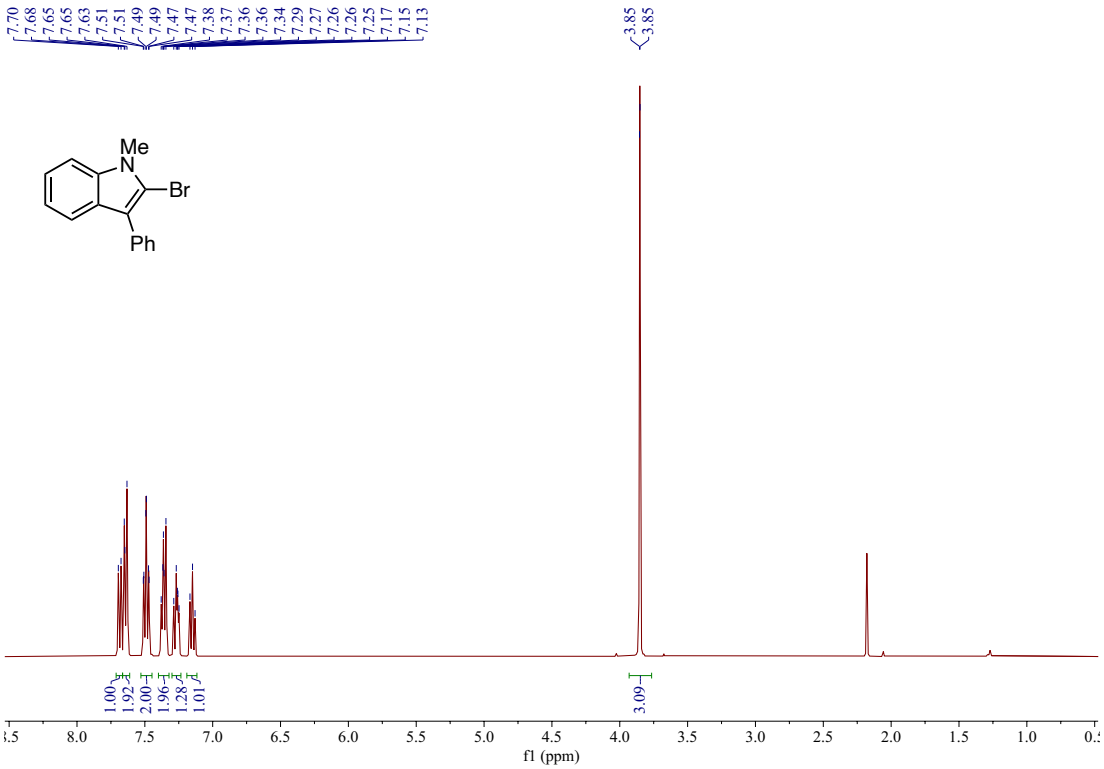

^{1}H NMR of 2-bromo-1-methyl-3-phenyl-1H-indole (**34**) (400 MHz, $CDCl_3$)

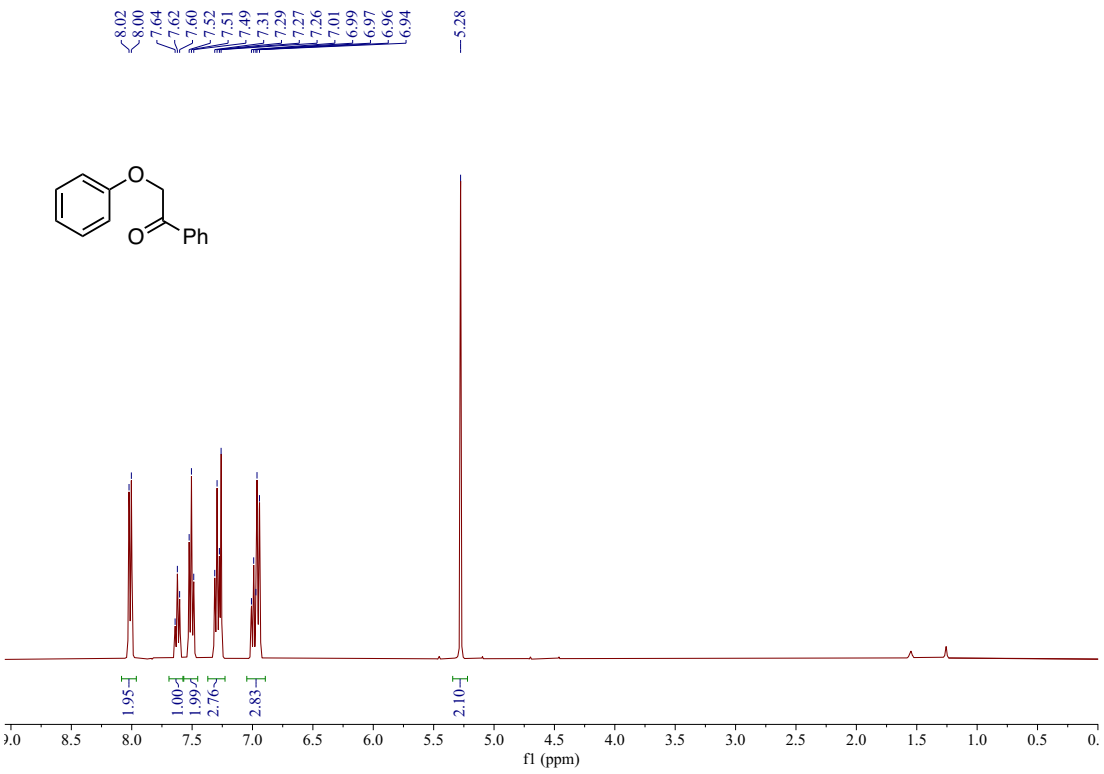

^{1}H NMR of phenyl benzoate (400 MHz, $CDCl_3$)

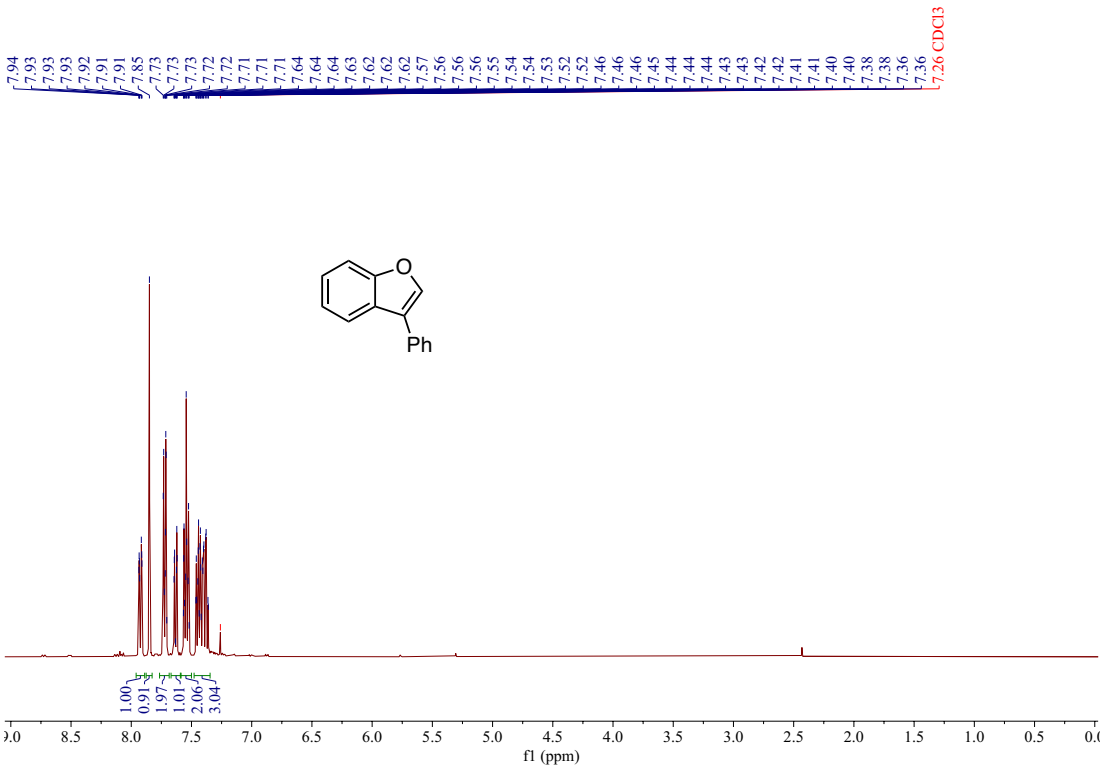

^{1}H NMR of 3-phenylbenzofuran (400 MHz, $CDCl_3$)

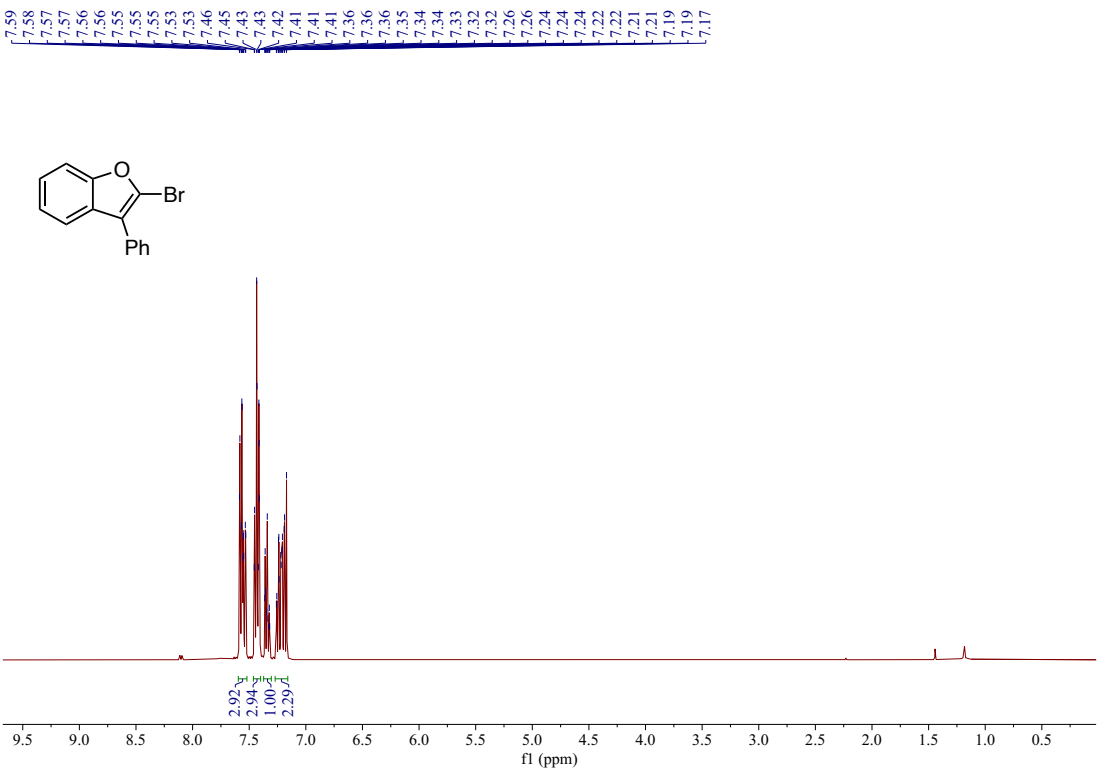

^{1}H NMR of 2-bromo-3-phenylbenzofuran (**33**) (400 MHz, $CDCl_3$)

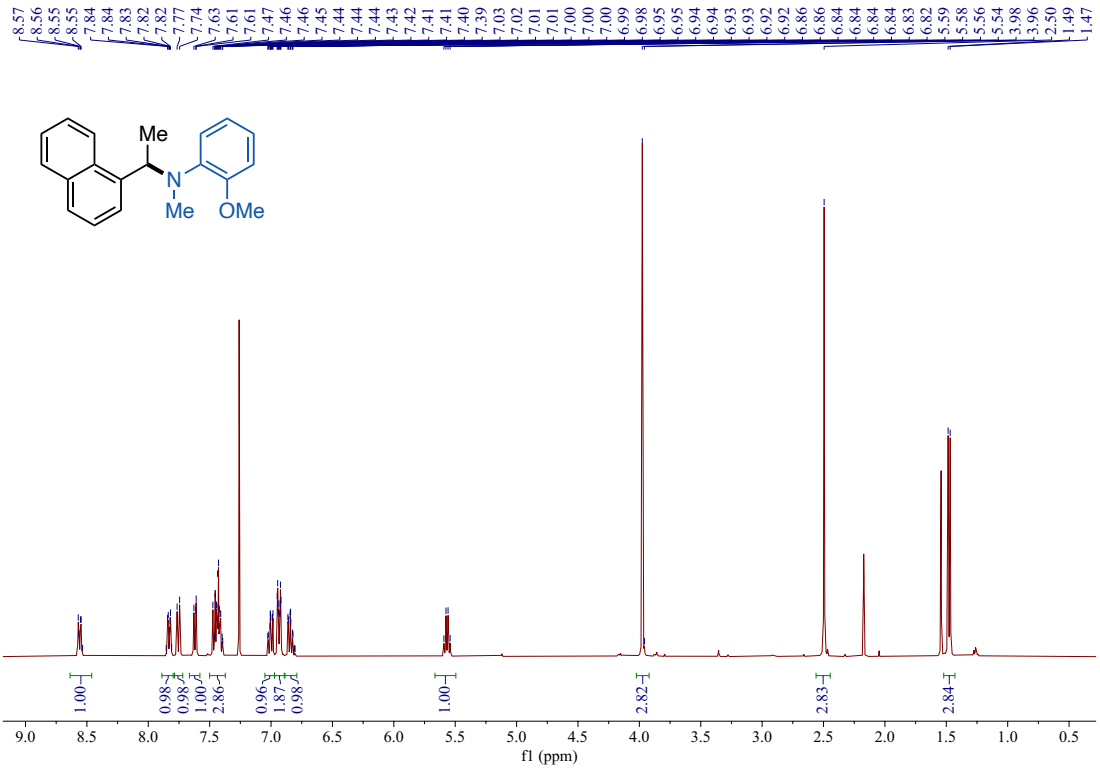

^{1}H NMR of 2-methoxy-*N*-methyl-*N*-(1-(naphthalen-1-yl)ethyl)aniline (400 MHz, $CDCl_3$)

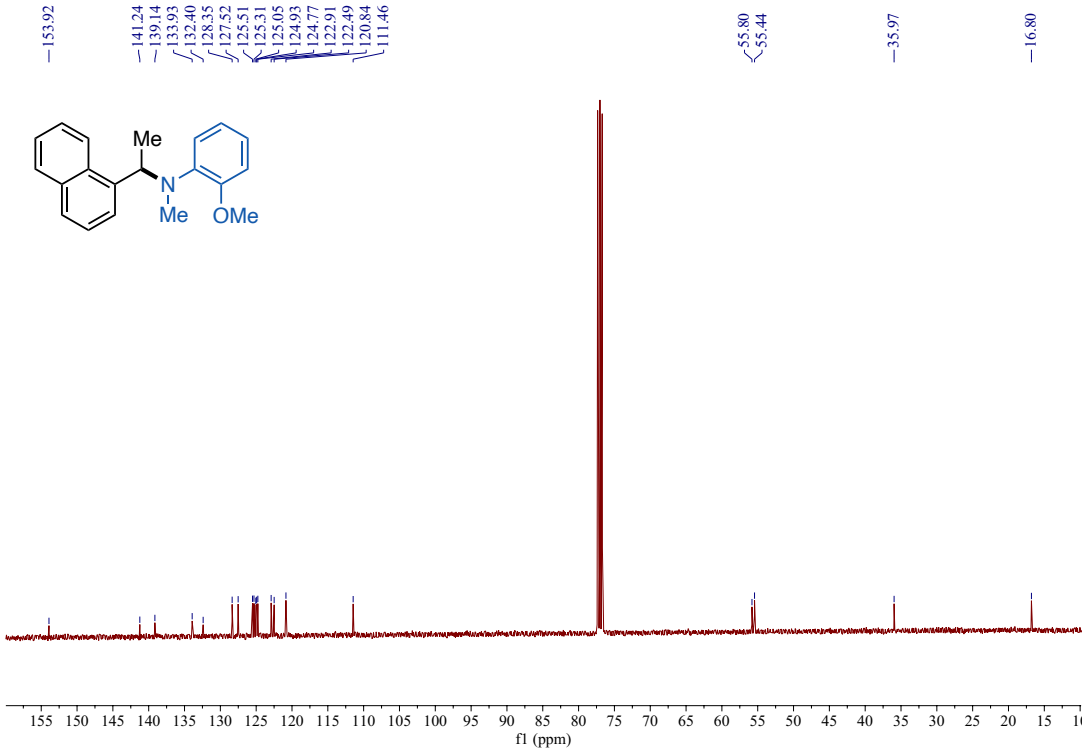

^{13}C NMR of 2-methoxy-*N*-methyl-*N*-(1-(naphthalen-1-yl)ethyl)aniline (101 MHz, $CDCl_3$)

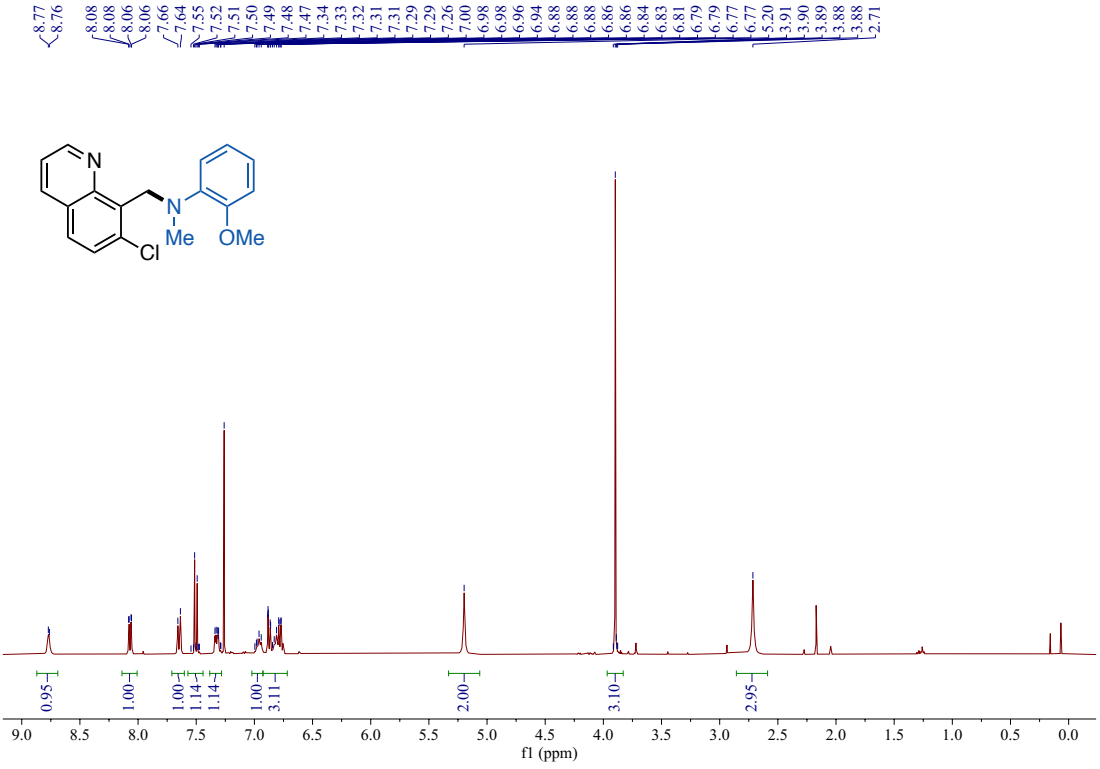

^{1}H NMR of *N*-(2-methoxyphenyl)-*N*-methyl-5,6,7,8-tetrahydroquinolin-8-amine (400 MHz, $CDCl_3$)

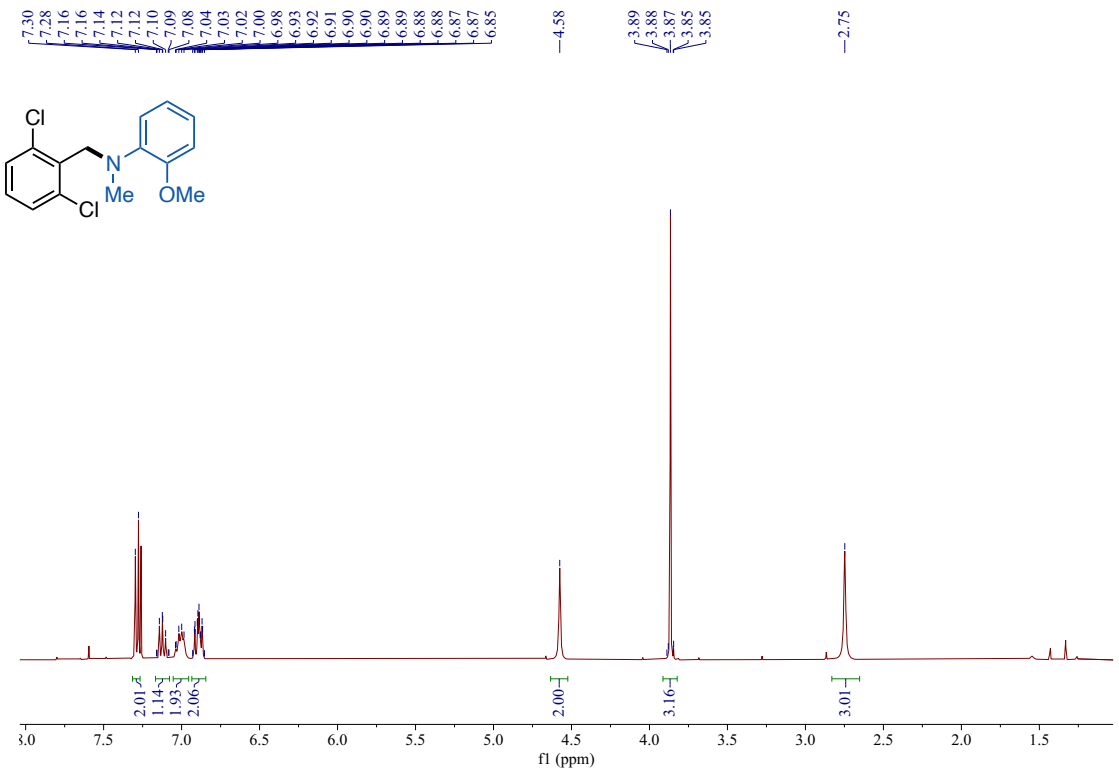

^{1}H NMR of *N*-(2,6-dichlorobenzyl)-2-methoxy-*N*-methylaniline (400 MHz, $CDCl_3$)

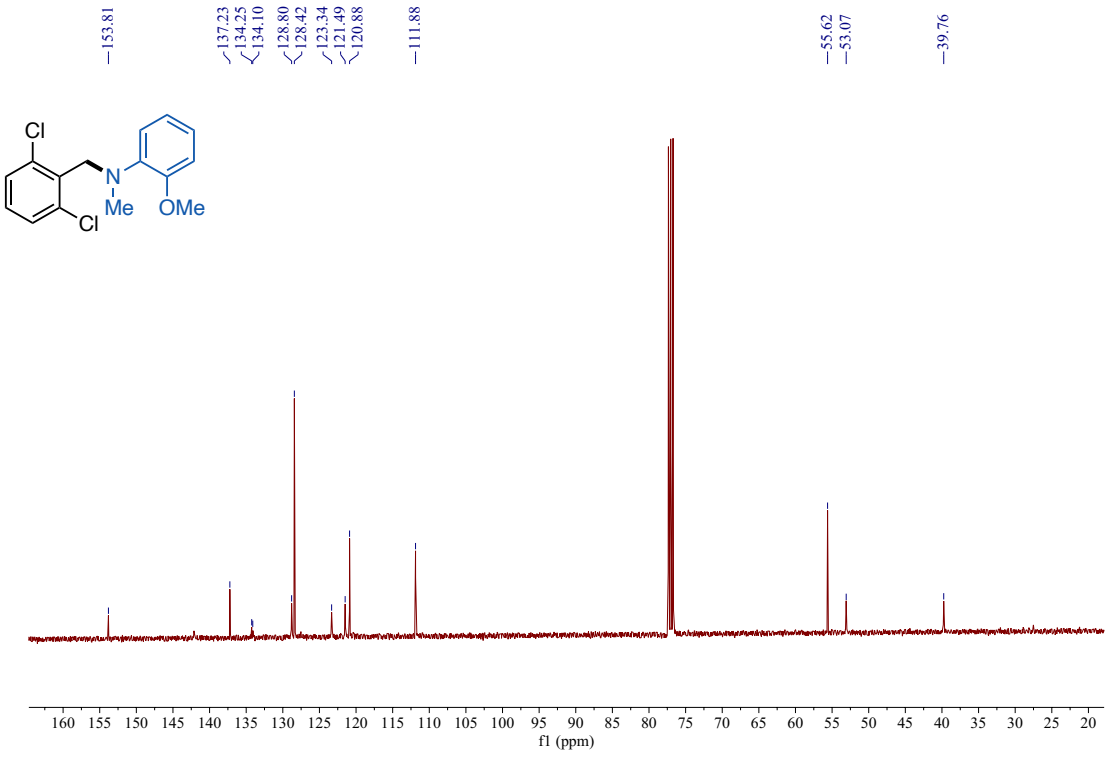

^{13}C NMR of *N*-(2,6-dichlorobenzyl)-2-methoxy-*N*-methylaniline (101 MHz, $CDCl_3$)

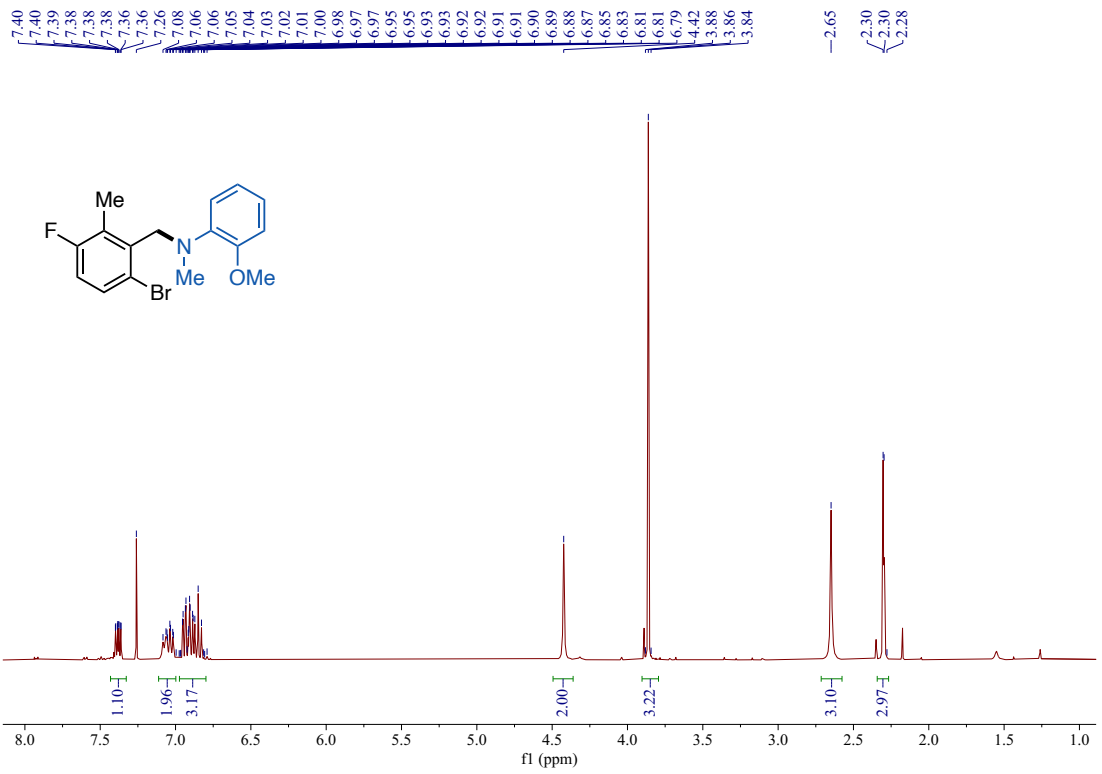

^{1}H NMR of *N*-(6-bromo-3-fluoro-2-methylbenzyl)-2-methoxy-*N*-methylaniline (400 MHz, $CDCl_3$)

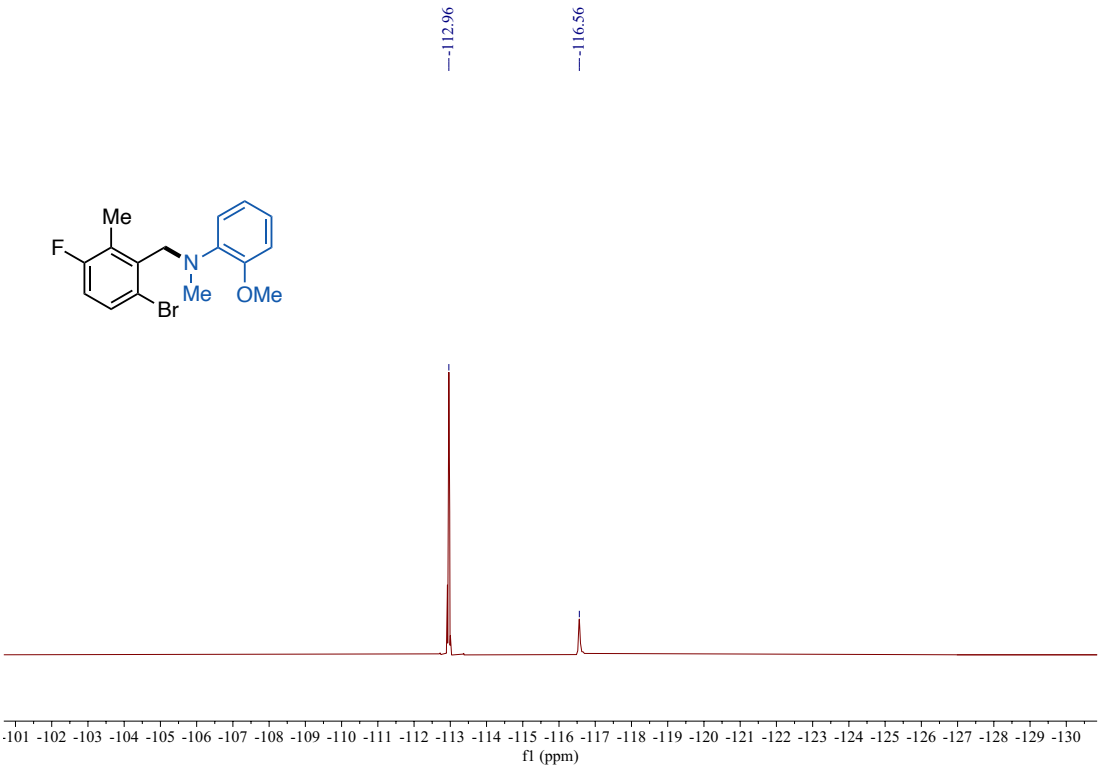

^{19}F NMR of *N*-(6-bromo-3-fluoro-2-methylbenzyl)-2-methoxy-*N*-methylaniline (376 MHz, $CDCl_3$)

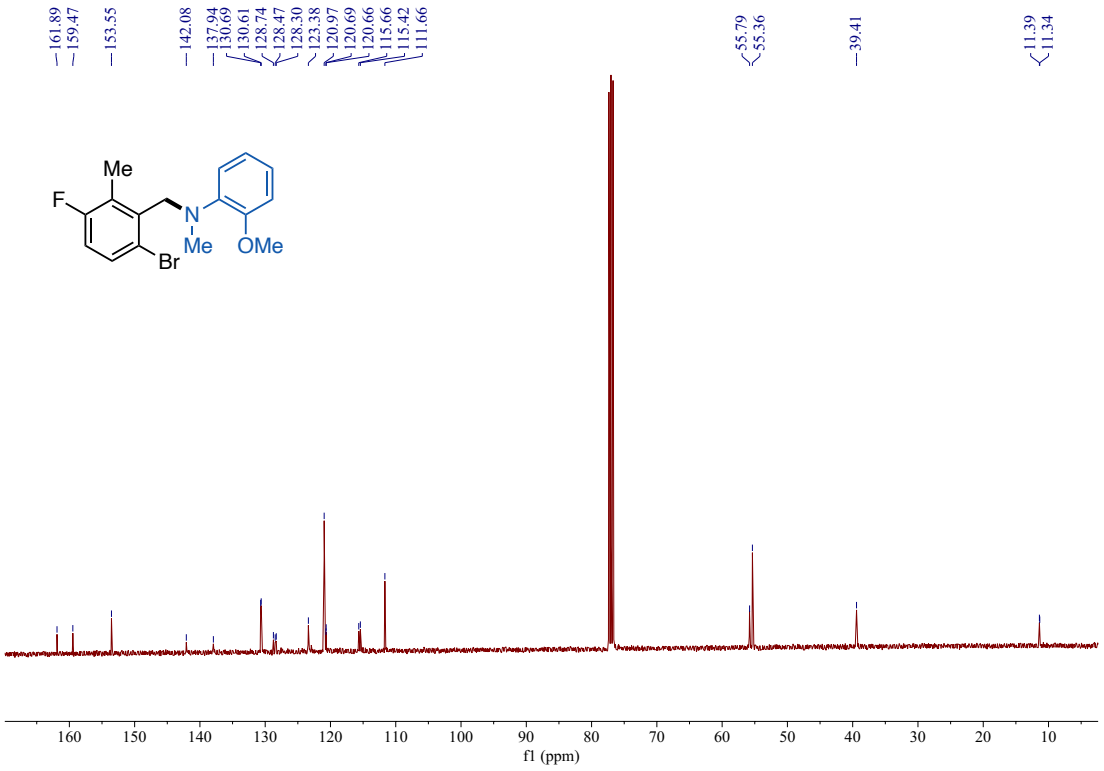

^{13}C NMR of *N*-(6-bromo-3-fluoro-2-methylbenzyl)-2-methoxy-*N*-methylaniline (101 MHz, $CDCl_3$)

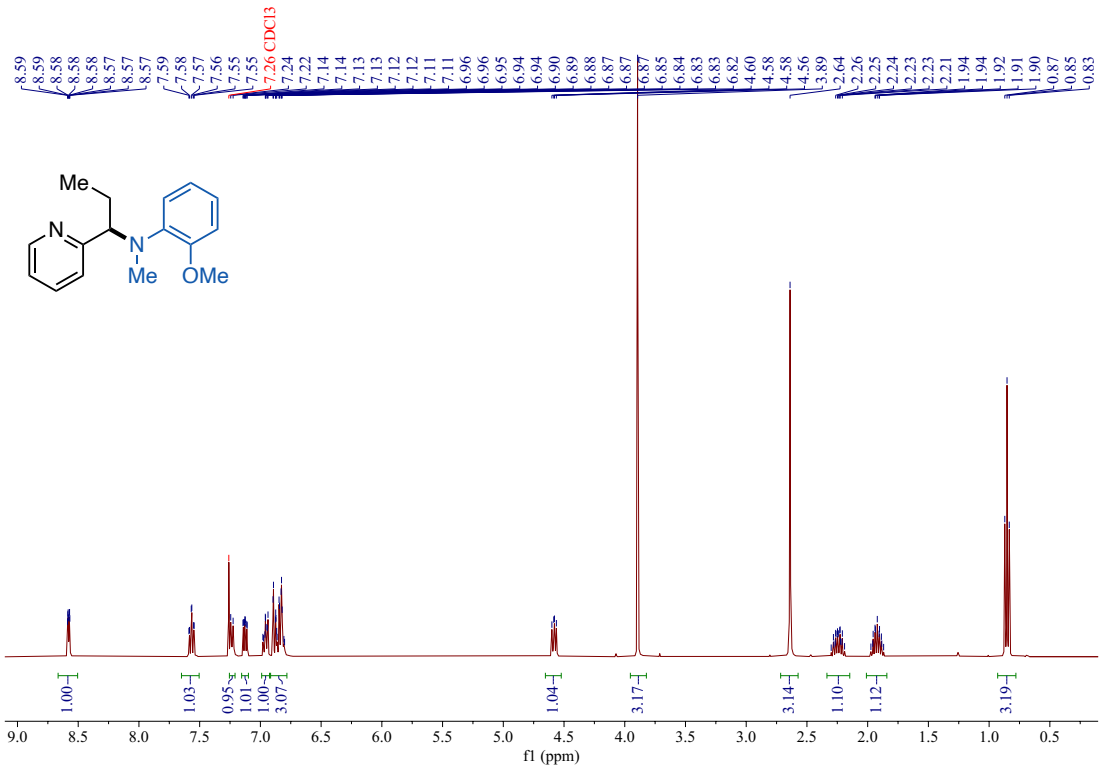

^{1}H NMR of 2-methoxy-*N*-methyl-*N*-(1-(pyridin-2-yl)propyl)aniline (400 MHz, $CDCl_3$)

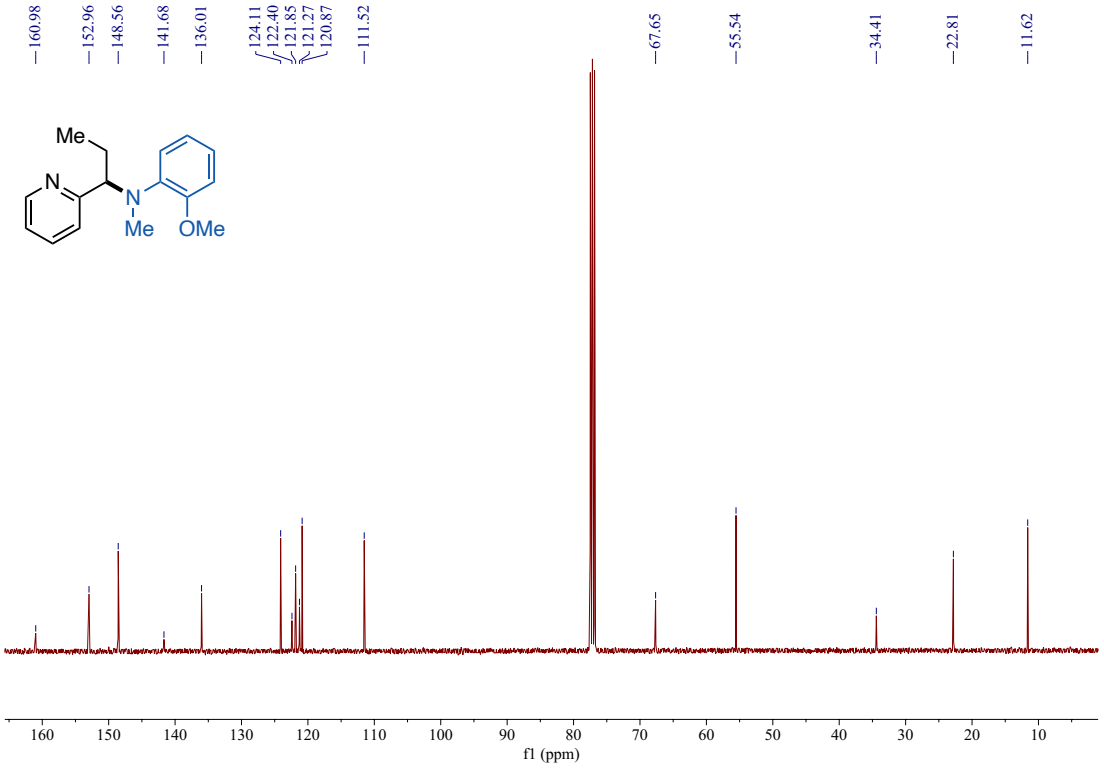

^{13}C NMR of 2-methoxy-*N*-methyl-*N*-(1-(pyridin-2-yl)propyl)aniline (101 MHz, $CDCl_3$)

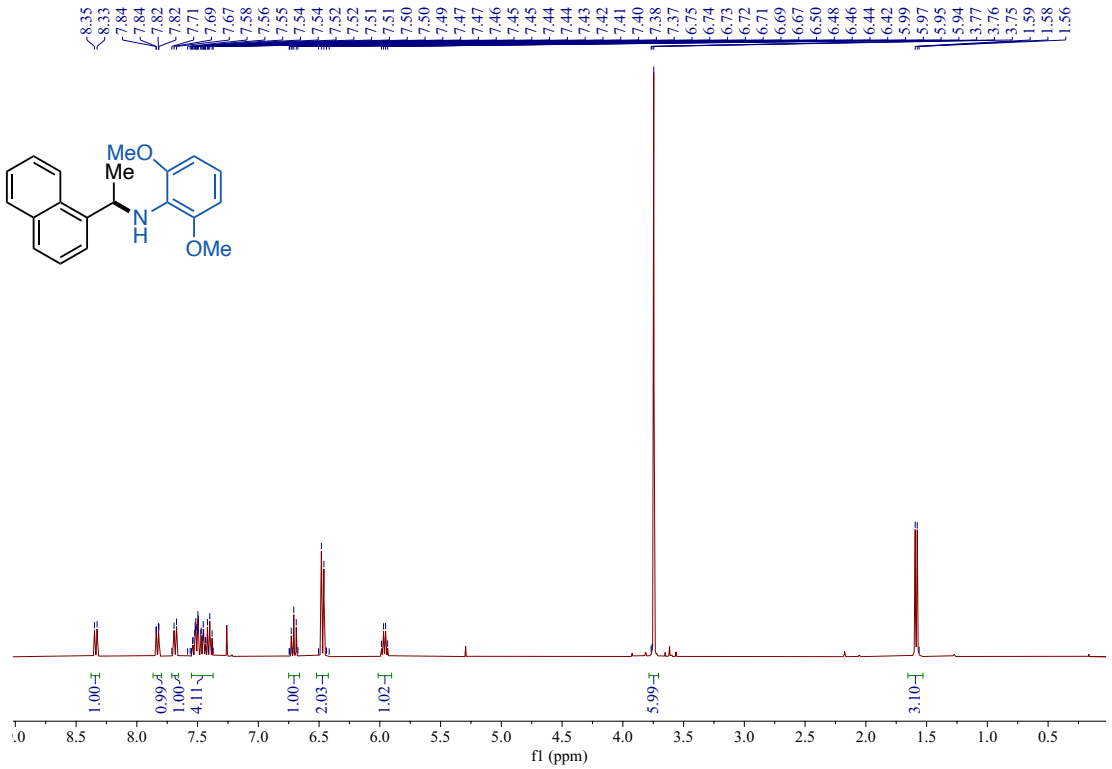

^{1}H NMR of 2,6-dimethoxy-*N*-(1-(naphthalen-1-yl)ethyl)aniline (400 MHz, $CDCl_3$)

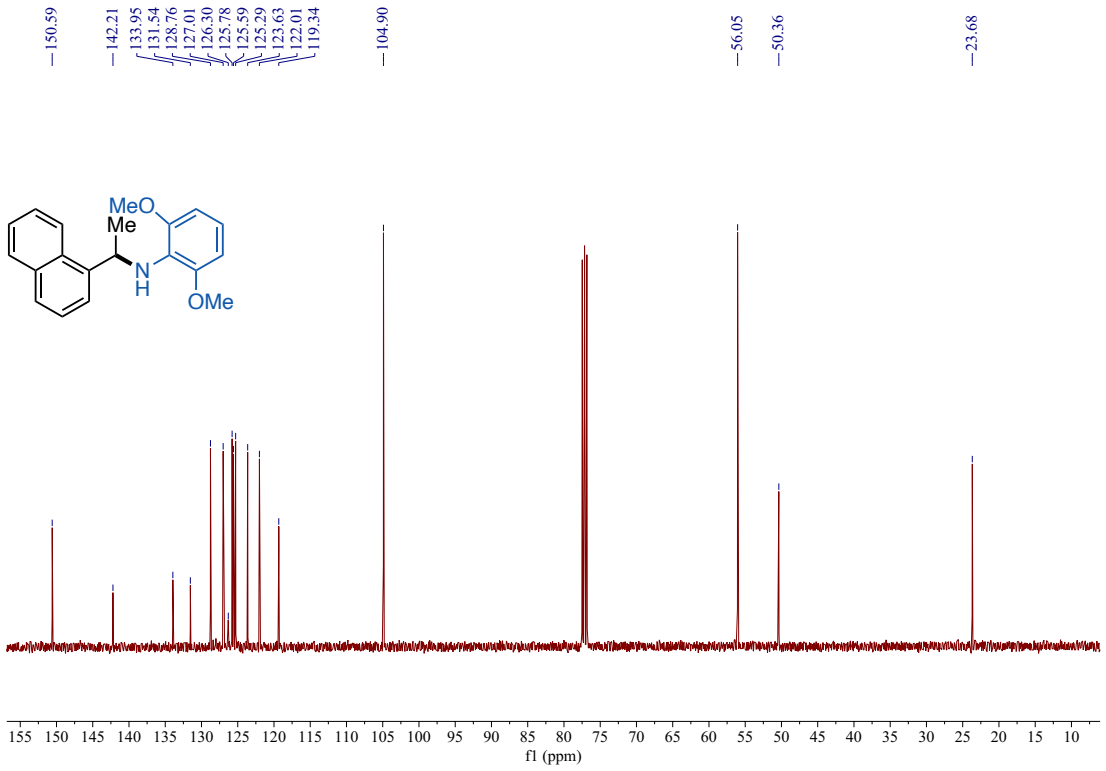

^{13}C NMR of 2,6-dimethoxy-*N*-(1-(naphthalen-1-yl)ethyl)aniline (101 MHz, $CDCl_3$)